LBL-15855
c.2

Lawrence Berkeley Laboratory
UNIVERSITY OF CALIFORNIA

Materials & Molecular Research Division

RECEIVED
LAWRENCE
BERKELEY LABORATORY

AUG 10 1983

LIBRARY AND
DOCUMENTS SECTION

MOLECULAR BEAM SCATTERING

M.F. Vernon
(Ph.D. Thesis)

July 1983

TWO-WEEK LOAN COPY

This is a Library Circulating Copy which may be borrowed for two weeks. For a personal retention copy, call Tech. Info. Division, Ext. 6782.

Prepared for the U.S. Department of Energy under Contract DE-AC03-76SF00098

LBL-15855 c.2

DISCLAIMER

This document was prepared as an account of work sponsored by the United States Government. While this document is believed to contain correct information, neither the United States Government nor any agency thereof, nor the Regents of the University of California, nor any of their employees, makes any warranty, express or implied, or assumes any legal responsibility for the accuracy, completeness, or usefulness of any information, apparatus, product, or process disclosed, or represents that its use would not infringe privately owned rights. Reference herein to any specific commercial product, process, or service by its trade name, trademark, manufacturer, or otherwise, does not necessarily constitute or imply its endorsement, recommendation, or favoring by the United States Government or any agency thereof, or the Regents of the University of California. The views and opinions of authors expressed herein do not necessarily state or reflect those of the United States Government or any agency thereof or the Regents of the University of California.

LBL-15855

MOLECULAR BEAM SCATTERING

Matthew Fowler Vernon

Materials and Molecular Research Division
Lawrence Berkeley Laboratory and
Department of Chemistry
University of California
Berkeley, California 94720

This work was supported by the Director, Office of Energy Research, Office of Basic Energy Sciences, Chemical Science Division of the U.S. Department of Energy under Contract No. DE-AC03-76SF00098.

MOLECULAR BEAM SCATTERING

Matthew Fowler Vernon

Materials and Molecular Research Division
Lawrence Berkeley Laboratory and
Department of Chemistry
University of California
Berkeley, California 94720

ABSTRACT

The molecular beam technique has been used in three different experimental arrangements to study a wide range of inter-atomic and molecular forces.

Chapter 1 reports results of a low energy (0.2 kcal/mole) elastic scattering study of the He-Ar pair potential. The purpose of the study was to accurately characterize the shape of the potential in the well region, by scattering slow He atoms produced by expanding a mixture of He in N_2 from a cooled nozzle. No new information was obtained, due to an inaccuracy of the measurement of the Ar beam velocity, and the large spread in He velocities produced by the mixed gas expansion.

Chapter 2 contains measurements of the vibrational predissociation spectra and product translational energy for clusters of water, benzene, and ammonia. The experiments show that most of the product energy remains in the internal molecular motions. The major hindrance to extracting potential information from the spectra is the inability to properly account, in model calculations, for large amplitude motion present in the clusters.

Chapter 3 presents measurements of the reaction $Na(3^2[_{3/2})$ + $HCl(^1\Sigma^+ v=0) \rightarrow NaCl\ (^1\Sigma^+) + H(^2S)$ at collision energies of 5.38 and 19.4 kcal/mole. This is the first study to resolve both scattering angle and velocity for the reaction of a short lived (16 nsec) electronic excited state. The large reaction enhancement observed in the excited state, as well as the absence of a measureable alignment or orientation polarization dependence, are consistent with the expected electron jump mechanism for this reaction. The product translational energy and recoil angle distributions are consistent with an early repulsive energy release.

Apendices I and II describe computer programs written to analyze molecular beam expansions to extract information characterizing their velocity distributions, and to calculate accurate laboratory elastic scattering differential cross sections accounting for the finite apparatus resolution. Appendix III contains experimental results which attempted to determine the efficiency of optically pumping the $Li(2^2P_{3/2})$ and $Na(3^2P_{3/2})$ excited states. A simple three level model for predicting the steady state fraction of atoms in the excited state is included.

Dedication

This thesis is dedicated to my parents, Marion and Atlee, for sacrificing much of their time and energy to enable me to pursue my academic interests, and to Julie Patrusky, for supporting me with her love.

ACKNOWLEDGMENTS

The diverse experiments of this thesis are a tribute to the foresight of Professor Yuan Lee. Working in his molecular beam laboratory has always been exciting. The hard work required usually paid off with astonishing success, and I will always be amazed by Yuan's "second sense" for thinking up qualitatively new experiments, or in ascertaining the origin of experimental trouble. In regards to the last point, I always thought that Yuan'a ability to find my mistakes (the closed gate valve incident) were a testiment to his long exposure to the daily comings and going of laboratory work, where sometime in the past, a graduate student, or himself, had committed a similar error.

The main advantage of working with Yuan were the graduate students and post docs he attracted. Everyone was helpful. In particular, Chris Becker, Piero Casavecchia, Carl Hayden, Hoi-Sing Kwok, Jim Lisy, Andre Tramer, Hartmut Schmidt and Paul Weiss all worked hard on the projects of this thesis. These experiments would never have been possible without them.

During my stay at Berkeley, I became especially close to Scott Anderson, Doug Krajnovich, and Dan Neumark. I could always talk to them about all matters of science, and they usually had good advice to offer. Doug, in particular, was helpful in steering my way through the interpretation of the reactive scattering work.

Professor Klemperer (Harvard) and Professor John Hemminger (Irvine) were the first to interest me in experimental chemistry,

especially molecular beam experiments. I owe much to them for guiding me at this impressionable stage.

Finally, special thanks go to the individuals at LBL - Fred and Ed, Ed Voronin, Charlie Taylor, Dick Escobales and especially Ann Weightman. These people were always helpful, and a pleasant reminder that there were some advantages to working at LBL.

This work was supported by the Director, Office of Energy Research, Office of Basic Energy Science, Chemical Science Division of the U.S. Department of Energy under Contract No. DE-AC03-76SF00098.

TABLE OF CONTENTS

	Page
ABSTRACT	1
DEDICATION	i
ACKNOWLEDGMENTS	iii
TABLE OF CONTENTS	v
I. ELASTIC SCATTERING OF Ar-He AT LOW ENERGIES	1
A. Introduction	1
B. Experimental Arrangement	4
C. Beam Velocity Characterization	15
D. Determination of the Interaction Potentials from Experimental Differential Cross Sections	17
E. Suggested Improvements	24
REFERENCES	26
TABLES	27
FIGURE CAPTIONS	29
FIGURES	32
APPENDIX I. TIME-OF-FLIGHT MEASUREMENT PROCEDURE	40
A. Theory and Methods for TOF Calibration	40
B. Time-of-Flight Program Kelvin and Directions for Use	50
REFERENCES	53
TABLES	54
FIGURE CAPTIONS	55
FIGURES	56
PROGRAM LISTING	58

Page

APPENDIX II. ELASTIC SCATTERING PROGRAM FOR THE COMPARISON OF LABORATORY ANGULAR DISTRIBUTIONS CALCULATED FROM THE CENTER OF MASS FRAME DIFFERENTIAL CROSS SECTION 75

A. Introduction. 75

B. Description of Program Methods. 77

C. Geometry of Scattering. 83

D. Input Record Structure. 87

E. Definition of Parameters. 88

F. Examples of Several Standard Program Uses 92

G. Changing the Potential Form 94

REFERENCES 96

PROGRAM LISTING. 97

II. INFRARED VIBRATIONAL PREDISSOCIATION OF C_6H_6, H_2O, and NH_3 CLUSTERS STUDIED BY THE CROSSED LASER-MOLECULAR BEAM TECHNIQUE. 174

A. Introduction. 174

B. Experimental Arrangement. 176

1. Infrared Laser. 176

2. Perpendicular Laser-Molecular Beam Arrangement. . . 177

3. Coaxial Laser-Molecular Beam Arrangement. 178

C. Experimental Observables. 179

D. Benzene 181

1. Introduction. 181

2. Results 183

3. Discussion. 188

E. Water 192

1. Introduction. 192

Page

2. Experimental Results. 196

3. Analysis. 199

4. Discussion. 203

a. Spectroscopy. 203

b. Dynamics. 210

F. NH_3 216

1. Introduction. 216

2. Experimental Results. 218

3. Discussion. 220

a. Spectroscopy. 220

b. Dynamics. 220

4. Summary 223

REFERENCES 226

TABLES 234

FIGURE CAPTIONS. 241

FIGURES. 245

III. REACTIVE SCATTERING OF $Na(3^2P_{3/2})$ + HCl. 265

A. Introduction. 265

B. Historical Review of Scattering Studies of Short Lived Atomic Excited States. 267

1. Na^* + H_2. 268

2. Na^* + CO. 269

3. Na^* + N_2. 270

4. Ca^* + HCl 277

Page

C. Experimental Arrangement. 279

1. Sodium Beam 280

2. HCl Beam. 283

3. Optical Preparation of $Na(3^2P_{3/2})$ 284

4. Angular Distribution Measurement Procedure. 288

5. Doppler Shift Measurements of Na Velocity Distributions 292

6. Product Velocity Measurements 293

7. Variation of Total Cross Section with Collision Energy 297

D. Experimental Results. 299

E. Data Analysis 306

F. Discussion. 313

G. Conclusion. 318

REFERENCES 319

FIGURE CAPTIONS. 322

FIGURES. 327

APPENDIX III. OPTICAL PUMPING STUDIES OF THE Li 2S⟶2P AND Na 3S⟶3P TRANSITIONS. 355

REFERENCES 369

FIGURE CAPTIONS. 370

FIGURES. 372

I. ELASTIC SCATTERING OF Ar-He AT LOW ENERGIES

A. INTRODUCTION

In the last decade, remarkable progress in understanding the theoretical basis of intermolecular forces has been made.[1] The development of the molecular beam technique has figured prominently in the experimental testing of the predictions of theories of intermolecular bonding. In particular, for the noble gas pair interactions, it has been possible to derive accurate experimental intermolecular potentials from measurements of the energy dependence of the angle-resolved differential cross-sections, and to relate these derived potentials to *ab initio* and semi-empirical theories of intermolecular forces.[2]

Despite general agreement between theory and experiment, the pair potentials involving He are still thought to be poorly characterized experimentally in the well region of the intermolecular potential.[3] Most theories assume that the long range potential follows the well-known dispersion series ($-C_6/r^6 - C_8/r^8 - \ldots$), while the short range repulsive core shape is modeled by the Born-Mayer $A*\exp(-\alpha r)$ function. The major difference between theories is the manner in which the potential is interpolated between these two limiting ranges, in the well region.

Experimental determinations of the He-rare gas potentials show differences outside of the stated errors of the respective experiments.[4,5,6,7] For example, the binding energy of the He-Ar potential is reported to be known to an accuracy of 3 percent,[1] yet, the best experiments were performed at collision energies 10-30 times

that of the derived well depths. This suggests that the well region may not be sensitively probed at these elevated collision energies, because the centrifugal potential screens it from contributing significantly to the scattering. In Fig. 1, the classical turning points are shown for a few partial waves at three collision energies using the best experimentally derived He-Ar potential. The effect of reducing the collision energy on the range of the potential probed is clearly seen.

An additional problem associated with the experimental determination of the potential involves the form of the model potential function chosen to be fit to the data. Many parameterizations use the well depth as a scaling factor, i.e., $V(r) = \varepsilon * f(r/r_m)$, where ε is the well depth, r_m the internuclear separation at the potential minimum, $f(x)$ the reduced, dimensionless potential, and $V(r)$ the intermolecular potential. Changing ε, consequently, affects the whole of the potential. If care is not exercised and several distinct parameterizations not tested, optimizing ε may result in an improved fit to the potential in the range of the experimental collision energy, but degrading the fit in the well region.[4] As the exact form of the potential is unknown, to construe this derived ε obtained at a high collision energy relative to the well depth, as the true well depth, is actually an extrapolation to low collision energy. Depending on the ratio of the collision energy to the true well depth, E/ε, this extrapolation may or may not be accurate.

Four differential cross-section measurements have been published on the He-Ar potential.[4-7] Table 1 summarizes the collision energy (E), energy resolution ($\Delta E/E$), the derived well depths (ϵ) and bond lengths (r_m) of these studies. The large variation in the potential parameters, especially ϵ, is evident. In the most recent and accurate study by Aziz, et al.,[7] it was suggested that the discrepancy between the published potential values is related to the method of analysis of the small angle ($\theta < 5^\circ$) scattering data. The authors say that the error in the data in this range is dominated by systematic experimental errors and not the statistical counting errors as assumed in several other studies.[4,6]

With this historical background, a new set of scattering experiments was planned for the He-Ar system. The goal of the experiments was to measure the differential cross-sections for a wide range of collision energies (E/ϵ = 30, 5, 2) and to simultaneously fit all the data to a single potential. By covering a large range of collision energies, and utilizing flexible potential forms, the above-mentioned problems with the ϵ scaling parameter can be avoided. To insure that the collision energy was chosen sufficiently low to accurately probe the potential minimum, a series of computer simulations were performed to show the sensitivity of the data at a particular energy to the potential parameters. Experimentally, the technique of aerodynamic deceleration of He by N_2 was used to achieve the low He velocities necessary for a reduced collision energy of $E/\epsilon = 2$. The characteristics of the velocity distributions produced in this manner and the

problems associated with this method of beam production were investigated.

The structure of this chapter is as follows: In the second section, the experimental method and data error analysis are described. The third section details the beam velocity measurements needed for an accurate knowledge of the absolute distribution of collision energies. The fourth section sketches the feasibility of a direct deconvolution of the experimental data to obtain a potential independent of a presupposed analytical form. The final section is devoted to suggested improvements in the experiment. Two appendicies describe general computer programs written to analyze the data and to plan experiments.

B. EXPERIMENTAL ARRANGEMENT

The differential cross-sections were measured in a new rotating detector, crossed beams apparatus the details of which are given elsewhere.[8] Briefly, two supersonic molecular beams, each doubly differentially pumped, are crossed in a collision chamber. The Ar beam is 100 percent amplitude modulated at 150 Hz by a tuning fork chopper located in the second differential pumping region. The scattered He atoms are detected by a rotating mass spectrometer consisting of an electron bombardment ionizer, r-f quadrupole mass filter, and a Daly ion counter. The detector rotates in the plane defined by the atomic beams. The pulses from the Daly counter are discriminated, then counted by standard pulse counting electronics. From the phase of the tuning fork modulation, the ion pulses are

scaling, a confidence limit for the scale factor, α, was calculated. This was done by expanding the X^2 error about the optimal scale value, α_0,

$$X^2(\alpha) = X^2(\alpha_0) + \frac{1}{2}\frac{d^2X^2}{d\alpha^2}(\alpha - \alpha_0)^2 \tag{1}$$

and using the curvature of the fit, $d^2X^2/d\alpha^2$, to measure the change in scale factor which produces a given change in the fit. The change in α_0 necessary to increase X^2 by 1/3 of the data error for the points used in the scaling was taken as a measure of the scaling error. This estimate of the scaling error was always less than $\alpha_0 * 10^{-6}$, and no correction for it was made.

The first order dead time correction was computed from the equation

$$TCR = \frac{MCR}{1 - MCR*PW} \quad , \tag{2}$$

where TCR is the true count rate, MCR is the measured count rate and PW is the discriminator pulse width (50 nanoseconds). The correction was applied to both data channels to obtain the true signal, the difference of the corrected channels. The error at each angle was incremented by the change in the signal introduced by the dead time correction.

Several additional systematic errors were investigated for their effects on the data, and found to be either negligible or uncorrectable with the measured experimental parameters. For example, there is

a variation in phase of the detected product with laboratory angle. The phase and gate width of the chopper gating circuit was set by first maximizing the modulated Ar signal looking directly at the modulated Ar beam, then adjusting for the difference in arrival time of the He atoms from the collision center using the measured He and Ar velocities (see Sec. C below). If the elastically scattered He atoms had the same laboratory velocity at all angles, and this velocity was the same as the He beam (reference) velocity, no correction would be necessary. In general, the He is moving faster in the laboratory at larger scattering angles. If the laboratory velocity at a given angle, θ, is $V_0(1 + \alpha)$, V_0 being the He beam velocity for which the phase/gate width is set, the time difference for arrival of the He at this angle from its reference value will be

$$\Delta t = \frac{L}{V_0} \frac{\alpha}{1 + \alpha} \quad . \tag{3}$$

In this equation, L is the flight distance to the detector from the collision volume (L = 30 cm). At the maximum angle detected, Δt = .06 msecs for the Newton diagram in Fig. 3(a) and Δt = .16 msecs for the diagram in Fig. 3(b). From the measured Ar beam modulation function, the rise time (10–90 percent of full scale) for the gated Ar beam is .5 msecs. These phase delays are thus neglected, being within the rise time of the chopper function.

Secondly, the angular calibration of the apparatus was checked by locating the first minimum/maximum in the laboratory cross sections on

routed to either of two counters, depending on whether the Ar beam is blocked or unblocked. The difference between the counters gives the signal at a particular detector angle.

To obtain sufficient signal to noise ratios for the complete angular range measured, separate scans were made of smaller intervals. The variation of the signal count rate with angle of three orders of magnitude meant that different detector settings (emission current or quadrupole transmission) were necessary to reduce pulse pile-up effects in the counting electronics at small angles, without sacrificing sensitivity at large angles.

Each of the smaller angular intervals was scanned an even number of times, alternating the scan direction to minimize the systematic errors introduced by the large He background which is correlated with the detector position (see Fig. 2). The high intensity of the He beam coupled with the low pumping speed for He by ion pumps, results in a background count rate roughly 10^3 - 10^4 times larger than the signal count rate. When the detector angle is changed, the finite time constant for the detector pressure to equilibrate to the different He gas load results in a monotonic increase or decrease in the He count rate at the new angle, depending on the direction of rotation of the detector. For example, if all scans were made in the same direction from small to large angles, the signals obtained would be systematically high. As the background channel is always accumulated after the signal and background channel, the background channel would be smaller by an amount proportional to the rate of the He background decrease with

time. By reversing the scan direction, the data is biased an equal amount in favor of the background channel. The sum of the bidirectional scans would subsequently average out all linear correlations of the He background with detector angle.

The above effect is most prominent at small angles where the background is largest, and the counting times usually shortest. To properly quantify the magnitude of this error, a careful study of the time dependence of the signal after rotating the detector to a small angle from either direction should be done. Likewise, if the detector is rotated directly from a small angle to a large angle at which the background is substantially lower, the time dependence of the signal at the new large angle position will show if, within the statistical errors, the decrease of the He background with time has measurable effects.

Within the data statistical uncertainty, there was no need to correct for long term fluctuations in detector response, beam intensities, etc. as done in a previous study.[4] It was found that for scans made on separate days with all machine indicators unchanged, the signal levels agreed within 1.5 percent. This was taken as the inherent stability of the experiment. No long term signal could be obtained more accurately than this error.

The smaller angular intervals were joined together to produce the complete angular scan. Care was taken to insure that adjacent scans overlapped for many points to reduce systematic scaling errors between large and small angles. To ascertain the error introduced by the

both sides of the He beam. These minima/maxima correspond to a common center-of-mass scattering angle. For the liquid nitrogen cooled He data, with a 1 percent velocity spread, a single Newton diagram determination of the location of the primary beam gives no angular offset within the expected accuracy. The absolute angular accuracy of the measurements is taken as better than $\pm 1/4^\circ$. A more precise determination of the offset could be obtained from a detailed fit to the first two oscillations on both sides of the He beam.

As noted above, the signal is derived from the difference between two large numbers. It is possible for the background to be incorrectly accounted for by this difference if the attenuation of the He beam by the presence of the Ar is of the order of the signal error. Figure 2 shows the background count rate as a function of angle. The asymptotic value for angles larger than 27° is the sum of the inherent detector background, and an effusive component from the main scattering chamber when the He beam is operating. The step in the He count rate over the angular range $22\text{-}27^\circ$ is from back scattered He beam gas which begins to hit the front of the detector at these angles, and increases the scattering of He beam gas into the detector. At angles less than 10°, the count rate begins to increase exponentially. At this position, the detector begins to view direct effusive He gas from the differential pumping region. Small angle scattering of the He beam from background gas and other He beam atoms moving at different velocities also begins to contribute at these small angles.

When the Ar beam is unblocked by the chopper, the He beam is attenuated by the amount $e^{-n\sigma L}$, where n is the Ar beam gas density

at the scattering zone, σ is the total cross section for scattering He out of the beam, and L is a characteristic length of the collision volume. The He background then changes when the Ar beam is blocked or unblocked. The difference between the two counters will give

$$(S + B_{on}) - B_{off} = S + (e^{-n\sigma l}-1)(B_{corr}) \quad . \tag{4}$$

Here, B_{on} and B_{off} are the background counts with the Ar beam on and off respectively, S is the true signal, $e^{-n\sigma l}$ the attenuation factor for the He beam, and B_{corr} the background He counts correlated with the Ar modulation.

To quantify this effect, an estimate of the Ar beam gas density at the collision zone, as well as the total scattering cross section, is needed. The number density at the scattering center, n, is given by

$$n = \frac{K}{4\pi} n_o(T_o, P_o) \left(\frac{r}{d}\right)^2 \quad , \tag{5}$$

where the peaking factor, K, is 2 for a monatomic gas, $n_o(T_o, P_o)$ is the gas density at the nozzle, r is the nozzle radius, and d is the distance between the nozzle and the collision volume. Equation (5) is derived from the total gas flow through the nozzle from a model developed by Habets.[9] The model assumes that the intensity is linear with gas flow. For the experimental conditions used in the present study, the beams are operated near the high pressure limit where non-ideal background gas interactions begin to affect the expansion. The beam

intensities are maximized, so small changes in nozzle backing pressure produce no increase in beam intensity. In this regime, there is no linear relation between beam intensity and backing pressure. Hence, Eq. (5) is an upper bound for the beam density in the scattering volume. For the Ar beam source the parameters are r = .0038 cm, d = 5.75 cm, and $n_o = 2 \times 10^{19}/cm^3$, giving a density of $1.5 \times 10^{12}/cm^3$ at the collision volume. The total cross section for scattering out of the He beam is conservatively assumed to be ~5Å^2. The fractional attenuation of the primary (He) beam is then 2.5×10^{-4}. Using Eq. (4), the error bars at each angle should be increased by the factor $2.5 \times 10^{-4} * B_{corr}$. B_{corr} is assumed bounded by the quantity $B(\theta) - B(\theta_{max})$ where $B(\theta)$ is the background count rate measured at the detector angle θ, and $B(\theta_{max})$ is the large angle background count rate which is taken to be uncorrelated with the tuning fork. The angle dependence of the background shown in Fig. 2 then gives the shape of this correction.

The attenuation correction, when applied to the signals measured here, gave a differently shaped cross section, suggesting that for angles larger than ~10°, the data is much less affected than this model predicts. The potentials derived from the data corrected for the modeled attenuation effect were substantially at odds with what one would reasonably expect on physical grounds, as well as having large X^2 errors. As a large component of the He count rate is a result of pressure buildup in the detector (and this should be uncorrelated with the chopper modulation), the upper bound chosen for

B_{corr} is probably too high. For this reason, no correction for the attenuation was made to the data as it affected the cross sections to an unreasonable extent, and the proper experimental measurements to account for it were not available.

To experimentally measure the attenuation effect, the background He level with and without the Ar beam must be measured. The background He levels can be measured by the time-of-flight (TOF) technique. To measure a fractional difference of 2×10^{-4} in the background would take ~1000 seconds if the average He count rate was $\sim 10^{+6}$/sec, ~1 millisecond of time of the TOF spectrum was averaged to determine the background, and the TOF wheel speed was ~400 Hz. As the Ar beam is on or off for large time intervals, this method would not measure the background correlated on the chopper time scale. It would indicate if the attenuation of the He beam had an observable effect which would need to be accounted for in the data analysis.

The final systematic effect investigated concerns the fraction of He atoms which undergo multiple collisions before leaving the collision volume. The intense He beam used at the .4 kcal/mole collision energy (660 psi backing pressure, 30 μ nozzle diameter, nozzle-collision volume distance of 6.75 cm) produces a He atom density of $1.4 \times 10^{14}/\mathrm{cm}^3$ at the scattering volume. The density of scattered He atoms in the collision volume, N_{He}^{*}, is given by

$$N_{He}^{*} = N_{He} \left(\frac{N_{He}\, N_{Ar}\, \sigma_{Ar-He}\, v_{Ar-He}^{rel}\, V}{N_{He}\, A\, v_{He}}\right) = 2.1 \times 10^{10}/\mathrm{cm}^3 \quad . \qquad (6)$$

In Eq. (6), N_{He} and N_{Ar} are the number densities of the He and Ar beams at the collision volume, σ_{Ar-He} is the total cross section for He-Ar scattering, v^{rel}_{Ar-He} is the relative velocity between the He and Ar beams, V the collision volume, v_{He} the He beam velocity, and A the cross sectional area of the He beam. The numerator of the parenthetical expression in Eq. (6) is the number of He atoms scattered per second from the collision volume, and the denominator is the number of He atoms entering the collision volume per second. Hence, the parenthetical expression is the percentage of He atoms scattered. The number of singly scattered atoms, N_{He**}, which collide with the undeflected He beam atoms (the most probable multiple collision event) is given by

$$N_{He**} = \frac{N^{*}_{He}\, N_{He}\, \sigma_{He*-He}\, v^{rel}_{He*-He}\, V}{2 \sin\theta} \quad , \tag{7}$$

where σ_{He*-He} is the collision cross section for He-He collisions and v^{rel}_{He*-He} the relative velocity between the colliding He atoms. The factor 2 sinθ accounts for the overlap of the incident He beam with the He scattered at an angle θ. Normalizing Eq. (7) to the singly scattered He signal will give the fraction of He atoms multiply scattered, $f_{He}{}^{**}$,

$$f_{He**} = \frac{N^{*}_{He}\, N_{He}\, \sigma_{He*-He}\, v^{rel}_{He*-He}\, V}{2 \sin\theta\, N_{Ar}\, N_{He}\, \sigma_{ArHe}\, v^{rel}_{Ar-He}\, V} \quad . \tag{8}$$

Combining Eqs. (6) and (8) one obtains for f_{He**}

$$f_{He**} = \frac{N_{He}\ \sigma_{He*-He}(\theta)\ v^{rel}_{He*-He}(\theta)\ L}{2\ \sin\theta\ \ v_{He}} \quad . \tag{9}$$

In Eq. (9), L is a characteristic length of the collision volume. The angular dependence of Eq. (9) is approximated by modeling the He*-He collision cross section by the classical cross section for orbiting collisions. For He atoms deflected by colliding with Ar through an angle θ with respect to the incident He beam, the orbiting cross section with the remaining undeflected He beam will be

$$\sigma_{orb}^{He*-He}(\theta) = \pi \left(\frac{6\ C_6}{\mu\ v_{rel}^2(\theta)}\right)^{1/3} \quad , \tag{10}$$

where C_6 is the C_6 coefficient for the He-He potential.[11] The laboratory solid angle into which these orbiting collisions are redistributed is $\sim\sin^2\theta$. The fraction of the signal lost at each angle, $f(\theta)$, after substituting numerical values in (9) and (10) is

$$f(\theta) = 3 \times 10^{-6}\ (\sin\theta)^{4/3} \quad . \tag{11}$$

Therefore, even at small angles, the effect is negligible under the strong assumption that all of the orbiting collisions are lost.

C. BEAM VELOCITY CHARACTERIZATION

A knowledge of the absolute velocity distribution of the atomic beams is necessary for the quantitative determination of the potentials. The method used to obtain the velocity distributions is described in Appendix 1. The extracted velocity distribution parameters are listed in Table II. The ion flight time delay (in microseconds) was not measured, but computed from the canonical $3(M(amu))^{1/2}$ relation established by previous tests for 75 volt ions with negligible initial velocity.

For the neat, high pressure He beam expanded from the liquid nitrogen cooled nozzle, the error in the velocity is determined by the ratio of the ionizer length to the neutral flight path, or 1/92.

The velocity distribution of this beam is extremely narrow. At the time the velocity was measured, no means of delaying the start of the multi-channel scaler (MCS) was available to allow a high resolution window to be centered about the peak He beam velocity. Consequently, a larger dwell time (decreased resolution) was necessary to bring the velocity distribution within the 255 channels available in the MCS.

A direct deconvolution of the He velocity data (see Appendix 1) shows the observed width to be dominated by the time response of the apparatus. The velocity distribution width parameter, β, is poorly determined for this beam, but must be greater than the value listed. The distribution in velocities is already so small, that the error in determining β does not affect the data analysis below.

The measured He flow velocity for the liquid nitrogen cooled nozzle determined an effective nozzle temperature of 88°K. At this temperature, the predicted flow velocity of a mixture of 30 percent N_2 in He would be 5.71×10^4 cm/sec from the average mass of the gas mixture. The measured value of 5.85×10^4 cm/sec is 2.5 percent faster, consistent with either (or both) a small 5 percent additional contribution to the heat capacity from the cooling of the N_2 rotations, or an error of 2 percent in the gas mixture ratio.

The aerodynamically decelerated He beam (30 percent N_2 in He) has a broad velocity distribution. When higher nozzle backing pressures were applied, the N_2/He beam would form various $(N_2)_m(He)_n$ clusters. With only moderate pressures, the ratio of clustered to unclustered He could be easily changed, obtaining totally condensed beams of large clusters if desired. The hydrodynamic deceleration, as noted above, does lower the velocity as predicted, but the onset of cluster formation ultimately restricts the speed ratios to small values.

The Ar beam was cooled by a 93°K copper block and measured on a third apparatus with a 62 cm flight path. This apparatus was used to reduce the gas load of Ar into the detector of the crossed beams scattering machine so subsequent experiments would have a small mass 20 background. The thermocouple temperature of the copper cooling block predicted an Ar velocity of 3.1×10^4 cm/sec if the Ar gas at the nozzle was in equilibrium with this temperature. The measured value of 4.08×10^4 cm/sec is much faster. The implications of this difference on the derived potentials will be discussed in more detail below.

D. DETERMINATION OF THE INTERACTION POTENTIALS FROM EXPERIMENTAL DIFFERENTIAL CROSS SECTIONS

The determination of interaction potentials from differential cross section data has followed two methods. The most desirable of these is to invert the scattering data to obtain a numerical potential using semiclassical[10,11,12] or quantum mechanical[13] algorithms. The inversion involves two steps. First, the laboratory differential cross section must be fit by a set of phase shifts. Three approaches to this problem have been published. The first, by Buck,[11] involves parameterizing the phase shifts by analytical functions, then varying the function parameters to fit the observed data. The second method, by Kleingbeil,[10] uses a non-linear least squares fit of the phase shifts to the observed data, assuming the Born approximation to be valid beyond a critical impact parameter. The third method, by Gerber and Shapiro,[13] is based on the unitary properties of the scattering wave equation to obtain the phase shifts. Shapiro[14] has devised a method for transforming experimental data to the center-of-mass frame which is necessary before the phase shifts can be obtained by the unitary scheme.[13] The only application of these techniques to derive a true quantum mechanical potential from experimental data is by Gerber, et al.[15] for the He-Ne potential.

All of the methods suffer from the necessity of assuming that either a single set of phase shifts is responsible for the observed scattering, or that an energy-angle scaling relationship, which can correct for the velocity averaging effects, is known. Any geometrical

averaging by the experiment from the finite detector or collision volume sizes can be accounted for by comparing the laboratory differential cross sections with transformed and geometrically averaged center-of-mass differential cross sections. For neat He beams where speed ratios in excess of 100 are possible,[16] a single set of phase shifts should dominate the observed scattering.

To test this assumption, the laboratory data taken at the .4 kcal/mole collision energy were fit under three different assumptions. First, a single Newton diagram was averaged only over the detector and collision volume dimensions. Second, allowance was made for the variation of the phase shifts at different positions in the collision volume. In general, this is necessary when the beam velocity spread, $\Delta v/v_0$, along a streamline is less than the beam's angular divergence, $\sin\theta \geq \Delta v/v_0$. If this inequality holds, the velocity transverse to the beam centerline will contribute more to the distribution of collision energies than the inherent velocity spread along the centerline. Third, a full averaging procedure including velocity averaging over each beam as well as positional averaging over the detector and collision volumes was done. The variation in the potentials determined under the three different sets of averaging conditions tests the ability of a single set of phase shifts to mimic the true laboratory measurements. For the .4 kcal/mole collision energy, all potential parameters were within 1 percent of each other for each of the three averaging conditions. It is, therefore, reasonable to assume the laboratory cross sections obtained with $\Delta v/v_0 \sim .01$ at the collision

energy .4 kcal/mole are well-approximated by a single set of phase shifts.

This brief discussion underscores the importance of using the highest speed ratios obtainable. Correcting for the finite velocity dispersion can only be done rigorously by the forward convolution method described below. If the experimental velocity averaging is small and well represented by a single set of phase shifts, the next step is to fit a sufficient number of laboratory angular measurements over an extensive angular range to obtain a converged set of phase shifts. For reasons cited below, we assume that this step can be done using available non-linear fitting routines.

The extraction of a potential from a set of phase shifts involves a semiclassical[10,11] or a quantum mechanical inversion.[13] The semi-classical procedure was tested first due to its relative computational simplicity. Two sets of quantum mechanical phase shifts for He-Ar were calculated at the energies of two experimental measurements from an assumed He-Ar potential. Parameterizing the potential, V(r), and internuclear separation, r, by u

$$V(r(u)) = E*(1 - \exp(-2*T(u))) \tag{12}$$

$$r(u) = u*\exp(-T(u)),\ 0 \leq u \leq \quad ,$$

it can be shown[10] that

$$T(u) = \frac{2}{\pi K} \int_u^{\infty} (b^2 - u^2)^{1/2} \frac{d\eta(b)}{db}\, db, \tag{13}$$

where $k = 2\pi(2\mu E)^{1/2}/h$, E is the collision energy, b the impact parameter, and $\eta(b)$, the phase shift curve. Given the phase shift curve and a value for u, Eq. (13) is solved for T(u) by an adaptive Chebeshev quadruture scheme discussed by Kleingbeil.[10] Once u, and T(u) are known, Eqs. (12) are used to obtain r(u) and V(r(u)). The potential V(r) is easily obtained by solving these equations for many values of u. The chief numerical obstacle (for the diffractive scattering of He-Ar at these energies) to the solution of Eq. (13) is computing the derivative of the phase shift curve, $\frac{d\eta}{db}$, at an arbitrary impact parameter, b. Spline, as well as 2, 3, 4, and 5 point Lagrangian interpolations were tested. The results are displayed in Fig. 4.

Since quantum mechanical phase shifts were computed and used as input to the inversion program, one does not expect to recover the exact potential by the semiclassical inversion scheme. By necessity, any phase shifts derived from experimental data would be quantum mechanical. The extracted potentials show two pathologies. First, the repulsive wall has oscillations which make the potential multivalued. In solving the equations for V and r in this range, V is always increasing with decreasing u while r oscillates as it approaches the classical turning point (u = 0). This oscillation results from the difficulty in interpolating a <u>derivative</u> which decreases monotonically with increasing impact parameters in this range due to the sparseness of negative phase shifts. Second, at the higher collision energy, the phase shifts produce a potential which

has a spurious hump, whose details are sensitive to the type of interpolation scheme. The hump is associated with the maximum of the phase shift curve. The density of phase shifts near the maximum is low, so the numerical interpolation of a first derivative is poor. The sign of the interpolated first derivative changes several times in this region, producing a second minimum. To avoid these shortcomings, the repulsive wall and well region of the phase shift curve need to be represented by functions whose first derivatives behave properly.

Shapiro[15] has outlined a quantum mechanical procedure for obtaining the potential from phase shifts using a distorted wave Born approximation. A set of reference potentials is used to continue the asymptotic dispersion series to smaller internuclear distances. The method improves if good reference potentials are available, and is not limited by a small number of significant phase shifts. For the He-Ar system, this method was not tested for its ability to recover a known potential from its phase shifts, because the computational complexity was too great to implement the algorithm from the published information.

The direct inversion procedures are seen to involve assumptions which are dependent on the system measured, as well as the experimental conditions. The errors introduced by these assumptions are difficult to assess. The only experimentally tested method[15] for removing the velocity dependence of the averaging assumes that a velocity-laboratory angle scaling relation holds for all angles over the spread of collision energies of the experiment (2 percent). For the He-Ne system,[15] the deconvoluted-inverted potential seemed as accurate as any derived

by assuming a potential form. For diffractive scattering, the method, although complex, appears promising. For these reasons, the forward convolution method was used to obtain potentials from the current measurements.

The forward convolution method uses a computer program to simulate an elastic scattering experiment, and through a least squares optimization of potential parameters, determine a best fit potential. The advantage of the forward convolution method is its stability. The method can achieve an accuracy dependent only on the knowledge of the experimental conditions. Moreover, because a single potential curve can be used to generate differential cross sections at different energies, multiple energy scattering experiments can be used simultaneously in the potential optimization. In the extreme case, a purely numerical potential consisting of a set of points $V(r_i)$, $\{i = 1\text{-}N\}$, can be optimized to derive a potential independent of any assumption of the potential shape, by using multiple experimental cross sections covering a wide range of collision energies. The convergence of this method to the correct potential should be easy, since a good guess of the initial potential can be made using flexible analytic potential forms.

The strong angular dependence of the diffractive oscillations necessitated writing a computer program which accurately accounts for the geometrical and velocity averaging of the experimental apparatus. Appendix 2 describes the program and numerical methods used to solve the scattering equations.

As an example of how the program can be used, a best fit SPHD[17] Ar-He potential was calculated assuming a range of approximations and

averaging effects. The solid line shown in Fig. 5(a) is a perfect experiment, consisting of one Newton diagram with an infinitesimally small detector. Curve A(•) allows for angular averaging of the detector (acceptance angle .56°) and beam divergences (1.40° He beam, 1.5° Ar beam), while restricting the scattering to a plane. The differential cross section of curve A(---) allows the phase shifts to vary with the position in the collision volume, to show the importance of beam angular divergence when the velocity dispersion along the centerline is small. Curves B(—) and B(---) are the three dimensional analogs of curves A(•), A(---). Here, the detector is treated as a two dimensional aperture and the collision volume has three dimensions. Curve C(—) includes velocity averaging over the atomic beam velocity distribution as determined by time-of-flight analysis. Finally, curve C(---) represents the fully averaged cross section for the actual experimental conditions. The detector size and collision volume are twice those of curve C(—). From this series of approximations, the role of finite apertures in determining the amplitude of the oscillations is seen to be especially important in the region of the minima.

The Ar-He data was analyzed by simultaneously fitting the potential parameters to the three different collision energy cross sections. Each data set was simulated by a different set of averaging parameters, chosen to give accuracy without sacrificing computational speed. The potential fit to the highest energy data [7] was the initial starting point for the optimization. Exhaustive variation of the potential parameters resulted in no major change from the starting potential

values, even though the two low energy data sets were poorly fit. Figure 6 shows the individually best fit cross sections and potential parameters for the three collision energies. Figure 7 compares the differential cross sections predicted by the individually best fit potentials for the other data sets.

Since the simultaneous fitting was unable to find a compromise "best" fit, it seemed best to investigate origins of other systematic errors in the experiments. As noted above, the Ar velocity for the low collision energies was higher than expected from the temperature of the cooling block. If the measured Ar velocity was in error, by changing its value we should be able to improve both of the low energy fits to the optimized high energy potential. Indeed, for v_{Ar} = 3.7×10^4 cm/sec, both low energy cross sections are predicted well within data errors by the Aziz[7] potential (see Fig. 8), and better than any potential optimized to them separately. The origin of the possible error in the Ar velocity is not clear. Most likely, the conditions of the Ar source during the scattering experiment were not the same as those measured in the time-of-flight apparatus. For this reason, no improvement in the potential was obtained from the present work.

E. SUGGESTED IMPROVEMENTS

The present study has shown that for an accurate determination of the He-Ar pair potential several experimental improvements are needed. First, an optimal size for the detector aperture and collision volume will yield more precise values for the amplitude of the diffractive

oscillations. These features are sensitive to the well shape. Second, initial experiments should measure the shape of the minimum of an oscillation for various beam conditions and aperture sizes. This would be fruitful in deciding the resolution of the experiment as well as verifying the computer simulations of the averaging effects.

The systematic errors noted above can also be reduced. The counting electronics can be maximized for minimum pile-up by using a 10 nanosecond discriminator pulse width. A smaller dwell time to measure the He beam velocity will provide a precise determination of the velocity distribution. Additional collimation of the He beam will reduce the small angle background. (A triple slit collimation arrangement as used in the cluster photofragmentation studies of Chapter 2 would be ideal.) A nonuniform angular grid near the minima and maxima of the oscillations to accurately determine positions on both sides of the primary beam, will be useful for determining angular offsets. Of course, modifications which reduce the background help minimize modulated background also. For He which is inefficiently pumped by ion pumps, turbomolecular pumps should offer substantial improvements.

REFERENCES

1. K. Tang, J. Toennies, J. Chem. Phys., 66, 1496 (1977).
2. G. Scoles, Ann. Rev. Phys. Chem., 31, 81 (1980).
3. Y. T. Lee, private communication.
4. C. H. Chen, P. E. Siska, Y. T. Lee, J. Chem. Phys., 59, 601 (1973).
5. K. M. Smith, A. M. Rulis, G. Scoles, R. A. Aziz, V. Nain, J. Chem. Phys. 67, 152 (1977).
6. M. Keil, J. T. Slankas, A. Kupperman, J. Chem. Phys., 70, 482 (1979).
7. R. Aziz, P. Riley, U. Buck, G. Maneke, J. Schleusener, G. Scoles, U. Valbusa, J. Chem. Phys., 71, 2637 (1979).
8. R. Sparks, Ph.D. thesis, University of California, Berkeley, 1979.
9. A. Habets, dissertation, Technische Hogeschool Eindhoven, 1977.
10. R. Klingbeil, J. Chem. Phys., 56, 132 (1972).
11. U. Buck, J. Chem. Phys., 54, 1923 (1971).
12. U. Buck, Rev. Mod. Phys., 46, 369 (1974).
13. R. Gerber, M. Shapiro, Chem. Phys., 13, 227 (1976), ibid., 234.
14. M. Shapiro, R. Gerber, U. Buck, J. Schleusener, J. Chem. Phys., 67, 3570 (1977).
15. R. Gerber, M. Shapiro, U. Buck, J. Schleusener, Phys. Rev. Lett., 41, 236 (1978).
16. J. Toennies, K. Winkelmann, J. Chem. Phys., 66, 3965 (1977).
17. R. Bickes, R. Bernstein, J. Chem. Phys., 66, 2408 (1977).

Table 1. Experimental parameters and conditions from previous scattering studies of He-Ar.

Author	Year	References	Collision Energy (kcal/mole)	Energy Resolution	Well Depth (kcal/mole)	r (Å)
Chen	1973	4	.48	.14	.048	3.54
Smith	1977	5	1.37	.18	.060	3.46
			.42	.18		
Keil	1978	6	1.45	.20	.0406	3.57
Aziz	1979	7	1.572	.028	.058	3.44

Table 2. Velocity distribution parameters.

Gas	Nozzle Temperature	$V_o(10^4$ cm/sec)	$\beta(10^{-8}$ sec^2/cm^2)	χ^2
He	88°K	9.57	75.5	2.8
He/N_2	88°K	5.85	1.47	29.
Ar	93°K	4.08	4.55	2.9

FIGURE CAPTIONS

Fig. 1. Collision energy and angular momentum dependence of the classical turning points for the He-Ar potential.

Fig. 2. Angular dependence of the He detector background.

Fig. 3. Newton diagrams for elastic He-Ar scattering at collision energies of .479 kcal/mole and .244 kcal/mole.

Fig. 4. Semiclassical inversion of phase shifts to determine the intermolecular potential.

(A) Potentials extracted from phase shifts computed for a collision energy of .479 kcal/mole using (—) -5 point Lagrange, (– – –) -4 point Lagrange, (· · ·) 3 point Lagrange, and (·-·) spline interpolations.

(B) Same as (A) except the phase shifts were computed at the collision energy .244 kcal/mole. Points are only indicated at positions where they differ from previously plotted points of the other interpolation types.

Fig. 5. Effect of experimental averaging on the observed cross sections.

(A) (—) Perfect experiment. (•) Spatial averaging over the detector aperture and collision volume for in-plane scattering only. (– – –) Same as (•) except the collision energy and phase shifts depend on the position in the collision volume.

(B) (—) Spatial averaging as for curve A(•), except now full three dimensional scattering allowed. (– – –) Same as curve B(—), but the phase shifts vary with position in the collision volume.

(C) (—) Same as curve A(•), with velocity averaging over the experimental velocity distributions. (---) Same as C(—), but in-plane collision volume dimensions and detector slits are twice as large. This corresponds to the conditions of the experiments performed here.

Fig. 6. Comparison of experimental and best fit cross sections obtained at each collision energy (—) calculated points, (---) experimental points with 1 standard deviation error bars.

(a) E = 1.57 kcal/mole, (b) .479 kcal/mole, (c) .244 kcal/mole.

Fig. 7. Comparison of best fits of Fig. 6 at the other two data sets. (—) - calculated points, (---) experimental points with 1 standard deviation error bar.

(A) Best fit .479 kcal/mole potential compared to 1.57 kcal/mole data.

(B) Best fit .244 kcal/mole potential compared to 1.57 kcal/mole data.

(C) Best fit 1.57 kcal/mole potential compared to .244 kcal/mole data.

(D) Best fit 1.57 kcal/mole potential compared to .479 kcal/mole data.

(E) Best fit .244 kcal/mole potential compared to .479 kcal/mole data.

(F) Best fit .479 kcal/mole potential compared to .244 kcal/mole data.

Fig. 8. Comparison of observed elastic scattering laboratory cross section with the Buck[7] Ar-He potential when the Ar velocity is 3.4×10^4 cm/sec. (a) $E_{col} = .45$ kcal. (b) $E_{col} = .20$ kcal/mole. (—) - Calculated cross section, (---) observed cross section with 1 σ error bars. The poor fit for angles smaller than 5° in part A is sensitive to details of the averaging procedure and to the outer well of the potential.

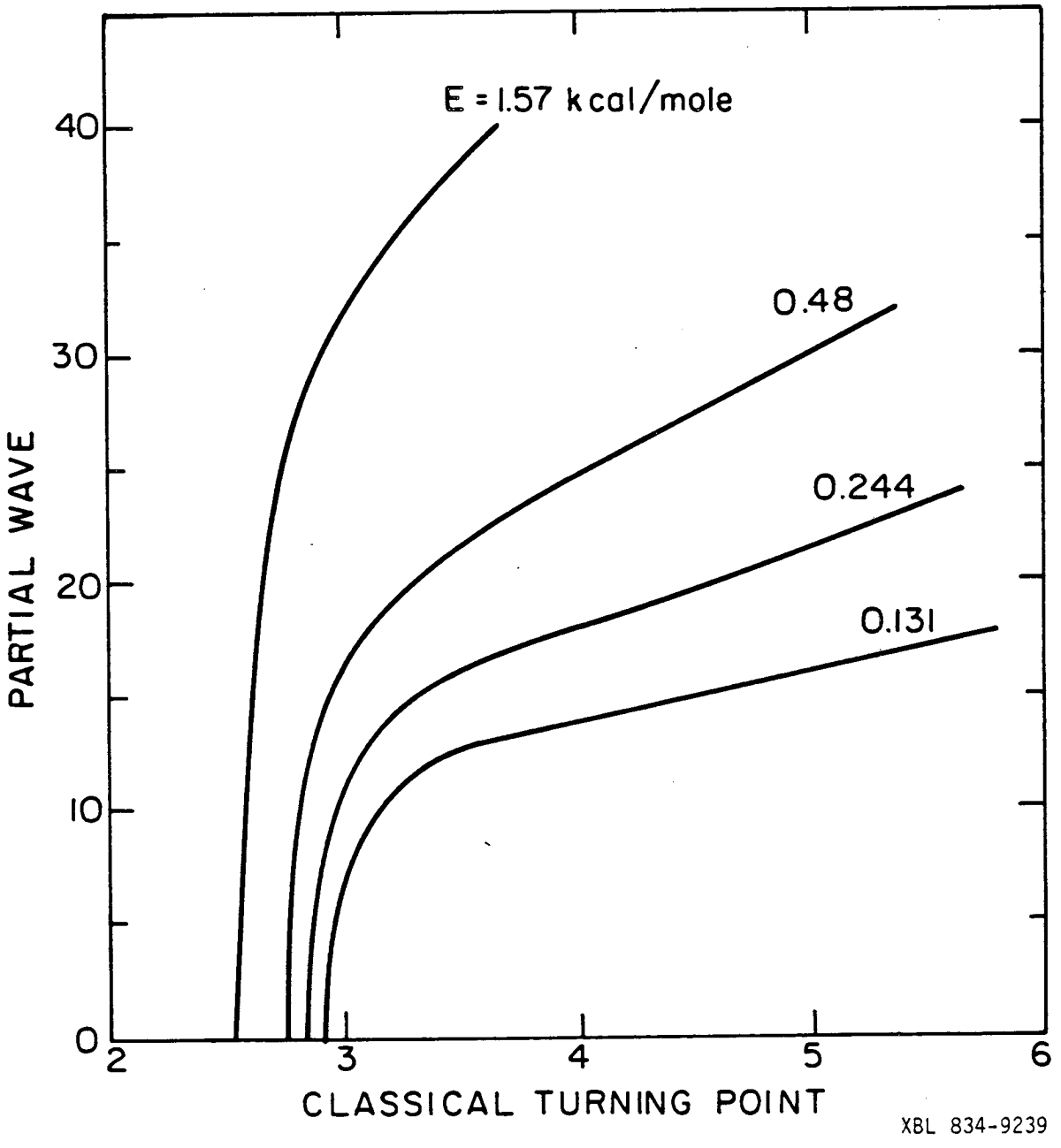
E = 1.57 kcal/mole
0.48
0.244
0.131
PARTIAL WAVE
0
10
20
30
40
2
3
4
5
6
CLASSICAL TURNING POINT
XBL 834-9239

Fig. 1

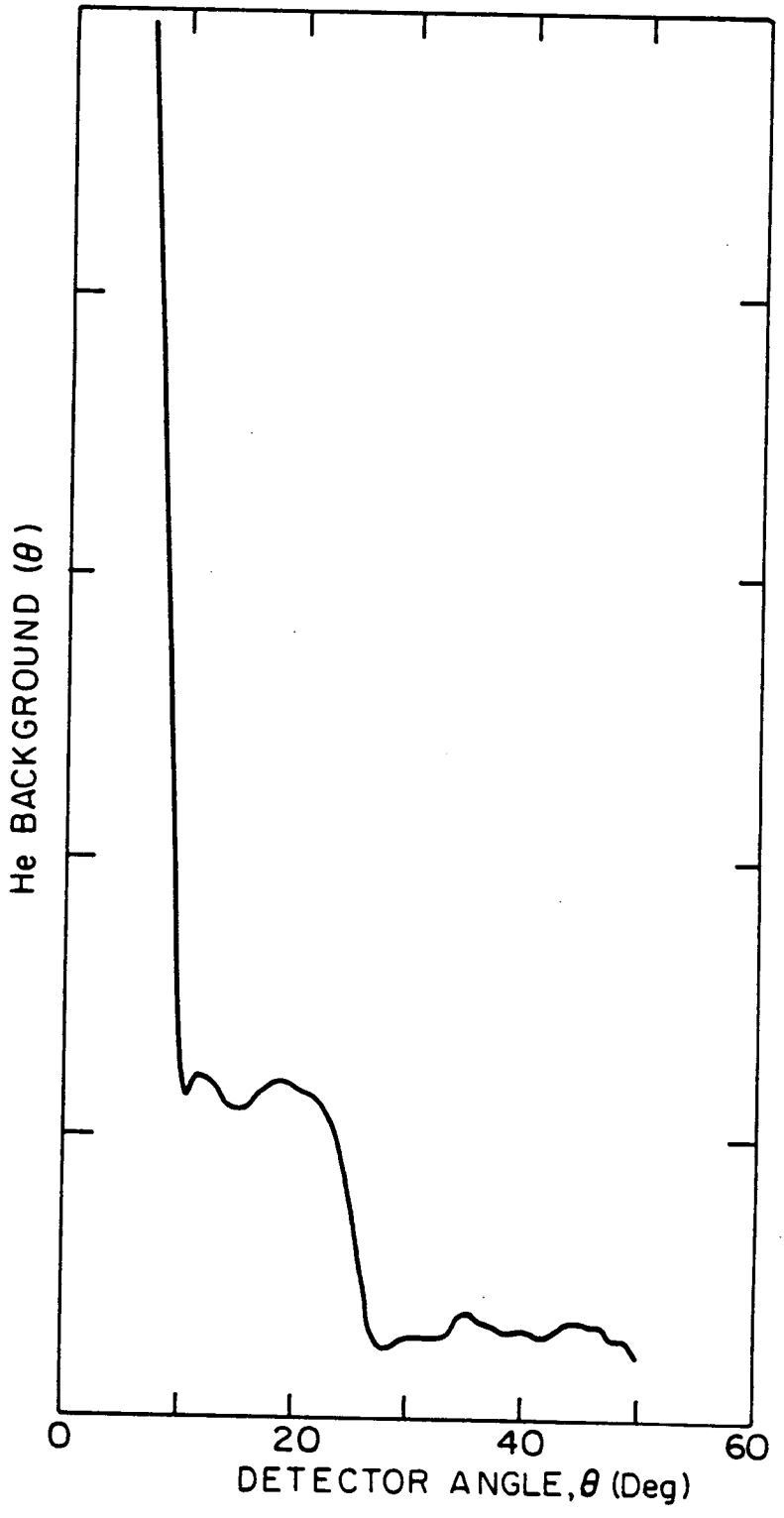

XBL 834-9240

Fig. 2

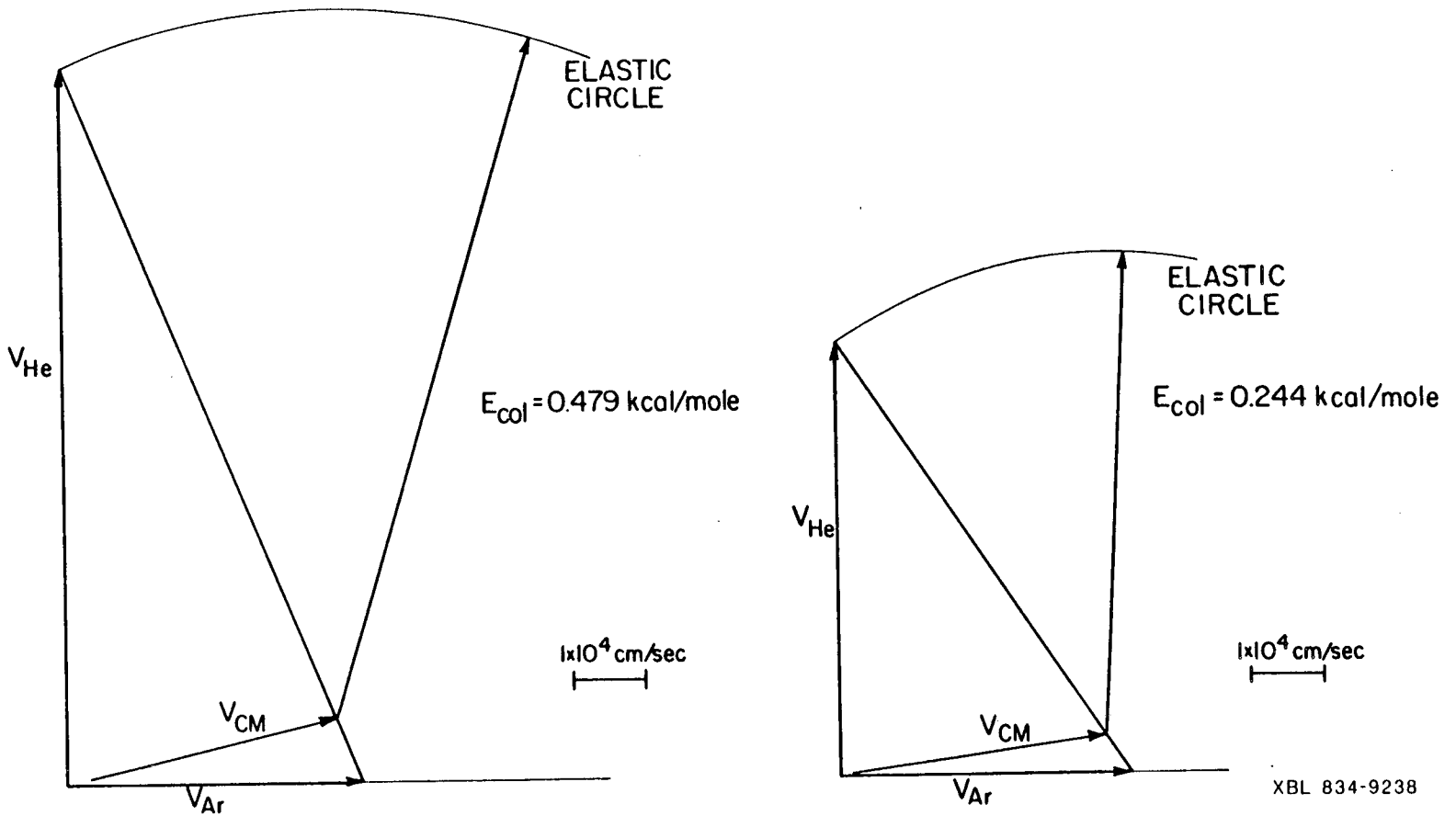
ELASTIC CIRCLE
V_{He}
E_{col} = 0.479 kcal/mole
1×10^4 cm/sec
V_{CM}
V_{Ar}
ELASTIC CIRCLE
E_{col} = 0.244 kcal/mole
V_{He}
1×10^4 cm/sec
V_{CM}
V_{Ar}
XBL 834-9238

Fig. 3

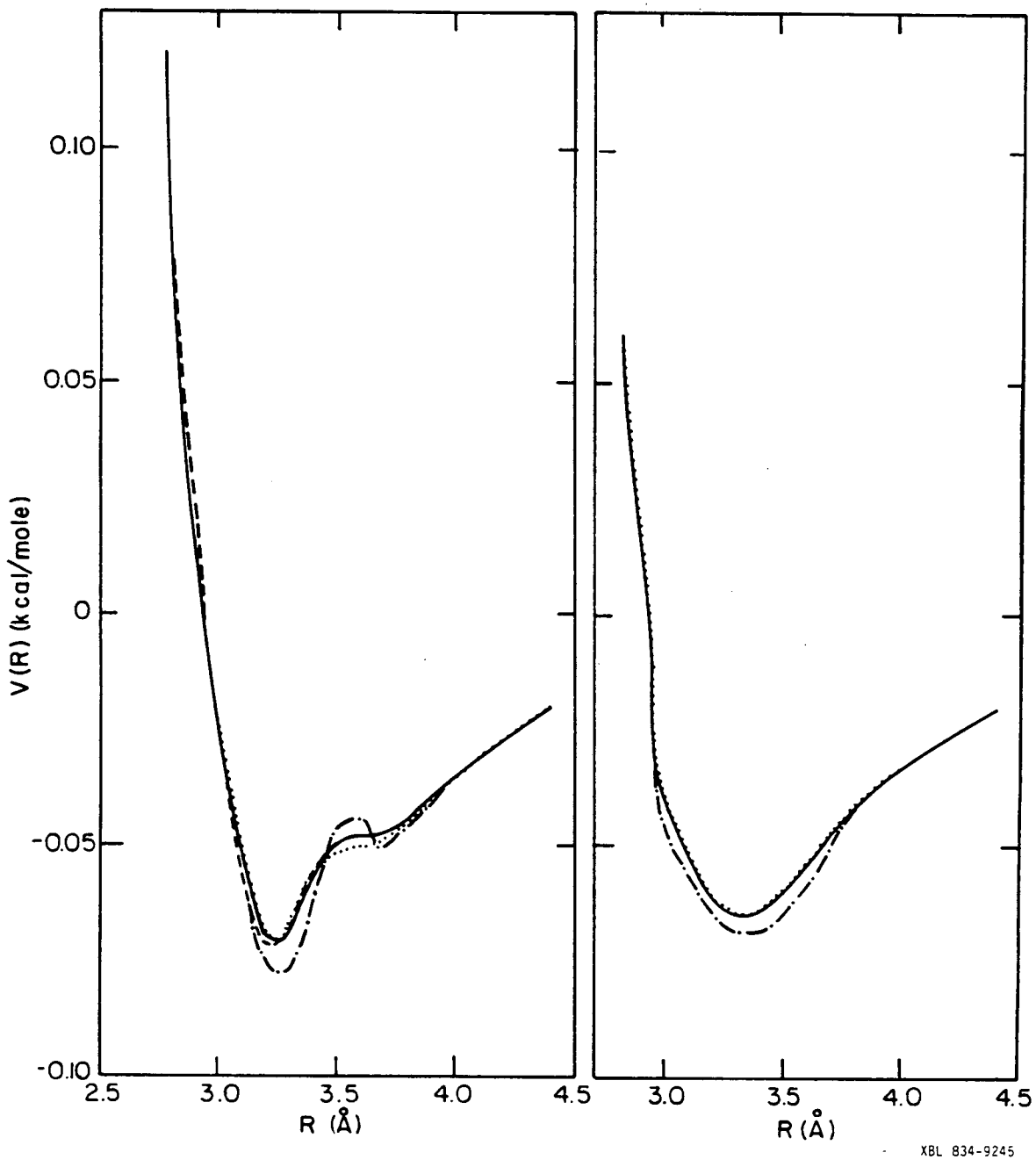
0.10
0.05
0
-0.05
-0.10
V(R) (kcal/mole)
2.5
3.0
3.5
4.0
4.5
R (Å)
3.0
3.5
4.0
4.5
R (Å)
XBL 834-9245

Fig. 4

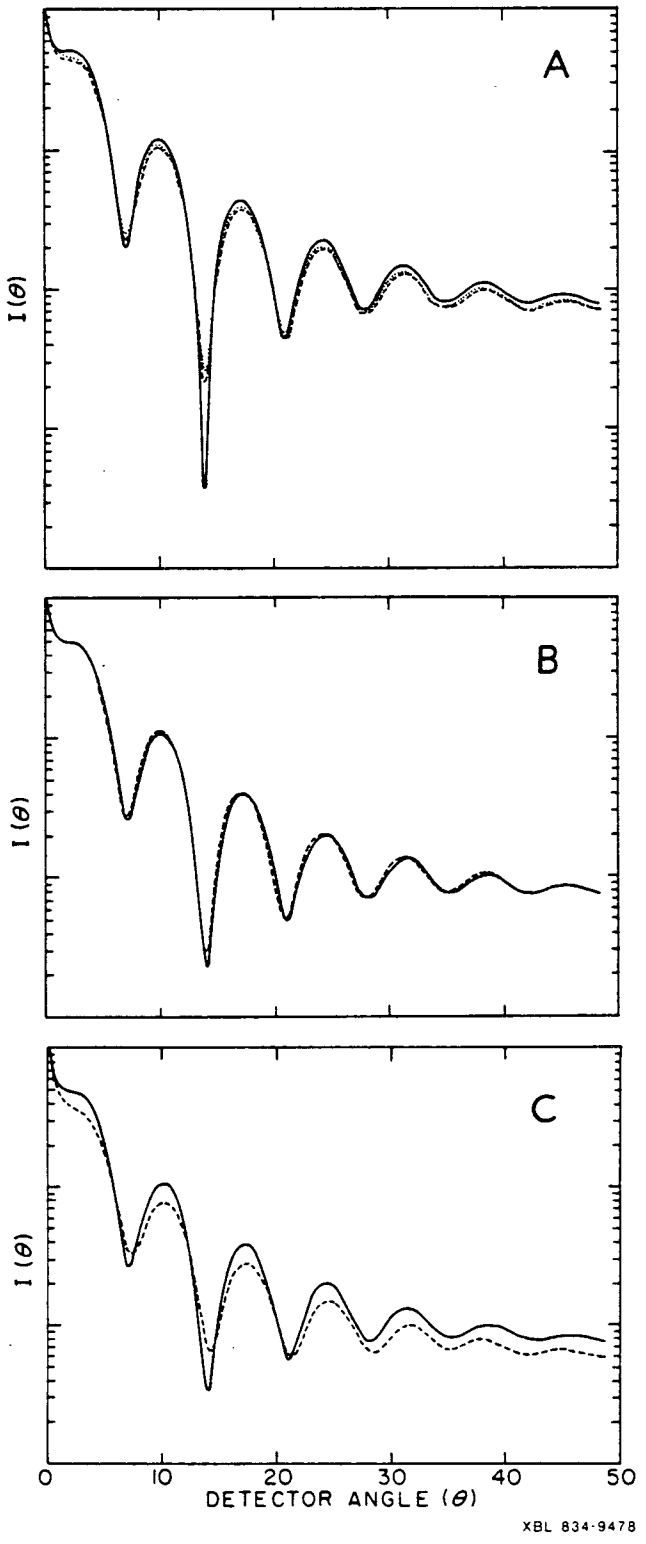

Fig. 5

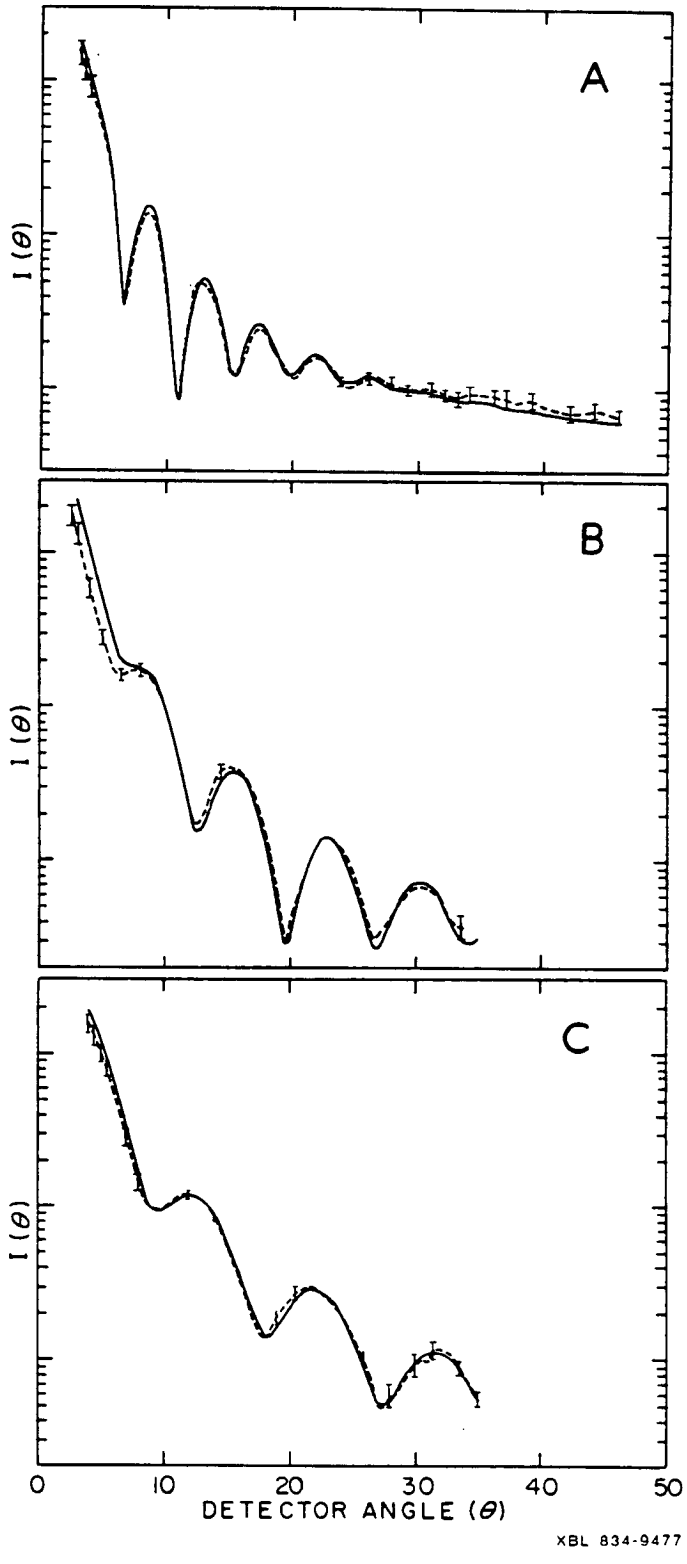

Fig. 6

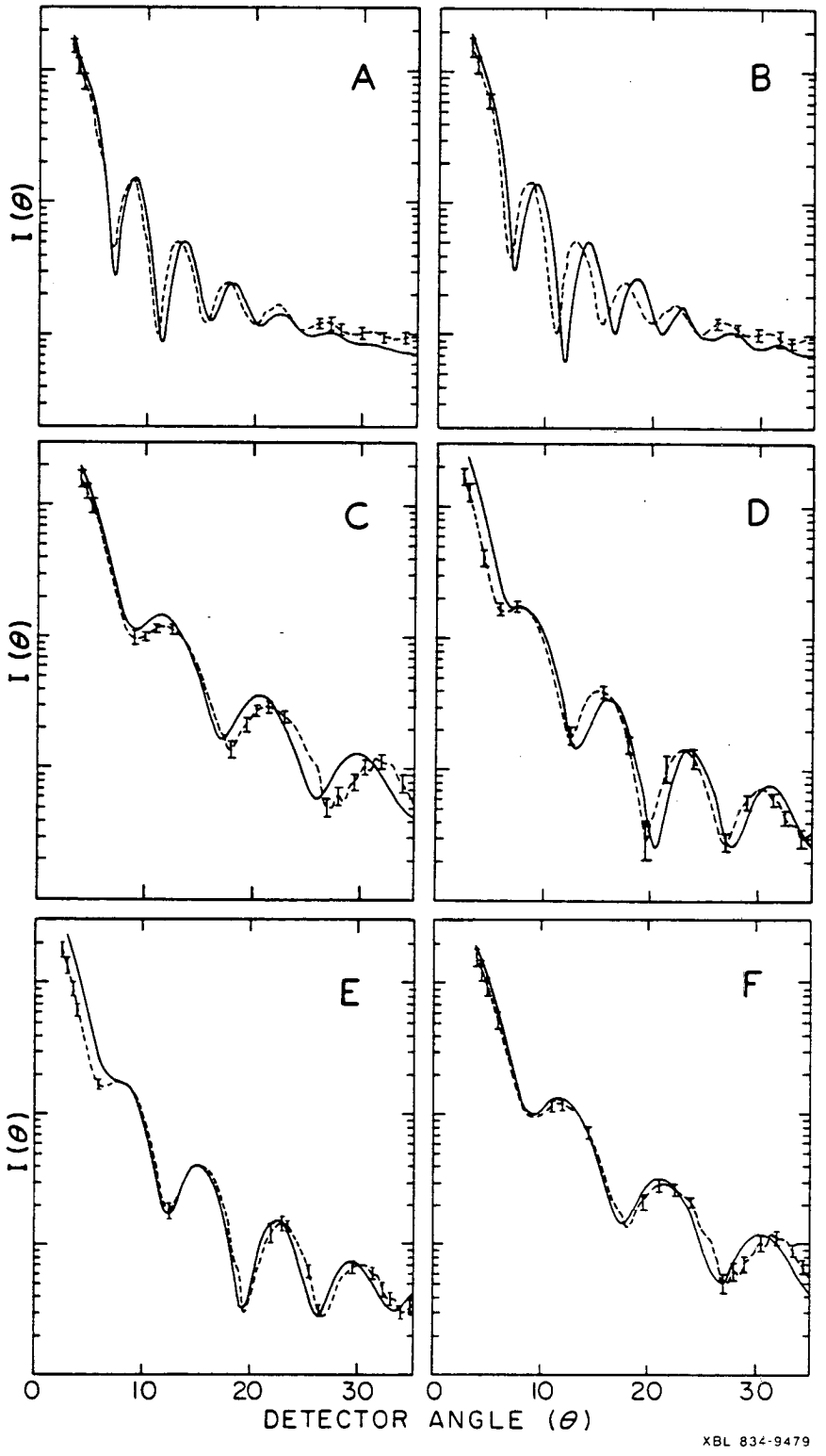
A
B
C
D
E
F
I (θ)
I (θ)
I (θ)
0
10
20
30
0
10
20
30
DETECTOR ANGLE (θ)
XBL 834-9479

Fig. 7

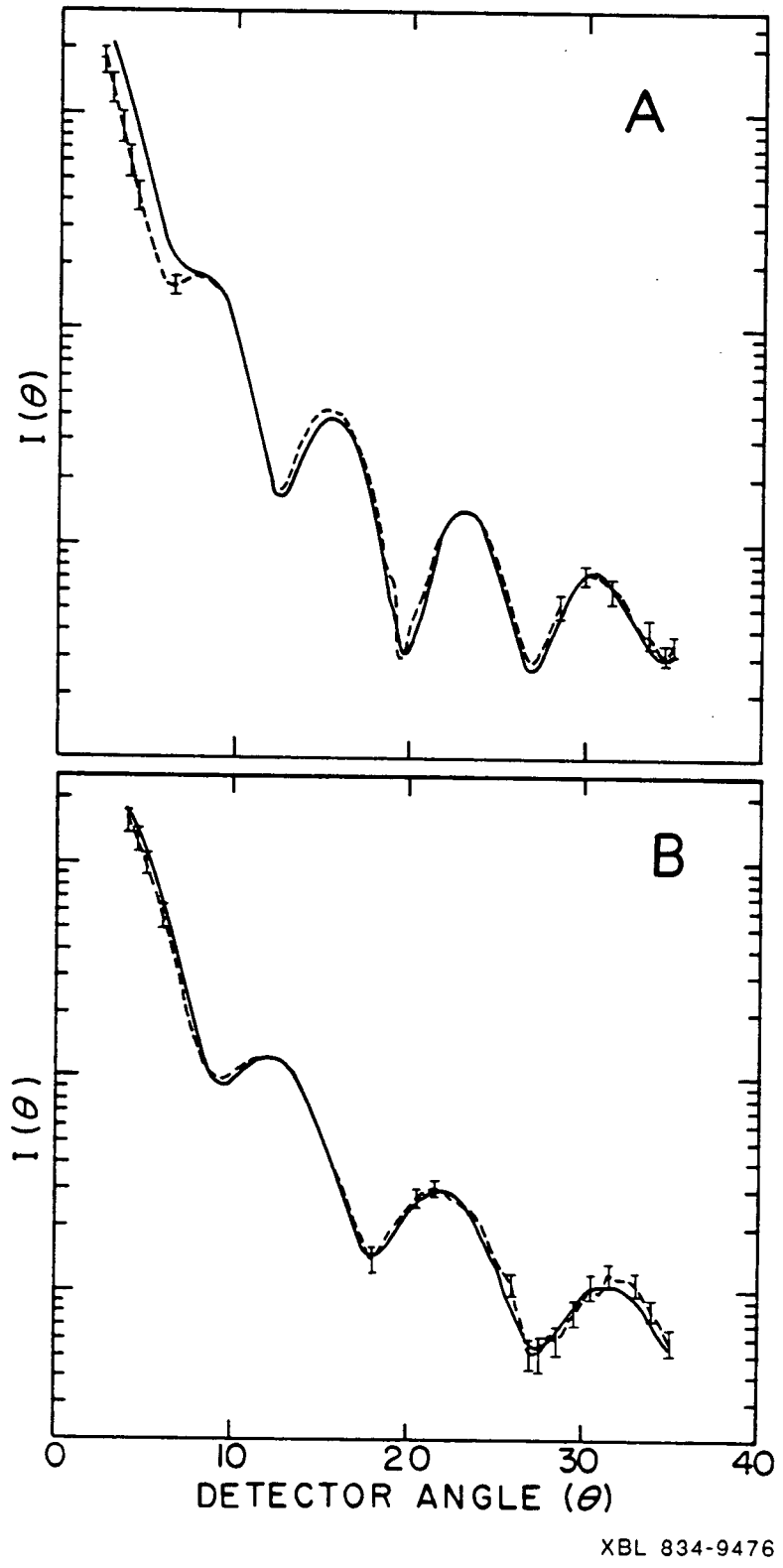

Fig. 8

APPENDIX I. TIME-OF-FLIGHT MEASUREMENT PROCEDURE

A. THEORY AND METHODS FOR TOF CALIBRATION

The purpose of this appendix is to explain in detail the procedure for performing time-of-flight (TOF) calibration measurements. The result of the calibration measurements is to assign a correct length (L) to the path the molecules travel in a particular experimental configuration. In conjunction with time information, (t), a velocity distribution, (L/t), can then be determined.

To measure the flight path from the interaction zone or TOF wheel to the ionizer, a known velocity distribution is used as calibrant. The standard practice is to use the rare gas nozzle distributions which are defined by assuming a Maxwellian velocity distribution superimposed on the bulk flow velocity. Because the electron bombardment ionizer is sensitive to number density, the velocity dependence of the assumed number density distribution is important. From standard texts[1] a Maxwellian velocity distribution is

$$e^{-\frac{M}{2kT_s}(v_x^2 + v_y^2 + v_z^2)} \, dv_x dv_y dv_z \qquad (1)$$

where T_s is the source temperature. For our model, this is the distribution an observer would see moving at the flow velocity, where T_s is the terminal beam temperature (usually $\leq 10^\circ$K for rare gases). However, the observations made in the laboratory frame distort the distribution because of the constraints imposed on the molecular

trajectories by the defining apertures. This distortion is now derived.

Let the +z direction be along the beam centerline. For practical measurements the nozzle can be treated as a point source[2a,2b] and the detector as a circular disk of radius r at a distance L from the nozzle. The beam flow velocity in the laboratory reference frame is (o, o, v_F). The laboratory frame molecular velocity including the random Maxwellian velocity is $(v_x, v_y, v_z + v_F)$, where (v_x, v_y, v_z) is the Maxwellian velocity in the mass flow frame of reference. The detector aperture limits the transverse velocity perpendicular to the beam axis by $(v_{transverse}) \leq \frac{r}{L}(v_z + v_F)$. The measured laboratory number density distribution of velocities (v_L) is then

$$e^{-\beta v_Z^2} dv_z \int_0^{\frac{r}{L}(v_z+v_F)} e^{-\beta\rho^2} \rho d\rho = e^{-\beta(v_L-v_F)^2} (e^{-\beta v_L^2 r^2/L^2} - 1) \; dv_L \quad (2)$$

where $\rho = (v_x^2 + v_y^2)^{1/2}$, $\beta = \frac{M}{2kT}$ and $v_L = v_Z + v_F$. For a standard detector arrangement, $\frac{r}{L} < \frac{0.005}{5}$ and the expression (2) can be expanded in a power series of the variable $x = (\alpha v_L r)/(v_F L)$, where $\alpha = v_F(\beta)^{1/2}$ is the speed ratio, i.e.

$$\exp\left(\frac{-\alpha^2(v_L-v_L)^2}{v_F^2}\right)\left(x^2 - \frac{x^4}{2} + \cdots\right) \quad (3)$$

When the exponential term is maximized ($v_L = v_F$), the second term in the power series expansion will contribute less than 1 percent when $\alpha \leq 100$. For all beams except high pressure He beams or He seeded beams, the speed ratios are usually much less than this value. For speed ratios near 100, the distributions are then sufficiently narrow with respect to the dwell time and ionizer resolution that the width cannot be directly measured with the present flight lengths, so the approximation can be used for all α.

In conclusion, the observed velocity distribution, $P(v_L)$ is proportional to

$$P(v_L)dv_L \sim v_L^2 \exp(-\beta(v_L - v_F)^2)\, dv_L \tag{4}$$

This expression agrees with that derived by Habets[2b] using somewhat different arguments. To compare with the result from the multichannel scaler (MCS), the Jacobian from velocity to time is

$$dv_L = \frac{v_L^2}{L}\, dt. \tag{5}$$

The number density distribution experimentally measured is then

$$\frac{v_L^4}{L}\, e^{-\beta(v_L - v_F)^2}\, dt \tag{6}$$

with $v_L = \frac{L}{t}$, and t regarded as the independent variable.

The procedure is to use Eq. (4) with known rare gas expansion conditions so that v_F and β can be determined. By using the time location of the observed peak (t_p) in the velocity distribution, the effective length L to the ionizer can be determined by $L = v_p * t_p$.

The direct output from the MCS can be used to obtain a good first approximation to L. First, the total time offset must be measured. The time offset is given by

$$t_{offset} = t_E - t_{ion} - t_{trigger} + t_D + t_{Wheel}. \tag{7}$$

t_E is the electronic offset given by the time between the leading edge of the trigger pulse at the MCS trigger input and the maximum of the photodiode signal. t_{ion} is the ion flight time to be described below. $t_{trigger}$ is the width of the trigger pulse sent to the MCS. t_D is a deliberate offset to displace the TOF for long flight paths. t_{wheel} is the time delay resulting from the offset between the peak of the photodiode signal and the time when the wheel slit is centered on the detector slit. t_{wheel} is measured by rotating the wheel clockwise and counterclockwise and averaging the two results. The $t_{trigger}$ delay results from the design of the MCS. The 1 MHz internal clock is disabled for the duration of the trigger pulse, so the clock begins to decrement the dwell time counter within 50 nsecs after the <u>end</u> of the trigger pulse. The ion flight time is determined by measuring the time difference between the peak velocities for different ion masses originating from a common molecule. The use of

multiply charged rare gas ions has been observed to result in incorrect (overestimation) of ion flight times. Krajnovich[3] has successfully used a 1 percent CF_3I mixture in He to obtain narrow velocity distributions with ion mass fragments over a large mass range. The possible source of error in this method is the translational energy released in the ion fragmentation which could distort the measurement. A comparison of the fragment distribution widths will indicate if this is important. The various mass fragment peaks can be used to fit the constant C in the expression $C(M)^{1/2}$ for the ion flight times. As all the ions originate from the same neutral velocity distribution, the difference in time between the ion fragment peaks is a result of the different fragment ion velocities in the mass spectrometer. Neglecting the initial neutral velocity, the ion velocity for a fixed ion energy will depend on the inverse square root of the mass. For 75 volt ions and 250 volt extraction voltage the canonical value for C is 3 μsecs/(amu)$^{1/2}$.

The predicted maximum velocity from Eq. (6) is

$$v_P = \frac{v_F}{2} + \frac{v_F}{2}\left(1 + \frac{8}{\beta v_F^2}\right)^{1/2} \quad \text{or} \quad v_F = \frac{v_P^2 - 2.0/\beta}{v_P} \quad , \tag{8}$$

where

$$v_F\ (\text{cm/sec}) = 2.039 \times 10^4 \left(\frac{T_{nozzle}(K^\circ) - T_{terminal}(^\circ K)}{M(\text{amu})}\right)^{1/2} . \tag{9}$$

The nozzle temperature is measured with a thermocouple using an ice bath reference. The terminal temperature is obtained from the half width of the velocity distribution by

$$T_{terminal}(K^{\circ}) = 8.679 \times 10^{-9}\ m(amu)\ (\Delta v(cm/sec))^2 \qquad (10)$$

where

$$\Delta v = \frac{L*\Delta t}{t'_{1/2}*t'_0*t_D} \quad . \qquad (11)$$

In Eq. (11), L is the flight length to be determined and can be guessed by previous knowledge for an initial correction. Δt is the number of channels between the maximum and half height of the distribution, $t'_{1/2}$ is the half height channel number corrected for the offset time, t'_0 is the peak channel number corrected for the offset time, and t_D is the dwell time. Using these values, L(cm) = v_p(cm/sec)*t'_0(sec). The agreement between L values determined from Ar, Kr, and Xe expansions should be ± 0.3 percent.

To compare the accuracy of this direct method, the more accurate peak fitting by the KELVIN program was used to iterate on $T_{terminal}$ and L until agreement was found. The results are reported in Table 1.

The sources of errors which can bias the above procedure, which are within experimental control, are the purity of rare gas used for calibration and the count rate limitations of the MCS. The first effect can be quite noticeable because several minutes after flowing a

new rare gas it is still possible to detect a clean TOF at the preceeding mass. The experimentalist should wait until all traces of the old gas disappear. Gas cylinders can contain impurities when they are low in pressure. A cursory mass scan at atmospheric and rare gas peaks during the purge time can check for this source of contamination.

The count rate limit cannot be determined by using the observed count rate on the count rate meter, since most of the signal is arriving in a small time interval, roughly 1/200 of the rate meter duty cycle. The MCS scalers are rated at ~30 MHz with a minimum data pulse width of 20 nanoseconds. For 1 percent accuracy in the largest channel, the instantaneous count rate should not exceed 1 MHz.

An additional source of bias was thought to be the manner in which the dual scalers toggle back and forth as the channels advance. If a data pulse is present at the transition from one channel to the next, then, depending on its width, four alternatives are possible. First, if the data pulse is short, then the partial pulse transmitted to either scaler will be too short to trigger the counters. Conversely, if each portion is sufficiently long then the pulse will be counted twice. The intermediate range occurs when one half of the pulse is sufficient, and the other insufficient to trigger the corresponding counter. These effects were empirically investigated using a digital delay generator/pulse generator arrangement to measure the delay between a single data pulse relative to the trigger pulse with an accuracy of 10 nanoseconds. The results are shown in Fig. 1. From these measurements, it is seen that for pulse widths greater than 30

nanoseconds, the multiple counting dominates. However, the effect of the problem is not significant except for very large total counts. The reason for this is as follows.

Assume the data in channels i, i+1 is fit by a linear equation to be determined below. If C_i, C_{i+1} are the total counts in these channels, then the linear fit will be

$$Y = \frac{(C_{i+1} + C_i)}{2t_i t_D} X + \frac{C_{i+1} + C_i}{2t_D} + \frac{(C_i - C_{i+1})t_i}{t_D^2} \tag{12}$$

where t_i is the ith channel time, t_D the dwell time, and

$$C_{i+1} = \int_{t_i}^{t_{i+1}} ydx; \qquad C_i = \int_{t_{i-1}}^{t_i} ydx. \tag{13}$$

The number of counts centered about the channel transition in a time interval 2Δ is

$$\int_{t_{i-\Delta}}^{t_{i+\Delta}} ydx = \frac{\Delta(C_{i+1} + C_i)}{t_D \quad 2} = \frac{\Delta}{t_D} N . \tag{14}$$

Consequently, for Δ = 30 nanoseconds, and t_D = 2 microseconds, the correction is 4.5×10^{-3} N, where 30 percent overcounting has been assumed. This compares with the statistical error $(N)^{1/2}$ when N = 5×10^5 counts. With longer dwell times the effect is even less

important. The behavior on the 1 microsecond dwell time scale is not nearly as good as the 2 microsecond results, and should be avoided. The data presented here refers to a particular MCS unit and may not be transferable to other units.

The imperfect gas correction to the enthalpy for Ar at 1000 torr, 288°K amounts to ~-0.2 [2b], and can be neglected here in determining V_o (Eq. (8)) from the nozzle temperature. Condensation effects will perturb the terminal temperature and velocity by the heat of condensation added to the flow and by ionizer fragmentation to the monomer mass. This can be checked by observing higher polymer masses, and lowering the pressure if necessary.

Several studies[2] have shown that a two component velocity distribution gives a much improved fit to the data. This was not investigated but the systematic differences observed in the calculated and experimental data here are similar to those reported by the above studies using a one component distribution. For most chemical experiments, the one component fit is adequate.

The assumption of the one component distribution was tested indirectly by attempting a direct deconvolution of the measured distribution. For every channel, a narrow velocity distribution ($\beta = 10^6$) centered on that channel was convoluted over the ionizer and shutter functions. The spread of this "delta function" input into adjacent channels defines a matrix C which takes the true channel distribution into the observed one. The inverse of this matrix $C^{-1} = D$ will then relate the observed channel distribution to the

true distribution free of ionizer and shutter effects. This deconvoluted distribution can then be transferred simply to a velocity distribution. In Fig. 2 the results for two rather different expansions, a high pressure He beam and a He/N_2 anti-seeded beam are shown. The high pressure beam indicates that the distribution is completely contained within the convolution effects. The large oscillations are a result of the narrow distribution and the change in sign of adjacent entries of the inverse matrix, D. A simple two channel average noticeably removes this effect. The anti-seeded distribution shows no significant difference between the measured and deconvoluted results. This is a consequence of the broadness of the distribution. The direct deconvolution result is not as useful as the trial and fit method, because the information is not as compact as the simple two parameter fit. However, it is useful as a guide to the magnitude of the broadening induced by the measurements.

For laser photofragmentation experiments the distance from the collision zone to the TOF wheel must be added to the TOF distance. The collision zone-wheel distance is measured with the transit while the wheel is spinning to reduce the warp error caused by the 5 mil stainless steel wheel material.

Finally, the emission current and extractor voltage affect the modeling of the detection process by a nonuniform electron distribution which can shield the ions from the extraction field or ionize the neutral species nonuniformly. These can be experimentally measured by using a narrow He beam whose experimental width is dominated by the

ionizer. Until this behavior is known, a more accurate deconvolution of the TOF spectra is not warranted.

B. TIME-OF-FLIGHT PROGRAM KELVIN AND DIRECTIONS FOR USE

This section describes the salient features of the FORTRAN program KELVIN used to fit time-of-flight data to deduce velocity distributions. The current version draws heavily on its predecessor written by J. Valentini. The basic difference is the improved efficiency in the calculation, by using a digital filter devised by R. Sparks. It also has an improved search procedure to find the best fit parameters.

The nominal structure is to simulate the effects of the finite ionizer length and slit widths on a measured velocity distribution by calculating a shutter function for the slit overlap which is used as a digital filter. This is applied to the trial velocity distribution which has been convoluted for the ionizer length. The ionizer is treated as a simple sum of 10 identical point ionizers with slightly different lengths from the collision zone. Using a Marquardt algorithm, the parameters are varied until one of three criteria is satisfied.

1) The change in parameters is less than 0.005 of their respective magnitudes.
2) The value of X^2 has reached a value such that the data has been fit to the 90 percent confidence limit.
3) Twenty complete iterations have occurred without either 1) or 2) occurring.

KELVIN can analyze any number of time-of-flight distributions. Each velocity distribution needs the same number of input parameter

records. The number of data records in each distribution will vary. The final data set is followed by a blank record. Input records needed for each velocity distribution (all numbers F10.1 format, except where noted) are:

Record

1. Title
2. Mass (amu), channel width (μ sec), nominal neutral flight length (cm), ionizer length (cm), channel offset (channels).
3. Beginning channel number (I5), ending channel number (I5).
4. Wheel frequency (Hz), wheel diameter (cm), wheel slit width (mm), collimating slit width (mm).
5. etc. Data (8F10.1)

Output consists of the title with a list of the parameters used, followed by the input data, and the shutter function calculated for the dwell time used. "Offset" should include all the corrections from Eq. (7) divided by the dwell time to obtain the number of channels (fractional values allowed) by which the observed TOF distribution is uniformly offset.

The intermediate reduced standard deviations and parameter changes are listed with each iteration.

The final parameters are listed along with the number of iterations, calculated data, and the change in the fitted parameters that would produce a fit which would differ by an additional standard deviation at each point.

A graph of the two distribution is also produced.

The parametrized velocity distribution has the form

$$P(v) \sim v^2 \, e^{-\beta(v-v_0)^2}$$

where v_0 is the mass flow velocity, and $\beta = 1/(\alpha)^2$, where α is the average relative velocity in the mass flow frame of reference. The speed ratio is the dimensionless number $v_0(\beta)^{1/2}$. The flow velocity is in units of 10,000 cm/sec.

REFERENCES

1. F. Reif, Fundamentals of Statistical and Thermal Physics, p. 264, McGraw-Hill (1965).

2. (a) U. Bossel, R. David, M. Faubel, K. Winkelmann, Rarified Gas Dynamics, p. 235.

   (b) A. Habets, "Supersonic Expansion of Argon into Vacuum," Ch. 2,5 Thesis, University of Eindhoven, Holland, 1977.

3. D. Krajnovich, private communication.

Table 1. Comparison of computer fitted parameters with those obtained by iteratively solving Eqs. (6) and (7) in the text.

	Computer Fit			First Iteration			Second Iteration		
	L(cm)	β	v_0	L	β	v_0	L	β	v_0
Ar	16.46	2.751	5.517	16.75	2.662	5.616	16.544	2.740	5.536
Kr	16.46	5.136	3.807	16.75	4.970	3.875	16.512	5.115	3.820
Xe	16.46	8.111	3.058	16.75	7.838	3.113	16.477	8.067	3.068

FIGURE CAPTIONS

Fig. 1. Transition effects in the dual scalers (a) 25 nanosecond data pulse width, 2 microsecond dwell time. (b) 40 nanosecond data pulse width, 2 microsecond dwell time. (c) 50 nanosecond data pulse width, 2 microsecond dwell time. (d) 40 nanosecond data pulse width, 3 microsecond dwell time. ▲ total counts in channels 10 and 11. ■ total counts in channel 10. ● total counts in channel 11.

Fig. 2. (a) Deconvoluted He beam. — Initial data. ● Deconvoluted data. △ Deconvoluted with 2 channel average.

(b) Deconvoluted He/N_2 beam. ● Initial data. △ Deconvoluted data (displaced by one channel).

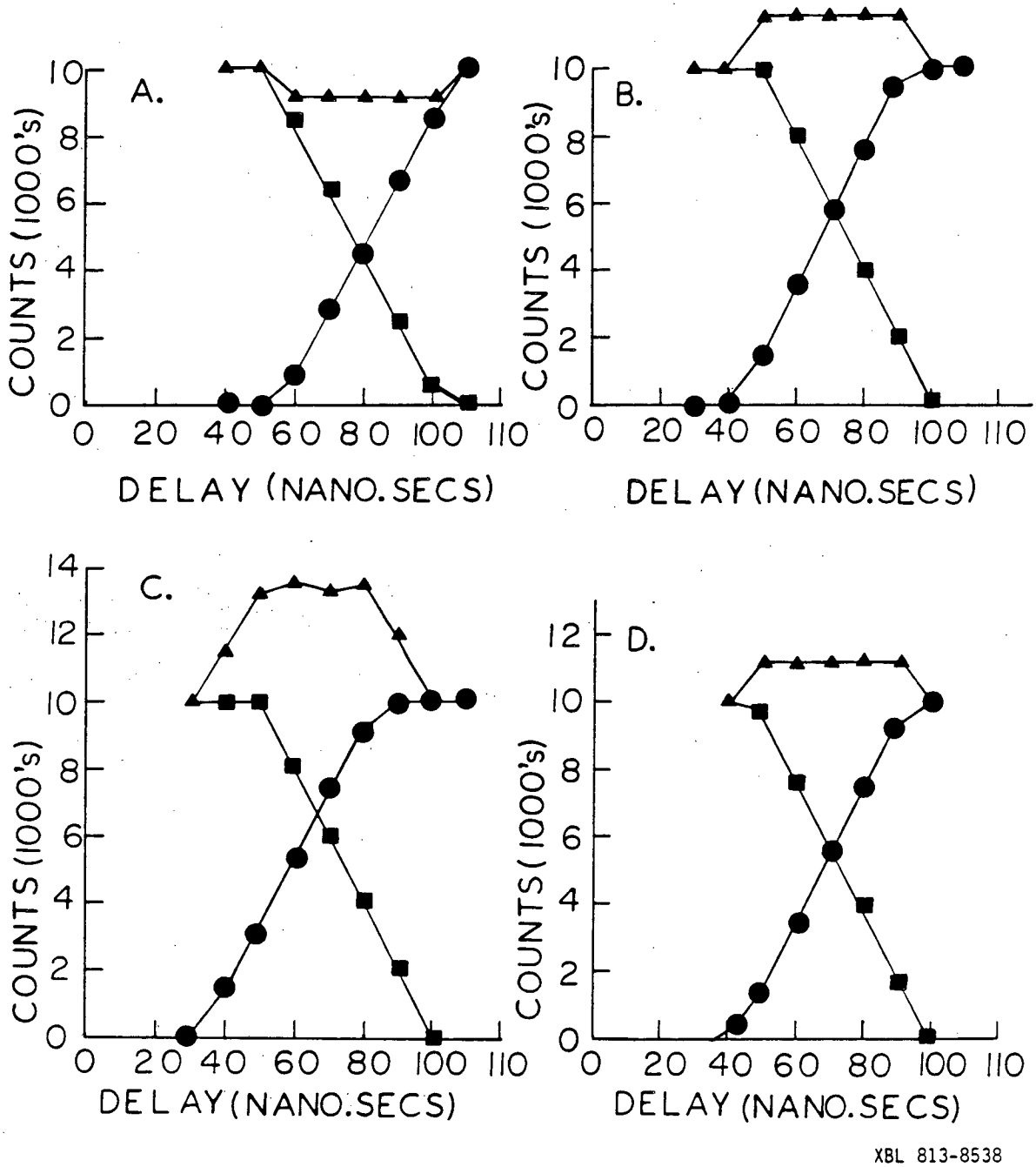
A.
B.
C.
D.
COUNTS (1000's)
DELAY (NANO.SECS)
0
2
4
6
8
10
12
14
20
40
60
80
100
110
XBL 813-8538

Fig. 1

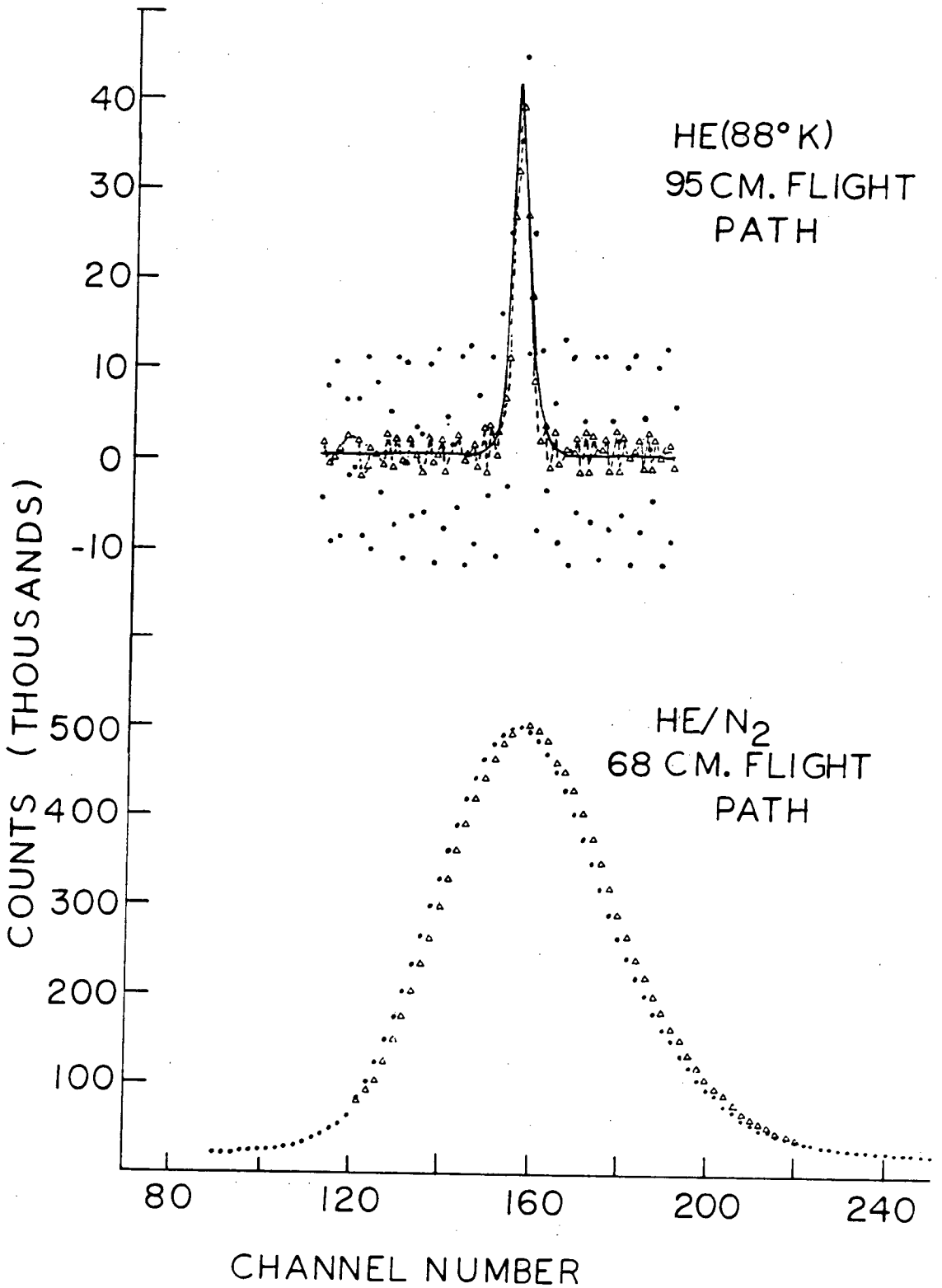

XBL 813-8537

Fig. 2

```
      PROGRAM KELVIN
C
C
C     FUNCTION- DETERMINES PARAMETERS VZRO AND BETA
C     CHARACTERIZING A SONIC NOZZLE VELOCITY DISTRIBUTION
C     FROM AN EXPERIMENTALLY MEASURED TIME-OF-FLIGHT
C     DISTRIBUTION,USING A LEAST SQUARES FITTING PROCEDURE.
C
C     INPUT-DESCRIBED IN SUBROUTINE 'INPUT'
C
C     OUTPUT- OUTPUT CONSISTS OF A TITLE WITH THE LIST OF
C     PARAMETERS USED,FOLLOWED BY THE INPUT DATA,AND THE
C     SHUTTER FUNCTION. THE INTERMEDIATE REDUCED STANDARD
C     DEVIATIONS AND THE PARAMETER CHANGES ARE LISTED WITH
C     EACH ITERATION. THE FINAL PARAMETERS ARE LISTED ALONG
C     WITH THE NUMBER OF ITERATIONS and THE FINAL CALCULATED
C     BEST FIT DISTRIBUTION. AN ESTIMATE OF THE ERROR IN THE
C     DERIVED PARAMETERS IS GIVEN. THIS ERROR IS THE CALCULATED
C     CHANGE THAT IS PREDICTED NEEDED TO UNIFORMLY INCREASE THE
C     FITTING ERROR AT EACH POINT BY ONE STANDARD DEVIATION.
C     A GRAPH OF THE INPUT AND CALCULATED DISTRIBUTIONS IS
C     PRODUCED. ALL OUTPUT IS FOR A LINE PRINTER.
C
C     ROUTINES CALLED- INDATA,VELO,FIT,LPPLT
C
C     AUTHOR-M. F. VERNON
C
C     LAST REVISION DATE- FEBRUARY 15,1983.
C
C
      COMMON/PAR/CHAN,LMID,DL,BCHAN,ECHAN,NCHAN,MASS,MAXE,OFFSET
      COMMON/TRIP/WIDTH,HZ,DIA,SA,SB,TRP(19),ITRSIZ,ITRSHF,IFLAG
      DIMENSION EXPT(255),SIGCAL(255),SIGCA1(255),SIGCA2(255)
      DIMENSION YPL1(256),YPL2(256),XPL(256)
      REAL MASS,LMID
      INTEGER BCHAN,ECHAN,NCHAN
C
C     INPUT DATA
C
 1003 CONTINUE
      CALL INDATA(EXPT,BETA,VZRO)
C
C     FITTING ROUTINE TAKEN FROM 'DATA REDUCTION AND ERROR ANALYSIS
C     FOR THE PHYSICAL SCIENCES' BY PHILIP R. BEVINGTON.
C     PROGRAM 11-5 CURFIT WHICH IS A MARQUARDT ALGORITHM FOR  A NON-
C     LINEAR LEAST SQUARES FIT WITH IMPROVED STABILITY NEAR A MINIMUM
C     WAS THE MODEL FOR THIS PROCEDURE.
C     ALL CALCULATIONS ARE PERFORMED WITH VZRO IN KILOMETERS/SECOND.
C     OUTPUT IS IN UNITS OF 10**4 CM/SEC
C
C
```

```
C      CALCULATE FIRST ATTEMPT AT A FIT WITH TRIAL VALUES.
C
       SF=0.
       CALL VELO(BETA,VZRO,SIGCAL,SIGCA1,SIGCA2)
       CALL FIT(SIGCAL,EXPT,SF,DC)
       ILOW=BCHAN+ITRSHF
       IHIGH=ECHAN-ITRSHF
       IFIT=20
       FLAMDA=.001
       CH=FLOAT(NCHAN-4-2*ITRSHF)
       WRITE(6,300)

C
C      THIS IS THE LEAST SQUARES FITTING LOOP
C
       DO 1000 JCYC=1,IFIT
C
C      DFDV IS THE FIRST DERIVATIVE WITH RESPECT TO PEAK VELOCITY.
C      DFDB IS THE FIRST DERIVATIVE WITH RESPECT TO PEAK WIDTH.
C
C      W IS THE WEIGHTING FACTOR.
C      B1 AND B2 IS THE BETA MATRIX.
C      A11,A12,A22 IS THE ALPHA MATRIX
C      THESE PARAMETERS ARE DEFINED IN BEVINGTON.
C
       B1=0.
       B2=0.
       A11=0.
       A12=0.
       A22=0.
       SUM=0.
C
C      DO LOOP ONLY EXTENDS OVER CHANNELS WHICH AREN'T TRUNCATED BY THE
C      SHUTTER FUNCTION.
C
       DO 1001 I=ILOW,IHIGH
       DFDB=SIGCA2(I)*SF
       DFDV=SIGCA1(I)*SF
       W=1./EXPT(I)
       D=EXPT(I)-SIGCAL(I)
       DW=D*W
       B1=B1+ DW*DFDV
       B2=B2+ DW*DFDB
       A11=A11+DFDV*DFDV*W
       A22=A22+DFDB*DFDB*W
       A12=A12+DFDV*DFDB*W
       SUM=SUM+D*DW
 1001  CONTINUE
C
C      CALCULATE THE CHI SQUARED ERROR.
C      NOTE THAT THERE ARE FOUR PARAMETERS IN THE FIT TO THE DATA.
```

```
C       THESE ARE THE  DC LEVEL, THE SCALE FACTOR, THE PEAK WIDTH AND
C       VELOCITY.
C
      CHI1=SUM/CH
C
C       ADJUST PARAMETERS AS NECESSARY
C       A1 AND A2 IS THE CURVATURE MATRIX. A1NV AND A2NV ITS INVERSE.
C       FLAMDA IS THE FACTOR WHICH DETERMINES THE EXTENT OF THE GRADIENT
C       INFLUENCE ON THE SEARCH.
C
 71   CONTINUE
      A1=1.+FLAMDA
      DEN2=SQRT(A11*A22)
      A2=A12/DEN2
      DEN1=A1*A1-A2*A2
      A1NV=A1/DEN1
      A2NV=-A2/DEN1
      DVZRO=B1*A1NV/ABS(A11)+B2*A2NV/DEN2
      DBETA=B1*A2NV/DEN2  +B2*A1NV/ABS(A22)
C
C       IF BETA IS FORCED TO GO NEGATIVE, THEN THE DISTRIBUTION IS
C       NARROW RELATIVE TO THE SHUTTER FUNCTION. DBETA IS HALVED UNTIL
C       THE VALUE OF BETA IS POSITIVE. IFLAG IS SET TO 1 SINCE THE MORE
C       ACCURATE INTEGRATION OVER THE CHANNEL WIDTH IS NECESSARY FOR THIS
C       CASE.
C
 221  IF(BETA+DBETA)225,225,220
 225  IFLAG=1
      DBETA=DBETA/2.
      GOTO 221
C
C       CALCULATE THE DISTRIBUTION AT THE NEW VALUE OF BETA AND VZRO.
C
 220  SF=0.
      CALL VELO(BETA+DBETA,VZRO+DVZRO,SIGCAL,SIGCA1,SIGCA2)
      CALL FIT(SIGCAL,EXPT,SF,DC)
      SUM=0.
      DO 1010 I=ILOW,IHIGH
 1010 SUM=SUM+(EXPT(I)-SIGCAL(I))**2/EXPT(I)
      CHI2=SUM/CH
      WRITE(6,216) CHI2,DBETA/100.,DVZRO*10.

C
C       IF THE NEW VALUE OF CHISQR. IS LARGER THAN THE  OLD VALUE, MAKE
C       THE GRADIENT CONTRIBUTION 10 TIMES LARGER AND TRY AGAIN.
C
      IF(CHI1-CHI2) 95,101,101
 95   FLAMDA=10.*FLAMDA
      GOTO 71
C
C       STOP FITTING IF PARAMETERS OPTIMIZED
```

```
C
C      A IS THE NUMBER OF STANDARD DEVIATIONS EACH CALCULATED POINT
C      DIFFERS FROM THE DATA ON THE AVERAGE
C
 101  A=SQRT(SUM/FLOAT(NCHAN-2*ITRSHF))
      VZRO=VZRO+DVZRO
      BETA=BETA+DBETA
      FLAMDA=FLAMDA/10.
C
C      THE SEARCH ENDS IF IFIT ITERATIONS HAVE HAPPENED WITHOUT THE
C      FOLLOWING CONDITIONS HAVING BEEN SATISFIED.
C      IF THE VALUES OF  BETA AND VZRO ARE CHANGING LESS THAN .005
C      OF THEIR PREVIOUS VALUE, OR THE DATA HAS BEEN FIT WITHIN THE 90
C      PER CENT CONFIDENCE LIMIT, I.E. A≤2.
C
      IF(A.LE.2.) GOTO 1002
      IF((ABS(DBETA).LE.(.005*BETA)).AND.(ABS(DVZRO).LE.(.005*VZRO)))
     1 GOTO 1002
 1000 CONTINUE
      JCYC=JCYC-1
 1002 WRITE(6,301)
      WRITE(6,1210)BETA/100.,VZRO*10.,VZRO*SQRT(BETA),10./SQRT(BETA),
     1JCYC,A
      IF(JCYC.EQ.IFIT) WRITE(6,219)
      EBETA=SQRT(A2NV/A22)
      EVZRO=SQRT(A1NV/A11)
      WRITE(6,217) EBETA/100.,EVZRO*10.
      T=DSQRT((1.+2.*A)*SUM)
      EB2=T*EBETA/100.
      EV2=T*EVZRO*10.
      WRITE(6,218) EB2,EV2
C
C      PLOT DATA
C
      WRITE(6,205)
C
C        DATA IS SCALED HERE FOR THE LINE PRINTER PLOTS
C
      NPTS=ECHAN-BCHAN-2*ITRSHF
      XSTEP=5./FLOAT(NPTS)
      J=1
      DC=EXPT(BCHAN+3)
      XPL(1)=0.
      TT=9.9/(EXPT(MAXE)-DC)
      WRITE(6,206)(I,SIGCAL(I),I=ILOW,IHIGH)
      DO 1005 I=ILOW,IHIGH
      YPL1(J)=(EXPT(I)-DC)*TT
      YPL2(J)=(SIGCAL(I)-DC)*TT
      J=J+1
      XPL(J)=XPL(J-1)+XSTEP
 1005 CONTINUE
```

```
      CALL LPPLT(XPL,YPL1,NPTS,XPL,YPL2,NPTS,1)
      GO TO 1003
C
C
C      FORMAT STATEMENTS
C
C
 300  FORMAT(1X,'INTERMEDIATE VALUES',/)
 216  FORMAT(5X,'STANDARD DEVIATION=',E10.3,5X,'DBETA=',E12.4,5X,'DVZRO=
     1',E12.4)
 301  FORMAT(/,1X,'FINAL PARAMETER VALUES',/)
 1210 FORMAT(1X,'BETA=',E12.4,3X,'VZRO=',E12.4,2X,'SPEED RATIO=',E12.4,
     12X,'ALPHA=',E12.4,2X,'ITERATIONS=',I3,2X,'AVERAGE DEVIATION=',F5.1
     1)
 219  FORMAT(5X,'C A U T I O N----- THE FULL NUMBER OF ITERATIONS HAS
     1OCCURED WITHOUT CONVERGENCE',/)
 217  FORMAT(' ESTIMATED ERROR IN LOCATION OF MINIUM ON SURFACE IN BETA
     1 AND VZRO=',E12.4,5X,E12.4)
 205  FORMAT(//,10X,'C A L C U L A T E D  D I S T R I B U T I O N ',/)
 206  FORMAT(8(3X,I3,1X,F9.1))
 218  FORMAT(2X,'ESTIMATED ERROR IN THE DERIVED PARAMETERS',
     1 ' BETA AND VZRO=',E12.4,5X,E12.4)
      END


       SUBROUTINE FIT(SIGCAL,EXPT,SCALE,DC)
C
C      FUNCTION- SCALES THE CALCULATED AND OBSERVED TOF SPECTRA
C
C      INPUT-SIGCAL AND EXPT CONTAIN THE CALCULATED AND
C      EXPERIMENTAL TOF DISTRIBUTIONS
C
C      OUTPUT-SCALE AND DC ARE THE SCALE FACTOR AND DC
C      BACKGROUND USED TO SCALE THE CALCULATED DATA TO THE
C      EXPERIMENTAL DATA. THE CALCULATED DATA IS REPLACED
C      BY ITS SCALED VALUES
C
C      ROUTINES CALLED- NONE
C
C      AUTHOR- M.F. VERNON
C
C
C      LAST REVISION DATE- FEBRUARY 15,1983
C
C
      DIMENSION SIGCAL(255),EXPT(255)
      COMMON/TRIP/WIDTH,HZ,DIA,SA,SB,TRP(19),ITRSIZ,ITRSHF,IFLAG
      COMMON/PAR/CHAN,LMID,DL,BCHAN,ECHAN,NCHAN,MASS,MAXE,OFFSET
      INTEGER BCHAN,ECHAN
      ILOW=BCHAN+ITRSHF
```

```
      IHIGH=ECHAN-ITRSHF
      RCHAN=0.
      XINV=0.
      X=0.
      Y=0.
      YX=0.
      YYX=0.
C
C      LEAST SQUARES DETERMINATION OF SCALE FACTOR AND DC BACKGROUND
C
      DO 30 I=ILOW,IHIGH
      Y=Y+SIGCAL(I)
      XINV=XINV+1./EXPT(I)
      YX=YX+SIGCAL(I)/EXPT(I)
      YYX=YYX+SIGCAL(I)*SIGCAL(I)/EXPT(I)
      RCHAN=RCHAN+1.
      X=X+EXPT(I)
 30   CONTINUE
      DELTA=XINV*YYX-YX*YX
      DC=(RCHAN*YYX-YX*Y )/DELTA
      SCALE=(XINV*Y-RCHAN*YX)/DELTA
C
C      FINALLY SCALE THE DATA
C
      DO 40 I=BCHAN,ECHAN
      SIGCAL(I)=SIGCAL(I)*SCALE+DC
 40   CONTINUE
      RETURN
      END



      SUBROUTINE BIG(SIGCAL,MAX)
C
C      FUNCTION- Finds the maximum in a tof spectrum
C
C      INPUT- SIGCAL, ARRAY TO BE SEARCHED FOR MAXIMUM
C
C      OUTPUT- MAX, THE INDEX OF THE ARRAY SIGCAL OF THE LARGEST ELEMENT
C
C      ROUTINES CALLED-NONE
C
C      AUTHOR-M.F. VERNON
C
C      LAST REVISION DATE-FEBRUARY 15,1983
C
C
C
      COMMON/PAR/CHAN,LMID,DL,BCHAN,ECHAN,NCHAN,MASS,MAXE,OFFSET
      INTEGER BCHAN,ECHAN
```

```
      DIMENSION SIGCAL(255)
      MAX=0
      SIGMAX=0.0
      DO 1 I=BCHAN,ECHAN
      IF (SIGCAL(I) .LT. SIGMAX) GO TO 1
      SIGMAX=SIGCAL(I)
      MAX=I
    1 CONTINUE
      IF(MAX .EQ. 0) WRITE (6,255)
  255 FORMAT('0  NO MAXIMUM FOUND')
      RETURN
      END


      SUBROUTINE TRAP1
C
C
C      FUNCTION- CALCULATE THE SHUTTER FUNCTION TRAPEZOID.
C
C      INPUT- ALL INPUT PASSED THROUGH THE COMMON ARRAY TRIP
C
C      OUTPUT-THE ELEMENTS OF THE COMMON BLOCK TRIP, TRP,
C      ITRSIZ,AND ITRSHF ARE COMPUTED IN THIS ROUTINE.
C
C      ROUTINES CALLED-NONE
C
C      AUTHOR-M.F. VERNON
C
C      LAST REVISION DATE-FEBRUARY 15,1983
C
C
      COMMON/TRIP/WIDTH,HZ,DIA,SA,SB,TRP(19),ITRSIZ,ITRSHF,IFLAG
      DATA PI,CON/3.14159265,100000./
C
C      DEFINITION OF INPUT PARAMETERs in common block trip
C      SA=WHEEL SLIT WIDTH IN MILLIMETERS
C      SB=DETECTOR SLIT WIDTH IN MILLIMETERS
C      WIDTH= CHANNEL TIME IN MICROSECONDS
C      DIA=DIAMETER FROM CENTER OF WHEEL TO DETECTOR SLIT IN CM.
C      T=ONE HALF THE NUMBER OF CHANNELS PER MILLIMETER TRAVEL OF WHEEL
C      TT=HALF THE NUMBER OF SLITS FOR BASE OF TRAPEZOID
C      TA=HALF THE NUMBER OF SLITS FOR THE TOP OF TRAPEZOID
C      ITT=INTEGRAL VERSION OF TT
C      ITA=INTEGRAL VERSION OF TA
C      ITRSIZ=NUMBER OF CHANNELS AFFECTED BY DIGITAL FILTER
C      ITRSHF DEFINED BY  ITRSIZ=2*ITRSHF+1
C
      T=CON/(PI*DIA*HZ*2.*WIDTH)
      TT=T*(SA+SB)
      SA=AMIN1(SA,SB)
      TA=TT-SA*T*2.
```

```
      ITT=INT(TT-.5)
      ITA=INT(TA-.5)
C
C      CHECK IF BASE OF TRAPEZOID LESS THAN ONE CHANNEL WIDE
C
      IF(TT.LE..5) GOTO 90
      ITRSIZ=1+2*(ITT+1)
      ITRSHF=ITT+1
C
C      CHECK IF TOP OF TRAPEZOID MORE THAN ONE CHANNEL WIDE
C
      IF(TA.GE..5) GOTO 40
C
C      TRAPEZOID CORNER OCCURS WITHIN THE FIRST CHANNEL
C
      TRP(10)=(TT-TA*TA-.25)/(TT-TA)
C
C      CHECK IF TRAPEZOID BASE OCCURS WITHIN FIRST CHANNEL
C
      IF(ITT.EQ.0) GOTO 30
C
C      TRAPEZOID EDGE SPREAD OVER ITT CHANNELS
C
      DO 20 I=1,ITT
      TRP(10+I)=(TT-FLOAT(I))/(TT-TA)
 20   TRP(10-I)=TRP(10+I)
C
C      CHANNEL WHERE EDGE HITS BASE
C
 30   TRP(11+ITT)=(TT-.5-FLOAT(ITT))**2/(2.*(TT-TA))
      TRP(9-ITT)=TRP(11+ITT)
      GOTO 75
C
C      CASE WHERE TOP OF TRAPEZOID AT LEAST ONE CHANNEL WIDE.
C
 40   TRP(10)=1.
C
C      DOES TOP OF TRAPEZOID EXTEND OVER MORE THAN ONE CHANNEL?
C
      IF(ITA.EQ.0.) GOTO 50
C
C      IF SO THAN ALL THESE CHANNELS HAVE UNIT AREA
C
      DO 45 I=1,ITA
      TRP(10+I)=1.
 45   TRP(10-I)=1.
C
C      IS EDGE OF TRAPEZOID CONTAINED WITHIN ONE CHANNEL.
C
 50   IF(ITT.EQ.ITA) GOTO 70
C
```

```
C       AREA FOR CORNER OF TRAPEZOID.
C
      TERM=FLOAT(ITA)+1.5-TA
      TRP(11+ITA)=1.-TERM*TERM/(2*(TT-TA))
      TRP(9-ITA)=TRP(11+ITA)
C
C       CHANNELS WITH EDGE OF TRAPEZOID, BUT NO CORNERS
C
C
C        CHECK IF THERE ARE PURE EDGE CHANNELS
C
      IF(2+ITA-ITT.GT.0) GOTO 60
      ILOW=2+ITA
      DO 55 I=ILOW,ITT
      TRP(I+10)=(TT-FLOAT(I))/(TT-TA)
 55   TRP(10-I)=TRP(10+I)
C
C       CHANNEL WHERE EDGE HITS BASE
C
 60   TRP(11+ITT)=(TT-.5-FLOAT(ITT))**2/(2.*(TT-TA))
      TRP(9-ITT)=TRP(11+ITT)
      GOTO 75
C
C       CASE WHERE EDGE CONTAINED IN ONE CHANNEL
C
 70   TRP(11+ITT)=(TA+TT-1)*.5-FLOAT(ITA)
      TRP(9-ITT)=TRP(11+ITT)
      GOTO 75
C
C       CASE WHERE ALL OF TRAPEZOID IN ONE CHANNEL
C
 90   TRP(10)=1.
      ITRSIZ=1
      ITRSHF=0
C
C       NORMALIZE SO TRAPEZOID HAS UNIT AREA
C
 75   SUM=0.
      AREA=TA+TT
      ILOW=10-ITRSHF
      IHIGH=10+ITRSHF
      DO 77 I=ILOW,IHIGH
      TRP(I)=TRP(I)/AREA
 77   SUM=SUM+TRP(I)
      WRITE(6,103)
 103  FORMAT(//)
      WRITE(6,1000)(TRP(I),I=ILOW,IHIGH)
 1000 FORMAT(1H ,'SHUTTER FUNCTION TRAPEZOID',  2X,19F4.3)
      WRITE(6,103)
      RETURN
      END
```

```
      SUBROUTINE HALF(EXPT,H)
C
C
C      FUNCTION- FIND THE VALUE OF THE HALF MAX POINT FOR
C      GUESSING AN INITIAL VALUE OF BETA
C
C      INPUT-EXPT, THE ARRAY OF EXPERIMENTAL POINTS FOR THE
C      TOF DISTRIBUTION
C
C      OUTPUT- H, THE VALUE OF THE LOCATION OF THE HALF MAXIMUM
C      POINT, IN REAL FORMAT. FRACTIONAL CHANNELS ARE NEEDED
C      FOR THE HIGH SPEED RATIO DISTRIBUTIONS
C
C      ROUTINES CALLED-NONE
C
C      AUTHOR-M.F. VERNON
C
C      LAST REVISION DATE- FEBRUARY 15,1983
C
C
      COMMON/PAR/CHAN,LMID,DL,BCHAN,ECHAN,NCHAN,MASS,MAXE,OFFSET
      DIMENSION EXPT(255)
      REAL MASS,LMID
      INTEGER BCHAN,ECHAN,NCHAN
C
C      CALCULATE CHANNEL NUMBER OF APPROXIMATE HALF HEIGHT
C
C
C      ASSUME DC LEVEL GIVEN BY THE COUNTS IN THE THIRD CHANNEL
C
      DC=EXPT(BCHAN+3)
C
C     MAXE IS THE CHANNEL NUMBER OF THE PEAK OF THE DISTRIBUTION
C
      H=(EXPT(MAXE)+DC)/2.
      DO 10 I=BCHAN,MAXE
C
C      ASSUME FIRST CHANNEL WHOSE SIGNAL IS LARGER THAN THE CALCULATED
C      HALF HEIGHT IS THE CORRECT CHANNEL
C
      IF(EXPT(I).LT.H) GOTO 10
C
C      LINEARLY INTERPOLATE TO FIND THE FRACTIONAL CHANNEL
C      LOCATION OF THE HALF HEIGHT POINT
C
      T1=(EXPT(I)-EXPT(I-1))
      B=EXPT(I)+EXPT(I-1)-T1*FLOAT(2*I-1)
```

```
      B=B/2.
      H=(H-B)/T1
      GOTO 20
 10   CONTINUE
 20   RETURN
      END
```

```
      SUBROUTINE INDATA(EXPT,BETA,VZRO)
C
C
C      FUNCTION- READ IN DATA AND PARAMETERS
C
C      INPUT ALL NUMBERS F10.1 FORMAT EXCEPT WHERE NOTED
C
C      CARD                    CONTENTS
C        1                      TITLE
C        2      MASS(AMU),CHANNEL WIDTH(MICROSECONDS),NOMIAL
C               NEUTRAL FLIGHT LENGTH(CM),IONIZER LENGTH(CM),
C               CHANNEL OFFSET(CHANNELS)
C        3      BEGINNING CHANNEL NUMBER, ENDING CHANNEL NUMBER(2I5)
C        4      WHEEL FREQUENCY(HZ),WHEEL DIAMETER(CM),WHEEL SLIT
C               WIDTH(MM),COLLIMATING SLIT WIDTH(MM)
C        5      DATA(8F10.1)
C       ETC.
C               A BLANK CARD TERMINATES PROGRAM. MULTIPLE DATA SETS
C               CAN BE RUN BY REPEATING THE CARDS 1-4 FOR EACH DATA
C               SET
C
C
C      OUTPUT- EXPT IS THE EXPERIMENTAL DATA, BETA AND VZRO
C      THE FIRST TRIAL VALUES FOR THE VELOCITY DISTRIBUTION
C      PARAMETERS
C
C      ROUTINE CALLED-NONE
C
C      AUTHOR-M.F. VERNON
C
C      LAST REVISION DATE- FEBRUARY 15, 1983
C
C
      DIMENSION EXPT(255),TITLE(20)
      COMMON/PAR/CHAN,LMID,DL,BCHAN,ECHAN,NCHAN,MASS,MAXE,OFFSET
      COMMON/TRIP/WIDTH,HZ,DIA,SA,SB,TRP(19),ITRSIZ,ITRSHF,IFLAG
      INTEGER BCHAN,ECHAN,BC,EC
      REAL MASS,LMID
      READ(5,102) TITLE
```

```
      READ(5,101)MASS,CHAN,LMID,DL,OFFSET
      IF(MASS .EQ. 0.0) STOP
      READ(5,100) BCHAN,ECHAN
      BC=BCHAN
      EC=ECHAN
      NCHAN=ECHAN-BCHAN+1
      READ(5,101)HZ,DIA,SA,SB
      READ(5,101) (EXPT (I), I=BCHAN,ECHAN)
      WRITE(6,204) TITLE
C
C      WRITE INPUT DATA TO OUTPUT FILE
C
      WRITE(6,200) MASS
      WRITE(6,201) CHAN,BC,EC,LMID,DL
      WRITE(6,104)OFFSET
      WRITE(6,211)HZ,DIA,SA,SB
      WRITE(6,103)
      WRITE(6,205)
      WRITE(6,215)(I,EXPT(I),I=BCHAN,ECHAN)
      WRITE(6,103)
      WIDTH =CHAN
      IFLAG=0
      CALL TRAP1
C
C      GENERATE ESTIMATE OF BETA AND VZRO
C
      CALL BIG(EXPT,MAXE)
      VZRO=LMID/(FLOAT(MAXE)+OFFSET)/.1/CHAN
      CALL HALF(EXPT,H)
      VTEM=LMID/(H+OFFSET)/.1/CHAN
      BETA=.693/((VTEM-VZRO)**2)
      VZRO=VZRO**2/(VZRO+1./BETA)
C
C
C      FORMAT STATEMENTS
C
C
  102 FORMAT(20A4)
  100 FORMAT(3I5)
  101 FORMAT(8F10.1)
  204 FORMAT(1H1,20A4)
  200 FORMAT('0  MASS =',F7.3)
  201 FORMAT('   CHANNEL WIDTH =',F4.1,' MICROSECONDS; BEGINNING CHANNEL
     1 =',I3,', ENDING CHANNEL =',I3,'; FLIGHT LENGTH =',F5.2,' CM; IONI
     1ZER LENGTH =',F5.2,' CM.')
  104 FORMAT(3X,'OFFSET= ',F4.1,' CHANNELS')
  211 FORMAT('   WHEEL FREQ. =',F4.0,' HZ; WHEEL DIAMETER =',F4.1,' CM;
     1SLOT WIDTH = ',F4.2,' MM; DETECTOR APERTURE =',F4.2,' MM')
  103 FORMAT(///)
  20  FORMAT(10X,'I N P U T  D I S T R I B U T I O N',/)
  25  FORMAT(8(3X,I3,1X,F9.1))
```

```
      RETURN
      END


      SUBROUTINE LPPLT (X1,Y1,NPT1,X2,Y2,NPT2,NO)
C
C      LINE PRINTER PLOT ROUTINE
C
C      AUTHOR- F. HUISKEN
C
C      LAST REVISION DATE- UNKNOWN
C
      DIMENSION IPA(120),IX1(300),IY1(300),IX2(300),IY2(300)
      DIMENSION X1(300),X2(300),Y1(300),Y2(300)
      DATA L1,L2,L3,L4,LS,LO,LA / 1H1,1H2,1H3,1H4,1HS,1HO,1H* /
      DATA LB,LI,LM,LP / 1H ,1HI,1H-,1H+ /
      DATA DX,DY / 0.025,0.125 /
      WRITE(6,2001)
      IF (NO .EQ. 9) GOTO 20
      IF (NO .EQ. 1) LNO=L1
      IF (NO .EQ. 2) LNO=L2
      IF (NO .EQ. 3) LNO=L3
      IF (NO .EQ. 4) LNO=L4
      GOTO 21
 20   CONTINUE
      LNO=LS
      WRITE (6,2003)
 21   CONTINUE
      DO 1 I=1,NPT1
      IF (X1(I) .LT. DX) X1(I)=DX
      IF (Y1(I) .LT. -3.+DY) Y1(I)=-3.+DY
      IX1(I)=INT((X1(I)+DX)/(2.*DX))
      IY1(I)=INT((Y1(I)+3.+DY)/(2.*DY))+4
 1    CONTINUE
      DO 10 I=1,NPT2
      IF (X2(I) .LT. DX) X2(I)=DX
      IF (Y2(I) .LT. -3.+DY) Y2(I)=-3.+DY
      IX2(I)=INT((X2(I)+DX)/(2.*DX))
      IY2(I)=INT((Y2(I)+3.+DY)/(2.*DY))+4
 10   CONTINUE
      DO 2 I=1,18
      IPA(I)=LB
 2    CONTINUE
      DO 7 N=1,57
      NZ=60-N+1
      DO 3 I=19,120
      IPA(I)=LB
 3    CONTINUE
      IPA(20)=LI
```

```
      IF ((FLOAT(NZ)/8.-NZ/8) .GT. 1.E-6) GOTO 5
      IPA(19)=LM
      IPA(20)=LM
      IF (NZ .NE. 16) GOTO 5
      DO 4 I=21,120
      IPA(I)=LM
      IF ((FLOAT(I)/10.-I/10) .LE. 1.E-6) IPA(I)=LP
 4    CONTINUE
 5    CONTINUE
      DO 6 I=1,NPT1
      IF (IY1(I) .NE. NZ) GOTO 6
      IPA(20+IX1(I))=LO
 6    CONTINUE
      DO 12 I=1,NPT2
      IF (IY2(I) .NE. NZ) GOTO 12
      IND=20+IX2(I)
      IF (IPA(IND) .EQ. LB) IPA(IND)=LNO
      IF (IPA(IND) .EQ. LO) IPA(IND)=LA
      IF (IPA(IND) .EQ. LM) IPA(IND)=LNO
 12   CONTINUE
 7    CONTINUE
C
C
C      FORMAT STATEMENTS
C
C
 2001 FORMAT (1H1)
 2003 FORMAT (1H /)
      WRITE (6,2000) (IPA(I),I=1,120)
 2000 FORMAT (120A1)
      RETURN
      END


      SUBROUTINE VELO(BETA,VZRO,SIGCAL,SIG1,SIG2)
C
C      FUNCTION-CALCULATES THE TOF SPECTRA AVERAGED OVER THE IONIZER
C                LENGTH AND SHUTTER FUNCTION
C
C
C      INPUT- BETA AND VZRO ARE THE PARAMETERS FOR THE TRIAL
C      VELOCITY DISTRIBUTION FUNCTION.
C
C      OUTPUT-SIGCAL,SIGCA1,SIGCA2 THE CALCULATED TOF DISTRIBUTION
C      AND ITS DERIVATIVE WITH RESPECT TO VZRO AND BETA RESPECTIVELY
C
C      ROUTINES CALLED-NONE
C
C      AUTHOR-M.F. VERNON
C
```

```
C
      COMMON/PAR/CHAN,LMID,DL,BCHAN,ECHAN,NCHAN,MASS,MAXE,OFFSET
      COMMON/TRIP/WIDTH,HZ,DIA,SA,SB,TRP(19),ITRSIZ,ITRSHF,IFLAG
      DIMENSION SIGTEM(255),SIGCAL(255)
      DIMENSION SIGCA1(255),SIGCA2(255),SIG1(255),SIG2(255)
      REAL MASS,LMID,L
      INTEGER BCHAN,ECHAN
      N=3
C
C      ZERO ARRAYS
C      SIGCA1, SIGCA2 CONTAIN THE ANALYTICAL DERIVATIVES OF THE
C      DISTRIBUTION WITH RESPECT TO VZRO AND BETA RESPECTIVELY.
C      THE SHUTTER FUNCTION CONVOLUTED RESULTS ARE RETURNED IN
C      SIG1, SIG2.
C
      DO 5 I=BCHAN,ECHAN
      SIGCAL(I)=0.
      SIGTEM(I)=0.
      SIGCA1(I)=0.
      SIGCA2(I)=0.
      SIG1(I)=0.
      SIG2(I)=0.
 5     CONTINUE
      ILOW=BCHAN+ITRSHF
      IHIGH=ECHAN-ITRSHF
C
C      NINT IS THE GRID SIZE FOR THE SIMPSON'S RULE INTEGRATION
C      OVER THE CHANNEL WIDTH. IF THE BEAM WIDTH IS VERY NARROW, THEN
C      SET IFLAG=1 AND THIS INTEGRATION IS PERFORMED, ELSE USE IFLAG=0
C      AND THE ROUTINE IS ROUGHLY 6 TIMES FASTER.
C      NINT SHOULD PROBABLY BE ODD.
C      SEE 'INTRODUCTION TO NUMERICAL ANALYSIS BY HILDEBRAND,SECOND
C      ED., PG. 93.
C      THE CURRENT VALUE OF NINT IS CHOOSEN SUCH THAT IF A FINER GRID
C      IS NEEDED, THEN THE SIMULATION OF THE EXPERIMENT BY THIS PROGRAM
C      IS PROBABLY MORE IN ERROR.
C
      NINT=11
C
C      DIVIDE IONIZER INTO NION INTERVALS
C      NOTE THAT NION SHOULD BE ODD
C
      NION=11
C
C      THESE CONSTANTS ARE USED IN THE INTERVALS FOR THE IONIZER
C      INTEGRATION AND THE CHANNEL WIDTH INTGRATION.
C
      S2=FLOAT(NINT-1)
      N12=NINT-2
      NMID=(NION+1)/2
      S=FLOAT(NION-1)
```

```
      C1=CHAN*.1
      C2=CHAN*.1*(-.5)
C
C      THE 40 DO LOOP TREATS EACH POINT IN THE IONIZER EQUALLY, AND
C      MODELS THE EXPERIMENT BY NION INDEPENDENT AND SLIGHTLY DISPLACED
C      IONIZERS.
C
      DO 40 I=1,NION
      L=LMID+FLOAT(I-NMID)*DL/S
      DO 35 J=BCHAN,ECHAN
      IF(IFLAG.EQ.0) GOTO 30
C
C      THE DO LOOP PERFORMS THE SIMPSON'S RULE INTEGRATION
C
C     T1 IS THE LEFT EDGE OF THE CHANNEL.
      T1=C1*(FLOAT(J-1)+OFFSET)
      V1=L/T1
      X1=V1**N*EXP(-BETA*((V1-VZRO)**2))/T1
      W1=0.
      W2=0.
      W=0.
C
C      DT IS THE STEP LENGTH IN TIME SPACE FOR THE INTEGRATION
C      OVER THE CHANNEL WIDTH
C
      DT=C1/S2
      DO 25 K=1,N12,2
      T2=T1+DT
      T3=T2+DT
      V2=L/T2
      V3=L/T3
      X2=V2**N*EXP(-BETA*((V2-VZRO)**2))/T2
      X3=V3**N*EXP(-BETA*((V3-VZRO)**2))/T3
      W=W+X1+4.*X2+X3
      W1=W1+X1*2.*BETA*(V1-VZRO)+X2*8.*BETA*(V2-VZRO)+X3*2.*BETA*(V3-VZR
     10)
      W2=W2-X1*(V1-VZRO)**2-X3*(V3-VZRO)**2-4.*X2*(V2-VZRO)**2
      X1=X3
      T1=T3
 25   CONTINUE
      SIGTEM(J)=SIGTEM(J)+W*DT/3.
C
C      DERIVATIVE OF INTENSITY WITH RESPECT TO VZRO.
C
      SIGCA1(J)=SIGCA1(J)+W1*DT/3.
C
C      DERIVATIVE OF INTENSITY WITH RESPECT TO BETA.
C
      SIGCA2(J)=SIGCA2(J)+W2*DT/3.
      GOTO 35
C
```

```
C       APPROXIMATE THE AREA OF THE VELOCITY DISTRIBUTION IN THIS
C       CHANNEL BY ITS VALUE AT THE MIDPOINT.
C
 30    T=C1*(FLOAT(J)+OFFSET)+C2
C
C       CALCULATE THE VELOCITY OF THE PARTICLE DETECTED IN CHANNEL J
C       IF IT WAS IONIZED AT THIS DISTANCE L FROM THE COLLISION ZONE
C
       V=L/T
C
C       USING THE GIVEN VELOCITY DISTRIBUTION, CALCULATE THE RELATIVE
C       AMOUNT EXPECTED TO HAVE THIS VELOCITY
C
       C=V**N*EXP(-BETA*(V-VZRO)**2) /T
C
C       DERIVATIVE OF INTENSITY WITH RESPECT TO VZRO.
C
       SIGCA1(J)=SIGCA1(J)+2.*BETA*(V-VZRO)*C
C
C       DERIVATIVE OF INTENSITY WITH RESPECT TO BETA.
C
       SIGCA2(J)=SIGCA2(J)+C*(-(V-VZRO)**2)
       SIGTEM(J)=SIGTEM(J)+C
 35    CONTINUE
 40    CONTINUE
       DO 60 I=ILOW,IHIGH
C
C       CONVOLUTE NOW OVER THE SHUTTER FUNCTION USING THE TRAP
C       ARRAY AS A DIGITAL FILTER
C
       ITEMP=10-I
       JLOW=I-ITRSHF
       JHIGH=I+ITRSHF
       DO 55 J=JLOW,JHIGH
       K=J+ITEMP
       SIG1(I)=SIG1(I)+TRP(K)*SIGCA1(J)
       SIG2(I)=SIG2(I)+TRP(K)*SIGCA2(J)
 55    SIGCAL(I)=SIGCAL(I)+TRP(K)*SIGTEM(J)
 60    CONTINUE
       RETURN
       END
```

APPENDIX II. ELASTIC SCATTERING PROGRAM FOR THE COMPARISON OF LABORATORY ANGULAR DISTRIBUTIONS CALCULATED FROM THE CENTER OF MASS FRAME DIFFERENTIAL CROSS SECTION

A. INTRODUCTION

The program described below was based on previous versions which already existed in our laboratory to allow the analysis of elastic scattering data to be handled at a level of accuracy comparable with the present experimental capabilities. This program begins with an assumed potential form and computes laboratory angular distributions, corresponding to the experimental conditions, from the differential center-of-mass cross section. Basically, the program accounts for the finite detector size, the finite velocity spread of the initial beams and the finite collision volume.

The program is designed to allow, in practice, the computation of the laboratory distribution to any numerical accuracy depending only on the limitation of the computing budget. It is based on a direct simulation of the experiment so that the program can be used to investigate the effects of misalignment, velocity distributions, and other experimental parameters on the observed scattering. This is helpful in designing a good experiment with the experimental conditions chosen to resolve the required features.

In the sections below, the input record structure, several basic program uses, and a program listing provides the user with the necessary information to quickly begin to make calculations.

A description of the scattering equation and the program's numerical methods to solving it is given in Section B. This section should be read before reading the program listing to gain a crude knowledge of the program layout.

Two different phase shift routines are included to fit a particular system's need. Both routines have the capability of interpolating phase shifts - that is, the phase shifts are calculated for a uniformly distributed subset of partial waves (the subset is under user control) and the remaining phase shifts interpolated between their values at these points as needed. In this way, when the number of partial waves becomes large, computing efficiency can still be realized. One routine calculates exact phase shifts using a slightly modified program written by R. J. Leroy at the University of Waterloo, while the other calculates JWKB phase shifts.[1] An alternative published method for the exact phase shift calculation uses the log-derivative integration scheme.[2] Also, a second order JWKB method[3] has been used to improve the accuracy of the semiclassical phase shifts. The latter two routines were not implemented here due to time limitations.

In developing this computer code, commercial software was used whenever possible. In particular, the least squares routine, based on the Levenberg-Marquardt algorithm, was taken from the Minpack library. The only machine dependent routines (CDC 7600) are "SECOND" and "VECPRO." "SECOND" returns the time since the program began execution and is used for locating the sections of the program which determine

the execution efficiency. "VECPRO" is a CDC assembly code routine for performing dot products quickly. Dummy routines to substitute for these are included.

Modifications to the program to perform other than elastic scattering with number density sensitive detectors can easily be implemented. To change the detector aperture shape, modify subroutines "FINT" and "MULSMP." To change the atomic beam cross sectional shapes, modify subroutine "WEIGHTS." To change the energy dependence of the cross section, the velocity dependence of the detection efficiency, or the Jacobian, modify subroutine "CMANG." To change the beam velocity distribution shape, modify subroutine "NOZZLE."

Proper execution of the computer program was checked by verifying internal selfconsistency or comparing with published data. Recovery of a known data set was used to check the least squares routine. The phase shifts were compared with published values for a reference Lennard-Jones potential.[5] A test of the averaging was done by comparing parameters derived from least square fits to the He-Ar data obtained by Aziz, et al.[4]

B. DESCRIPTION OF PROGRAM METHODS

The DFCS is calculated by directly simulating the scattering process. The basic equation to be solved is

$S(\theta)$ = number of scattered particles/sec into the detector positioned at laboratory angle θ

$$= \int_0^\infty n_1(|\vec{v}_1|)\, dv_1 \int_0^\infty n_2(|\vec{v}_2|)\, dv_2 * |\vec{v}_2 - \vec{v}_1| * \int_{-Lx}^{Lx} dx \int_{-Ly}^{Ly} dy \int_{-Lz}^{Lz} dz \int_A \frac{d\sigma}{d\Omega}(\theta)\, dA \quad , \tag{1}$$

where $n_1(|\vec{v}_1|)$ and $n_2(|\vec{v}_2|)$ are the number densities of the primary and secondary beams at the speeds $|\vec{v}_1|$, $|\vec{v}_2|$, respectively. $|\vec{v}_2-\vec{v}_1|$ is the relative collision velocity. $\frac{d\sigma}{d\Omega}(\theta)$ is the center-of-mass cross section for scattering at the center-of-mass angle which correlates to the detector positioned at the nominal laboratory angle θ. The integration over the beam velocities (dv_1, dv_2) and the collision volume (dx, dy, dz) is handled by choosing discrete samples of each variable with a suitable weighting factor, and summing the results, i.e.,

$$S(\theta) = \sum_{\substack{i,j \\ k,l,m}} W_{ijklm}\, n_1(|\vec{v}_i|) * n_2(|\vec{v}_j|) * |\vec{v}_i - \vec{v}_j| * \int_A \frac{d\sigma}{d\Omega}(\theta_{ijklm})\, dA \tag{2}$$

Gauss-Hermite quadrature is used for the velocity integrals. The collision volume integration is performed by Gauss-Legendre quadrature.

For fixed values of the primary and secondary beam speeds and for each point in the collision volume, the scattering to a fixed point on

the detector is a simple matter of geometry, using the center-of-mass → laboratory transformation characterizing the intersection. The finite dimensions of the detector are accounted for by an adaptive Simpson's rule integration which chooses points on the detector and calculates the lines between these points and the collision volume grid points. Such lines intersect the Newton sphere in 0, 1, or 2 points. The partial waves are then summed at the center-of-mass scattering angles determined by the intersections, and the center-of-mass cross section is computed by summing the partial waves. The cross sections at the intersection points are weighted by both their inverse lab velocities (since the electron bombardment detector is sensitive to density, not flux), and the Jacobian factor which transforms areas in the center-of-mass to areas in the laboratory frame. The adaptive Simpson's rule continues to calculate by adding points at the detector until the scattering has converged to 1/10 the error in the data, or 1 percent if no data errors are supplied.

This procedure has the advantage that by increasing the volume grid and the number of Newton diagrams, an effectively exact treatment of the scattering can be realized. The two dimensional detector integration proceeds as in the one dimensional case until the desired convergence has been obtained.

Singular behavior in the Jacobian will result in numerical problems when the detector is tangent to the Newton sphere. Numerically, the only way to properly account for this is to transform the domain of integration from the detector to the center-of-mass. By

conservation of flux, the center-of-mass flux scattered through the boundary viewed by the detector is the same flux that would be experimentally observed in the laboratory frame. This removes the singularity but replaces it with an integration which has a complicated boundary. Although this boundary can be defined parametrically through the intersection equation, several cases can occur, each of which deserves separate treatment. Also, it is unclear whether any new physical information would be contained in treating this case properly. For this reason, the program will not handle this case.

The summation of the partial waves involves the product of trigonometric functions of the phase shifts along with the Legendre functions of the scattering angle. These vector products are performed using a fast vector product routine written in CDC assembly code. The "vectors" are defined from the scattering amplitude, $f(\theta)$, as follows:

$$
\begin{aligned}
f(\theta) &= \frac{1}{2ik} \sum_{\ell} (2\ell + 1) P_{\ell}(c\theta)(e^{2i\eta_{\ell}} - 1) \\
&= \sum_{\ell} \frac{1}{k} \left(\frac{2\ell + 1}{2}\right) P_{\ell}(c\theta) \sin 2\eta_{\ell} \\
&+ i \sum_{\ell} \frac{1}{k} \left(\frac{2\ell + 1}{2}\right) P_{\ell}(c\theta)(1 - \cos 2\eta_{\ell}) \\
&= \frac{1}{k} \left(\sum_{\ell} \vec{P}_{\ell} * \vec{S}_{\ell} + i \sum_{\ell} \vec{P}_{\ell} * \vec{C}_{\ell}\right) ,
\end{aligned}
\tag{3}
$$

where

$$\vec{P} = (\tfrac{1}{2}P_0(c\theta), \frac{3P_1(c\theta)}{2}, \ldots, \frac{(2\ell+1)}{2}P_\ell(c\theta), \ldots),$$

$$\vec{S} = (\sin 2\eta_0, \sin 2\eta_1, \ldots, \sin 2\eta_\ell, \ldots),$$

$$\vec{C} = (\cos 2\eta_0 - 1, \cos 2\eta_1 - 1 \ldots, \cos 2\eta_\ell - 1, \ldots), \tag{4}$$

$$\frac{d\sigma}{d\Omega}(\theta) = |f(\theta)|^2 = \frac{1}{k^2}\left(\sum \vec{P}_\ell * \vec{C}_\ell\right)^2 + \left(\sum \vec{P}_\ell * \vec{S}_\ell\right)^2 \quad \text{, and}$$

$$c\theta = \cos\theta.$$

The center-of-mass angles at which these summations are performed are determined in the subroutine CMANG. Therefore, at every detector angle, CMANG calculates the angles, and INTENS sums the partial waves at those angles.

The approximation which sets all phase shifts for the collision volume points equal to the most probable one can be used whenever the beam velocity spread ($\Delta v/v_0$) is larger than the beam spatial angular divergence ($\frac{XL}{PRINOZ}$).

If both input masses are equal, the program only sums over even (odd) phase shifts depending on the parameter IBOSE. This is to allow for nuclear symmetry oscillations. If one wants to avoid this option when scattering particles of the same mass, merely change one of the input masses by a small amount so that the particles are not mathematically equal, yet for all practical purposes they will be physically equal.

The program produces a timing summary which allows one to locate those parts of the program to optimize. For JWKB phase shifts, approximately 70-80 percent of the total computing time is used to sum the partial waves at the center-of-mass angles and compute Legendre functions. The fast dot product code uses IINT * NVOL * (285 + 8 * NETA) μsecs where NVOL = NCOLX * NCOLY * NCOLZ and IINT is the number of calls to the INTENSE subroutine. This is typically about 30 percent of the total computing time. Therefore, there is little optimization possible without additional assumptions which limit the number of center-of-mass scattering angles where the intensity is evaluated.

C. GEOMETRY OF SCATTERING

Let: (x,y,z) label a point in the region where the particles collide.

$(-x_1, 0, 0)$ locate the primary nozzle considered as a point source.

$(0, -y_2, 0)$ locate the secondary nozzle considered as a point source.

v_1 be the <u>speed</u> of the primary beam.

v_2 be the <u>speed</u> of the secondary beam.

$$\frac{v_1 * (x_1 + x,\ y,\ z)}{(x_1 + x)^2 + y^2 + z^2)^{1/2}}$$

is the velocity of the primary beam which passes through the point (x,y,z) with speed v_1.

$$= (v_1^x,\ v_1^y,\ v_1^z)$$

$$\frac{v_2 (x,\ y + y_2,\ z)}{(x^2 + (y+y_2)^2 + z^2)^{1/2}}$$

is the velocity of the secondary beam which passes through the point (x,y,z) with speed v_2.

$$= (v_2^x,\ v_2^y,\ v_2^z)$$

$$(v_{cm}^x,\ v_{cm}^y,\ v_{cm}^z) = (M_1 v_1^x + M_2 v_2^x,\ M_1\ v_1 + M_2 v_2^y,$$

$$M_1\ v_1^z + M_2 v_2^z)/(M_1 + M_2) + (x,y,z)$$

are the lab coordinates for the location of the tip of the center-of-mass velocity vector.

$$\frac{M_2}{(M_1 + M_2)} * \left((v_1^x - v_2^x)^2 + (v_1^y - v_2^y)^2 + (v_1^z - v_2^z)^2\right)^{1/2} = v_{1S}$$

is the speed of the primary product or the radius of the Newton sphere.

(x_D, y_D, z_D) is a point in the laboratory on the detector surface.

$(r_D c\theta_D, r_D s\theta_D, z_D)$ is this same point on the detector, now labeled by r_D, the distance from the collision zone center to the detector entrance, and θ_D is the angle the detector makes with respect to the primary beam.

Now we wish to derive an expression which relates the line connecting this point on the detector to the point (x,y,z) in the collision volume, and find the points where this line will intersect the Newton sphere.

Let (x^1, y^1, z^1) be a point of intersection. It must satisfy the following equations:

$$(x^1 - v^x_{cm})^2 + (y^1 - v^y_{cm})^2 + (z^1 - v^z_{cm})^2 = v^2_{1S} \tag{5}$$

$$(x^1, (\frac{y-y_D}{x-x_D})\, x^1 + \frac{xy_D - x_D y}{x-x_D}, (\frac{z-z_D}{x-x_D})\, x^1 + \frac{xz_D - x_D z}{x-x_D}) = (x^1, y^1, z^1) \tag{6}$$

Equation (5) is the Newton sphere equation and Eq. (6) is the linear line sight equation between the detector point and the collision volume point.

When Eq. (6) is substituted into Eq. (5), two solutions are obtained for x^1 which are the front/back sides of the Newton sphere. Of course, the solutions can be degenerate or nonexistent.

To simply the solution, redefine Eq. (6) as

$$y^1 = M_y x^1 + b_y \tag{7}$$

$$z^1 = M_z x^1 + b_z$$

Equation (5) then gives for x^1

$$A(x^1)^2 + Bx^1 + C = 0, \quad \text{where} \tag{8}$$

$$A = (1 + M_y^2 + M_z^2)$$

$$B = -2(v_{cm}^x + M_y(v_{cm}^y - b_y) + M_z(v_{cm}^z - b_z))$$

$$C = (v_{cm}^x)^2 + (b_y - v_{cm}^y)^2 + (b_z - v_{cm}^z)^2 - (v_{1S})^2 \quad .$$

Depending on the discriminate of the quadratic equation, a number of distinct solutions are possible. Even if two distinct solutions are found, they still must be checked to see that the laboratory velocity is in the detector's direction. For light particles, the backward scattered product may be traveling away from the detector. If $x^1 > 0$, then this condition will be satisfied.

To find the cosine of the angle in the center-of-mass frame between the scattered product and the relative velocity vector, the equations are

$$\cos(\theta_{cm}) = \frac{\vec{N} * \vec{\theta}}{|\vec{N}||\vec{\theta}|} \quad , \tag{9}$$

$$\vec{N} = (x^1 - v_{cm}^x, y^1 - v_{cm}^y, z^1 - v_{cm}^z) \quad ,$$

$$\vec{\theta} = (v_1^x - v_2^x, v_1^y - v_2^y, v_1^z - v_2^z) \quad .$$

Zare[6] has shown in a straightforward way that the transformation of the center-of-mass flux through a surface to the same flux in a different surface in the laboratory frame involves the elastic Jacobian factor, J,

$$J = \frac{v_{lab}^2}{\vec{u}_{cm}^2 \cos(\vec{v}_{lab}, \vec{u}_{cm})} \quad , \tag{10}$$

where $\vec{v}_{lab}$ is the particle's laboratory velocity, $\vec{u}_{cm}$ is the particle's velocity in the center-of-mass frame, and $\cos(\vec{v}_{lab}, \vec{u}_{cm})$ is the cosine of the angle between the velocity of the particle in the two frames. To compare with number density detection, we must scale by an additional factor of $1/\ |\vec{v}_{lab}|$. Therefore,

$$I(\theta) = \frac{d\sigma}{d\Omega}(\theta) * \frac{|\vec{v}_{lab}|}{(\vec{u}_{cm})^2 \cos(\vec{u}_{cm}, \vec{v}_{lab})} \tag{11}$$

relates the flux in the center-of-mass frame for the area viewed by the detector at the laboratory scattering angle θ, to the number density detected in the laboratory frame, $I(\theta)$.

The above equations for the intersection point are not valid if the detector is looking into the secondary beam. To treat this case or general placement of the detector, the subroutine CMANG must be modified so that a new set of non-singular quadratic equations are defined.

D. INPUT RECORD STRUCTURE

All real numbers are in F10.3 format, all integers are in I10 format. Record numbers in parentheses are optional depending on the choice of input parameters. Examples are provided in Section F.

Record	Type	Parameters
1	20A4	Title
2	Real	MPRI, BETA1, VZRO1, PRINOZ
3	Real	MSEC, BETA2, VZRO2, SECNOZ
4	Real	XL, YL, ZL, ALIM(1), BLIM(1), ALIM(2), BLIM(2), DETRAD
5	Real	RANGE(2), RANGE(3), RANGE(4), RANGE(5)
6	Int	NCOLX, NCOLY, NCOLZ, NPRI, NSEC, NANG, IINT, IAPPRX
7	Int	NETA, NSKP, NPRI1, NSETS, NOPT, NLST, NPAR, NITER
8	Int	NPRI2, MAXIT, IBOSE
9	Real	XSTART, XSTEP, RNPHAS, ERROR Note: For JWKB phase shifts, all parameters on Card 9 must be zero.
10,11	Real	A(1) → A(15)
(Optional)	Int	INDEX(1) → INDEX(NLST)
(Optional)	Real	FTOL, XTOL, FACTOR, EPSFCN
12	Real	(ANGLE(1), DATA (1)) → (ANGLE(NANG), DATA(NANG))
(Optional)	Real	(EDAT(1) → EDAT(NANG))
13	Int	IRPT
etc.		

E. DEFINITION OF PARAMETERS

MPRI/MSEC	Mass (amu) of primary/secondary beams.
BETA1/BETA2 VZRO1/VZRO2	Primary/secondary nozzle beam number density velocity distribution parameters, defined by $P(v) = v^2 \exp(-\beta(v-v_0)^2)$.
PRINOZ/SECNOZ	Distance of primary and secondary nozzles from collision center.
XL, YL, ZL	Dimensions of collision volume in X,Y,Z directions as determined by the molecular beam defining slits.
ALIM(2), BLIM(2)	Bottom and top positions of detector aperture, i.e., BLIM(2)-ALIM(2)=Detector height.
ALIM(1), BLIM(1)	Detector width = BLIM(1)-ALIM(1). Note: The ALIM, BLIM arrays can be used to see the effects of detector aperture misalignment. The center of the detector coordinates are determined by the laboratory angle. The symmetric, aligned limits are ALIM(1) = -Detector width/2. BLIM(1) = -ALIM(1) ALIM(2) = -Detector height/2 BLIM(2) = -ALIM(2). To give a net in plane offset, add (or subtract) the offset from both ALIM(1) and BLIM(1). Similarly, for vertical offsets, add (or subtract) the offset to ALIM(2) and BLIM(2). To improve speed when using the full two dimensional detector integration, set ALIM(2) = 0. This assumes that the scattering is symmetric with respect to the scattering plane, and therefore, only the top half of the detector needs to be integrated.
DETRAD	Distance from collision center to defining aperture on detector.
RANGE(2), RANGE(3)	RMIN, RMAX for plotting the potential.
RANGE(4), RANGE(5)	VMIN, VMAX for plotting the potential. Note: RANGE defines a rectangle for plotting the potential. Any points outside the rectangle are not plotted. RANGE can be used to focus on a particular region of the potential.

NCOLX, NCOLY, NCOLZ	Number of integration points in X,Y,Z directions for collision volume integration. Maximum of 5 in any single direction.
NPR1, NSEC	Number of integration quadrature points for the primary/secondary beams. Limited to a maximum of 10 each.
NANG	Number of laboratory angles where calculations are to be performed. Limited to 100 maximum.
IINT	=0, treats the detector as a point located at the center of the detector coordinates. =1, treats the detector as a horizontal slit in the plane of the molecular beams. =2, treats the detector as a full two-dimensional aperture.
IAPPRX	=0, each point in the collision volume has its own phase shifts, computed from the intersection angles defined by the nozzle positions and intersection point. =1, all points have the same phase shifts corresponding to the dominate collision point as determined by the integration weighting scheme. =2, all collision volume points for all Newton diagrams have the same phase shifts.
NETA	Number of phase shifts or maximum phase shift.
NSKP	Interval used in interpolating phase shifts.
NPRI1	=0, no phase shift printing. =1, lists the collision energies and phase shifts for each Newton diagram. Caution - this generates much output if more than 1 Newton diagram and 1 collision volume point are used.
NSETS	The number of data sets to be used simultaneously in a least squares fit. NSETS must be less than 4.

NOPT	=1, calculates differential cross sections (DFCS) with no data.
	=2, calculates DFCS with data, but no data errors.
	=3, calculates DFCS with data and data errors.
NLST	=0, no least squares fitting.
	=1, a least squares fit to the data will be performed for NLST variables.
NPAR	Number of parameters in potential function.
NITER	The maximum number of cross sections allowed in the least squares fitting. If N parameters are varied, then N+1 cross sections per iteration are needed if the first try at improving the fit is successful. If three parameters are simultaneously changed, and three iterations are desired, then approximately 13 cross sections will be calculated.
NPRI2	=0, no printing.
	=1, intermediate values for the detector integration are printed. This is useful in estimating the change of the scattering intensity over the detector height.
MAXIT	Maximum number of iterations in the adoptive Simpson's integration over the detector (usually 4 is sufficient).
IBOSE	=1, then only even Legendre terms are summed over when the nuclei are identical.
	=2, then only odd Legendre terms are summed over when the nuclei are identical.
XSTART	In reduced distance units, the starting point for the Numerov integration for the exact phase shifts.
XSTEP	In reduced distance units, the step size for the Numerov integration.
RNPHAS	The number of steps in the Numerov phase shift integration.

ERROR	Maximum error, in radians, for the phase shifts calculated by the exact Numerov method.
A(1)-A(15)	Potential parameters needed as defined in the subroutines, "POT" and "PREPOT."
INDEX(I)	Array containing the list of variables to be varied in least squares fit. If a potential has 10 parameters (NPAR=10), but only the third, fifth and seventh are to be varied, then INDEX(1)=3, INDEX(2)=5, INDEX(3)=7, with NLST=3.
XTOL	Fractional change in parameters used as a convergence test in least square fits. Fitting terminates when all parameters are changing by less than XTOL of their value.
FTOL	Same as XTOL, but refers to the fractional change in the chi square value.
FACTOR	Controls length of initial step size in least squares fitting of parameters. Values between 0.1 - 1000.0 are normal, with larger values representing larger parameter changes on first iteration.
EPSFCN	An estimate of the reliability of the numerical derivatives. This parameter should be several orders of magnitude smaller than XTOL or FTOL.
(ANGLE(I), DATA(I))	Pairs giving the experimental intensity at a given detector angle. The angles are measured relative to the primary beam, positive direction measured toward the secondary beam.
EDAT(I)	Errors associated with the measured data.
IRPT	=0, the program stops. =1, read in a new set of potential parameters, all data and other input remaining unchanged from previous values, and calculate a DFCS for this potential. This parameter assumes NLST=0. =2, begin again at card 1, with completely new input.

F. EXAMPLES OF SEVERAL STANDARD PROGRAM USES.

The control variables are designed to allow easy interchange among several basic uses. These uses are:

a) Calculate a hypothetical DFCS to test various resolution effects including collision volume size, velocity beam spreads, phase shift accuracy, and detector integration mode. In this case, read in records 1-12 inclusive. Record 12 contains the two numbers, ANGLE(1) = Starting Lab Angle, and DATA(1) = Angle Step Size, which differs from the standard definition for these parameters. If a single job testing several sets of resolution effects is desired, follow this record with either IRPT=1, if only the potential is to be changed, or IRPT=2 if, in addition, any other parameters are to be changed. For this last case records 1-12 need to be input again. A blank record terminates the program's execution. Make NLST=0, NOPT=1, and NITER=1, on record 7.

b) Calculate a DFCS with data and possibly data errors. Read in records 1-12 inclusive with NOPT = 2 or 3, NLST = 0, and NITER = 1. Again, IRPT will allow several runs of this type in a single job. Previously calculated data points can be input producing a graph comparing the angular distributions corresponding to different machine parameters, to locate where the data are most affected. The program will scale the calculation to the input cross section.

Obviously, if no least squares fitting is desired, this mode allows one to test potentials in a trial and error mode which is helpful in determining the general range for the potential parameters.

c) Least Squares. The optional records between 11 and 12 are needed, with the parameters described above. Because the calculation can be expensive, it is a good practice to begin with NITER=1 to see how long a single iteration takes.

G. CHANGING THE POTENTIAL FORM

To change the potential form, the user must supply two subroutines for each potential.

1. JWKB phase shifts

```
SUBROUTINE POT (X, A, V, VP, L, RM)
DIMENSION X(10), A(15), V(10), VP(10)
```

The array X, on input, contains the reduced, dimensionless, distances needed for the semi-classical phase shifts. X*A(2) is the distance in angstroms. The two potential parameters A(1) and A(2) must be the well depth and r_m. L is the number of entries in the X array ($L \leq 10$). The subroutine POT must evaluate the reduced potential at the points, x, and return the potential values and first derivatives in the corresponding entries of the arrays V and VP, respectively.

```
SUBROUTINE PREPOT (A, RM)
DIMENSION A(15)
```

PREPOT checks the potential parameters to insure that they are self-consistent. It is called once each time the potential is changed. For example, the HFD potential includes r_m explicity in its form, so PREPOT insures that r_m is consistent with all the other parameters. The ESMSV and similar forms use PREPOT to determine spline coefficients. If your particular potential does not need to use PREPOT, then supply the following dummy routine.

```
SUBROUTINE PREPOT (A, RM)
DIMENSION A(15)
Return
End
```

Since all phase shift routines work in reduced units, they assume that A(1) = ϵ, and A(2) = r_m. The potential subroutines must be consistent with this convention.

2. Numerov Phase Shifts

```
SUBROUTINE POT (X, A, V, VP, L, RM)
DIMENSION A(15), X(10), V(10), VP(10)
```

On input, X contains the reduced positions where the potential needs to be calculated for JWKB corrections to the exact phase shift. On output, V(I) is the reduced potential at X(I), and X(I) equals $1/X^2(I)$, i.e. the reduced centrifugal potential.

```
SUBROUTINE PREPOT (A, RM)
DIMENSION A(15)
Common/PTNL/V(6001), XM2(6001), XSTART, XSTEP, RNPHAS, ERROR
```

On input, RNPHAS is the number of points used in the Numerov integration, XSTART is the starting point for the integration and XTEP is the step size. The routine calculates the reduced potential for the RNPHAS points starting at XSTART, and stepping by XSTEP, and stores the results in the V array. The XM2 array contains the corresponding values of the fraction 1./X(I)**2 for the centrifugal potential. The routine must insure the self-consistency of the potential parameters as described above for the JWKB shifts.

REFERENCES

1. J. Cohen, J. Chem. Phys., 68, 1841 (1978).
2. B. R. Johnson, J. Comput. Phys. 13, 445 (1973).
3. M. Keil, J. T. Slankas, A. Kuppermann, J. Chem. Phys. 70, 482 (1979).
4. R. A. Aziz, et al., J. Chem. Phys., 71, 2637 (1979).
5. R. Bernstein, J. Chem. Phys. 33, 795 (1960).
6. R. N. Zare, J. Chem. Phys., 69, 1737 (1978).

```
      PROGRAM ELASTIC(INPUT,OUTPUT,TAPE6,TAPE8,TAPE10,TAPE5=INPUT)      TEST.2
C                                                                       TEST.3
C                                                                       TEST.4
C     ELASTIC SCATTERING PROGRAM FOR SPHERICALLY SYMMETRIC INTERACTIONS TEST.5
C     INPUT VARIABLES ARE DEFINED IN THE ROUTINE INPUT.                 TEST.6
C                                                                       TEST.7
C                                                                       TEST.8
C       AUTHOR- M.F.F VERNON
C
C       LAST REVISION DATA- APRIL 17, 1983
C
C
      COMMON/SAVE/IDIN(5),PNOZ(5),SNOZ(5),NTA(5),DTA(5),ID(5),NCX(5),   SAVE.2
     $NCY(5),NCZ(5),IIRR(5),IS1MAX(5),IP1MAX(5),NBP(5),NBS(5),HT(5),    SAVE.3
     $ WD(5),NAGL(5),DRD(5),ALM1(5),ALM2(5),BLM1(5),BLM2(5),NPRIN1(5),  SAVE.4
     $VELO1(5,10),VLWT1(5,10),VELO2(5,10),VLWT2(5,10),CC1(7,5),XCV(5,5) SAVE.5
     $,YCV(5,5),ZCV(5,5),WXCV(5,5),WYCV(5,5),WZCV(5,5),ANGUM(3,100),    SAVE.6
     $ ERRPT(3,100),DATUM(3,100),DTSN1(3,100),DTCN1(3,100),NSETS        SAVE.7
      COMMON/LST/EINV(300),INDEX(15),VFAR(15),RM,FTOL,XTOL,MAXFEV,FACTORLST.2
     $,EPSFCN                                                           LST.3
      DIMENSION A(15),DMMY(100),SCAL(100),DMMY3(100)                    TEST.11
      COMMON/GEOMTY/PRINOZ,SECNOZ,PRISPD,SECSPD,XCOL,YCOL,ZCOL,MPRI,    GEOMTRY.2
     1MSEC,SNDT,CSDT,NOPT,NPRI1                                         GEOMTRY.3
     $,NPRI2 ,MAXIT                                                     GEOMTRY.4
      REAL MPRI,MSEC,MTOT                                               GEOMTRY.5
      COMMON/DAT/ANGLE(100),SDAT(100),EDAT(100),NANG,SF                 DAT.2
      COMMON/TM/TIME(10),ICM,INTS,SPMAX,SPMIN                           TM.2
      DIMENSION TITLE(20)                                               TEST.15
      DIMENSION RANGE(5)                                                TEST.16
9     CONTINUE                                                          TEST.17
      CALL SECOND(TIME(10))                                             TEST.18
C                                                                       TEST.19
C      READ IN DATA AND EXPERIMENTAL  CONDITIONS                        TEST.20
C                                                                       TEST.21
      CALL INPUT(A,RM1,NTERMS,NPAR,TITLE)                               TEST.22
      NN=1                                                              TEST.23
      IF(NTERMS.NE.0) GOTO 200                                          TEST.24
C                                                                       TEST.25
C      NO LEAST SQUARES FIT                                             TEST.26
C                                                                       TEST.27
 3    WRITE(6,117)                                                      TEST.28
      WRITE(6,2)(A(I),I=1,NPAR)                                         TEST.30
      CALL SECOND(T1)                                                   TEST.32
      CALL POTPLOT(A,RM1)                                               TEST.33
      CALL SECOND(T2)                                                   TEST.34
      TIME(9)=T2-T1+TIME(9)                                             TEST.35
C                                                                       TEST.36
C     CALCULATE DFCS FOR INITIAL PARAMETERS                             TEST.37
C                                                                       TEST.38
      CALL DFCS(A,SCAL,CHI,RM1)                                         TEST.39
      IF(NOPT-1) 250,250,275                                            TEST.40
C                                                                       TEST.41
C     PLOT ANGULAR DISTRIBUTION, NO DATA                                TEST.42
```

```
C                                                                       TEST.43
 250  CALL SECOND(T1)                                                   TEST.44
      CALL XPPLOT(-118101,1,-1,0,1,-1,0,0.,1,ANGLE,SCAL,NANG,1HX)       TEST.45
      CALL SECOND(T2)                                                   TEST.46
      TIME(9)=T2-T1+TIME(9)                                             TEST.47
      GOTO 10                                                           TEST.48
 275  CALL SECOND(T1)                                                   TEST.49
C                                                                       TEST.50
C     PLOT ANGULAR DISTRIBUTION WITH DATA                               TEST.51
C                                                                       TEST.52
      WRITE(6,14)                                                       TEST.53
      WRITE(6,8)CHI                                                     TEST.54
      RANGE(1)=1.                                                       TEST.55
      RANGE(2)=ANGLE(1)                                                 TEST.56
      RANGE(3)=ANGLE(NANG)                                              TEST.57
      RANGE(5)=SPMAX                                                    TEST.58
      RANGE(4)=SPMIN                                                    TEST.59
      CALL XPPLOT(-118101,1,-1,0,1,-1,0,RANGE,2,ANGLE,SDAT,NANG,1HE,ANGLTEST.60
     -E,SCAL,NANG,1HC)                                                  TEST.61
C                                                                       TEST.62
C      PLOT ANGULAR DISTRIBUTION DIFFERENCES                            TEST.63
C                                                                       TEST.64
      RANGE(1)=0.                                                       TEST.65
      DO 274 I=1,NANG                                                   TEST.66
      DMMY(I)=SCAL(I)-SDAT(I)                                           TEST.67
      DMMY3(I)=-EDAT(I)                                                 TEST.68
 274   CONTINUE                                                         TEST.69
      CALL XPPLOT( -59101,1,-1,0,1,-1,0,RANGE,3,ANGLE,DMMY,NANG,1HX,ANGLTEST.70
     -E,EDAT,NANG,1HO,ANGLE,DMMY3,NANG,1H+)                             TEST.71
      CALL SECOND(T2)                                                   TEST.72
      TIME(9)=TIME(9)+T2-T1                                             TEST.73
      GOTO 10                                                           TEST.74
C                                                                       TEST.75
C     LEAST SQUARES SECTION     ****************************************TEST.76
C                                                                       TEST.77
 200  CONTINUE                                                          TEST.78
      CALL SECOND(T1)                                                   TEST.79
C                                                                       TEST.80
C     PLOT POTENTIAL                                                    TEST.81
C                                                                       TEST.82
      CALL POTPLOT(A,RM1)                                               TEST.83
      CALL SECOND(T2)                                                   TEST.84
      TIME(9)=T2-T1+TIME(9)                                             TEST.85
      CALL SECOND(TS)                                                   TEST.86
      WRITE(6,14)                                                       TEST.87
      WRITE(6,4)                                                        TEST.88
      DO 4445 I=1,15                                                    TEST.90
      VPAR(I)=A(I)                                                      TEST.91
4445  CONTINUE                                                          TEST.92
      CALL LSTSQR(NTERMS,SCAL)                                          TEST.93
C                                                                       TEST.94
C      PLOT FITTED DISTRIBUTIONS FOR EACH DATA SET AFTER LEAST SQUARES  TEST.95
C      TERMINATES                                                       TEST.96
```

```
C                                                                       TEST.97
4459  CONTINUE                                                          TEST.98
      CALL SWITCH (NN)                                                  TEST.99
      CALL DFCS(A,SCAL,CHI,RM1)                                         TEST.100
      WRITE(6,72) SF                                                    TEST.101
      WRITE(6,73)CHI                                                    TEST.102
C                                                                       TEST.105
C     PLOT ANGULAR DISTRIBUTION DIFFERENCES                             TEST.106
C                                                                       TEST.107
      CALL SECOND(T1)                                                   TEST.108
      DO 190 I=1,NANG                                                   TEST.109
      DMMY(I)=SCAL(I)-SDAT(I)                                           TEST.110
      DMMY3(I)=-EDAT(I)                                                 TEST.111
 190  CONTINUE                                                          TEST.112
      CALL XPPLOT(-118101,1,-1,0,1,-1,0,0.,3,ANGLE,DMMY,NANG,1HX,ANGLE, TEST.113
     -EDAT,NANG,1HO,ANGLE,DMMY3,NANG,1H+)                               TEST.114
C                                                                       TEST.115
C     PLOT ANGULAR DISTRIBUTION                                         TEST.116
C                                                                       TEST.117
      CALL XPPLOT(-118101,1,-1,0,1,-1,0,0.,2,ANGLE,SDAT,NANG,1HE,ANGLE, TEST.118
     -SCAL,NANG,1HO)                                                    TEST.119
      CALL SECOND(T2)                                                   TEST.120
      TIME(9)=TIME(9)+T2-T1                                             TEST.121
 10   WRITE(6,12)                                                       TEST.122
C                                                                       TEST.124
C      WRITE OUT CALCULATED TABLES                                      TEST.125
C                                                                       TEST.126
      WRITE(6,221)                                                      TEST.127
      WRITE(6,13)                                                       TEST.130
      WRITE(6,5)(ANGLE(I),SCAL(I),I=1,NANG)                             TEST.131
      WRITE(10,18)(TITLE(I),I=1,20)                                     TEST.133
      DO 17 I=1,NANG                                                    TEST.135
      SCAL(I)=EXP(SCAL(I))                                              TEST.136
 17   CONTINUE                                                          TEST.137
      WRITE(10,7)(ANGLE(I),SCAL(I),I=1,NANG)                            TEST.138
      WRITE(6,13)                                                       TEST.140
      WRITE(6,11)                                                       TEST.141
      WRITE(6,13)                                                       TEST.143
      WRITE(6,5)(ANGLE(I),SCAL(I),I=1,NANG)                             TEST.144
      NN=NN+1                                                           TEST.145
      IF(NN.LE.NSETS) GOTO 4459                                         TEST.146
C                                                                       TEST.147
C      READ IN PARAMETER TO SEE IF AN ADDITIONAL DATA SET TO BE ANALYZEDTEST.148
C                                                                       TEST.149
      READ(5,1)IRPT                                                     TEST.150
      IF(IRPT.NE.1) GOTO 15                                             TEST.152
      READ(5,2)(A(I),I=1,15)                                            TEST.153
      CALL PREPOT(A,RM)                                                 TEST.154
      GOTO 3                                                            TEST.155
 15   CONTINUE                                                          TEST.156
C                                                                       TEST.157
C     TIMING INFORMATION                                                TEST.158
C                                                                       TEST.159
```

```
      T=0.                                                              TEST.160
      CALL SECOND(XX)                                                   TEST.161
      TT=XX-TIME(10)                                                    TEST.162
      TIME(5)=TIME(5)-TIME(4)-TIME(3)                                   TEST.163
      TIME(8)=TIME(9)                                                   TEST.164
      DO 106 I=1,10                                                     TEST.165
  106 TIME(I)=TIME(I)/TT*100.                                           TEST.166
      WRITE(6,14)                                                       TEST.167
      WRITE(6,107)                                                      TEST.168
      WRITE(6,100)(TIME(I),I=2,4)                                       TEST.171
      WRITE(6,13)                                                       TEST.173
      WRITE(6,138) TT                                                   TEST.174
      WRITE(6,14)                                                       TEST.176
      WRITE(6,101) INTS                                                 TEST.177
      IF(IRPT.EQ.2)GOTO 9                                               TEST.179
      STOP                                                              TEST.180
C
C
C       FORMAT STATEMENTS
C
C
 117  FORMAT(10X,*INPUT POTENTIAL PARAMETERS*,/)                        TEST.29
  2   FORMAT(8F10.3)                                                    TEST.31
  4   FORMAT(//,40X,*L E A S T  S Q U A R E S  S E C T I O N*,//)       TEST.89
 73   FORMAT(10X,*CHI SQUARE ERROR=*,E14.7,/)                           TEST.103
 72   FORMAT(2X,*SCALE FACTOR= *,2X,E14.7)                              TEST.104
 12   FORMAT(/////)                                                     TEST.123
 221  FORMAT(30X,*F I N A L  C A L C U L A T E D  D I S T R I B U T I O TEST.128
     1N*)                                                               TEST.129
 5    FORMAT(5(3X,F6.1,2X,F10.3))                                       TEST.132
 18   FORMAT(20A4)                                                      TEST.134
 7    FORMAT(8F10.3)                                                    TEST.139
 11   FORMAT(30X,*FINAL DISTRIBUTION CONVERTED TO INPUT FORM*)          TEST.142
 1    FORMAT(8I10)                                                      TEST.151
 107  FORMAT(30X,*P E R  C E N T  T I M E  S P E N T  I N  S U B R O U TTEST.169
     $ I N ES*,/,3X,*PHSHFT*,6X,*CMANG*, 7X,*INTENS*,/)                 TEST.170
 100  FORMAT(6X,10(2X,F10.5))                                           TEST.172
 138  FORMAT( 2X,*TOTAL TIME FOR CALCULATION=*,2X,F12.5)                TEST.175
 101  FORMAT (1X,*CALLS TO FINT ROUTINE*,I10)                           TEST.178
 14   FORMAT(/////)                                                     TEST.181
 13    FORMAT(/)                                                        TEST.182
 8    FORMAT(10X,*CHISQR FOR INPUT PARAMETERS=*,E14.7,/)                TEST.183
      END                                                               TEST.184


                                                                        TEST.185
      SUBROUTINE SWITCH(J)                                              SWITCH.2
C                                                                       SWITCH.3
C      FUNCTION- SWITCHES DATA SETS AND AVERAGING PARAMETERS WHEN
C                SIMULTANEOUS FITTING MORE THAN ONE DATA SET            SWITCH.5
C                                                                       SWITCH.6
C      ON INPUT J IS THE DATA SET TO BE CALCULATED NEXT.                SWITCH.7
```

```
C                                                                       SWITCH.8
C
C      OUTPUT- ALL COMMON BLOCKS CONTAIN THE DATA FOR SET J
C
C        ROUTINES CALLED-NONE
C
C        AUTHOR-M.F. VERNON
C
C        LAST REVISION DATE-FEBRUARY 16,1983
C
      COMMON/TRIG/DETSIN(100),DETCOS(100)                               SWITCH.9
      COMMON/ETA/STHE(8000),CTHE(8000),NETA,DETA,IDENT                  ETA.2
     $,IBOSE                                                            ETA.3
      COMMON/AA/DETWD,DETHT,DETRAD,E                                    AA.2
      COMMON/GEOMTY/PRINOZ,SECNOZ,PRISPD,SECSPD,XCOL,YCOL,ZCOL,MPRI,    GEOMTRY.2
     1MSEC,SNDT,CSDT,NOPT,NPRI1                                         GEOMTRY.3
     $,NPRI2 ,MAXIT                                                     GEOMTRY.4
      REAL MPRI,MSEC,MTOT                                               GEOMTRY.5
      COMMON/SAVE/IDIN(5),PNOZ(5),SNOZ(5),NTA(5),DTA(5),ID(5),NCX(5),   SAVE.2
     $NCY(5),NCZ(5),IIRR(5),IS1MAX(5),IP1MAX(5),NBP(5),NBS(5),HT(5),    SAVE.3
     $ WD(5),NAGL(5),DRD(5),ALM1(5),ALM2(5),BLM1(5),BLM2(5),NPRIN1(5),  SAVE.4
     $VELO1(5,10),VLWT1(5,10),VELO2(5,10),VLWT2(5,10),CC1(7,5),XCV(5,5) SAVE.5
     $,YCV(5,5),ZCV(5,5),WXCV(5,5),WYCV(5,5),WZCV(5,5),ANGUM(3,100),    SAVE.6
     $ ERRPT(3,100),DATUM(3,100),DTSN1(3,100),DTCN1(3,100),NSETS        SAVE.7
      COMMON/DAT/ANGLE(100),SDAT(100),EDAT(100),NANG,SF                 DAT.2
      COMMON/INTEG/IINT                                                 INTEG.2
      COMMON/EN/ENERGY(125),CMTH1(125),CMTH2(125),WGHT1(125),WGHT2(125),EN.2
     1NCOLX,NCOLY,NCOLZ,IAPPRX                                          EN.3
      COMMON/LIMITS/ALIM(2),BLIM(2)                                     LIMITS.2
      COMMON/VOL/X(5),Y(5),Z(5),WX(5),WY(5),WZ(5)                       VOL.2
      COMMON/BEAM/VPRI(10),VSEC(10),WPRI(10),WSEC(10),NPRI,NSEC,IPRIM,  BEAM.2
     +ISECON                                                            BEAM.3
      COMMON/WH/C1,C2,C3,C4,C5,C6,C7,C8,C9,C10,MTOT                     WH.2
      IINT=IDIN(J)                                                      SWITCH.21
      PRINOZ=PNOZ(J)$ SECNOZ=SNOZ(J) $ NETA=NTA(J) $DETA=DTA(J)         SWITCH.22
      IDENT=ID(J) $ NCOLX=NCX(J) $NCOLY=NCY(J)$NCOLZ=NCZ(J)             SWITCH.23
      IAPPRX=IIRR(J) $ISECON=IS1MAX(J)$IPRIM=IP1MAX(J)$NPRI=NBP(J)      SWITCH.24
      NSEC=NBS(J)$DETHT=HT(J)  $DETWD=WD(J)  $NANG=NAGL(J)              SWITCH.25
      DETRD=DRD(J) $ ALIM(1)=ALM1(J) $ ALIM(2)=ALM2(J) $ BLIM(1)=BLM1(J)SWITCH.26
      BLIM(2)=BLM2(J)$ NPRI1=NPRIN1(J)                                  SWITCH.27
      DO 4020 I=1,NPRI                                                  SWITCH.28
      VPRI(I)=VELO1(J,I)                                                SWITCH.29
      WPRI(I)=VLWT1(J,I)                                                SWITCH.30
 4020 CONTINUE                                                          SWITCH.31
      DO 4025 I=1,NSEC                                                  SWITCH.32
      VSEC(I)=VELO2(J,I)                                                SWITCH.33
      WSEC(I)=VLWT2(J,I)                                                SWITCH.34
 4025 CONTINUE                                                          SWITCH.35
      DO 4030 I=1,NCOLX                                                 SWITCH.36
      X(I)=XCV(J,I)                                                     SWITCH.37
      WX(I)=WXCV(J,I)                                                   SWITCH.38
 4030 CONTINUE                                                          SWITCH.39
      DO 4035 I=1,NCOLY                                                 SWITCH.40
```

```
      Y(I)=YCV(J,I)                                                     SWITCH.41
      WY(I)=WYCV(J,I)                                                   SWITCH.42
 4035 CONTINUE                                                          SWITCH.43
      DO 4040 I=1,NCOLZ                                                 SWITCH.44
      Z(I)= ZCV(J,I)                                                    SWITCH.45
      WZ(I)=WZCV(J,I)                                                   SWITCH.46
 4040 CONTINUE                                                          SWITCH.47
      IMAX=NAGL(J)                                                      SWITCH.48
      DO 4050 I=1,IMAX                                                  SWITCH.49
      ANGLE(I)=ANGUM(J,I)                                               SWITCH.50
      EDAT(I)=ERRPT(J,I)                                                SWITCH.51
      SDAT(I)= DATUM(J,I)                                               SWITCH.52
      DETSIN(I)= DTSN1(J,I)                                             SWITCH.53
      DETCOS(I)= DTCN1(J,I)                                             SWITCH.54
 4050   CONTINUE                                                       SWITCH.55
      C1=CC1(1,J)                                                       SWITCH.56
      C2=CC1(2,J)                                                       SWITCH.57
      C3=CC1(3,J)                                                       SWITCH.58
      C4=CC1(4,J)                                                       SWITCH.59
      C5=CC1(5,J)                                                       SWITCH.60
      C6=CC1(6,J)                                                       SWITCH.61
      C7=CC1(7,J)                                                       SWITCH.62
      RETURN                                                            SWITCH.63
      END                                                               SWITCH.64


      SUBROUTINE LSTSQR(NTERMS,FVEC)                                    LSTSQR.2
      DIMENSION FVEC(1)                                                 LSTSQR.3
C                                                                       LSTSQR.4
C      FUNCTION- LSTSQR CONTROLS THE NONLINEAR LEAST SQUARES FITTING OF LSTSQR.5
C      THE OBSERVED DATA TO THE CALCULATED SIMULATION.                  LSTSQR.6
C                                                                       LSTSQR.7
C      ARGUMENTS- NTERMS, AN INTEGER VARIABLE EQUAL TO THE NUMBER OF    LSTSQR.8
C      PARAMETERS VARIED IN THE LEAST SQUARES FIT                       LSTSQR.9
C      FVEC- THE ARRAY OF FUNCTIONS TO BE MINIMIZED.                    LSTSQR.10
C            FVEC(I)=(DATA(I)-CALC(I))/SQRT(ERROR(I))                   LSTSQR.11
C      WHERE DATA(I) IS THE OBSERVED INTENSITY AT THE ITH ANGLE         LSTSQR.12
C      CALC(I) IS THE CALCULATED INTENSITY AT THIS ANGLE, AND           LSTSQR.13
C      ERROR(I) IS THE ERROR IN THE OBSERVED DATA AT THIS ANGLE         LSTSQR.14
C                                                                       LSTSQR.15
C      SUBPROGRAMS- SQRT                                                LSTSQR.16
C                 - FCN,LMDIF                                           LSTSQR.17
C                                                                       LSTSQR.18
C        AUTHOR-M.F. VERNN
C
C
C        LAST REVISION DATE -FEBRUARY 16,1983
C
C
      DIMENSION FJAC(300,10),DIAG(10),IPVT(10),QTF(10),WA1(10),WA2(10)  LSTSQR.21
      DIMENSION WA3(10),WA4(300),VTMP(10)                               LSTSQR.22
```

```
      COMMON/SAVE/IDIN(5),PNOZ(5),SNOZ(5),NTA(5),DTA(5),ID(5),NCX(5),   SAVE.2
     $NCY(5),NCZ(5),IIRR(5),IS1MAX(5),IP1MAX(5),NBP(5),NBS(5),HT(5),    SAVE.3
     $ WD(5),NAGL(5),DRD(5),ALM1(5),ALM2(5),BLM1(5),BLM2(5),NPRIN1(5),  SAVE.4
     $VELO1(5,10),VLWT1(5,10),VELO2(5,10),VLWT2(5,10),CC1(7,5),XCV(5,5) SAVE.5
     $,YCV(5,5),ZCV(5,5),WXCV(5,5),WYCV(5,5),WZCV(5,5),ANGUM(3,100),    SAVE.6
     $ ERRPT(3,100),DATUM(3,100),DTSN1(3,100),DTCN1(3,100),NSETS        SAVE.7
      COMMON/LST/EINV(300),INDEX(15),VPAR(15),RM,FTOL,XTOL,MAXFEV,FACTORLST.2
     $,EPSFCN                                                           LST.3
      COMMON/DAT/ANGLE(100),SDAT(100),EDAT(100),NANG,SF                 DAT.2
      EXTERNAL FCN                                                      LSTSQR.26
C                                                                       LSTSQR.27
C      INITIAL PARAMETERS TO LEAST SQUARE ROUTINE                       LSTSQR.28
C      FOR A MORE COMPLETE DESCRIPTION OF THESE PARAMETERS SEE THE      LSTSQR.29
C      LISTING FOR THE PROGRAM LMDIF.                                   LSTSQR.30
C                                                                       LSTSQR.31
      LDFJAC=300                                                        LSTSQR.32
      NPRINT=1                                                          LSTSQR.33
      GTOL=0.                                                           LSTSQR.34
      MODE=1                                                            LSTSQR.35
      M=0                                                               LSTSQR.36
      DO 100 I=1,NSETS                                                  LSTSQR.37
      M=M+NAGL(I)                                                       LSTSQR.38
 100   CONTINUE                                                          LSTSQR.39
      N=NTERMS                                                          LSTSQR.40
      WRITE(6,12)(VPAR(I),I=1,15)                                       LSTSQR.41
      WRITE(6,559) XTOL,FTOL                                            LSTSQR.44
C                                                                       LSTSQR.47
C      LOAD THE ARRAY OF THE PARAMETERS TO BE VARIED                    LSTSQR.48
C                                                                       LSTSQR.49
      DO 10 I=1,NTERMS                                                  LSTSQR.50
      VTMP(I)=VPAR(INDEX(I))                                            LSTSQR.51
 10    CONTINUE                                                         LSTSQR.52
C                                                                       LSTSQR.53
C      SINCE THE NONLINEAR FUNCTIONS ARE JUST THE DIFFERENCES BETWEEN   LSTSQR.54
C      THE CALCULATED AND OBSERVED SIGNAL,WEIGHTED BY THE ERROR,        LSTSQR.55
C      THE SQRT OF THE DATA ERROR IS NEEDED SO THAT THE SUM OF THE      LSTSQR.56
C       SQUARES OF THE FUNCTIONS IS THE CHI SQUARE ERROR.               LSTSQR.57
C                                                                       LSTSQR.58
      IJ=0                                                              LSTSQR.59
      DO 16 J=1,NSETS                                                   LSTSQR.60
      IMAX=NAGL(J)                                                      LSTSQR.61
      DO 15 I=1,IMAX                                                    LSTSQR.62
      EINV(I+IJ)=1./SQRT(ERRPT(J,I))                                    LSTSQR.63
 15    CONTINUE                                                          LSTSQR.64
      IJ=IJ+NAGL(J)                                                     LSTSQR.65
 16    CONTINUE                                                          LSTSQR.66
      WRITE(6,1)                                                        LSTSQR.67
      WRITE(6,889)                                                      LSTSQR.68
C                                                                       LSTSQR.71
C      LMDIF IS THE MINPACK DRIVER FOR THE NONLINEAR LEAST SQUARES FIT  LSTSQR.72
C                                                                       LSTSQR.73
      CALL LMDIF(FCN,M,N,VTMP,FVEC,FTOL,XTOL,GTOL, MAXFEV,EPSFCN,DIAG,  LSTSQR.74
     *MODE,FACTOR,NPRINT,INFO,NFEV,FJAC,LDFJAC,IPVT,QTF,WA1,WA2,WA3,WA4)LSTSQR.75
```

```
C                                                                       LSTSQR.76
C      WRITE OUT RESULTS OF LEAST SQUARES FIT WITH INFORMATION ON THE   LSTSQR.77
C      EXIT CONDITION FROM THE MINPACK ROUTINE                          LSTSQR.78
C                                                                       LSTSQR.79
      WRITE(6,2)                                                        LSTSQR.80
      WRITE(6,1000) NFEV                                                LSTSQR.83
      WRITE(6,13)(VPAR(I),I=1,15)                                       LSTSQR.85
      WRITE(6,2)                                                        LSTSQR.88
      WRITE(6,1001) INFO                                                LSTSQR.89
      IF(INFO.EQ.0) WRITE(6,550)                                        LSTSQR.91
      IF(INFO.EQ.1) WRITE(6,551)                                        LSTSQR.92
      IF(INFO.EQ.2) WRITE(6,552)                                        LSTSQR.93
      IF(INFO.EQ.3) WRITE(6,553)                                        LSTSQR.94
      IF(INFO.EQ.4) WRITE(6,554)                                        LSTSQR.95
      IF(INFO.EQ.5) WRITE(6,555)                                        LSTSQR.96
      IF(INFO.EQ.6) WRITE(6,556)                                        LSTSQR.97
      IF(INFO.EQ.7) WRITE(6,557)                                        LSTSQR.98
      IF(INFO.EQ.8) WRITE(6,558)                                        LSTSQR.99
C                                                                       LSTSQR.119
C      ON RETURN TO THE MAIN PROGRAM, REPLACE THE OLD PARAMETERS BY THE LSTSQR.120
C      NEW ONES.                                                        LSTSQR.121
C                                                                       LSTSQR.122
      DO 20 I=1,NTERMS                                                  LSTSQR.123
      VPAR(INDEX(I))=VTMP(I)                                            LSTSQR.124
 20    CONTINUE                                                         LSTSQR.125
      RETURN                                                            LSTSQR.126
C
C
C      FORMAT STATEMENTS
C
C
 12   FORMAT(10X,* ON INPUT TO THE LEAST SQUARES PROGRAM, PARAMETERS ARELSTSQR.42
     $=*,/,10(2X,E10.3),/,10(2X,E10.3))                                 LSTSQR.43
 559  FORMAT(10X,*VARIABLE CONVERGENCE (XTOL)=*,E14.7,/,10X,            LSTSQR.45
     $*CONVERGENCE FOR NORM OF RESIDUALS (FTOL)=*,E14.7)                LSTSQR.46
889   FORMAT(1X,*L2 NORM OF RESIDUALS*,30X,*INTERMEDIATE PARAMETER VALUELSTSQR.69
     $S*,/)                                                             LSTSQR.70
 2    FORMAT(/)                                                         LSTSQR.81
 1    FORMAT(//)                                                        LSTSQR.82
 1000 FORMAT(5X,*NUMBER OF FUNCTION EVALUATIONS *,I5,/)                 LSTSQR.84
 13   FORMAT(10X,* ON EXIT FROM THE LEAST SQUARES PROGRAM, PARAMETERS   LSTSQR.86
     $ARE=*,/,5(2X,E14.7),/,5(2X,E14.7),/,5(2X,E14.7))                  LSTSQR.87
 1001 FORMAT(10X,*EXIT CONDITION PARAMETER *,I5)                        LSTSQR.90
 550  FORMAT(2X,*IMPROPER INPUT PARAMETERS TO LMDIF ROUTINE*,/)         LSTSQR.100
 551  FORMAT(2X,*BOTH ACTUAL AND PREDICTED RELATIVE REDUCTIONS IN THE   LSTSQR.101
     $SUM OF SQUARES ARE AT MOST FTOL*,/)                               LSTSQR.102
 552  FORMAT(2X,*RELATIVE ERROR BETWEEN TWO CONSECUTIVE ITERATES OF THE LSTSQR.103
     $PARAMETERS IS AT MOST XTOL*,/)                                    LSTSQR.104
 553  FORMAT(2X,*RELATIVE ERROR BETWEEN TWO CONSECUTIVE ITERATES OF THE LSTSQR.105
     $PARAMETERS ON TWO CONSECUTIVE ITERATIONS IS LESS*,/,2X,* THAN FTOLLSTSQR.106
     $ AND XTOL RESPECTIVELY*,/)                                        LSTSQR.107
 554  FORMAT(2X,*SOLUTION VECTOR IS ORTHOGONAL TO JACOBIAN. TRY A NEW *,LSTSQR.108
     $*STARTING POINT TO INSURE THIS IS NOT*,/,2X,* A MAXIMUM OR SADDLE LSTSQR.109
```

```
     $POINT*,/)                                                         LSTSQR.110
 555  FORMAT(2X,*MAXIMUM ALLOWED NUMBER OF FUNCTION EVALUATIONS HAS BE  LSTSQR.111
     $EN REACHED*,/)                                                    LSTSQR.112
 556  FORMAT(2X,*FTOL IS TOO SMALL. NO FURTHER REDUCTION IN SUM OF SQUARLSTSQR.113
     $ES IS POSSIBLE*,/)                                                LSTSQR.114
 557  FORMAT(2X,*XTOL IS TOO SMALL. NO FURTHER IMPROVEMENT IN THE*      LSTSQR.115
     $* APPROXIMATE SOLUTION X IS POSSIBLE*,/)                          LSTSQR.116
 558  FORMAT(2X,*GTOL IS TOO SMALL. THE FUNCTION IS ORTHOGONAL TO THE   LSTSQR.117
     $JACOBIAN WITHIN THE MACHINE PRECISION*,/)                         LSTSQR.118
      END                                                               LSTSQR.127


                                                                        LSTSQR.128
      SUBROUTINE FCN(M,N,X,FVEC,IFLAG)                                  FCN.2
C                                                                       FCN.3
C      FUNCTION-FCN IS THE INTERFACE ROUTINE WHICH CALCULATES THE
C              FUNCTIONS                                                FCN.4
C      USED IN THE NONLINEAR LEAST SQUARES ROUTINE.                     FCN.5
C
C      PARAMETERS-M, ON INPUT, IS THE NUMBER OF DATA POINTS             FCN.6
C      N- ON INPUT IS THE NUMBER OF PARAMETERS IN THE LEAST SQUARES FIT FCN.7
C      X, ON INPUT, IS THE ARRAY OF POTENTIAL PARAMETER VALUES          FCN.8
C      FVEC- ON OUTPUT IS AN ARRAY WHICH IS THE DIFFERENCE IN THE       FCN.9
C      OBSERVED AND CALCULATED DATA WEIGHTED BY THE SQUARE ROOT OF THE  FCN.10
C      ERROR FOR EACH ANGLE.                                            FCN.11
C      IFLAG- ON INPUT CONTROLS THE PRINTING OF INTERMEDIATE            FCN.12
C      ITERATION VALUES                                                 FCN.13
C                                                                       FCN.14
C      SUBPROGRAMS- DFCS,PREPOT,ENORM                                   FCN.15
C                 -SWITCH                                               FCN.16
C                                                                       FCN.17
C       AUTHOR M.F. VERNON
C                                                                       FCN.19
C                                                                       FCN.20
C       LAST REVISION DATE- FEBRUARY 16,1983
C
      COMMON/SAVE/IDIN(5),PNOZ(5),SNOZ(5),NTA(5),DTA(5),ID(5),NCX(5),   SAVE.2
     $NCY(5),NCZ(5),IIRR(5),IS1MAX(5),IP1MAX(5),NBP(5),NBS(5),HT(5),    SAVE.3
     $ WD(5),NAGL(5),DRD(5),ALM1(5),ALM2(5),BLM1(5),BLM2(5),NPRIN1(5),  SAVE.4
     $VELO1(5,10),VLWT1(5,10),VELO2(5,10),VLWT2(5,10),CC1(7,5),XCV(5,5) SAVE.5
     $,YCV(5,5),ZCV(5,5),WXCV(5,5),WYCV(5,5),WZCV(5,5),ANGUM(3,100),    SAVE.6
     $ ERRPT(3,100),DATUM(3,100),DTSN1(3,100),DTCN1(3,100),NSETS        SAVE.7
      COMMON/LST/EINV(300),INDEX(15),VPAR(15),RM,FTOL,XTOL,MAXFEV,FACTORLST.2
     $,EPSFCN                                                           LST.3
      COMMON/TM/TIME(10),ICM,INTS,SPMAX,SPMIN                           TM.2
      COMMON/DAT/ANGLE(100),SDAT(100),EDAT(100),NANG,SF                 DAT.2
      INTEGER M,N,IFLAG                                                 FCN.25
      REAL X(N),FVEC(M),SCAL1(100)                                      FCN.26
C                                                                       FCN.27
C      PLACE THE PARAMETERS TO BE VARIED IN THEIR PROPER POSITION       FCN.28
C                                                                       FCN.29
      DO 10 I=1,N                                                       FCN.30
```

```
      VPAR(INDEX(I))=X(I)                                               FCN.31
 10    CONTINUE                                                         FCN.32
C                                                                       FCN.33
C       CALCULATE THE DFCS                                              FCN.34
C                                                                       FCN.35
      RM1=RM                                                            FCN.36
      CALL PREPOT(VPAR,RM1)                                             FCN.37
      IJ=0                                                              FCN.38
      DO 30 J=1,NSETS                                                   FCN.39
      CALL SWITCH(J)                                                    FCN.40
      CALL DFCS(VPAR,SCAL1,DMY,RM1)                                     FCN.41
C                                                                       FCN.42
C       SET UP NON-LINEAR FUNCTIONS                                     FCN.43
C                                                                       FCN.44
      DO 20 I=1,NANG                                                    FCN.45
      FVEC(IJ+I)=(SDAT(I)-SCAL1(I))*EINV(IJ+I)                          FCN.46
 20    CONTINUE                                                          FCN.47
      IJ=IJ+NANG                                                        FCN.48
30    CONTINUE                                                          FCN.49
C                                                                       FCN.50
C       IF INTERMEDIATE PRINTING INFORMATION IS NEEDED, DO SO HERE.     FCN.51
C                                                                       FCN.52
      IF(IFLAG.NE.0) GOTO 50                                            FCN.53
      FNORM=ENORM(M,FVEC)                                               FCN.54
      WRITE(6,111) FNORM,(INDEX(I),X(I),I=1,N)                          FCN.55
 50   RETURN                                                            FCN.57
C
C
C       FORMAT STATEMENTS
C
C
 111   FORMAT(1X,F10.4,20X,5(2X,I2,1X,F10.4),/,31X,5(2X,I2,1X,F10.4))    FCN.56
      END                                                               FCN.58


                                                                        FCN.59
      SUBROUTINE POTPLOT(A,RM)                                          POTPLOT.2
C                                                                       POTPLOT.3
C       FUNCTION- PLOTS THE POTENTIAL ON A LINE PRINTER. THE AREA PLOTED POTPLOT.4
C       IS DEFINED BY                                                   POTPLOT.5
C       XMIN=RANGE(2),XMAX=RANGE(3),YMIN=RANGE(4),YMAX=RANGE(5)         POTPLOT.6
C       IF ANY POINTS ARE OUTSIDE THIS BOUNDARY THEY ARE NOT PLOTTED.   POTPLOT.7
C       THIS ENABLES ONE TO COMPARE DIFFERENT POTENTIALS ON AN          POTPLOT.8
C       INDEPENDENT SCALE. IF EXACT OR JWKB PHASE SHIFTS ARE USED, THEN POTPLOT.9
C       THE POTENTIAL IS EXPRESSED IN DIFFERENT UNITS. ISKP DETERMINES  POTPLOT.10
C       WHICH TYPE OF PHASE SHIFTS ARE USED                             POTPLOT.11
C                                                                       POTPLOT.12
C       PARAMETERS- A, ON INPUT CONTAINS THE POTENTIAL PARAMETERS       POTPLOT.13
C       RM IS THE REDUCED MASS                                          POTPLOT.14
C                                                                       POTPLOT.15
C       SUBPROGRAMS- POT,XPPLOT,SQRT                                    POTPLOT.16
C                                                                       POTPLOT.17
```

```
C       AUTHOR M.F. VERNON
C                                                                       POTPLOT.19
C       LAST REVISION DATE- FEBRUARY 16,1983
C
C
      COMMON/PTNL/V(2001),XM2(2001),XSTART,XSTEP,RNPHAS,ERROR           PTNL.2
      COMMON/RNG/RANGE(5)                                               RNG.2
      DIMENSION XX(100),VV(100),VT(10),X(10),VP(10),A(15)               POTPLOT.22
      DIMENSION RN(5)                                                   POTPLOT.23
C                                                                       POTPLOT.24
C      MAKE A COPY OF THE COMMON BLOCK TO PASS AS A SUBROUTINE ARGUMENT POTPLOT.25
C                                                                       POTPLOT.26
      DO 10 I=1,5                                                       POTPLOT.27
      RN(I)=RANGE(I)                                                    POTPLOT.28
 10    CONTINUE                                                         POTPLOT.29
      XMIN=RANGE(2)                                                     POTPLOT.30
C                                                                       POTPLOT.31
C      DETERMINE THE UNITS OF THE POTENTIAL ENERGY BY DECIDING WHAT     POTPLOT.32
C      TYPE OF PHASE SHIFTS ARE USED                                    POTPLOT.33
C                                                                       POTPLOT.34
      ISKP=0                                                            POTPLOT.35
      IF(XSTART*XSTEP*RNPHAS.NE.0.) ISKP=1                              POTPLOT.36
      BZ=RM*A(1)*A(2)*A(2)*349.757/16.8573                              POTPLOT.37
      STEP=(RANGE(3)-RANGE(2))/100.                                     POTPLOT.38
      TEST=ABS(RANGE(4))                                                POTPLOT.39
      DO 100 I=1,10                                                     POTPLOT.40
      ISTART=10*(I-1)                                                   POTPLOT.41
C                                                                       POTPLOT.42
C      CALCULATE POTENTIAL IN BLOCKS OF 10 POINTS                       POTPLOT.43
C                                                                       POTPLOT.44
      DO 90 J=1,10                                                      POTPLOT.45
      X(J)=XMIN/A(2)                                                    POTPLOT.46
 90   XMIN=XMIN+STEP                                                    POTPLOT.47
      CALL POT(X,A,VT,VP,10,RM)                                         POTPLOT.48
      DO 80 J=1,10                                                      POTPLOT.49
      II=ISTART+J                                                       POTPLOT.50
C                                                                       POTPLOT.51
C      IF EXACT PHASE SHIFTS ARE USED, THEN THE POSITION AND ENERGY HAVEPOTPLOT.52
C       TO BE CONVERTED TO BE CONSISTENT WITH THE JWKB UNITS            POTPLOT.53
C                                                                       POTPLOT.54
      IF(ISKP.EQ.1) VT(J)=VT(J)/BZ                                      POTPLOT.55
      IF(ISKP.EQ.1) X(J)=SQRT(1./X(J))                                  POTPLOT.56
C                                                                       POTPLOT.57
C      CONVERT FROM REDUCED TO REAL UNITS                               POTPLOT.58
C                                                                       POTPLOT.59
      VV(II)=VT(J)*A(1)                                                 POTPLOT.60
      XX(II)=X(J) *A(2)                                                 POTPLOT.61
 80   CONTINUE                                                          POTPLOT.62
 100  CONTINUE                                                          POTPLOT.63
C                                                                       POTPLOT.64
C      XPPLOT IS THE SANDIA LINE PRINTER PLOT ROUTINE                   POTPLOT.65
C                                                                       POTPLOT.66
      CALL XPPLOT(-180100,1,-1,0,1,-1,0,RN,1,XX,VV,100,1H*)             POTPLOT.67
```

```
      RETURN                                                            POTPLOT.68
      END                                                               POTPLOT.69


                                                                        POTPLOT.70
      SUBROUTINE SCALE(X,V)                                             SCALE.2
C                                                                       SCALE.3
C     FUNCTION-SCALES CALCULATED TO  OBSERVED CROSS SECTIONS.           SCALE.4
C     CHOOSE BEST ADDITIVE CONSTANT WHICH MINIMIZES CHISQR              SCALE.5
C     ON INPUT, X CONTAINS THE SCATTERING DISTRIBUTION. ON OUTPUT, X    SCALE.6
C     CONTAINS THE LOG OF THE CALCULATED SCATTERING DISTRIBUTION,       SCALE.7
C     SCALED TO MINIMIZE CHI SQUARE ERROR.                              SCALE.8
C     V, ON OUTPUT, IS THE CHI SQUARE ERROR.                            SCALE.9
C                                                                       SCALE.10
C      SUBPROGRAMS-ALOG                                                 SCALE.11
C                                                                       SCALE.12
C      AUTHOR-M.F. VERNON
C                                                                       SCALE.14
C      LAST REVISION DATE-FEBRUARY 16,1983
C
C
      COMMON/DAT/ANGLE(100),SDAT(100),EDAT(100),NANG,SF                 DAT.2
      DIMENSION X(1)                                                    SCALE.16
C                                                                       SCALE.17
C      CONVERT TO LOG SCALE                                             SCALE.18
C                                                                       SCALE.19
      DO 9 I=1,NANG                                                     SCALE.20
      X(I)=ALOG(X(I))                                                   SCALE.21
 9    CONTINUE                                                          SCALE.22
C                                                                       SCALE.23
C     FIND ADDITIVE CONSTANT TO MINIMIZE LEAST SQUARE ERROR             SCALE.24
C                                                                       SCALE.25
      S=0.                                                              SCALE.26
      V=0.                                                              SCALE.27
      R=0.                                                              SCALE.28
      DO 10 I=1,NANG                                                    SCALE.29
      R=R+(X(I)-SDAT(I))/EDAT(I)                                        SCALE.30
      S=S+1./EDAT(I)                                                    SCALE.31
 10   CONTINUE                                                          SCALE.32
C                                                                       SCALE.33
C      SF IS THE SCALE FACTOR, OR ADDITIVE CONSTANT ON A LOG SCALE      SCALE.34
C                                                                       SCALE.35
      SF=R/S                                                            SCALE.36
C                                                                       SCALE.37
C      RETURN SCALED DATA AND CHI SQUARE ERROR                          SCALE.38
C                                                                       SCALE.39
      DO 11 I=1,NANG                                                    SCALE.40
      X(I)=X(I)-SF                                                      SCALE.41
      V=V+(X(I)-SDAT(I))**2/EDAT(I)                                     SCALE.42
 11   CONTINUE                                                          SCALE.43
      RETURN                                                            SCALE.44
      END                                                               SCALE.45
```

```
                                                                        SCALE.46
      SUBROUTINE INPUT(A,RM1,NLST,NPAR,TITLE)                           INPUT.2
C                                                                       INPUT.3
C      FUNCTION- INPUT READS THE DATA AND PARAMETERS WHICH DESCRIBE THE INPUT.4
C      EXPERIMENTAL CONDITIONS FROM DEVICE 6. IT CONVERTS THE DATA      INPUT.5
C      TO A LOG SCALE, CHECKS THAT THE ARRAY DIMENSIONS ARE             INPUT.6
C      COMPATIBLE WITH THE PARAMETERS, AND CALLS ROUTINE TO SET UP      INPUT.7
C      NEWTON DIAGRAMS AND INTEGRATION WEIGHTS                          INPUT.8
C                                                                       INPUT.9
C      PARAMETERS- A- ON OUTPUT CONTAINS THE POTENTIAL PARAMETERS       INPUT.10
C      RM1- ON OUTPUT, CONTAINS THE REDUCED MASS IN AMU                 INPUT.11
C      NLST- ON OUTPUT, CONTAINS THE NUMBER OF PARAMETERS INVOLVED IN A INPUT.12
C      LEAST SQUARE FIT                                                 INPUT.13
C      NPAR- ON OUTPUT CONTAINS THE NUMBER OF PARAMETERS IN THE         INPUT.14
C      POTENTIAL FUNCTION                                               INPUT.15
C      TITLE- ON OUTPUT CONTAINS A CHARACTER STRING FOR  IDENTIFYING    INPUT.16
C      PUNCHED CARD OUTPUT                                              INPUT.17
C                                                                       INPUT.18
C      SUBPROGRAMS- ALOG,COS,SIN                                        INPUT.19
C                  -NOZZLE,PREPOT,WEIGHTS                               INPUT.20
C                  - SWITCH                                             INPUT.21
C                                                                       INPUT.22
C       AUTHOR-M.F. VERNON
C
C       LAST REVISION DATE-FEBRUARY 16,1983
C
C                                                                       INPUT.24
C      ALL REAL PARAMETERS ARE READ USING 8F10.3 FORMAT.                INPUT.25
C      ALL INTEGERS ARE READ USING 8I10 FORMAT                          INPUT.26
C***********************************************************************INPUT.27
C  CARD  TYPE                    PARAMETERS                            INPUT.28
C***********************************************************************INPUT.29
C    1        TITLE                                                     INPUT.30
C    2   REAL MPRI1,BETA1,VZRO1,PRINOZ,WDTH1                            INPUT.31
C    3   REAL MSEC,BETA2,VZRO2,SECNOZ,WDTH2                             INPUT.32
C    4   REAL XL,YL,ZL,ALIM(1),BLIM(1),ALIM(2),BLIM(2),DETRAD           INPUT.33
C    5   REAL RANGE(2),RANGE(3),RANGE(4),RANGE(5)                       INPUT.34
C    6   INT. NCOLX,NCOLY,NCOLZ,NPRI,NSEC,NANG,IINT,IAPPRX              INPUT.35
C    7   INT. NETA,NSKP,NPRI1,IDFPLT,NOPT,NLST,NPAR,NITER               INPUT.36
C    6   REAL XSTART,XSTEP,RNPHAS,ERROR                                 INPUT.37
C  8,9   REAL A(I),I=1,15                                               INPUT.38
C  9OPT  INT  INDEX(I),I=1,NLST                                         INPUT.39
C 10 OPT REAL FTOL,XTOL,FACTOR,EPSFCN                                   INPUT.40
C 11...  REAL (ANGLE(I),DATA(I)), I=1,NANG                              INPUT.41
C  ...   REAL EDAT(I),I=1,NANG                                          INPUT.42
C        INT  IRPT                                                      INPUT.43
C***********************************************************************INPUT.44
C     DESCRIPTION OF INPUT PARAMETERS                                   INPUT.45
C     TITLE- TITLE IS USED TO IDENTIFY OUTPUT (PUNCHED CARDS)           INPUT.46
C                                                                       INPUT.47
```

```
C     MPRI/MSEC; MASS(AMU) OF PRIMARY/SECONDARY BEAMS                    INPUT.48
C                                                                        INPUT.49
C     BETA1,BETA2,VZRO1,VZRO2; PRIMARY/SECONDARY NOZZLE BEAM VELOCITY    INPUT.50
C     DISTRIBUTION PARAMETERS. SEE SUBROUTINE NOZZLE FOR FUNCTIONAL      INPUT.51
C     DEPENDENCE. IDEALLY, THESE PARAMETERS SHOULD BE FIT USING THE      INPUT.52
C     KELVIN PROGRAM                                                     INPUT.53
C                                                                        INPUT.54
C     PRINOZ/SECNOZ;DISTANCE OF PRIMARY/SECONDARY NOZZLE FROM CENTER OF INPUT.55
C     COLLISION ZONE                                                     INPUT.56
C                                                                        INPUT.57
C                                                                        INPUT.58
C     XL,YL,ZL; DIMENSIONS OF COLLISION VOLUME IN X,Y,Z DIRECTIONS AS    INPUT.59
C     DETERMINED BY THE MOLECULAR BEAM DEFINING SLITS.                   INPUT.60
C     ALIM(1),BLIM(1)-- ARE THE DETECTOR WIDTH ENDPOINTS RELATIVE TO THEINPUT.61
C     DETECTOR CENTER.                                                   INPUT.62
C     ALIM(2),BLIM(2)-- ARE THE DETECTOR HEIGHT ENDPOINTS RELATIVE TO    INPUT.63
C     THE DETECTOR CENTER. ALIM IS THE LOWER INTEGRATION LIMIT AND       INPUT.64
C     MUST BE LESS THAN BLIM.                                            INPUT.65
C                                                                        INPUT.66
C     DETRAD; LOCATION OF DETECTOR DEFINIG APERTURE FROM THE CENTER OF   INPUT.67
C     THE COLLISION ZONE.                                                INPUT.68
C                                                                        INPUT.69
C     RANGE(2)=XMIN,RANGE(3)=XMAX,RANGE(4)=YMIN,RANGE(5)=YMAX FOR THE    INPUT.70
C     POTENTIAL PLOT.                                                    INPUT.71
C                                                                        INPUT.72
C     NCOLX,NCOLY,NCOLZ;  NUMBER OF INTEGRATION POINTS IN X,Y,Z          INPUT.73
C     DIRECTIONS FOR COLLISION VOLUME INTEGRATION. MAXIMUM OF 5 IN EACH INPUT.74
C     DIRECTION.                                                         INPUT.75
C                                                                        INPUT.76
C     NPRI,NSEC; NUMBER OF NEWTON DIAGRAMS FOR PRIMARY/SECONDARY BEAMS. INPUT.77
C     LIMITED TO A MAXIMUM OF 10 EACH.                                   INPUT.78
C                                                                        INPUT.79
C     NANG; NUMBER OF LABORATORY ANGLES WHERE CALCULATION IS TO BE PER- INPUT.80
C     FORMED.                                                            INPUT.81
C                                                                        INPUT.82
C     IINT=0, THEN POINT DETECTOR LOCATED AT CENTER OF DETECTOR .        INPUT.83
C     IINT=  1 IF ONLY INTEGRATE OVER DETECTOR WIDTH(IN PLANE)           INPUT.84
C     IINT=  2 IF FULL TWO DIMENSIONAL DETECTOR INTEGRATION TO BE DONE. INPUT.85
C                                                                        INPUT.86
C     IAPPRX=1 THEN ALL THE POINTS IN THE COLLISION VOLUME HAVE THE      INPUT.87
C     SAME PHASE SHIFTS.                                                 INPUT.88
C     IAPPRX=0, THEN ALL POINTS IN THE COLLISION ZONE HAVE THEIR OWN     INPUT.89
C     PHASE SHIFTS COMPUTED FROM THE ANGLES DEFINED BY THE NOZZLE        INPUT.90
C     POSITIONS AND THE INTERSECTION POINT.                              INPUT.91
C     IAPPRX=2, THEN ALL POINTS IN THE COLLISION VOLUME FOR ALL NEWTON   INPUT.92
C     DIAGRAMS HAVE THE SAME PHASE SHIFTS- NAMELY THOSE FOR THE MOST     INPUT.93
C     PROBABLE NEWTON DIAGRAM.                                           INPUT.94
C                                                                        INPUT.95
C     NPRI1 =1 PRINTS OUT COLLISION ENERGIES OF EACH NEWTON DIAGRAM      INPUT.96
C     AND THE PHASE SHIFTS. CAUTION-MUCH PRINT.                          INPUT.97
C     NPRI1=0  ; NO PHASE SHIFT PRINTING.                                INPUT.98
C                                                                        INPUT.99
C     NSETS- THE NUMBER OF DATA SETS USED IN A SINGLE LEAST SQUARE FIT. INPUT.100
```

```
C     ALL DATA SETS MUST HAVE A COMPLETE DATA DECK AS THOUGH IRPT=2      INPUT.101
C     (SEE BELOW). ADDITIONALLY, NSETS MUST BE THE SAME FOR EACH DATA    INPUT.102
C     SET. A DUMMY VALUE FOR IRPT MUST BE GIVEN FOR EACH DATA SET,       INPUT.103
C     EXCEPT FOR THE LAST ONE READ    WHICH WILL BE EXECUTED AS NORMAL.  INPUT.104
C                                                                        INPUT.105
C                                                                        INPUT.106
C     NITER IS THE ALLOWED NUMBER OF FUNCTION CALLS BY THE LEAST         INPUT.107
C     SQUARES ROUTINE BEFORE TERMINATION.                                INPUT.108
C                                                                        INPUT.109
C     NETA; MAXIMUM VALUE OF THE ORBITAL ANGULAR MOMENTUM                INPUT.110
C                                                                        INPUT.111
C     NSKP; STEP SIZE IN THE ORBITAL ANGULAR MOMENTUM QUANTUM NUMBER     INPUT.112
C     FOR CONSTRUCTING PHASE SHIFT GRID FOR INTERPOLATION.               INPUT.113
C                                                                        INPUT.114
C     NOPT =1, DFCS CALCULATED BUT NO DATA SUPPLIED.                     INPUT.115
C     NOPT =2, DFCS CALCULATED WITH DATA, BUT NO ERRORS.                 INPUT.116
C     NOPT =3, DFCS CALCULATED WITH DATA AND ERRORS.                     INPUT.117
C                                                                        INPUT.118
C     NLST$0, THEN LEAST SQUARES FIT TO DATA WILL BE PERFORMED FOR       INPUT.119
C     NLST VARIABLES. IF NLST=0, NO LEAST SQUARES FIT.                   INPUT.120
C                                                                        INPUT.121
C     NPAR  ; THE NUMBER OF PARAMETERS IN THE POTENTIAL.                 INPUT.122
C                                                                        INPUT.123
C     NPRI2=1, THEN EACH APPROXIMATION TO THE DETECTOR INTEGRAL IS       INPUT.124
C     PRINTED.                                                           INPUT.125
C          =0, THEN PRINTING SUPPRESSED                                  INPUT.126
C                                                                        INPUT.127
C     MAXIT- MAXIMUM NUMBER OF ITERATIONS IN THE ADAPTIVE SIMPSON'S      INPUT.128
C     INTEGRATION OVER THE DETECTOR.                                     INPUT.129
C                                                                        INPUT.130
C     XSTART- BEGINNING POINT FOR THE NUMEROV INTEGRATION OF PHASE       INPUT.131
C     SHIFTS (IN REDUCED UNITS)                                          INPUT.132
C                                                                        INPUT.133
C     XSTEP- STEP LENGTH FOR NUMEROV INTEGRATION, IN REDUCED UNITS.      INPUT.134
C     RNPHAS- NUMBER OF STEPS IN NUMEROV INTEGRATION                     INPUT.135
C                                                                        INPUT.136
C     ERROR- WHEN THE JWKB CORRECTED PHASE SHIFTS AGREE TO WITHIN        INPUT.137
C     ERROR RADIANS ON TWO CONSECUTIVE NODES, THE PHASE SHIFT IS CON-    INPUT.138
C     SIDERED CONVERGED                                                  INPUT.139
C                                                                        INPUT.140
C     IBOSE- WHEN NUCLEI ARE IDENTICAL, IBOSE=1 SUMS OVER EVEN PARTIAL   INPUT.141
C     WAVES ONLY.                                                        INPUT.142
C     IBOSE=2, SAME BUT OVER ODD PARTIAL WAVES.                          INPUT.143
C     IF NUCLEI ARE NOT IDENTICAL, IBOSE SET TO 1 INTERNALLY AND NEED    INPUT.144
C     NOT BE SUPPLIED                                                    INPUT.145
C                                                                        INPUT.146
C                                                                        INPUT.147
C     NOTE---------                                                      INPUT.148
C     XSTART,XSTEP,RNPHAS,ERROR ALL MUST BE ZERO WHEN JWKB PHASE SHIFTS  INPUT.149
C     ARE USED.                                                          INPUT.150
C                                                                        INPUT.151
C     A; VECTOR CONTAING THE POTENTIAL PARAMETERS                        INPUT.152
C     ALL 15 ENTRIES OF A ARE READ ON INPUT, SO DUMMY VALUES MUST BE     INPUT.153
```

```
C     GIVEN FOR THE UNUSED ENTRIES.                                     INPUT.154
C                                                                       INPUT.155
C     INDEX; CONTAINS THE LIST OF WHICH PARAMETERS ARE TO BE VARIED IN  INPUT.156
C     LEAST SQUARES FIT. IF POTENTIAL HAS, SAY, 10 PARAMETERS, BUT      INPUT.157
C     ONLY THE THIRD,  FIFTH, AND SEVENTH ARE TO BE VARIED, THEN        INPUT.158
C     INDEX(1)=3,INDEX(2)=5,INDEX(3)=7 WITH NLST=3.                     INPUT.159
C                                                                       INPUT.160
C     FTOL IS THE UPPER BOUND FOR THE RELATIVE VARIATION IN THE CHI-    INPUT.161
C     SQUARE ERROR. TO STOP THE LEAST SQUARES FIT AFTER CHI SQUARE IS   INPUT.162
C     CHANGING BY LESS THAN 1 PER CENT, SET FTOL=.01                    INPUT.163
C                                                                       INPUT.164
C     XTOL- SIMILAR TO FTOL EXCEPT THIS IS THE RELATIVE VARIATION IN    INPUT.165
C     THE PARAMETERS THEMSELVES. THE LEAST SQUARES ROUTINE WILL TERMIN- INPUT.166
C     ATE WHEN THE  RELATIVE CHANGE IN THE PARAMETERS IS LESS THAN      INPUT.167
C     XTOL PER CENT.                                                    INPUT.168
C                                                                       INPUT.169
C     FACTOR- CONTROLS THE LENGTH OF THE FIRST PARAMETER STEP. 100 IS   INPUT.170
C     THE SUGGESTED VALUE. IT SHOULD LIE IN THE RANGE .1-100.           INPUT.171
C                                                                       INPUT.172
C     EPSFCN-THE RELATIVE ACCURACY OF THE DERIVATIVES. MAKE THIS        INPUT.173
C     SEVERAL ORDERS OF MAGNITUDE SMALLER THAN FTOL,XTOL.               INPUT.174
C                                                                       INPUT.175
C                                                                       INPUT.176
C     IRPT IS READ IN THE MAIN PROGRAM UNIT TEST. ITS FUNCTION IS AS    INPUT.177
C     FOLLOWS                                                           INPUT.178
C     IRPT=1  , THEN A NEW SET OF POTENTIAL  PARAMETERS A(I) IS READ,   INPUT.179
C     AND THE CALCULATION REPEATED WITH THE EXPERIMENTAL AVERAGING      INPUT.180
C     PARAMETERS REMAINING UNCHANGED FROM THEIR PREVIOUS VALUE.         INPUT.181
C     IRPT=2,  THEN A COMPLETE NEW DATA SET IS INPUT, BEGINNING WITH    INPUT.182
C     CARD 1.                                                           INPUT.183
C     IRPT=0, OR A BLANK CARD WILL TERMINATE PROGRAM.                   INPUT.184
C*********************************************************************INPUT.185
C                                                                       INPUT.186
C                                                                       INPUT.187
      COMMON/TRIG/DETSIN(100),DETCOS(100)                               INPUT.188
      COMMON/VOL/X(5),Y(5),Z(5),WX(5),WY(5),WZ(5)                       VOL.2
      COMMON/SAVE/IDIN(5),PNOZ(5),SNOZ(5),NTA(5),DTA(5),ID(5),NCX(5),   SAVE.2
     $NCY(5),NCZ(5),IIRR(5),IS1MAX(5),IP1MAX(5),NBP(5),NBS(5),HT(5),    SAVE.3
     $ WD(5),NAGL(5),DRD(5),ALM1(5),ALM2(5),BLM1(5),BLM2(5),NPRIN1(5),  SAVE.4
     $VELO1(5,10),VLWT1(5,10),VELO2(5,10),VLWT2(5,10),CC1(7,5),XCV(5,5) SAVE.5
     $,YCV(5,5),ZCV(5,5),WXCV(5,5),WYCV(5,5),WZCV(5,5),ANGUM(3,100),    SAVE.6
     $ ERRPT(3,100),DATUM(3,100),DTSN1(3,100),DTCN1(3,100),NSETS        SAVE.7
      COMMON/PTNL/V(2001),XM2(2001),XSTART,XSTEP,RNPHAS,ERROR           PTNL.2
      COMMON/LST/EINV(300),INDEX(15),VPAR(15),RM,FTOL,XTOL,MAXFEV,FACTORLST.2
     $,EPSFCN                                                           LST.3
      COMMON/BEAM/VPRI(10),VSEC(10),WPRI(10),WSEC(10),NPRI,NSEC,IPRIM,  BEAM.2
     +ISECON                                                            BEAM.3
      COMMON/GEOMTY/PRINOZ,SECNOZ,PRISPD,SECSPD,XCOL,YCOL,ZCOL,MPRI,    GEOMTRY.2
     1MSEC,SNDT,CSDT,NOPT,NPRI1                                         GEOMTRY.3
     $,NPRI2 ,MAXIT                                                     GEOMTRY.4
      REAL MPRI,MSEC,MTOT                                               GEOMTRY.5
      COMMON/TM/TIME(10),ICM,INTS,SPMAX,SPMIN                           TM.2
      COMMON/INTEG/IINT                                                 INTEG.2
```

```
      COMMON/ETA/STHE(8000),CTHE(8000),NETA,DETA,IDENT                  ETA.2
     $,IBOSE                                                            ETA.3
      COMMON/WH/C1,C2,C3,C4,C5,C6,C7,C8,C9,C10,MTOT                     WH.2
      COMMON/EN/ENERGY(125),CMTH1(125),CMTH2(125),WGHT1(125),WGHT2(125),EN.2
     1NCOLX,NCOLY,NCOLZ,IAPPRX                                          EN.3
      COMMON/RNG/RANGE(5)                                               RNG.2
      COMMON/AA/DETWD,DETHT,DETRAD,E                                    AA.2
      COMMON/LIMITS/ALIM(2),BLIM(2)                                     LIMITS.2
      COMMON/DAT/ANGLE(100),SDAT(100),EDAT(100),NANG,SF                 DAT.2
      DIMENSION VB(20),A(15)                                            INPUT.204
      DIMENSION TITLE(20)                                               INPUT.205
      RANGE(1)=1.                                                       INPUT.206
C                                                                       INPUT.207
C      READ PROGRAM PARAMETERS AND TRANSLATE THEM INTO THEIR APPROPRIATEINPUT.208
C      VALUES WHERE NECESSARY                                           INPUT.209
C                                                                       INPUT.210
      NN=0                                                              INPUT.211
4100   CONTINUE                                                         INPUT.212
      READ(5,2)(TITLE(I),I=1,20)                                        INPUT.213
      READ(5,1000) MPRI,BETA1,VZRO1,PRINOZ                              INPUT.215
      READ(5,1000) MSEC,BETA2,VZRO2,SECNOZ                              INPUT.216
      IDENT=1                                                           INPUT.217
      IF(MPRI.EQ.MSEC) IDENT=2                                          INPUT.218
      READ(5,1000)XL,YL,ZL,ALIM(1),BLIM(1),ALIM(2),BLIM(2),DETRAD       INPUT.219
C                                                                       INPUT.220
C     ALIM,BLIM SETS LIMITS FOR DETECTOR SLIT INTEGRALS                 INPUT.221
C                                                                       INPUT.222
      DETHT=BLIM(2)-ALIM(2)                                             INPUT.223
      DETWD=BLIM(1)-ALIM(1)                                             INPUT.224
      READ(5,1000) RANGE(2),RANGE(3),RANGE(4),RANGE(5)                  INPUT.225
      READ(5,1001) NCOLX,NCOLY,NCOLZ,NPRI,NSEC,NANG,IINT,IAPPRX         INPUT.226
      READ(5,1001) NETA,NSKP,NPRI1,NSETS,NOPT,NLST,NFAR,NITER           INPUT.227
      READ(5,1001) NPRI2,MAXIT,IBOSE                                    INPUT.228
      IF(IDENT.EQ.1) IBOSE=1                                            INPUT.229
      READ(5,1000) XSTART,XSTEP,RNPHAS,ERROR                            INPUT.230
      DETA=FLOAT(NSKP)                                                  INPUT.231
      READ(5,1000)(A(I),I=1,15)                                         INPUT.232
      IF(NLST.NE.0) READ(5,1001)(INDEX(I),I=1,NLST)                     INPUT.233
      IF(NLST.NE.0) READ(5,1000) FTOL,XTOL,FACTOR,EPSFCN                INPUT.234
C                                                                       INPUT.235
C      WRITE OUT INFORMATION ON THE PROGRAM PARAMETERS                  INPUT.236
C                                                                       INPUT.237
      MAXFEV=NITER                                                      INPUT.238
      WRITE(6,1002)                                                     INPUT.239
      WRITE(6,1003)                                                     INPUT.241
      WRITE(6,1004)XL,YL,ZL                                             INPUT.243
      WRITE(6,1005)DETWD,DETHT,DETRAD                                   INPUT.245
      WRITE(6,1006)NCOLX,NCOLY,NCOLZ                                    INPUT.248
      WRITE(6,1007) IINT                                                INPUT.251
      WRITE(6,1012) NETA,DETA                                           INPUT.253
      IF(IAPPRX.EQ.2) WRITE(6,1017)                                     INPUT.256
      IF(XSTART*XSTEP*RNPHAS*ERROR.NE.0.) WRITE(6,1018) XSTART,XSTEP,   INPUT.259
     $ RNPHAS,ERROR                                                     INPUT.260
```

```
      IF(IAPPRX.EQ.1) WRITE(6,1013)                                     INPUT.263
      WRITE(6,13)                                                       INPUT.266
C                                                                       INPUT.267
C      READ IN DATA OR ANGULAR RANGE                                    INPUT.268
C                                                                       INPUT.269
      IF(NOPT-2) 800,810,820                                            INPUT.270
C                                                                       INPUT.271
C      NO DATA                                                          INPUT.272
C                                                                       INPUT.273
  800 READ(5,1000) ANG1,DANG                                            INPUT.274
      ANG1=ANG1-DANG                                                    INPUT.275
      DO 1110 I=1,NANG                                                  INPUT.276
      EDAT(I)=1.                                                        INPUT.277
      ANG1=ANG1+DANG                                                    INPUT.278
 1110 ANGLE(I)=ANG1                                                     INPUT.279
      WRITE(6,30)                                                       INPUT.280
      WRITE(6,1009)(ANGLE(I),I=1,NANG)                                  INPUT.283
      NVOL=NCOLX*NCOLY*NCOLZ                                            INPUT.284
      GOTO 2222                                                         INPUT.285
C                                                                       INPUT.286
C      DATA, NO ERRORS                                                  INPUT.287
C                                                                       INPUT.288
  810 READ(5,1000)(ANGLE(I),SDAT(I),I=1,NANG)                           INPUT.289
      DO 1120 I=1,NANG                                                  INPUT.290
 1120 EDAT(I)=1.                                                        INPUT.291
      GOTO 830                                                          INPUT.292
C                                                                       INPUT.293
C      DATA AND ERRORS                                                  INPUT.294
C                                                                       INPUT.295
  820 READ(5,1000)(ANGLE(I),SDAT(I),I=1,NANG)                           INPUT.296
      READ(5,1000)(EDAT(I),I=1,NANG)                                    INPUT.297
  830 CONTINUE                                                          INPUT.298
C                                                                       INPUT.299
C      WRITE OUT DATA AND ANGULAR RANGE                                 INPUT.300
C                                                                       INPUT.301
      WRITE(6,1008) NANG                                                INPUT.302
      WRITE(6,1009)(ANGLE(I),SDAT(I),I=1,NANG)                          INPUT.304
      IF(NOPT.NE.3) GOTO 831                                            INPUT.306
      WRITE(6,13)                                                       INPUT.307
      WRITE(6,1019)                                                     INPUT.308
      WRITE(6,1021)(EDAT(I),I=1,NANG)                                   INPUT.310
  831 NVOL=NCOLX*NCOLY*NCOLZ                                            INPUT.314
C                                                                       INPUT.315
C      CONVERSION OF ERRORS APPROPRIATE FOR LOG SCALING                 INPUT.316
C                                                                       INPUT.317
      IF(NOPT.EQ.2) GOTO 2223                                           INPUT.318
      DO 1039 I=1,NANG                                                  INPUT.319
      EDAT(I)=ALOG(1.+EDAT(I)/SDAT(I))                                  INPUT.320
C                                                                       INPUT.321
 1039 CONTINUE                                                          INPUT.322
 2223 CONTINUE                                                          INPUT.323
      WRITE(6,13)                                                       INPUT.324
C                                                                       INPUT.325
```

```
C      CONVERT DATA TO LOG SCALE                                        INPUT.326
C                                                                       INPUT.327
      SMAX=ALOG(SDAT(1))                                                INPUT.328
      SMIN=SMAX                                                         INPUT.329
      DO 1022 I=1,NANG                                                  INPUT.330
      SDAT(I)=ALOG(SDAT(I))                                             INPUT.331
      SMIN=AMIN1(SDAT(I),SMIN)                                          INPUT.332
      SMAX=AMAX1(SDAT(I),SMAX)                                          INPUT.333
 1022  CONTINUE                                                         INPUT.334
C                                                                       INPUT.335
C      THESE ARE THE SCALE FACTORS FOR THE LINE PRINTER PLOTS OF THE    INPUT.336
C      ANGULAR DISTRIBUTIONS                                            INPUT.337
C                                                                       INPUT.338
      SPMAX=SMAX*1.05                                                   INPUT.339
      SPMIN=SMIN*.95                                                    INPUT.340
      WRITE(6,1023)                                                     INPUT.341
      WRITE(6,1009)(ANGLE(I),SDAT(I),I=1,NANG)                          INPUT.344
      IF(NOPT.EQ.2) GOTO 2222                                           INPUT.345
      WRITE(6,1019)                                                     INPUT.346
      WRITE(6,1021)(EDAT(I),I=1,NANG)                                   INPUT.347
 2222  CONTINUE                                                         INPUT.348
C                                                                       INPUT.349
C     CHECK THAT DIMENSIONS ARE O.K.                                    INPUT.350
C                                                                       INPUT.351
      IF(NANG.LE.100) GOTO 9                                            INPUT.352
      WRITE(6,16)                                                       INPUT.353
      GOTO 5000                                                         INPUT.355
 9    IF(NVOL.LE.125) GOTO 10                                           INPUT.356
      WRITE(6,11)                                                       INPUT.357
      GOTO 5000                                                         INPUT.360
 10   IF(NETA*NVOL.LE.8000) GOTO 18                                     INPUT.361
      WRITE(6,12)                                                       INPUT.362
      GOTO 5000                                                         INPUT.365
C                                                                       INPUT.366
C     INITIALIZE PARAMETERS                                             INPUT.367
C
 18   DO 499 I=1,9                                                      INPUT.368
 499  TIME(I)=0.                                                        INPUT.369
      ICM=0                                                             INPUT.370
      INTS=0                                                            INPUT.371
      RM=MSEC*MPRI/(MSEC+MPRI)                                          INPUT.372
      RM1=RM                                                            INPUT.373
C                                                                       INPUT.374
C     CALCULATE QUADRUTURE WEIGHTS FOR NEWTON DIAGRAMS AND PHASE SHIFT  INPUT.375
C     ROUTINE                                                           INPUT.376
C                                                                       INPUT.377
      CALL WEIGHTS(XL,YL,ZL,NPRI2)                                      INPUT.378
C                                                                       INPUT.379
C     THESE ARE CONSTANTS NEEDED IN CMANG                               INPUT.380
C                                                                       INPUT.381
      MTOT=MPRI+MSEC                                                    INPUT.382
      C1=2.*PRINOZ                                                      INPUT.383
      C2=PRINOZ*PRINOZ                                                  INPUT.384
```

```
      C3=2.*SECNOZ                                                      INPUT.385
      C4=SECNOZ*SECNOZ                                                  INPUT.386
      C5=MSEC*MSEC/MTOT/MTOT                                            INPUT.387
      C6=.601408*MPRI*MTOT/MSEC*1.98717E-03                             INPUT.388
      C7=MSEC/MTOT                                                      INPUT.389
C                                                                       INPUT.390
C     SET UP PRIMARY BEAM NEWTON DIAGRAMS                               INPUT.391
C                                                                       INPUT.392
      WRITE(6,13)                                                       INPUT.393
      WRITE(6,1010)                                                     INPUT.394
      N=NPRI                                                            INPUT.397
      CALL NOZZLE(N,VB(1),VB(11),VZRO1,BETA1)                           INPUT.398
      IPRIM=0                                                           INPUT.399
      PMAX=0.                                                           INPUT.400
      DO 1014 I=1,N                                                     INPUT.401
      VPRI(I)=VB(I)                                                     INPUT.402
      WPRI(I)=VB(10+I)                                                  INPUT.403
C                                                                       INPUT.404
C     FIND MOST PROBABLE VELOCITY                                       INPUT.405
C                                                                       INPUT.406
      IF(WPRI(I).LT.PMAX) GOTO 1014                                     INPUT.407
      PMAX=WPRI(I)                                                      INPUT.408
      IPRIM=I                                                           INPUT.409
 1014  CONTINUE                                                         INPUT.410
      WRITE(6,1011) MPRI,BETA1,VZRO1,PRINOZ                             INPUT.411
C                                                                       INPUT.414
C     SET UP SECONDARY BEAM NEWTON DIAGRAMS                             INPUT.415
C                                                                       INPUT.416
      WRITE(6,13)                                                       INPUT.418
      WRITE(6,1016)                                                     INPUT.419
      N=NSEC                                                            INPUT.422
      CALL NOZZLE(N,VB(1),VB(11),VZRO2,BETA2)                           INPUT.423
      PMAX=0.                                                           INPUT.424
      ISECON=0                                                          INPUT.425
      DO 1015 I=1,N                                                     INPUT.426
      VSEC(I)=VB(I)                                                     INPUT.427
      WSEC(I)=VB(I+10)                                                  INPUT.428
C                                                                       INPUT.429
C     FIND MOST PROBABLE VELOCITY                                       INPUT.430
C                                                                       INPUT.431
      IF(WSEC(I).LT.PMAX) GOTO 1015                                     INPUT.432
      PMAX=WSEC(I)                                                      INPUT.433
      ISECON=I                                                          INPUT.434
 1015  CONTINUE                                                         INPUT.435
      WRITE(6,1011) MSEC,BETA2,VZRO2,SECNOZ                             INPUT.436
      CALL PREPOT(A,RM)                                                 INPUT.437
C                                                                       INPUT.438
C      CALCULATE THE SIN, COSINE ARRAYS FOR THE DETECTOR'S POSITION     INPUT.439
C      TO SAVE FUNCTION EVALUATIONS IN THE DFCS ROUTINE                 INPUT.440
C                                                                       INPUT.441
      DO 5 II=1,NANG                                                    INPUT.442
      DET=ANGLE(II)*3.14159/180.                                        INPUT.443
      DETSIN(II)=SIN(DET)                                               INPUT.444
```

```
      DETCOS(II)=COS(DET)                                               INPUT.445
 5     CONTINUE                                                         INPUT.446
C                                                                       INPUT.447
C      THIS SECTION COPIES THE INPUT PARAMETERS WHEN MORE THAN ONE      INPUT.448
C      DATA SET IS TO BE FIT SIMULTANEOUSLY IN THE LEAST SQUARES ROUTINEINPUT.449
C                                                                       INPUT.450
      IF(NSETS.LT.1) GOTO 4000                                          INPUT.451
      NN=NN+1                                                           INPUT.452
      DETRD=DETRAD                                                      INPUT.453
      IDIN(NN)=IINT$PNOZ(NN)=PRINOZ$SNOZ(NN)=SECNOZ$NTA(NN)=NETA        INPUT.454
      DTA(NN)=DETA$ID(NN)=IDENT$NCX(NN)=NCOLX$NCY(NN)=NCOLY$NCZ(NN)=    INPUT.455
     $NCOLZ $ IIRR(NN)=IAPPRX$ IS1MAX(NN)= ISECON $IP1MAX(NN)=IPRIM     INPUT.456
      NBP(NN)=NPRI$NBS(NN)=NSEC$HT(NN)=DETHT$WD(NN)=DETWD$NAGL(NN)=NANG INPUT.457
      DRD(NN)=DETRD$ALM1(NN)=ALIM(1)$ALM2(NN)=ALIM(2)$BLM1(NN)=BLIM(1)  INPUT.458
      BLM2(NN)=BLIM(2)                                                  INPUT.459
      NPRIN1(NN)=NPRI1                                                  INPUT.460
      DO 4020 I=1,NPRI                                                  INPUT.461
      VELO1(NN,I)=VPRI(I)                                               INPUT.462
      VLWT1(NN,I)=WPRI(I)                                               INPUT.463
4020   CONTINUE                                                         INPUT.464
      DO 4025 I=1,NSEC                                                  INPUT.465
      VELO2(NN,I)=VSEC(I)                                               INPUT.466
      VLWT2(NN,I)=WSEC(I)                                               INPUT.467
4025   CONTINUE                                                         INPUT.468
      CC1(1,NN)=C1                                                      INPUT.469
      CC1(2,NN)=C2                                                      INPUT.470
      CC1(3,NN)=C3                                                      INPUT.471
      CC1(4,NN)=C4                                                      INPUT.472
      CC1(5,NN)=C5                                                      INPUT.473
      CC1(6,NN)=C6                                                      INPUT.474
      CC1(7,NN)=C7                                                      INPUT.475
      DO 4030 I=1,NCOLX                                                 INPUT.476
      XCV(NN,I)=X(I)                                                    INPUT.477
      WXCV(NN,I)=WX(I)                                                  INPUT.478
4030   CONTINUE                                                         INPUT.479
      DO 4035 I=1,NCOLY                                                 INPUT.480
      YCV(NN,I)=Y(I)                                                    INPUT.481
      WYCV(NN,I)=WY(I)                                                  INPUT.482
4035   CONTINUE                                                         INPUT.483
      DO 4040 I=1,NCOLZ                                                 INPUT.484
      ZCV(NN,I)=Z(I)                                                    INPUT.485
      WZCV(NN,I)=WZ(I)                                                  INPUT.486
4040   CONTINUE                                                         INPUT.487
      DO 4050 I=1,NANG                                                  INPUT.488
      ANGUM(NN,I)=ANGLE(I)                                              INPUT.489
      ERRPT(NN,I)=EDAT(I)                                               INPUT.490
      DATUM(NN,I)=SDAT(I)                                               INPUT.491
      DTSN1(NN,I)=DETSIN(I)                                             INPUT.492
      DTCN1(NN,I)=DETCOS(I)                                             INPUT.493
4050   CONTINUE                                                         INPUT.494
      IF(NN.EQ.NSETS) GOTO 4000                                         INPUT.495
      READ(5,1000) IRPT                                                 INPUT.496
      GOTO 4100                                                         INPUT.497
```

```
4000   CONTINUE                                                         INPUT.498
      RETURN                                                            INPUT.499
 5000 STOP                                                              INPUT.500
C
C
C      FORMAT STATEMENTS
C
C
 2    FORMAT(20A4)                                                      INPUT.214
 1002 FORMAT(/)                                                         INPUT.240
 1003 FORMAT(1H1,45X,*I N P U T  P A R A M E T E R S *,/)               INPUT.242
 1004 FORMAT(5X,*COLLISION VOLUME DIMENSIONS (X,Y,Z)*,3F10.3,/)         INPUT.244
 1005 FORMAT(5X,*DETECTOR WIDTH, HEIGHT, AND DISTANCE FROM COLLISION CENINPUT.246
     1TER*,3F10.3,/)                                                    INPUT.247
 1006 FORMAT(5X,*NUMBER OF POINTS IN X,Y,Z DIRECTIONS USED IN APPROXIMATINPUT.249
     1ING COLLISION VOLUME INTEGRATION*,3I5,/)                          INPUT.250
 1007 FORMAT(5X,*DETECTOR IS TREATED AS A *,I3,2X,*DIMENSIONAL SLIT*,/) INPUT.252
 1012 FORMAT(5X,*NUMBER OF PHASE SHIFTS=*,I5,2X,* PHASE SHIFT INCREMENT INPUT.254
     -=*,F5.1)                                                          INPUT.255
 1017 FORMAT(10X,*ALL NEWTON DIAGRAMS HAVE THE SAME PHASE SHIFTS-IAPPRX=INPUT.257
     $2*,/)                                                             INPUT.258
 1018 FORMAT( 5X,*FOR NUMEROV INTEGRATION, XSTART,XSTEP,RNPHAS,ERROR=*, INPUT.261
     $ 4(2X,F9.4))                                                      INPUT.262
 1013 FORMAT(5X,*ONLY ONE SET OF PHASE SHIFTS CALCULATED PER NEWTON DIA INPUT.264
     1GRAM*,/)                                                          INPUT.265
 30   FORMAT(10X,* INPUT OPTION 1- ANGLES WHERE DFCS WILL BE CALCULATED*INPUT.281
     1,/)                                                               INPUT.282
 1008 FORMAT(45X,*I N P U T  D A T A   F O R *,I3,2X,*A N G L E S *,/)  INPUT.303
 1009 FORMAT(10(2X,F10.3))                                              INPUT.305
 1019 FORMAT(/,55X,*E R R O R S *,/)                                    INPUT.309
 1021 FORMAT( 5(12X,F10.3))                                             INPUT.311
 1000 FORMAT(8F10.3)                                                    INPUT.312
 1001 FORMAT(8I10)                                                      INPUT.313
 1023 FORMAT(30X,*I N P U T  D A T A  C O N V E R T E D  T O  L O G  S CINPUT.342
     - A L E*,/)                                                        INPUT.343
 16   FORMAT(1X,*TOO MANY ANGLES*,/)                                    INPUT.354
 11   FORMAT(10X,*NVOL EXCEEDS DIMENSION FOR ARRAYS IN COMMON BLOACK EN*INPUT.358
     1,/)                                                               INPUT.359
 12   FORMAT(10X,*TOTAL NUMBER OF PHASE SHIFTS EXCEEDS DIMENSIONS IN    INPUT.363
     +PHASE SHIFT ROUTINE. CURRENT VALUE IS 8000*,/)                    INPUT.364
 1010 FORMAT(/,40X,*P R I M A R Y  B E A M  N E W T O N  D I A G R A M  INPUT.395
     1S*,/)                                                             INPUT.396
 1011 FORMAT(1X,*MASS=*,F10.3,2X,*BETA=*,F10.3,2X,*VZRO=*,F10.3,5X,*    INPUT.412
     $NOZZLE DISTANCE FROM COLLISION CENTER=*,F10.3)                    INPUT.413
 13   FORMAT(/////)                                                     INPUT.417
 1016 FORMAT(/,35X,*S E C O N D A R Y  B E A M  N E W T O N  D I A G R  INPUT.420
     1A M S*,/)                                                         INPUT.421
      END                                                               INPUT.501


                                                                        INPUT.502
      SUBROUTINE INTENS(TOTAL)                                          INTENS.2
```

```
      COMMON/TM/TIME(10),ICM,INTS,SPMAX,SPMIN                           TM.2
      COMMON/ETA/STHE(8000),CTHE(8000),NETA,DETA,IDENT                  ETA.2
     $,IBOSE                                                            ETA.3
      COMMON/EN/ENERGY(125),CMTH1(125),CMTH2(125),WGHT1(125),WGHT2(125),EN.2
     1NCOLX,NCOLY,NCOLZ,IAPPRX                                          EN.3
      DIMENSION P(1000)                                                 INTENS.6
      INTS=INTS+1                                                       INTENS.7
      CALL SECOND(BG)                                                   INTENS.8
C                                                                       INTENS.9
C      FUNCTION- GIVEN THE PHASE SHIFTS AND CENTER OF MASS SCATTERING   INTENS.10
C      ANGLES, THIS SUBROUTINE EVALUATES THE LEGRENDRE EXPANSION        INTENS.11
C      TO OBTAIN THE SCATTERING AMPLITUDE. THE MODULUS                  INTENS.12
C      OF THE SCATTERING AMPLITUDE IS USED TO FIND THE SCATTERED        INTENS.13
C      INTENSITY.                                                       INTENS.14
C                                                                       INTENS.15
C      PARAMETERS- ON INPUT, THE COMMON BLOCK ETA CONTAINS THE SIN AND  INTENS.16
C      COSINE FUNCTIONS OF THE PHASE SHIFTS WHICH ARE INDEPENDENT OF    INTENS.17
C      THE SCATTERING ANGLE. THE COSINE OF THE CENTER OF MASS SCATTERINGINTENS.18
C       ANGLES ARE CONTAINED IN THE ARRAYS CMTH1,CMTH2 FOR THE TWO      INTENS.19
C      POSSIBLE INTERSECTIONS WITH THE NEWTON SPHERE.                   INTENS.20
C      ON OUTPUT, THE PARAMETER TOTAL CONTAINS THE SCATTERED INTENSITY  INTENS.21
C       FROM EACH OF THESE CENTER OF MASS ANGLES.                       INTENS.22
C                                                                       INTENS.23
C      SUBPROGRAMS- FLOAT,SECOND,VECPRO                                 INTENS.24
C                                                                       INTENS.25
C       AUTHOR-M.F. VERNON
C                                                                       INTENS.27
C
C        LAST REVISION DATE-FEBRUARY 16,1983
C
      TOTAL=0.                                                          INTENS.28
      NVOL=NCOLX*NCOLY*NCOLZ                                            INTENS.29
      DO 100 II=1,NVOL                                                  INTENS.30
C                                                                       INTENS.31
C     CALCULATE STARTING INDEX FOR THE NEXT SET OF PHASE SHIFTS, STORED INTENS.32
C     SEQUENTIALLY IN STHE AND CTHE ARRAYS.                             INTENS.33
C     NETA IS THE NUMBER OF PHASE SHIFTS.                               INTENS.34
C                                                                       INTENS.35
      ITEMP=NETA*(II-1)                                                 INTENS.36
C                                                                       INTENS.37
C     IF THERE IS NO INTERSECTION WITH NEWTON SPHERE, SKIP TO BACK SIDE INTENS.38
C                                                                       INTENS.39
      IF(WGHT1(II).EQ.0.) GOTO 110                                      INTENS.40
      X=CMTH1(II)                                                       INTENS.41
C                                                                       INTENS.42
C     INITIALIZE SUMS OF THE REAL AND IMAGINARY CONTRIBUTIONS           INTENS.43
C     FROM THE L=0,1 PARTIAL WAVES.                                     INTENS.44
C                                                                       INTENS.45
C                                                                       INTENS.46
C     SET UP INITIAL VALUES FOR LEGENDRE RECURSION FORMULA.             INTENS.47
C                                                                       INTENS.48
      P(1)=1.                                                           INTENS.49
      P(2)=X                                                            INTENS.50
```

```
      P0=1.                                                             INTENS.51
      P1=X                                                              INTENS.52
      IDEL=3                                                            INTENS.53
C                                                                       INTENS.54
C     PARTIAL WAVE LOOP                                                 INTENS.55
C                                                                       INTENS.56
      DO 50 I=3,NETA                                                    INTENS.57
C                                                                       INTENS.58
C     LEGENDRE RECURSION FORMULA.                                       INTENS.59
C                                                                       INTENS.60
      P2=(FLOAT(IDEL)*X*P1-FLOAT(I-2)*P0)/FLOAT(I-1)                    INTENS.61
      P(I)=P2                                                           INTENS.62
C                                                                       INTENS.63
C     UPDATE RECURSION FORMULA INITIAL VALUES.                          INTENS.64
C                                                                       INTENS.65
      P0=P1                                                             INTENS.66
      P1=P2                                                             INTENS.67
      IDEL=IDEL+2                                                       INTENS.68
 50   CONTINUE                                                          INTENS.69
C                                                                       INTENS.70
C     TOTAL INTENSITY IS SUM OF SQUARES OF REAL AND IMAGINARY PARTS.    INTENS.71
C     THE WEIGHT FACTOR INCLUDES THE VOLUME INTEGRATION WEIGHT, THE     INTENS.72
C     INVERSE ENERGY WEIGHT FROM THE SCATTERING FORMULA, AND THE        INTENS.73
C     INVERSE VELOCITY WEIGHT FOR THE ELECTROM BOMBARDMENT DETECTOR.    INTENS.74
C                                                                       INTENS.75
C     IDENT ACCOUNTS FOR SYMMETRIC NUCLEI                               INTENS.76
C     IF IBOSE=1 (2), SUM ONLY OVER EVEN (ODD) PARTIAL WAVES WHEN       INTENS.77
C     NUCLEI ARE IDENTICAL.                                             INTENS.78
C                                                                       INTENS.79
      ITM=ITEMP+IBOSE                                                   INTENS.80
      NPROD=NETA/IDENT -(IBOSE-1)                                       INTENS.81
      TP=VECPRO(NPROD,CTHE(ITM),IDENT,P(IBOSE),IDENT,0.)                INTENS.82
      SP=VECPRO(NPROD,STHE(ITM),IDENT,P(IBOSE),IDENT,0.)                INTENS.83
      TOTAL=TOTAL+(TP*TP+SP*SP)*WGHT1(II)                               INTENS.84
C                                                                       INTENS.85
C     BACK SIDE OF NEWTON SPHERE                                        INTENS.86
C     THE LOGIC AND PARAMTERS ARE DEFINED  AS ABOVE                     INTENS.87
C                                                                       INTENS.88
C                                                                       INTENS.89
C     IF THERE IS NO INTERSECTION WITH THE BACK SIDE OF THE NEWTON      INTENS.90
C     SPHERE, GO TO THE NEXT COLLISION VOLUME POINT.                    INTENS.91
C                                                                       INTENS.92
 110  IF(WGHT2(II).EQ.0.) GOTO 100                                      INTENS.93
C                                                                       INTENS.94
C     INITIALIZE VALUES OF THE L=0,1 PARTIAL WAVES FOR THE LEGENDRE     INTENS.95
C     RECURSION FORMULA.                                                INTENS.96
C                                                                       INTENS.97
      X=CMTH2(II)                                                       INTENS.98
      P(1)=1.                                                           INTENS.99
      P(2)=X                                                            INTENS.100
      P0=1.                                                             INTENS.101
      P1=X                                                              INTENS.102
      IDEL=3                                                            INTENS.103
```

```
C                                                                       INTENS.104
C      LEGRENDRE RECURSION LOOP                                         INTENS.105
C                                                                       INTENS.106
      DO 60 I=3,NETA                                                    INTENS.107
      P2=(FLOAT(IDEL)*X*P1-FLOAT(I-2)*P0)/FLOAT(I-1)                    INTENS.108
      P(I)=P2                                                           INTENS.109
      P0=P1                                                             INTENS.110
      P1=P2                                                             INTENS.111
      IDEL=IDEL+2                                                       INTENS.112
 60   CONTINUE                                                          INTENS.113
C                                                                       INTENS.114
C      IDENT ACCOUNTS FOR SYMMETRIC NUCLEI                              INTENS.115
C      IF IBOSE=1 (2), SUM ONLY OVER EVEN (ODD) PARTIAL WAVES WHEN      INTENS.116
C      NUCLEI ARE IDENTICAL.                                            INTENS.117
C                                                                       INTENS.118
      ITM=ITEMP+IBOSE                                                   INTENS.119
      NPROD=NETA/IDENT -(IBOSE-1)                                       INTENS.120
      TP=VECPRO(NPROD,CTHE(ITM),IDENT,P(IBOSE),IDENT,0.)                INTENS.121
      SP=VECPRO(NPROD,STHE(ITM),IDENT,P(IBOSE),IDENT,0.)                INTENS.122
C                                                                       INTENS.123
C      SQUARE REAL AND IMAGINARY PARTS OF THE SCATTERING AMPLITUDE TO   INTENS.124
C      OBTAIN THE OBSERVED INTENSITY.                                   INTENS.125
C                                                                       INTENS.126
      TOTAL=TOTAL+(TP*TP+SP*SP)*WGHT2(II)                               INTENS.127
 100  CONTINUE                                                          INTENS.128
      CALL SECOND(ED)                                                   INTENS.129
      TIME(4)=TIME(4)+ED-BG                                             INTENS.130
      RETURN                                                            INTENS.131
      END                                                               INTENS.132


                                                                        INTENS.133
      SUBROUTINE DFCS(A,SCAT,CHI,RM)                                    DFCS.2
C                                                                       DFCS.3
C      FUNCTION- SUM THE SCATTERING INTENSITY FOR ALL NEWTON DIAGRAMS   DFCS.4
C      OVER ALL ANGLES TO OBTAIN THE COMPUTED SCATTERING INTENSITY      DFCS.5
C      APPROPRIATE FOR THE EXPERIMENTAL CONDITIONS.                     DFCS.6
C
C      PARAMETERS-A, ON INPUT THE POTENTIAL PARAMETERS                  DFCS.7
C      RM- THE REDUCED MASS IN AMU.                                     DFCS.8
C      SCAT- ON OUTPUT, THE CALCULATED SCATTERING INTENSITY FOR THE SET DFCS.9
C      OF ANGLES SPECIFIED IN THE ARRAY ANGLE.                          DFCS.10
C      CHI- THE CHI SQUARE ERROR IN THE FIT OF THE CALCULATED DATA TO   DFCS.11
C      THE OBSERVED DATA, IF GIVEN.                                     DFCS.12
C      IF IAPPRX=2, ALL NEWTON DIAGRAMS HAVE THE SAME PHASE SHIFT.      DFCS.13
C      IAPPRX=1, ALL COLLISION VOLUME POINTS HAVE THE SAME PHASE SHIFT  DFCS.14
C      FOR EACH NEWTON DIAGRAM                                          DFCS.15
C      IAPPRX=0, ALL COLLISION VOLUME POINTS HAVE THEIR OWN PHASE SHIFTSDFCS.16
C                                                                       DFCS.17
C                                                                       DFCS.18
C      IF NOPT=1, THEN CALCULATED DISTRIBUTION IS SCALED TO A MAXIMUM   DFCS.19
C      VALUE OF 10000, AND CHI SET TO 1.                                DFCS.20
```

```
C                                                                       DFCS.21
C       SUBPROGRAMS CALLED-CMANG,PHSHFT,FINT,FILL,MULSMP,SCALE,SQRT,    DFCS.22
C       SECOND                                                          DFCS.23
C                                                                       DFCS.24
C        AUTHOR-M.F. VERNON
C
C        LAST REVISION DATE-FEBRUARY 16,1983
C
C
C                                                                       DFCS.26
                                                                        DFCS.27
      COMMON/TRIG/DETSIN(100),DETCOS(100)                               DFCS.28
      COMMON/GEOMTY/PRINOZ,SECNOZ,PRISPD,SECSPD,XCOL,YCOL,ZCOL,MPRI,    GEOMTRY.2
     1MSEC,SNDT,CSDT,NOPT,NPRI1                                         GEOMTRY.3
     $,NPRI2 ,MAXIT                                                     GEOMTRY.4
      REAL MPRI,MSEC,MTOT                                               GEOMTRY.5
      COMMON/DAT/ANGLE(100),SDAT(100),EDAT(100),NANG,SF                 DAT.2
      COMMON/BEAM/VPRI(10),VSEC(10),WPRI(10),WSEC(10),NPRI,NSEC,IPRIM,  BEAM.2
     +ISECON                                                            BEAM.3
      COMMON/TM/TIME(10),ICM,INTS,SPMAX,SPMIN                           TM.2
      COMMON/INTEG/IINT                                                 INTEG.2
      COMMON/EN/ENERGY(125),CMTH1(125),CMTH2(125),WGHT1(125),WGHT2(125),EN.2
     1NCOLX,NCOLY,NCOLZ,IAPPRX                                          EN.3
      COMMON/AA/DETWD,DETHT,DETRAD,E                                    AA.2
      COMMON/LIMITS/ALIM(2),BLIM(2)                                     LIMITS.2
      DIMENSION SCAT(1),A(1)                                            DFCS.37
      EXTERNAL FINT                                                     DFCS.38
      IBUG=NPRI2                                                        DFCS.39
      MAXI=MAXIT                                                        DFCS.40
      NVOL=NCOLX*NCOLY*NCOLZ                                            DFCS.41
C                                                                       DFCS.42
C     IF IAPPRX=2, THEN ONLY ONE SET OF PHASE SHIFTS IS USED FOR ALL    DFCS.43
C     NEWTON DIAGRAMS                                                   DFCS.44
C                                                                       DFCS.45
      IF(IAPPRX.NE.2) GOTO 15                                           DFCS.46
      SECSPD=VSEC(ISECON)                                               DFCS.47
      PRISPD=VPRI(IPRIM)                                                DFCS.48
C                                                                       DFCS.49
C      GET COLLISION ENERGY FOR THIS MOST PROBABLE NEWTON DIAGRAM       DFCS.50
C                                                                       DFCS.51
      CALL SECOND(BG)                                                   DFCS.52
      IOPT=0                                                            DFCS.53
      XL=DETRAD/SQRT(2.)                                                DFCS.54
      YL=XL                                                             DFCS.55
      ZL=0.                                                             DFCS.56
      CALL CMANG(XL,YL,ZL,IOPT)                                         DFCS.57
C                                                                       DFCS.58
C      GET PHASE SHIFTS FOR THIS MOST PROBABLE NEWTON DIAGRAM           DFCS.59
C                                                                       DFCS.60
      CALL PHSHFT(A,RM,NPRI1)                                           DFCS.61
C                                                                       DFCS.62
C     COPY SAME SET OF PHASE SHIFTS INTO REMAINING PHASE SHIFT ENTRIES  DFCS.63
C      FOR EACH COLLISION VOLUME POINT                                  DFCS.64
C                                                                       DFCS.65
```

```
      CALL FILL                                                         DFCS.66
      CALL SECOND(ED)                                                   DFCS.67
      TIME(2)=TIME(2)+ED-BG                                             DFCS.68
 15   CONTINUE                                                          DFCS.69
C                                                                       DFCS.70
C      ZERO CALCULATED SCATTERING INTENSITY AT EACH ANGLE               DFCS.71
C                                                                       DFCS.72
      DO 10 I=1,NANG                                                    DFCS.73
      SCAT(I)=0.                                                        DFCS.74
 10    CONTINUE                                                         DFCS.75
      DO 200 NN=1,NPRI                                                  DFCS.76
C                                                                       DFCS.77
C     CHOOSE PRIMARY SPEED                                              DFCS.78
C                                                                       DFCS.79
      PRISPD=VPRI(NN)                                                   DFCS.80
      DO 200 MM=1,NSEC                                                  DFCS.81
C                                                                       DFCS.82
C     CHOOSE SECONDARY SPEED                                            DFCS.83
C                                                                       DFCS.84
      SECSPD=VSEC(MM)                                                   DFCS.85
      CALL SECOND(BG)                                                   DFCS.86
      IF(IAPPRX.EQ.2) GOTO 16                                           DFCS.87
C                                                                       DFCS.88
C     IOPT=0 CALLS CMANG FOR COLLISION ENERGIES ONLY                    DFCS.89
C                                                                       DFCS.90
      IOPT=0                                                            DFCS.91
      XL=DETRAD/SQRT(2.)                                                DFCS.92
      YL=XL                                                             DFCS.93
      ZL=0.                                                             DFCS.94
      CALL CMANG(XL,YL,ZL,IOPT)                                         DFCS.95
C                                                                       DFCS.96
C     CALCULATE PHASE SHIFTS FOR COLLISION ENERGIES AT EACH POINT IN    DFCS.97
C     VOLUME GRID.                                                      DFCS.98
C                                                                       DFCS.99
      CALL PHSHFT(A,RM,NPRI1)                                           DFCS.100
C                                                                       DFCS.101
C     IAPPRX=1, THEN ALL POINTS IN THE COLLISION VOLUME HAVE THE SAME   DFCS.102
C     PHASE SHIFTS, SO ONLY NEED ONE SET OF PHASE SHIFTS FOR THIS       DFCS.103
C     WHOLE NEWTON DIAGRAM                                              DFCS.104
C                                                                       DFCS.105
      IF(IAPPRX.EQ.1) CALL FILL                                         DFCS.106
 16   CONTINUE                                                          DFCS.107
      CALL SECOND(ED)                                                   DFCS.108
      TIME(2)=TIME(2)+ED-BG                                             DFCS.109
C                                                                       DFCS.110
C     CALCULATE INTENSITY AT EACH DETECTOR ANGLE                        DFCS.111
C                                                                       DFCS.112
      DO 20 II=1,NANG                                                   DFCS.113
      DETANG=ANGLE(II)                                                  DFCS.114
      SNDT=DETSIN(II)                                                   DFCS.115
      CSDT=DETCOS(II)                                                   DFCS.116
C                                                                       DFCS.117
C    MULSMP INTEGRATES INTENSITY OVER  DETECTOR AREA.                   DFCS.118
```

```
C                                                                       DFCS.119
C                                                                       DFCS.120
C     CALCULATE SCATTERING ACCURATE TO 1 PERCENT OR 1/10 OF DATA ERROR. DFCS.121
C                                                                       DFCS.122
      ER=.01                                                            DFCS.123
      IF(EDAT(II).NE.1.) ER =EDAT(II)/10.                               DFCS.124
      CALL MULSMP(IINT,MAXI,ER,FINT,VALUE,IXIT,IBUG)                    DFCS.125
      IF(IXIT.NE.1) WRITE(6,501)IXIT,NN,MM,DETANG                       DFCS.126
C                                                                       DFCS.131
C     ADD THE NEWTON DIAGRAM WEIGHT.                                    DFCS.132
C                                                                       DFCS.133
      SCAT(II)=SCAT(II)+VALUE*WPRI(NN)*WSEC(MM)                         DFCS.134
 20   CONTINUE                                                          DFCS.135
 200  CONTINUE                                                          DFCS.136
C                                                                       DFCS.137
C      NORMALIZE FOR DETECTOR AREA,COLLISION VOLUME,NUMBER OF NEWTON    DFCS.138
C      DIAGRAMS                                                         DFCS.139
C                                                                       DFCS.140
      RNORM=DETWD                                                       DFCS.141
      IF(IINT.EQ.2) RNORM=RNORM*DETHT                                   DFCS.142
      RNORM=1./RNORM                                                    DFCS.143
      DO 21 II=1,NANG                                                   DFCS.144
      SCAT(II)=SCAT(II)*RNORM                                           DFCS.145
 21   CONTINUE                                                          DFCS.146
      IF(NOPT.NE.1) GOTO 4900                                           DFCS.147
C                                                                       DFCS.148
C      SCALE CROSS SECTION TO HAVE A MAXIMUM OF 10000                   DFCS.149
C                                                                       DFCS.150
      CALMAX=SCAT(1)                                                    DFCS.151
      DO 30 I=1,NANG                                                    DFCS.152
      CALMAX=AMAX1(CALMAX,SCAT(I))                                      DFCS.153
      SCAT(I)=ALOG(SCAT(I))                                             DFCS.154
30    CONTINUE                                                          DFCS.155
      DO 31 I=1,NANG                                                    DFCS.156
      SCAT(I)=SCAT(I)-ALOG(CALMAX)+4.*ALOG(10.)                         DFCS.157
31    CONTINUE                                                          DFCS.158
      CHI=1                                                             DFCS.159
      GOTO 5000                                                         DFCS.160
4900   CONTINUE                                                         DFCS.161
C                                                                       DFCS.162
C      SCALE CROSS SECTION TO DATA TO MINIMIZE CHI SQUARE               DFCS.163
C                                                                       DFCS.164
      CALL SCALE(SCAT,CHI)                                              DFCS.165
 5000 RETURN                                                            DFCS.166
C
C
C      FORMAT STATEMENTS
C
C
 501  FORMAT(10X,*MULSMP ROUTINE (INTEGRATES OVER DETECTOR AREA) DID NOTDFCS.127
     *TERMINATE PROPERLY- EXIT PARAMETER= *,I5,/,10X,*CALCULATION IS CONDFCS.128
     *TINUING, BUT RESULTS MAY LACK DESIRED ACCURACY*,/,10X,*ERROR OCCURDFCS.129
     *ED FOR NEWTON DIAGRAM*,2I5,10X,*AT ANGLE*,3X,F10.5,/)             DFCS.130
```

```
      END                                                               DFCS.167


                                                                        DFCS.168
      SUBROUTINE CMANG(XD,YD,ZD,IOPT)                                   CMANG.2
      COMMON/GEOMTY/PRINOZ,SECNOZ,PRISPD,SECSPD,XCOL,YCOL,ZCOL,MPRI,    GEOMTRY.2
     1MSEC,SNDT,CSDT,NOPT,NPRI1                                         GEOMTRY.3
     $,NPRI2 ,MAXIT                                                     GEOMTRY.4
      REAL MPRI,MSEC,MTOT                                               GEOMTRY.5
      COMMON/WH/C1,C2,C3,C4,C5,C6,C7,C8,C9,C10,MTOT                     WH.2
      COMMON/EN/ENERGY(125),CMTH1(125),CMTH2(125),WGHT1(125),WGHT2(125),EN.2
     1NCOLX,NCOLY,NCOLZ,IAPPRX                                          EN.3
      COMMON/VOL/X(5),Y(5),Z(5),WX(5),WY(5),WZ(5)                       VOL.2
      COMMON/TM/TIME(10),ICM,INTS,SPMAX,SPMIN                           TM.2
      ICM=ICM+1                                                         CMANG.8
      CALL SECOND(BG)                                                   CMANG.9
C                                                                       CMANG.10
C      FUNCTION- GIVEN A POINT ON THE DETECTOR LOCATED AT (XD,YD,ZD) IN CMANG.11
C      THE LABORATORY, FIND THE CENTER OF MASS SCATTERING ANGLES FOR    CMANG.12
C      EACH NEWTON DIAGRAM REPRESENTING THE DIFFERENT POINTS IN THE     CMANG.13
C      COLLISION VOLUME TO THIS POINT ON THE DETECTOR. ADDITIONALLY,    CMANG.14
C      DETERMINE THE GEOMETRICAL WEIGHT FACTORS TO ACCOUNT FOR          CMANG.15
C      1. THE COLLISION VOLUME WEIGHT,                                  CMANG.16
C      2. THE INVERSE LABORATORY VELOCITY DEPENDENCE OF THE IONIZER     CMANG.17
C      DETECTOR EFFICIENCY,                                             CMANG.18
C      3. THE INVERSE ENERGY DEPENDENCE OF THE ELASTIC SCATTERING CROSS CMANG.19
C      SECTION,                                                         CMANG.20
C      4. THE RELATIVE VELOCITY FACTOR FOR THE TOTAL SCATTERING         CMANG.21
C      PROBABILITY, AND                                                 CMANG.22
C      5. THE TRANSFORMATION JACOBIAN FROM THE CENTER OF MASS TO THE    CMANG.23
C      LABORATORY FRAME APPROPRIATE FOR ELASTIC SCATTERING.             CMANG.24
C                                                                       CMANG.25
C      THE WEIGHT FACTORS COMPUTED HERE ARE USED IN THE SUBROUTINE      CMANG.26
C      INTENS.                                                          CMANG.27
C                                                                       CMANG.28
C      PARAMETERS                                                       CMANG.29
C      XD,YD,ZD- ARE THE INPUT LABORATORY COORDINATES FOR THE POINT ON  CMANG.30
C      THE DETECTOR WHERE THE SCATTERING INTENSITY IS TO BE FOUND.      CMANG.31
C      IOPT=0, THEN ONLY THE COLLISION ENERGIES ARE FOUND FOR THE       CMANG.32
C      DIFFERENT POINTS IN THE COLLISION VOLUME. THIS IS USED TO FIND   CMANG.33
C      THE ENERGIES AT WHICH THE PHASE SHIFTS ARE TO BE COMPUTED.       CMANG.34
C      IOPT=1, FIND COLLISION ENERGIES, SCATTERING ANGLES, AND WEIGHT   CMANG.35
C      FACTORS.                                                         CMANG.36
C                                                                       CMANG.37
C      ON OUTPUT, THE COMMON BLOCK EN CONTAINS THE COLLISION ENERGIES   CMANG.38
C      IN THE ARRAY ENERGY, THE CENTER OF MASS SCATTERING ANGLES AND    CMANG.39
C      WEIGHTS FOR THE FORWARD SIDE SCATTERING IN THE ARRAYS CMTH1,WGHT1CMANG.40
C      AND THE SCATTERING ANGLES AND WEIGHTS FOR THE BACK SIDE NEWTON   CMANG.41
C      SPHERE SCATTERING IN THE ARRAYS CMTH2,WGHT2                      CMANG.42
C      IF THE BACK SIDE SCATTERING IS AWAY FROM THE DETECTOR, OR THE    CMANG.43
C      DETECTOR DOES NOT INTERSECT THE NEWTON SPHERE, THEN THE WEIGHT   CMANG.44
C      FACTORS FOR THAT POINT ARE SET TO ZERO. IF THE DETECTOR IS       CMANG.45
```

```
C      TANGENT TO THE NEWTON SPHERE, THE WEIGHT FACTOR IS ALSO SET TO   CMANG.46
C      ZERO, SINCE THIS SINGULARITY CANNOT BE INTEGRATED BY THE SIMPLE  CMANG.47
C      COORDINATE SYSTEM USED HERE. A MESSAGE IS PRINTED IF THIS HAPPENSCMANG.48
C                                                                       CMANG.49
C      SUBPROGRAMS USED--- SQRT, SECOND                                 CMANG.50
C                                                                       CMANG.51
C       AUTHOR M.F. VERNON
C                                                                       CMANG.53
C       LAST REVISION DATE-FEBRUARY 16,1983
C                                                                       CMANG.54
C                                                                       CMANG.55
C     ZERO ARRAYS                                                       CMANG.56
C                                                                       CMANG.57
      NVOL=NCOLX*NCOLY*NCOLZ                                            CMANG.58
      DO 10 I=1,NVOL                                                    CMANG.59
      CMTH1(I)=0.                                                       CMANG.60
      CMTH2(I)=0.                                                       CMANG.61
      WGHT1(I)=0.                                                       CMANG.62
      WGHT2(I)=0.                                                       CMANG.63
 10   CONTINUE                                                          CMANG.64
      INDEX=0                                                           CMANG.65
C                                                                       CMANG.66
C     LOOP OVER EACH POINT IN COLLISION ZONE                            CMANG.67
C                                                                       CMANG.68
      DO 100 I=1,NCOLX                                                  CMANG.69
      XCOL=X(I)                                                         CMANG.70
      DO 100 J=1,NCOLY                                                  CMANG.71
      YCOL=Y(J)                                                         CMANG.72
      DO 100 K=1,NCOLZ                                                  CMANG.73
C                                                                       CMANG.74
C      CALCULATE CONSTANTS NEEDED FOR DETERMINING VELOCITY VECTOR       CMANG.75
C      COMPONENTS                                                       CMANG.76
C                                                                       CMANG.77
      ZCOL=Z(K)                                                         CMANG.78
      INDEX=INDEX+1                                                     CMANG.79
      T=XCOL*XCOL+YCOL*YCOL+ZCOL*ZCOL                                   CMANG.80
      T3=T+C1*XCOL+C2                                                   CMANG.81
      T4=T+C3*YCOL+C4                                                   CMANG.82
      T1=PRISPD/SQRT(T3)                                                CMANG.83
      T2=SECSPD/SQRT(T4)                                                CMANG.84
C                                                                       CMANG.85
C     PRIMARY VELOCITY VECTOR=(VX1,VY1,VZ1)                             CMANG.86
C                                                                       CMANG.87
      VX1=T1*(PRINOZ+XCOL)                                              CMANG.88
      VY1=T1*YCOL                                                       CMANG.89
      VZ1=T1*ZCOL                                                       CMANG.90
C                                                                       CMANG.91
C     SECONDARY VELOCITY VECTOR=(VX2,VY2,VZ2)                           CMANG.92
C                                                                       CMANG.93
      VX2=T2*XCOL                                                       CMANG.94
      VY2=T2*(SECNOZ+YCOL)                                              CMANG.95
      VZ2=T2*ZCOL                                                       CMANG.96
C                                                                       CMANG.97
```

```
C     RELATIVE VELOCITY VECTOR=(RELVX,RELVY,RELVZ)                      CMANG.98
C                                                                       CMANG.99
      RELVLX=VX1-VX2                                                    CMANG.100
      RELVLY=VY1-VY2                                                    CMANG.101
      RELVLZ=VZ1-VZ2                                                    CMANG.102
C                                                                       CMANG.103
C     CENTER OF MASS VELOCITY VECTOR=(CMVELX,CMVELY,CMVELZ)             CMANG.104
C                                                                       CMANG.105
      CMVELX=(MPRI*VX1+MSEC*VX2L)/MTOT    +XCOL                         CMANG.106
      CMVELY=(MPRI*VY1+MSEC*VY2)/MTOT     +YCOL                         CMANG.107
      CMVELZ=(MPRI*VZ1+MSEC*VZ2)/MTOT     +ZCOL                         CMANG.108
C                                                                       CMANG.109
C     CALCULATE RADIUS OF NEWTON CIRCLE                                 CMANG.110
C                                                                       CMANG.111
      RDNWT2=C5*(RELVLX*RELVLX+RELVLY*RELVLY+RELVLZ*RELVLZ)             CMANG.112
      RELVEL=SQRT(RDNWT2/C5)                                            CMANG.113
C                                                                       CMANG.114
C     CENTER OF MASS COLLISION ENERGY =E                                CMANG.115
C                                                                       CMANG.116
      E=C6*RDNWT2                                                       CMANG.117
      ENERGY(INDEX)=E                                                   CMANG.118
C                                                                       CMANG.119
C     IF IOPT=0 THEN ONLY WANT TO KNOW THE COLLISION ENERGY TO COMPUTE  CMANG.120
C     PHASE SHIFTS.                                                     CMANG.121
C                                                                       CMANG.122
      IF(IOPT.EQ.0) GOTO 100                                            CMANG.123
      RR=C7/RDNWT2                                                      CMANG.124
C                                                                       CMANG.125
C     CALCULATE LINEAR EQN. PARAMETERS FOR Y AND Z COMPONENTS OF        CMANG.126
C     INTERSECTION BETWEEN DETECTOR RAY AND NEWTON CIRCLE.              CMANG.127
C                                                                       CMANG.128
      TEMP=XCOL-XD                                                      CMANG.129
      SLPY=(YCOL-YD)/TEMP                                               CMANG.130
      BY=(XCOL*YD-XD*YCOL)/TEMP                                         CMANG.131
      SLPZ=(ZCOL-ZD)/TEMP                                               CMANG.132
      BZ=(XCOL*ZD-XD*ZCOL)/TEMP                                         CMANG.133
C                                                                       CMANG.134
C     A,B,C ARE DEFINED BY THE EQN.                                     CMANG.135
C     A*XNWT*XNWT+B*XNWT+C=0.                                           CMANG.136
C     THE TWO SOLUTIONS (XNWT1,XNWT2) ARE THE X CORRDINATES OF THE TWO  CMANG.137
C     POINTS ON THE NEWTON CIRCLE.                                      CMANG.138
C                                                                       CMANG.139
      A=1.+SLPY*SLPY+SLPZ*SLPZ                                          CMANG.140
      B=-2.*(CMVELX+SLPY*(CMVELY-BY)+SLPZ*(CMVELZ-BZ))                  CMANG.141
      C=CMVELX*CMVELX+(BY-CMVELY)*(BY-CMVELY)+(BZ-CMVELZ)*(BZ-CMVELZ)   CMANG.142
     1-RDNWT2                                                           CMANG.143
      TEMP=B*B-4.*A*C                                                   CMANG.144
      T5=1./2./A                                                        CMANG.145
      IF(TEMP) 100,40,30                                                CMANG.146
C                                                                       CMANG.147
C     EDGE OF NEWTON CIRCLE                                             CMANG.148
C                                                                       CMANG.149
 40   XNWT1=-B*T5                                                       CMANG.150
```

```
      XNWT2=XNWT1                                                       CMANG.151
      WRITE(6,31)                                                       CMANG.152
      GOTO 100                                                          CMANG.154
C                                                                       CMANG.155
C     TWO DISTINCT ROOTS                                                CMANG.156
C                                                                       CMANG.157
 30   TEMP=SQRT(TEMP)                                                   CMANG.158
      XNWT1=(-B+TEMP)*T5                                                CMANG.159
      XNWT2=(-B-TEMP)*T5                                                CMANG.160
C                                                                       CMANG.161
C     Y,Z CORRDINATES DETERMINED BY THE LINEAR EQNS. DEFINED ABOVE.     CMANG.162
C                                                                       CMANG.163
 35   YNWT1=SLPY*XNWT1+BY                                               CMANG.164
      YNWT2=SLPY*XNWT2+BY                                               CMANG.165
      ZNWT1=SLPZ*XNWT1+BZ                                               CMANG.166
      ZNWT2=SLPZ*XNWT2+BZ                                               CMANG.167
C                                                                       CMANG.168
C     CHECK THAT THE LAB VELOCITY WILL SCATTER PRODUCT INTO THE DETECTORCMANG.169
C                                                                       CMANG.170
      IF((XNWT1-XCOL)*XD.LT.0.) GOTO 45                                 CMANG.171
      IF((YNWT1-YCOL)*YD.LT.0.) GOTO 45                                 CMANG.172
      VCNTX1=(XNWT1-CMVELX)                                             CMANG.173
      VCNTY1=(YNWT1-CMVELY)                                             CMANG.174
      VCNTZ1=ZNWT1-CMVELZ                                               CMANG.175
C                                                                       CMANG.176
C     CALCULATE COSINE OF THE CENTER OF MASS SCATTERING ANGLE           CMANG.177
C                                                                       CMANG.178
      CMANG1=(VCNTX1*RELVLX+VCNTY1*RELVLY+VCNTZ1*RELVLZ)*RR             CMANG.179
      CMTH1(INDEX)=CMANG1                                               CMANG.180
C                                                                       CMANG.181
C     CALCULATE LABORATORY SPEED OF PRODUCT                             CMANG.182
C                                                                       CMANG.183
      VLAB1=SQRT((XNWT1-XCOL)**2+(YNWT1-YCOL)**2+(ZNWT1-ZCOL)**2)       CMANG.184
C                                                                       CMANG.185
C     CALCULATE LAB CARTESIAN COMPONENTS OF PRODUCT VELOCITY VECTOR     CMANG.186
C                                                                       CMANG.187
      VLAB1X=XNWT1-XCOL                                                 CMANG.188
      VLAB1Y=YNWT1-YCOL                                                 CMANG.189
      VLAB1Z=ZNWT1-ZCOL                                                 CMANG.190
C                                                                       CMANG.191
C     CALCULATE CENTER OF MASS SCATTERING VECTOR                        CMANG.192
C                                                                       CMANG.193
      CM1X=XNWT1-CMVELX                                                 CMANG.194
      CM1Y=YNWT1-CMVELY                                                 CMANG.195
      CM1Z=ZNWT1-CMVELZ                                                 CMANG.196
C                                                                       CMANG.197
C     CALCULATE THE ABSOLUTE VALUE OF THE COSINE OF THE ANGLE BETWEEN   CMANG.198
C     THE LAB PRODUCT VELOCITY VECTOR AND THE CENTER OF MASS SCATTERING CMANG.199
C     VECTOR                                                            CMANG.200
C                                                                       CMANG.201
      T1=CM1X*VLAB1X+CM1Y*VLAB1Y+CM1Z*VLAB1Z                            CMANG.202
      COSUV1=SQRT(T1*T1/RDNWT2)/VLAB1                                   CMANG.203
C                                                                       CMANG.204
```

```
C     CALCULATE JACOBIAN FACTORS                                        CMANG.205
C                                                                       CMANG.206
      FJAC1=VLAB1*VLAB1/COSUV1/RDNWT2                                   CMANG.207
      WGHT1(INDEX)=WX(I)*WY(J)*WZ(K)*RELVEL/VLAB1/ENERGY(INDEX)         CMANG.208
      WGHT1(INDEX)=WGHT1(INDEX)*FJAC1                                   CMANG.209
C                                                                       CMANG.210
C     CHECK THAT THE LAB VELOCITY WILL SCATTER PRODUCT INTO THE DETECTORCMANG.211
C                                                                       CMANG.212
 45   IF((XNWT2-XCOL)*XD.LT.0.) GOTO 100                                CMANG.213
      IF((YNWT2-YCOL)*YD.LT.0.) GOTO 100                                CMANG.214
      VCNTX2=XNWT2-CMVELX                                               CMANG.215
      VCNTY2=YNWT2-CMVELY                                               CMANG.216
      VCNTZ2=ZNWT2-CMVELZ                                               CMANG.217
C                                                                       CMANG.218
C     CALCULATE COSINE OF THE CENTER OF MASS SCATTERING ANGLE           CMANG.219
C                                                                       CMANG.220
      CMANG2=(VCNTX2*RELVLX+VCNTY2*RELVLY+VCNTZ2*RELVLZ)*RR             CMANG.221
      CMTH2(INDEX)=CMANG2                                               CMANG.222
C                                                                       CMANG.223
C     CALCULATE LABORATORY SPEED OF PRODUCT                             CMANG.224
C                                                                       CMANG.225
      VLAB2=SQRT((XNWT2-XCOL)**2+(YNWT2-YCOL)**2+(ZNWT2-ZCOL)**2)       CMANG.226
C                                                                       CMANG.227
C     CALCULATE LAB COMPONENTS OF PRODUCT VELOCITY VECTOR               CMANG.228
C                                                                       CMANG.229
      VLAB2X=XNWT2-XCOL                                                 CMANG.230
      VLAB2Y=YNWT2-YCOL                                                 CMANG.231
      VLAB2Z=ZNWT2-ZCOL                                                 CMANG.232
C                                                                       CMANG.233
C     CALCULATE CENTER OF MASS SCATTERING VECTOR                        CMANG.234
C                                                                       CMANG.235
      CM2X=XNWT2-CMVELX                                                 CMANG.236
      CM2Y=YNWT2-CMVELY                                                 CMANG.237
      CM2Z=ZNWT2-CMVELZ                                                 CMANG.238
C                                                                       CMANG.239
C     CALCULATE THE ABSOLUTE VALUE OF THE COSINE OF THE ANGLE BETWEEN   CMANG.240
C     THE LAB PRODUCT VELOCITY VECTOR AND THE CENTER OF MASS SCATTERING CMANG.241
C     VECTOR                                                            CMANG.242
C                                                                       CMANG.243
      T2=CM2X*VLAB2X+CM2Y*VLAB2Y+CM2Z*VLAB2Z                            CMANG.244
      COSUV2=SQRT(T2*T2/RDNWT2)/VLAB2                                   CMANG.245
C                                                                       CMANG.246
C     CALCULATE JACOBIAN FACTORS                                        CMANG.247
C                                                                       CMANG.248
      FJAC2=VLAB2*VLAB2/COSUV2/RDNWT2                                   CMANG.249
      WGHT2(INDEX)=WGHT1(INDEX)*VLAB1/VLAB2                             CMANG.250
      WGHT2(INDEX)=WGHT2(INDEX)*FJAC2/FJAC1                             CMANG.251
 100  CONTINUE                                                          CMANG.252
C                                                                       CMANG.253
C     IF IAPPRX=1, THEN FIND THE POINT IN THE COLLISION ZONE WITH THE   CMANG.254
C     LARGEST WEIGHT FACTOR AND COMPUTE PHASE SHIFTS FOR THIS ENERGY    CMANG.255
C     ONLY. THE CANONICAL ENERGY IS STORED IN ENERGY(1).                CMANG.256
C                                                                       CMANG.257
```

```
 70   IF(IAPPRX.EQ.0) GOTO 80                                          CMANG.258
      RMAX=0.                                                          CMANG.259
      DO 50 I=1,INDEX                                                  CMANG.260
      IF(WGHT1(I).LT.RMAX) GOTO 55                                     CMANG.261
      RMAX=WGHT1(I)                                                    CMANG.262
      IMAX=I                                                           CMANG.263
 55   IF(WGHT2(I).LE.RMAX) GOTO 50                                     CMANG.264
      RMAX=WGHT2(I)                                                    CMANG.265
      IMAX=I                                                           CMANG.266
 50   CONTINUE                                                         CMANG.267
      ENERGY(1)=ENERGY(IMAX)                                           CMANG.268
 80   CALL SECOND(ED)                                                  CMANG.269
      TIME(3)=TIME(3)+ED-BG                                            CMANG.270
      RETURN                                                           CMANG.271
C
C
C       FORMAT STATEMENTS
C
C
 31   FORMAT(10X,*DETECTOR TANGENT TO NEWTON SPHERE.*)                 CMANG.153
      END                                                              CMANG.272


                                                                       CMANG.273
      FUNCTION FINT(X)                                                 FINT.2
C                                                                      FINT.3
C      FINT IS THE FUNCTION WHICH RETURNS THE VALUE OF THE SCATTERED   FINT.4
C      INTENSITY AT A POINT ON THE DETECTOR LOCATED AT (XD,YD) IN THE  FINT.5
C      LAB FRAME, FROM EACH POINT IN THE COLLISION VOLUME GRID         FINT.6
C      PARAMETERS                                                      FINT.7
C      X- ON INPUT CONTAINS THE (X,Y)=(X(1),X(2)) POSITION ON THE      FINT.8
C      DETECTOR WHERE THE SCATTERING INTENSITY IS TO BE CALCULATED.    FINT.9
C      X(1) MEASURES HORIZONTAL DISPLACEMENT FROM THE DETECTOR MIDPOINT FINT.10
C      X(2) MEASURES VERTICAL DISPLACEMNET                             FINT.11
C                                                                      FINT.12
C      SUBPROGRAMS CALLED- INTENS, CMANG                               FINT.13
C                                                                      FINT.14
C                                                                      FINT.15
      COMMON/INTEG/IINT                                                INTEG.2
      COMMON/GEOMTY/PRINOZ,SECNOZ,PRISPD,SECSPD,XCOL,YCOL,ZCOL,MPRI,   GEOMTRY.2
     1MSEC,SNDT,CSDT,NOPT,NPRI1                                        GEOMTRY.3
     $,NPRI2 ,MAXIT                                                    GEOMTRY.4
      REAL MPRI,MSEC,MTOT                                              GEOMTRY.5
      COMMON/AA/DETWD,DETHT,DETRAD,E                                   AA.2
      DIMENSION X(2)                                                   FINT.19
C                                                                      FINT.20
C     TRANSLATE FROM DETECTOR COORDINATES TO LAB COORDINATES           FINT.21
C                                                                      FINT.22
      XD=DETRAD*CSDT+X(1)*SNDT                                         FINT.23
      YD=DETRAD*SNDT-X(1)*CSDT                                         FINT.24
      ZD=X(2)                                                          FINT.25
C                                                                      FINT.26
```

```
C     IF ONLY INTEGRATING IN -PLANE SCATTERING, THEN SET Z COORDINATE   FINT.27
C     OF DETECTOR TO ZERO.                                              FINT.28
C                                                                       FINT.29
      IF(IINT.EQ.1) ZD=0.                                               FINT.30
      IOPT=1                                                            FINT.31
C                                                                       FINT.32
C      FIND C.M. ANGLES WHERE INTENSITY IS TO BE EVALUATED              FINT.33
C                                                                       FINT.34
      CALL CMANG(XD,YD,ZD,IOPT)                                         FINT.35
C                                                                       FINT.36
C      COMPUTE THE INTENSITY AT THESE ANGLES                            FINT.37
C                                                                       FINT.38
      CALL INTENS(F)                                                    FINT.39
      FINT=F                                                            FINT.40
      RETURN                                                            FINT.41
      END                                                               FINT.42


                                                                        FINT.43
      SUBROUTINE FILL                                                   FILL.2
C                                                                       FILL.3
C                                                                       FILL.4
C      FUNCTION- WHEN ALL THE COLLISION VOLUME POINTS HAVE THE SAME     FILL.5
C      PHASE SHIFTS, THIS ROUTINE COPIES THE ONE SET OF PHASE SHIFTS
C      THAT ARE CALCULATED INTO THE PHASE SHIFT ARRAYS FOR THE
C      REMAINING POINTS. THE COLLISION ENERGY ARRAY IS ALSO COMPLETED
C      WITH THEENERGY CORRESPONDING TO THAT OF THE CALCULATED PHASE
C      SHIFTS.                                                          FILL.9
C                                                                       FILL.10
C      SUBPROGRAMS- NONE                                                FILL.11
C                                                                       FILL.12
C      REFERENCE M.F. VERNON, MAY 1982.                                 FILL.13
C                                                                       FILL.14
C                                                                       FILL.15
      COMMON/ETA/STHE(8000),CTHE(8000),NETA,DETA,IDENT                  ETA.2
     $,IBOSE                                                            ETA.3
      COMMON/EN/ENERGY(125),CMTH1(125),CMTH2(125),WGHT1(125),WGHT2(125),EN.2
     1NCOLX,NCOLY,NCOLZ,IAPPRX                                          EN.3
      NVOL=NCOLX*NCOLY*NCOLZ                                            FILL.18
      DO 50 II=2,NVOL                                                   FILL.19
      ENERGY(II)=ENERGY(1)                                              FILL.20
      ITEMP=(II-1)*NETA                                                 FILL.21
      DO 25 J=1,NETA                                                    FILL.22
      CTHE(ITEMP+J)=CTHE(J)                                             FILL.23
      STHE(ITEMP+J)=STHE(J)                                             FILL.24
 25   CONTINUE                                                          FILL.25
 50   CONTINUE                                                          FILL.26
      RETURN                                                            FILL.27
      END                                                               FILL.28
```

```
                                                                        FILL.29
      SUBROUTINE MULSMP(N,MAXI,E,FINT,VALUE,IXIT,IBUG)                  MULSMP.2
C                                                                       MULSMP.3
C     SIMPSON'S RULE MULTIPLE INTEGRATION FROM BKY SOURCE LIBRARY AND   MULSMP.4
C     MODIFIED SLIGHTLY BY M. VERNON.                                   MULSMP.5
C     N = MULTIPLICITY OF THE INTEGRATION.  N .LE. 5.                   MULSMP.6
C                                                                       MULSMP.7
C     IF N.EQ.0 THEN VALUE IS RETURNED WITH THE INTENSITY AT THE CENTER MULSMP.8
C     OF THE DETECTOR.                                                  MULSMP.9
C                                                                       MULSMP.10
C     ALIM = NAME OF FUNCTION ROUTINE DEFINING THE LOWER LIMITS.        MULSMP.11
C     BLIM = NAME OF FUNCTION ROUTINE DEFINING THE UPPER LIMITS.        MULSMP.12
C     THE CURRENT VERSION OF THE PROGRAM ASSUMES  RECTANGULAR           MULSMP.13
C     DETECTOR SLITS. THE ALIM, BLIM  VALUES ARE CONSTANTS. IF THE      MULSMP.14
C     BOUNDARIES DEPEND ON THE COORDINATES, THEN THE ALIM, BLIM         MULSMP.15
C     CALLS MUST BE REPLACED BY FUNCTIONS, WITH ARGUMENTS BEING THE     MULSMP.16
C     DIMENSION AND XNEW VALUES. NOTE THAT THE LIMIT FUNCTIONS MUST BE  MULSMP.17
C     DEFINED SO THAT LOWER DIMENSION LIMITS DEPEND ONLY ON THE HIGHER  MULSMP.18
C     DIMENSIONAL COORDINATES.                                          MULSMP.19
C                                                                       MULSMP.20
C     MAXI = THE MAX. NO. OF ITERATIONS THE ROUTINE MAY DO.             MULSMP.21
C                                                                       MULSMP.22
C      FOR ANY DIMENSION, BY THE NTH ITERATION, A TOTAL OF              MULSMP.23
C      2**N  +2**(N-1) + ... + 2**2 + 2**1 + 3  FUNCTION EVALUATIONS    MULSMP.24
C      WILL HAVE BEEN NECESSARY. IF N>3 , AN 8 POINT GAUSS- LEGENDRE    MULSMP.25
C      QUADRUTURE MAY BE MORE EFFICIENT.                                MULSMP.26
C                                                                       MULSMP.27
C     E = FRACTIONAL ERROR, MEANING                                     MULSMP.28
C         IF V(I)=VALUE OF THE INTEGRAL ON THE ITH ITERATION,           MULSMP.29
C         THEN THE PROBLEM IS CONSIDERED SOLVED WHEN                    MULSMP.30
C         E * ABS(V(I)) .GT. ABS(V(I)-V(I+1)).                          MULSMP.31
C     FINT = NAME OF FUNCTION ROUTINE DEFINING THE INTEGRAND.           MULSMP.32
C     VALUE = LAST APPROXIMATION TO THE INTEGRAL.                       MULSMP.33
C     IXIT = 1 MEANS NORMAL RETURN                                      MULSMP.34
C            2 MEANS NO CONVERGENCE                                     MULSMP.35
C            3 MEANS LOWER .GT. UPPER LIMIT.                            MULSMP.36
C     IBUG = 1 MEANS PRINT EACH APPROXIMATION TO INTEGRAL.              MULSMP.37
C                                                                       MULSMP.38
C      SUBPROGRAMS- ABS,FINT                                            MULSMP.39
C                                                                       MULSMP.40
C      REFERENCE- M. F. VERNON, 1982                                    MULSMP.41
C                                                                       MULSMP.42
      DIMENSION A(5),B(5),FA(5),FB(5),XH(5),XIR(5),XHA(5),XJ(5),INDEX(5)MULSMP.43
     X          ,XNEW(5),FNEWX(5),XI(5),S(5),XE(5),K(5),XIP(5)          MULSMP.44
      COMMON/LIMITS/ALIM(2),BLIM(2)                                     LIMITS.2
C                                                                       MULSMP.46
      IF(IBUG.NE.0) WRITE(6,100)                                        MULSMP.47
      I=N                                                               MULSMP.50
C                                                                       MULSMP.51
C      IF DIMENSION IS ZERO, RETURN VALUE AT CENTER OF DETECTOR         MULSMP.52
C                                                                       MULSMP.53
      IF(N.EQ.0) GOTO 2001                                              MULSMP.54
C                                                                       MULSMP.55
```

```
C      LOAD LOWER LIMITS, BEGINNING WITH THE HIGHEST DIMENSION FIRST    MULSMP.56
C      IN CASE THE LOWER DIMENSIONAL LIMITS DEPEND ON THESE COORDINATES MULSMP.57
C                                                                       MULSMP.58
C      SET LIMITS FOR THE NEXT PASS AT THE INTEGRAL. K IS USED TO DECIDEMULSMP.59
C      THE STAGE OF THE INTEGRATION OVER THE HIGHER DIMENSIONS (SEE     MULSMP.60
C      BELOW)                                                           MULSMP.61
C                                                                       MULSMP.62
    3 DO 1 L=1,I                                                        MULSMP.63
      J=I + 1 - L                                                       MULSMP.64
      K(J)=1                                                            MULSMP.65
      A(J)=ALIM(J)                                                      MULSMP.66
    1 XNEW(J)=A(J)                                                      MULSMP.67
C                                                                       MULSMP.68
C      BEGIN INTEGRATION OVER LOWEST DIMENSIONS WITH NEW VALUES OF      MULSMP.69
C      HIGHER DIMENSIONAL COORDINATES                                   MULSMP.70
C                                                                       MULSMP.71
    2 I=1                                                               MULSMP.72
C                                                                       MULSMP.73
C      GET VALUE OF INTEGRAND AT THE LOWER LIMIT OF LOWEST DIMENSION    MULSMP.74
C                                                                       MULSMP.75
      XNEW(1)=A(1)                                                      MULSMP.76
      FA(1)=FINT(XNEW)                                                  MULSMP.77
C                                                                       MULSMP.78
C      GET VALUE OF INTEGRAND AT UPPER LIMIT OF LOWEST DIMENSION        MULSMP.79
C                                                                       MULSMP.80
      B(1)=BLIM(1)                                                      MULSMP.81
      XNEW(1)=B(1)                                                      MULSMP.82
      FB(1)=FINT(XNEW)                                                  MULSMP.83
C                                                                       MULSMP.84
 1000 XH(I)=B(I)-A(I)                                                   MULSMP.85
      IF (.25 * XH(I) .EQ. 0.) GO TO 4                                  MULSMP.86
      IF (XH(I) .LT. 0.) GO TO 5                                        MULSMP.87
C                                                                       MULSMP.88
C      XIR,XHA,XJ ARE CONSTANTS NEEDED TO INITIALIZE ADAPTIVE SIMPSON'S MULSMP.89
C      INTEGRAL.AT THIS POINT, INTEGRAL IS APPROXIMATED USING  2 POINTS MULSMP.90
C      , THE VALUES OF THE INTEGRAND AT THE UPPER AND LOWER LIMITS OF   MULSMP.91
C      THE LOWEST DIMENSION                                             MULSMP.92
C                                                                       MULSMP.93
      XIR(I)=0.5*XH(I)                                                  MULSMP.94
      XHA(I)=XIR(I)/3.                                                  MULSMP.95
      XJ(I)=XIR(I)*(FA(I)+FB(I))                                        MULSMP.96
      INDEX(I)=0                                                        MULSMP.97
C                                                                       MULSMP.98
C      NOW BEGIN HALVING STEP SIZE                                      MULSMP.99
C                                                                       MULSMP.100
      XNEW(I)=A(I)+XIR(I)                                               MULSMP.101
C                                                                       MULSMP.102
 1006 IF (I .EQ. 1) GO TO 14                                            MULSMP.103
C                                                                       MULSMP.104
C      IF NOT INTEGRATING LOWEST DIMENSION, THEN MUST DO SO. AT THIS    MULSMP.105
C      POINT, A  NEW POINT INVOLVING A CHANGE IN THE HIGHER DIMENSIONAL MULSMP.106
C      COORDINATES IS NEEDED, SO MUST BEGIN AT THE LOWEST DIMENSION AND MULSMP.107
C      INTEGRATE UP TO THE  DIMENSION WHERE THE NEW MESH POINT IS NEEDEDMULSMP.108
```

```
C                                                                       MULSMP.109
   15 I=I-1                                                             MULSMP.110
      GO TO 3                                                           MULSMP.111
   14 FNEWX(1)=FINT(XNEW)                                               MULSMP.112
C                                                                       MULSMP.113
 1001 IF (INDEX(I) .GT. 0) GO TO 1003                                   MULSMP.114
C                                                                       MULSMP.115
C      FIRST APPROXIMATION,XI, IS 3 POINT SIMPSON'S RULE                MULSMP.116
C                                                                       MULSMP.117
 1002 INDEX(I)=INDEX(I)+1                                               MULSMP.118
      XI(I)=XHA(I)*(FB(I)+FA(I)+4.*FNEWX(I))                            MULSMP.119
C                                                                       MULSMP.120
C     XJ CONTAINS THE CONTRIBUTION TO THE NEXT APPROXIMATION WHICH      MULSMP.121
C     DEPENDS ON THE POINTS ALREADY CALCUALTED IN THE ADAPTIVE          MULSMP.122
C     SIMPSON'S INTEGRAL.                                               MULSMP.123
C                                                                       MULSMP.124
 1004 XJ(I)=0.25*(XJ(I)+3.*XI(I))                                       MULSMP.125
      INDEX(I)=INDEX(I)+1                                               MULSMP.126
      IF (INDEX(I) .GT. MAXI) GO TO 1011                                MULSMP.127
C                                                                       MULSMP.128
C      HALVE STEP SIZE FOR NEXT APPROXIMATION                           MULSMP.129
C                                                                       MULSMP.130
 1010 XH(I)=0.5*XH(I)                                                   MULSMP.131
      IF (.5 * XH(I) .EQ. 0.) GO TO 7                                   MULSMP.132
C                                                                       MULSMP.133
C      XNEW IS THE FIRST POINT AT THE NEW STEP SIZE. NOTE THAT ONLY     MULSMP.134
C      THE POINTS WHICH ARE AN ODD MULTIPLE OF THE CURRENT STEP SIZE    MULSMP.135
C      ARE CALCULATED, AND THESE ARE OBTAINED BY STARTING AT XNEW AND   MULSMP.136
C      INCREMENTING BY TWICE THE CURRENT STEP SIZE.                     MULSMP.137
C                                                                       MULSMP.138
      XNEW(I)=0.5*XH(I)+A(I)                                            MULSMP.139
C                                                                       MULSMP.140
C      S= THE SUM OF THE INTEGRAND VALUES AT ALL ODD MULTIPLES OF THE   MULSMP.141
C      CURRENT STEP SIZE, I.E. THE VALUES OF THE INTEGRAND AT POINTS    MULSMP.142
C      NOT PREVIOUSLY CALCULATED.                                       MULSMP.143
C                                                                       MULSMP.144
      S(I)=0.0                                                          MULSMP.145
C                                                                       MULSMP.146
C      CHECK IF CURRENT MESH POINT EXCEEDS UPPER LIMIT. IF IT DOES,     MULSMP.147
C      THEN CURRENT MESH SIZE IS FINISHED.                              MULSMP.148
C                                                                       MULSMP.149
 1005 IF (XNEW(I) .LT. B(I)) GO TO 1006                                 MULSMP.150
C                                                                       MULSMP.151
C      CURRENT DIMENSION INTEGRATED, ITS VALUE GIVEN BY XIP.            MULSMP.152
C                                                                       MULSMP.153
 1007 XIP(I)=(XJ(I)+XH(I)*2.*S(I))/3.                                   MULSMP.154
C                                                                       MULSMP.155
C      CHECK FOR CONVERGENCE                                            MULSMP.156
C                                                                       MULSMP.157
      XE(I)=ABS (E*XIP(I))                                              MULSMP.158
      IF(IBUG.NE.0) WRITE(6,101)I,INDEX(I),XIP(I),XE(I),XIP(I)-XI(I)    MULSMP.159
      IF (ABS(XIP(I) - XI(I)) .LE. XE(I)) GO TO 1009                    MULSMP.161
C                                                                       MULSMP.162
```

```
C      NOT CONVERGED, SO CURRENT APPROXIMATION NOW BECOMES THE LAST     MULSMP.163
C      APPROXIMATION, AND INTEGRATION CONTINUES BY DECREASING THE       MULSMP.164
C      STEP SIZE                                                        MULSMP.165
C                                                                       MULSMP.166
 1008 XI(I)=XIP(I)                                                      MULSMP.167
      GO TO 1004                                                        MULSMP.168
C                                                                       MULSMP.169
C      SUM UP S WITH CURRENT VALUE OF INTEGRAND, AND INCREMENT TO NEXT  MULSMP.170
C      MESH POINT                                                       MULSMP.171
C                                                                       MULSMP.172
 1003 S(I)=FNEWX(I)+S(I)                                                MULSMP.173
      XNEW(I)=XNEW(I)+XH(I)                                             MULSMP.174
      GO TO 1005                                                        MULSMP.175
C                                                                       MULSMP.176
    4 XIP(I) = 0.                                                       MULSMP.177
C                                                                       MULSMP.178
 1009 IF (I .EQ. N) GO TO 16                                            MULSMP.179
C                                                                       MULSMP.180
C      BEGIN INTEGRATION OVER THE NEXT DIMENSION                        MULSMP.181
C                                                                       MULSMP.182
   17 I1=I+1                                                            MULSMP.183
      J=K(I1)                                                           MULSMP.184
      GO TO (11,12,13),J                                                MULSMP.185
C                                                                       MULSMP.186
C                                                                       MULSMP.187
C      VALUE OF INTEGRAND AT LOWER LIMIT OF NEXT DIMENSION IS THE       MULSMP.188
C      CURRENT VALUE OF XIP.                                            MULSMP.189
C                                                                       MULSMP.190
   11 FA(I1)=XIP(I)                                                     MULSMP.191
C                                                                       MULSMP.192
C      SET K  SO THAT AT COMPUTED GOTO WILL BRANCH TO UPPER LIMIT       MULSMP.193
C      (STATEMENT 12) .                                                 MULSMP.194
C                                                                       MULSMP.195
      K(I1)=2                                                           MULSMP.196
C                                                                       MULSMP.197
C      SET COORDINATES TO UPPER LIMIT OF CURRENT DIMENSION.             MULSMP.198
C                                                                       MULSMP.199
      B(I1)=BLIM(I1)                                                    MULSMP.200
      XNEW(I1)=B(I1)                                                    MULSMP.201
C                                                                       MULSMP.202
C      NOW BEGIN INTEGRATION OVER ALL LOWER DIMENSIONS WITH THE HIGHEST MULSMP.203
C      DIMENSION SET AT ITS UPPER LIMIT                                 MULSMP.204
C                                                                       MULSMP.205
      GO TO 3                                                           MULSMP.206
C                                                                       MULSMP.207
C                                                                       MULSMP.208
C      SAVE VALUE OF INTEGRAND AT UPPER LIMIT OF CURRENT MAXIMUM        MULSMP.209
C      DIMENSION.                                                       MULSMP.210
C                                                                       MULSMP.211
   12 FB(I1)=XIP(I)                                                     MULSMP.212
C                                                                       MULSMP.213
C      SET K TO BRANCH TO STATEMENT 13 ON COMPUTED GOTO TO BEGIN        MULSMP.214
C      SIMPSON'N INTEGRATION FOR CURRENT DIMENSION, NOW THAT THE UPPER  MULSMP.215
```

```
C      LOWER LIMITS OF THE INTGRAND ARE DEFINED.                          MULSMP.216
C                                                                         MULSMP.217
      K(I1)=3                                                             MULSMP.218
      I=I1                                                                MULSMP.219
      GO TO 1000                                                          MULSMP.220
C                                                                         MULSMP.221
C                                                                         MULSMP.222
C      FNEWX CONTAINS THE VALUE OF THE INTEGRAND AT CURRENT MESH POINT. MULSMP.223
C      STORE IT AND CONTINUE INTEGRATION OVER ALL LOWER DIMENSIONS TO   MULSMP.224
C      ACHIEVE INTEGRAND VALUE AT NEXT MESH POINT.                        MULSMP.225
C                                                                         MULSMP.226
   13 FNEWX(I1)=XIP(I)                                                    MULSMP.227
      I=I1                                                                MULSMP.228
      GO TO 1001                                                          MULSMP.229
C                                                                         MULSMP.230
C      INTEGRAL COMPLETED WITH CONVERGENCE OBTAINED.                      MULSMP.231
C                                                                         MULSMP.232
   16 VALUE=XIP(N)                                                        MULSMP.233
      IXIT = 1                                                            MULSMP.234
 1014 RETURN                                                              MULSMP.235
C                                                                         MULSMP.236
C     ERROR EXITS                                                         MULSMP.237
C                                                                         MULSMP.238
C                                                                         MULSMP.239
C      NO CONVERGENCE WITHIN SPECIFIED NUMBER OF ITERATIONS               MULSMP.240
C                                                                         MULSMP.241
 1011  CONTINUE                                                           MULSMP.242
      WRITE(6,1013)                                                       MULSMP.243
      WRITE(6,1012) I,INDEX(I)                                            MULSMP.244
      VALUE=0.                                                            MULSMP.247
      IXIT = 2                                                            MULSMP.248
      GO TO 1014                                                          MULSMP.250
C                                                                         MULSMP.251
 5     CONTINUE                                                           MULSMP.252
C                                                                         MULSMP.253
C      UPPER BOUND LESS THAN LOWER BOUND                                  MULSMP.254
C                                                                         MULSMP.255
       WRITE(6,1013)                                                      MULSMP.256
      WRITE(6,6) I,A(I),I,B(I)                                            MULSMP.257
      VALUE = 0.                                                          MULSMP.260
      IXIT = 3                                                            MULSMP.261
      GO TO 1014                                                          MULSMP.262
C                                                                         MULSMP.263
7     CONTINUE                                                            MULSMP.264
C                                                                         MULSMP.265
C      STEP SIZE IS ZERO                                                  MULSMP.266
C                                                                         MULSMP.267
      WRITE(6,1013)                                                       MULSMP.268
      WRITE(6,8) I,INDEX(I),I,A(I),I,B(I)                                 MULSMP.269
      XIP(I) = XI(I)                                                      MULSMP.273
      GO TO 1009                                                          MULSMP.274
C                                                                         MULSMP.275
C      RETURN VALUE AT THE CENTER OF THE DETECTOR COORDINATES FOR         MULSMP.276
```

```
C      POINT DETECTOR APPROXIMATION                                      MULSMP.277
C                                                                        MULSMP.278
 2001 XNEW(1)=(ALIM(1)+BLIM(1))/2.                                       MULSMP.279
      XNEW(2)=(ALIM(2)+BLIM(2))/2.                                       MULSMP.280
      VALUE=FINT(XNEW)                                                   MULSMP.281
      IXIT=1                                                             MULSMP.282
      GOTO 1014                                                          MULSMP.283
C
C
C       FORMAT STATEMENST
C
C
 100  FORMAT(10X,*DIMENSION*,10X,*ITERATION*,10X,*APPROXIMATION*,10X,*ERMULSMP.48
     $ROR*,10X,*DIFFERENCE*)                                             MULSMP.49
 101  FORMAT(10X,I5,15X,I5,11X,E14.7,5X,E14.7,10X,E14.7)                 MULSMP.160
 1012 FORMAT (4HOTHE,I3,34H INTEGRAL HAS NOT CONVERGED AFTER ,I3,        MULSMP.245
     X        11H ITERATIONS)                                            MULSMP.246
 1013 FORMAT(10X,* ERROR FROM MULSMP INTEGRATION ROUTINE*)               MULSMP.249
    6 FORMAT (///12H NOTE.....A(I2,2H)=1PE20.8/                          MULSMP.258
    61        10X2HB(I2,2H)=E20.8)                                       MULSMP.259
    8 FORMAT (///23H THE STEP SIZE FOR THE I1,21H INTEGRAL = 0 ON THE    MULSMP.270
    81        I5,11H ITERATION.//3H A(I1,3H) =1PE15.4/3H B(I1,3H) =      MULSMP.271
    82        E15.4)                                                     MULSMP.272
      END                                                                MULSMP.284


                                                                         MULSMP.285
      SUBROUTINE WEIGHTS(XL,YL,ZL,NPRI1)                                 WEIGHTS.2
C                                                                        WEIGHTS.3
C      FUNCTION- DETERMINE QUADRUTURE POINTS AND WEIGHTS FOR THE         WEIGHTS.4
C      COLLISION VOLUME INTEGRATION AND THE SEMI-CLASSICAL PHASE SHIFT   WEIGHTS.5
C      INTEGRATION.                                                      WEIGHTS.6
C                                                                        WEIGHTS.7
C      ARGUMENTS- XL,YL,ZL ON INPUT ARE THE X,Y,Z DIMENSIONS OF THE      WEIGHTS.8
C      COLLISION VOLUME.                                                 WEIGHTS.9
C      NPRI1 =1, THEN THE COLLISION VOLUME GRID IS PRINTED               WEIGHTS.10
C            =0, NO PRINTING                                             WEIGHTS.11
C      ON OUTPUT, THE COMMON BLOCK VOL CONTAINS THE INTEGRATION POInts   weights.12
C      AND WEIGHTS FOR THE COLLISION VOLUME INTEGRATION                  WEIGHTS.13
C      THE COMMON BLOCK PHSWTS CONTAINS THE INTEGRATION POINTS AND       WEIGHTS.14
C      WEIGHTS FOR THE SEMICLASSICAL PHASE SHIFT INTEGRALS               WEIGHTS.15
C                                                                        WEIGHTS.16
C      SUBPROGRAMS- NONE                                                 WEIGHTS.17
C                                                                        WEIGHTS.18
C      REFERENCE- M.F. VERNON                                            WEIGHTS.19
C                                                                        WEIGHTS.20
      COMMON/EN/ENERGY(125),CMTH1(125),CMTH2(125),WGHT1(125),WGHT2(125),EN.2
     1NCOLX,NCOLY,NCOLZ,IAPPRX                                           EN.3
      COMMON/PHSWTS/XQ(10),WQ(10),NXQ                                    PHSWTS.2
      COMMON/VOL/X(5),Y(5),Z(5),WX(5),WY(5),WZ(5)                        VOL.2
      DIMENSION GXQ(10),GWQ(10)                                          WEIGHTS.24
      DATA(GXQ(I),I=1,7)/.20119,.39415,.57097,.72442,.84821,.93727,.9879WEIGHTS.25
```

```
     19/                                                                WEIGHTS.26
      DATA(GWQ(I),I=1,7)/.19843,.18616,.16627,.13957,.10716,.07037,.0307WEIGHTS.27
     15/                                                                WEIGHTS.28
C                                                                       WEIGHTS.29
C     SET UP GAUSSIAN QUADRUTURE POINTS AND WEIGHTS FOR THE SEMI-       WEIGHTS.30
C     CLASSICAL PHASE SHIFT ROUTINE                                     WEIGHTS.31
C                                                                       WEIGHTS.32
      NXQ=7                                                             WEIGHTS.33
      DO 5 I=1,NXQ                                                      WEIGHTS.34
      XQ(I)=1.-GXQ(I)*GXQ(I)                                            WEIGHTS.35
      WQ(I)=2.*GXQ(I)*GXQ(I)*GWQ(I)                                     WEIGHTS.36
 5     CONTINUE                                                         WEIGHTS.37
C                                                                       WEIGHTS.38
C     THIS COMPUTES THE POSITIONS AND WEIGHTS USED IN THE INTEGRATION   WEIGHTS.39
C     OVER THE COLLISION VOLUME. CURRENTLY THE MAXIMUM NUMBER OF POINTS WEIGHTS.40
C     IN ANY ONE DIMENSION IS FIVE. IF A LARGER VALUE IS TRIED, IT IS   WEIGHTS.41
C     SET TO THIS MAXIMUM VALUE AND A MESSAGE PRINTED.                  WEIGHTS.42
C                                                                       WEIGHTS.43
      NMAX=5                                                            WEIGHTS.44
      IF(NCOLX.LE.NMAX) GOTO 10                                         WEIGHTS.45
      NCOLX=NMAX                                                        WEIGHTS.46
      WRITE(6,1) NMAX                                                   WEIGHTS.47
 10   IF(NCOLX-2) 11,12,13                                              WEIGHTS.49
C     NCOLX=1                                                           WEIGHTS.50
 11   X(1)=0.                                                           WEIGHTS.51
      WX(1)=1.                                                          WEIGHTS.52
      GOTO 19                                                           WEIGHTS.53
C     NCOLX=2                                                           WEIGHTS.54
 12   CONTINUE                                                          WEIGHTS.55
      X(1)=-.577   $X(2)=-X(1)$WX(1)=1.$WX(2)=1.                        WEIGHTS.56
      GOTO 19                                                           WEIGHTS.57
 13   IF(NCOLX-4) 14,15,16                                              WEIGHTS.58
C     NCOLX=3                                                           WEIGHTS.59
 14   CONTINUE                                                          WEIGHTS.60
      X(1)=-.775$X(2)=0.$X(3)=-X(1)$WX(1)=5./9.$WX(2)=8./9.$WX(3)=WX(1) WEIGHTS.61
      GOTO 19                                                           WEIGHTS.62
C     NCOLX=4                                                           WEIGHTS.63
 15   CONTINUE                                                          WEIGHTS.64
      X(1)=-.861$X(2)=-.339$X(3)=-X(2)$X(4)=-X(1)$WX(1)=.348$WX(2)=.652 WEIGHTS.65
     1$WX(3)=WX(2)$WX(4)=WX(1)                                          WEIGHTS.66
      GOTO 19                                                           WEIGHTS.67
C     NCOLX=5                                                           WEIGHTS.68
 16   CONTINUE                                                          WEIGHTS.69
      X(1)=-.906$X(2)=-.538$X(3)=0.$X(4)=-X(2)$X(5)=-X(1)               WEIGHTS.70
      WX(1)=.237$WX(2)=.478$WX(3)=.569$WX(4)=WX(2)$WX(5)=WX(1)          WEIGHTS.71
 19   IF(NCOLY.LE.NMAX) GOTO 20                                         WEIGHTS.72
      NCOLY=NMAX                                                        WEIGHTS.73
      WRITE(6,2) NMAX                                                   WEIGHTS.74
 20   IF(NCOLY-2) 21,22,23                                              WEIGHTS.76
C     NCOLY=1                                                           WEIGHTS.77
 21   Y(1)=0.                                                           WEIGHTS.78
      WY(1)=1.                                                          WEIGHTS.79
      GOTO 29                                                           WEIGHTS.80
```

```
C     NCOLY=2                                                           WEIGHTS.81
 22   CONTINUE                                                          WEIGHTS.82
      Y(1)=-.577$Y(2)=-Y(1)$WY(1)=1.$WY(2)=1.                           WEIGHTS.83
      GOTO 29                                                           WEIGHTS.84
 23   IF(NCOLY-4) 24,25,26                                              WEIGHTS.85
C     NCOLY=3                                                           WEIGHTS.86
 24   CONTINUE                                                          WEIGHTS.87
      Y(1)=-.775$Y(2)=0.$Y(3)=-Y(1)$WY(1)=5./9.$WY(2)=8./9.$WY(3)=WY(1) WEIGHTS.88
      GOTO 29                                                           WEIGHTS.89
C     NCOLY=4                                                           WEIGHTS.90
 25   CONTINUE                                                          WEIGHTS.91
      Y(1)=-.861$Y(2)=-.340$Y(3)=-Y(2)$Y(4)=-Y(1)$WY(1)=.237$WY(2)=.478 WEIGHTS.92
      WY(3)=WY(2)$WY(4)=WY(1)                                           WEIGHTS.93
      GOTO 29                                                           WEIGHTS.94
C     NCOLY=5                                                           WEIGHTS.95
 26   CONTINUE                                                          WEIGHTS.96
      Y(1)=-.906$Y(2)=-.538$Y(3)=0.$Y(4)=-Y(2)$Y(5)=-Y(1)               WEIGHTS.97
      WY(1)=.237$WY(2)=.479$WY(3)=.569$WY(4)=WY(2)$WY(5)=WY(1)          WEIGHTS.98
 29   IF(NCOLZ.LE.NMAX) GOTO 30                                         WEIGHTS.99
      NCOLZ=NMAX                                                        WEIGHTS.100
      WRITE(6,3) NMAX                                                   WEIGHTS.101
 30   IF(NCOLZ-2) 31,32,33                                              WEIGHTS.103
C     NCOLZ=1                                                           WEIGHTS.104
 31   Z(1)=0.                                                           WEIGHTS.105
      WZ(1)=1.                                                          WEIGHTS.106
      GOTO 39                                                           WEIGHTS.107
C     NCOLZ=2                                                           WEIGHTS.108
 32   CONTINUE                                                          WEIGHTS.109
      Z(1)=-.577$Z(2)=-Z(1)$WZ(1)=1.$WZ(2)=1.                           WEIGHTS.110
      GOTO 39                                                           WEIGHTS.111
 33    IF(NCOLZ-4) 34,35,36                                             WEIGHTS.112
C     NCOLZ=3                                                           WEIGHTS.113
 34   CONTINUE                                                          WEIGHTS.114
      Z(1)=-.775$Z(2)=0.$Z(3)=-Z(1)$WZ(1)=5./9.$WZ(2)=8./9.$WZ(3)=WZ(1) WEIGHTS.115
      GOTO 39                                                           WEIGHTS.116
C     NCOLZ=4                                                           WEIGHTS.117
 35   CONTINUE                                                          WEIGHTS.118
      Z(1)=-.861$Z(2)=-.340$Z(3)=-Z(2)$Z(4)=-Z(1)$WZ(1)=.349$WZ(2)=.652 WEIGHTS.119
      WZ(3)=WZ(2)$WZ(4)=WZ(1)                                           WEIGHTS.120
      GOTO 39                                                           WEIGHTS.121
C     NCOLZ=5                                                           WEIGHTS.122
 36   CONTINUE                                                          WEIGHTS.123
      Z(1)=-.906$Z(2)=-.538$Z(3)=0.$Z(4)=-Z(2)$Z(5)=-Z(1)               WEIGHTS.124
      WZ(1)=.237$WZ(2)=.479$WZ(3)=.569$WZ(4)=WZ(2)$WZ(5)=WZ(1)          WEIGHTS.125
C                                                                       WEIGHTS.126
C      CONVERT FROM UNIT INTERVAL TO ACTUAL COLLISION VOLUME DIMENSIONS WEIGHTS.127
C                                                                       WEIGHTS.128
 39   DO 40 I=1,NCOLX                                                   WEIGHTS.129
      X(I)=X(I)*XL/2.                                                   WEIGHTS.130
 40   CONTINUE                                                          WEIGHTS.131
      DO 45 I=1,NCOLY                                                   WEIGHTS.132
      Y(I)=Y(I)*YL/2.                                                   WEIGHTS.133
 45   CONTINUE                                                          WEIGHTS.134
```

```
      DO 50 I=1,NCOLZ                                                   WEIGHTS.135
      Z(I)=Z(I)*ZL/2.                                                   WEIGHTS.136
 50   CONTINUE                                                          WEIGHTS.137
      IF(NPRI1.EQ.0) GOTO 80                                            WEIGHTS.138
      WRITE(6,1037)                                                     WEIGHTS.139
      WRITE(6,99)                                                       WEIGHTS.141
      WRITE(6,100)                                                      WEIGHTS.143
      DO 60 I=1,NCOLX                                                   WEIGHTS.145
      DO 60 J=1,NCOLY                                                   WEIGHTS.146
      DO 60 K=1,NCOLZ                                                   WEIGHTS.147
 60   WRITE(6,70) X(I),Y(J),Z(K),WX(I)*WY(J)*WZ(K)                      WEIGHTS.148
 80   RETURN                                                            WEIGHTS.150
C
C
C      FORMAT STATEMENTS
C
C
 1    FORMAT(10X,*NCOLX LARGER THAN NMAX, THEREFORE SET TO NMAX=*,I5)   WEIGHTS.48
 2    FORMAT(10X,*NCOLY EXCEEDS NMAX. SET TO NMAX=*,I5)                 WEIGHTS.75
 3    FORMAT(10X,*NCOLZ EXCEEDS NMAX, SET TO NMAX=*,I5)                 WEIGHTS.102
 1037 FORMAT(///)                                                       WEIGHTS.140
 99   FORMAT(30X,*C O L L I S I O N  V O L U M E   G R I D*,/)         WEIGHTS.142
 100  FORMAT(4X,*X*,9X,*Y*,9X,*Z*,6X,*WEIGHT*,/)                       WEIGHTS.144
 70   FORMAT(4(F7.4,3X),5X,4(F7.4,3X),5X,4(F7.4,3X))                   WEIGHTS.149
      END                                                               WEIGHTS.151
                                                                        WEIGHTS.152
      SUBROUTINE NOZZLE(NVL,VB,FB,VZRO,BETA)                            NOZZLE.2
      DIMENSION FB(1),VB(1)                                             NOZZLE.3
C                                                                       NOZZLE.4
C      FUNCTION -GIVEN A NOZZLE BEAM VELOCITY DISTRIBUTION DESCRIBED BY NOZZLE.5
C      THE TWO PARAMETERS VZRO,BETA, CALCULATE A SET OF VELOCITIES AND  NOZZLE.6
C      RELATIVE WEIGHTS USED IN AVERAGING EXPERIMENTAL SCATTERING DATA  NOZZLE.7
C      OVER THE FINITE VELOCITY DISTRIBUTIONS OF THE MOLECULAR BEAMS.   NOZZLE.8
C      THE NOZZLE BEAM NUMBER DENSITY DISTRIBUTION IS ASSUMED TO BE OF  NOZZLE.9
C      THE FORM                                                         NOZZLE.10
C
C         I(V)=V*V*EXP(-BETA*(V-VZRO)**2)                               NOZZLE.11
C                                                                       NOZZLE.12
C      THE DETERMINATION OF THE PARAMETERS BETA AND VZRO IS DONE USING  NOZZLE.13
C      THE PROGRAM KELVIN DESCRIBED IN LBL REPORT                       NOZZLE.14
C      THE CONTINUOUS DISTRIBUTION I(V) IS REPLACED BY A DISCRETE SET   NOZZLE.15
C      OF VELOCITIES,VB(I),WITH RELATIVE WEIGHT FACTORS,FB(I).          NOZZLE.16
C      ARGUMENTS                                                        NOZZLE.17
C      NVL- THE NUMBER OF DISCRETE VELOCITIES USED IN APPROXIMATING THE NOZZLE.18
C      CONTINUOUS VELOCITY DISTRIBUTION.                                NOZZLE.19
C      VB- ON OUTPUT CONTAINS THE AVERAGE VELOCITY FOR THE NVL INTERVALSNOZZLE.20
C      FB- ON OUTPUT CONTAINS THE NORMAIZED INTENSITY OF THE NVL        NOZZLE.21
C      VELOCITY SEGMENTS                                                NOZZLE.22
C      VZRO,BETA- ON INPUT THE TWO PARAMETERS DEFINING THE BEAM VELOCITYNOZZLE.23
C      DISTRIBUTION                                                     NOZZLE.24
C                                                                       NOZZLE.25
C      SUBPROGRAMS CALLED- FLOAT,SQRT,EXP                               NOZZLE.26
C                                                                       NOZZLE.27
```

```
C      REFERENCE- M.F. VERNON, 1982                                    NOZZLE.28
C
C
      PI=3.1415926                                                     NOZZLE.29
      RNORM=SQRT(PI/BETA)*(1./VZRO**2+1./2./BETA)                      NOZZLE.30
      S=1./SQRT(BETA)                                                  NOZZLE.31
      IF(NVL-1) 100,110,120                                            NOZZLE.32
 120  IF(NVL-3)130,140,150                                             NOZZLE.33
 150  IF(NVL-5) 160,170,180                                            NOZZLE.34
 180  IF(NVL-7) 190,200,210                                            NOZZLE.35
 210  IF(NVL-9) 220,230,240                                            NOZZLE.36
 100   CONTINUE                                                        NOZZLE.37
      WRITE(6,101)                                                     NOZZLE.38
      STOP                                                             NOZZLE.40
C ONE                                                                  NOZZLE.41
 110   CONTINUE                                                        NOZZLE.42
      VB(1)=VZRO                                                       NOZZLE.43
      FB(1)=VZRO**2/RNORM                                              NOZZLE.44
      GOTO 250                                                         NOZZLE.45
C      TWO                                                             NOZZLE.46
 130   CONTINUE                                                        NOZZLE.47
      T=.7071*S                                                        NOZZLE.48
      VB(1)=VZRO-T                                                     NOZZLE.49
      VB(2)=VZRO+T                                                     NOZZLE.50
      FB(1)=VB(1)**2*.88623/RNORM                                      NOZZLE.51
      FB(2)=VB(2)**2*.88623/RNORM                                      NOZZLE.52
      GOTO 250                                                         NOZZLE.53
C      THREE                                                           NOZZLE.54
 140   CONTINUE                                                        NOZZLE.55
      T=1.2247*S                                                       NOZZLE.56
      VB(1)=VZRO-T                                                     NOZZLE.57
      VB(2)=VZRO                                                       NOZZLE.58
      VB(3)=VZRO+T                                                     NOZZLE.59
      FB(1)=VB(1)**2*2.95409E-01/RNORM                                 NOZZLE.60
      FB(2)=VB(2)**2*1.18164/RNORM                                     NOZZLE.61
      FB(3)=VB(3)**2*.295409/RNORM                                     NOZZLE.62
      GOTO 250                                                         NOZZLE.63
C      FOUR                                                            NOZZLE.64
 160   CONTINUE                                                        NOZZLE.65
      T1=.5246*S                                                       NOZZLE.66
      T2=1.6507*S                                                      NOZZLE.67
      VB(1)=VZRO-T2                                                    NOZZLE.68
      VB(2)=VZRO-T1                                                    NOZZLE.69
      VB(3)=VZRO+T1                                                    NOZZLE.70
      VB(4)=VZRO+T2                                                    NOZZLE.71
      FB(1)=VB(1)**2*8.13128E-02/RNORM                                 NOZZLE.72
      FB(2)=VB(2)**2*8.04914E-01/RNORM                                 NOZZLE.73
      FB(3)=VB(3)**2*8.04914E-01/RNORM                                 NOZZLE.74
      FB(4)=VB(4)**2*8.13128E-02/RNORM                                 NOZZLE.75
      GOTO 250                                                         NOZZLE.76
C     FIVE                                                             NOZZLE.77
 170   CONTINUE                                                        NOZZLE.78
      T1=.95857*S                                                      NOZZLE.79
```

```
      T2=2.02018*S                                                      NOZZLE.80
      VB(1)=VZRO-T2                                                     NOZZLE.81
      VB(2)=VZRO-T1                                                     NOZZLE.82
      VB(3)=VZRO                                                        NOZZLE.83
      VB(4)=VZRO+T1                                                     NOZZLE.84
      VB(5)=VZRO+T2                                                     NOZZLE.85
      FB(1)=VB(1)**2*1.99532E-02/RNORM                                  NOZZLE.86
      FB(2)=VB(2)**2*3.93619E-01/RNORM                                  NOZZLE.87
      FB(3)=VB(3)**2*9.45309E-01/RNORM                                  NOZZLE.88
      FB(4)=VB(4)**2*.393619/RNORM                                      NOZZLE.89
      FB(5)=VB(5)**2*1.99532E-02/RNORM                                  NOZZLE.90
      GOTO 250                                                          NOZZLE.91
C      SIX                                                              NOZZLE.92
  190   CONTINUE                                                        NOZZLE.93
      T1=.436077*S                                                      NOZZLE.94
      T2=1.335849*S                                                     NOZZLE.95
      T3=2.35060*S                                                      NOZZLE.96
      VB(1)=VZRO-T3                                                     NOZZLE.97
      VB(2)=VZRO-T2                                                     NOZZLE.98
      VB(3)=VZRO-T1                                                     NOZZLE.99
      VB(4)=VZRO+T1                                                     NOZZLE.100
      VB(5)=VZRO+T2                                                     NOZZLE.101
      VB(6)=VZRO+T3                                                     NOZZLE.102
      FB(1)=VB(1)**2*4.53001E-03/RNORM                                  NOZZLE.103
      FB(2)=VB(2)**2*1.57067E-01/RNORM                                  NOZZLE.104
      FB(3)=VB(3)**2*7.246296E-01/RNORM                                 NOZZLE.105
      FB(4)=VB(4)**2*7.246296E-01/RNORM                                 NOZZLE.106
      FB(5)=VB(5)**2*1.57067E-01/RNORM                                  NOZZLE.107
      FB(6)=VB(6)**2*4.53001E-03/RNORM                                  NOZZLE.108
      GOTO 250                                                          NOZZLE.109
C      SEVEN                                                            NOZZLE.110
  200   CONTINUE                                                        NOZZLE.111
      T1=.81629*S                                                       NOZZLE.112
      T2=1.67355*S                                                      NOZZLE.113
      T3=2.65196*S                                                      NOZZLE.114
      VB(1)=VZRO-T3                                                     NOZZLE.115
      VB(2)=VZRO-T2                                                     NOZZLE.116
      VB(3)=VZRO-T1                                                     NOZZLE.117
      VB(4)=VZRO                                                        NOZZLE.118
      VB(5)=VZRO+T1                                                     NOZZLE.119
      VB(6)=VZRO+T2                                                     NOZZLE.120
      VB(7)=VZRO+T3                                                     NOZZLE.121
      FB(1)=VB(1)**2*9.71781E-04/RNORM                                  NOZZLE.122
      FB(2)=VB(2)**2*5.45156E-02/RNORM                                  NOZZLE.123
      FB(3)=VB(3)**2*4.25607E-01/RNORM                                  NOZZLE.124
      FB(4)=VB(4)**2*8.10264E-01/RNORM                                  NOZZLE.125
      FB(5)=VB(5)**2*4.25607E-01/RNORM                                  NOZZLE.126
      FB(6)=VB(6)**2*5.45156E-02/RNORM                                  NOZZLE.127
      FB(7)=VB(7)**2*9.71781E-04/RNORM                                  NOZZLE.128
      GOTO 250                                                          NOZZLE.129
C      EIGHT                                                            NOZZLE.130
  220   CONTINUE                                                        NOZZLE.131
      T1=.381187*S                                                      NOZZLE.132
```

```
      T2=1.15719*S                                                      NOZZLE.133
      T3=1.98166*S                                                      NOZZLE.134
      T4=2.93064*S                                                      NOZZLE.135
      VB(1)=VZRO-T4                                                     NOZZLE.136
      VB(2)=VZRO-T3                                                     NOZZLE.137
      VB(3)=VZRO-T2                                                     NOZZLE.138
      VB(4)=VZRO-T1                                                     NOZZLE.139
      VB(5)=VZRO+T1                                                     NOZZLE.140
      VB(6)=VZRO+T2                                                     NOZZLE.141
      VB(7)=VZRO+T3                                                     NOZZLE.142
      VB(8)=VZRO+T4                                                     NOZZLE.143
      FB(1)=VB(1)**2*1.99604E-04/RNORM                                  NOZZLE.144
      FB(2)=VB(2)**2*1.707798E-02/RNORM                                 NOZZLE.145
      FB(3)=VB(3)**2*.207802/RNORM                                      NOZZLE.146
      FB(4)=VB(4)**2*.661147/RNORM                                      NOZZLE.147
      FB(5)=VB(5)**2*.661147/RNORM                                      NOZZLE.148
      FB(6)=VB(6)**2*.207802/RNORM                                      NOZZLE.149
      FB(7)=VB(7)**2*1.707798E-02/RNORM                                 NOZZLE.150
      FB(8)=VB(8)**2*1.96604E-04/RNORM                                  NOZZLE.151
      GOTO 250                                                          NOZZLE.152
C      NINE                                                             NOZZLE.153
 230   CONTINUE                                                          NOZZLE.154
      T1=.72355*S                                                       NOZZLE.155
      T2=1.46855*S                                                      NOZZLE.156
      T3=2.26658*S                                                      NOZZLE.157
      T4=3.19099*S                                                      NOZZLE.158
      VB(1)=VZRO-T4                                                     NOZZLE.159
      VB(2)=VZRO-T3                                                     NOZZLE.160
      VB(3)=VZRO-T2                                                     NOZZLE.161
      VB(4)=VZRO-T1                                                     NOZZLE.162
      VB(5)=VZRO                                                        NOZZLE.163
      VB(6)=VZRO+T1                                                     NOZZLE.164
      VB(7)=VZRO+T2                                                     NOZZLE.165
      VB(8)=VZRO+T3                                                     NOZZLE.166
      VB(9)=VZRO+T4                                                     NOZZLE.167
      FB(1)=VB(1)**2*3.96070E-05/RNORM                                  NOZZLE.168
      FB(2)=VB(2)**2*4.94362E-03/RNORM                                  NOZZLE.169
      FB(3)=VB(3)**2*8.84745E-02/RNORM                                  NOZZLE.170
      FB(4)=VB(4)**2*4.32652E-01/RNORM                                  NOZZLE.171
      FB(5)=VB(5)**2*7.20235E-01/RNORM                                  NOZZLE.172
      FB(6)=VB(6)**2*4.32652E-01/RNORM                                  NOZZLE.173
      FB(7)=VB(7)**2*8.84745E-02/RNORM                                  NOZZLE.174
      FB(8)=VB(8)**2*4.94362E-03/RNORM                                  NOZZLE.175
      FB(9)=VB(9)**2*3.96070E-05/RNORM                                  NOZZLE.176
      GOTO 250                                                          NOZZLE.177
C      TEN                                                              NOZZLE.178
 240   CONTINUE                                                          NOZZLE.179
      T1=.34290*S                                                       NOZZLE.180
      T2=1.03661*S                                                      NOZZLE.181
      T3=1.75668*S                                                      NOZZLE.182
      T4=2.53273*S                                                      NOZZLE.183
      T5=3.43616*S                                                      NOZZLE.184
      VB(1)=VZRO-T5                                                     NOZZLE.185
```

```
      VB(2)=VZRO-T4                                                     NOZZLE.186
      VB(3)=VZRO-T3                                                     NOZZLE.187
      VB(4)=VZRO-T2                                                     NOZZLE.188
      VB(5)=VZRO-T1                                                     NOZZLE.189
      VB(6)=VZRO+T1                                                     NOZZLE.190
      VB(7)=VZRO+T2                                                     NOZZLE.191
      VB(8)=VZRO+T3                                                     NOZZLE.192
      VB(9)=VZRO+T4                                                     NOZZLE.193
      VB(10)=VZRO+T5                                                    NOZZLE.194
      FB(1)=VB(1)**2*7.6404E-06/RNORM                                   NOZZLE.195
      FB(2)=VB(2)**2*1.34364E-03/RNORM                                  NOZZLE.196
      FB(3)=VB(3)**2*3.3874E-02/RNORM                                   NOZZLE.197
      FB(4)=VB(4)**2*2.40139E-01/RNORM                                  NOZZLE.198
      FB(5)=VB(5)**2*6.10862E-01/RNORM                                  NOZZLE.199
      FB(6)=VB(6)**2*6.10862E-01/RNORM                                  NOZZLE.200
      FB(7)=VB(7)**2*2.40139E-01/RNORM                                  NOZZLE.201
      FB(8)=VB(8)**2*3.3874E-02/RNORM                                   NOZZLE.202
      FB(9)=VB(9)**2*1.34364E-03/RNORM                                  NOZZLE.203
      FB(10)=VB(10)**2*7.6404E-06/RNORM                                 NOZZLE.204
 250   CONTINUE                                                         NOZZLE.205
      WRITE(6,30)                                                       NOZZLE.206
      WRITE(6,40)(VB(I)   ,I=1,NVL)                                     NOZZLE.209
      WRITE(6,40)(FB(I)   ,I=1,NVL)                                     NOZZLE.210
      WRITE(6,41)                                                       NOZZLE.212
      RETURN                                                            NOZZLE.214
C
C
C       FORMAT STATEMENTS
C
C
 101   FORMAT(5X,*NUMBER OF NEWTON DIAGRAMS ZERO*)                      NOZZLE.39
  30   FORMAT(10X,*VELOCITIES (UNITS OF 10,000 CM/SEC)  /RELATIVE WEIGHTSNOZZLE.207
     1*,/)                                                              NOZZLE.208
  40   FORMAT(10(1X,F11.4))                                             NOZZLE.211
  41   FORMAT(/)                                                        NOZZLE.213
      END                                                               NOZZLE.215


      SUBROUTINE PHSHFT(A,RM,NPRI1)                                     PHASE1.2
C                                                                       PHASE1.3
C     JWKB PHASE SHIFTS EVALUATED WITH GAUSS QUADRATURE                 PHASE1.4
C     CODED BY CARL HAYDEN                                              PHASE1.5
C     SQRT(1-X) WEIGHTING FUNCTION                                      PHASE1.6
C     FOR DETAILS SEE JAMES S. COHEN, JCP,68,PG.1841 (1978).            PHASE1.7
C                                                                       PHASE1.8
      COMMON/ETA/STHE(8000),CTHE(8000),NETA,DETA,IDENT                  ETA.2
     $,IBOSE                                                            ETA.3
      COMMON/PHSWTS/XQ(10),WQ(10),NXQ                                   PHSWTS.2
      COMMON/EN/ENERGY(125),CMTH1(125),CMTH2(125),WGHT1(125),WGHT2(125),EN.2
     1NCOLX,NCOLY,NCOLZ,IAPPRX                                          EN.3
      DIMENSION A(15),X(10),V(10),VP(10)                                PHASE1.12
      DIMENSION Y(250),YPP(250),Z(250),ZPP(250),W(750)                  PHASE1.13
```

```
      REAL KR2,KR,KEX,KEX2                                              PHASE1.14
      NSTEP=INT(DETA)                                                   PHASE1.15
C                                                                       PHASE1.16
C     FOR INTERPOLATED PHASE SHIFTS, NEED ADDITIONAL NETAS.             PHASE1.17
C                                                                       PHASE1.18
      IF(NSTEP.NE.1) NETA=NETA+NSTEP                                    PHASE1.19
      NPHASE=NETA/NSTEP                                                 PHASE1.20
      ISX=0                                                             PHASE1.21
      NVOL=NCOLX*NCOLY*NCOLZ                                            PHASE1.22
C                                                                       PHASE1.23
C     IAPPRX=1, THEN ALL POINTS IN THE COLLISION VOLUME HAVE THE SAME   PHASE1.24
C     PHASE SHIFT. CALCULATE ONLY ONE SET OF PHASE SHIFTS FOR THIS      PHASE1.25
C     NEWTON DIAGRAM.                                                   PHASE1.26
C                                                                       PHASE1.27
      IF(IAPPRX.EQ.1) NVOL=1                                            PHASE1.28
      IF(NPRI1.NE.1) GOTO  99                                           PHASE1.29
      WRITE(6,104)                                                      PHASE1.30
      WRITE(6,103)(ENERGY(I),I=1,NVOL)                                  PHASE1.32
      WRITE(6,105)                                                      PHASE1.33
      WRITE(6,102)                                                      PHASE1.35
 99   DO 500 II=1,NVOL                                                  PHASE1.38
C                                                                       PHASE1.39
C     ER IS THE REDUCED COLLISION ENERGY                                PHASE1.40
C                                                                       PHASE1.41
      ER=ENERGY(II)/A(1)                                                PHASE1.42
C                                                                       PHASE1.43
C     ITEMP IS INDEX FOR STORING PHASE SHIFTS AT EACH ENERGY.           PHASE1.44
C                                                                       PHASE1.45
      ITEMP=(II-1)*NETA                                                 PHASE1.46
      ERSR=SQRT(ER)                                                     PHASE1.47
      KR2=20.7481*RM*A(1)*(A(2)**2)                                     PHASE1.48
      KR=SQRT(KR2)                                                      PHASE1.49
      CONST=KR*ERSR                                                     PHASE1.50
C                                                                       PHASE1.51
C      FIRST GUESS AT TURNING POINT                                     PHASE1.52
C                                                                       PHASE1.53
      XC=0.6                                                            PHASE1.54
C                                                                       PHASE1.55
C     AMQN IS THE ORBITAL ANGULAR MOMENTUM                              PHASE1.56
C                                                                       PHASE1.57
      AMQN=0                                                            PHASE1.58
C                                                                       PHASE1.59
C     FOR EACH PARTIAL WAVE                                             PHASE1.60
C                                                                       PHASE1.61
      J=0                                                               PHASE1.62
      DO 60 I=1,NETA,NSTEP                                              PHASE1.63
      J=J+1                                                             PHASE1.64
      AM=AMQN+0.5                                                       PHASE1.65
      AM2=AM*AM                                                         PHASE1.66
      L=1                                                               PHASE1.67
C                                                                       PHASE1.68
C     CALCULATE CLASSICAL TURNING POINT                                 PHASE1.69
C                                                                       PHASE1.70
```

```
      DO 10 M=1,199                                                     PHASE1.71
      X(L)=XC                                                           PHASE1.72
      CALL POT(X,A,V,VP,L,RM)                                           PHASE1.73
      X2=X(L)*X(L)                                                      PHASE1.74
      XC=X(L)-((ER-V(L)-(AM2/(KR2*X2)))/((2*AM2)/(KR2*X2*X(L))-VP(L)))  PHASE1.75
      IF(ABS(XC-X(L)).LE.1.E-6*XC) GO TO 20                             PHASE1.76
      IF(M.GE.199) GO TO 50                                             PHASE1.77
   10 CONTINUE                                                          PHASE1.78
   20 F=0                                                               PHASE1.79
      ETA=0                                                             PHASE1.80
      KEX=CONST*XC                                                      PHASE1.81
      KEX2=KEX*KEX                                                      PHASE1.82
      AMR2=AM2/KEX2                                                     PHASE1.83
C                                                                       PHASE1.84
C     CALCULATE PHASE SHIFT USING QUAD. SCHEME                          PHASE1.85
C                                                                       PHASE1.86
      PS=0                                                              PHASE1.87
      DO 25 K=1,NXQ                                                     PHASE1.88
C                                                                       PHASE1.89
C     QUAD. POINTS DEPEND ON TURNING POINT.                             PHASE1.90
C                                                                       PHASE1.91
      X(K)=XC/XQ(K)                                                     PHASE1.92
   25 CONTINUE                                                          PHASE1.93
C                                                                       PHASE1.94
C     FIND POTENTIAL AT TURNING POINTS                                  PHASE1.95
C                                                                       PHASE1.96
      CALL POT(X,A,V,VP,NXQ,RM)                                         PHASE1.97
C                                                                       PHASE1.98
C     SUM UP POTENTIAL CONTRIBUTIONS AT QUAD. POINTS.                   PHASE1.99
C                                                                       PHASE1.100
      DO 26 K=1,NXQ                                                     PHASE1.101
      XLT1=XQ(K)                                                        PHASE1.102
      AMRX2=AMR2*XLT1**2                                                PHASE1.103
      VR=V(K)                                                           PHASE1.104
      TEMP=(1.-AMRX2-VR/ER)/(1.-XLT1)                                   PHASE1.105
      IF(TEMP.LT.0.) GOTO 106                                           PHASE1.106
      F=(SQRT(TEMP)-SQRT(1.+XLT1))/XLT1/XLT1                            PHASE1.107
      PS=WQ(K)*F+PS                                                     PHASE1.108
   26 CONTINUE                                                          PHASE1.109
      ETA=KEX*PS+((AM-KEX)*1.5707963)                                   PHASE1.110
      THE=2*ETA                                                         PHASE1.111
      T=2*AMQN+1                                                        PHASE1.112
C                                                                       PHASE1.113
C     CTHE CONTAINS (2*L+1)*(COS(2*ETA)-1)                              PHASE1.114
C     STHE CONTAINS (2*L+1)*SIN(2*ETA)                                  PHASE1.115
C                                                                       PHASE1.116
      IF(NSTEP-1) 27,27,28                                              PHASE1.117
 27   CTHE(ITEMP+I)=T*(COS(THE)-1.)                                     PHASE1.118
      STHE(ITEMP+I)=SIN(THE)*T                                          PHASE1.119
      GOTO 29                                                           PHASE1.120
 28   Y(J)=T*(COS(THE)-1.)                                              PHASE1.121
      Z(J)=T*SIN(THE)                                                   PHASE1.122
 29   CONTINUE                                                          PHASE1.123
```

```
      IF(NPRI1.EQ.1) WRITE(6,100) AMQN,XC,M,ETA                         PHASE1.124
  100 FORMAT(10X,F6.1,5X,F10.5,5X,I5,5X,E14.7)                          PHASE1.125
      AMQN=AMQN+DETA                                                    PHASE1.126
   60 CONTINUE                                                          PHASE1.127
      IF(NSTEP.EQ.1) GOTO 500                                           PHASE1.128
      CALL SPLIFT(NSTEP,Y,YPP,NPHASE,W,IERR,ISX,0.,0.,0.,0.)            PHASE1.129
      ISX=1                                                             PHASE1.130
      CALL SPLIFT(NSTEP,Z,ZPP,NPHASE,W,IERR,ISX,0.,0.,0.,0.)            PHASE1.131
      CALL SPLINT(NSTEP,Y,YPP,NPHASE,ITEMP,Z,ZPP)                       PHASE1.132
      IF(NPRI1.NE.1)GOTO 500                                            PHASE1.133
      WRITE(6,400)                                                      PHASE1.134
      WRITE(6,402)                                                      PHASE1.136
      WRITE(6,401)(CTHE(IJJ+ITEMP),IJJ=1,NETA)                          PHASE1.138
      WRITE(6,403)                                                      PHASE1.140
      WRITE(6,401)(STHE(IJJ+ITEMP),IJJ=1,NETA)                          PHASE1.142
  500 CONTINUE                                                          PHASE1.143
C                                                                       PHASE1.144
C     RESET NETA IF INTERPOLATED ETA'S USED                             PHASE1.145
C                                                                       PHASE1.146
      IF(NSTEP.NE.1) NETA=NETA-NSTEP                                    PHASE1.147
      GOTO 70                                                           PHASE1.148
   50 WRITE(6,101)                                                      PHASE1.149
      GOTO 51                                                           PHASE1.151
  106 WRITE(6,107) AMQN                                                 PHASE1.152
      WRITE(6,108) VR,ER                                                PHASE1.154
  51  STOP                                                              PHASE1.156
   70 RETURN                                                            PHASE1.157
C
C
C       FORMAT STATEMENTS
C
C
  104 FORMAT(10X,*COLLISION ENERGIES (KCAL/MOLE)*,/)                    PHASE1.31
  105 FORMAT(//)                                                        PHASE1.34
  103 FORMAT(10(2X,E10.4))                                              PHASE1.36
  102 FORMAT(12X,*L*,11X,*TURNING POINT*,2X,*ITRNS.*,5X,*PHASE*,//)     PHASE1.37
  400 FORMAT(//,10X,*INTERPOLATED PHASE SHIFT FUNCTIONS*,/)             PHASE1.135
  402 FORMAT(//,10X,*CTHE ARRAY*,/)                                     PHASE1.137
  401 FORMAT(10(1X,E12.6))                                              PHASE1.139
  403 FORMAT(//,10X,*STHE ARRAY*,/)                                     PHASE1.141
  101 FORMAT(10X,* XC CALCULATION NOT CONVERGED IN PHASE SHIFT ROUTINE*)PHASE1.150
  107 FORMAT(10X,*SQRT ARGUMENT NEGATIVE AT AMQN= *,F10.3)              PHASE1.153
  108 FORMAT(10X,*COLLISION ENERGY=*,F8.4,*  POTENTIAL ENERGY=*,F8.4)   PHASE1.155
      END                                                               PHASE1.158


                                                                        PHASE1.159
      SUBROUTINE BSELFX(L,ARG,SBJ,SBN)                                  PHASE2.2
      IMPLICIT REAL (A-H,O-Z)                                           PHASE2.3
C.......................................................................PHASE2.4
C** SUBROUTINE TO CALCULATE SPHERICAL BESSEL FUNCTIONS OF THE FIRST AND PHASE2.5
C   SECOND KINDS,  SBJ  AND  SBN  , RESPECTIVELY, OF ORDER  L  , WITH   PHASE2.6
```

```
C   ARGUMENT  ARG.                                                    PHASE2.7
C.......................................................................PHASE2.8
      LH=L/2                                                          PHASE2.9
      PM=1.0E0                                                        PHASE2.10
      LE=L                                                            PHASE2.11
      AR1=1.E0/ARG                                                    PHASE2.12
      XQ=SQRT(1.570796326794896E+00*ARG)                              PHASE2.13
      AQ=COS(ARG)/XQ                                                  PHASE2.14
      BQ=SIN(ARG)/XQ                                                  PHASE2.15
      XQ=XQ*AR1                                                       PHASE2.16
  100 CQ=PM                                                           PHASE2.17
      IF (LE) 110,170,120                                             PHASE2.18
  110 QQ=AQ                                                           PHASE2.19
      RQ=BQ                                                           PHASE2.20
      GO TO 130                                                       PHASE2.21
  120 IF (ARG.LT.(1.E0*L)) GO TO 180                                  PHASE2.22
      QQ=BQ                                                           PHASE2.23
      RQ=AQ                                                           PHASE2.24
  130   DO 140 IQ=1,L                                                 PHASE2.25
        PQ=QQ*(CQ+CQ-PM)*AR1-RQ                                       PHASE2.26
        CQ=CQ+PM                                                      PHASE2.27
        RQ=QQ                                                         PHASE2.28
  140   QQ=PQ                                                         PHASE2.29
      PQ=PQ*XQ                                                        PHASE2.30
      IF (PM.LT.0.E+00) GO TO 160                                     PHASE2.31
      SBJ=PQ                                                          PHASE2.32
  150 PM=-1.0E0                                                       PHASE2.33
      LE=-L                                                           PHASE2.34
      GO TO 100                                                       PHASE2.35
  160 SBN=PQ                                                          PHASE2.36
      K=L-2*LH                                                        PHASE2.37
      IF (K.EQ.0) SBN=-PQ                                             PHASE2.38
      RETURN                                                          PHASE2.39
  170 SBJ=BQ*XQ                                                       PHASE2.40
      SBN=-AQ*XQ                                                      PHASE2.41
      RETURN                                                          PHASE2.42
C.......................................................................PHASE2.43
C** CALCULATE FX OF 1-ST KIND FOR SMALL ARGUMENT BY ASCENDING POWER    PHASE2.44
C   EXPANSION.                                                        PHASE2.45
C.......................................................................PHASE2.46
  180 QQ=1.0E0                                                        PHASE2.47
        DO 190 I=1,L                                                  PHASE2.48
  190   QQ=QQ*ARG/(2*I+1)                                             PHASE2.49
      SBJ=QQ                                                          PHASE2.50
      L4=50                                                           PHASE2.51
      IF (L.GT.12) L4=4*L                                             PHASE2.52
      CQ=(2*L+1)                                                      PHASE2.53
      QQ=-0.5E0*ARG*ARG                                               PHASE2.54
      RQ=1.0E0                                                        PHASE2.55
      PQ=RQ                                                           PHASE2.56
        DO 200 I=1,L4                                                 PHASE2.57
        K=I                                                           PHASE2.58
        RQ=RQ*QQ/(I*(CQ+2*I))                                         PHASE2.59
```

```
      PQ=PQ+RQ                                                          PHASE2.60
      IF (ABS(RQ/PQ).LT.1.E-10) GO TO 210                               PHASE2.61
  200 CONTINUE                                                          PHASE2.62
     RQ=RQ/PQ                                                           PHASE2.63
     WRITE (6,1000) L,ARG,L4,RQ                                         PHASE2.64
  210 SBJ=SBJ*PQ                                                        PHASE2.65
     GO TO 150                                                          PHASE2.66
 1000 FORMAT(18H0  ERROR IN   SBJ(,I3,1H,,E10.5,9H) . AFTER,I4,26H ASCENPHASE2.67
    XDING TERMS   RATIO =,E10.5 )                                       PHASE2.68
     END                                                                PHASE2.69
     SUBROUTINE PHSHFT(A,RM,IWR)                                        PHASE2.70
C.......................................................................PHASE2.71
C**** R.J.LE ROY  SUBROUTINE -PHSHFT- , AS OF 16 NOVEMBER, 1978  ***    PHASE2.72
C** SUBROUTINE TO CALCULATE THE ABSOLUTE PHASE SHIFT  -ADLT- FOR        PHASE2.73
C  THE POTENTIAL -V(I)- (REDUCED BY THE FACTOR  BZ/RSC) AT ENERGY -ZE-  PHASE2.74
C  AND PARTIAL WAVE -L-.                                                PHASE2.75
C** SOLVE THE RADIAL SCHROEDINGER EQUATION IN THE REDUCED FORM?         PHASE2.76
C    D2S/DR2=-(ZE*BZ/ESC-V(I)-L*(L+1)*XM2)*S , WHERE XM2=1/X**2  AND    PHASE2.77
C  S  IS THE WAVE FUNCTION.  ** USE NUMEROV-S METHOD.                   PHASE2.78
C** INTEGRATE OUTWARD FROM  -XMIN- WITH AN INCREMENT OF  -XH- (BOTH     PHASE2.79
C  IN REDUCED UNITS, I.E. SCALED BY -RSC-),  FOR UP TO -N- STEPS.       PHASE2.80
C** IF(IWR.GT.0) PRINTS ALL TRIAL PHASE SHIFTS AND NODE POSITIONS.      PHASE2.81
C  IF(IWR.NE.0) PRINT CONVERGED PHASE SHIFTS AND NODE POSITIONS         PHASE2.82
C** RADIAL INTEGRATION STOPS WHEN JWKB-CORRECTED VALUES AT 3            PHASE2.83
C  SUCCESSIVE NODES AGREE TO WITHIN -PHTST- (RADIANS).                  PHASE2.84
C-----------------------------------------------------------------      PHASE2.85
C.......................................................................PHASE2.86
      IMPLICIT REAL (A-H,O-Z)                                           PHASE2.87
      COMMON/ETA/STHE(8000),CTHE(8000),NETA,DETA,IDENT                  ETA.2
     $,IBOSE                                                            ETA.3
      COMMON/EN/ENERGY(125),CMTH1(125),CMTH2(125),WGHT1(125),WGHT2(125),EN.2
     1NCOLX,NCOLY,NCOLZ,IAPPRX                                          EN.3
      COMMON/PTNL/V(2001),XM2(2001),XSTART,XSTEP,RNPHAS,ERROR           PTNL.2
      DIMENSION Z(15),X(10),VP(1),A(15)                                 PHASE2.91
      DIMENSION            VV(8),RR2(8),XX(8),WW(8),XG(4),WG(4)         PHASE2.92
      DIMENSION Y(250), YPP(250), W(750)                                PHASE2.93
      DATA Z0/0.E0/,ZH/0.5E0/,Z1/1.E0/,Z2/2.E0/,Z3/3.E0/,Z4/4.E0/,      PHASE2.94
     X  Z5/5.E0/,Z6/6.E0/,PI/3.141592653589793E0/,IFIRST/0/             PHASE2.95
C.......................................................................PHASE2.96
C** GAUSSIAN WEIGHTS AND POINTS FOR QUADRATURES.                        PHASE2.97
C.......................................................................PHASE2.98
      DATA  XG/-0.8611363115940526E0,-0.3399810435848563E0,1.E0,1.E0/,  PHASE2.99
     X  WG/0.3478548451374539E0,0.6521451548625461E0,0.E0,0.E0/         PHASE2.100
C.......................................................................PHASE2.101
C** ON VERY FIRST ENTRY TO -PHSHFT- ONLY, PREPARE POINTS AND WEIGHTS    PHASE2.102
C  FOR GAUSSIAN QUADRATURE JWKB EDGE CORRECTION TO NODAL PHASE SHIFT    PHASE2.103
C.......................................................................PHASE2.104
      IF (IFIRST.GT.0) GO TO 120                                        PHASE2.105
      IFIRST=1                                                          PHASE2.106
      NGT=4                                                             PHASE2.107
      NGH=2                                                             PHASE2.108
      IF(IWR.GT.0) WRITE(6,1140)                                        PHASE2.109
      IF (IWR.GT.0) WRITE (6,1130) NGT,(XG(I),WG(I),I=1,NGH)            PHASE2.111
```

```
      DO 110 I=1,NGT                                                    PHASE2.112
      J=I                                                               PHASE2.113
      IF (I.LE.NGH) GO TO 100                                           PHASE2.114
      J=NGT+1-I                                                         PHASE2.115
      XX(I)=ZH*(Z1-XG(J))                                               PHASE2.116
      GO TO 110                                                         PHASE2.117
  100 XX(I)=ZH*(Z1+XG(J))                                               PHASE2.118
  110 WW(I)=WG(J)/XX(I)**2                                              PHASE2.119
    IF (IWR.GT.0) WRITE (6,1120) NGT,(XX(I),WW(I),I=1,NGT)              PHASE2.120
C.......................................................................PHASE2.121
C** DEFINE AND INITIALIZE VARIOUS CONSTANTS AND PARAMETERS.             PHASE2.122
C.......................................................................PHASE2.123
    X12=Z1/12.E0                                                        PHASE2.124
  120 CONTINUE                                                          PHASE2.125
     PHTST=ERROR                                                        PHASE2.126
    NVOL=NCOLX*NCOLY*NCOLZ                                              PHASE2.127
    IF(IAPPRX.NE.0) NVOL=1                                              PHASE2.128
    NSTEP=INT(DETA)                                                     PHASE2.129
    ISX=0                                                               PHASE2.130
C FOR INTERPOLATED ETA'S NEED ADDITIONAL NETA.                          PHASE2.131
    IF(NSTEP.NE.1) NETA=NETA+NSTEP                                      PHASE2.132
    NPHASE=NETA/NSTEP                                                   PHASE2.133
C   JJ IS THE NUMBER OF COMPUTED PHASE SHIFTS                           PHASE2.134
    IF(IWR.NE.1) GOTO 99                                                PHASE2.135
     WRITE(6,1150)                                                      PHASE2.136
    WRITE(6,104)                                                        PHASE2.138
    WRITE(6,103)(ENERGY(I),I=1,NVOL)                                    PHASE2.140
 99 DO 500 IJ=1,NVOL                                                    PHASE2.142
    ZE=ENERGY(IJ)*349.757                                               PHASE2.143
    ESC=A(1)                                                            PHASE2.144
    XH=XSTEP                                                            PHASE2.145
    JJ=0                                                                PHASE2.146
    XMIN=XSTART                                                         PHASE2.147
    N=INT(RNPHAS)                                                       PHASE2.148
    ITEMP=(IJ-1)*NETA                                                   PHASE2.149
    BZ=RM*A(1)*A(2)*A(2)/16.85763                                       PHASE2.150
    DO 60 K=1,NETA,NSTEP                                                PHASE2.151
    JJ=JJ+1                                                             PHASE2.152
    L=K-1                                                               PHASE2.153
    T=FLOAT(2*L+1)                                                      PHASE2.154
    EJ=L*(L+1)                                                          PHASE2.155
    H2=XH*XH                                                            PHASE2.156
    E=ZE*BZ/ESC                                                         PHASE2.157
    SQE=SQRT(E)                                                         PHASE2.158
    NODE=0                                                              PHASE2.159
    DLT2=Z0                                                             PHASE2.160
    DLT3=Z0                                                             PHASE2.161
    COR2=Z0                                                             PHASE2.162
    COR3=Z0                                                             PHASE2.163
    XND2=-.000001E+00                                                   PHASE2.164
    XND3=-.000001E+00                                                   PHASE2.165
    IF (IWR.GT.0) WRITE (6,1110)                                        PHASE2.166
C.......................................................................PHASE2.167
```

```
C** START TESTING FOR PHASE SHIFT CONVERGENCE AT NODES PAST THE          PHASE2.168
C  MESH POINT -ILK- WHERE   E = L*(L+1)/R**2                              PHASE2.169
C.......................................................................PHASE2.170
      XLK=SQRT(Z1/E)                                                     PHASE2.171
      IF (L.GT.0) XLK=SQRT(EJ/E)                                         PHASE2.172
      ILK=(XLK-XMIN)/XH+1                                                PHASE2.173
      IF (ILK.GT.N) GO TO 320                                            PHASE2.174
C.......................................................................PHASE2.175
C** IF HAVE POTENTIAL (SUCH AS EXP-6) WITH NEGATIVE  V(R)  AT VERY       PHASE2.176
C  SMALL  R , OR IF (V(I)-E) SO HIGH THAT -XH- IS (LOCALLY) MUCH TOO     PHASE2.177
C  LARGE, THEN SHIFT INNER STARTING POINT OUTWARD.                       PHASE2.178
C.......................................................................PHASE2.179
      IST=1                                                              PHASE2.180
  130 IST=IST+1                                                          PHASE2.181
      IF (IST.GE.(N-8)) GO TO 310                                        PHASE2.182
      GI=H2*(V(IST)+EJ*XM2(IST)-E)                                       PHASE2.183
      IF ((GI.LE.Z0).OR.(GI.GT.11.E0)) GO TO 130                         PHASE2.184
      IF ((IWR.GT.0).AND.(IST.GT.2)) WRITE (6,1000) L,ZE,IST             PHASE2.185
      GN=H2*(V(IST-1)+EJ*XM2(IST-1)-E)                                   PHASE2.186
      IF (GN.LE.0) GO TO 130                                             PHASE2.187
      IST=IST+1                                                          PHASE2.188
C.......................................................................PHASE2.189
C** INITIALIZE WAVE FUNCTION FOR OUTWARD INTEGRATION.                    PHASE2.190
C.......................................................................PHASE2.191
      IF ((XMIN+(IST-3)*XH).LE.Z0) GO TO 140                             PHASE2.192
C.......................................................................PHASE2.193
C** IF INTEGRATION STARTS AT  R.GT.0 , INITIALIZE WAVE FUNCTION AS       PHASE2.194
C  THE EXPONENTIALLY INCREASING JWKB SOLUTION.                           PHASE2.195
C.......................................................................PHASE2.196
      SRTGI=SQRT(GI)                                                     PHASE2.197
      SRTGN=SQRT(GN)                                                     PHASE2.198
      SB=Z1                                                              PHASE2.199
      SI=SQRT(SRTGN/SRTGI)*EXP(ZH*(SRTGN+SRTGI))                         PHASE2.200
      IF (SI.GE.SB) GO TO 150                                            PHASE2.201
      WRITE (6,1040) L,ZE,SB,SI                                          PHASE2.202
  140 SB=Z0                                                              PHASE2.203
      SI=Z1                                                              PHASE2.204
  150 Y1=SB*(Z1-GN*X12)                                                  PHASE2.205
      Y2=SI*(Z1-GI*X12)                                                  PHASE2.206
      RATIN=SI                                                           PHASE2.207
C.......................................................................PHASE2.208
C** INTEGRATE OUT TO MESH POINT -ILK- OR CLASSICALLY ALLOWED REGION      PHASE2.209
C.......................................................................PHASE2.210
      DO 200 I=IST,N                                                     PHASE2.211
      II=I                                                               PHASE2.212
      SC=SB                                                              PHASE2.213
      SB=SI                                                              PHASE2.214
      Y3=Y2+Y2-Y1+GI*SB                                                  PHASE2.215
      GI=H2*(V(I)+EJ*XM2(I)-E)                                           PHASE2.216
      SI=Y3/(Z1-GI*X12)                                                  PHASE2.217
      IF (SI.LE.1.E+30) GO TO 160                                        PHASE2.218
C.......................................................................PHASE2.219
C** NORMALIZE IN CASE OF OVERFLOW FROM WAVE FUNCTION GROWTH UNDER POTENTPHASE2.220
```

```
C.......................................................................PHASE2.221
      SP=Z1/SI                                                          PHASE2.222
      IF (ABS(RATIN).GT.1.E-40) RATIN=RATIN*SP                          PHASE2.223
      SC=SC*SP                                                          PHASE2.224
      SB=SB*SP                                                          PHASE2.225
      SI=Z1                                                             PHASE2.226
      Y3=Y3*SP                                                          PHASE2.227
      Y2=Y2*SP                                                          PHASE2.228
  160 Y1=Y2                                                             PHASE2.229
      Y2=Y3                                                             PHASE2.230
C.......................................................................PHASE2.231
C** TEST FOR AND COUNT NODES                                            PHASE2.232
C.......................................................................PHASE2.233
      IF (SB) 170,180,170                                               PHASE2.234
  170 IF ((SB*SC).GE.Z0) GO TO 190                                      PHASE2.235
  180 NODE=NODE+1                                                       PHASE2.236
  190 IF ((GI.LT.Z0).AND.(I.GE.ILK)) GO TO 210                          PHASE2.237
  200 CONTINUE                                                          PHASE2.238
    GO TO 320                                                           PHASE2.239
C.......................................................................PHASE2.240
C** AT THIS POINT, NORMALIZE BEFORE PROCEEDING                          PHASE2.241
C.......................................................................PHASE2.242
  210 SP=Z1/(ABS(SI)+ABS(SC))                                           PHASE2.243
    IF (ABS(RATIN).GT.1.E-40) RATIN=RATIN*SP                            PHASE2.244
    SC=SC*SP                                                            PHASE2.245
    SB=SB*SP                                                            PHASE2.246
    SI=SI*SP                                                            PHASE2.247
    Y1=Y1*SP                                                            PHASE2.248
    Y2=Y2*SP                                                            PHASE2.249
    IF (IWR.GT.0) WRITE (6,1090)                                        PHASE2.250
C.......................................................................PHASE2.251
C** NUMERICAL INTEGRATION CALCULATING TRIAL PHASE SHIFTS STARTS HERE    PHASE2.252
C.......................................................................PHASE2.253
    ILK1=II+1                                                           PHASE2.254
      DO 280 I=ILK1,N                                                   PHASE2.255
      Y3=Y2+Y2-Y1+GI*SI                                                 PHASE2.256
      GI=H2*(V(I)+EJ*XM2(I)-E)                                          PHASE2.257
      SN=Y3/(Z1-GI*X12)                                                 PHASE2.258
C.......................................................................PHASE2.259
C** LOOK FOR WAVE FUNCTION NODE                                         PHASE2.260
C.......................................................................PHASE2.261
      IF (SI) 220,230,220                                               PHASE2.262
  220 IF ((SB*SI).GE.Z0) GO TO 270                                      PHASE2.263
  230 NODE=NODE+1                                                       PHASE2.264
C.......................................................................PHASE2.265
C** EVALUATE NODAL PHASE SHIFTS AND TEST FOR CONVERGENCE.               PHASE2.266
C.......................................................................PHASE2.267
      JN=I                                                              PHASE2.268
      XJN=XMIN+(JN-1)*XH                                                PHASE2.269
      XJC=XJN-Z3*XH                                                     PHASE2.270
      XND1=XND2                                                         PHASE2.271
      XND2=XND3                                                         PHASE2.272
      XND3=XJN+XH*(SN*SB*SC/((SI-SN)*(SI-SB)*(SI-SC))+Z2*SN*SI*SC/      PHASE2.273
```

```
     X   ((SB-SN)*(SB-SI)*(SB-SC))+Z3*SN*SI*SB/((SC-SN)*(SC-SI)*(SC-SB))PHASE2.274
     X   )                                                             PHASE2.275
         IF ((XND3.GT.XJC).AND.(XND3.LT.XJN)) GO TO 240                PHASE2.276
         WRITE (6,1100)  NODE,L,ZE,JN,XND3                             PHASE2.277
         XND3=XJN-XH*(Z1+SI/(SI-SB))                                   PHASE2.278
         IF ((XND3.GT.XJC).AND.(XND3.LT.XJN)) GO TO 240                PHASE2.279
         WRITE (6,1080)  NODE,L,ZE,JN,XND3                             PHASE2.280
         GO TO 270                                                     PHASE2.281
  240    ARG=XND3*SQE                                                  PHASE2.282
         CALL BSELFX(L,ARG,SBJ,SBN)                                    PHASE2.283
         DLTX=ATAN(SBJ/SBN)                                            PHASE2.284
         DLT1=DLT2                                                     PHASE2.285
         DLT2=DLT3                                                     PHASE2.286
         DLT3=DLTX                                                     PHASE2.287
C.......................................................................PHASE2.288
C** ADD JWKB PHASE SHIFT CORRECTION DUE TO POTENTIAL TAIL BEYOND -XND3- PHASE2.289
C.......................................................................PHASE2.290
         COR1=COR2                                                     PHASE2.291
         COR2=COR3                                                     PHASE2.292
C.......................................................................PHASE2.293
C** START QUADRATURE CALCULATION OF TRUNCATION CORRECTION              PHASE2.294
C** FIRST EVALUATE POTENTIAL AT APPROPRIATE GAUSSIAN POINTS             PHASE2.295
C.......................................................................PHASE2.296
           DO 250 IK=1,NGT                                             PHASE2.297
  250      RR2(IK)=XND3/XX(IK)                                         PHASE2.298
       CALL POT(RR2,A,VV,VP,NGT,RM)                                    PHASE2.299
C.......................................................................PHASE2.300
C** NOW PERFORM ACTUAL QUADRATURE                                       PHASE2.301
C.......................................................................PHASE2.302
         PSC=Z0                                                        PHASE2.303
           DO 260 IK=1,NGT                                             PHASE2.304
  260      PSC=PSC+WW(IK)*(SQRT(E-VV(IK)-EJ*RR2(IK)) - SQRT(E-EJ*RR2(IK))PHASE2.305
     X       )                                                         PHASE2.306
         COR3=PSC*ZH*XND3                                              PHASE2.307
         DLT3=DLT3+COR3                                                PHASE2.308
         SNRM=Z1/SN                                                    PHASE2.309
C.......................................................................PHASE2.310
C** TEST FOR PHASE SHIFT CONVERGENCE                                   PHASE2.311
C.......................................................................PHASE2.312
         IF (IWR.GT.0) WRITE (6,1050) NODE,XND3,DLTX,DLT3,COR3         PHASE2.313
         IF ((ABS(DLT2-DLT3).LT.PHTST).AND.(ABS(DLT1-DLT2).LT.PHTST)) GO PHASE2.314
     X   TO 290                                                        PHASE2.315
  270    SC=SB                                                         PHASE2.316
         SB=SI                                                         PHASE2.317
         SI=SN                                                         PHASE2.318
         Y1=Y2                                                         PHASE2.319
  280    Y2=Y3                                                         PHASE2.320
C.......................................................................PHASE2.321
C** END OF INTEGRATION LOOP WHICH CALCULATES NODAL PHASE SHIFTS        PHASE2.322
C.......................................................................PHASE2.323
       WRITE (6,1070) DLT3,COR3,DLT2,COR2,DLT1,COR1,XND3,XND2,XND1     PHASE2.324
C.......................................................................PHASE2.325
C** GET ABSOLUTE PHASE SHIFT USING EQ.(9.2.29) OF ABRAMOWITZ AND STEGUN PHASE2.326
```

```
C.......................................................................PHASE2.327
  290 ZU=Z4*EJ+Z1                                                       PHASE2.328
      R4=Z4*ARG                                                         PHASE2.329
      SIR4=Z1/R4**2                                                     PHASE2.330
      TH=ARG-ZH*L*PI+(ZH+SIR4*((ZU-25.E0)/Z6+SIR4*((1073.E0-ZU*(114.E0- PHASE2.331
     X ZU))/Z5-SIR4*(375733E0-ZU*(54703.E0-ZU*(1535.E0-Z5*ZU)))/14.E0)))PHASE2.332
     X *(ZU-Z1)/R4                                                      PHASE2.333
      XNDT=(TH+DLTX)/PI                                                 PHASE2.334
      NDT=(XNDT+ZH)                                                     PHASE2.335
      ADLT=DLT3+(NODE-NDT)*PI                                           PHASE2.336
      RATIN=RATIN*SNRM                                                  PHASE2.337
      IF (ABS(RATIN).GT.1.0E-10) WRITE (6,1060) L,ZE,RATIN              PHASE2.338
      IF (IWR.EQ.0) GO TO 300                                           PHASE2.339
      WRITE (6,1020) L,ZE,ADLT,XND3,COR3                                PHASE2.340
  300 CONTINUE                                                          PHASE2.341
      THE=2.*ADLT                                                       PHASE2.342
      IF(NSTEP-1) 27,27,28                                              PHASE2.343
  27  CTHE(ITEMP+K)=T*(COS(THE)-1.)                                     PHASE2.344
      STHE(ITEMP+K)=T*SIN(THE)                                          PHASE2.345
      GOTO 60                                                           PHASE2.346
  28  Y(JJ)=THE                                                         PHASE2.347
  60  CONTINUE                                                          PHASE2.348
      IF(NSTEP.EQ.1) GOTO 500                                           PHASE2.349
      CALL SPLIFT(NSTEP,Y,YPP,NPHASE,W,IERR,ISX,0.,0.,0.,0.)            PHASE2.350
      ISX=1                                                             PHASE2.351
      CALL SPLINT (NSTEP, Y, YPP, NPHASE, ITEMP)                        PHASE2.352
      IF(IWR.NE.1) GOTO 500                                             PHASE2.353
      WRITE(6,404)                                                      PHASE2.354
      WRITE(6,402)                                                      PHASE2.356
      WRITE(6,401)(CTHE(IJJ+ITEMP),IJJ=1,NETA)                          PHASE2.358
      WRITE(6,403)                                                      PHASE2.360
      WRITE(6,401)(STHE(IJJ+ITEMP),IJJ=1,NETA)                          PHASE2.362
  500 CONTINUE                                                          PHASE2.363
      IF(NSTEP.NE.1) NETA=NETA-NSTEP                                    PHASE2.364
  400 RETURN                                                            PHASE2.365
  310 WRITE (6,1010) L,ZE,IST                                           PHASE2.366
      GOTO 400                                                          PHASE2.367
  320 WRITE (6,1030) L,ZE,ILK                                           PHASE2.368
      GOTO 400                                                          PHASE2.369
C
C
C     FORMAT STATEMENTS
C
C
 1140   FORMAT(1H1)                                                     PHASE2.110
 1150  FORMAT(//)                                                       PHASE2.137
 104  FORMAT(10X,*COLLISION ENERGIES*)                                  PHASE2.139
 103  FORMAT(10(2X,E10.4))                                              PHASE2.141
 404  FORMAT(//,10X,*INTERPOLATED PHASE SHIFT FUNCTIONS*,/)             PHASE2.355
 402  FORMAT(//,10X,*CTHE ARRAY*,/)                                     PHASE2.357
 401  FORMAT(10(1X,E12.6))                                              PHASE2.359
 403  FORMAT(//,10X,*STHE ARRAY*,/)                                     PHASE2.361
 1000 FORMAT(13H0   FOR   L =,I3,7H    E =,F9.3,70H   POTENTIAL SUCH THAPHASE2.370
```

```
      XT INTEGRATION CANNOT START TILL PAST MESH POINT @,I5)              PHASE2.371
 1010 FORMAT(26H0  *** ERROR *** FOR   L =,I3,6H   E =,F9.3,65H   INTEGRPHASE2.372
      XATION INTERVAL APPARENTLY CANNOT START TILL MESH POINT @,I5)       PHASE2.373
 1020 FORMAT(10H0 AT   L =,I3,6H   E =,F10.4,23H(1/CM)    PHASE SHIFT =,PHASE2.374
      X    F12.8,13H    FOR   X =,F7.4,10H    COR3 =,F11.8)               PHASE2.375
 1030 FORMAT(27H0 *** ERROR ***   FOR   L =,I3,7H    E =,F9.3,9H    ILK PHASE2.376
      X=  ,I5,66H ,  REACH END OF RANGE BEFORE START LOOKING FOR NODAL PHPHASE2.377
      XASE SHIFTS  )                                                      PHASE2.378
 1040 FORMAT(27H0 *** WARNING *** FOR   L =,I3,7H    E =,F9.3,39H    JWKPHASE2.379
      XB INITIALIZATION GIVES   SB/SI =,D10.3,1H/,D10.3,17H,  SO SET   SBPHASE2.380
      X=0. )                                                              PHASE2.381
 1050 FORMAT(I6,F15.10,F14.10,F16.10,F14.10)                              PHASE2.382
 1060 FORMAT(20H0 *** CAUTION    L =,I3,6H   E =,F9.3,47H   WAVE FUNCTIOPHASE2.383
      XN MAY BE UNRELIABLE AS   RATIN =,D10.3,25H,  SO MAKE  XMIN  SMALLEPHASE2.384
      XR)                                                                 PHASE2.385
 1070 FORMAT(54H *** CAUTION *** NOT CONVERGED BY END OF RANGE   DLT =, PHASE2.386
      X  3(F11.8,1H(,F11.8,1H))/46X,8HAT   X =,3(F11.8,13X) )             PHASE2.387
 1080 FORMAT(1H0,5X,51HINSTABILITY **** IN LINEAR INTERPOLATION AT  NODEPHASE2.388
      X =,I3,10H , FOR  L=,I3,5H   E=,E11.5,12H(1/CM)   JN=,I4,8H   XND3=PHASE2.389
      X,    F10.6)                                                        PHASE2.390
 1090 FORMAT(62H0  NODE    X(NODE)      DLT(NODE)        DLT(COR3)       PHASE2.391
      X COR3 ,/2X,30(2H**))                                               PHASE2.392
 1100 FORMAT(1H0,5X,51HINSTABILITY ***** IN CUBIC INTERPOLATION AT  NODEPHASE2.393
      X =,I3,10H , FOR  L=,I3,5H   E=,E11.5,12H(1/CM)   JN=,I4,8H   XND3=PHASE2.394
      X,    F10.6)                                                        PHASE2.395
 1110 FORMAT(/1X,60(2H-- ))                                               PHASE2.396
 1120 FORMAT(50H0   POINTS   X = RST/R   AND EFFECTIVE WEIGHTS FOR,        PHASE2.397
      X   I3,44H-POINT QUADRATURE FOR PHASE SHIFT CORRECTION,/(3(F22.16, PHASE2.398
      X     F20.16)))                                                     PHASE2.399
 1130 FORMAT(51H0   REGULAR GAUSSIAN POINTS AND WEIGHTS FOR REGULAR,      PHASE2.400
      X  I3,18H-POINT QUADRATURES,/(3(F22.16,F20.16)))                    PHASE2.401
       END                                                                PHASE2.402


                                                                          PHASE2.403
       SUBROUTINE POT(X,A,V,VP,L,RM)                                      POT1.2
C                                                                         POT1.3
C ESMMSV JWKB                                                             POT1.4
C      DEFINITION OF POTENTIAL PARAMETERS- SEE JCP,70,PG. 488 (1979)      POT1.5
C      EQUATION 7 AND JCP,59,PG.602 (1973) FOR DETAILS.                   POT1.6
C      A(1)=EPSILON                                                       POT1.7
C      A(2)=RMIN                                                          POT1.8
C      A(3)= A                                                            POT1.9
C      A(4)=ALPHA                                                         POT1.10
C      A(5)=X1                                                            POT1.11
C      A(6)=X2                                                            POT1.12
C      A(7)=X3                                                            POT1.13
C      A(8)=X4                                                            POT1.14
C      A(9)=BETA FOR REPULSIVE WALL MORSE                                 POT1.15
C      A(10)=C6                                                           POT1.16
C      A(11)=C8                                                           POT1.17
C      A(12)=BETA ATTRACTIVE WELL                                         POT1.18
```

```
C     A(13)=C10                                                         POT1.19
C                                                                       POT1.20
      DIMENSION X(10),A(15),V(10),VP(10)                                POT1.21
      COMMON/POTPRE/C6,C8,C10,B1,B2,B3,B4,A1,A2,A3,A4                   POTPRE.2
      RT=ALOG(2.)                                                       POT1.23
      DO 100 I=1,L                                                      POT1.24
      T1=X(I)-A(5)                                                      POT1.25
      IF(T1)5,5,6                                                       POT1.26
C                                                                       POT1.27
C     EXPONENTIAL WALL                                                  POT1.28
C                                                                       POT1.29
 5    V(I)=A(3)*EXP(-A(4)*(X(I)-1.))                                    POT1.30
      VP(I)=-A(4)*V(I)                                                  POT1.31
      GOTO 100                                                          POT1.32
 6     T2=X(I)-A(6)                                                     POT1.33
      IF(T2)7,8,8                                                       POT1.34
C                                                                       POT1.35
C      EXPONENTIAL SPLINE                                               POT1.36
C                                                                       POT1.37
 7    V(I)=EXP(A1+T1*(A2+T2*(A3+A4*T1)))                                POT1.38
      VP(I)=V(I)*(A2+A3*(T1+T2)+A4*T1*(T1+2.*T2))                       POT1.39
      GOTO 100                                                          POT1.40
 8    T3=X(I)-1.+RT/A(12)                                               POT1.41
      IF(T3)9,9,10                                                      POT1.42
C                                                                       POT1.43
C      FIRST MORSE (R%SIGMA)                                            POT1.44
C                                                                       POT1.45
 9    W=(A(9)-RT)/(A(12)-RT)                                            POT1.46
      E1=EXP(A(9)-X(I)*A(12)*W)                                         POT1.47
      V(I)=E1*(E1-2.)/W                                                 POT1.48
      VP(I)=2.*E1*A(12)*(1./W-E1)                                       POT1.49
      GOTO 100                                                          POT1.50
 10   T4=X(I)-A(7)                                                      POT1.51
      IF(T4) 11,12,12                                                   POT1.52
C                                                                       POT1.53
C      SECOND MORSE                                                     POT1.54
C                                                                       POT1.55
 11   E1=EXP(-2.*A(12)*(X(I)-1.))                                       POT1.56
      E2=EXP(-A(12)*(X(I)-1.))                                          POT1.57
      V(I)=E1-2.*E2                                                     POT1.58
      VP(I)=-2.*A(12)*(E1-E2)                                           POT1.59
      GOTO 100                                                          POT1.60
 12   T4=X(I)-A(8)                                                      POT1.61
      T3=X(I)-A(7)                                                      POT1.62
      IF(T4)13,14,14                                                    POT1.63
C                                                                       POT1.64
C      POLYNOMIAL SPLINE TO DISPERSION SERIES                           POT1.65
C                                                                       POT1.66
 13   V(I)=B1+T3*(B2+T4*(B3+T3*B4))                                     POT1.67
      VP(I)=B2+B3*(T4+T3)+B4*T3*(T3+2.*T4)                              POT1.68
      GOTO 100                                                          POT1.69
C                                                                       POT1.70
C      DISPERSION SERIES                                                POT1.71
```

```
C
 14   RR=X(I)**2                                                        POT1.72
      R6=RR**3                                                          POT1.73
      R8=RR*R6                                                          POT1.74
      R10=RR*R8                                                         POT1.75
      V(I)=-C6/R6-C8/R8-C10/R10                                         POT1.76
      VP(I)=6.*C6/R6/X(I)+8.*C8/R8/X(I)+10.*C10/R10/X(I)                POT1.77
 100  CONTINUE                                                          POT1.78
      RETURN                                                            POT1.79
      END                                                               POT1.80
                                                                        POT1.81


                                                                        POT1.82
      SUBROUTINE PREPOT(A,RM)                                           PREPOT1.2
C                                                                       PREPOT1.3
C     ESMMSV JWKB                                                       PREPOT1.4
C     DETERMINES THE SPLINE COEFFICIENTS AND REDUCED PARAMETERS FOR POT1PREPOT1.5
C     SEE THAT SUBROUTINE FOR  A LISTING OF THE CORRELATION OF THE      PREPOT1.6
C      PARAMETERS AND THE ENTRIES OF THE A ARRAY                        PREPOT1.7
C                                                                       PREPOT1.8
      DIMENSION A(15)                                                   PREPOT1.9
      COMMON/POTPRE/C6,C8,C10,B1,B2,B3,B4,A1,A2,A3,A4                   POTPRE.2
      ERM6=A(1)*A(2)**6                                                 PREPOT1.11
C                                                                       PREPOT1.12
C      REDUCED UNITS FOR DISPERSION COEFFICIENTS                        PREPOT1.13
C                                                                       PREPOT1.14
      C6=A(10)/ERM6                                                     PREPOT1.15
      C8=A(11)/ERM6/A(2)**2                                             PREPOT1.16
      C10=A(13)/ERM6/A(2)**4                                            PREPOT1.17
C                                                                       PREPOT1.18
C      SPLINE COEFFICIENTS FOR THE REPULSIVE WALL                       PREPOT1.19
C                                                                       PREPOT1.20
      A1=ALOG(A(3))-A(4)*(A(5)-1.)                                      PREPOT1.21
      TEMP=EXP(-2.*A(9)*(A(6)-1.))-2.*EXP(-A(9)*(A(6)-1.))              PREPOT1.22
      A2=(ALOG(TEMP)-A1)/(A(6)-A(5))                                    PREPOT1.23
      A3=-(A(4)+A2)/(A(5)-A(6))                                         PREPOT1.24
      A4=2.*A(9)*(EXP(-A(9)*(A(6)-1.))-EXP(-2.*A(9)*(A(6)-1.)))*EXP(-(A1PREPOT1.25
     1+A2*(A(6)-A(5))))-A2-A3*(A(6)-A(5))                               PREPOT1.26
      A4=A4/(A(6)-A(5))**2                                              PREPOT1.27
C                                                                       PREPOT1.28
C      SPLINE COEFFICIENTS FOR THE DISPERSION SERIES.                   PREPOT1.29
C                                                                       PREPOT1.30
      TT=A(12)*(A(7)-1.)                                                PREPOT1.31
      B1=EXP(-2.*TT)-2.*EXP(-TT)                                        PREPOT1.32
      TEMP=-C6/A(8)**6-C8/A(8)**8-C10/A(8)**10                          PREPOT1.33
      B2=(TEMP-B1)/(A(8)-A(7))                                          PREPOT1.34
      TEMP=-2.*A(12)*EXP(-2.*TT)+2.*EXP(-TT)*A(12)                      PREPOT1.35
      B3=(TEMP-B2)/(A(7)-A(8))                                          PREPOT1.36
      TEMP=6.*C6/A(8)**7+8.*C8/A(8)**9+10.*C10/A(8)**11                 PREPOT1.37
      B4=(TEMP-B2-B3*(A(8)-A(7)))/(A(8)-A(7))**2                        PREPOT1.38
      RETURN                                                            PREPOT1.39
      END                                                               PREPOT1.40
```

```
                                                                        PREPOT1.41
      SUBROUTINE POT(X,A,V,VP,L,RM)                                     POT2.2
      COMMON/POTPRE/C6,C8,C10,B1,B2,B3,B4,A1,A2,A3,A4                   POTPRE.2
C                                                                       POT2.4
C      HFD POTENTIAL- SEE JCP,67,PG.152(1977) EQN. (1) FOR DEFINITION OFPOT2.5
C      THE FUNCTIONAL FORM                                              POT2.6
C      A(1)=EPSILON                                                     POT2.7
C      A(2)=RMIN                                                        POT2.8
C      A(3)=A                                                           POT2.9
C      A(4)=ALPHA                                                       POT2.10
C      A(5)=C6                                                          POT2.11
C      A(6)=C8                                                          POT2.12
C      A(7)=C10                                                         POT2.13
C                                                                       POT2.14
      DIMENSION A(15),X(10),V(10),VP(10)                                POT2.15
      DO 10 I=1,L                                                       POT2.16
      R=X(I)*A(2)                                                       POT2.17
      RR=R*R                                                            POT2.18
      R6=RR**3                                                          POT2.19
      F=A(3)*EXP(-A(4)*R)                                               POT2.20
      G=-C6/R6-C8/R6/RR-C10/R6/RR/RR                                    POT2.21
      D=1.                                                              POT2.22
      IF(X(I).LE.1.28)D=EXP(-(1.28/X(I)-1.)**2)                         POT2.23
      V(I)=(F+G*D)/A(1)                                                 POT2.24
      FP=-F*A(4)                                                        POT2.25
      GP=6.*C6/R6/R+8.*C8/R6/RR/R+10.*C10/R6/RR/RR/R                    POT2.26
      DP=0.                                                             POT2.27
      IF(X(I).LE.1.28)DP=2.*1.28*D*(1.28*A(2)/R-1.)*A(2)/R/R            POT2.28
      VP(I)=(FP+GP*D+DP*G)/A(1)*A(2)                                    POT2.29
 10   CONTINUE                                                          POT2.30
      RETURN                                                            POT2.31
      END                                                               POT2.32


                                                                        POT2.33
      SUBROUTINE PREPOT(A,RM)                                           PREPOT2.2
      COMMON/POTPRE/C6,C8,C10,B1,B2,B3,B4,A1,A2,A3,A4                   POTPRE.2
C                                                                       PREPOT2.4
C     HFD POTENTIAL- SEE POT2 FOR DESCRIPTION OF FUNCTIONAL FORM AND    PREPOT2.5
C     DESCRIPTION  AND LITERATURE REFERENCE.                            PREPOT2.6
C                                                                       PREPOT2.7
      DIMENSION A(15)                                                   PREPOT2.8
      C6=A(5)                                                           PREPOT2.9
      C8=A(6)                                                           PREPOT2.10
      C10=A(7)                                                          PREPOT2.11
      H=EXP(-.28**2)                                                    PREPOT2.12
      T=2.*.28*1.28                                                     PREPOT2.13
      C1=(6.-T)*C6                                                      PREPOT2.14
      C2=(8.-T)*C8                                                      PREPOT2.15
```

```
      C3=(10.-T)*C10                                                    PREPOT2.16
      C4=2.*T                                                           PREPOT2.17
      C5=4.*1.28-6.*1.28*1.28                                           PREPOT2.18
      D6=C6*(6.*C4-42.-C5)                                              PREPOT2.19
      D8=C8*(-72.+8.*C4-C5)                                             PREPOT2.20
      D10=C10*(-110.+10.*C4-C5)                                         PREPOT2.21
C                                                                       PREPOT2.22
C      A MAXIMUM OF 100 ITERATIONS ALLOWED TO FIND RM.                  PREPOT2.23
C                                                                       PREPOT2.24
      DO 10 I=1,100                                                     PREPOT2.25
      RMIN=A(2)                                                         PREPOT2.26
      R=RMIN                                                            PREPOT2.27
      F=A(3)*EXP(-A(4)*A(2))                                            PREPOT2.28
      RR=RMIN*RMIN                                                      PREPOT2.29
      R6=RR**3                                                          PREPOT2.30
      G=-C6/R6-C8/R6/RR-C10/R6/RR/RR                                    PREPOT2.31
C                                                                       PREPOT2.32
C      COMPUTE FIRST AND SECOND DERIVATIVES                             PREPOT2.33
C                                                                       PREPOT2.34
      FP=-A(4)*F                                                        PREPOT2.35
      FPP=-A(4)*FP                                                      PREPOT2.36
      GP=H*(C1+C2/RR+C3/RR/RR)/R/R6                                     PREPOT2.37
      GPP=H*(D6+D8/RR+D10/RR/RR)/R6/RR                                  PREPOT2.38
      VP=FP+GP                                                          PREPOT2.39
      VPP=FPP+GPP                                                       PREPOT2.40
C                                                                       PREPOT2.41
C      NEWTON'S FORMULA FOR NEW VALUE OF RMIN                           PREPOT2.42
C                                                                       PREPOT2.43
      RNEW=RMIN-VP/VPP                                                  PREPOT2.44
      A(2)=RNEW                                                         PREPOT2.45
      IF(ABS(RNEW-RMIN).GT.1.E-05) GOTO 10                              PREPOT2.46
      A(1)=F+G*H                                                        PREPOT2.47
      A(1)=ABS(A(1))                                                    PREPOT2.48
      GOTO 20                                                           PREPOT2.49
 10   CONTINUE                                                          PREPOT2.50
      WRITE(6,15)                                                       PREPOT2.51
 15   FORMAT(10X,*PREPOT NOT CONVERGED*)                                PREPOT2.52
      STOP                                                              PREPOT2.53
 20   CONTINUE                                                          PREPOT2.54
      RETURN                                                            PREPOT2.55
      END                                                               PREPOT2.56


                                                                        PREPOT2.57
      SUBROUTINE POT(X,A,V,VP,L,RM)                                     POT3.2
      COMMON/POTPRE/C6,C8,C10,B1,B2,B3,B4,A1,A2,A3,A4                   POTPRE.2
C                                                                       POT3.4
C     LENNARD-JONES, JWKB                                               POT3.5
C      DEFINITION OF POTENTIAL PARAMETERS                               POT3.6
C      A(1)=EPSILON                                                     POT3.7
C      A(2)=RMIN                                                        POT3.8
C                                                                       POT3.9
```

```
      DIMENSION A(15),X(10),V(10),VP(10)                                POT3.10
      DO 10 I=1,L                                                       POT3.11
      XIN=1./X(I)                                                       POT3.12
      TEMP=XIN**6                                                       POT3.13
      V(I)=4.*TEMP*(TEMP-1)                                             POT3.14
      VP(I)=24.*TEMP*XIN*(1.-2.*TEMP)                                   POT3.15
   10 CONTINUE                                                          POT3.16
      RETURN                                                            POT3.17
      END                                                               POT3.18


                                                                        POT3.19
      SUBROUTINE PREPOT(A,RM)                                           PREPOT10.2
C     DUMMY PREPOT                                                      PREPOT10.3
      COMMON/POTPRE/C6,C8,C10,B1,B2,B3,B4,A1,A2,A3,A4                   POTPRE.2
      DIMENSION A(15)                                                   PREPOT10.5
      RETURN                                                            PREPOT10.6
      END                                                               PREPOT10.7


                                                                        PREPOT10.8
      SUBROUTINE POT(X,A,V,VP,L,RM)                                     POT11.2
C                                                                       POT11.3
C      HFD POTENTIAL- LEROY PHASE SHIFTS                                POT11.4
C      FOR DESCRIPTION OF FUNCTIONAL FORM,LITERATURE REFERENCE AND      POT11.5
C      EXPLANATION OF VARIABLES,SEE POT2                                POT11.6
C                                                                       POT11.7
      COMMON/POTPRE/C6,C8,C10,B1,B2,B3,B4,A1,A2,A3,A4                   POTPRE.2
      DIMENSION A(15),X(10),V(10),VP(10)                                POT11.9
      BZ=RM*A(1)*A(2)*A(2)*349.757/16.85763                             POT11.10
      DO 130 I=1,L                                                      POT11.11
      R=X(I)*A(2)                                                       POT11.12
      RR=R*R                                                            POT11.13
      R6=RR**3                                                          POT11.14
      F=A(3)*EXP(-A(4)*R)                                               POT11.15
      G=-C6/R6-C8/R6/RR-C10/R6/RR/RR                                    POT11.16
      D=1.                                                              POT11.17
      IF(X(I).LE.1.28) D=EXP(-(1.28/X(I)-1.)**2)                        POT11.18
C                                                                       POT11.19
C      CONVERT TO REDUCED ENERGY AND WAVENUMBERS                        POT11.20
C                                                                       POT11.21
      V(I)=BZ*(F+G*D)/A(1)                                              POT11.22
C                                                                       POT11.23
C      SET UP REDUCED CENTRIFUGAL ENERGY                                POT11.24
C                                                                       POT11.25
      TEMP=1./X(I)                                                      POT11.26
      X(I)=TEMP*TEMP                                                    POT11.27
  130 CONTINUE                                                          POT11.28
      RETURN                                                            POT11.29
      END                                                               POT11.30
```

```
                                                                        POT11.31
      SUBROUTINE PREPOT(A,RM)                                           PREPOT11.2
      COMMON/POTPRE/C6,C8,C10,B1,B2,B3,B4,A1,A2,A3,A4                   POTPRE.2
      COMMON/PTNL/V(2001),XM2(2001),XSTART,XSTEP,RNPHAS,ERROR           PTNL.2
      DIMENSION A(15)                                                   PREPOT11.5
C                                                                       PREPOT11.6
C       HFD POT ENT IAL- LEROY EXACT PHASE SHIFTS                       PREPOT11.7
C      FOR DESCRIPTION OF FUNCTIONAL FORM,LITERATURE REFERENCE, AND     PREPOT11.8
C      EXPLANATION OF VARIABLES SEE POT2.                               PREPOT11.9
C                                                                       PREPOT11.10
      XMIN=XSTART                                                       PREPOT11.11
      XH=XSTEP                                                          PREPOT11.12
      N=INT(RNPHAS)                                                     PREPOT11.13
      C10=A(13)/ERM6/A(2)**4                                            PREPOT11.14
      C6=A(5)                                                           PREPOT11.15
      C8=A(6)                                                           PREPOT11.16
      C10=A(7)                                                          PREPOT11.17
C                                                                       PREPOT11.18
C     SELF CONSISTENCY SECTION                                          PREPOT11.19
C     NEWTON SEARCH FOR RMIN.                                           PREPOT11.20
C                                                                       PREPOT11.21
      H=EXP(-.28**2)                                                    PREPOT11.22
      T=2.*.28*1.28                                                     PREPOT11.23
      C1=(6.-T)*C6                                                      PREPOT11.24
      C2=(8.-T)*C8                                                      PREPOT11.25
      C3=(10.-T)*C10                                                    PREPOT11.26
      C4=2.*T                                                           PREPOT11.27
      C5=4.*1.28-6.*1.28*1.28                                           PREPOT11.28
      D6=C6*(6.*C4-42.-C5)                                              PREPOT11.29
      D8=C8*(-72.+8.*C4-C5)                                             PREPOT11.30
      D10=C10*(-110.+10.*C4-C5)                                         PREPOT11.31
C                                                                       PREPOT11.32
C      A MAXIMUM OF 100 ITERATIONS ALLOWED TO FIND RM.                  PREPOT11.33
C                                                                       PREPOT11.34
      DO 10 I=1,100                                                     PREPOT11.35
      RMIN=A(2)                                                         PREPOT11.36
      R=RMIN                                                            PREPOT11.37
      F=A(3)*EXP(-A(4)*A(2))                                            PREPOT11.38
      RR=RMIN*RMIN                                                      PREPOT11.39
      R6=RR**3                                                          PREPOT11.40
      G=-C6/R6-C8/R6/RR-C10/R6/RR/RR                                    PREPOT11.41
C                                                                       PREPOT11.42
C      COMPUTE FIRST AND SECOND DERIVATIVES                             PREPOT11.43
C                                                                       PREPOT11.44
      FP=-A(4)*F                                                        PREPOT11.45
      FPP=-A(4)*FP                                                      PREPOT11.46
      GP=H*(C1+C2/RR+C3/RR/RR)/R/R6                                     PREPOT11.47
      GPP=H*(D6+D8/RR+D10/RR/RR)/R6/RR                                  PREPOT11.48
      VP=FP+GP                                                          PREPOT11.49
      VPP=FPP+GPP                                                       PREPOT11.50
C                                                                       PREPOT11.51
```

```
C      NEWTON'S FORMULA FOR NEW VALUE OF RMIN                          PREPOT11.52
C                                                                      PREPOT11.53
      RNEW=RMIN-VP/VPP                                                 PREPOT11.54
      A(2)=RNEW                                                        PREPOT11.55
      IF(ABS(RNEW-RMIN).GT.1.E-05) GOTO 10                             PREPOT11.56
      A(1)=F+G*H                                                       PREPOT11.57
      A(1)=ABS(A(1))                                                   PREPOT11.58
      GOTO 20                                                          PREPOT11.59
 10   CONTINUE                                                         PREPOT11.60
      WRITE(6,15)                                                      PREPOT11.61
 15    FORMAT(10X,*HFD PREPOT SEARCH FOR RMIN NOT CONVERGED AFTER 100 *  PREPOT11.62
     $*ITERATIONS*)                                                    PREPOT11.63
      STOP                                                             PREPOT11.64
 20   CONTINUE                                                         PREPOT11.65
      XST=XMIN-XH                                                      PREPOT11.66
C                                                                      PREPOT11.67
C      SET UP ARRAY OF POINTS FOR POTENTIAL CALCULATION NEEDED FOR PHASEPREPOT11.68
C      SHIFTS                                                          PREPOT11.69
C                                                                      PREPOT11.70
      DO 110 I=1,N                                                     PREPOT11.71
 110  XM2(I)=XST+I*XH                                                  PREPOT11.72
      DO 130 I=1,N                                                     PREPOT11.73
      R=XM2(I)*A(2)                                                    PREPOT11.74
      RR=R*R                                                           PREPOT11.75
      R6=RR**3                                                         PREPOT11.76
      F=A(3)*EXP(-A(4)*R)                                              PREPOT11.77
      G=-C6/R6-C8/R6/RR-C10/RR/RR/R6                                   PREPOT11.78
      D=1.                                                             PREPOT11.79
      IF(XM2(I).LE.1.28)D=EXP(-(1.28/XM2(I)-1.)**2)                    PREPOT11.80
C                                                                      PREPOT11.81
C      CONVERT TO WAVENUMBERS. ADDITIONAL FACTOR OF A(1) RESULTS FROM  PREPOT11.82
C      HFD BEING CALCULATED IN REAL ENERGY UNITS                       PREPOT11.83
C                                                                      PREPOT11.84
      V(I)=BZ*(F+G*D)/A(1)                                             PREPOT11.85
C                                                                      PREPOT11.86
C      SET UP ARRAY OF THE REDUCED CENTRIFUGAL POTENTIAL               PREPOT11.87
C                                                                      PREPOT11.88
      TEMP=1./XM2(I)                                                   PREPOT11.89
      XM2(I)=TEMP*TEMP                                                 PREPOT11.90
 130  CONTINUE                                                         PREPOT11.91
      RETURN                                                           PREPOT11.92
      END                                                              PREPOT11.93


                                                                       PREPOT11.94
      SUBROUTINE POT(X,A,V,VP,L,RM)                                    POT12.2
      DIMENSION A(15),V(10),X(10),VP(10)                               POT12.3
C                                                                      POT12.4
C LJ 6-12 EXACT PHASE SHIFTS                                           POT12.5
C      FOR DESCRIPTION OF FUNCTIONAL FORM, LITERATURE REFERENCE AND    POT12.6
C      EXPLANATION OF VARIABLES, SEE POT3.                             POT12.7
C                                                                      POT12.8
```

```
      BZ=RM*A(1)*A(2)*A(2)*349.757/16.85763                             POT12.9
      DO 10 I=1,L                                                       POT12.10
      XIN=1./X(I)                                                       POT12.11
      TEMP=XIN**6                                                       POT12.12
      V(I)=4.*TEMP*(TEMP-1.)                                            POT12.13
      V(I)=V(I)*BZ                                                      POT12.14
      X(I)=XIN*XIN                                                      POT12.15
 10   CONTINUE                                                          POT12.16
      RETURN                                                            POT12.17
      END                                                               POT12.18
```

```
                                                                        POT12.19
      SUBROUTINE PREPOT(A,RM)                                           PREPOT12.2
      COMMON/PTNL/V(2001),XM2(2001),XSTART,XSTEP,RNPHAS,ERROR           PTNL.2
      COMMON/POTPRE/C6,C8,C10,B1,B2,B3,B4,A1,A2,A3,A4                   POTPRE.2
      DIMENSION A(15)                                                   PREPOT12.5
C                                                                       PREPOT12.6
C     LJ 6-12 ^XACT PHASE SHIFTS                                        PREPOT12.7
C      FOR A DESCRIPTION OF FUNCTIONAL FORM,LITERATURE REFERENCE AND    PREPOT12.8
C      EXPLANATION OF VARIABLES, SEE POT3.                              PREPOT12.9
C                                                                       PREPOT12.10
      XMIN=XSTART                                                       PREPOT12.11
      BZ=RM*A(1)*A(2)*A(2)*349.757/16.85763                             PREPOT12.12
      XH=XSTEP                                                          PREPOT12.13
      L=INT(RNPHAS)                                                     PREPOT12.14
      XS=XMIN-XH                                                        PREPOT12.15
      DO 10 I=1,L                                                       PREPOT12.16
      XS=XS+XH                                                          PREPOT12.17
      XIN=1./XS                                                         PREPOT12.18
      TEMP=XIN**6                                                       PREPOT12.19
      V(I)=4.*TEMP*(TEMP-1.)                                            PREPOT12.20
      V(I)=V(I)*BZ                                                      PREPOT12.21
      XM2(I)=XIN*XIN                                                    PREPOT12.22
 10   CONTINUE                                                          PREPOT12.23
      RETURN                                                            PREPOT12.24
      END                                                               PREPOT12.25
```

```
                                                                        PREPOT12.26
      SUBROUTINE POT(X,A,V,VP,L,RM)                                     POT13.2
      COMMON/POTPRE/C6,C8,C10,B1,B2,B3,B4,A1,A2,A3,A4                   POTPRE.2
      DIMENSION A(15),V(10),VP(10),X(10)                                POT13.4
C                                                                       POT13.5
C     EXACT PHASE SHIFT SPHD POTENTIAL                                  POT13.6
C     JCP,71,PG.2638 (1979).                                            POT13.7
C     DEFINITION OF A ARRAY                                             POT13.8
C     A(1)=EPSILON,A(2)=RM,A(3)=A      ,A(4)=ALPHA,A(5)=B0,A(6)=B1,     POT13.9
C     A(7)=B2,A(8)=B3,A(9)=XF,A(10)=TAU,A(11)=X0.                       POT13.10
C      A(12)=C6,A(13)=C8,A(14)=C10                                      POT13.11
C                                                                       POT13.12
```

```
      BZ=RM*A(1)*A(2)*A(2)*349.757/16.85763                             POT13.13
      DO 10 I=1,L                                                       POT13.14
      Z=X(I)-A(9)                                                       POT13.15
      IF(Z.LT.0.) GOTO 20                                               POT13.16
C                                                                       POT13.17
C      DISPERSION SERIES                                                POT13.18
C                                                                       POT13.19
      XT=X(I)**6                                                        POT13.20
      X2=X(I)**2                                                        POT13.21
      V(I)=-(C6/XT+C8/XT/X2+C10/XT/X2/X2)                               POT13.22
      GOTO 30                                                           POT13.23
C                                                                       POT13.24
C      SPHD SERIES                                                      POT13.25
C                                                                       POT13.26
 20   Z=1.-1./X(I)                                                      POT13.27
      H=1./(1.+EXP(A(10)*(X(I)-A(11))))                                 POT13.28
      G=A(5)*Z*Z*(1.+Z*(A(6)+Z*(A(7)+Z*A(8))))-1.                       POT13.29
      V(I)=H*A(3)*EXP(-A(4)*A(2)*X(I)  )/A(1)+(1.-H)*G                  POT13.30
C                                                                       POT13.31
C      CONVERT POTENTIAL TO WAVENUMBERS AND CALCULATE REDUCED           POT13.32
C      CENTRIFUGAL POTENTIAL ARRAY                                      POT13.33
C                                                                       POT13.34
 30   X(I)=1./X(I)/X(I)                                                 POT13.35
      V(I)=V(I)*BZ                                                      POT13.36
 10   CONTINUE                                                          POT13.37
      RETURN                                                            POT13.38
      END                                                               POT13.39


                                                                        POT13.40
      SUBROUTINE PREPOT(A,RM)                                           PREPOT13.2
      COMMON/PTNL/V(2001),XM2(2001),XSTART,XSTEP,RNPHAS,ERROR           PTNL.2
      COMMON/POTPRE/C6,C8,C10,B1,B2,B3,B4,A1,A2,A3,A4                   POTPRE.2
      DIMENSION A(15)                                                   PREPOT13.5
C                                                                       PREPOT13.6
C   SPHD EXACT POTENTIAL                                                PREPOT13.7
C                                                                       PREPOT13.8
      BZ=RM*A(1)*A(2)*A(2)*349.757/16.85763                             PREPOT13.9
      XMIN=XSTART                                                       PREPOT13.10
      XH=XSTEP                                                          PREPOT13.11
       L=INT(RNPHAS)                                                    PREPOT13.12
      XS=XMIN-XH                                                        PREPOT13.13
C                                                                       PREPOT13.14
C      CONVERT DISPERSION CONSTANTS TO REDUCED UNITS                    PREPOT13.15
C                                                                       PREPOT13.16
      D6=A(12)                                                          PREPOT13.17
      D8=A(13)                                                          PREPOT13.18
      D10=A(14)                                                         PREPOT13.19
      ERM6=A(1)*A(2)**6                                                 PREPOT13.20
      C6=D6/ERM6                                                        PREPOT13.21
      C8=D8/ERM6/A(2)**2                                                PREPOT13.22
      C10=D10/ERM6/A(2)**4                                              PREPOT13.23
C                                                                       PREPOT13.24
```

```
C      B2,B3 ARE USED TO MATCH DISPERSION SERIES AND ITS FIRST          PREPOT13.25
C      DERIVATIVE AT XF.                                                PREPOT13.26
C                                                                       PREPOT13.27
      XF=A(9)                                                           PREPOT13.28
      H=1./(1.+EXP(A(10)*(XF-A(11))))                                   PREPOT13.29
      H1=-H*H*EXP(A(10)*(XF-A(11)))*A(10)                               PREPOT13.30
      XF6=XF**6                                                         PREPOT13.31
      XF2=XF*XF                                                         PREPOT13.32
      F=-(C6/XF6+C8/XF6/XF2+C10/XF6/XF2/XF2)                            PREPOT13.33
      F1=(6.*C6/XF6+8.*C8/XF2/XF6+10.*C10/XF2/XF6)/XF                   PREPOT13.34
      G=H*A(3)*EXP(-A(4)*XF)                                            PREPOT13.35
      G1=G*(H1/H-A(4))                                                  PREPOT13.36
      RL=1.-1./XF                                                       PREPOT13.37
      T=-1.+RL*RL*(A(5)+A(6)*RL)                                        PREPOT13.38
      RL1=1./XF2                                                        PREPOT13.39
      CNST1=(F+1.)/RL/RL/A(5)                                           PREPOT13.40
      CNST1=CNST1-1.-RL*A(6)                                            PREPOT13.41
      CNST2=F1/A(5)/RL/RL1                                              PREPOT13.42
      CNST2=CNST2-2.-3.*A(6)*RL                                         PREPOT13.43
      A(7)=(5.*CNST1-CNST2)/RL**2                                       PREPOT13.44
      A(8)=(CNST2-4.*CNST1)/RL**3                                       PREPOT13.45
      DO 10 I=1,L                                                       PREPOT13.46
      XS=XS+XH                                                          PREPOT13.47
      XM2(I)=XS                                                         PREPOT13.48
      Z=XM2(I)-A(9)                                                     PREPOT13.49
      IF(Z.LT.0.) GOTO 20                                               PREPOT13.50
C                                                                       PREPOT13.51
C      DISPERSION SERIES                                                PREPOT13.52
C                                                                       PREPOT13.53
      XT=XM2(I)**6                                                      PREPOT13.54
      X2=XM2(I)**2                                                      PREPOT13.55
      V(I)=-(C6/XT+C8/XT/X2+C10/XT/X2/X2)                               PREPOT13.56
      GOTO 30                                                           PREPOT13.57
C                                                                       PREPOT13.58
C      SPHD SERIES                                                      PREPOT13.59
C                                                                       PREPOT13.60
 20   Z=1.-1./XM2(I)                                                    PREPOT13.61
      H=1./(1.+EXP(A(10)*(XM2(I)-A(11))))                               PREPOT13.62
      G=A(5)*Z*Z*(1.+Z*(A(6)+Z*(A(7)+Z*A(8))))-1.                       PREPOT13.63
      V(I)=H*A(3)*EXP(-A(4)*A(2)*XM2(I))/A(1)+(1.-H)*G                  PREPOT13.64
 30   XM2(I)=1./XM2(I)/XM2(I)                                           PREPOT13.65
      V(I)=V(I)*BZ                                                      PREPOT13.66
 10   CONTINUE                                                          PREPOT13.67
      RETURN                                                            PREPOT13.68
      END                                                               PREPOT13.69


                                                                        PREPOT13.70
      SUBROUTINE POT(X,A,V,VP,L,RM)                                     POT14.2
C                                                                       POT14.3
C      ESMMSV-EXACT PHASE SHIFTS                                        POT14.4
C                                                                       POT14.5
C      DEFINITION OF POTENTIAL PARAMETERS? SEE JCP,71,P. 2638 (1979).   POT14.6
```

```
C       FOR BASIC REFERENCE                                              POT14.7
C       A(1)=EPSILON, A(2)=RM,A(3)=A,A(4)=ALPHA,A(5)=X1,A(6)=X2,A(7)=X3, POT14.8
C       A(8)=X4,A(9)=BETA1,A(10)=C6,A(11)=C8,A(12)= BETA2                POT14.9
C                                                                        POT14.10
C       NOTE THAT THE FOLLOWING MODIFICATIONS HAVE BEEN MADE TO THIS     POT14.11
C       VERSION OF THE POTENTIAL.                                        POT14.12
C       1. THE FIRST MORSE POTENTIAL EXTENDS FROM X2 TO RM.              POT14.13
C       2. THE SECOND MORSE POTENTIAL EXTENDS FROM RM TO X3.             POT14.14
C       3. THE SECOND MORSE IS SPLINED TO THE DISPERSION SERIES USING A  POT14.15
C       TRIGONOMETRIC SWITCHING FUNCTION, INSTEAD OF A POLYNOMIAL SPLINE.POT14.16
C                                                                        POT14.17
      COMMON/POTPRE/C6,C8,C10,B1,B2,B3,B4,A1,A2,A3,A4                    POTPRE.2
      DIMENSION X(10),A(15),V(10),VP(10)                                 POT14.19
      RZ=RM*A(1)*A(2)*A(2)*349.757/16.85763                              POT14.20
      DO 200 I=1,L                                                       POT14.21
       T4=X(I)-A(5)                                                      POT14.22
      IF(T4)1,1,2                                                        POT14.23
C                                                                        POT14.24
C      EXPONENTIAL REPULSIVE WALL                                        POT14.25
C                                                                        POT14.26
 1     V(I)=A(3)*EXP(-A(4)*(X(I)-1.))                                    POT14.27
      VP(I)=-A(4)*V(I)                                                   POT14.28
      GOTO 100                                                           POT14.29
 2     T5=X(I)-A(6)                                                      POT14.30
      IF(T5)3,4,4                                                        POT14.31
C                                                                        POT14.32
C      EXPONENTIAL SPLINE                                                POT14.33
C                                                                        POT14.34
  3     V(I)=EXP(A1+T4*(A2+T5*(A3+A4*T4)))                               POT14.35
      VP(I)=V(I)*(A2+A3*(T4+T5)+A4*T4*(T4+2.*T5))                        POT14.36
      GOTO 100                                                           POT14.37
 4     T1=X(I)-1.                                                        POT14.38
      IF(T1)5,5,6                                                        POT14.39
C                                                                        POT14.40
C      FIRST MORSE (X<1)                                                 POT14.41
C                                                                        POT14.42
 5    TEMP=EXP(-A(9)*T1)                                                 POT14.43
      V(I)=TEMP*(TEMP-2.)                                                POT14.44
      VP(I)=2.*A(9)*TEMP*(1.-TEMP)*(-1)                                  POT14.45
      GOTO 100                                                           POT14.46
 6    T2=X(I)-A(7)                                                       POT14.47
      IF(T2) 7,8,8                                                       POT14.48
C                                                                        POT14.49
C      SECOND MORSE                                                      POT14.50
C                                                                        POT14.51
 7    TEMP=EXP(-A(12)*T1)                                                POT14.52
      V(I)=TEMP*(TEMP-2.)                                                POT14.53
      VP(I)=2.*A(9)*TEMP*(1.-TEMP)*(-1)                                  POT14.54
      GOTO 100                                                           POT14.55
 8     T3=X(I)-A(8)                                                      POT14.56
      IF(T3) 9,9,10                                                      POT14.57
 9     CONTINUE                                                          POT14.58
C                                                                        POT14.59
```

```
C      TRIGONOMETRIC SWITCHING REGION FROM SECOND MORSE TO DISPERSION   POT14.60
C      SERIES                                                           POT14.61
C                                                                       POT14.62
      TEMP=EXP(-A(12)*T1)                                               POT14.63
      RR=X(I)**2                                                        POT14.64
      R6=RR**3                                                          POT14.65
      R8=RR*R6                                                          POT14.66
      R10=R8*RR                                                         POT14.67
      D=-C6/R6-C8/R8-C10/R10                                            POT14.68
      RTT2=3.141592/(A(8)-A(7))                                         POT14.69
      RTT1=(X(I)-A(7))*RTT2                                             POT14.70
      S=.5*(COS(RTT1)+1.)                                               POT14.71
      DS=-RTT2*SIN(RTT1)/2.                                             POT14.72
      RMORSE=TEMP*(TEMP-2.)                                             POT14.73
      V(I)=RMORSE*S+(1.-S)*D                                            POT14.74
      VP(I)=(RMORSE-D)*DS+S*2.*A(12)*TEMP*(1.-TEMP)                     POT14.75
      VP(I)=VP(I)+(1.-S)*6.*C6/R6/X(I)+8.*C8/R8/X(I)+10.*C10/R10/X(I)   POT14.76
      GOTO 100                                                          POT14.77
C                                                                       POT14.78
C      DISPERSION SERIES                                                POT14.79
C                                                                       POT14.80
 10   RR=X(I)**2                                                        POT14.81
      R6=RR**3                                                          POT14.82
      R8=RR*R6                                                          POT14.83
      R10=RR*R8                                                         POT14.84
      V(I)=-C6/R6-C8/R8-C10/R10                                         POT14.85
      VP(I)=6.*C6/R6/X(I)+8.*C8/R8/X(I)+10.*C10/R10/X(I)                POT14.86
 100  CONTINUE                                                          POT14.87
C                                                                       POT14.88
C      CONVERT TO WAVENUMBERS AND RETURN REDUCED CENTRIFUGAL POTENTIAL  POT14.89
C                                                                       POT14.90
      V(I)=V(I)*BZ                                                      POT14.91
      X(I)=1./X(I)/X(I)                                                 POT14.92
 200  CONTINUE                                                          POT14.93
      RETURN                                                            POT14.94
      END                                                               POT14.95


                                                                        POT14.96
      SUBROUTINE PREPOT(A,RM)                                           PREPOT14.2
      DIMENSION A(15)                                                   PREPOT14.3
      COMMON/PTNL/V(2001),XM2(2001),XSTART,XSTEP,RNPHAS,ERROR           PTNL.2
      COMMON/POTPRE/C6,C8,C10,B1,B2,B3,B4,A1,A2,A3,A4                   POTPRE.2
C                                                                       PREPOT14.6
C      ESMMSV - EXACT PHASE SHIFTS.                                     PREPOT14.7
C      SEE POT 14 FOR DETAILS ON THE POTENTIAL PARAMETERS. IN THIS      PREPOT14.8
C      VERSION OF THE ESMMSV POTENTIAL, THE TWO MORSE POTENTIALS JOIN ATPREPOT14.9
C      RM, AND THE DISPERSION SERIES IS SWITCHED ON WITH A TRIGONOMETRICPREPOT14.10
C       FUNCTION, NOT A POLYNOMIAL SPLINE.                              PREPOT14.11
C                                                                       PREPOT14.12
      BZ=RM*A(1)*A(2)*A(2)*349.757/16.85763                             PREPOT14.13
      XMIN=XSTART                                                       PREPOT14.14
      XH=XSTEP                                                          PREPOT14.15
```

```
      L=INT(RNPHAS)                                                     PREPOT14.16
      XS=XMIN-XH                                                        PREPOT14.17
C                                                                       PREPOT14.18
C      CONVERT DISPERSION CONSTANTS TO REDUCED UNITS                    PREPOT14.19
C                                                                       PREPOT14.20
      ERM6=A(1)*A(2)**6                                                 PREPOT14.21
      C6=A(10)/ERM6                                                     PREPOT14.22
      C8=A(11)/ERM6/A(2)**2                                             PREPOT14.23
      C10=A(13)/ERM6/A(2)**4                                            PREPOT14.24
C                                                                       PREPOT14.25
C      CHECK THAT THE MORSE CURVATURE AND SPLINE POINTS ARE COMPATIBLE  PREPOT14.26
C                                                                       PREPOT14.27
      IF(.5.GT. EXP(A(9)*(A(6)-1.))) GOTO 20                            PREPOT14.28
      WRITE(6,11) A(9),A(6)                                             PREPOT14.29
 11   FORMAT(10X,* IN SUBROUTINE PREPOT14, THE MORSE CURVATURE PARAMETERPREPOT14.30
     $ A(9) IS INCOMPATIBLE WITH THE EXPONENTIAL*,/,10X,*SPLINE POINT X PREPOT14.31
     $3. THEIR VALUES ARE*,2(2X,E14.7),10X,*RESPECTIVELY*,/)            PREPOT14.32
      STOP                                                              PREPOT14.33
20     CONTINUE                                                         PREPOT14.34
C                                                                       PREPOT14.35
C      COMPUTE SPLINE CONSTANTS FOR EXPONENTIAL WALL ,FIRST MORSE       PREPOT14.36
C                                                                       PREPOT14.37
      A1=ALOG(A(3))-A(4)*(A(5)-1.)                                      PREPOT14.38
      TEMP=EXP(-2.*A(9)*(A(6)-1.))-2.*EXP(-A(9)*(A(6)-1.))              PREPOT14.39
      A2=(ALOG(TEMP)-A1)/(A(6)-A(5))                                    PREPOT14.40
      A3=-(A(4)+A2)/(A(5)-A(6))                                         PREPOT14.41
      A4=2.*A(9)*(EXP(-A(9)*(A(6)-1.))-EXP(-2.*A(9)*(A(6)-1.)))*EXP(-(A1PREPOT14.42
     ;+A2*(A(6)-A(5))))-A2-A3*(A(6)-A(5))                               PREPOT14.43
      A4=A4/(A(6)-A(5))**2                                              PREPOT14.44
C                                                                       PREPOT14.45
C      SET UP POTENTIAL ARRAY FOR PHASE SHIFT CALCULATION               PREPOT14.46
C                                                                       PREPOT14.47
      DO 500 I=1,L                                                      PREPOT14.48
      XS=XS+XH                                                          PREPOT14.49
      T4=XS-A(5)                                                        PREPOT14.50
      IF(T4)1,1,2                                                       PREPOT14.51
C                                                                       PREPOT14.52
C      REPULSIVE WALL                                                   PREPOT14.53
C                                                                       PREPOT14.54
 1     V(I)=A(3)*EXP(-A(4)*(XS-1.))                                     PREPOT14.55
      GOTO 100                                                          PREPOT14.56
 2     T5=XS-A(6)                                                       PREPOT14.57
      IF(T5)3,4,4                                                       PREPOT14.58
C                                                                       PREPOT14.59
C      EXPONENTIAL SPLINE                                               PREPOT14.60
C                                                                       PREPOT14.61
 3     V(I)=EXP(A1+T4*(A2+T5*(A3+A4*T4)))                               PREPOT14.62
      GOTO 100                                                          PREPOT14.63
 4     T1=XS-1.                                                         PREPOT14.64
      IF(T1)5,5,6                                                       PREPOT14.65
C                                                                       PREPOT14.66
C      FIRST MORSE (X<1.)                                               PREPOT14.67
C                                                                       PREPOT14.68
```

```
  5    TEMP=EXP(-A(9)*T1)                                                PREPOT14.69
       V(I)=TEMP*(TEMP-2.)                                               PREPOT14.70
       GOTO 100                                                          PREPOT14.71
    6  T2=XS-A(7)                                                        PREPOT14.72
       IF(T2) 7,8,8                                                      PREPOT14.73
C                                                                        PREPOT14.74
C       SECOND MORSE                                                     PREPOT14.75
C                                                                        PREPOT14.76
  7    TEMP=EXP(-A(12)*T1)                                               PREPOT14.77
       V(I)=TEMP*(TEMP-2.)                                               PREPOT14.78
       GOTO 100                                                          PREPOT14.79
  8    T3=XS-A(8)                                                        PREPOT14.80
       IF(T3) 9,9,10                                                     PREPOT14.81
  9     CONTINUE                                                         PREPOT14.82
C                                                                        PREPOT14.83
C       SWITCHING FUNCTION FROM SECOND MORSE TO DISPERSION SERIES        PREPOT14.84
C                                                                        PREPOT14.85
       TEMP=EXP(-A(12)*T1)                                               PREPOT14.86
       RR=XS**2                                                          PREPOT14.87
       R6=RR**3                                                          PREPOT14.88
       R8=RR*R6                                                          PREPOT14.89
       R10=R8*RR                                                         PREPOT14.90
       D=-C6/R6-C8/R8-C10/R10                                            PREPOT14.91
       RTT2=3.141592/(A(8)-A(7))                                         PREPOT14.92
       RTT1=T2*RTT2                                                      PREPOT14.93
       S=.5*(COS(RTT1)+1.)                                               PREPOT14.94
       RMORSE=TEMP*(TEMP-2.)                                             PREPOT14.95
       V(I)=RMORSE*S+(1.-S)*D                                            PREPOT14.96
       GOTO 100                                                          PREPOT14.97
C                                                                        PREPOT14.98
C       DISPERSION SERIES                                                PREPOT14.99
C                                                                        PREPOT14.100
 10    RR=XS**2                                                          PREPOT14.101
       R6=RR**3                                                          PREPOT14.102
       R8=RR*R6                                                          PREPOT14.103
       R10=RR*R8                                                         PREPOT14.104
       V(I)=-C6/R6-C8/R8-C10/R10                                         PREPOT14.105
 100   CONTINUE                                                          PREPOT14.106
C                                                                        PREPOT14.107
C       CONVERT POTENTIAL TO WAVENUMBERS AND SET UP CENTRIFUGAL POTENTIALPREPOT14.108
C      IN REDUCED UNITS                                                  PREPOT14.109
C                                                                        PREPOT14.110
       XM2(I)=1./XS/XS                                                   PREPOT14.111
       V(I)=V(I)*BZ                                                      PREPOT14.112
 500   CONTINUE                                                          PREPOT14.113
       RETURN                                                            PREPOT14.114
       END                                                               PREPOT14.115


                                                                         PREPOT14.116
       SUBROUTINE POT(X,A,V,VP,L,RM)                                     POT15.2
C                                                                        POT15.3
C      ESMMSV EXACT ETA'S                                                POT15.4
```

```
C
C      DEFINITION OF POTENTIAL PARAMETERS? SEE JCP,70,P. 489 (1979)
C      A(1)=EPSILON,A(2)=RM,A(3)=A,A(4)=ALPHA,A(5)=X1,A(6)=X2,A(7)=X3,
C      A(8)=X4,A(9)=BETA1,A(10)=C6,A(11)=C8,A(12)=BETA2
C
C      THE FOLLOWING ARE THE MAIN DIFFERENCES BETWEEN THIS VERSION AND
C      POT14
C      1. THE OUTER MORSE IS SPLINED TO THE DISPERSION SERIES
C     2. THE TWO MORSE PARTS ARE JOINED AT THE SIGMA POINT.
C
      COMMON/POTPRE/C6,C8,C10,B1,B2,B3,B4,A1,A2,A3,A4
      DIMENSION X(10),A(15),V(10),VP(10)
      RT=ALOG(2.)
      BZ=RM*A(1)*A(2)*A(2)*349.757/16.85763
      DO 200 I=1,L
      T1=X(I)-A(5)
      IF(T1)5,5,6
C
C      EXPONENTIAL REPULSIVE WALL
C
 5    V(I)=A(3)*EXP(-A(4)*(X(I)-1.))
      GOTO 100
 6     T2=X(I)-A(6)
      IF(T2)7,8,8
C
C      EXPONENTIAL SPLINE
C
 7    V(I)=EXP(A1+T1*(A2+T2*(A3+A4*T1)))
      GOTO 100
 8    T3=X(I)-1.+RT/A(12)
      IF(T3)9,9,10
C
C      FIRST MORSE (R< SIGMA)
C
 9    W=(A(9)-RT)/(A(12)-RT)
      E1=EXP(A(9)-X(I)*A(12)*W)
      V(I)=E1*(E1-2.)/W
      GOTO 100
 10   T4=X(I)-A(7)
      IF(T4) 11,12,12
C
C      SECOND MORSE
C
 11   E1=EXP(-2.*A(12)*(X(I)-1.))
      E2=EXP(-A(12)*(X(I)-1.))
      V(I)=E1-2.*E2
      GOTO 100
 12   T4=X(I)-A(8)
      T3=X(I)-A(7)
      IF(T4)13,14,14
C
C      POLYNOMIAL SPLINE TO DISPERSION SERIES
C
```

```
 13   V(I)=B1+T3*(B2+T4*(B3+T3*B4))                                    POT15.58
      GOTO 100                                                         POT15.59
C                                                                      POT15.60
C      DISPERSION SERIES                                               POT15.61
C                                                                      POT15.62
 14   RR=X(I)**2                                                       POT15.63
      R6=RR**3                                                         POT15.64
      R8=RR*R6                                                         POT15.65
      R10=RR*R8                                                        POT15.66
      V(I)=-C6/R6-C8/R8-C10/R10                                        POT15.67
 100  CONTINUE                                                         POT15.68
C                                                                      POT15.69
C       CONVERT TO REDUCED UNITS, SET UP CENTRIFUGAL POTENTIAL.        POT15.70
C                                                                      POT15.71
      V(I)=V(I)*BZ                                                     POT15.72
      X(I)=1./X(I)/X(I)                                                POT15.73
 200  CONTINUE                                                         POT15.74
      RETURN                                                           POT15.75
      END                                                              POT15.76


                                                                       POT15.77
      SUBROUTINE PREPOT(A,RM)                                          PREPOT15.2
      DIMENSION A(15)                                                  PREPOT15.3
      COMMON/PTNL/V(2001),XM2(2001),XSTART,XSTEP,RNPHAS,ERROR          PTNL.2
      COMMON/POTPRE/C6,C8,C10,B1,B2,B3,B4,A1,A2,A3,A4                  POTPRE.2
C                                                                      PREPOT15.6
C      ESMMSV- EXACT PHASE SHIFTS                                      PREPOT15.7
C      MORSE POTENTIALS JOINED AT THE SIGMA POINT                      PREPOT15.8
C      POLYNOMIAL SPLINE TO THE DISPERSION SERIES                      PREPOT15.9
C                                                                      PREPOT15.10
      RT=ALOG(2.)                                                      PREPOT15.11
      BZ=RM*A(1)*A(2)*A(2)*349.757/16.85763                            PREPOT15.12
      XMIN=XSTART                                                      PREPOT15.13
      XH=XSTEP                                                         PREPOT15.14
      L=INT(RNPHAS)                                                    PREPOT15.15
      XS=XMIN-XH                                                       PREPOT15.16
C                                                                      PREPOT15.17
C      CONVERT DISPERSION CONSTANTS TO REDUCED UNITS                   PREPOT15.18
C                                                                      PREPOT15.19
      ERM6=A(1)*A(2)**6                                                PREPOT15.20
      C6=A(10)/ERM6                                                    PREPOT15.21
      C8=A(11)/ERM6/A(2)**2                                            PREPOT15.22
      C10=0.                                                           PREPOT15.23
C                                                                      PREPOT15.24
C      CALCULATE SPLINE COEFFICIENTS TO EXPONENTIAL WALL               PREPOT15.25
C                                                                      PREPOT15.26
      A1=ALOG(A(3))-A(4)*(A(5)-1.)                                     PREPOT15.27
      TEMP=EXP(-2.*A(9)*(A(6)-1.))-2.*EXP(-A(9)*(A(6)-1.))             PREPOT15.28
      IF(TEMP.GT.0.) GOTO 20                                           PREPOT15.29
      WRITE(6,21) A(6),A(9)                                            PREPOT15.30
 21    FORMAT(2X,*IN PREPOT15, SPLINE POINT AND MORSE CURVATURE NOT *  PREPOT15.31
     $*COMPATIBLE*,2(2X,E10.4))                                        PREPOT15.32
```

```
      STOP                                                              PREPOT15.33
20     CONTINUE                                                         PREPOT15.34
      A2=(ALOG(TEMP)-A1)/(A(6)-A(5))                                    PREPOT15.35
      A3=-(A(4)+A2)/(A(5)-A(6))                                         PREPOT15.36
      A4=2.*A(9)*(EXP(-A(9)*(A(6)-1.))-EXP(-2.*A(9)*(A(6)-1.)))*EXP(-(A1PREPOT15.37
     1+A2*(A(6)-A(5))))-A2-A3*(A(6)-A(5))                               PREPOT15.38
      A4=A4/(A(6)-A(5))**2                                              PREPOT15.39
      TT=A(12)*(A(7)-1.)                                                PREPOT15.40
C                                                                       PREPOT15.41
C      CALCULATE SPLINE CONSTANTS  TO DISPERSION SERIES                 PREPOT15.42
C                                                                       PREPOT15.43
      B1=EXP(-2.*TT)-2.*EXP(-TT)                                        PREPOT15.44
      TEMP=-C6/A(8)**6-C8/A(8)**8-C10/A(8)**10                          PREPOT15.45
      B2=(TEMP-B1)/(A(8)-A(7))                                          PREPOT15.46
      TEMP=-2.*A(12)*EXP(-2.*TT)+2.*EXP(-TT)*A(12)                      PREPOT15.47
      B3=(TEMP-B2)/(A(7)-A(8))                                          PREPOT15.48
      TEMP=6.*C6/A(8)**7+8.*C8/A(8)**9+10.*C10/A(8)**11                 PREPOT15.49
      B4=(TEMP-B2-B3*(A(8)-A(7)))/(A(8)-A(7))**2                        PREPOT15.50
      DO 500 I=1,L                                                      PREPOT15.51
      XS=XS+XH                                                          PREPOT15.52
      T1=XS-A(5)                                                        PREPOT15.53
      IF(T1)5,5,6                                                       PREPOT15.54
C                                                                       PREPOT15.55
C      REPULSIVE EXPONENTIAL WALL                                       PREPOT15.56
C                                                                       PREPOT15.57
 5    V(I)=A(3)*EXP(-A(4)*(XS-1.))                                      PREPOT15.58
      GOTO 100                                                          PREPOT15.59
 6     T2=XS-A(6)                                                       PREPOT15.60
      IF(T2)7,8,8                                                       PREPOT15.61
C                                                                       PREPOT15.62
C      EXPONENTIAL SPLINE                                               PREPOT15.63
C                                                                       PREPOT15.64
 7    V(I)=EXP(A1+T1*(A2+T2*(A3+A4*T1)))                                PREPOT15.65
      GOTO 100                                                          PREPOT15.66
 8    T3=XS  -1.+RT/A(12)                                               PREPOT15.67
      IF(T3)9,9,10                                                      PREPOT15.68
C                                                                       PREPOT15.69
C      FIRST MORSE (X<SIGMA)                                            PREPOT15.70
C                                                                       PREPOT15.71
 9    W=(A(9)-RT)/(A(12)-RT)                                            PREPOT15.72
      E1=EXP(A(9)-XS  *A(12)*W)                                         PREPOT15.73
      V(I)=E1*(E1-2.)/W                                                 PREPOT15.74
      GOTO 100                                                          PREPOT15.75
 10   T4=XS  -A(7)                                                      PREPOT15.76
      IF(T4) 11,12,12                                                   PREPOT15.77
C                                                                       PREPOT15.78
C      SECOND MORSE                                                     PREPOT15.79
C                                                                       PREPOT15.80
 11   E1=EXP(-2.*A(12)*(XS  -1.))                                       PREPOT15.81
      E2=EXP(-A(12)*(XS  -1.))                                          PREPOT15.82
      V(I)=E1-2.*E2                                                     PREPOT15.83
      GOTO 100                                                          PREPOT15.84
 12   T4=XS  -A(8)                                                      PREPOT15.85
```

```
      T3=XS  -A(7)                                                      PREPOT15.86
      IF(T4)13,14,14                                                    PREPOT15.87
C                                                                       PREPOT15.88
C      POLYNOMIAL SPLINE                                                PREPOT15.89
C                                                                       PREPOT15.90
 13   V(I)=B1+T3*(B2+T4*(B3+T3*B4))                                     PREPOT15.91
      GOTO 100                                                          PREPOT15.92
C                                                                       PREPOT15.93
C      DISPERSION SERIES                                                PREPOT15.94
C                                                                       PREPOT15.95
 14   RR=XS  **2                                                        PREPOT15.96
      R6=RR**3                                                          PREPOT15.97
      R8=RR*R6                                                          PREPOT15.98
      R10=RR*R8                                                         PREPOT15.99
      V(I)=-C6/R6-C8/R8-C10/R10                                         PREPOT15.100
 100  CONTINUE                                                          PREPOT15.101
C                                                                       PREPOT15.102
C      CONVERT POTENTIAL TO REDUCED UNITS AND SET UP CENTRIFUGAL POTENT.PREPOT15.103
C                                                                       PREPOT15.104
      XM2(I)=1./XS/XS                                                   PREPOT15.105
      V(I)=V(I)*BZ                                                      PREPOT15.106
 500  CONTINUE                                                          PREPOT15.107
      RETURN                                                            PREPOT15.108
      END                                                               PREPOT15.109
```

CHAPTER II. INFRARED VIBRATIONAL PREDISSOCIATION OF C_6H_6, H_2O, and NH_3 CLUSTERS STUDIED BY THE CROSSED LASER-MOLECULAR BEAM TECHNIQUE

A. INTRODUCTION

Since the observation by Welsh and McKellar of fine structure in the pressure induced infra-red spectra of H_2 with various gases (D_2, H_2, Ar, Kr, Xe, N_2, etc.) at low temperatures,[1] van der Waals molecules and molecular clusters have exhibited a number of intriguing properties which test our understanding of intermolecular forces. One property, in particular, which has been recently studied both experimentally and theoretically, is the vibrational predissociation lifetime of a van der Waals molecule when one of the vibrations of the strong chemical bonds is excited. This vibrational energy is typically 5-50 times the van der Waals bond energy. Early calculations by Child[2] on the lifetimes of Ar...HCl(v=1) suggested that the vibrationally excited complex was stable to dissociation for times comparable to the infrared radiative lifetime. The spectra of McKellar and Welsh showed that for systems such as Ar...H_2(v=1), the lifetimes are sufficiently long to resolve rotational motions of the H_2 molecule within the complex.

In 1978, Scoles, Gough, and their coworkers[3] first observed directly the vibrational predissociation of a van der Waals molecule, $(N_2O)_2$, in the ground electronic state, obtaining a lifetime in the range 10^{-12} - 10^{-4} seconds. The clusters were excited by a diode laser and the predissociation observed as a decrease in signal

at a bolometer which monitored the molecular beam. Since that time, the Waterloo group has studied CO_2 clusters using an F-center laser for excitation.[4] Levy and coworkers have performed many experiments on the vibrational predissociation of rare gas-iodine clusters in an excited electronic state.[5] The predissociation was observed in the dispersed fluorescence spectrum of the I_2 fragment produced by the predissociation. Limits to the lifetimes could be determined from the absorption linewidths or by using competing I_2 electronic predissociation or fluorescence rates as an internal clock. From these results, a detailed picture of the propensity rules in vibrational predissociation has been obtained. In addition to earlier work in our laboratory on $(NH_3)_2$,[6] Reuss,[7] Gentry,[8] and Janda[9] and their coworkers have observed vibrational predissociation of various clusters with CW or pulsed CO_2 lasers and mass spectrometer detectors. In particular, Janda was able to argue convincingly that on the basis of the observed linewidths and signal strengths, the predissociation was occurring on a timescale of 0.3 - 1.0 picoseconds for ethylene complexes. Current theoretical and experimental studies have considered small clusters as simple model systems for condensed phases. To test the accuracy of cluster models, experimental data for a wide range of compounds with different strengths of intermolecular forces is needed.

In the remainder of this chapter, results are presented on vibrational predissociation studies of C_6H_6, H_2O, and NH_3 molecular clusters. First, a general description of the experimental techniques and measured quantities is presented. Next, the detailed analyses for

each system are presented. Finally, a summary will generalize the individual results where possible.

B. EXPERIMENTAL ARRANGEMENT

The two experimental methods described below utilize a supersonic expansion to prepare a spatially well defined molecular beam containing molecular clusters, an infrared laser to excite the vibrational motions of interest, and a mass spectrometer to detect the effects on the clusters of laser excitation. One scheme is based on looking for the disappearance of clusters in the molecular beam correlated with the pulsed laser, similar to the method of Janda, et al.,[9] while a second scheme monitors the appearance of molecular fragments created by the predissociation as in photofragment translational energy spectroscopy.[10]

1. Infrared Laser

Tunable, infra-red radiation is generated by a Nd:YAG pumped optical parametric oscillator (OPO) based on the L-shaped cavity design of Byer, et al.[22] The far-field pumping arrangement, cavity design, and optics are shown in Fig. 1. The idler frequency easily tunes in the 2800-4000 cm^{-1} range spanning CH, OH, NH, and F-H stretching motions. The repetition rate is 10 Hz, and the output power is 1-4 millijoules/pulse, with 1 joule/cm^{-2} of Nd:YAG pump energy fluence. The OPO linewidth (the frequency difference between the half power points) in this wavelength range is measured to be 3-4 cm^{-1}. The duration of the OPO pulse is less than 10 nanoseconds.

2. Perpendicular Laser-Molecular Beam Arrangement

An in-plane view of this molecular beam configuration is shown in Fig. 2. In this arrangement, the vibrational predissociation process is observed by the detection of the predissociation products. The laser and molecular beams intersect at right angles, and a rotating mass spectrometer pivots about the intersection point. A series of defining slits restricts the acceptance angle of the mass spectrometer's ionizer to 2 degrees so that only those molecules whose velocities are oriented in the detector's direction and whose positions are within the acceptance cone can be detected. The background pressure in the intersection chamber is 1.0×10^{-7} torr, which ensures that all molecules which enter the detector from events in the intersection region are collision-free, primary products. The molecular beam, produced by a supersonic expansion, is collimated by three apertures to an angular divergence of 1.5°. The cluster distribution of the molecular beam is measured by using the rotating mass spectrometer to directly sample the molecular beam.

The laser is coupled into the vacuum chamber by a BaF_2 lens held in a moveable tube which allows the OPO to be focused at the center of rotation of the detector, where it intersects the molecular beam. An aperture in this tube spatially defines the laser beam diameter to a 2 mm cross section at the intersection point. The laser is linearly polarized perpendicular to the plane defined by the laser and molecular beams. The output energy of the OPO idler frequency is measured with a germanium filter masked power meter placed a few inches beyond

the intersection point. This scheme allows the power dependence of the absorption to be determined, and accounts for frequency variations in the photon number.

The signal produced by OPO photons is recovered from the background by gating a 255 channel, variable channel width, multichannel scaler (LBL 13X3381) with the laser pulse. The time delay between the OPO pulse and the arrival of molecules at the detector which were affected by the OPO photons, is the sum of the neutral molecule flight time from the intersection region to the ionizer, and the ion flight time through the quadrupole mass spectrometer to the ion counting electronics. The ion flight time is independently determined and subtracted prior to analysis.

3. Coaxial Laser-Molecular Beam Arrangement

A cross sectional view of this arrangement is shown in Fig. 3. In this configuration, the laser is colinear with the molecular beam. The electron bombardment ionizer and ion extraction optics are perpendicular to the laser and molecular beams. The quadrupole mass spectrometer directly monitors the molecular beam so the predissociation of clusters appears as a decrease in signal at the ion related to the predissociating parent clusters.

The signal is also gated by the laser and time resolved by the multichannel scaler. The initial delay between the laser pulse and the onset of a change in the time resolved mass spectrometer signal, is the sum of the ion flight time from the ionizer to the counting electronics, and the flight time for the effects of the first cluster

predissociations to reach the ionizer. The 65 cm flight path can detect lifetimes as long as 1.0 millisecond (for the nominal molecular beam velocities of these experiments), while all lifetimes shorter than one microsecond (after correcting for the ion flight time) will appear to be "instantaneous". The power variation of the OPO is measured by monitoring a reflection of the OPO photons from a beam splitter.

C. EXPERIMENTAL OBSERVABLES

From the experimental observations, two quantities are derived: the wavelength dependence of the predissociation cross sections, and the translational energy distributions of the predissociation fragments. The photon energy is sufficient at the wavelengths 2800-3800 cm^{-1} corresponding to the various hydrogen atom stretching frequencies to break the weak intermolecular bond. The perpendicular molecular beam experiment uses the translational recoil velocity of the dissociated fragment clusters (which carries them away from the molecular beam) to detect the absorption of radiation. As shown in Fig. 4, the cluster predissociation fragments must have sufficient recoil energy to reach the detector when it is placed at a fixed angle relative to the molecular beam. Rotating the detector to successively larger angles favors those fragments which have higher translational energy. Through the energy balance equation

$$E'_{int} = E_{h\nu} + E_{int} - D_o - E'_t \quad , \tag{1}$$

the internal energy in rotation and vibration of the fragments (E'_{int}) can be obtained from the photon energy ($E_{h\nu}$), the initial internal energy of the clusters (E_{int}), the dissociation energy (D_o and the product recoil energy (E'_t). E'_t can be derived from the measurements of laboratory angular and velocity distributions.

For the measured product yield at a fixed detector angle to be proportional to the photon absorption cross section of the parent cluster, the time scale, τ, for the predissociation process must adhere to two restrictions. First, for the predissociation to be detected, the vibrationally excited clusters must not travel outside the detector's viewing region before dissociating. For the nominal beam velocities 1×10^5 cm/sec, this places an upper limit of 2 microseconds on τ. Secondly, τ cannot vary with the OPO wavelength in such a way as to produce a change in the shape of the laboratory angular distribution. Within the experimental statistical counting error, this has been verified for the systems reported here. Changing the orientation of the laser polarization with respect to the detector-molecular beam plane had no effect on the signals.

The coaxial arrangement directly measures the depletion of the clusters and is not sensitive to the translational energy distribution. As such, it is free from any assumptions regarding the angular shape of the laboratory photofragment distributions, and is limited only by the upper bound on the lifetime given by the 65 cm flight path. It is to be pointed out that, in the colinear experiment, the signal is proportional to the number of polymers dissociating within 1

millisecond after excitation, while in the perpendicular beam experiment only the fragments formed during the first 2 microseconds after the laser pulse may be detected. Both spectra being identical, we can assume that $\tau \leq 2$ microseconds for all wavelengths measured, and that the above assumptions concerning the shape of the laboratory distributions made in the perpendicular arrangement are valid.

D. BENZENE

1. Introduction

Benzene is a natural choice as an experimental model system for learning about intermolecular interactions due to its widespread use in simulations of liquid behavior,[11,12,13] and the existence of a large body of spectroscopic data in different phases.[14,15,16] Extensive modeling of the intermolecular potential function for benzene has been done by Evans and Watts[11] who have derived a six-centered Lennard-Jones potential which adequately describes the second virial coefficient, the static lattice energy, the solid state crystal structure, liquid phase distribution functions, viscosity, and thermal conductivity. Simpler models have been proposed by Lowden and Chandler[13] and MacRury, Steele, and Berne,[12] and where comparison is possible, there is qualitative agreement on the interpretation of the results. For example, all have predicted that the local structure in the room temperature liquid should be similar to the solid with a preferred T-shaped nearest neighbor geometry.

In a molecular beam electric resonance study, Janda et al.[17] have shown that benzene dimer is polar, strongly suggesting that the

gas phase dimer is also T-shaped. The similar near neighbor geometry in the dimer and condensed phases is the basis for assuming that a simple model for some condensed phase properties might be found in the small, gas phase clusters.

Two general theories have addressed the vibrational predissociation rate question - the "momentum gap" model of Ewing[18] and the "energy gap" model of Beswick and Jortner.[19] The basic prediction of both theories is that the most efficient predissociation mechanism minimizes the translational energy of the predissociation products. The physical basis for this minimization of the translational energy was shown to be the poor overlap between the continuum translational wavefunction of the products and the initial "bound" state intermolecular wavefunction of the vibrationally excited cluster.

To date, these models have been applied only to binary complexes such as $He...I_2$.[20] A recent theoretical study of $(N_2O)_2$ by Ewing[21] is especially intriguing. According to the momentum gap model, Ewing predicted that the most probable dissociation channel involves a V→V,T energy transfer to the ν_1=1 vibrational state of the N_2O monomer when the ν_3=1 mode is excited. This product state minimizes the translational energy of the fragments. Using a realistic model function for the intermolecular potential, Ewing also concluded that a dipole-dipole coupling was more consistent with the dissociation lifetime than the Morse coupling of the intermolecular vibrational (and dissociation) coordinate. Beswick and Jortner, using a different dimer geometry and intermolecular potential, predict that the two N_2O monomer products

will be left in the $\nu_2 = 1$ and $\nu_1 = 1$ states respectively.[19] The energy gap and product states for this process are different than those predicted by Ewing. Therefore, the theoretical models are sensitive to details of both the intermolecular potential and the physical mechanism which determines the predissociation lifetime. The simplicity of the Ewing and Beswick/Jortner models for a wide range of molecules invites further experimental confirmation. Using benzene as a "large molecule" test case to investigate cluster dissociation, other factors in the intermolecular vibrational energy relaxation might be necessary to understand the product state distributions when more than one vibrational state has a small momentum gap.[19]

2. Results

Benzene clusters were formed by bubbling He through room temperature liquid benzene and expanding the gas mixture through a 0.18 mm diameter nozzle heated to 70°C. The distribution of cluster sizes was controlled by changing the He pressure.

In Fig. 6, the off axis predissociation spectra taken at the parent ions of benzene monomer (mass 78) and pentamer (mass 390) using the perpendicular laser-molecular beam configuration are shown. The signals represent the total laser induced signal corrected for background and photon number, and, consequently, are proportional to the absorption cross section. These masses, to have reached the detector, must have originated from a cluster containing at least two or six benzene molecules, respectively. Therefore, the spectra are labeled according to the smallest polymer capable of contributing to that

mass, although fragmentation of larger clusters to these masses either in the predissociation process or by the electron bombardment ionization may also contribute. From Fig. 6, it can be concluded that the frequency shifts of the different polymers are small compared to the laser spectral bandwidth. The atypical beam conditions for these spectra, (Ar carrier gas and a room temperature nozzle), can produce large clusters. The principal spectral change is in the relative intensities of the three bands, showing that a unique spectral identification of the absorbing clusters is not possible at this resolution.

To assign the off-axis predissociation fragment signals to a parent cluster, the pressure dependence of the off-axis signals were compared to the pressure dependence of the polymers in the molecular beam, obtained by rotating the mass spectrometer to 0° along the molecular beam axis. In Fig. 7, the ratios of the off-axis predissociation fragment signals at mass 78, to the parent molecular beam mass 156 and 234 signals with the detector placed at 0°, are plotted as a function of the nozzle stagnation pressure. The 78 (off-axis fragments)/156 (0° molecular beam parent) ratio is flat, while the 78 (off-axis fragments)/234 (0° molecular beam parent) ratio falls sharply. This is consistent with the assumption that the off-axis mass 78 signal comes from the molecular beam cluster detected at 0° at mass 156, presumed to be the dimer. Under these expansion conditions, the signals in the molecular beam which relate to clusters containing more than three monomers are negligible. The ratios of mass 156:mass 234:mass 312 in the molecular beam are 100:3:0.3.

In a molecular beam study on the polarity of benzene polymers,[17] it was concluded that only 1/10 of the benzene dimers were ionized to the parent mass peak. With this known proclivity for fragmentation of the neutral clusters by electron bombardment, other evidence is necessary to show that the mass 78 off-axis signal is indeed that of the monomer photofragment from predissociation dimers, and not the ionization by-product of dimer photofragments originating from the predissociation of trimer and larger clusters. To verify these mass assignments, the coaxial laser-molecular beam configuration is used.

Figure 8 shows two time-resolved signals obtained with the coaxial method, as well as a time-of-flight spectra obtained with the perpendicular method by placing the detector at zero degrees. This simulates the depletion scheme of the coaxial configuration. The increase in sensitivity is dramatic, a consequence of the increased interaction volume between the laser and molecular beams. From the decrease in signal at mass 78 in the coaxial arrangement, it is clear that the clusters are fragmented by electron impact to mass 78 ions. That is, when the laser dissociates the benzene clusters, they are no longer present at the ionizer to fragment by electron bombardment to mass 78. The slight positive signal at mass 50 comes from the increase in the neutral <u>monomer</u> density resulting from the photodissociation of benzene clusters in or near the ionizer. Its shorter time duration is a result of the progressively smaller solid angle of acceptance for cluster photofragments more than a few centimeters from the ionizer. This different temporal behavior from the mass 78 signal shows that

mass 50 ions correlate only to neutral benzene monomers. It also shows that the mass 78 signal cannot be explained as a change in the monomer fragmentation pattern which might occur should the monomer beam component be vibrationally excited by the laser. Since the mass spectra of benzene monomer has prominent peaks at mass 78 and 50-52,[23] one would expect the laser related signals at these masses to extend for a time equal to the neutral monomer flight time from the nozzle to the detector, if the monomer were absorbing radiation. The mass 50-52 signals are inconsistent with this explanation. The experimentally derived partial electron bombardment fragmentation pattern is summarized by

Parent Cluster		Ion	Mass	
$(C_6H_6)_2 + e^-$	$\longrightarrow$	$(C_6H_6)_2^+$	(156)	
	$\longrightarrow$	$(C_6H_6)^+$	(78)	(2)
$C_6H_6 + e^-$	$\longrightarrow$	$C_4H^+_{2,3,4}$	(50-52)	

From the preceding analysis, it is clear that if the mass 50-52 angular scan in the perpendicular laser-molecular beam geometry is the same as the mass 78 scan, then the mass 78 data relates to benzene monomer predissociation fragments and not ionization fragments from higher clusters. Figure 9 shows the time-of-flight data taken at the two masses for two laboratory angles, establishing the validity of the previous assumption that the mass 78 off-axis signal results from ionizing monomers. The mass 156 off-axis signal is assigned to the

trimer predissociation based on the strength of the observed signal; the tetramer and larger clusters in the molecular beam are present in negligible amounts.

The angular distributions of the mass 78 and 156 products, shown in Fig. 10, are similar in shape and extend only 10 degrees from the molecular beam. By measuring the beam velocity, V_b, of the initial clusters using a rotating slotted disk placed at a known distance from the ionizer,[24] and if the functional form of the center-of-mass angular distribution is known, the transverse velocity of the predissociation fragments can be computed from the laboratory angle. The observed steep monotonic increase of the dissociation signal with decreasing laboratory angle can only be fit with a translational energy distribution which also has a decrease with increasing translational energy and peaks very near zero translational energy.

An analytical function of the form

$$P(E) = \alpha e^{-\alpha E} \tag{3}$$

was used to quantitatively fit the measured laboratory angular and time-of-flight distributions. This center-of-mass energy distribution is convoluted over the experimental conditions (the finite aperture sizes, initial velocity distribution of the molecular beam, and ionizer length) assuming an isotropic center-of-mass angular distribution. The small range of laboratory angles where product is observed is insensitive to details of the center-of-mass angular distribution. Furthermore, it is shown below that it is reasonable to assume that

the vibrationally excited complex rotates several times before predissociating. An isotropic center-of-mass distribution is appropriate in this case. In Fig. 10, the best fit curves for the mass 78 (α=5) $(kcal/mole)^{-1}$ and 156 (α=7) $(kcal/mole)^{-1}$ signals are compared with the experimental data.

From the measured wavelength dependence of the predissociation cross sections, it is clear that the perturbations of the three monomer vibrational bands in the 3000-3100 cm^{-1} range are small. The resolution of the laser is insufficient to observe rotational fine structure. No additional vibrational bands were observed which could be attributed to different bonding sites in the clusters or to a reduction of D_{6H} symmetry in the monomers. Combination bands involving intermolecular vibrations with an absorption strength greater than 1/5 of the fundamentals were not detected in this wavelength range. The absence of P, R rotational branches in the predissociation spectra limits either the internal temperature of the clusters or the size of the potential barrier hindering individual molecular rotation, as in liquid, room temperature benzene.

The observed signals were all linear in photon number. Additional absorption of photons by the predissociation products was not observed at this photon flux (~7 x 10^{17} photons/cm^2 pulse).

3. Discussion

From the results of these experiments, three properties of the vibrational predissociation can be determined: the identification of the main product channels, the lifetime of the vibrationally excited clusters, and the internal energy distribution of the products.

The main product channels established by the pressure dependence and mass spectroscopy of the OPO induced signals for the predissociation of benzene dimers and trimers are

$$
\begin{aligned}
(C_6H_6)_2 + h\nu &\longrightarrow 2C_6H_6 \\
(C_6H_6)_3 + h\nu &\longrightarrow (C_6H_6)_2 + C_6H_6.
\end{aligned}
\tag{4}
$$

From the consistency of the wavelength dependence of the two predissociation signals measured in the perpendicular and coaxial configurations, it is clear that the clusters are predissociating within several microseconds of the laser pulse. A lower limit to the vibrationally excited state lifetime of 1 picosecond may be deduced by ascribing all of the observed linewidths (neglecting the ~3-4 cm^{-1} spectral bandwidth of the OPO and the initial internal state distribution of the clusters) to homogeneous broadening caused by the predissociation. This lower limit is consistent with the lack of a polarization dependence for the observed signals in the perpendicular configuration. If the rotational distribution of the dimers is characterized by the same temperature as the molecular beam translational energy distribution (50°K), and can be modeled as a simple diatomic with 5 Å bond length, the most probable rotational state has a classical rotational frequency of 1 picosecond. A polarization dependence would be expected if the predissociation lifetime was significantly shorter than this rotational frequency <u>and</u> if the transition dipole had a fixed orientation with respect to the intermolecular

axis. Since the intermolecular forces are poorly understood, large amplitude motion of the low frequency vibrations may well preclude such a fixed transition moment. Consequently, the lack of a polarization dependence is consistent with the lower lifetime limit deduced from the linewidth, but does not supply an independent determination of it. Recently, predissociation attributed to benzene dimers near 1040 cm^{-1} has been observed[25,26] with a linewidth of less than 3 cm^{-1}.[25]

The translational energy distribution which adequately fits the data peaks at zero translational energy and has a very narrow energy spread. Therefore, the energy in internal excitation of the fragments for the most probable case is

$$E'_{int} = E_{int} + E_{h\nu} - D_0 \quad . \tag{5}$$

For simplicity, the initial internal energy is neglected. The adiabatic cooling in the nozzle expansion is expected to make this term small compared to the errors in the remaining larger contributions to the internal energy.

An estimate for the bond energy between two benzene molecules may be obtained from the crystal sublimation energy at 0°K. Model calculations[11,12] which reproduce this value give ~750 cm^{-1} for the pair potential zero point binding energy. Therefore, the internal energy of the fragments determined from Eq. (5) is 2300 cm^{-1}.

How is this energy distributed among the available internal states of the monomer and dimer fragments from the trimer predissociation?

If all the excess energy were placed in the dimer fragment, it would be far in excess of the dimer bond energy, and the dimer would be expected to predissociate before reaching the ionizer. The observation of dimer product places a lower limit of 1550 cm^{-1} on the internal energy in the monomer. The rate of energy migration among the three benzene molecules in the trimer, for this unequal energy distribution to be observed, is then slower than the predissociation rate. Likewise, the photon excitation is to a particular monomer, and that is the monomer which is vibrationally excited in the predissociation products. This implies that the benzene monomers are located at distinguishable sites in the trimer. If this were not true, the zeroth order vibrational wavefunction would be delocalized over the three monomers.

One can tentatively generalize this conclusion to the case of dimers; we expect the dissociation to yield one "vibrationally hot" and one "vibrationally cold" molecule. This is consistent with the postulated T-shaped dimer structure where the two molecules are not equivalent.

The above predissociation mechanism qualitatively agrees with the momentum gap model proposed by Ewing. The substantial internal excitation of the products automatically reduces the momentum gap to a small value. The density of internal vibrational states near 2000 cm^{-1} in benzene monomer is sufficient to ensure that there will always be a resonant state within 10 cm^{-1}, even if the rotational excitation is not significant. This high density of states is

advantageous for testing in finer detail the predissociation process, because there are probably several product states with nearly the same momentum gap. Other factors to date not explicitly considered in the momentum gap model, especially the detailed predissociation dynamics, will have to be understood in order to predict the relative vibrational, rotational state populations in the products. Such state distributions are expected to become available in the near future for some of these systems from laboratory measurements. An accurate determination of the ground state binding energy can also be deduced from such measurements from the highest vibrational-rotational state populated in the products.

E. WATER

1. Introduction

Understanding the structure and dynamics of condensed phases from intermolecular potentials is an important problem. Substantial agreement between theory and experiment has been made for the weakly interacting rare gases[27] where, due to the domination of pairwise additive potentials in these systems, a single realistic pair interaction potential has been able to accurately fit experimental data of all phases. Conversely, for strongly interacting molecules such as water, no single pair potential has yet been proposed which accurately reproduces the known physical properties of this substance in all phases.[28] The strong orientational forces responsible for hydrogen bonding are notoriously difficult to theoretically model.

In 1951 Rowlinson[29] proposed the first molecular model aimed at a quantitative prediction of solid state properties, beginning with

known gas phase properties. Subsequently, many different pair potentials have been published. The Ben-Naim Stillinger potential,[30(a,b)] for example, was an "effective" pair potential for the liquid which partially accounted for many-body effects. An extensive series of ab initio calculations have also been performed by Clementi and co-workers.[31a-g] Beginning with Hartree-Fock potentials for the water dimer, studies were made of the effects of configuration interaction, empirical dispersion terms, and many-body effects on the structure of the liquid and small polymers predicted by these pairwise additive potentials. The conclusions of these studies were: (a) that the liquid state structural properties were predicted as well as by any other current potential, (b) that the three body interaction accounts for approximately 10 percent of the binding energy and has no strong angular dependence, and (c) that analytical fits to Hartree-Fock calculations, suitably corrected for the dispersion interaction, can reproduce results in an economical form.

When potentials which have been designed to predict liquid state structural properties are used to calculate the properties mainly dependent on the pair interaction potential or vice versa, agreement has not been very satisfactory. The determination of the potential parameters from experimental results is difficult because the available experimental data are largely integral quantities which depend on many different regions of the potential surface. Consequently, errors in the repulsive interaction can be compensated for by errors in the attractive well so that a single experimental observable can always be

fit. Moreover, even when disagreement is observed in the computed properties, it is not clear which region of the potential is responsible, and a trial and error method of adjusting the potential parameters has been the method of choice in improving agreement with experimental data. To better discriminate against potential forms, microscopic data sensitive to well defined regions of the potential energy surface are needed.

Infrared spectra of clusters of water have been experimentally available since the original matrix isolation work of Pimentel and co-workers.[32] In these studies, the dependence of infrared absorption linestrengths on the matrix to absorber ratio was used to assign the various absorption bands to specific polymers. The problems of overlapping absorptions bands limited the application of the matrix isolation technique to principally the dimer and trimer. No similarity with the broad, structureless infrared spectrum of liquid water was observed. More recently, Luck[33] has carefully followed the concentration dependence of the infrared matrix absorptions to extend the correlations between bands and polymer sizes.

An additional property sensitive to features of the interaction potential of water clusters is the time scale for predissociation of vibrationally excited clusters containing energy in excess of the hydrogen bond energy. In 1946, Stepanov[34] proposed that the broadening of the hydrogen bonded infrared vibrational spectra might be a result of predissociation. More recently, Hagen and Kassner[35] have calculated the decay rate for water trimers as a function of temperature based on a Slater type model. Robertson and Coulson,[36a-c]

Ewing,[37] and Beswick and Jortner[38] have all calculated predissociation rates for binary complexes using first order time dependent perturbation theory. This current theoretical work has shown that the dissociation rate is intimately connected with the mode of energy disposal.

Experimental studies on relaxation lifetimes in liquid H_2O have included dielectric,[39] nuclear quadrupole resonance (NQR),[40] inelastic neutron scattering,[41] and depolarized Rayleigh scattering (DPRS).[42] The 2-5 picosecond relaxation times observed in the room temperature dielectric and NQR studies have been related to orientational lifetimes in liquid water. The DPRS experiments measure two lifetimes. The slower component is similar to the reorientational time scale of the NQR and neutron scattering results, while the fast component of 0.6 picoseconds has an Arrhenius temperature dependence with a 3 kcal/mole activation energy. This fast lifetime was interpreted as the time constant for breaking a hydrogen bond, with the activation energy measuring the energy difference between waters oriented in the proper direction for hydrogen bonding and those that are not. The induction period for the other relaxation processes which depend on reorientation suggests that the breaking of a hydrogen bond is the rate-determining step before reorientation can occur. The vibrational predissociation lifetimes would then be expected to be longer than 1 picosecond, depending also on the hydrogen bond breaking rate.

The current work was undertaken to provide infrared spectra of selected clusters of water molecules in order to assign the features

in the vibrational spectra and relate these assignments to current interaction potentials of water. Using the crossed laser-molecular beam technique, the frequency dependence of the predissociation fragment yield is measured, improving spectroscopic assignments as a result of careful control of cluster size distribution and the mass selective detection scheme. Additional measurements of the velocity distributions of the predissociation fragments give directly the translational energy released in the predissociation. From these new observations, an explanation for the discrepancy between the condensed phase water and gas phase pair interactions is given. The infrared spectra are seen to be quite sensitive to the proposed intermolecular potential model and should figure prominently in determining future intermolecular water potentials.

2. Experimental Results

A molecular beam of water (nozzle diameter 0.18 mm, nozzle temperature 125°C) containing a small percentage of water clusters was crossed at right angles by the infrared radiation in the perpendicular laser-molecular beam configuration. Because there is always a distribution of polymer species in the molecular beam, and because of problems associated with ion fragmentation, unique identification of the water clusters in the electron bombardment ionizer is not possible. However, one important feature of the mass selective detection scheme is that it acts as a "high-pass" filter; that is, for a given detected ion mass, only clusters <u>larger</u> than a certain size can possibly contribute to the signal. This represents a significant advantage

over the matrix isolation technique, where strong absorption by monomers and smaller clusters often obscures absorption peaks due to larger clusters.

As an example, suppose we set the quadrupole mass filter to pass $(H_2O)_3H^+$ (m/e = 55). The smallest water cluster which could produce this ion in the ionizer is $(H_2O)_4$, and the smallest cluster which could produce $(H_2O)_4$ by vibrational predissociation is $(H_2O)_5$. Thus, only pentamers and larger clusters can contribute to the vibrational predissociation signal measured at m/e = 55. Contamination from higher polymers can be minimized by carefully controlling the expansion conditions of the molecular beam. For example, in the investigation of $(H_2O)_3$, the nozzle stagnation pressure was adjusted so that the concentration of the next higher polymer $(H_2O)_4$ was substantially less than $(H_2O)_3$. The combination of working on the largest observable clusters in the beam and the mass selective detection scheme, while not able to completely eliminate the contamination, allows the main features and trends in the cluster spectra to be obtained.

Vibrational predissociation spectra were measured using four different nozzle stagnation pressures. For each stagnation pressure, the ion mass detected was chosen to be the largest mass whose signal was 10 times larger than the background after 2000 laser shots at the absorption maximum. The experimental conditions are summarized in Table 1. In all cases, the detector was positioned at a fixed angle of 4° from the molecular beam. At each frequency, the signal was accumulated for at least 2000 laser shots and normalized to the

average laser power. To ensure long-term stability, the spectra were scanned in two directions and checked for agreement within statistical counting error. Also, for each spectrum, the power dependence of the signal was checked at the major peaks to guarantee linearity of the predissociation yield with photon flux. The large error bars near 3550 cm^{-1} result from anomalously low idler power attributed to OH impurity in the $LiNbO_3$ crystal. For these points, the counting times were extended to ~20,000 laser shots. Finally, the power normalized signals were divided by frequency to convert from power to photon flux.

To obtain information on the dynamics of the vibrational predissociation process, angular and velocity distributions of the predissociation products were also measured at selected laser frequencies.

In the coaxial configuration, preliminary frequency scans at H_3O^+ and $(H_2O)_2H^+$ were taken. The perpendicular configuration does not allow one to measure the water dimer spectrum because of a large monomer background from the molecular beam at small detector angles. Additionally, as shown below, the larger clusters predissociate by loss of a monomer. This latter monomer background is correlated with the laser and can be removed only by reducing the polymerization conditions in the molecular beam. At mild water vapor pressures where there was no detectable signal at H_3O^+, there was no signal detected at H_2O^+ after 2000 laser shots in the frequency range 3600-3750 cm^{-1}.

A preliminary frequency scan and power dependence was measured in the coaxial configuration for large water clusters. The large clusters

were formed by passing 100 torr of Ar through an 80°C water bath and expanding the mixture from a 0.07 mm, 102°C nozzle. The count rate for all $(H_2O)_nH^+$ masses up to n=19 were at least 400 kHz from this source. The power dependence was linear up to the maximum energy of 8 mj/pulse.

3. Analysis

The water cluster vibrational predissociation spectra are shown in Fig. 11. The relatively high binding energies of the water clusters compared to the photon excitation energy substantially reduce the possible vibrational predissociation channels. Using four different intermolecular potentials,[43-46] the equilibrium bond energies (D_e) relative to complete dissociation of an n-mer into n water monomers were calculated[47] and are listed in Table 2.

There are two major energy classifications of the allowed dissociation processes. The lowest energy channel for all polymers includes a monomer fragment and is called monomeric dissociation (MD). It is defined by the equation:

$$(H_2O)_n + h\nu \xrightarrow{MD} (H_2O)_{n-1} + H_2O \quad . \tag{6}$$

The next energetically accessible dissociation process divides the parent cluster into two smaller clusters. This channel is called cluster dissociation (CD) and is defined by the equation:

$$(H_2O)_n + h\nu \xrightarrow{CD} (H_2O)_m + (H_2O)_{n-m} \quad , \; m > 1 \quad . \tag{7}$$

The CD channel computed from the D_e bond energies in Table 2 is not always accessible over the frequency range probed. The simplest explanation consistent with the spectral observations discussed here and the dynamic properties presented below, would attribute all dissociations as occurring through the energetically favorable MD channel. The time-of-flight and angular distributions (see below) do not change with frequency within experimental error, as might be expected if a new dissociation channel became energetically accessible.

The electron impact fragmentation behavior of water clusters has recently been analyzed in the literature.[48,49] Briefly, the exceptional stability of the H_3O^+ ion explains the dominance of the mass peaks $(H_2O)_nH^+$ in the mass spectrum. The electron bombardment ionization of the neutral $(H_2O)_n$ clusters presumably first proceeds by the ionization of a water monomer subunit. A unimolecular ion-molecule reaction follows in which the H_3O^+ ion is formed (solvated by the remaining water molecules) and an OH radical is ejected from the cluster. The dominant ionization mechanism, then, is assumed to be

$$(H_2O)_n + e^- \rightarrow (H_2O)_{n-1}\ H_2O^+ + 2e^- \rightarrow (H_2O)_{n-1}\ H^+ + OH + 2e^- \quad . \quad (8)$$

If this simple picture were complete, each water cluster, $(H_2O)_n$, would be correlated with a single ion, $(H_2O)_{n-1}\ H^+$, in the mass spectrometer, and assignment of the vibrational predissociation spectra would be straightforward. Unfortunately, in the electron bombardment ionization process, the $(H_2O)_{n-1}\ H^+$ ion may be formed with substantial

vibrational energy, such that one or more water molecules may evaporate from the cluster ion. Therefore, the mass spectrum of each water cluster, $(H_2O)_n$, also contains smaller $(H_2O)_m H^+$ mass peaks (where $m < n - 1$). This source of contamination is impossible to eliminate by mass spectroscopy alone. The fact that this contamination can potentially be very serious is demonstrated in Figs. 11(a),(e). The two spectra shown were measured by tuning the mass spectrometer to H_3O^+, nominally assigned to the trimer dissociation by Eqs. (7) and (8), but using very different nozzle expansion conditions. The Fig. 11(a) spectrum was obtained with the water reservoir held at 67.5°C, giving a nozzle stagnation pressure of 209 torr (see Table 1). The H_3O^+ signal amounted to 1.2 counts/laser pulse at 3400 cm^{-1}, with 0.7 counts/pulse at $(H_2O)_2H^+$ and much less signal at all higher masses. The spectrum in Fig. 11(e) was obtained with the water reservoir held at 90°C, giving a nozzle stagnation pressure of 526 torr. Under these conditions the water beam was heavily polymerized. The H_3O^+ signal at 3400 cm^{-1} was 5.3 counts/pulse, and at least 1 count/pulse was obtained at all $(H_2O)_n H^+$ masses up to $(H_2O)_6 H^+$. While we believe that the spectrum in Fig. 11(a) is largely due to predissociation of water trimers, it is clear that the spectrum in Fig. 11(e) is heavily contaminated by fragmentation of the predissociation products of larger water clusters in the ionizer.

However, we can still get some idea of how the water cluster distribution varied with nozzle stagnation pressure, by assuming that $(H_2O)_nH^+$ is the major ion fragment of $(H_2O)_{n+1}$. We list in Table 3

the pressure dependence of the ion ratios $(H_2O)_n H^+:H_3O^+$, n = 1-3, measured by pointing the mass spectrometer directly into the water beam.

Information on the predissociation product energy distributions is obtained from the laboratory angular and time-of-flight distributions of the products. The experimental angular distributions, shown in Fig. 12, exhibit a steep monotonic decrease with increasing laboratory angle, and can only be fit with a center-of-mass energy distribution which peaks at or near zero translational energy and rapidly decreases with increasing product translational energy. A simple analysis relating the laboratory angle, nominal beam velocity, and center-of-mass velocity shows that the recoil energy necessary to scatter fragments to 4° is merely tens of wavenumbers, while the particles scattered 10° have several hundred wavenumbers of translational energy. This means that most of the excess energy is in the internal excitation of the fragment molecules.

The observation of a reasonable signal level (~1 count/laser pulse) in the experiment implies an upper limit of ~1 microsecond to the vibrationally excited cluster lifetime. If the lifetime of the excited state was longer than the four microsecond residence time of the clusters in the viewing range of the detector, then only a fraction of the predissociated clusters could be detected. For the signal level to be 1 count/pulse, a large fraction of the clusters in the beam must have predissociated within 1 microsecond of the laser pulse.

4. Discussion

a. Spectroscopy

As a first attempt to assign the features of the water cluster spectra, normal mode calculations have been performed using water potentials which allow the intramolecular monomer bonds to distort. For each potential, the configuration of the atoms was varied using a multi-parameter minimization procedure to find locally stable polymer configurations (Fig. 13). For the Watts potential,[43] a single minimum was found for the water trimer, a cyclic structure shown in Fig. 13b. Larger polymers had several local minima, but in each case the lowest energy configuration found was cyclic. For the Stillinger central force[44] and polarization potentials[45], the minimum energy configurations found beginning at the minimum energy structures of the Watts potential were also cyclic, except for the polarization model where the linear trimer is most stable. At the minima, the harmonic frequencies of the normal modes were calculated using finite differences to obtain the second derivative force constants of the potential. Table 4 contains the normal mode frequencies for several water polymer configurations obtained using the published potential forms. Using the harmonic frequencies, the harmonic zero point energies (HZPE) were also obtained.

The observed absorption spectra are characterized by two features: a sharp, narrow absorption 15 cm^{-1} wide located at 3715 cm^{-1}, and a 600 cm^{-1} broad absorption extending from 3000-3600 cm^{-1} with an approximate 150 cm^{-1} superimposed fine structure. The sharp peak is

midway between the gas phase monomer symmetric (3657 cm^{-1}) and antisymmetric (3756 cm^{-1}) stretching vibrations, and is representative of an uncoupled, non-hydrogen bonded intramolecular OH stretch. For comparison, the OH stretch in HOD occurs at 3705 cm^{-1}. This narrow band is also what would be expected for the free hydrogens of the equilibrium ring structures determined in the energy minimization calculations. If neither hydrogen atom of a particular water molecule is involved in hydrogen bonding, there should appear two absorption peaks correlating to perturbed symmetric and antisymmetric stretching frequencies for this "hydrogen accepting" monomer. The single sharp peak is taken as evidence that the isolated polymers containing three or more molecules are cyclic with at least one hydrogen atom of each water molecule hydrogen bonded. Additional experimental evidence for the cyclic structures is given by the small to undetectable dipole moments of water polymers in a molecular beam polarity study.[50]

The calculated harmonic normal mode frequencies of the Watts potential show the tight frequency grouping of the free hydrogens, midway between the calculated monomer normal mode frequencies obtained with the same potential model. The Stillinger potential frequencies show a blue shift relative to the Stillinger monomer frequencies with little grouping. This is presumably a result of the compromise the Stillinger model was forced to make when attempting to fit with the same form of the OH interaction potential both the infrared absorption frequencies and electrostatic properties of the monomer. The potential was not sufficiently flexible to enable an exact fit to all of these observables.

The second major feature of the spectra--the broad, hydrogen bonded absorption--is not as easily understood. The broadness of the hydrogen bonded infrared spectra has been experimentally well documented.[51] The theoretical models which have explained the extensive absorption in other systems (such as carboxylic acid dimers[52]) conclude that a strong coupling picture, involving at least the hydrogen bond and intramolecular stretching coordinates common to the hydrogen bonded hydrogen atom, is necessary. Additional complications may arise from the resonant first overtone of the intramolecular bending frequency near 3200 cm^{-1}.[53] The breadth of other hydrogen bonded systems has been explained without resorting to a Fermi resonance picture. Hence, the fundamental coupling mechanism producing the broad water cluster absorptions is taken to involve the O . . . HO group, with Fermi resonance (involving $2\nu_2$) possibly accounting for a portion of the intensity pattern near 3200 cm^{-1}. Even without an exact quantum number assignment of the vibrational bands, the similarity of the frequencies and number of bands for the series of polymers measured, as compared to the matrix isolated dimer,[54] means that once the cyclic structures are formed, the basic near neighbor interactions dominate. A proper treatment of the large amplitude intermolecular motion is necessary before the strong coupling picture can be adequately tested. If more than one local minimum structure is accessible to the ground state wave function, it is not known how the infrared spectra would be affected.

Liquid water infrared spectra have been quantitativly analyzed by assuming the Badger-Bauer relation between frequency and bond length

to be operative.[55] Using an empirical curve of frequencies and bond lengths, the distribution of oxygen-oxygen distances in the liquid has been calculated from the infrared spectra. The near Gaussian shape of the liquid infrared spectra does not show any of the fine structure seen in the polymer spectrum, although the existence of four components comprising the broad infrared absorption can be inferred from curve decomposition.[56] These four bands were then suggested to be characteristic of water molecules bound to different numbers of, or in different ways to, neighboring water molecules.

Additional evidence for distinct water bonding types in the liquid has been derived from the temperature dependence of the first stretching overtones. Using the overtone region to separate the congested fundamental infrared bands, Luck[57] and others[56] have performed many experiments which show clear isosbestic behavior in this region, suggesting an equilibrium between at least two species of water molecules. Recently, Sceats[58] has reinterpreted the overtone region using a quantum mechanical picture, showing that reasonable values for the electrical and mechanical anharmonicities in the liquid phase can explain the observed isosbestic behavior. Consequently, the apparent isosbestic behavior is not a sufficient condition for the mixture model of water.

More recently, Byer et al.[59] have measured the depolarization CARS spectra of liquid H_2O and have observed spectral structure in the regions of the bands observed here, excepting the free OH stretch. Their experiment shows that the broad liquid absorption is composed of

several overlapping vibrational bands. Despite the fact that the room temperature infrared bands are so overlapped giving the appearance of a single broad band, the depolarization CARS experiment can resolve these features using the different depolarization ratios of the vibrational transitions. The cooling of the water clusters in the molecular beam expansion, and mass selective detection enable the features to be resolved in the work reported here. With this clear evidence for substructure in the liquid phase spectrum, a confident analogy can be drawn between the interactions present in the gas phase clusters and the liquid.

Matrix isolation results beginning with the pioneering work of Pimentel[32] have used the concentration dependence of spectral features to assign bands to particular water polymers. Host materials have included Ar, N_2, and D_2.[54] The dimer has attracted the most attention because the original N_2 matrix work suggested a cyclic structure for the dimer, contrary to later theoretical calculations. Subsequent higher resolution matrix studies have identified the expected number of intramolecular vibrations for a trans-linear structure, the same given by the most extensive quantum mechanical calculations, although the D_2 matrix appears exceptional, supporting only a cyclic structure.[60] Molecular beam electric resonance spectroscopy[50] has definitely established that the gas phase dimer is stable in the trans-linear form. The conclusion seems to be that the difference in energy of different water dimer geometries is insufficient to result in one matrix dimer independent of the host material.

The vibrational predissociation spectra obtained in this study disagree with some of the matrix assignments for trimer and multimer spectra. Primarily, the gas phase clusters are all seen to absorb over the same frequency range, principally distinguished by variations in intensity, not frequency. It is difficult for the matrix technique to distinguish between different species absorbing at the same frequency. The molecular beam method with mass selectivity can limit the size of the parent polymers which are measured, and to some degree, circumvents this problem.

For the assignments of the matrix trimer spectra to be correct, the matrix trimer would either have to be trapped in a different intermolecular geometry than exists in the gas phase (such as a linear arrangement), or the contributions from higher polymers in the present molecular beam experiments dominated the signal assigned to the trimer. However, the trend with decreasing beam polymerization (lower nozzle stagnation pressures) in the series of spectra reported here, indicates a decrease in intensity of the 3550 cm^{-1} band relative to the 3200 and 3350 cm^{-1} bands. The 3550-3700 cm^{-1} frequency range in the matrix studies is assigned to the trimer, with the 3300 cm^{-1} range assigned to tetramer and higher clusters. Thus, the pressure dependence of the H_3O^+ spectrum in the molecular beam study is in the opposite direction to be consistent with the assignments obtained from the matrix studies.

The similarities of the liquid water and cluster spectra allows us to conclude that small, cyclic polymers form an excellent zeroth order model for explaining the infrared absorptions of liquid water.

McDonald and Klein[61(a)] used the Watts central force model based on fitting known monomer/dimer properties and found a disappointingly poor fit to liquid properties. Similarly, those potentials based on bulk phase properties, most notably the Stillinger-Rahman central force potential, give poor agreement with gas phase properties such as second virial coefficients and dimer geometries.[62] It has been suggested,[28] therefore, that large, non-additive, many body effects in water may preclude the existence of a simple central force model which can explain gas phase and cluster properties as well as liquid/solid behavior.

Perhaps the key to this problem is contained in the cluster spectra shown here. If one takes the known results for the infrared spectra of water dimers from matrix isolation work,[54] there is observed to be a dramatic spectral change between the matrix dimer and the gas phase trimer of this work. The dimer spectra are confined to a narrower frequency range (3530-3715 cm^{-1}), and bear little similarity to liquid water. In contrast, the trimer and higher clusters absorb over the complete range that liquid water does. To verify the conclusions of the molecular beam experiments, the water dimer and trimer spectra were measured using the coaxial molecular beam configuration shown in Fig. 1b. The dimer mass peak, H_3O^+, shows the expected high frequency ν_1, ν_3 doublet of the perturbed, hydrogen-accepting water monomer. This feature is absent in the trimer spectra, indicating the abrupt change to the cyclic configuration. To concentrate on dimer properties may then be misleading if one wishes to predict liquid properties.

From the sophisticated SCF calculations by Clementi et al.[31] using large basis sets, it was concluded that within the frozen monomer approximation, the non-additive, three-body interaction is only 10 percent of the pair interaction energy and shows no pronounced directional character. This implies that the Watts potential should show excellent agreement with experiment, predicting the pair interaction properties especially well. Correcting the calculated dimer "intramolecular" frequencies from the Watts model by the previous procedure of insuring that the calculated and observed monomer transitions agree, Table 5 shows the rather remarkable agreement between the Watts model normal mode frequencies and the assigned matrix transitions for the dimer. The cyclic polymers of the Watts model, however, are seen to have normal modes in the same range as the dimer. Therefore, the empirical pair potential does not predict a lowering of the hydrogen-bonded intramolecular harmonic frequency upon forming a cyclic structure. The calculations show, therefore, that changes in the reduced mass cannot account for the experimentally observed red shifts. Nonadditive effects must be quite important for the intramolecular properties, so far unexplored in theoretical calculations within the frozen monomer approximation.

b. Dynamics

The experimental results establish that predissociation is occurring within microseconds of the laser pulse and that most of the excess energy remains as internal excitation of the fragments (based on the negligible amount of energy appearing in fragment translational motion).

The two current theories of vibrational predissociation by Ewing, and Beswick and Jortner have only addressed the case of binary complexes. These are dynamical models, the rate of dissociation being sensitive to the coupling between the wave functions of intermolecular motion and final translational motion. On the other hand, since the coupling is sufficiently strong in the water clusters and there are so many vibrational degrees of freedom, it is possible that a statistical product energy distribution is more appropriate.

In order to understand the dynamics of dissociation, three calculations have been performed using the Watts potential to investigate the predissociation mechanism. The first consists in determining a local, minimum energy dissociation coordinate (LDC). The minimization computer program was modified to allow the distance between two of the oxygen atoms to be fixed at one value while varying the remaining atomic positions to minimize the total energy. Starting at the minimum energy configurations for the dimer, trimer and tetramer, the LDC's are shown in Fig. 14.

The dimer dissociation is straightforward, resembling a simple diatomic molecule. The trimer, however, shows a two-step process to dissociation. First, the ring structure is broken (R = 2.75Å to 5.50Å). Afterwards, a monomer dissociates from the cluster as in the dimer. The tetramer indicates more exotic behavior which also should be characteristic of larger clusters. Curve C in Fig. 14 shows the dissociation when two adjacent water molecules of the tetramer are pulled apart. The plateau is again characteristic of the opening of

the cyclic equilibrium structure. However, the dissociation of the linear tetramer does not proceed concertedly with the reforming of the cyclic trimer. The configuration of the trimer subunit near dissociation is extended and far removed from its equilibrium geometry. It is expected, therefore, to contain substantial internal energy. Repeating the calculation in the reverse direction (adding a monomer to a cyclic trimer) results in curve D of Fig. 14. The reverse path has a relative minimum with the approaching water monomer bonded to one of the free OH groups of the cyclic trimer. The energy barrier to adding a water molecule to form a cyclic tetramer from this relative minimum is ~0.5 kcal. The "hysteresis" of the two paths is a result of the numerous local minima on the potential surface. Since the LDC is generated by small sequential displacements (~0.2Å) of the oxygen-oxygen distance, these curves are not global minima.

The LDC's suggest that there are two timescales analogous to the liquid phase relaxation measurements: the hydrogen bond breaking rate; and the cluster dissociation rate. The hydrogen bond breaking rate will nominally be that of the transfer rate of the photon energy from the high frequency, "intramolecular," optically excited vibrations into the intermolecular motions. This process should be describable by the vibrational predissociation theories of Ewing or Beswick/Jortner. The second time scale, that for dissociation of the clusters once the energy has been coupled into the lower frequency intermolecular motions, is not expected to be negligible. The LDC's indicate that the cyclic polymers must undergo substantial configurational changes

before dissociation. This is expected to strongly couple all of the allowed exit channels satisfying energy and angular momentum conservation.

To explore this strong coupling in the exit channels, several molecular dynamics calculations were performed. The tetramer was the first system studied. The initial positions were chosen to correspond to the minimum energy cyclic configuration. When the energy was set equal to the HZPE, the trajectories indicated that the ring structure was preserved with no interchange of the hydrogen-bonded and free OH groups. Therefore, the initial configuration of the polymers could be fixed at the cyclic minimum without substantial error, since the gross bonding topology was satisfied. The velocities were chosen randomly according to a Boltzmann distribution with a temperature of 100°K. The residual velocity components in the zero angular momentum frame were scaled so that this "internal" kinetic energy equaled the sum of the HZPE and the photon energy. The original rotational motion was then replaced, thus allowing the internal vibrational energy to be constant, and independent of the rotational temperature. This accounts for the presumed disequilibrium between the vibrational and rotational degrees of freedom of the polymers produced in the adiabatic beam expansion. The trajectories were integrated using the CLAMPS[63] simulation package and displayed on the NRCC interactive graphics system.[64]

Twenty trajectories were followed for 30 picoseconds with no dissociation. Even though the bonding topology changed every few

picoseconds between cyclic, linear, tetrahedral, and similar configurations, and the effective temperature of the cluster was 2200°K, the heat capacity was still sufficiently large to insure that $\tau > 1500$ psecs. Subsequently, three ensembles of fifty, 20 picosecond trajectories were followed for the water dimer. The rotational temperatures for these ensembles were 10°K, 100°K, and 200°K, and the total internal energy fixed at 3000°K (which is the sum of the photon energy and HZPE). The minimum potential energy configuration was chosen as the starting configuration. The decay curves are shown in Fig. 15. Additionally, 50 trajectories were followed in which the hydrogen-bonded proton was initially extended along its OH intramolecular bond axis so that it had 10 kcal/mole of potential energy. This was investigated to determine the time required for the high frequency vibrational energy to couple into the low frequency motions. None of the trajectories for this last set dissociated, even though for several of the trajectories, the energy was seen to be transferred into intermolecular motions. The conclusion from these computer studies is that the lifetime of the clusters is composed of two contributions: the energy transfer time from the optically excited high frequency modes into the intermolecular cluster modes, and the decay time of the excited cluster (in which the energy is distributed progressively throughout the cluster) into products. The primary energy transfer time is expected to decrease with increasing cluster size, since the number of internal energy states resonant with the optically excited state will increase (the energy gaps approach zero), while the

decay time to products after the energy transfers from the optically excited state will increase with cluster size as the effective heat capacity increases.

Finally, RRKM calculations were attempted for a series of points along the LDC, but the results indicated lifetimes too short compared to the classical trajectory calculations. For these small systems in which rotational motions are nearly unhindered in the critical configuration, it is difficult to obtain reasonable values for the vibrational frequencies from simple "normal mode" type analyses. On the other hand, with the level of excitation being not much higher than the fundamental intramolecular vibrational energies and the hydrogen bond dissociation energy, one would expect dynamic factors to be more important than statistical ones.

If extensive energy randomization is occurring, by increasing the cluster size, the predissociation rates could be reduced. A series of experiments was tried in the coaxial configuration to see if the rate could be slowed to a timescale measurable on that apparatus, $\sim 10^6$ sec^{-1}. The results of these measurements indicated that for clusters containing at least 20 water molecules, the time scales were too short to resolve. However, several complications serve to increase the ambiguity of these results. For example, if the photon absorption rate for large clusters is proportional to the cluster size, while the predissociation rate is inversely dependent on the cluster size, the rate of predissociation observed would be independent of cluster size, but possibly power dependent. For the dimer and trimer, we can be

reasonably sure that the predissociation rate is much faster than the rate of sequential photon absorption. If the photon density is sufficiently high to dissociate 50 percent of the trimers, we can expect that on the average, all hexamers will have absorbed at least one photon, while dodecamers will have absorbed two photons, etc. The large clusters may be expected to absorb more than one photon within the ~5 nanosecond laser pulse. If they still predissociate faster than 10^6 sec^{-1}, but slower than 10^8 sec^{-1}, one can expect some secondary dissociation. Additionally, for the large clusters, the translational recoil is so small that the products are not scattered out of the beam. What is observed, in the worst case, is a difference in the rate of predissociation from the given cluster, to the rate at which that cluster mass is repopulated by predissociations from larger clusters. Hence, the desired conditions are difficult to verify, namely, a power level where only one photon is absorbed for the large clusters, and a cluster distribution rapidly decreasing in intensity with increasing cluster size in order to minimize repopulation. The experimental data in Fig. 17 show that when the power is reduced, the time dependence of the signal does not change over one order of magnitude in laser power, where signal is observable. Figure 18 shows the absorption spectra for mass 289, corresponding to clusters equal to or larger than $(H_2O)_{17}$.

F. NH_3

1. Introduction

NH_3 monomer has three strong infrared bands in the 3000-3500 cm^{-1} frequency range - the symmetric (ν_1, A symmetry) and

antisymmetric (ν_3, E symmetry) NH stretches, and the first overtone of the antisymmetric band ($2\nu_2$, A+E symmetry). For the monomer, the ν_3 band is well separated to higher frequency and easily assigned, whereas the ν_1 and $2\nu_2$ bands are in Fermi resonance and mixed. For hydrogen-bonded liquids, the monomer bending frequencies are expected to increase, because the preferred hydrogen-bonded geometry has a strong orientational dependence. The stretching frequencies should decrease because electron density is removed from the NH intramolecular bonding orbitals to form the intermolecular hydrogen bonds. These effects have been observed in recent experiments,[65] and microscopic models have been able to explain their physical origins.[66] For NH_3, the ν_1 and $2\nu_2$ bands in condensed phases are reversed with respect to their gas phase ordering. Because the liquid and gas phase ν_1-$2\nu_2$ regions look similar at first glance, this interchange was noticed only after the combined infrared[69] and Raman spectra,[65,68-70] (including polarization dependence) of several isotopic forms of NH_3 were studied. In addition, condensed phases of NH_3 have been studied by x-ray and neutron scattering,[72] matrix isolation spectroscopy,[73-75] and a molecular beam polarity study.[76]

Recent theoretical work on the NH_3 intermolecular potential has included <u>ab initio</u> studies of the pairwise,[77] and three-body terms[78,79,80] of the intermolecular potential, as well as empirical atom-atom potential functions[81-83] based on condensed phase properties of NH_3. These latter potentials have been used in Monte Carlo and molecular dynamics simulations of liquid NH_3.[84-85] Even within

the fixed monomer geometry approximation of these theoretical treatments, non-additive effects appear to be very important, contributing 25 percent of the trimer binding energy at its equilibrium configuration.[78]

The effect of intermolecular forces on the Fermi resonance of the ν_1 and $2\nu_2$ modes, including resonant energy exchange, has been elegantly treated by McHale and Wang.[66] Using a Mori-Zwanzig projection operator formalism, they have derived expressions relating the observed Raman spectrum to the microscopic potential terms governing the inter- and intramolecular anharmonicity and Fermi resonances. From these results, the nonlinear concentration dependence of portions of the Raman spectra can be understood. No equivalent treatment of the infrared spectra of liquid NH_3 has been reported.

2. Experimental Results

NH_3 polymers were studied using the perpendicular laser-molecular beam configuration. They were formed by expanding pure ammonia vapor through a 0.18 mm diameter, room temperature, glass nozzle. The distribution of clusters was controlled by changing the ammonia pressure behind the nozzle. The predissociation spectra were obtained by measuring the variation in signal with laser frequency at a fixed detector angle of 4° relative to the ammonia beam. The shape of the angular distributions did not change within the 10 percent statistical error of the measurements. The laser power dependence of the signal was measured at the absorption peaks, and the spectra recorded in the linear response region. The spectra then represent

the absorption cross sections for the clusters. Figure 19 shows the spectra recorded at different masses. The angular distributions of the detected masses are presented in Fig. 20. For the spectra in Fig. 19, the next polymer signal was 50 percent that of the recorded mass.

As in the previous cluster studies, the parentage of the detected masses is complicated by fragmentation in the electron bombardment ionization and by multiple vibrational predissociation channels. Unlike water clusters, where the intermolecular bond energies are quantitatively known, the energetics of neutral ammonia clusters are smaller and experimentally poorly determined.[86-89] A molecular beam photoionization study[86] has derived total binding energies of ammonia polymers through the hexamer of -4.6, -13.7, and -17.5 kcal/mole respectively. Two spectroscopic studies[88,89] have used the quadratic dependence of some absorption features to derive enthalpies of -3.5 kcal/mole and -4.5 kcal/mole for the ammonia dimer. Analysis of imperfect gas properties[87] deduces a dimer binding energy of -3.2 kcal/mole. Consequently, it is impossible to preclude predissociation by channels involving the breaking of more than one hydrogen bond. Based on analogies to previous work, the most probable product channel contributing to each mass is assigned by the following predissociation-ionization steps:

$$(NH_3)_n + h\nu \longrightarrow (NH_3)_{n-1} + NH_3 \tag{9}$$

$$(NH_3)_m + e^- \longrightarrow (NH_3)_{m-1}H^+ + NH_2 + 2e^- \quad . \tag{10}$$

The separation of different product masses in the angular distributions of Fig. 20 indicates that ion fragmentation is not as severe as for the water clusters. The dominant uncertainty in the ammonia spectra mass assignment is taken to be the predissociation process of Eq. (9).

3. Discussion

a. Spectra

The differences between the ammonia monomer and cluster spectra are smaller than for water. Hence, the strength of hydrogen-bonding in NH_3 is noticeably weaker. The main trends with increasing cluster size are an increase in the intensity of the 3375 cm^{-1} band relative to the 3225 cm^{-1} doublet, and a merging of the low frequency doublet to a single broad peak. The relationship of these spectral changes to the intermolecular forces is complicated by the anharmonicity and Fermi resonance of the ν_1, $2\nu_2$ and ν_3 bands. These intramolecular couplings are of the order of the intermolecular perturbations. To analyze the observed results, all of these effects must be considered. Such a task is beyond the scope of the work presented here. A theory incorporating these effects has been developed for the Raman spectra of strongly intermolecularly coupled vibrational modes in Fermi resonance,[66] but no equivalent treatment for the infrared spectra has appeared.

b. Dynamics

The lifetimes of the vibrationally excited ammonia clusters are less than a microsecond, as observed in the other cluster studies.

The well-resolved differences of the angular distribution shapes enable a more detailed treatment of the energy disposal than in the water clusters. Two distinct cases for the vibrational predissociation will be considered.

The first mechanism is a direct predissociation whereby the monomer fragment absorbing the radiation dissociates from the cluster as the energy redistributes into the intermolecular bonds.

In this case, regardless of cluster size, the maximum energy which appears as relative translational motion (E_{max}) of the departing monomer is the same, independent of cluster size. Momentum and energy balance determine the maximum angle where the heavier product is observed for a cluster containing N monomers (monomer mass M) and moving with laboratory velocity v,

$$\sin(\theta^{N}_{max}) = \frac{1}{v}\left(\frac{2E_{max}}{M}\ \frac{1}{N(N-1)}\right)^{1/2} \tag{11}$$

The ratio of the maximum scattering angles for sequential cluster sizes is dependent only on the cluster size

$$\frac{\sin(\theta^{N}_{max})}{\sin(\theta^{N+1}_{max})} = \left(\frac{(N+1)}{(N-1)}\right)^{1/2} \quad . \tag{12}$$

The second model assumes energy randomization over the cluster, and the maximum translational energy is inversely dependent on cluster

size. Momentum and energy balance determine the ratio of maximum scattering angles for adjacent masses as defined above:

$$\frac{\sin(\theta^{N}_{max})}{\sin(\theta^{N-1}_{max})} = \frac{(N+1)}{N} \left(\frac{N}{N-1}\right)^{1/2} . \tag{13}$$

Table 6 shows the experimental ratios and the predictions of each model. The important point is that the direct model predicts the observed angles of maximum scattering to within experimental error for the mass assignments made according to Eqs. (9) and (10), while the randomization model does not.

Does the direct model have a physical basis, based on the knowledge we have for ammonia and a probable predissociation mechanism? As noted previously, the intramolecular motions in NH_3 are highly coupled. Also, the translational energy distributions indicate that the most probable predissociation will have negligible translational energy. Any mechanism postulated should be consistent with internally excited fragments but not randomization. Analogous to benzene, the ammonia polymers seem to predissociate by first redistributing the energy among lower frequency intramolecular vibrations of the monomer which absorbed the photon. Subsequently, the minimum energy necessary to break the intermolecular bonds is lost from these lower frequency vibrations. This model assumes rapid intramolecular energy redistribution, with a slower rate of energy migration into the intermolecular bond. Most probably, the binding energy for an ammonia monomer is

similar to the lowest frequency intramolecular vibration, ν_2 = 950 cm^{-1}. In this case, the intermolecular bond is required to absorb at once sufficient energy to dissociate. The monomer products are predicted to be internally excited by this model, while the cluster fragments should be characterized by the internal temperature of the cluster before photoexcitation.

4. Summary

For the C_6H_6, NH_3, and H_2O clusters studied, the rate of vibrational predissociation is greater than 10^6 sec^{-1}. In all cases, the measured translational energy distributions of the fragments indicate no detectable variation with excitation wavelength, partially a consequence of the small amount of energy released into translational motion. The rapid vibrational predissociation rate and small kinetic energy release are in qualitative agreement with the predictions of Ewing and Beswick/Jortner. Although these models have heretofore only been applied to binary clusters, they predict that for predissociation rates of the magnitude observed here, the energy will be concentrated in internal motions of the products.

For the NH_3 and C_6H_6 clusters, where the intermolecular forces do not radically perturb the monomer intramolecular spectrum, the translational energy distributions suggest a rather detailed scenario for the infrared intermolecular energy flow leading to predissociation. After one photon is absorbed into the H atom intramolecular stretching frequencies, the intermolecular perturbations induce this energy to flow into combinations and overtones of the lower frequency intramolecular motions, namely NH or CH bends. Once these lower frequency

motions are populated, the energy can more resonantly flow into the intermolecular modes in units of these low frequency vibrations. As the lowest frequency intramolecular vibrations in C_6H_6 and NH_3 are comparable to the intermolecular binding energy, little energy randomization can occur in the cluster before predissociation. The intermolecular bond is forced to accept at one time an amount of energy which exceeds the intermolecular bond strength, so predissociation occurs before intermolecular energy migration.

The infrared spectra obtained for water clusters containing three or more water monomers show a pronounced similarity with liquid water. This is a result of the cyclic structures of these polymers, where each water monomer is acting as both a hydrogen bond donor and acceptor. This last conclusion has been important in explaining the poor agreement between the potential models based on dimer properties and those based on liquid or solid properties. The modifications to the intramolecular potential based on the work by Sceats shows that physically reasonable models can reproduce the gross red shifts without modifying the intermolecular force fields. This decoupling of the intramolecular and intermolecular forces to first order should enable most properties to be fit in a systematic way.

The analysis presented here for H_2O should also explain the observed features of HF clusters,[90] which show the same dramatic change between the dimer and trimer and provide additional evidence for the favored cyclic equilibrium structures of small hydrogen bonded clusters containing three or more molecules.

Several issues still remain unsolved. First of all, the reasons for the breadth of the hydrogen bond absorption is unexplained, as well as the exact assignments of the bands observed. The recent classical linear response theory methods of Behrens and Wilson,[91] if extended to handle combination and overtone bands, will enable the larger cluster spectra to be calculated. Although there are uncertainties in the dipole moment and potential functions, the special trends with cluster size outlined in these experiments might be properly accounted for, considering the large amplitude motion of these clusters, by the classically based spectral response theory.

REFERENCES

1. A. R. W. McKellar and H. L. Welsh, J. Chem. Phys. 61, 4636 (1974).

2. C. J. Ashton, Part II B.A. Thesis, Oxford University (1976) unpublished, M. S. Child, Faraday Discussions, Chem. Soc. 62, 307 (1977); C. J. Ashton, Ph.D. Thesis, Oxford University (1979).

3. T. E. Gough, R. E. Miller and G. Scoles, J. Chem. Phys. 69, 1588 (1978).

4. Infrared Laser Spectroscopy of Molecular Beams, Roger Miller, Ph.D. Thesis, University of Waterloo, Waterloo, Ontario (1980).

5. Donald Levy, Adv. Chem. Phys. XL VII, Part 2, p.323-362 (1981), Wiley and Sons.

6. A. Sudbo, P. A. Schulz, Y. T. Lee and Y. R. Shen, Proc. of the First International School on Laser Applications to Atoms, Molecules and Nuclear Physics, (Vilhuis, USSR, 1978).

7. "Laser Induced Predissociation of SF_6 Clusters", J. Geraedts, S. Setiadi, S. Stolte and J. Reuss, to be published.

8. W. R. Gentry, Mark A. Hoffbauer, Clayton F. Giese, VII International Symposium on Molecular Beams (Trento, 1979).

9. Michael P. Casassa, David S. Bomse, J. L. Beauchamp and Kenneth C. Janda, J. Chem. Phys. 72, 6805 (1980), ibid, 74, 5044 (1981).

10. R. K. Sparks, L. R. Carlson, K. Shobatake, M. L. Kowalczyk and Y. T. Lee, J. Chem. Phys. 72, 1401 (1980).

11. (a) D. J. Evans and R. O. Watts, Mol. Phys. 29, 777 (1975); (b) ibid, 31, 83; (c) ibid, 32, 93.

12. T. B. MacRury, W. A. Steele, Bruce J. Berne, J. Chem. Phys. 64, 1288 (1976).

13. Lawrence J. Lowden, David Chandler, J. Chem. Phys. 61, 5228 (1974).

14. Paul C. Painter and Jack L. Koenis, Spectro. Acta 33A, 1003 (1977).

15. Peter Pulay, Geza Fogaraji, James Boggs, J. Chem. Phys. 74, 3999 (1981).

16. M. Spoliti, S. Nunziante Cesaro, V. Grosso, Spectro. Acta 32A, 145 (1976).

17. Kenneth Janda, John C. Hemminger, John J. Winn, Stewart E. Novick, Stephen J. Harris, and William Klemperer, J. Chem. Phys. 63, 1419 (1975).

18. George Ewing, J. Chem. Phys. 71, 3143 (1979).

19. J. A. Beswick and J. Jortner, Adv. Chem. Phys., XL VII, Part 2, p. 363-506 (1981).

20. J. A. Beswick and G. Delgado-Barrio, J. Chem. Phys. 73, 3653 (1980); and J. A. Beswick, J. Jortner, Mol. Phys. 34, 1137 (1980).

21. Daniel A. Morales and George E. Ewing, Chem. Phys. 53, 141 (1980).

22. Stephen Brosnan and Robert Byer, IEEE Jour. Quant. Elect. QE-15, 415 (1979).

23. E. Stenhasen, S. Abrahamsson, F. McLafferty, Atlas of Mass Spectral Data, Vol. 1, Interscience 1969, 101. The ratios of mass 78:52:51:50 are 1000:177:157:126.

24. Kelvin rare gas time-of-flight program, Matthew Vernon, LBL Report 12422 (1981).

25. Kenneth Janda, private communication.

26. R. Gentry, unpublished results.

27. J. A. Barker, R. A. Fisher and R. O. Watts, Mol. Phys. 21, 657 (1970).

28. I. R. McDonald, M. Klein, Dis. Fara. Soc. 66, 48 (1978).

29. J. R. Rowlinson, Trans. Fara. Soc. 47, 120 (1951).

30. (a) F. H. Stillinger, J. Chem. Phys. 57, 1780 (1972), (b) F. H. Stillinger, J. Phys. Chem. 74, 3677 (1970).

31. (a) G. Lie, E. Clementi, M. Yoshimine, J. Chem. Phys. 64, 2314 (1976).

(b) G. Lie, E. Clementi, ibid, 62, 2195 (1975).

(c) H. Kistenmacher, H. Popkie, E. Clementi, R. O. Watts, ibid, 60, 4455 (1974).

(d) H. Popkie, H. Kistenmacher, E. Clementi, ibid, 59, 1325 (1973).

(e) O. Matsuoka, E. Clementi, M. Yoshimine, ibid, 64, 1351 (1976).

(f) H. Kistenmacher, G. Lie, H. Popkie, E. Clementi, ibid, 61, 546 (1974).

(g) E. Clementi, W. Kolos, G. Lie, G. Ranghino, Int. J. Quant. Chem. 17, 377 (1980).

32. M. Van Thiel, E. Becker, and G. Pimentel, J. Chem. Phys. 27, 486 (1957).

33. V. B. Mann, T. Neikes, E. Schmidt, W. Luck, Berichte der Bunsen-Gesellschaft 78, 1236 (1974).

34. B. I. Stepanov, Nature 157, 808 (1946).

35. D. Hagen, J. L. Kassner, J. Chem. Phys. 61, 4285 (1974).

36. (a) C. A. Coulson, G. N. Robertson, Proc. Roy. Soc. London A 337, 167 (1974).

(b) C. A. Coulson, G. N. Robertson, ibid, A342, 289 (1975).

(c) G. N. Robertson, ibid, A286, 25 (1977).

37. G. Ewing, J. Chem. Phys. 72, 2096 (1980).

38. J. A. Beswick and J. Jortner, Adv. Chem. Phys., vol. XLVII, 363 (1981).

39. B. B. Owen, Robert C. Miller, Clifford E. Milner, Harold L. Logan, J. Phys. Chem. 65, 2065 (1961).

40. J. C. Hindman, A. J. Zielen, A. Svirmickas, M. Wood, J. Chem. Phys. 54, 621 (1971).

41. K. E. Larsson, V. Dahlborg, Physica 30, 1561 (1964).

42. C. J. Montrose, J. A. Bucaro, J. Marshall-Coakley, T. A. Litovitz, J. Chem. Phys. 60, 5025 (1974).

43. R. O. Watts, Chem. Phys. 26, 367 (1977).

44. (a) H. Lemberg, F. Stillinger, J. Chem. Phys. 62, 1677 (1975).
(b) F. Stillinger, A. Rahman, ibid, 68, 666 (1978).

45. (a) F. Stillinger, C. David, J. Chem. Phys. 69, 1473 (1978).
(b) F. Stillinger, C. David, ibid, 73, 3384 (1980).

46. J. Owicki, L. Shipman, H. Scheraga, J. Phys. Chem. 79, 1794 (1975).

47. NPL Subroutine BCNDQ1-Quasi Newton algorithm to find the minimum of a function of N simply bounded variables using function values only.

48. "Evidence for the existence of structures in gas-phase homomolecular clusters of water," V. Hermann, Bruce Kay, A. W. Castleman, Jr., sub. to J. Chem. Phys.

49. A. W. Castleman, B. Kay, V. Hermann, P. M. Holland, and T. D. Mark, Sur. Sci. 106, 179 (1981).

50. (a) T. Dyke, K. Mack, J. S. Muenter, J. Chem. Phys. 66, 498 (1977).

(b) T. Dyke, J. S. Muenter, ibid, 60, 2929 (1974).

(c) T. Dyke, J. S. Muenter, ibid, 57, 5011 (1972).

(d) J. A. Odutola, T. Dyke, ibid, 72, 5062 (1980).

51. D. Hadzi, S. Bratos, "Vibrational Spectroscopy of the Hydrogen Bond," Chapter 12, The Hydrogen Bond, P. Schuster, G. Zundel, and G. Sandorfy eds., North Holland, Amsterdam, 1976.

52. (a) G. C. Hofaker, Y. Marechal, M. A. Ratner, "Dynamical Properties of Hydrogen Bonded Systems," Chapter 6 of reference 25.

(b) Y. Marechal, A. Witkowski, J. Chem. Phys. 48, 3697 (1968).

(c) M. Wojcik, Mol. Phys. 36, 1757 (1978).

53. M. Sceats, M. Stavola, S. Rice, J. Chem. Phys. 71, 983 (1979).

54. (a) A. Tursi, E. Nixon, J. Chem. Phys. 52, 152 (1970).

(b) L. Fredin, B. Nelander, G. Ribbegard, Chem. Phys. Lett. 36, 375 (1975).

(c) L. Fredin, B. Nelander, G. Ribbegard, J. Chem. Phys. 66, 4065 (1977), 4073 (1977).

(d) G. Ayers, A. Pullin, Spectra. Acta. 32A, 1689 (1976), 1695 (1976).

(e) R. M. Bentwood, A. J. Barnes, W. J. Orville-Thomas, J. Mol. Spectro. 84, 391 (1980).

(f) P. V. Hong, J. C. Cornut, J. Chim. Phys. 72, 534 (1975).

(g) D. Strommen, D. Gruen, R. McBeth, J. Chem. Phys. 58, 4028 (1973).

(h) H. Hallam, "Matrix Isolation of Hydrogen Bonding," Chapter 22 of Ref. 25.

55. Reference 25, page 575.

56. (a) W. A. Senior, R. E. Verrall, J. Phys. Chem. 73, 4242 (1969).
(b) G. Walrafen, J. Chem. Phys. 114 (1967).

57. W. Luck, "Infrared Fundamental Region," Structure of Water and Aqueous Solutions, W. A. P. Luck, ed., Verlag Chemie, Weinheim, 1974.

58. M. Sceats, K. Belsley, Mol. Phys. 40, 1389 (1980).

59. N. Koroteev, M. Endemann, R. Byer, Phys. Rev. Lett. 43, 398 (1979).

60. E. John Murby and D. Pullin, Aust. J. Chem., 32, 1167 (1979).

61. (a) I. R. McDonald and M. L. Klein, ibid, 68, 4875 (1978).
(b) R. W. Impey, M. L. Klein, I. R. McDonald, ibid, J. Chem. Phys. 74, 647 (1981).

62. (a) R. O. Watts, Chem. Phys. 57, 185 (1981).
(b) R. O. Watts, Mol. Phys. 28, 1069 (1974).
(c) J. A. Barker, R. O. Watts, Chem. Phys. Lett. 3, 144 (1969).
(d) J. A. Barker, R. O. Watts, Mol. Phys. 26, 789 (1973).
(e) D. T. Evans, R. O. Watts, Mol. Phys. 28, 1233 (1974).

63. CLAMPS—Classical Many Particle Simulator, Author-D. Ceperley, program developed for the National Resource for Computational Chemistry under Grants DOE W-7405-Eng-48 and NSF CHE-7721305.

64. GRAMPS—Graphics language for use with Evans and Sutherland multipicture system, Author-T. J. O'Donnell, program developed for the National Resource for Computational Chemistry under Grants DOE W-7405-Eng-48 and NSF CHE-7721305.

65. S. Kinumaki, K. Aida, Sendia University Research Institutes Science Reports A, p. 186 (1954).

66. J. McHale, C. Wang, J. Chem. Phys., 73, 3600 (1980).

67. F. Reding, D. Hornig, J. Chem. Phys., 19, 594 (1951).

68. C. Plint, R. Small, H. Welsh, Can. Jour. Phys., 32, 653 (1954).

69. A. Lemley, J. Roberts, K. Plowman, J. Lagowski, J. Phys. Chem., 77, 2185 (1973).

70. M. Schwartz, C. Wang, J. Chem. Phys., 59, 5258 (1973).

71. A. Narten, J. Chem. Phys., 66, 3117 (1977).

72. J. Reed, P. Harris, J. Chem. Phys., 35, 1730 (1961).

73. G. Ribbegard, Chem. Phys., 8, 185 (1975).

74. G. Pimentel, M. Bulanin, M. Van Thiel, J. Chem. Phys., 36, 500 (1962).

75. S. Suzuki, A. Barnes, D. Cowieson, Z. Mielke, C. Purnell, Molecular Spectroscopy of Dense Phases, 12, European Conference on Molecular Spectroscopy, ed. Grossmann, p. 385.

76. J. Odutola, T. Dyke, B. Howard, J. Muenter, J. Chem. Phys., 70, 4884 (1979).

77. A. Hinchliffe, D. G. Bounds, M. L. Klein, I. R. McDonald, R. Righini, J. Chem. Phys., 74, 1211 (1981).

78. O. Novaro, S. Cruz, S. Castillo, W. Kolos, A. Les, J. Chem. Phys., 74, 1118 (1981).

79. Y. Jean, Chem. Phys. Lett., 69, 217 (1980).

80. S. Goren, Phys. Lett., 42A, 185 (1972).

81. G. Duquette, T. H. Ellis, G. Scoles, R. O. Watts, M. L. Klein, J. Chem. Phys., 68, 2544 (1978).

82. P. J. Turner, C. W. David, J. Phys. Chem., 85, 3501 (1981).

83. P. J. Turner, C. W. David, J. Chem. Phys., 74, 512 (1981).

84. I. R. McDonald, M. L. Klein, J. Chem. Phys., 64, 4790 (1976).

85. M. L. Klein, I. R. McDonald, B. J. Berne, M. Rao, D. L. Beveridge, P. K. Mehrotra, J. Chem. Phys., 71, (1979).

86. J. W. Taylor, Cook, Int. Jour. Mass Spectr. and Ion Phys., 30, 345 (1979).

87. C. S. Lee, J. P. O'Connell, C. D. Myrat, J. M. Prausnitz, Can. Jour. Chem., 48, 2993 (1970).

88. G. Gimmestad, G. Pardoe, H. Gebbie, J. Quant. Spectrosc. Radiat. Transfer, 12, 559 (1972).

89. J. Lowder, J. Quant. Spectrosc. Radiat. Transfer, 10, 1085 (1970).

90. J. M. Lisy, A. Tramer, M. F. Vernon, and Y. T. Lee, J. Chem. Phys., 75, 4733 (1981).

91. P. Berens, K. Wilson, J. Chem. Phys., 74, 4872 (1981).

Table 1. Experimental conditions used to measure the vibrational predissociation spectra in Fig. 1. In all cases the angle between the detector and the molecular beam was 4°, and the nozzle temperature was 125°C.

Temperature of water reservoir	Pressure at nozzle (torr)	Ion mass detected	Fig. 1 label	Smallest water cluster capable of contribution to signal
67.5	209	H_3O^+	a	trimer
72	255	$(H_2O)_2\ H^+$	b	tetramer
80	355	$(H_2O)_3\ H^+$	c	pentamer
84	417	$(H_2O)_4\ H^+$	d	hexamer

Table 2. Water polymer energetics.

$D_e(cm^{-1})$	Fig. 3 Label	Watts	Owicki	Stillinger (C.F.)	Stillinger (Pol.)
H_2O		0.0	0.0	0.0	0.0
$(H_2O)_2$	a	2122.0	1904.0	1993.0	2388.0
$(H_2O)_3$	b	5450.0	5183.0	5472.0	3774.0
$(H_2O)_3$	c	—	—	—	5387.0
$(H_2O)_4$	d	9187.0	8624.0	7667.0	10147.0
$(H_2O)_4$	e	7526.0	—	—	—
$(H_2O)_5$	f	12100.0	12429.0	11980.0	15789.0

Harmonic ZPE (cm^{-1})	Fig. 3 Label	Watts	Owicki*	Stillinger (C.F.)	Stillinger (Pol.)
(H_2O)		4723.0	0.0	4739.0	5107.0
$(H_2O)_2$	a	10224.0	854.0	10320.0	11863.0
$(H_2O)_3$	b	16088.0	1876.0	18417.0	18870.0
$(H_2O)_3$	c	—	—	—	18597.0
$(H_2O)_4$	d	21682.0	3094.0	23897.0	26611.0
$(H_2O)_4$	e	21406.0	—	—	—
$(H_2O)_5$	f	27145.0	3941.0	28891.0	36252.0

*Rigid H_2O molecule. ZPE's of $(H_2O)_n$ are only from the motions associated with hydrogen bonding.

Table 3. Pressure dependence of the water cluster distribution in the molecular beam.

Pressure at Nozzle (Torr)	$\frac{(H_2O)_2\ H^+}{H_3O^+}$	$\frac{(H_2O)_3\ H^+}{H_3O^+}$	$\frac{(H_2O)_4\ H^+}{H_3O^+}$
150	0.19	0.02	---
185	0.34	0.10	0.02
235	0.54	0.25	0.08
290	0.66	0.43	0.17
355	0.78	0.46	0.32
435	0.92	0.68	0.48
525	1.0	0.75	0.57

Table 4. High frequency vibrations for potential models. The values in parentheses are the integrated band intensities (using a linear approximation to the dipole moment function) for the normal coordinates, normalized to the most intense free OH transition.

	Watts		Stillinger Central Force		Stillinger Polarization	
Monomer	3951(1.00)	1653(0.99)	4283(0.34)	1375(1.20)	4354(0.82)	1642(5.29)
	3841(0.52)		3820(1.00)		4203(1.00)	
	Fig. 3(a)		Fig. 3(a)		Fig. 3(a)	
Dimer	3920.(1.00)	1708.(0.90)	4363.(0.95)	1495.(3.09)	4689.(0.25)	1811.(0.25)
	3914.(0.87)	1670.(1.12)	4303.(1.00)	1415.(3.53)	4485.(1.00)	1638.(0.32)
	3815.(0.45)		3877.(2.68)		4455.(0.25)	
	3760.(0.73)		3834.(2.74)		4157.(0.28)	

	Fig. 3(b)		Fig. 3(b)		Fig. 3(b)		Fig. 3(c)	
Trimer	3890.(0.00)	1773.(0.00)	4545.(1.00)	2918.(0.00)	4680.(0.99)	1780.(0.03)	4848.(0.22)	1840.(0.13)
	3884.(1.00)	1727.(0.85)	4545.(1.00)	1840.(0.31)	4657.(1.00)	1703.(0.46)	4657.(0.22)	1816.(0.06)
	3884.(1.00)	1727.(0.85)	4422.(0.0)	1840.(0.31)	4464.(0.06)	1647.(0.39)	4517.(1.00)	1629.(0.14)
	3696.(0.80)		3959.(2.05)		4415.(0.11)		4496.(0.13)	
	3969.(0.80)		3959.(2.05)		4375.(0.53)		4412.(0.27)	
	3660.(0.00)		3894.(0.0)		4337.(0.75)		4138.(0.15)	

Table 4. Continued.

	Watts				Stillinger Central Force		Stillinger Polarization	
	Fig. 3(d)		Fig. 3(e)		Fig. 3(d)		Fig. 3(d)	
Tetramer	3888.(0.00)	1749.(0.00)	3924.(0.90)	1791.(0.17)	4677.(0.59)	2269.(1.44)	4864.(0.02)	1858.(0.06)
	3884.(1.00)	1733.(1.16)	3892.(0.47)	1748.(1.14)	4636.(0.65)	2138.(1.69)	4766.(1.0)	1772.(0.08)
	3884.(1.00)	1733.(1.16)	3886.(1.00)	1727.(1.27)	4461.(0.81)	1579.(1.12)	4766.(1.0)	1770.(0.08)
	3883.(0.00)	1733.(0.00)	3819.(0.27)	1669.(0.99)	4403.(1.00)	1548.(4.96)	4507.(0.0)	1770.(0.0)
	3741.(0.00)		3779.(1.01)		3994.(1.59)		4483.(0.0)	
	3727.(0.76)		3701.(0.95)		3982.(1.200)		4409.(0.48)	
	3727.(0.76)		3687.(0.69)		3949.(1.29)		4409.(0.48)	
	3704.(0.00)		3653.(0.12)		3911.(1.32)		4384.(0.18)	
	Fig. 3(f)				Fig. 3(f)		Fig. 3(f)	
Pentamer	3886.(0.02)	1737.(0.10)			4512.(0.0)	1652.(0.13)	4812.(0.12)	2173.(0.00)
	3882.(0.98)	1736.(0.27)			4506.(0.0)	1629.(2.92)	4747.(0.29)	2068.(0.08)
	3882.(1.00)	1736.(0.01)			4463.(1.00)	1627.(2.78)	4672.(1.00)	2059.(0.04)
	3881.(0.10)	1732.(1.31)			4463.(1.00)	1611.(0.14)	4663.(0.77)	2051.(0.04)
	3880.(0.26)	1731.(1.02)			4431.(0.0)	1606.(0.05)	4612.(0.28)	2001.(0.01)
	3744.(0.00)				3959.(1.61)		4408.(1.08)	
	3743.(0.00)				3957.(1.70)		4325.(0.42)	
	3729.(0.91)				3943.(2.14)		4272.(5.99)	
	3728.(0.91)				3943.(2.14)		4248.(7.40)	
	3713.(0.00)				3934.(0.0)		3985.(0.32)	

Table 5. Comparison of assigned matrix $(H_2O)_2$ transitions with the Watts potential model.

Watts' Harmonic Frequencies	Watts' Scaled Frequencies	Ar Matrix	Diff.
	(X.951)		
3920.	3729.	3726.	+3
3914.	3723.	3709.	+14
3815.	3629.	3634.	-5
3760.	3577.	3574.	+3
		N_2 Matrix	
		3715	+19
		3699	+24
		3627	+2
		3550	+22

Table 6. Comparison of energy disposal mechanisms for direct and random models of NH_3 cluster predissociation.

N Cluster size	Experimental Ratios of Maximum Scattering Angles	Direct Model (Eq. 12)	Energy Randomization Model (Eq. 13)
3	1.41	1.41	1.63
4	1.20	1.29	1.44
5	1.11	1.22	1.34

FIGURE CAPTIONS

Fig. 1. Schematic diagram of the Nd:YAG pumped OPO. Components indicated are: 1. Telescope, 2. Input coupler (100 transmittance at 1.06 μ, 100 reflectance at 1.4–2.1 μ), 3. Gold mirror, 4. 30°C temperature stabilized, angle tuned $LiNbO_3$ crystal, 5. Output coupler (100% transmittance at 1.06 μ, 50% reflectance at 1.4–2.1 μ), 6. Double pass YAG mirror (100% reflectance at 1.06 μ, 100% transmittance at 1.4–4.0 μ), 7. BaF_2 lens.

Fig. 2. In plane view of perpendicular laser molecular beam apparatus. Labeled components are: 1. 0.007" quartz nozzle heated to 70°C, 2. First skimmer, 3. Second skimmer, 4. Third skimmer, 5. Power meter, 6. Germanium filter, 7. Ionizer assembly. 8. Quadrupole mass spectrometer. θ measures the angle of rotation of the detector from the molecular beam.

Fig. 3. Side view of the coaxial laser-molecular beam apparatus. Labeled components are: 1. BaF_2 entrance window for the OPO beam, 2. Quadrupole mass spectrometer, 3. Ionizer assembly, 4. Final molecular beam defining aperture, 5. Second skimmer, 6. First skimmer, 7. Nozzle.

Fig. 4. Schematic view of the perpendicular arrangement showing how the recoil velocity of the predissociation fragment relates to the detector's laboratory angle, θ, relative to the molecular beam. The insert shows that the angle is

determined from the vector addition of the recoil velocity (dotted arrows) and the initial beam velocity (thick arrow). The final laboratory velocities are the solid arrows, also shown at the intersection point of the OPO and molecular beams.

Fig. 5. Wavelength dependence of the mass 78 angular distributions. Open circles $\nu_{OPO} = 3040\ cm^{-1}$, solid circles, $\nu_{OPO} = 3095\ cm^{-1}$. The $3040\ cm^{-1}$ data have been displaced +0.5° relative to the $3095\ cm^{-1}$ data to allow easier comparison.

Fig. 6. Wavelength dependence of the predissociation cross sections. A) Mass 390, $(C_6H_6)_5^+$, at 400 torr Ar with $T_{nozzle} = 25°C$, B) Mass 78, $C_6H_6^+$, at 250 torr Ar with $T_{nozzle} = 25°C$.

Fig. 7. Pressure dependence of the mass 78 signal in the perpendicular arrangement with the detector angle at $\theta = 4°$. The solid points are the ratio mass 78($\theta = 4°$)/mass 156($\theta = 0°$), the open circles are the ratio mass 78($\theta = 4°$)/mass 234($\theta = 0°$).

Fig. 8. Comparison of the time resolved mass spectrometer signals of the perpendicular and colinear configurations. A) Mass 78 data taken at $\theta = 0°$ in the perpendicular laser-molecular beam arrangement, B), C), D) are masses 156, 78, and 50 respectively of the colinear configuration.

Fig. 9. Time of flight spectra at masses 78 (solid points) and 50 (open circles). A) Detector angle $\theta = 4°$, B) Detector angle $\theta = 5°$.

Fig. 10. Angular distribution of predissociation fragments. Solid points are mass 156, open circles are mass 78. The curves are the calculated distributions using the center-of-mass energy distribution given by Eqn. 3. For mass 78 and 156, the best fit values for α are 5 and 7 $(\text{kcal/mole})^{-1}$ respectively.

Fig. 11. Water cluster and condensed phase spectra. Panels (a)-(d) are spectra observed in the present work for the conditions given in Table I. Panel (e) conditions are described in the text. Panel (f) is taken from Ref. 6, Panel (g) from Ref. (30b), Panel (h) from E. Whalley and J. E. Bertie, J. Chem. Phys. 46, 1264 (1967).

Fig. 12. Laboratory angular distributions for the detected mass ○ - H_3O^+; + - $(H_2O)_2\ H^+$; □ - $(H_2O)_3\ H^+$; ● - $(H_2O)_4\ H^+$.

Fig. 13. Minimum energy cluster geometries for the Watts potential energy function (a,b,d,e,f), for the polarization model trimer (c), and for the configuration characterizing a transition state for the tetramer dissociating into a trimer and a monomer (g).

Fig. 14. Locally adiabatic dissociation energy curves for A. $(H_2O)_2 \rightarrow 2H_2O$, B. $(H_2O)_3 \rightarrow (H_2O)_2 + H_2O$, C. $(H_2O)_4 \rightarrow (H_2O)_3 + H_2O$ when adjacent hydrogen bonded waters are separated, D. $(H_2O)_4 \leftarrow (H_2O)_3 + H_2O$ when it is formed from a monomer adding to a cyclic trimer, E. $(H_2O)_4 \rightarrow (H_2O)_3 + H_2O$ when opposing nonhydrogen bonded water molecules of the cyclic tetramer are separated.

Fig. 15. The decay curves of the molecular dynamics trajectories for the conditions

● $T_{vib} = 3000°K$, $T_{rot} = 0°K$

+ $T_{vib} = 3000°K$, $T_{rot} = 100°K$

□ $T_{vib} = 3000°K$, $T_{rot} = 200°K$

○ $T_{vib} = 5000°K$, $T_{rot} = 100°K$

Fig. 16. Absorption cross section observed in the coaxial configuration at (A) H_3O^+ and (B) $(H_2O)_2H^+$, corresponding to $(H_2O)_2$ and $(H_2O)_3$ respectively.

Fig. 17. Time resolved signal observed in the coaxial configuration at mass 217(○) and mass 145 (●). The offset of the two peaks is from the different ion delays.

Fig. 18. Absorption cross section observed at mass 289 in the coaxial configuration, corresponding to $(H_2O)_{17}$.

Fig. 19. Ammonia polymer spectra

(A) Mass 18 corresponding to $(NH_3)_3$ predissociation products

(B) Mass 35 corresponding to $(NH_3)_4$ predissociation products

(C) Mass 52 corresponding to $(NH_3)_5$ predissociation products

Fig. 20. Angular distributions for the ammonia cluster predissociation products.

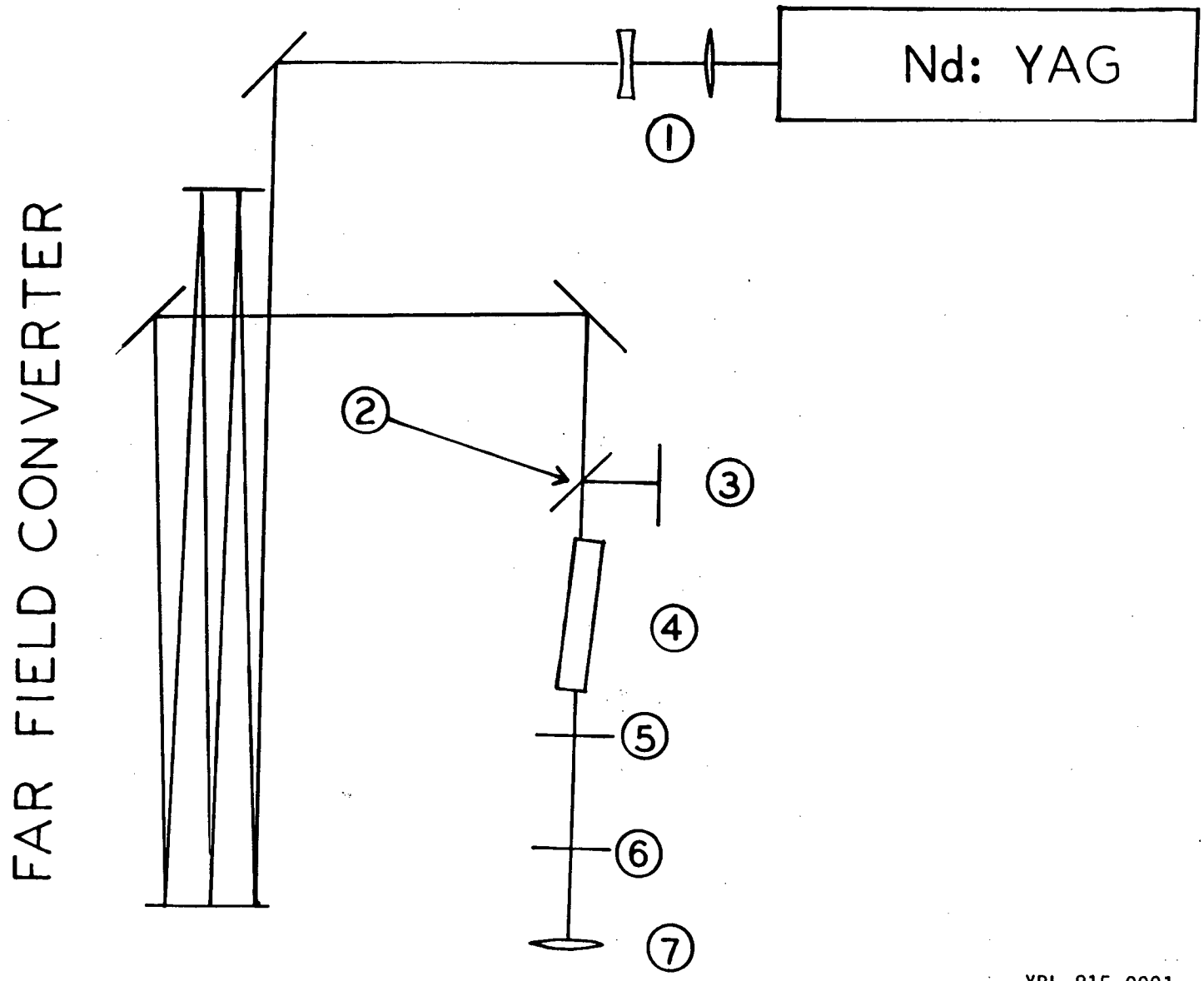

XBL 815-9991

Fig. 1

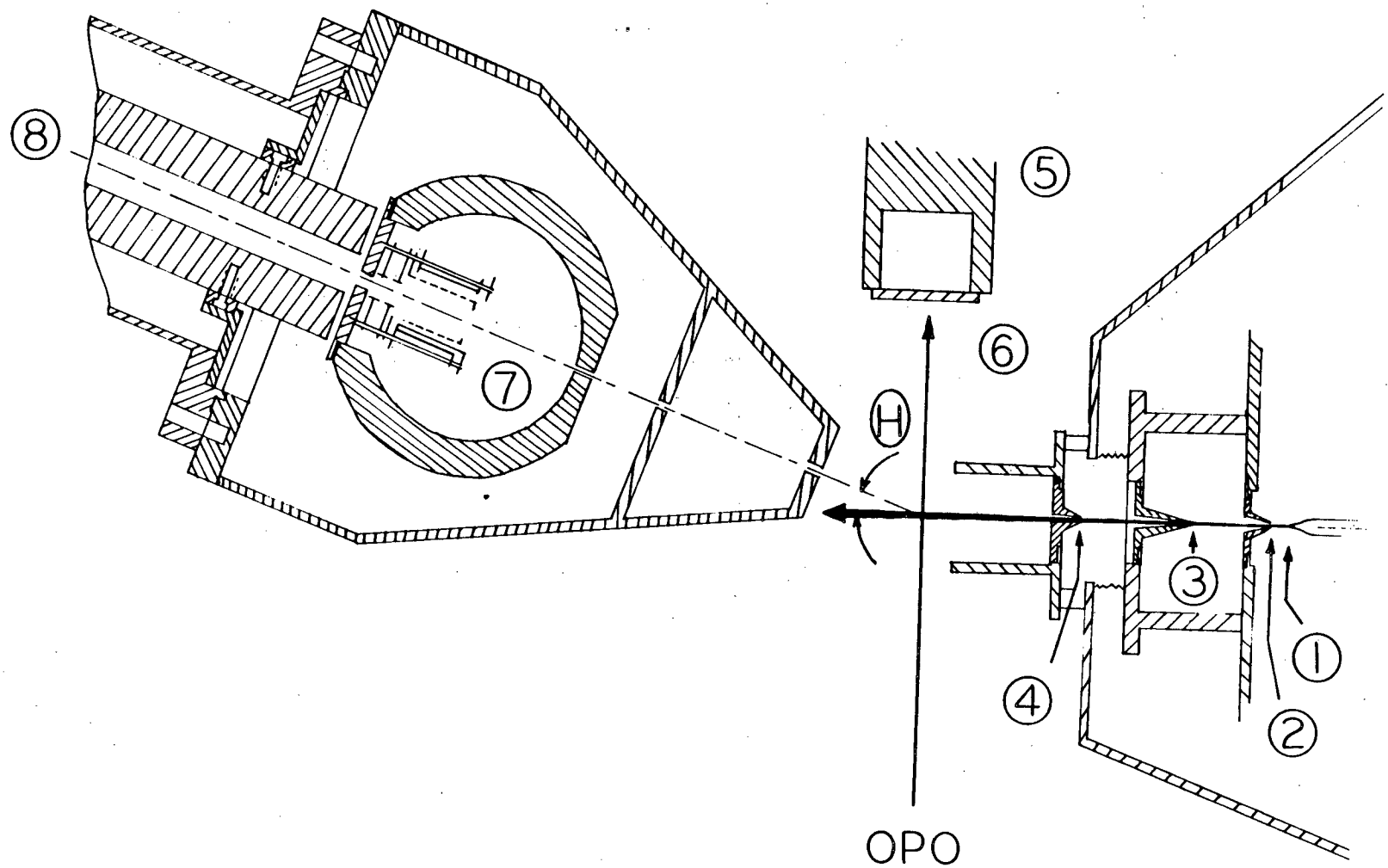

XBL 815-9990

Fig. 2

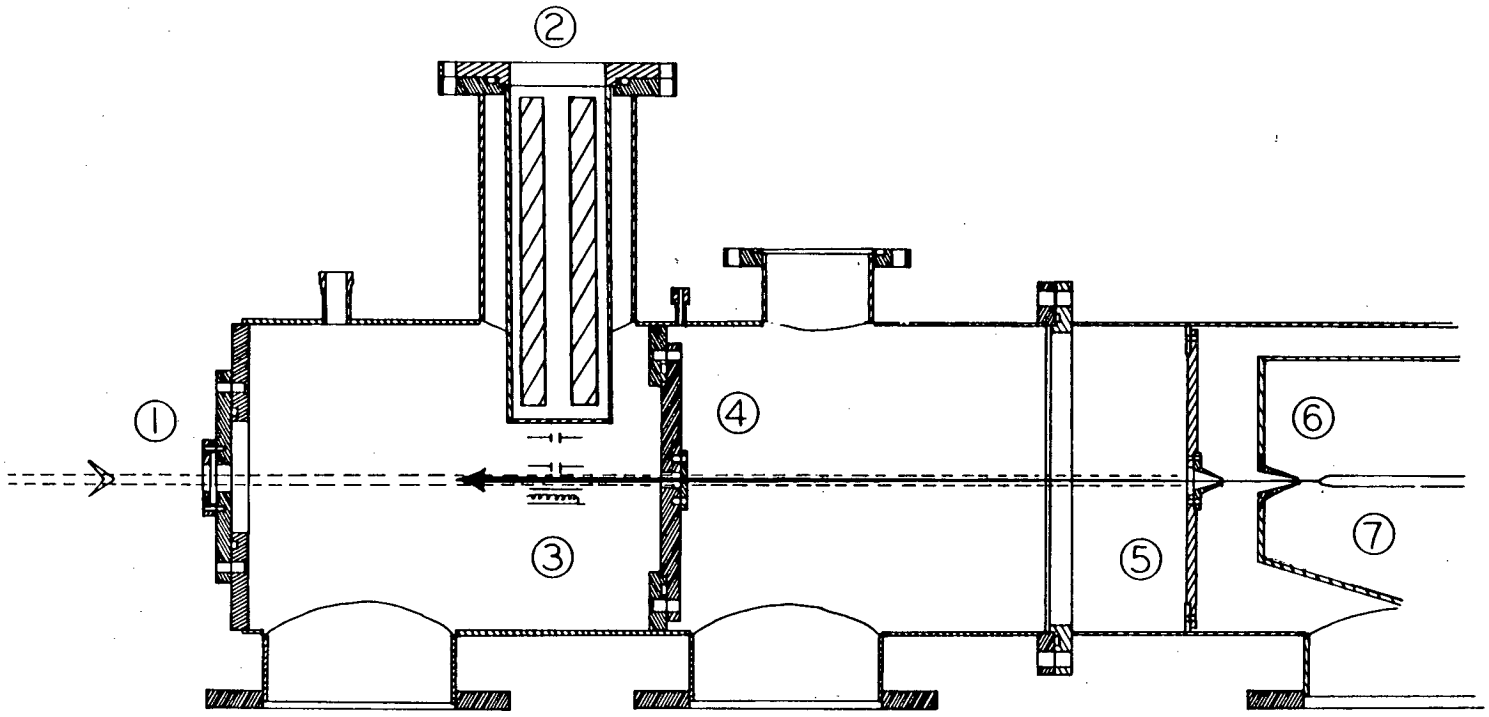

XBL 815-9994

Fig. 3

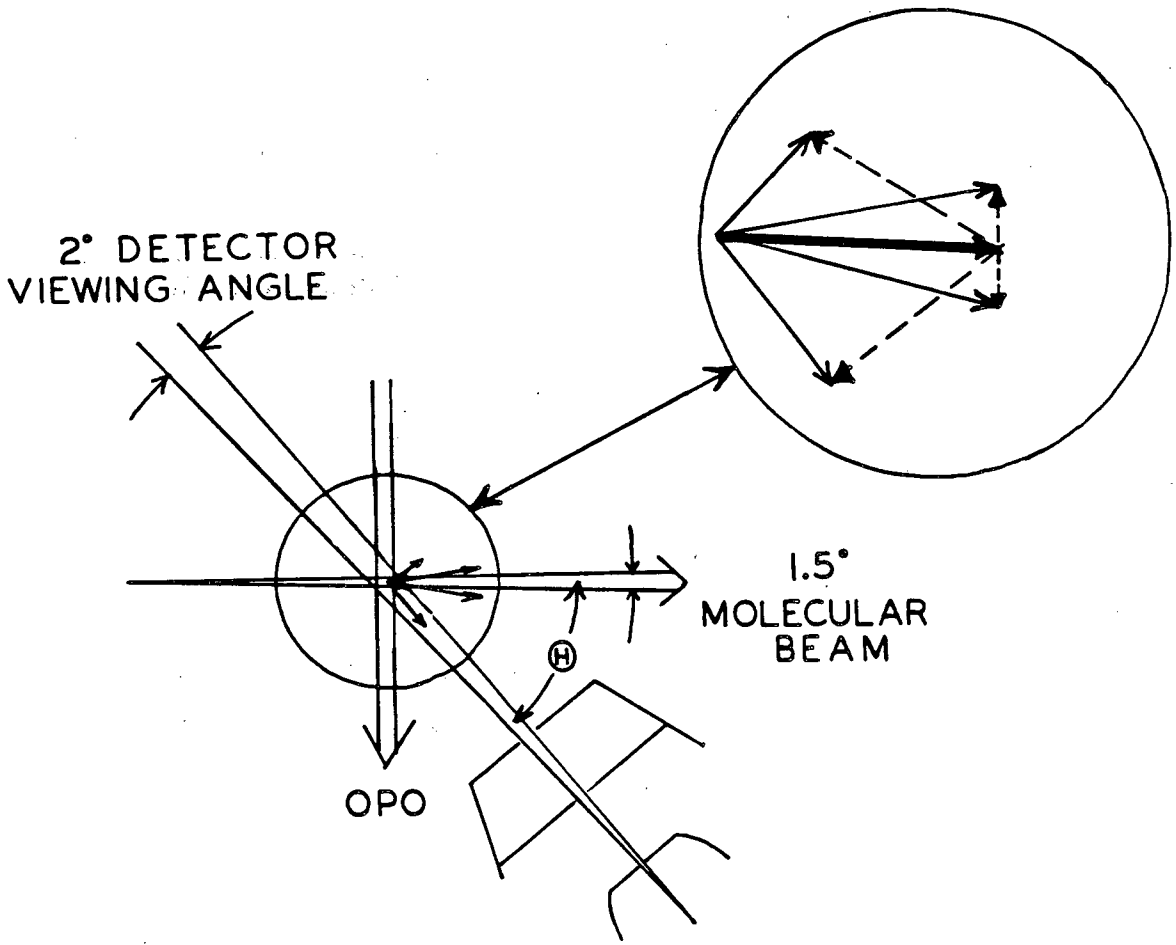

XBL 816-9998

Fig. 4

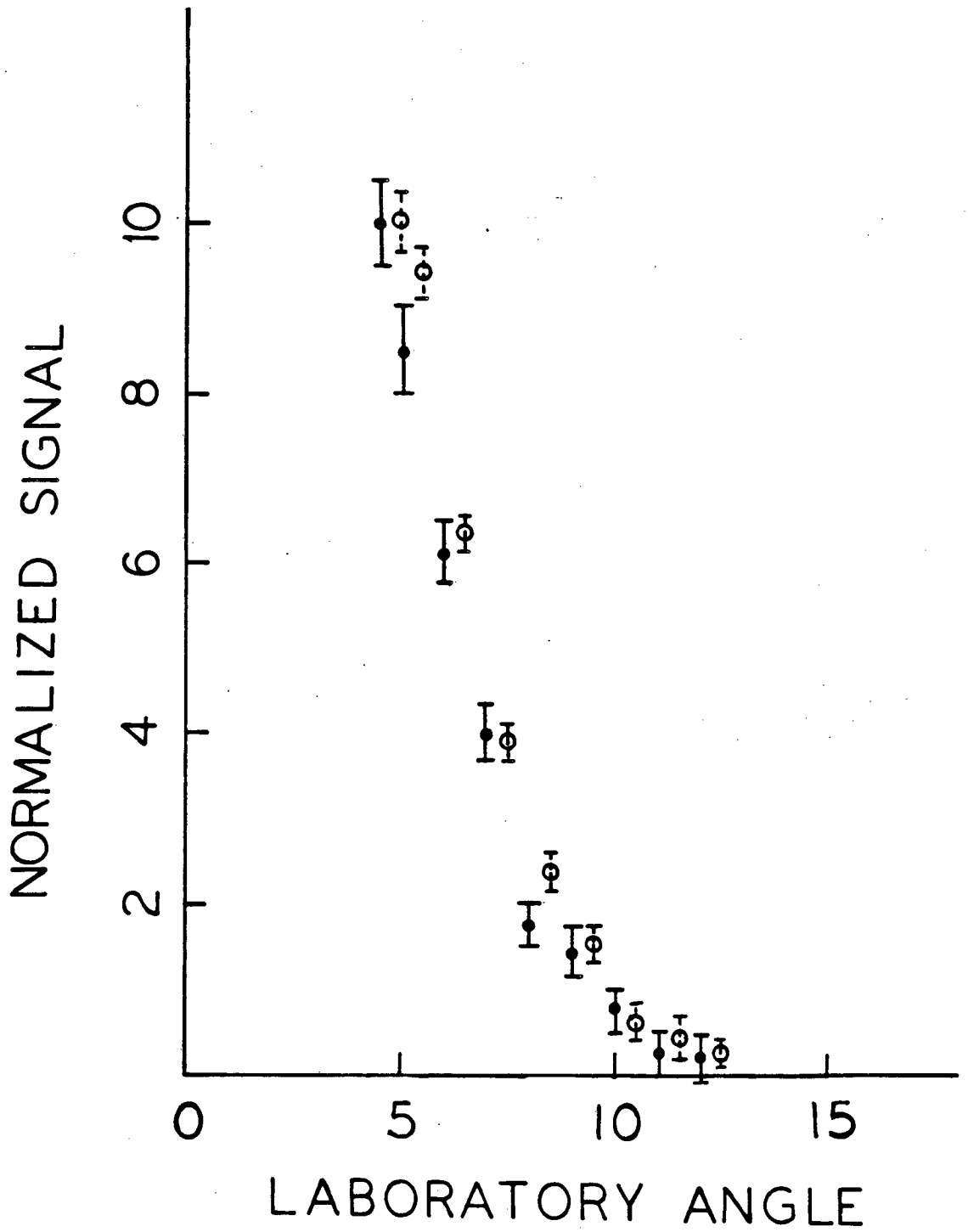

XBL 816-9996

Fig. 5

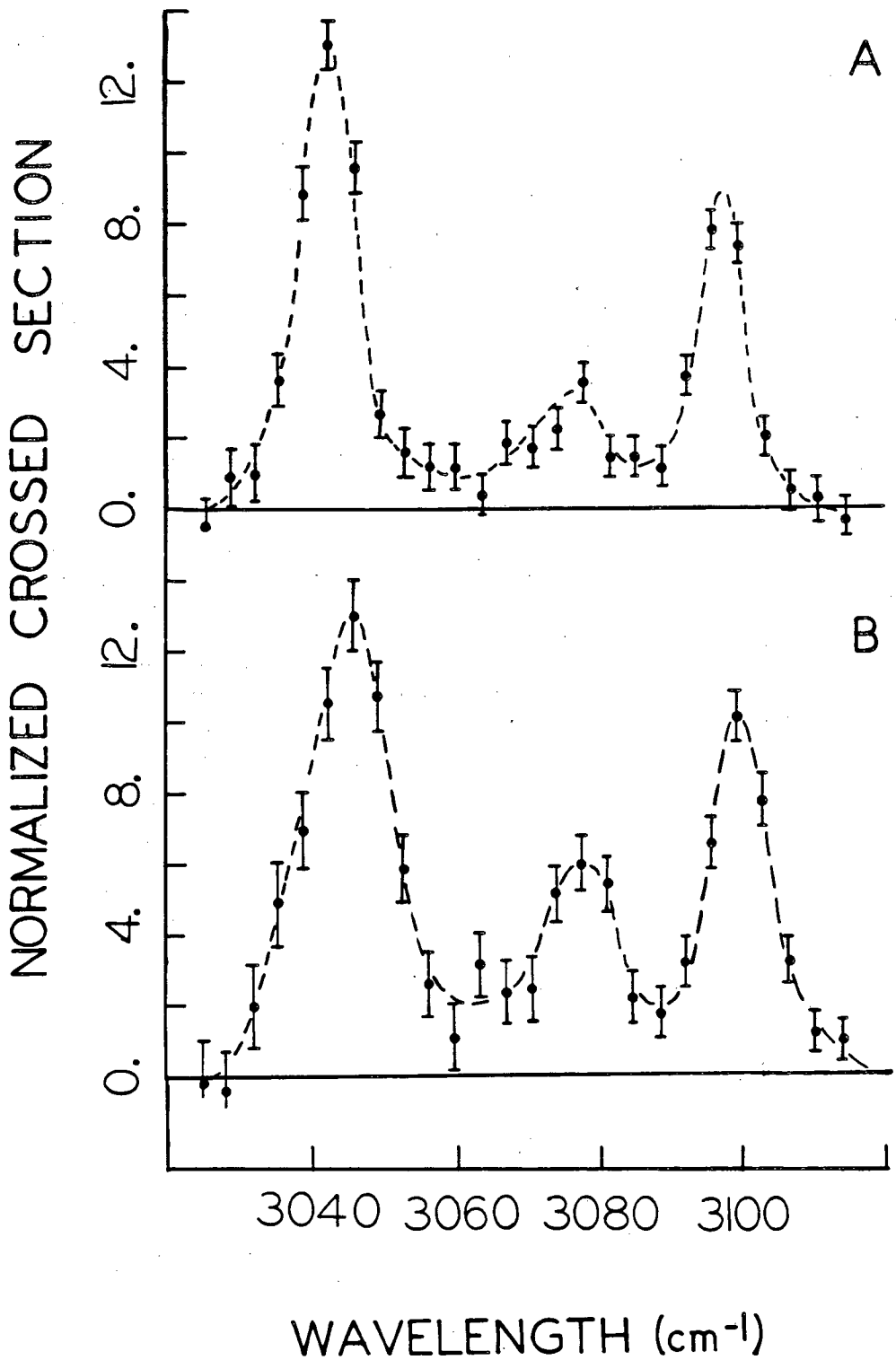

XBL 815-9992

Fig. 6

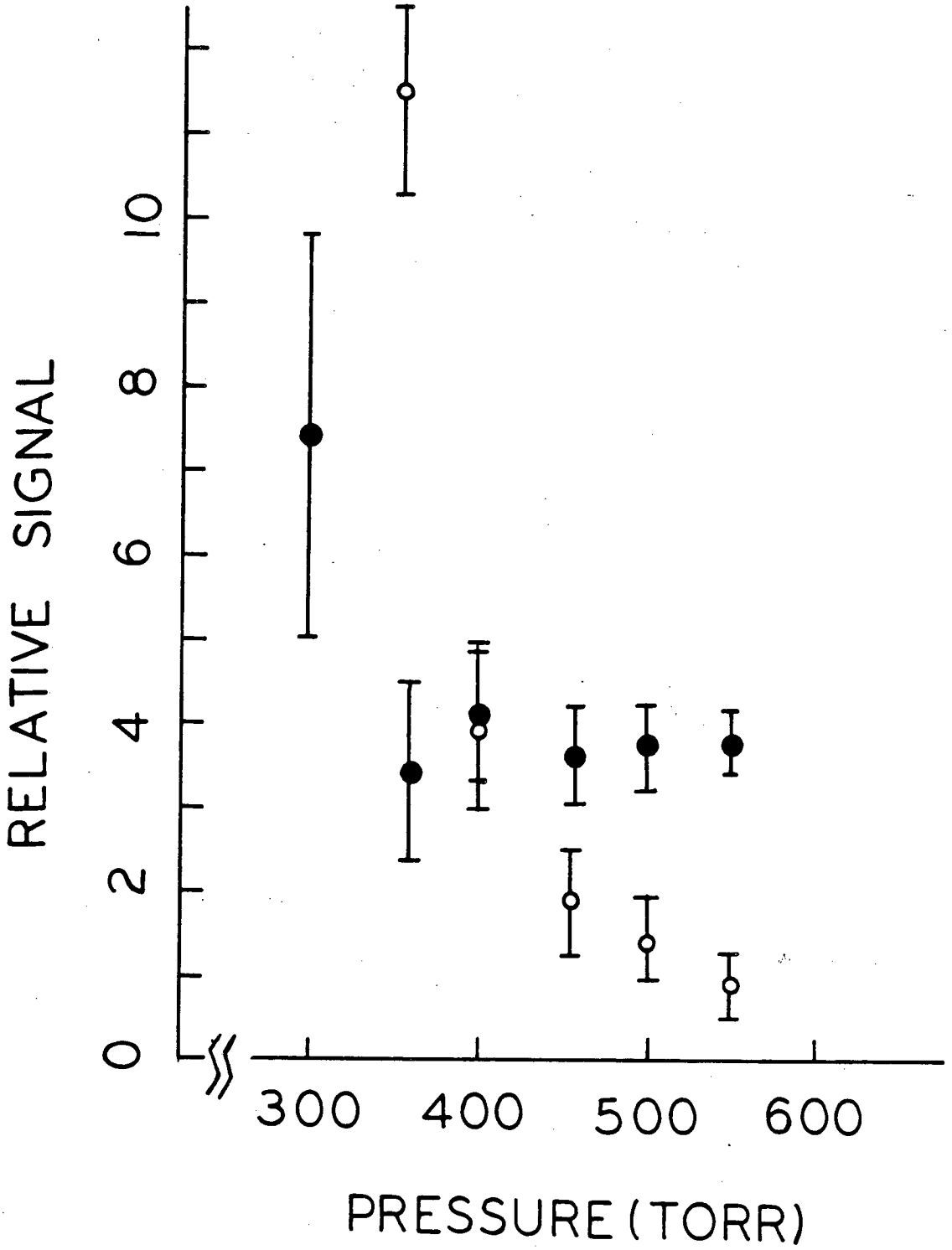

XBL 816-9997

Fig. 7

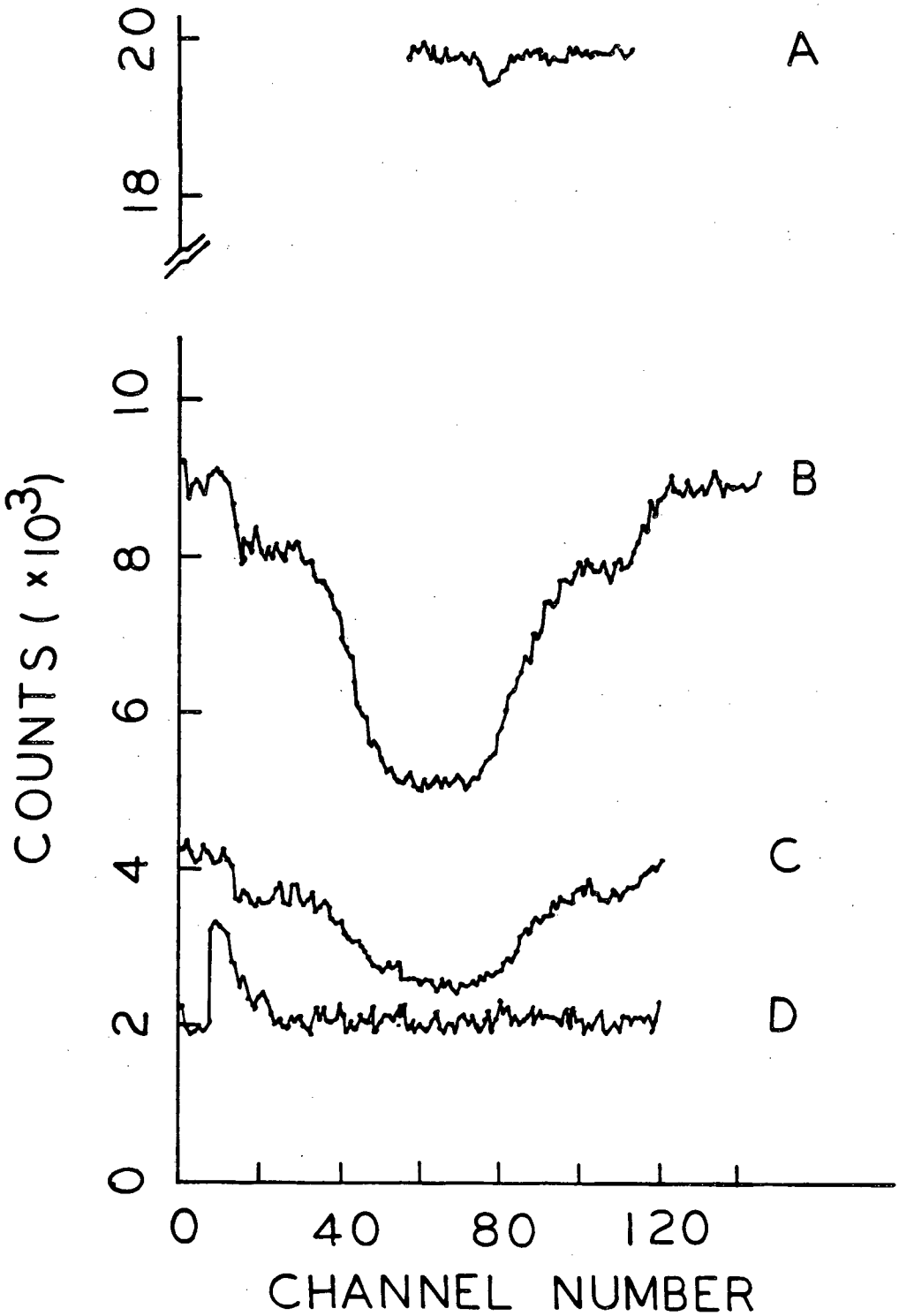

XBL 815-9989

Fig. 8

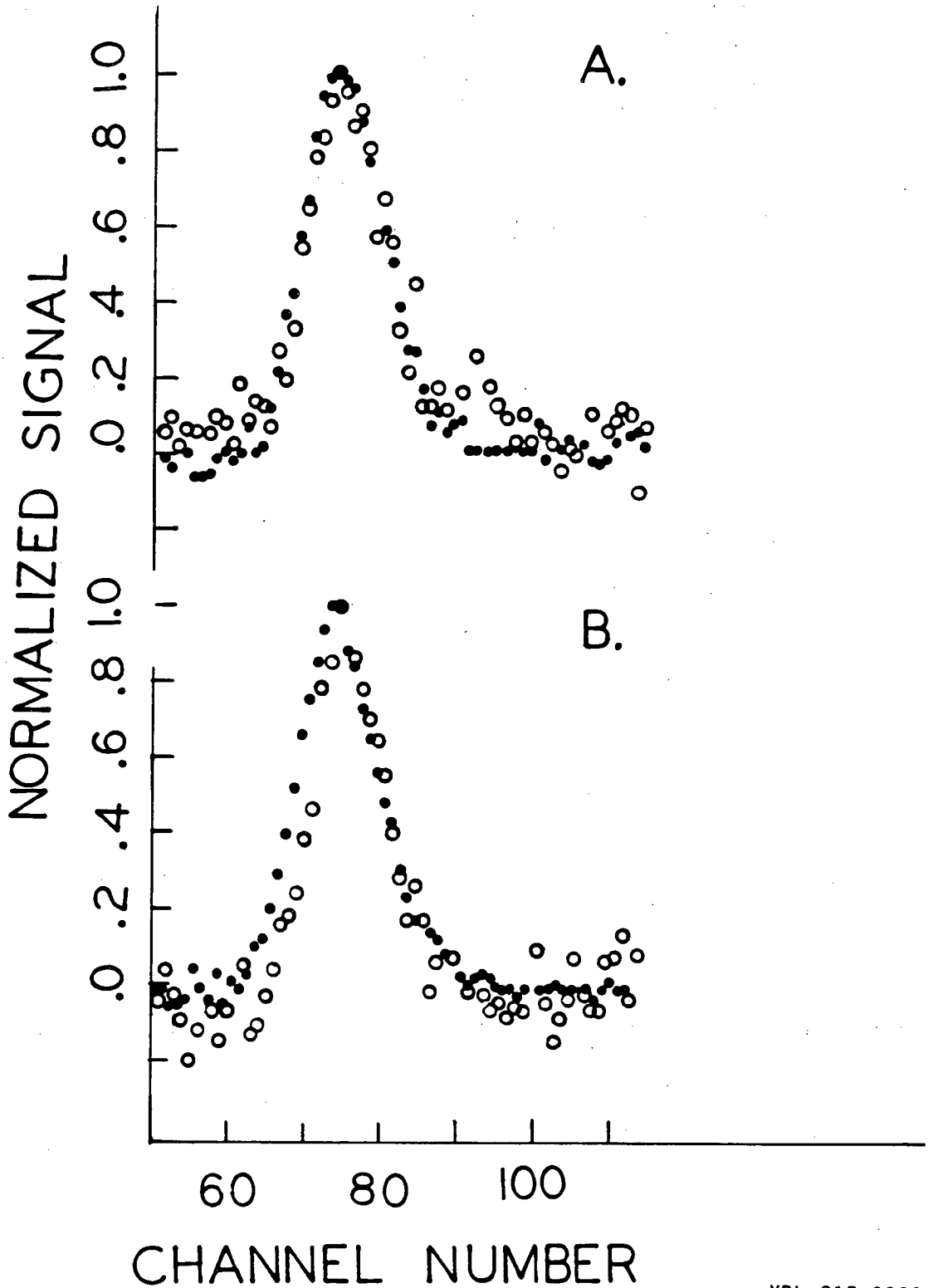

XBL 815-9993

Fig. 9

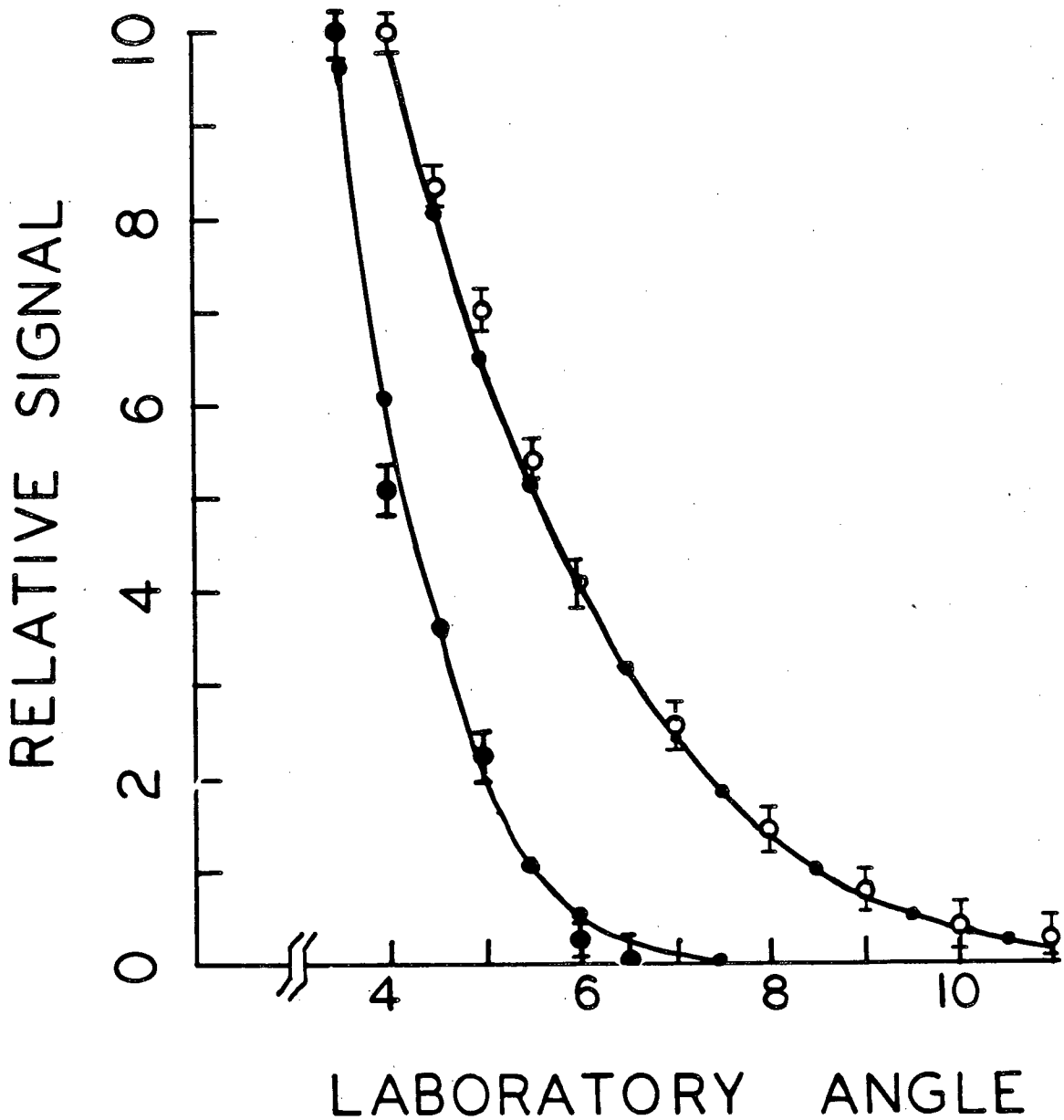

XBL 816-9995

Fig. 10

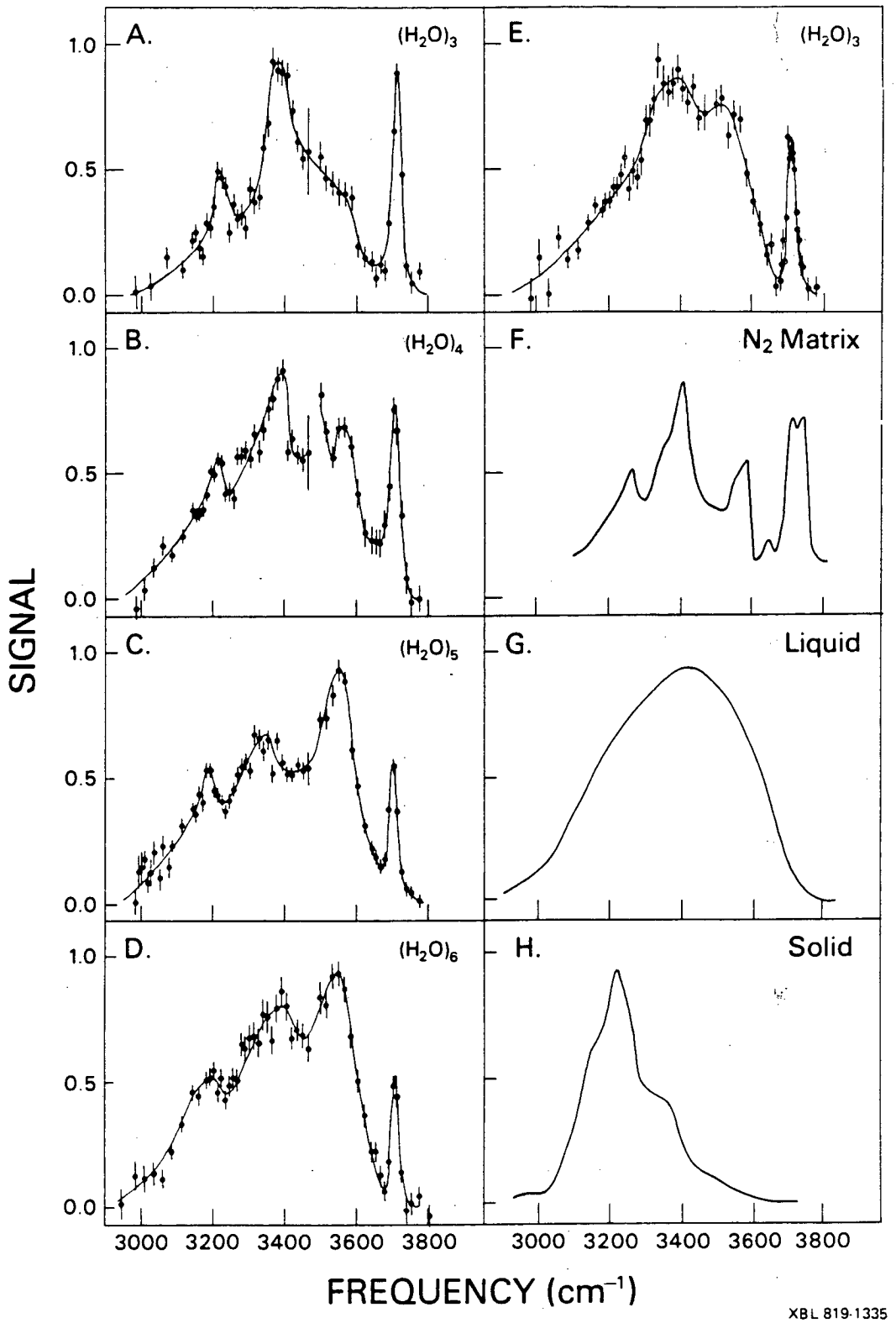
A.
$(H_2O)_3$
B.
$(H_2O)_4$
C.
$(H_2O)_5$
D.
$(H_2O)_6$
E.
$(H_2O)_3$
F.
N_2 Matrix
G.
Liquid
H.
Solid
SIGNAL
1.0
0.5
0.0
3000
3200
3400
3600
3800
FREQUENCY (cm^{-1})
XBL 819-1335

Fig. 11

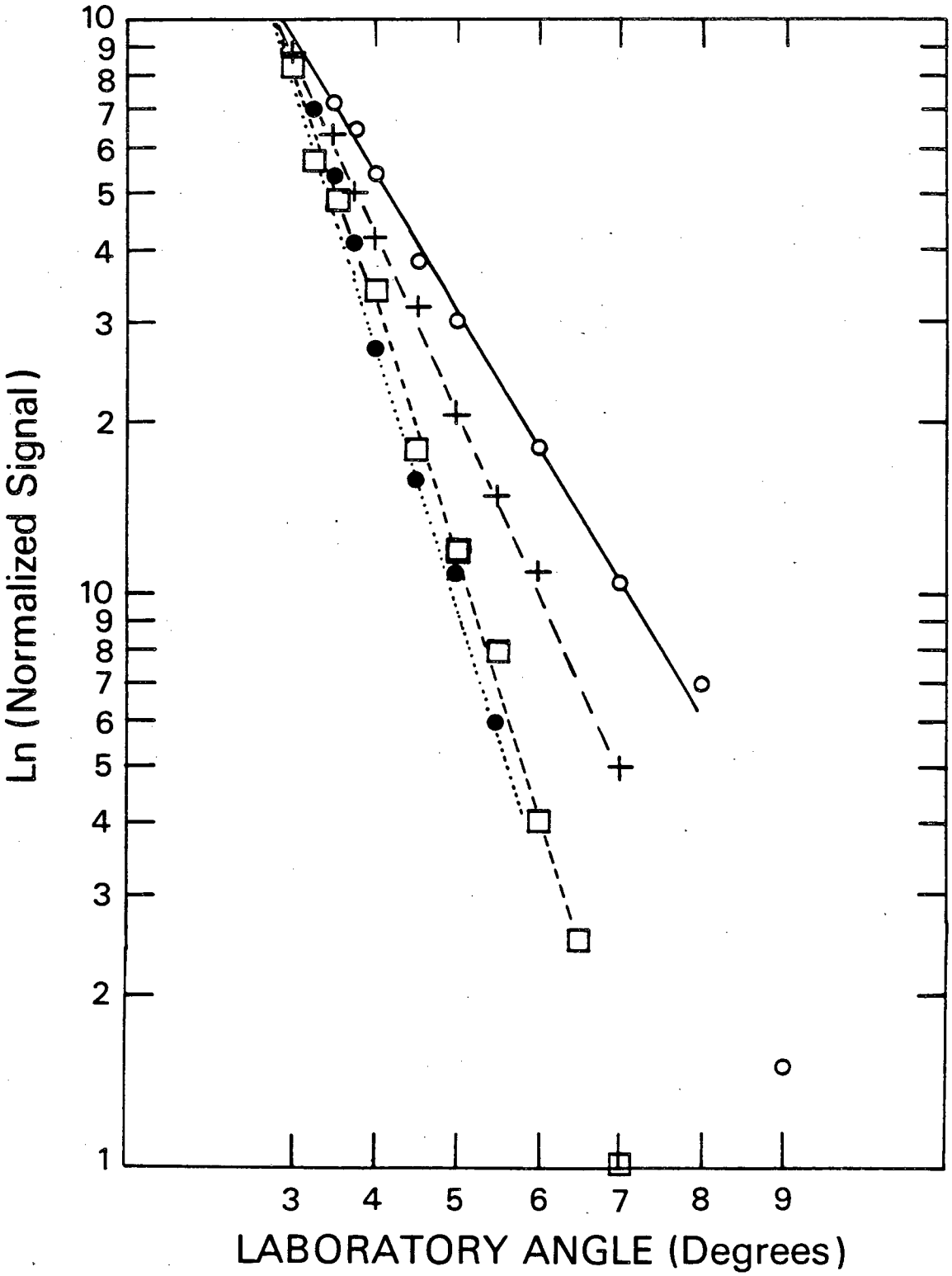

XBL 819-1333

Fig. 12

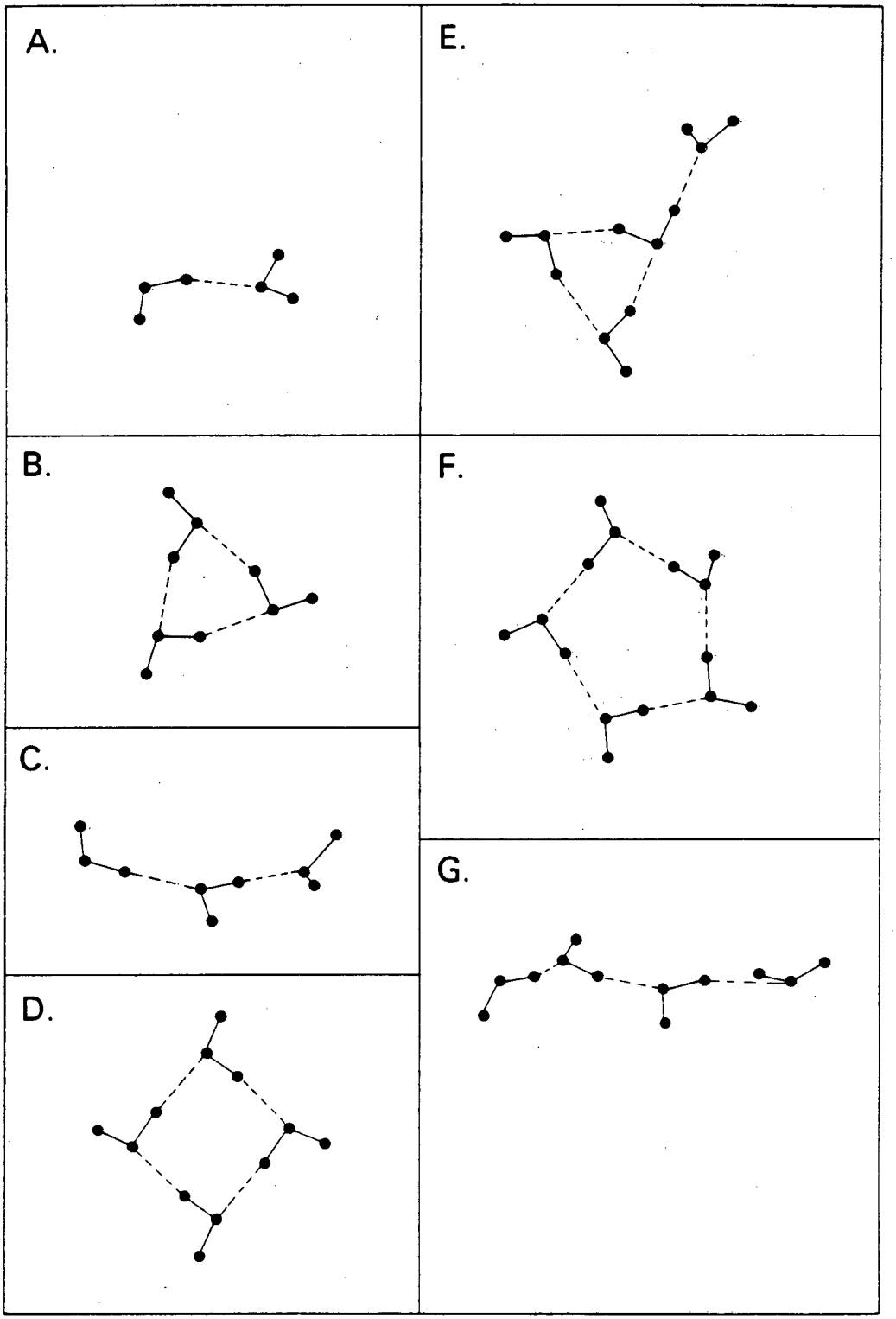

XBL 819-1334

Fig. 13

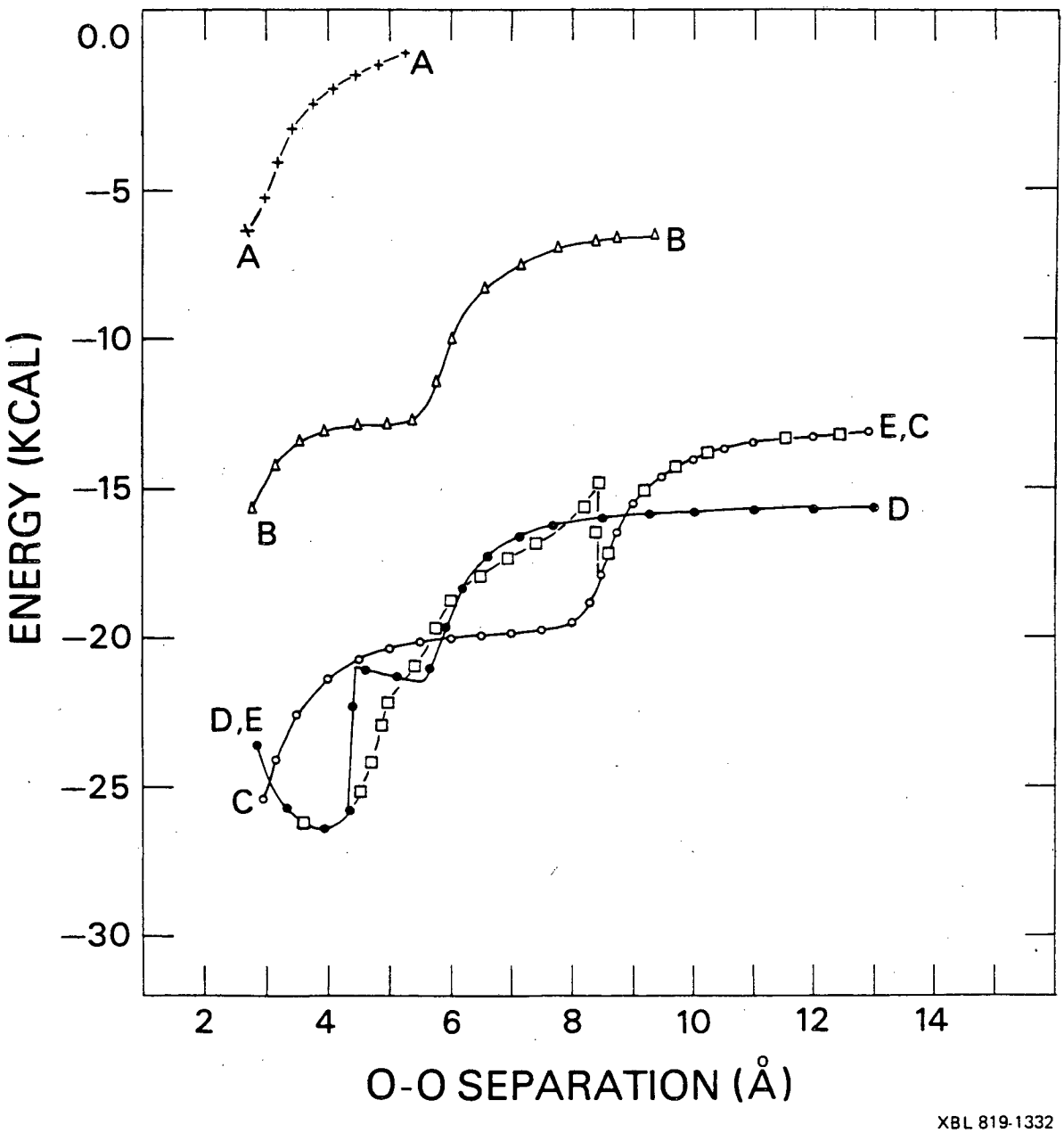
0.0
−5
−10
−15
−20
−25
−30
ENERGY (KCAL)
2
4
6
8
10
12
14
O-O SEPARATION (Å)
A
A
B
B
E,C
D
D,E
C
XBL 819-1332

Fig. 14

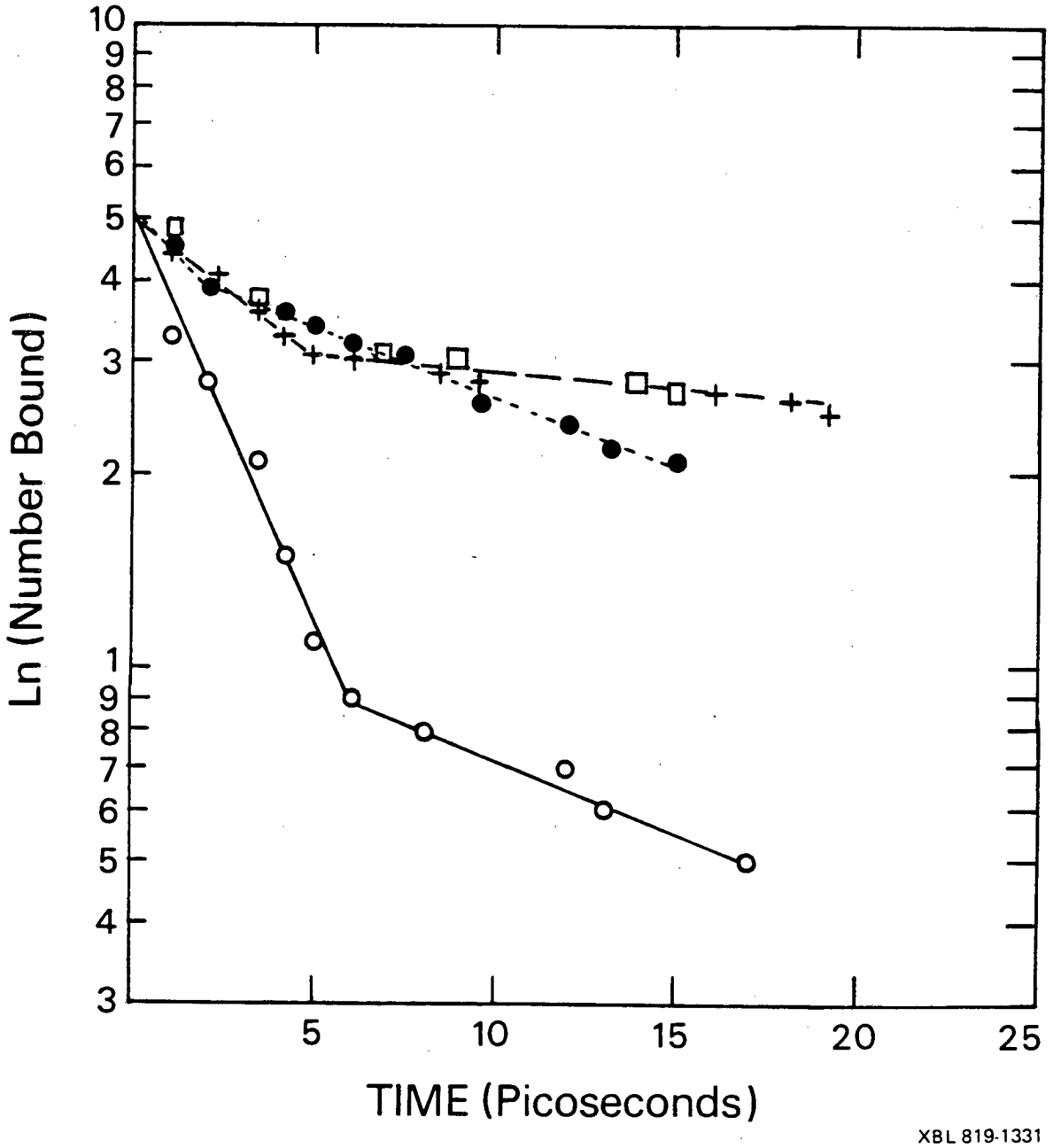
Ln (Number Bound)
10
9
8
7
6
5
4
3
2
1
9
8
7
6
5
4
3
5
10
15
20
25
TIME (Picoseconds)
XBL 819-1331

Fig. 15

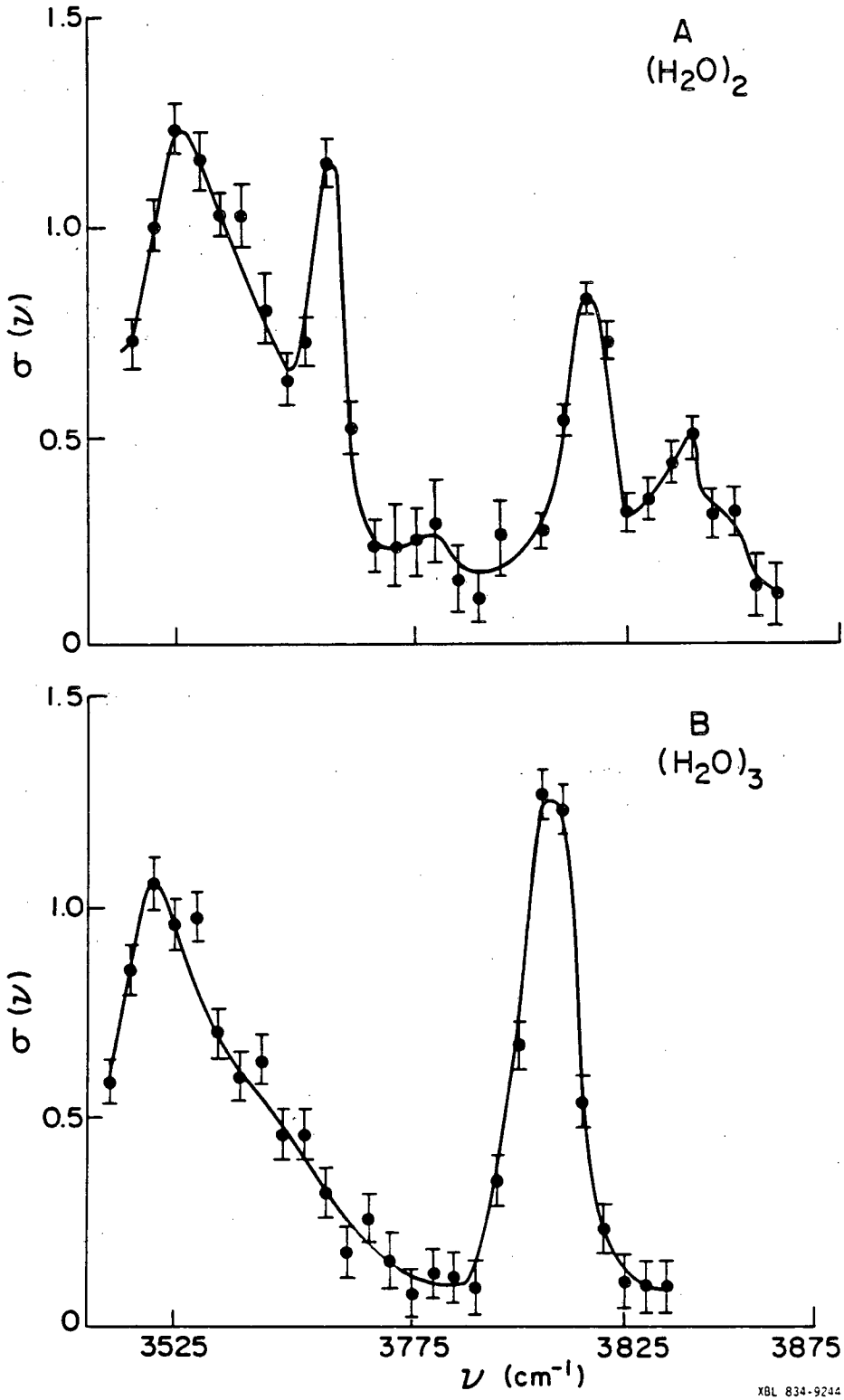
A
$(H_2O)_2$
B
$(H_2O)_3$
1.5
1.0
0.5
0
$\sigma(\nu)$
3525
3775
3825
3875
ν (cm^{-1})
XBL 834-9244

Fig. 16

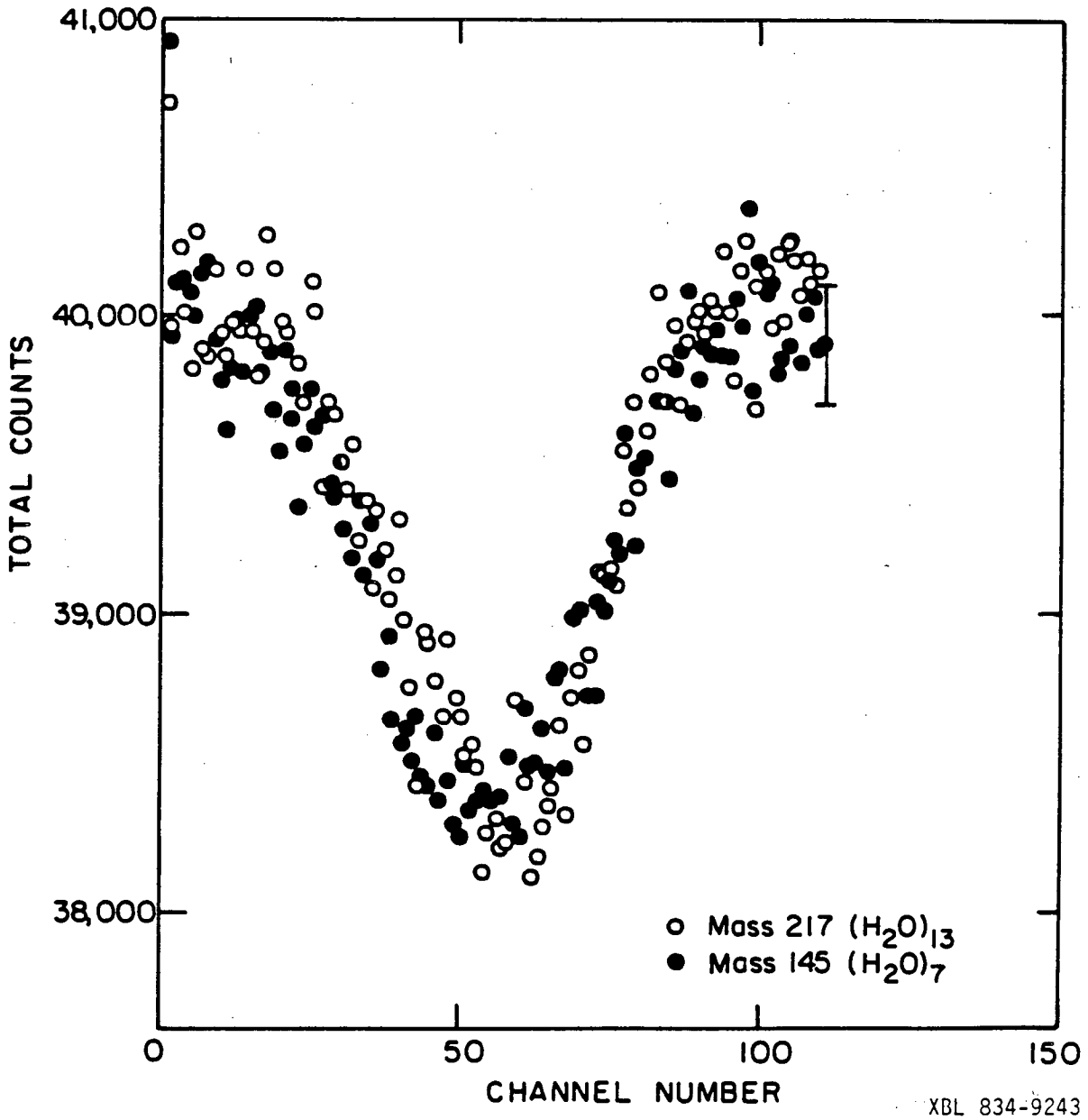
41,000
40,000
39,000
38,000
TOTAL COUNTS
0
50
100
150
CHANNEL NUMBER
Mass 217 $(H_2O)_{13}$
Mass 145 $(H_2O)_7$
XBL 834-9243

Fig. 17

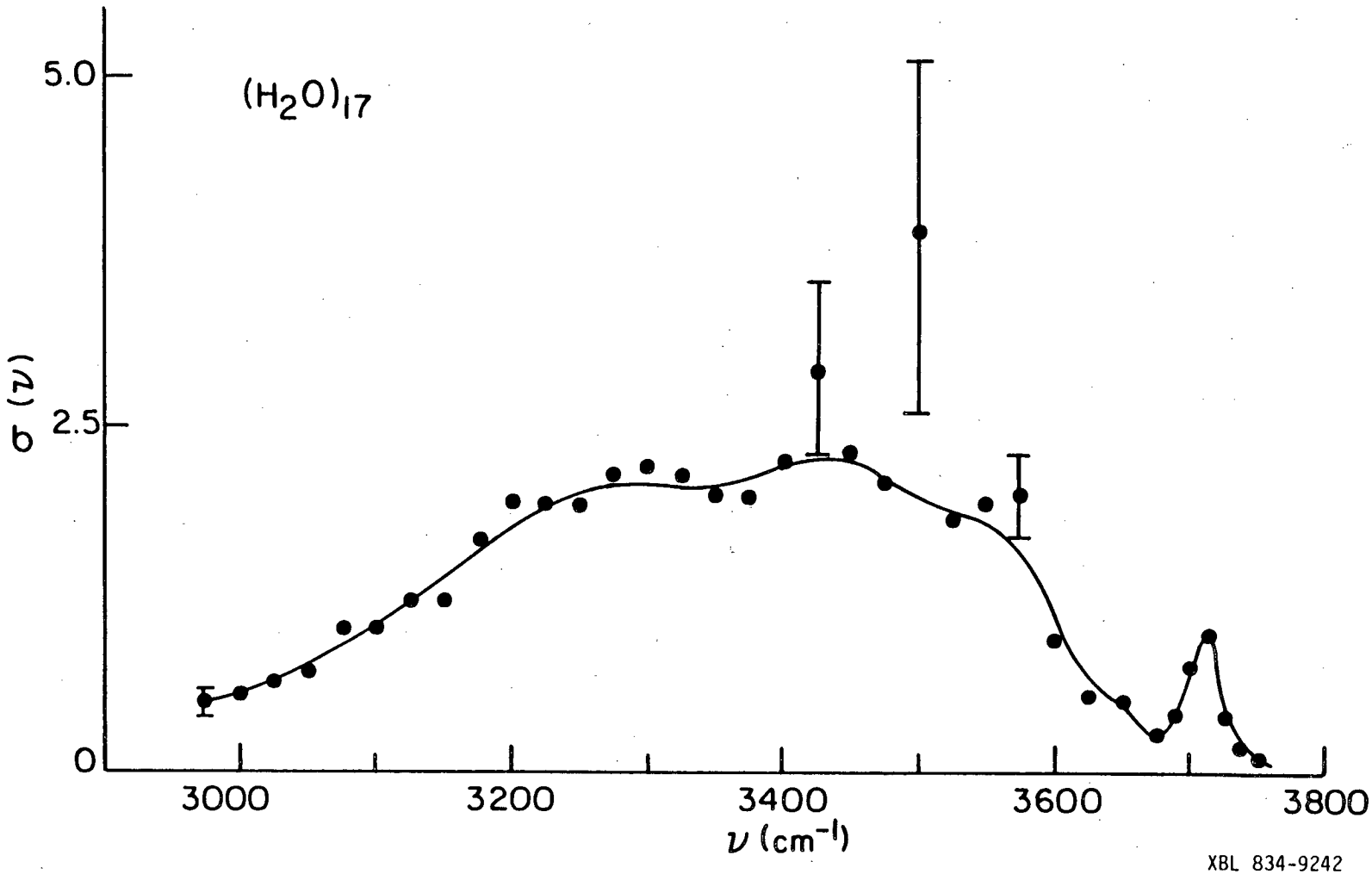
5.0
2.5
0
$(H_2O)_{17}$
$\sigma(\nu)$
3000
3200
3400
3600
3800
ν (cm^{-1})
XBL 834-9242

Fig. 18

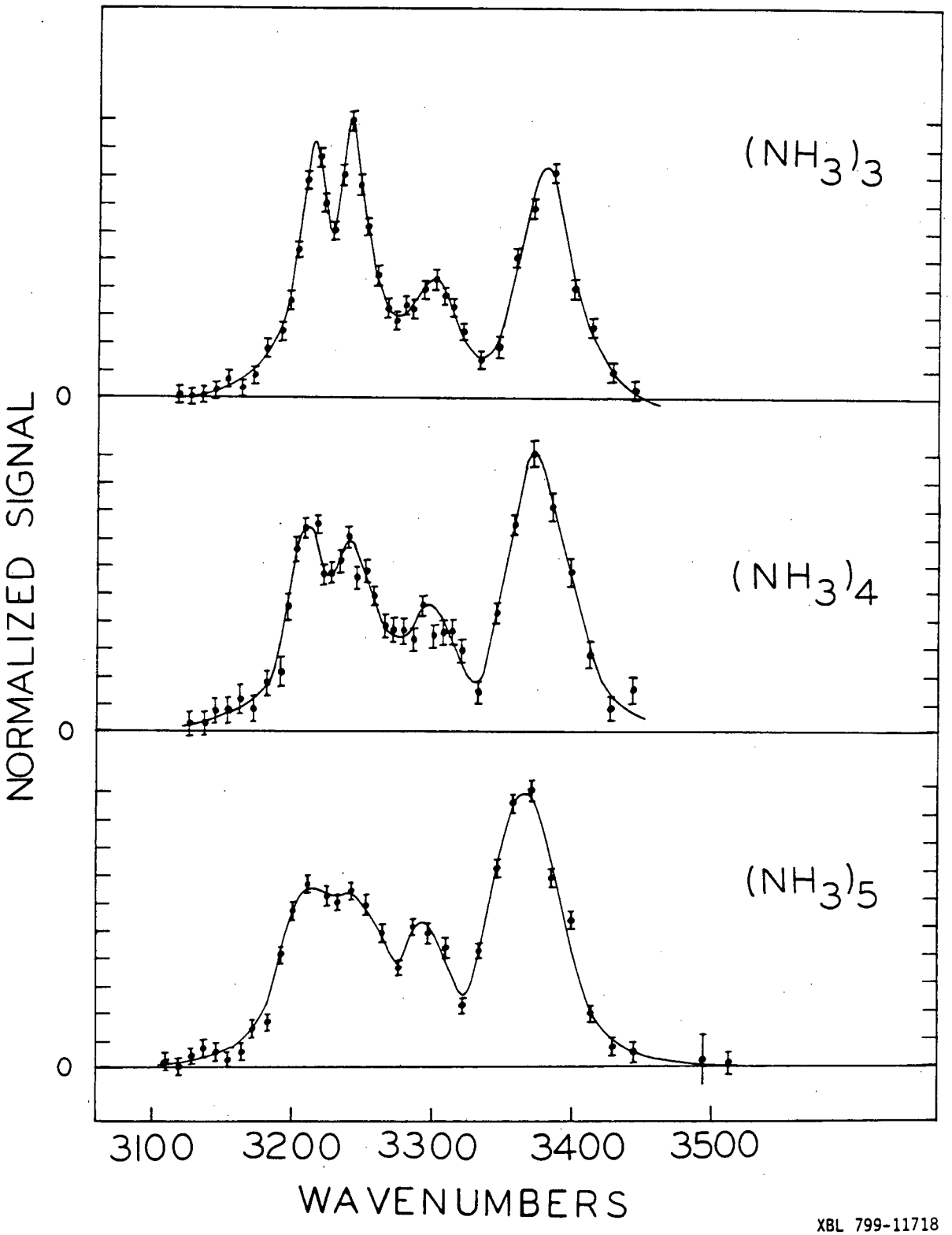

XBL 799-11718

Fig. 19

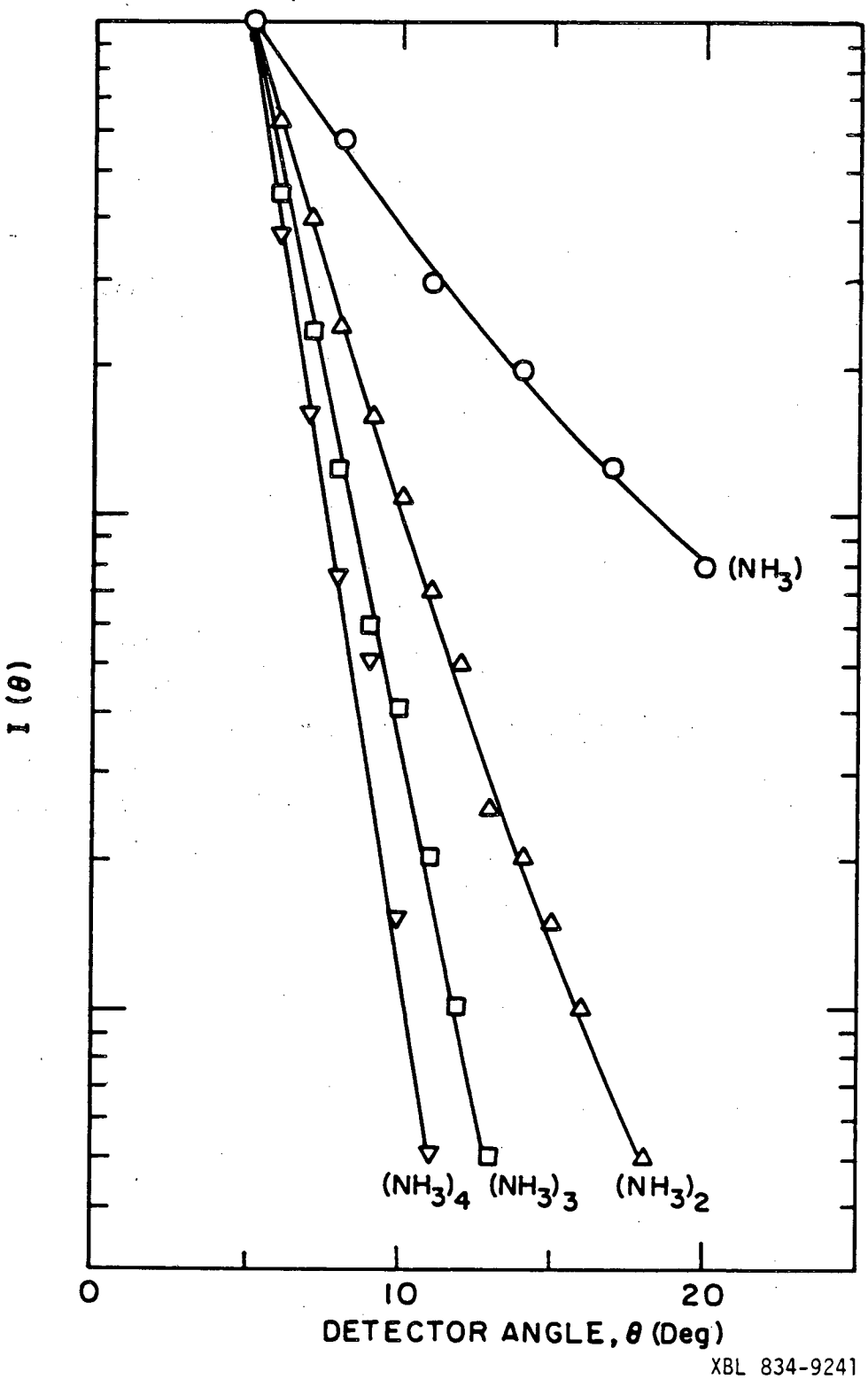

Fig. 20

III. REACTIVE SCATTERING OF $Na(3^2P_{3/2})$ + HCl

A. INTRODUCTION

Since the establishment of the non-relativistic Schrodinger equation in the 1930's, it has been known that the basic principles necessary to explain simple atom-molecule collision phenomena were well-defined. However, the realistic prediction of observations based on these first principles had to await the development of the modern computer, which could solve the large set of equations governing even a simple three body quantum mechanical system. Now that realistic, theoretical treatment of the interparticle forces and dynamics is computationally possible, current interest in the field of reaction dynamics is focused on detailed quantitative comparisons of theory with experiment.[1] The primary goals are to understand how the forces between particles affect the outcome of a collision, and how, through a judicious choice of initial conditions, the chemist can exert control over a collision to produce some desired product.

Although exact quantum treatments are possible for simple collisions (within the Born-Oppenheimer approximation) involving three structureless particles, governed by a single potential energy surface, and with a sparse internal energy level structure,[2] (i.e., $H + H_2 \longrightarrow H + H_2$), it is clear that such numerical approaches are not of general utility. First, the insight gained from this black box treatment is difficult to generalize. Each reaction appears unique, dominated by its individual parameters. Second, projected computer advancement will not enable substantial progress in the complexity of

the problems approached by ab initio methods much beyond the current level of treatment, i.e., three atom systems. Although the successful ab initio treatment of the forces and dynamics of a collision is important, and will continue to be an active area of study, simplifications of exact treatments through all manners of approximation are equally important. Through cleverly chosen approximations, one hopes to understand the particular details of a reaction as well as the general rules they suggest for other reactions of that type.

The work of Polanyi is an outstanding example of this approach. Using generalized mass combinations and potentials, the classical trajectory method was used to derive product energy distributions and rules which govern the energy disposal of reactant translational, vibrational, or rotational energy. These models have been applied to halogen atom reactions forming hydrogen halides[3] as well as many alkali reactions.[4]

The current experimental work was undertaken hoping to stimulate theoretical work on simple three atom reactions where one of the reactants is in an excited electronic state. Previous molecular beam work in this area has been confined mostly to metastable states of the rare gases[5] or oxygen atoms.[6] Notable exceptions are the work of Zare and coworkers on $Ca(^1P)$[7-10] and $I_2^*(^3\pi)$[11] reactions, and the work of Hertel, et al. on the nonreactive quenching of $Na(3^2P_{3/2})$.[12-21]

In the present study, a crossed beams, reactive scattering apparatus has been modified to enable scattering studies of $Na(3^2P_{3/2})$ atoms. The crossed molecular beams method is a powerful experimental technique

to probe reactions dynamics. Coupled with the selectivity of laser excitation of the reactant atoms, a new class of reactions involving short-lived excited states can now be studied by the crossed beams method.

The structure of this chapter is as follows. First, a short review of pertinent scattering work on excited electronic states created by laser optical pumping is reviewed in order to understand what quantities and features of a reaction can be measured, and to develop the framework within which such features are related to the physics of the scattering process. Second, the experimental method used here to study the $Na(3^2P_{3/2}) + HCl \longrightarrow NaCl\ (^1\Sigma+) + H(^2S)$ reaction is described. Next, experimental data for the $Na^* + HCl$ reaction (an asterisk is used to denote the $^2P_{3/2}$ state) are presented at collision energies of 5.38 and 19.4 kc/m. The data at the lower collision energy are analyzed to obtain the center-of-mass product energy and recoil angle distribution. These derived distributions are subsequently discussed to understand the features of the potential energy surface which might be responsible for the observations, as well as the role of angular momentum conservation in the reaction dynamics. A final section summarizes what we have learned from this study, and the questions raised by it.

B. HISTORICAL REVIEW OF SCATTERING STUDIES OF SHORT LIVED ATOMIC EXCITED STATES

The Hertel group has published three extensive works on the quenching of $Na(3^2P_{3/2})$ by H_2,[16,17] CO,[15] and N_2.[12-14] We now briefly

review the main conclusions of these studies which will form the basis for discussion of the "pre-reaction" interaction between $Na(3^2P_{3/2})$ + HCl . For each reaction, extensive quantum mechanical structure calculations were included of the relevant potential energy surfaces, and the scattering dynamics were explained in terms of the calculated potential energy surface features.

1. $\underline{Na^* + H_2}$

From the electronic potential energy surface calculations, the A^2B_2 Na^* - H_2 excited state surface was found to be energetically lowest, favoring a C_{2v} configuration. The location of the crossing seam with the ground state surface occurs at a Na - H_2 distance of R = 2.42Å with an H_2 bond length of r = 1.15Å. The H_2 (or D_2) bond is elongated at the crossing point and corresponds approximately to that of free $H_2(v = 2)$ and $D_2(v = 3)$. The observed vibrational $H_2(D_2)$ distributions peak at these values, with a Poisson-like distribution. The fact that the H_2 and D_2 energy transfer spectra are similar means that no special resonance effects are occurring. A projection of the H_2 (D_2) bond length at the crossing seam onto the ground state surface $H_2(D_2)$ vibrational basis set is sufficient to explain the observed features. The potential energy surface calculations indicate that the ground state surface is strongly repulsive in the R coordinate at the crossing seam. As the H_2 bond begins to contract after quenching, the Na atom and H_2 molecule rapidly separate. The calculated ground state surface shows negligible R-r coupling. Consequently, the asymptotic H_2 vibrational state distribution is taken to be that formed

at the crossing seam, with negligible H_2 vibrational state interaction as the products separate.

The magnitude of the experimental quenching cross section is large. The A^2B_2 state has a significant attractive well in the quantum calculations. The absorbing sphere model, using the calculated potential parameters, predicts a capture radius,or maximum impact parameter leading to quenching, of 3.91Å. This is less than the orbiting impact parameter calculated from the attractive well parameters of the excited state potential energy surface. Therefore, orbiting will not affect this result.

The calculated surface is also consistent with the 5 kc/m ($\Delta j = 5$) rotational excitation of H_2 experimentally estimated from the breadth of the final vibrational state distributions. The strong preference for the C_{2v} geometry (the potential surface increases rapidly as the sodium-H_2 angle deviates from 90°) means that the Na^*-H_2 complex will stay locked in a C_{2v} geometry as the reactants approach. Depending on the initial impact parameter, the known location of the quenching seam can be used to calculate the Na^*-H_2 collision complex rotational frequency at the quenching configuration. Since the products recede rapidly from each other, and the departing Na atom exerts little torque on the H_2 molecule, the H_2 rotational energy is given by that at the critical configuration.

2. <u>Na^* + CO</u>

The potential energy surfaces (PES) for Na(3P) + CO favor <u>linear</u> quenching configurations. When Na^* approaches the carbon end,

electron density plots indicate 30-60 percent of the Na(3P) electron is transferred to CO. Of the two excited state PESs at the linear configuration, the A state is bound by 24.4 kc/m, while the B state is repulsive. As observed for H_2, the ground state surface at the crossing seam is highly repulsive in R with little R-r coupling. To first approximation, the asymptotic vibrational distributions are taken to be those created by the "Franck-Condon" transfer to the ground state surface at the crossing seam. If Na^* approaches the oxygen end, the attraction is not as great, and a larger CO bond extension with a smaller Na*-CO distance is needed to reach the crossing seam.

The experimental results show very large rotational excitation which is explained by the calculated potential energy surface features as follows. If Na^* is quenched at the carbon end, the ground state surface prefers the Na-OC configuration by over 24 kc/m. There being no barrier in the calculated ground state surface for achieving this rotated configuration, a large torque is felt by the CO, resulting in substantial rotational excitation.

The presence of two active, distinct quenching sites leads to different internal energy distributions. Quenching at the oxygen produces larger CO vibrational excitation, while the carbon atom causes significant CO rotational excitation.

3. $\underline{Na^* + N_2}$

This system has been studied at the highest level of resolution. From the experimental energy and angular distributions, forward scattering has significant rotational excitation ($\Delta j>60$), while vibrational

excitation dominates the backward scattering angles. The final N_2 vibrational distribution is similar to the H_2 results, and the general quenching mechanism is presupposed to be analogous. As the Na^* approaches N_2, the sodium 3P electron is partially transferred to an anti-bonding orbital of N_2. Since N_2^- has a longer equilibrium bond length, the N_2 molecule stretches. At the crossing seam between the ground and excited states, the asymptotic N_2 vibrational distribution is obtained by projecting the stretched N_2 bond length onto the free N_2 molecular vibrational wavefunctions. Again, the C_{2v} configuration is favored, with the absorbing sphere model predicting the large quenching cross sections observed.

For this system, the effect of the Na(3P) orbital alignment and orientation on the scattering was measured. When polarized radiation is used to excite the Na atoms, the m sublevels are not equally repopulated do to the different Clebsh-Gordon coefficients coupling the ground state m sublevels by spontaneous decay. Laser excitation for many spontaneous decay cycles redistributes the Na atoms among the m sublevels. As a result, after many spontaneous decays, an anisotropic distribution of the three degenerate 3P orbitals is created. The ratio of the populations of the P orbitals is, at best, 2.5:1:1. The hyperfine structure determines this anisotropy ratio. By directing the k vector of the laser to intersect the collision volume either perpendicular or parallel to the scattering plane, and by rotating the laser polarization vector or circularly polarizing the light, the initial distribution of P orbitals can be selected.

In Fig. 1, the major laser beam, scattering plane configurations are shown. On the left are two different alignments of the linearly polarized electric field vector relative to the scattering plane, when the k vector of the laser is in the scattering plane. When the E-vector is perpendicular to the scattering plane, the $|p\pi^-\rangle$ orbital is favored, having negative reflection symmetry relative to the collision plane. When the E vector is rotated into the scattering plane, a mixture of $|p\pi^+\rangle$ and $|p\sigma\rangle$ states is made, depending on the angle the E vector makes with the relative velocity vector. When the laser propagates perpendicularly to the collision plane, and the linear polarization rotated, the asymptotic distribution can be predominately $|p\sigma\rangle$ if the E vector is parallel to the relative velocity vector, or $|p\pi^+\rangle$ if it is perpendicular. Since the P orbital axis is in the scattering plane, these states have positive reflection symmetry. If the laser is circularly polarized and directed perpendicular to the scattering plane, then the electronic angular momentum of the P orbital is also perpendicular to the scattering plane.

The polarization study of $Na^* + N_2$ consisted in measuring the effect on the scattering signal of the different initial Na $|p\pi^+\rangle$, $|p\pi^-\rangle$, and $|p\sigma\rangle$ distributions. Hertel and Hermann[21] have shown in a detailed way how these polarization dependencies relate to the density matrix representing the collision process. Experimentally, the polarization of the Na resonance fluorescence determines the actual moments of the Na charge distributions created by the optical pumping. Using these parameters, which characterize the initial distribution of P

orbitals, at each detector scattering angle four additional numbers are determined from ratios of the scattering intensity. These are: (a) the difference in the scattering signal with left and right handed circularly polarized light, normalized to their sum, (b) the ratio of the minimum to maximum scattering intensity when the E vector is linear polarized and rotated in the scattering plane, (c) the angle between the relative velocity vector and the laser polarization axis which maximizes the scattering for part (b) above, and finally, (d) the ratio of the scattering intensity with the P orbital perpendicular to the scattering plane to the P orbital axis in the scattering plane, scaled to the value of the scattered intensity of part (b) for the same in-plane polarization angle.

From these four ratios, the complete Na atom density matrix is known, as a function of scattering angle. Physically, these quantities are interpreted and understood by considering the time-inverse quenching process, $Na(3S) + N_2(v') \longrightarrow Na(3P) + N_2(v=0)$. Here, a collision produces an excited Na atom, and the polarization of the fluorescence emitted at a certain angle reflects the different $|p\pi^+\rangle$, $|p\pi^-\rangle$, and $|p\sigma\rangle$ contributions to the Na atom wavefunction for scattering to that angle. By rotating to a basis which has the Z axis along the laser k vector, and the X axis along the polarization angle producing maximum scattering for linearly polarized light with the polarization vector in the scattering plane, the resulting diagonal density matrix elements are then the length, width, and height of the Na(3P) charge cloud formed in the inverse quenching process at that Na scattering

angle. Alternatively, the height also measures the relative differential cross section for changing the molecular reflection symmetry, while the sum of the width and length gives the relative differential cross section for preserving the molecular symmetry. Of course, the overall symmetry of the total collision is preserved. As a result, these two processes are incoherent. The measurements show that the molecular symmetry changing cross section is a minimum at the peak of the energy transfer. This is interpreted to result from the locking of the Na^* to the body fixed Na^*-N_2 frame. At a distance of ~5.3Å, where the body fixed frame is established (see below), the $Na^* - N_2$ complex will have the Na^* symmetry prepared by the optical pumping, i.e. $|p\pi^+\rangle$, $|p\pi^-\rangle$, or $|p\sigma\rangle$. The minimum in the symmetry changing cross section implies that it is difficult to change only the Na^* symmetry, because the tight binding of the $Na^* - N_2$ interaction forces the $Na^* - N_2$ complex symmetry to change as well.

The variation in the laser polarization angle for maximum quenching with scattering angle reflects which state, $|p\pi^+\rangle$ or $|p\sigma\rangle$, is more effective at quenching, as a function of the impact parameter. For a given impact parameter, as the Na^* atom approaches the N_2 molecule, Coriolis coupling will cause continuous $|p\pi^+\rangle \longleftrightarrow |p\sigma\rangle$ transitions. The Na* atomic wave function at a $Na^* - N_2$ separation, R, and impact parameter, b, is composed of both $|p\sigma\rangle$ and $|p\pi^+\rangle$ states in the mixture

$$|\chi\rangle = \cos\alpha\ |p\sigma\rangle + \sin(\alpha)\ |p\pi^+\rangle, \qquad (1)$$

where $\cos\alpha = \frac{b}{R}$. At some distance, R', the potential interactions between Na^* and N_2 will split the asymptotically degenerate $|p\sigma\rangle$ and $|p\pi\rangle$ potential surfaces. At this distance, the Na^* will begin to change from a space fixed to body fixed frame. When the $|p\sigma\rangle$ and $|p\pi\rangle$ potential curves are split by the rotational energy of the P orbital, it is said that the body fixed axis now dominates. For a long range potential of the form $V_{\sigma,\pi} \sim C_n R^{-n}$, this locking or merging distance is

$$R_m = \left(\frac{\Delta C}{\hbar v b}\right)^{1/(n-2)} \tag{2}$$

where $\Delta C = |C_\sigma - C_\pi|$. The angle of maximum quenching shows what direction the P orbital prefers, at the merging distance to the body fixed frame, to maximize quenching. The observations show that this angle is approximately one-half the scattering angle. If the merging distance is approximately independent of the impact parameter, then this observation shows that the P orbital wishes to be tangent to the merging sphere, i.e., $|p\pi\rangle$ states are preferred.

At large Na scattering angles, the polarization asymmetry is small. As large angle scattering corresponds to smaller impact parameters, the locking radius is largest from Eq. (2). Of course, in the limit $b = 0$, the space and body fixed frames are equal. If the Na^* atom spends more time in the mixing region (where the $V_\sigma - V_\pi$ potential separation is comparable to the centrifugal energy of the P orbital), it will have more opportunities to forget its initial, asymptotically prepared

state distribution. An equal mixture of $\tilde{A}$ and $\tilde{A}'$ Na^* - N_2 collision complex states will be formed, reducing the observed anisotropy.

Finally, the measurements of the left-right asymmetry when the laser is circularly polarized and propagating perpendicularly to the scattering plane, gives information on the impact parameter dependence of the transfer of the Z component of the electronic orbital angular momentum into the heavy particle, nuclear motion. Quantum mechanically, $|p\sigma\rangle$ and $|p\pi^+\rangle$ states have the same overall symmetry, and can be coherently excited in a collision. If we again picture the inverse quenching process, the sign of this transfer will depend on the phase difference between the $|p\sigma\rangle$ and $|p\pi\rangle$ amplitudes in the final Na^* atom wavefunction. If the measured angular momentum transfer passes through zero at some Na scattering angle, then the phase difference between the $|p\sigma\rangle$ and $|p\pi^+\rangle$ states is a multiple of 180°, <u>or</u> the average trajectory has switched from predominately repulsive to predominately attractive in nature.

Additionally, if the cross section is larger for the electronic orbital angular momentum (L*) aligned antiparallel to the nuclear orbital angular momentum (L), then in a scattering experiment with the products detected in the scattering plane, we can say that the Na^* atom prefers to pass on the left of the N_2 molecule rather than on the right. If the detector samples a cylindrically symmetric distribution about the relative velocity vector, no circular asymmetry can be observed. The observed circular asymmetry in a crossed beam experiment is a result of detecting only a small, biased subset of the scattering angles.

To summarize the results of Hertel, the product distributions from Na(3P) quenching can be understood from the geometry of the collision complex at the crossing seam with the ground state. Polarization studies provide detailed information on the transformation of the Na(3P) atom from a spaced to body fixed basis, and on the efficiency of angular momentum transfer from the 3P orbital motion to the heavy particle, nuclear motion.

4. $Ca^* + HCl$

Rettner and Zare[7-10] have published the only studies using optical pumping to investigate the effects of alignment on a chemical reaction. They have measured the chemiluminesence for a series of $Ca(^1P) + XCl \longrightarrow CaCl\ (^2\pi,\ ^2\Sigma) + X$ reactions in a beam-gas experiment, and observed the dependence of the branching ratio between the $^2\Sigma$ and $^2\pi$ CaCl electronic states on the angle between the Ca atom velocity vector and the laser polarization vector.

For the $Ca^* + HCl$ reaction, a large reaction cross section was observed. The total fluorescence was independent of the laser polarization, but the dispersed fluorescence indicated that the product state electronic symmetry correlated with the initial atomic symmetry, i.e., $|p\sigma\rangle \longleftrightarrow {}^2\Sigma$, $|p\pi\rangle \longleftrightarrow {}^2\pi$. The independence of the total cross section on the laser polarization was interpreted by invoking an electron transfer harpoon mechanism. Reactions with the large cross sections typical of the observed $Ca^* + HCl$ magnitudes usually favor such ionic intermediates. The probability of the electron jump was concluded to be independent of the orbital alignment. However, the ion core formed by the electron transfer is aligned, and the different molecular states

coupling to the ion core will decide whether a $^2\pi$ or $^2\Sigma$ CaCl state is formed. From the experimental results, the Ca^+ orbital symmetry is preserved (adiabatic behavior), correlating to the Ca^+Cl^- molecular state with the most similar Ca^+ character.

For the reaction $Ca^* + Cl_2$, the total fluorescence cross section was dependent on the $Ca(^1P)$ orbital alignment. The added symmetry of Cl_2 vs. HCl causes some of the $Ca-Cl_2$ molecular states to not correlate with fluorescent product states. By varying the polarization, the Ca atoms can be preferentially directed on or off these dark potential surfaces.

With this historical background, we have modified a scattering apparatus to study reactive collisions of $Na(3^2P_{3/2})$ following the basic design configuration of Hertel, et al.[12-21] The major difference between the two apparati is the scattered product detector. Hertel and coworkers use a hot wire filament, sensitive to alkali atoms, while in this case, an electron bombardment ionization universal mass spectrometer is used. The added flexibility of detecting product at any mass comes with approximately a 10^5 loss in detection efficiency compared to the hot wire filament. HCl was chosen as a scattering partner for the initial reaction because the detector background at m/e = 58 is low, and the reaction is 4.68 kc/m endothermic in the ground state. The endothermicity enables a test of the experimental procedure with different amounts of competing ground state reaction by simply changing the collision energy. In addition, the kinematics of the reaction restricts all the product to observable

detector angles. The alkali-hydrogen halide family of reactions has been extensively studied by the molecular beam technique, including the efficiency of vibration, rotation and translation for promoting reaction.[22,23,24] Some ab initio[25] and semiempirical[26] potential energy surfaces are available and several classical trajectory studies[27] of reactions on these surfaces have been reported. Related theoretical studies of the H + HL mass combination have been published.[28,29]

Finally, Polanyi[3,30] has reported measurements of the relative reaction cross sections for the Na + HCl (v,j) reaction for v = 1 - 4, j = 5 - 15. The vibrational enhancement indicated gas kinetic reaction cross sections. The rotational dependence, with a minimum at j = 10, was rationalized in terms of the preferred HCl - Na orientations for reaction. Barker and Weston[31] studied the translational energy dependence of the quenching of Na(3P) atoms by a number of reactive and nonreactive molecules. The absorbing sphere model for the total cross section was consistent with their results.

C. EXPERIMENTAL ARRANGEMENT

In this section, modifications to an already existing crossed molecular beams apparatus which enable scattering studies of $Na(3^2P_{3/2})$ atoms are described. Characteristics of the basic apparatus are given elsewhere.[24] Briefly, two sonic beams are crossed at right angles (beam overlap volume $\sim 10^{-3}$ cm^3) in a liquid nitrogen cooled chamber, under single collision conditions. The collision chamber ambient background pressure is 1×10^{-7} torr. Scattered product is detected with a rotatable mass spectrometer which rotates in the plane defined

by the two reactant beams. The mass spectrometer detector consists of an electron bombardment ionizer, quadrupole mass filter, and a Daly ion counter, enclosed in a triply differentially pumped, ultra-high vacuum chamber. The experimental improvements described below include the development of a stable, seeded, Na atom source and the ability to excite a sizeable fraction of the Na atoms in the collision volume to the $3^2P_{3/2}$ excited state by the method of optical pumping. In addition, the experiment can measure moments of the $Na(3^2P_{3/2})$ charge distribution created by the polarized, exciting laser radiation, and the dependence of the observed scattering on these moments.

1. Sodium Beam

The sodium atom beam is produced by a two chamber stainless steel oven shown in Fig. 2. The main section, of volume 150cc, is the reservoir for the molten sodium metal. It is heated by .090 inch diameter thermal coax heating cable (SEMCO, Inc.) brazed into contact with the oven body. The braze melting point is 1050°C. At the top of the reservoir is a stainless steel gas inlet tube affixed onto a mini-conflat flange and sealed by a .005 inch thick nickel gasket. The gas inlet tube is radiatively heated by a .080 inch wide, 24 inch long tungsten ribbon. The gas inlet tube serves two functions. First, the sodium metal is easily loaded into the reservoir through the mini-conflat flange opening. Second, rare gases, introduced through the inlet tube, enable the velocity of the sodium atoms to be varied over the range 1. - 3. x 10^5 cm/sec at a constant nozzle temperature, here chosen to be 740°C. A plug constriction in the inlet tube increases

the local rare gas flow velocity so sodium vapor will not diffuse upstream and clog the inlet tube where the temperature is cooler. Additionally, the radiation heater is kept 50°-100°C warmer than the reservoir temperature to help impede the sodium from diffusing up the inlet tube. The sodium reservoir is the coldest part of the oven and determines the sodium vapor pressure.

The nozzle chamber consists of a 3.0 inch long, .25 inch diameter stainless steel tube, heated by .060 inch diameter thermal coax heating cable, again brazed into contact with the stainless steel tube. The nozzle aperture is formed by drilling a .003-.005 inch diameter hole in a .020 inch thick stainless steel disk, which in turn is welded onto the stainless steel tube. This additional chamber for the nozzle allows the nozzle to be hotter than the reservoir, thus preventing the formation of sodium polymers.

All connections to the thermal coax heating cable follow the design suggestions of Amperex.[32] Basically, a precision machined ceramic jacket is used to reduce rotational and bending mechanical stresses to the exposed center conductor at the junction to the electrical power leads. The ceramic piece is brazed to the sheathing on one side and the electrical power connector on the other. This arrangement reduces the heat dissipated at the junction to the power leads because good thermal contact is made with the high thermal conductivity of the copper power cable. Up to 150 watts of power can be delivered to the oven with the lengths of cable chosen. This is sufficient to raise the oven temperature above the melting point of

the braze material before the heating cable itself fails. All ovens are surrounded by two radiation shields.

The reservoir and nozzle heater power supplies are actively controlled to stabilize their temperature to within ±2°C of any desired set point. This is necessary to maintain stable intensity and velocity for the sodium beam. For the worst case, He seeding, small changes in the sodium partial pressure changes the average mass of the He/Na mixture, affecting the velocity distribution. With the actively controlled temperatures of both reservoir and nozzle, long term variations in the Na beam's average flow velocity are well within the short time scale velocity spread characterizing the isentropic expansion.

The oven assembly is supported by a water-cooled copper block. It is attached to the nozzle chamber vacuum bulkhead by three screws, which also enable it to be aligned along the beam axis. Except for the skimmer described below, care was taken to remove all obstructions from the nozzle and to maximize gas conductance away from the nozzle-skimmer region. The nozzle tube, with heaters, is approximately 3/8 inch diameter. The nearest support is approximately one inch further away.

The central portion of the Na beam is skimmed by a single piece, heated, stainless steel skimmer. The skimmer aperture is .045 inch diameter and is located .26 - .30 inches from the nozzle. The skimmer is also heated by coax heating cable. A second heated surface is placed to mask the edge where the skimmer fits through the nozzle chamber bulkhead. Without this mask, sodium would condense on the

cooler bulkhead eventually bridging over to the heated skimmer. When this happens, the liquid sodium conducts sufficient heat from the skimmer that it soon becomes clogged by the incident flux of sodium from the nozzle.

The final size of the sodium beam was determined by a rectangular aperture made from razor blades located in the second differential pumping region. The heat radiated from the skimmer is sufficient to keep the defining slit from clogging by the small amount of sodium incident upon it.

Balzers 71 diffusion pump fluid was used in the Na source and differential diffusion pumps. Octoil showed some signs of deterioration with time, as well as depositing thin films on the surfaces of these pumping regions. A full charge of DC704 would completely react to form a white, oilish, crystalline precipitate in less than one Na oven charge. Before loading Na metal into the oven, its oxide coating was removed in an inert atmosphere. Care was taken to clean the nozzle and differential chambers of sodium residue between runs. Also, each new charge of sodium, after evacuation of the source chamber, was held at just above the Na melting point (~150°C) for many hours to remove all impurities and vapor trapped in the solid. Ultra high purity rare gases, as well as an all metal, leak tight gas inlet system were found to be necessary to avoid slow clogging of the nozzle.

2. HCl Beam

The HCl beam was formed from a heated tube with an interchangeable nozzle affixed on the end, as shown in Fig. 3. A platinum electron

beam aperture (Ted Pella, Inc.) of 70 micron diameter was used in this study. The nozzle tube slides in a fixture which allows the nozzle-skimmer distance to be changed while the nozzle remains on the beam center-line axis. The nozzle temperature was actively stabilized to 180°C, to prohibit HCl polymer formation. Typically, 350 torr HCl nozzle backing pressure was used. A low pressure regulator, in addition to the standard cylinder regulator, was necessary to stabilize the delivery pressure at these low values. A 150 Hz tuning fork chopper was mounted on a water-cooled copper block attached to the nozzle chamber bulkhead. The cooling block was needed because the heated nozzle, via the alignment fixture, would heat the front of the nozzle chamber sufficient (70°C) to stop the chopper modulation.

The nozzle backing pressure of HCl was optimized at the same time the phase and gate width of the chopper modulation function were measured. The latter were measured by time resolving the signal at the mass spectrometer and displaying several chopping cycles. The gate width was set to the minimum of the chopper open or closed time interval. The phase and pressures were set by optimizing the contrast between the channels with the chopper open and closed.

3. Optical Preparation of $Na(3^2P_{3/2})$

The creation of a large, stationary fraction of $Na(3^2P_{3/2})$ atoms by optical pumping has been exhaustively and elegantly studied by Hertel and coworkers.[18-21] Their experimental technique has been adopted here. Briefly, the selection rules on ΔF, the change in total angular momentum, insure that all atoms excited from $^2S_{1/2}(F=2) \longrightarrow {}^2P_{3/2}(F=3)$ will form an isolated, two level system. The

level structure appropriate to the 3S → 3P transition is shown in Fig. 4. Spontaneous decay from the $^2P_{3/2}$(F=3) level can only repopulate the $^2S_{1/2}$(F=2) level of the ground state. Assuming all ground state levels are equally populated before the atoms enter the laser beam, at most 31.25 percent of the Na beam can be in the $^2P_{3/2}$ state.

Several details are pertinent to achieving this 3P excitation efficiency. Power broadening must be less than 60 MHz, the separation of the $^2P_{3/2}$(F=2,3) hyperfine levels. If this condition is not met, and the $^2P_{3/2}$(F=2) level is excited, it can spontaneously decay to the $^2S_{1/2}$(F=1) ground state HPF level and be lost from further optical pumping cycles. As the power broadening follows the laser profile, it is important to expand the laser beam so that the central portion is not power broadened beyond 60 MHz. Secondly, the sodium beam angular divergence along the laser beam propogation direction produces an associated transverse doppler shift. If this doppler shift is larger than 60 MHz, then some fraction of the sodium beam will be shifted off the $^2P_{3/2}$(F=3) resonance. For Na seeded in He, this limits the angular divergence to 1°.

At the time this experimental work was performed, it was thought that the published work by Hertel, et al. on the optical pumping of Na had definitely established that 30 percent of the Na atoms are excited to the $3^2P_{3/2}$ state. Recently, unpublished work[34] has appeared by this group suggesting that perhaps only 15-20 percent excitation is achieved. The reason for this is thought to be the weak coupling to the $3^2P_{3/2}$(F=2) hpf level, which removes atoms from the desired

isolated, two level system. Empirically, in the work by Schmidt and coworkers[12] on the scattering of $Na^+ + Na(3S) \rightarrow Na^+ + Na(3P)$ a 12 percent reduction in the inelastic $Na^+ + Na(3S) \rightarrow Na^+ + Na(3P)$ transition was observed when the sodium beam was optically pumped. Unfortunately, in the Na + HCl scattering experiments, there is no feature in the angular or velocity distributions which can be assigned only to ground state Na(3S) scattering. If such a feature can be found, the depletion of it by exciting Na atoms to the excited state would measure the effective Na fraction optically pumped to the $3^2P_{3/2}$ state. Consequently, in the analysis below, both cases of 15 percent (empirical) and 30 percent (theoretical) excitation efficiency are analyzed. Where the differences are important, they will be noted.

A combination of commercial camera lenses is used to image the sodium fluorescence onto a phototube (RCA IP28). The lenses magnify the fluorescence region tenfold, and in conjunction with a moveable iris aperture, located at an intermediate focal plane, spatially selected regions of the fluorescence can be measured. In this way, any spatial dependence of the fluorescence intensity can be observed, as well as the average polarization characteristics of the fluorescence determined for the entire collision volume.

The signal from the camera phototube, after current amplification (Kiethly Model 427) drives a lock-in stabilizer (Lansing 80-214) which corrects for short term (~1 sec) frequency drifts. The necessary reduction of the transverse doppler width noted above causes a 50 percent pumping loss if the laser frequency drifts 20 MHz off line center.

The manufacturer's specifications for the dye laser's drift rate is less than 100 MHz/hour. However, the experimental environment of the molecular beam laboratory is not suited to meet these requirements. Luckily, only a small feedback is needed to correct for these slow drifts.

The commercial lock-in stabilizer produces a DC correction voltage and AC (510 Hz) modulation reference frequency. These are appropriately scaled and summed, then input to the external voltage controlled frequency drive of the CR-599-21 dye laser scan electronics. In this manner, the Fabrey-Perot cavity of the 599-21 is dithered at 510 Hz with ~5 MHz amplitude. The intracavity feedback elements of the dye laser assured the laser frequency exactly tracks this reference cavity. The DC correction voltage (when the lock-in phase is properly set) applied to the reference cavity then maximizes the fluorescence. When properly aligned, the laser stability is sufficient for greater than 24 hour continuous operation.

As will be discussed in detail below, the polarization properties of the laser can be utilized to create oriented or aligned Na(3P) charge distributions. To perform alignment and orientation experiments, all windows and mirrors are anti-reflection coated for 5890Å with measured ellipticities of less than 1/2 percent. This insures that the polarization properties of the laser are preserved at the scattering center. Care was taken to remove oil from windows and mirrors in the vacuum chamber. The final 45° beam stirring mirror, located at the base of the scattering chamber, is heated to 100°C to

prevent oil accumulation. The aligned or oriented 3P orbital can be affected by stray magnetic fields or radiation trapping. Hertel[18] has shown that as long as the magnetic fields are smaller than 1 gauss and the Na atom density $<10^{11}/cm^3$, such effects are negligible. The magnetic field was measured and found to be less than 1 gauss. As long as the sodium partial pressure is kept below 10 torr for the 3 inch nozzle-collision volume distance, radiation trapping will be negligible. The actual charge alignment is measured concurrently with the polarization studies by recording the polarization of the fluorescence using the fluorescence monitor.

4. Angular Distribution Measurement Procedure

The laser beam can be directed to the scattering volume from three directions. A 45° crossing relative to the Na beam is used to measure the velocity of the Na atoms by the doppler shift method. Apertures on the entrance flanges to the collision chamber and internal photodiodes allow the laser beam to be positioned within 1 mm of its optimum position without breaking vacuum. After laser induced signal at the mass spectrometer is seen, fine tuning of the laser position to maximize the contrast of the mass spectrometer signal with and without the laser is done. The fluorescence monitor is then positioned to image the central region of the fluorescence onto the phototube for maximum phototube signal.

Most of the data acquisition is computer controlled. Five basic quantities are measured in an angular scan; the laser fluorescence (LF), the mass spectrometer signals with the laser on and HCl beam on

(L_+X_+), the laser off and HCl beam on (L_-X_+), the laser on and HCl beam off (L_+X_-), and the laser off and HCl beam off (L_-X_-). With the laser off, the difference

$$(L_-X_+) - (L_-X_-) \propto \frac{d\sigma}{d\Omega}(3^2S_{1/2}) \tag{3}$$

is proportional to the 3S ground state scattering. When the laser is on and if the optical pumping is saturated, the signal has contributions of 31.25 percent from $3^2P_{3/2}$ scattering and 68.75 percent from $3^2S_{1/2}$ scattering. The following combination of the four mass spectrometer signals is proportional to the $3^2P_{3/2}$ differential cross section

$$\frac{d\sigma}{d\Omega}(3^2P_{3/2}) \propto (L_+X_+ - L_+X_-) - .6875 * (L_-X_+ - L_-X_-) \tag{4}$$

The HCl beam is 100 percent amplitude modulated by the 150 Hz tuning fork chopper mounted in the HCl beam differential chamber. The laser beam is 100 percent amplitude modulated at 6 Hz by a stepping motor controlled beam stop. For 24 tuning fork chopper cycles, the signals are accumulated with the laser on. On the 25th chopper cycle, no signal is obtained to allow time for the laser beam flag to block the laser beam. Then, 24 chopper cycles with the laser blocked are accumulated. On the 25th cycle, no signal is obtained while the laser beam flag unblocks the laser. The above process is then repeated for a preset number of times determined by the user. In this way, once

the phase and gate width of the tuning fork modulation are known, the gating is automatically accomplished without significant loss of duty cycle or computer intervention.

When the laser is blocked, the fluorescence signal is lost. To stop the lock-in from wandering, a 1/6 sec blanking pulse is sent to the error loop of the lock-in. This freezes the lock-in at the frequency present when the blanking pulse arrived for the duration of time the laser is blocked. Feedback then resumes with fluorescence signal at the lock-in input.

The computer accumulates data at each angle for a preset time. When completed, the five signal channels are read, the contents displayed and written to disk. The fluorescence is checked to insure that it has not varied significantly from the maximum value recorded. If it has changed, the experimenter is informed of this fact. If the laser optics had moved, or laser frequency lock lost, these errors can be corrected at this time and the data point repeated. Approximately every 30 minutes, the computer program directs the user to return to a reference angle where the signals are measured for several of the preset time intervals. When the data file is processed, these periodic reference points are used to scale the laser on and laser off channels seperately by linear interpolation. This accounts for beam intensity drifts, and changes in detector sensitivity. The scale factors for the laser on and off channels should be equal if only the Na number density is varying. For stable scans, these scale factors empirically varied less than ±4 percent. For all data presented, the

error bars for the mean are one standard deviation for the statistical error associated with the finite signal count, or the variance of the mean of the actual measurements, whichever is larger. Typically, four separate angular scans are averaged to obtain approximately 10 percent error in the derived 3P distributions. The total counting time at ecah angle is usually eight minutes.

It is instructive to trace the effect of errors in the five measured angular data signals on the derived Na(3P) scattering cross sections. If we allow each of these signals to have an associated error, and we correct Eq. (4) for the unequal fluxes of Na(3S) and Na(3P) atoms, then the error in the differential cross section corresponding to the hypothetical case of 100 percent optical pumping efficiency is:

$$\Delta \frac{d\sigma^*}{d\Omega} = \frac{\Delta_{on} + (1-P)\Delta_{off}}{P} + \frac{\Delta P}{P^2} \; S_{on} - S_{off} \tag{5}$$

In Eq. (5), Δ_{on} and Δ_{off} are the statistical errors in the signals observed with the laser on (S_{on}) and the laser off (S_{off}). P and ΔP are the true optical pumping efficiency and error in this efficiency, respectively. The first term in Eq. (5) is the error resulting from statistical fluctuation in the mass spectrometer signals, while the second term is the error from the uncertainty or variation in the optical pumping efficiency. By accumulating data for sufficiently long time intervals, the first term can be made small, assuming, of course, that all source and detector conditions are stable. We note

at this stage that if only 15 percent of the sodium atoms are excited, then compared to a typical ground state scattering experiment, the error is ~7 times as large for equal counting times.

The second term in Eq. (5) is proportional to the difference in the laser on - laser off signal. If the laser frequency were to drift, causing a change in pumping efficiency, ΔP, then the variations would be larger at the higher signals. This underscores the need to actively stabilize the laser frequency and operate at saturation to reduce $\Delta P/P \sim .01$, where one can safely assume the second term in Eq.(5) is negligible compared to the statistical data fluctuations.

5. Doppler Shift Measurements of Na Velocity Distributions

At each normalization point, the sodium velocity distribution is measured by monitoring the doppler shifted fluorescence from the 45° laser crossing, and scanning the laser frequency. This can also be performed by the computer. First, a shutter is opened to allow the laser to pass at 45° to the sodium beam. Next, an analog switch changes the computer external frequency drive input from the lock-in amplifier to the computer D/A output. The computer scans the laser, recording the fluorescence intensity and the intensity of the Fabrey-Perot used as a relative frequency standard. The fluorescence intensity has the characteristic patterns shown in Fig. 5. There are four peaks. The two narrow and intense peaks are from the orthogonal Na beam intersection used in the optical pumping. Their separation is the ground state HPF splitting (1.77 GHz) minus a weighted sum of the $3^2P_{3/2}$ HPF structure determined by the fluorescence transition

strengths from the $3^2P_{3/2}$(F=3, 2 and 1) HPF levels. Empirically, this weighting produces a splitting of 1.67-1.70 GHz for the narrow peaks. This separation is consistent with the splitting derived from the fringe spacing (1.5 GHz) of the Fabrey-Perot and with the location of the center-of-mass for the Na + HCl scattering. If only the 1.77 GHz ground state HPF splitting is used, the center of mass shifts 2° towards the Na beam from where it is empirically observed and predicted by the 1.67 GHz spacing.

The two broad, red shifted peaks of Fig. 5 are the doppler shifted analogs of the orthogonal crossing peaks. The separation, in GHz, from the orthogonal crossing and the corresponding 45° crossing transition, Δf, is related to the average flow velocity, v_o, by the equation

$$v_o(\text{cm/sec}) = 83300. * \Delta f(\text{GHz}) \tag{6}$$

The Na beam velocity distribution is found by fitting the observed fluorescence intensity to the functional form

$$I(v)dv = Cve^{-\beta(v-v_o)^2} dv \tag{7}$$

appropriate for the number density velocity distribution. The distribution is weighted by 1/v in the doppler shift measurements, as the faster moving atoms spend less time in the laser beam, and execute less spontaneous radiation cycles.

6. Product Velocity Measurements

Time-of-flight measurements of the product velocity distributions at selected detector angles are obtained by the cross correlation

method. As for the angular data, two velocity distribution measurements are needed at each angle, with and without laser excitation. These are obtained in two different experiments.

Without laser excitation, the scattered products are correlated by a 255 channel pseudo-random sequence encoded onto a spinning disk placed between the reaction volume and mass spectrometer. The basic details of this procedure are given elsewhere.[24] The only major difference here is the use of a digital function module to synchronize the rotation of the disk to the channel advance of the multi-channel scaler (MCS). The digital function module contains 14 bit phase resolution for sin and cosine analog wavefunctions. The channel advance is used to generate the sin and cosine phases. These two analog signals are amplified and used to drive an asynchronous motor (Globe 75A 1003-2). Because every 1/255 of an MCS cycle the phase of the wheel is advanced, the synchronization is nearly exact for the applied restoring force to the motor.

With laser excitation, the laser beam itself is correlated. In this way, the full flight path from the collision zone to the detector of 20 cm is utilized. When the correlation wheel is placed between the detector and the mass spectrometer, as done without laser excitation, the flight distance is only 17 cm. Additionally, the entire signal from the interaction volume is modulated by the laser without the need to reduce the entrance aperture to the detector to match the smallest slit in the pseudo-random sequence. Normally, when the scattered product is modulated, this is done to achieve higher resolution. Using lenses to focus the laser light on the rotating disk, the

resolution is limited only by the slit size variation of the pseudo-random sequence and the uncertainty in the point where the product is ionized in the mass spectrometer. By cross correlating the fluorescence, the modulation function is directly obtained including the variation in slit size and wheel rotation synchronization. In the TOF data analysis, the correlation matrix generated by this measured modulation sequence can be inverted and used to decorrelate to the TOF data as outlined by Comsa, et al.[33]

When correlating the laser, the 3P Na population is modulated by the pseudo-random sequence. For every Na atom excited, one is removed from the ground state. Hence, equal densities of 3S and 3P sodium atoms are modulated by the laser correlation. In general, the 3P atoms contribute a positive signal, while 3S atoms contribute a negative signal by the laser modulation.

The different reactivity of the two types of atoms determine the TOF pattern observed. The excited state reactivity, compared to the ground state reactivity, is derived from the angular data for 31 percent excitation efficiency by the equation

$$R(\theta) = \frac{d\sigma^*/d\Omega(\theta)}{d\sigma/d\Omega(\theta)} = \frac{(L_+X_+ - L_+X_-) - .69\ (L_-X_+ - L_-X_-)}{.31\ (L_-X_+ - L_-X_-)} \tag{8}$$

If X(t) and Y(t) are the observed TOF spectra with and without the laser at the angle θ, normalized to equal areas (i.e. same total signal counts corrected for background), then these signals are related to P(t) and S(t), the 3P and 3S TOF distributions by

$$X(t) = a\,P(t) - b\,S(t)$$
$$Y(t) = S(t) \tag{9}$$

Integrating the total signals in X and Y, using Eq. (6) and assuming that X and Y are normalized for unit areas, then

$$a = \frac{R}{R-1}\ ,\ b = \frac{1}{R-1} \quad . \tag{10}$$

If R = 1, then the normalization condition in Eq. (10) is undefined.

In performing TOF measurements, overlap of the laser and molecular beam volumes is not as critical as in the angular measurements. For the angular measurements, one must know the actual percentage of Na atoms excited. For TOF measurements, the laser correlated 3S and 3P densities are always equal. Finally, the 3P TOF distribution is given by

$$P(t) = \frac{(R-1)}{R}\,X(t) + \frac{1}{R}\,Y(t) \tag{11}$$

For the long term operation necessary for obtaining good signal to noise ratios, a second lock-in scheme for the laser stabilization was needed for the TOF measurements. The 510 Hz reference frequency of the lock-in stabilizer with blanking, used for angular measurements, is in the same frequency range as the laser modulation by the correlation sequence. A second lock-in, operating at 100 Hz, dithered the laser frequency well below the range of the correlation sequence, and

made the TOF measurements easy to perform for many continuous hours. To improve the TOF signals at different collision energies, the sodium beam divergence determined by the defining slits can be adjusted to match the transverse doppler shift.

7. Variation of Total Cross Section with Collision Energy

For fixed collision energy, measurements of the angular and time-of-flight product distributions enable the determination of a center-of-mass frame product flux distribution. A fitted functional form to the product energy and angular distribution in the center-of-mass frame can be integrated to give an estimate of the total cross section for product formation at this energy. However, because absolute reactant densities and detection efficiency are unknown, this estimate is poor.

One method for obtaining total cross sections uses the nonreactive sodium scattering at several collision energies to fit a spherical long range potential that matches the small angle scattering.[24] The depletion of the large angle, nonreactive scattering from that predicted by the spherical potential can be used to estimate a maximum impact parameter for reaction. When extensive product ion fragmentation occurs, this method is difficult to apply unless the elastic contribution can be differentiated in the time-of-flight distributions.

A second method[24] is based on estimating the relative detection efficiency of Na/NaCl, then using the fitted spherical potential to give the absolute scale. Besides the errors introduced by the spherical potential approximation to the nonreactive scattering, the

estimation of ionization efficiencies and fragmentation patterns usually introduce absolute errors of 100 percent.

To further improve this latter method, the fluorescence signal can be used to very accurately compare cross sections at different collision energies. With different seed gases, the sodium density and speed are different for each collision energy. By measuring the fluorescence (LF), velocity distributions, and the mass spectrometer signals with fixed detector sensitivity and fluorescence photomultiplier gain, an accurate, relative sodium density for each collision energy can be derived. The relative scale factor, β, for data obtained at different collision energies is simply then

$$\frac{n(Na)\ g}{n'(Na)\ g'} = \beta \tag{12}$$

where $g = |V_{Na} - V_{HCl}|$ is the relative speed of the reactants and n(Na) is the relative sodium density. The primes in Eq.(12) refer to parameters at a different collision energy. The sodium density is proportional to the fluorescence signal <u>and</u> the velocity. (The saturated fluorescence signal is proportional to the time the sodium atoms spend in the laser beam, $1/V_{Na}$, and the number density of atoms with that velocity.) Hence, Eq. (12) can be written

$$\frac{LF*V_{Na}*g}{LF'*V'_{Na}*g'} = \beta \quad . \tag{13}$$

For the He/Ne seeding cases of the data shown below, the relative scale factor is $\beta = 8.7$, favoring He. Using these accurate relative scale factors, the shape of the total cross section can be established, although an absolute scale must still be provided by comparison with the nonreactive scattering. The advantages now are that all data can be used simultaneously in determining a single detection efficiency, because the relative scale factors are known quite well. Finally, the shape of the total cross section with collision energy is very important when fitting the angle-velocity data and allowing for a distribution of reactant velocities. If the collision cross section changes quickly with energy (for example, near threshold) the weighting of the different velocity groups can have a pronounced effect on the derived product energy and angle distributions.

D. EXPERIMENTAL RESULTS

The Na atom velocity distributions were derived from the doppler shifted fluorescence measurements shown in Fig. 5. The HCl velocity distribution was taken from the previous work of Becker, et al.[24] by scaling their measured flow velocity to be consistent with the 180°C nozzle temperature of this experiment. The value obtained, 8.45×10^4 cm/sec, is consistent with 99 percent relaxation of the HCl rotations in the adiabatic expansion. Unrelaxed, the HCl flow velocity would be 7.23×10^4 cm/sec. An independent check of the accuracy of the reactant beam flow velocities is provided by the sodium ground electronic state reactive NaCl angular distribution measured at the 5.38 kc/m collision energy. At this collision energy, only 0.7

kc/m is available for product translation. The maximum NaCl center-of-mass recoil velocity is then 4×10^3 cm/sec. Consequently, the observed laboratory angular distribution shown in Fig. 6 reflects only the distribution of center-of-mass angles from the velocity dispersion of the reactant beams. The maximum of the NaCl angular distribution located at 40° in the laboratory frame is correctly predicted by these beam velocities. A product flux distribution which is independent of both the recoil angle and energy reproduces the observed angular variation as shown in Fig. 7.

The Newton diagrams corresponding to the two collision energies for which data will be presented are shown in Fig. 8. The full widths at half-maximum for the reactant beam velocities, as well as the distribution of center-of-mass angles generated using the flow velocity of one beam and the half-maximum velocities of the other beam, are shown as hatched areas on the Newton diagrams. The approximate angular broadening caused by these distributions, $\Delta\theta_{cm}$, is also given.

The maximum center-of-mass product velocity allowed in the Na(3P) reaction, U^*_{NaCl}, is determined from the reaction endothermicity of 4.68 kc/m, the photon energy of 48.53 kc/m, and the translational energy corresponding to the flow velocities of each beam. The maximum laboratory scattering angles where product can appear from the excited state reaction are also indicated.

The angular distributions measured at masses 23 and 58 without laser excitation are shown in Fig. 6. As noted above, the reaction Na(3S) + HCl$\longrightarrow$NaCl + H at 5.38 kc/m collision energy is barely

allowed. For the mass combination of this reaction, the product parent mass angular distribution contains no detailed information on the product energy or center-of-mass scattering angle distribution, given the current detector resolution and reactant beams velocity dispersions.

The angular distribution at mass 23 is predominately non-reactive, elastic scattering, with a minor contribution from reactively scattered NaCl detected at mass 23 from fragmentation in the ionization process. As the detection sensitivities for mass 23 and mass 58 in the experiment are approximately equal, the fragmentation ratio for NaCl formed near threshold and ionized by 160 volt electrons can be estimated by subtracting different multiples of the mass 58 angular distribution from the mass 23 angular distribution. The family of curves generated using multiplicative factors in the range 1-2 is shown in Fig. 9. Assuming the depletion of the large angle, non-reactive scattering is negligible for this near threshold collision energy, a fragmentation ratio of 50-55 percent results in a smooth, monotonic mass 23 angular distribution for the corrected, non-reactive sodium scattering.

Varying the electron energy from 50-200 volts did not markedly change the fragmentation ratio. Future measurements of mass 23 ground state reactive and non-reactive time-of-flight distributions at angles where NaCl fragmentation is important can, of course, distinguish the NaCl ion fragment contribution to the Na(3S) elastic scattering by their different, and, distinct laboratory velocities.

A similar analysis of the non-reactive Na(3S) scattering at the 19.4 kc/m collision energy is ambiguous. Here, the mass 23 data is

dominated by NaCl reaction product fragments. Figure 9 shows the corrected mass 23 non-reactive distribution when fragmentation ratios of 50, 66, and 70 percent are assumed for the NaCl product formed at this collision energy. The large errors on the derived non-reactive scattering distributions indicate that non-reactive scattering contributes very little to the observed intensity. At this energy and for this angular range, no realiable non-reactive distributions can be derived from the angular measurements alone. The strong reactive signal at this collision energy suggests that the large angle, non-reactive scattering should be largely depleted by reaction. Unlike the 5.38 kc/m mass 23 distribution, there is no obvious pure, non-reactive scattering at large or small angles to enable an interpolation through the angular range dominated by reaction product fragmentation. Again, time-of-flight measurements can resolve the non-reactive contribution at each angle. The conclusion that the reactive NaCl product fragments more at this higher collision energy is firmly grounded. Fragmentation ratios less than 70 percent always leave a residual bump near the center-of-mass. Rainbow or inelastic scattering are physically unlikely to produce such results.

The laboratory differential cross sections observed with and without laser excitation are shown in Fig. 10 for the two collision energies. The Na(3P) angular distributions derived from Eq. (4) for both energies at masses 23 and 58 are shown in Fig. 11. A 50 percent error in the fraction of Na atoms assumed to be in the 3P state significantly affects the derived Na(3P) differential cross sections

for the 19.4 kc/m collision energy data, while the 5.38 kc/m collision energy data is basically unchanged within the stated measurement errors. Figure 12 shows the non-reactive mass 23 distributions derived by assuming several fixed values for the NaCl fragmentation ratio, with an optical pumping efficiency of 30 percent. These fragmentation curves are not qualitatively different if only 15 percent of the atoms are assumed excited to the $3^2P_{3/2}$ state.

Laser correlated time-of-flight (TOF) measurements at selected angles for masses 23 and 58 at the 5.38 kc/m collision energy are shown in Figs. 13-14 . The mass 23 data at the laboratory angles 25° and 30° clearly exhibit a fast, Na(3P) elastic peak as well as a slower, broader, reactive ion fragment peak. At all angles, a fluorescence induced signal, not displayed in Figs. 13-14 appears in the first channels. This signal is also observed when the mass spectrometer is set to pass an arbitrary mass well separated from the masses of the products and reactants. This signal is thought to result from scattered fluorescence striking the Daly ion counter photomultiplier. When correlated, this signal appears in the first channel. The magnitude of this artifact is small, and can be separated from the true heavy particle scattering which appears well displaced to longer product arival times. When the ion flight time is used to displace the laser correlated TOF data, this artifact moves to channels 254-255. The displayed TOF data is then the actual data measured. The only numerical transformation applied was to interpolate the convoluted data over the channels 254, 255, 1, and 2, to correct for the multi-channel scaler reset and synchronization error.

Time-of-flight measurements of the ground electronic state scattering have not been performed to date. To obtain only the Na(3P) contribution to the laser correlated TOFs, they were corrected according to Eq. (8) using computed ground state TOF distributions. As stated above, at this near threshold collision energy, the ground state reactive scattering is severely convoluted by the distribution of center-of-mass angles. The TOF distributions obtained from a fit to the mass 58 ground state angular distribution are expected to closely approximate the true ground state TOFs. The corrected, mass 23 distributions derived differ little from the original laser correlated TOFs. The chief effect is to boost the signal at 35°, 40°, and 45° for the channels near the center-of-mass. As the reactivity is approximately a factor of ten larger in the 3P state, the corrected channels are displaced within the statistical error of the orignal TOFs.

At this point, it should be stated that the error in the assumed fraction of Na(3P) atoms in the collision volume can have a dramatic effect on the correction of the TOF data. The weighting of the Na(3S) TOF to the laser correlated TOF depends on the ratio of the reactivity of Na(3P) to Na(3S) atoms at that laboratory angle. In turn, this depends on what fraction of the Na atoms we assume cause the difference in the angular distributions when the laser excites the Na beam. At the collision energy 5.38 kc/m, the laser effect is large compared to the ground state scattering signal. Large errors in the fraction of Na atoms excited do not have significant results on the derived

center-of-mass energy and angle distributions. For the 19.4 kc/m collision energy, the ground state signal is comparable to the laser induced signal and the assumed value for the Na(3P) fraction can qualitatively affect the shape of the angular and TOF data used to obtain the center-of-mass product flux distributions.

Polarization measurements performed at laboratory angles of 40° and 55° were independent of the direction of the laser electric field vector in the scattering plane, and on the handedness of the light. From the statistical accuracy of these measurements, the polarization dependence for rotation of the electric field vector in the scattering plane is estimated to be less than 20 percent. The two detector angles were chosen to sample the center-of-mass and back scattered product. For the back scattered product, we expect a limited range of contributing impact parameters. Although velocity resolved polarization studies might show a dependence, we feel that for this particular reaction, the intrinsic polarization dependence is small and is expected for the reaction mechanism postulated below.

Finally, in Fig. 15 , the laser induced mass spectrometer signal is plotted against the laser fluorescence. These data were obtained by attenuating the laser power over two orders of magnitude using filters. An "eyeball" fit to the data is drawn, indicating that within the experimental accuracy, a linear dependence is observed. We take this as evidence that the mass spectrometer, fluorescence detector, and optical pumping are properly functioning as a system within the statistical errors of the observed signal strengths.

E. DATA ANALYSIS

In this section, the experimental data is analyzed to find what center-of-mass recoil energy and angular distributions are consistent with the measurements. First, the type of the collision process responsible for the measurements is identified. Next, the data is quantitatively reduced, within the framework of the identified collision process, to the fundamental center-of-mass frame product flux distributions. The effect of the reactant beam velocity dispersions, finite detector apertures, and other experimental broadening mechanisms are taken into account.

The Na(3P) scattering distributions measured at masses 23 and 58 can be reasonably ascribed to one of the following collision processes.

<u>Reaction</u> $Na(3P) + HCl \longrightarrow NaCl(^1\ ) + H(^2S)$ (14)

$Na(3P) + HCl \longrightarrow NaH(^1\ ) + Cl(^2P_{3/2})$ (15)

<u>Quenching</u> $Na(3P) + HCl \longrightarrow Na(3S) + HCl$ (16)

<u>Elastic</u> $Na(3P) + HCl \longrightarrow Na(3P) + HCl$ (17)

Analogous to the Na(3S) reactive scattering, NaCl product is expected to be favored over NaH. However, unlike the ground state scattering, the mass 23 angular distributions do not have the same shape as the mass 58 distributions. As shown in Fig. 12, the curves derived from the measured 5.38 kc/m collision energy mass 23 distribution correcting for NaCl fragmentation, always have residual intensity in the backward scattered direction peaking at a laboratory angle of 50°. This conclusion is independent of the fraction of atoms assumed in the 3P state. If we followed the logic applied to the Na(3S) scattering,

we would conclude that there is significant Na(3P) scattering which is not attributable to elastic or NaCl reactive scattering. It will now be argued that this conclusion is an artifact of the electron bombardment ionization process and the dependency of the NaCl fragmentation ratio on internal energy.

From the ground state Na(3S) reactive scattering analysis, it was noted that from threshold to 15 kc/m above threshold, the NaCl fragmentation ratio changed from 50 to 70 percent. In this case, the absolute signal levels of the Na^+ ions ascribed to NaCl fragments were within a factor of two of the NaCl parent signal. For the Na(3P) angular distributions, this approximate equivalence no longer holds. The $NaCl^+$ parent signal is only 1/10 of the mass 23 signal. If we presume the mass 23 signal is from NaCl ion fragments, then the mass 23 angular distribution is a more accurate measure of the true NaCl reactive product distribution, than the comparably weak parent mass distribution. For example, a relative change in the fragmentation ratio of 2 percent will affect the shape of the mass 58 distribution by 20 percent. Since there is sound evidence for a rapid increase in the fragmentation ratio in the ground state reaction, and the NaCl parent mass is a minor ion in the excited state reaction, the mass 23 distribution is taken to reflect the true NaCl product distribution. Of course, corrections for the Na(3P) elastic scattering must be done at small angles.

In the above discussion, it was tacitly assumed that all of the mass 23 data (correcting for elastic scattering) was from NaCl ion

fragmentation, and that NaH formation or quenching were unnecessary to explain any of the mass 23 intensity. The derived energy and recoil angle distributions, to be presented below, are physically plausible and fit the data well. Therefore, our argument is self-consistent. Having assumed the mass 23 distribution is mostly NaCl ion fragments, we could analyze the data without resorting to nonphysical mechanisms. To make the argument definitive, we now reason that quenching or NaH formation cannot account for the observations with the same success without ridiculous constraints on these two processes.

Figure 16 shows the kinematically allowed recoil velocities for different HCl vibrational states if Na(3P) is quenched by HCl. The indicated rotational states are those allowed by energy conservation for that vibrational state. The mass combination of the quenching channel differs markedly from the NaCl reactive channel. Consequently, the quenching channel can scatter product to all laboratory angles. Recalling that the residual mass 23 intensity is at 50° in the laboratory frame for the 5.38 kc/m collision energy, if this signal is assigned to quenching, then the quenching process is extraordinarily resonant. From Fig. 16, not only must HCl be vibrationally excited to scatter Na only in the laboratory range 15°-70°, but only a narrow range of rotational states are accessible as well. From the experimental results of Na quenching by N_2, H_2, and CO measured by Hertel and coworkers, this final state selectivity was never observed. Moreover, when an additional 15 kc/m of translational energy is available at the 19.4 kc/m collision energy, the Na(3P) scattering follows the

kinematic constraints characteric of the NaCl product. At this higher collision energy, if the mass 23 distribution was from quenching, then the final state distribution is even more restricted than at the 5.38 kc/m collision energy. These absurd conclusions rule out quenching as an important source of the Na scattering for the angular range of these measurements.

A similar argument applies for NaH formation; its mass combination is essentially identical to the quenching channel. Here too, the data at the two collision energies can only be explained by assuming a decrease in the product translational energy at the higher collision energy.

Center-of-mass energy and angular distributions were obtained using the CMLAB program written by R. Buss.[35] Two modifications of the program were made. First, the laser correlated TOFs were corrected for any DC offset using the cross correlated data in channels 55-200. Next, the sum of the first 50 channels where the elastic and reactive product is observed, was normalized to the difference between the Na(3P) and Na(3S) angular distributions for that angle. The Na(3P) angular distribution was multiplied by a term to correct for the different number densities contributing to the laser correlated TOFs and angular distributions, assuming 15 percent of the Na atoms are in the excited state. The program then scaled the calculated TOFs to have a total signal count equal to the calculated angular intensity at their respective angles. Trial and error fits to reduce the chi-square error in the TOF data were done to obtain final translational

energy, P(E), and recoil angle, T(θ) distributions. The manner with which the integration over the beam velocities was performed was changed to a proper quadrature appropriate for nozzle beam speed distributions.

Five different data sets were optimized for best fit, uncoupled P(E) and T(θ) distributions. These were

(1) Mass 23 laser correlated TOF's, uncorrected for the Na(3S), NaCl, mass 23 ion fragment depleted by the laser.

(2) Same as (1) but corrected for laser depletion of the Na(3S), NaCl fragment appearing at mass 23. Fifteen percent of the Na atoms were assumed excited by the laser in the collision volume.

(3) Mass 58 laser correlated TOF's, uncorrected for laser depletion of the mass 58 ground state reactive scattering.

(4) Same as (3), but corrected for laser depletion of ground state reaction assuming 15 percent of the Na atoms are optically excited.

(5) The sum of (2) and (4) assuming equal detection efficiencies for masses 23 and 58.

The derived contour maps of the scattered flux, the observed and calculated TOF's, the observed and calculated angular distributions, and the P(E), T(θ) functions corresponding to the best fits are shown in Figs. 17-24. Some fitted distributions assuming foward-backward symmetry are also shown in Figs. 25-28.

The best center-of-mass scattering distributions derived from the uncoupled recoil angle-translational energy assumption, shown in Fig.

19, provide a good overall fit to the data. Two features of the calculated curves, which are not in accord with the experimental results, are the enhanced intensity of the leading edges of the 25° and 30° laboratory TOF distributions, and a resolved, double peak structure in the 35°, 40° and 45° TOF distributions for channels near the center-of-mass.

The double peak structure is sensitive to the shape of the product translational energy distribution, P(E), in the interval 0-5 kcal/m. Increasing the widths of the reactant velocity distribution by 50 percent also reduces the double peaking without seriour alterations to the fit of the remaining angular and TOF data. Additionally, the numerical method used to integrate the product scattering with negligible recoil velocity distorts the calculated distributions for these channels, further enhanced by the Jacobian transformation from the cm→laboratory frame.

With allowance for the above errors introduced by the method of data analysis, the poorer fits to the TOF data near the center-of-mass can also result from the RRK functional form[35] used to model the product translational energy distributions. The broad, flat P(E) restricts the shapes allowed for the slow product. Only one parameter in the RRK function describes the rise of the P(E) from E=0. To match the product translational energy distribution needed to fit the remaining fast product, this parameter cannot assume any arbitrary value, and a compromise value is assumed.

The fast laboratory product calculated, but not observed, in the 25° and 30° TOF distributions is probably an artifact of assuming an

uncoupled P(E) and T(θ) distribution for the center-of-mass scattering. The fit to the data indicates that there should be less product with translational energy in the range 35-50 kc/m for center-of-mass scattering angles, $\theta < 30^\circ$.

Attempts using a tabular form for the energy and angular distributions, or radically different initial values for the Legendre series and RRK analytical scattering distributions, eventually converged to distributions similar to the best fits shown here. If the mass 58 data was added to the mass 23 data, assuming equal detection efficiencies for both masses, the best fits obtained were within the range found acceptable for the mass 23 data only. The main difference was a further reduction in the scattering intensity at 0° and 180° in the center-of-mass frame.

Fits attempted for the mass 58 data alone were poor. Reaction exothermicities 30 percent above the thermochemical value were needed to obtain even a coarse fit. The calculated and observed data were most in error for the backward scattered, slow product.

In Fig. 19, the range of angular distributions consistent with the best data fits for the mass 23 or combined mass 23 and mass 58 data are shown. The relative variations in the derived P(E) distributions were much less. The indicated allowed variations are based on a reasonable guess of the sensitivity of the data to the fits.

We conclude this discussion of the derivation of the center-of-mass scattering distributions by noting that the energy dependence of the total reaction cross section was neglected. The large reaction

exothermicity diminishes the effect of the spread in collision energies produced by the reactant beam velocity distributions. In addition, the RRK form of the P(E) naturally accounts for the different total energies for each Newton diagram generated in the integration over the beam velocity distributions. There is no need for the product translational energy to extend to values which apparently violate the reaction exothermicity[24].

In the derivation of the P(E) distribution, the reaction exothermicity was a free variable. The final value obtained, 45.4 kc/m agrees favorably with the value 43.9 kc/m calculated from the Na(3S→3P) transition energy (48.53 kc/m) and the Na(3S) + HCl→NaCl + H reaction endothermicity of 4.68 kc/m. The good agreement for the value of the exothermicity obtained from the data analysis is taken as confirmation that the mass 23 data are NaCl product fragments, and that the measured and derived distributions are faithful representations of the true Na(3P) + HCl→NaCl + H reaction.

F. DISCUSSION

In this section, we strive to understand what detailed reaction mechanism could account for the experimental observations. Any mechanism must successfully explain the four major experimental findings. These are the derived center-of-mass recoil angle and product translational energy distributions, the large enhancement in the reactivity of Na(3P) compared to Na(3S), and the lack of an observable laser polarization dependence on the NaCl product scattering. Because there are no reliable potential energy surface calculations for the Na(3P) + HCl reaction, the discussion will be qualitative. We stress that the

collision process is complex, involving several electronic states, and that simple explanations are probably not possible. Even for the simpler reactions Li(2S) + HX⟶LiX + H, X = F,Cl[24], subsequent trajectory studies[27] indicated an involved mechanism which could not be reduced to a simple description.

For the Na + HCl⟶NaCl + H reaction, with a covalent to ionic bond change, an electron transfer mechanism in the spirit of the alkali-halogen "harpoon" model is a good, first model for the reaction. The electron jump distance, calculated from the -23 kc/m vertical electron affinity for HCl(v=o) and the 76 kc/m ionization potential of Na(3P), is 3.5Å. A negative electron affinity indicates the anion in unstable with respect to the neutral molecule and a free electron. The reaction cross section is 38Å^2 for this jump distance. If Na(3P) interacts at large distances with HCl in an analogous way as Hertel, et al. observed for N_2, H_2 and CO, then the HCl bond is expected to stretch as the Na(3P) approaches. The HCl electron affinity is increased as the bond stretches, enlarging the reaction cross section. The large reaction cross section observed is then consistent with our expectations of an electron jump initiating reaction step.

The total reaction cross section is expected to be affected in approximately the same way by either Na electronic energy or HCl vibrational energy.[3] This is because the vibrational excitation increases the HCl electron affinity, while electronic excitation reduces the Na ionization potential. To first order, the reaction

cross section will depend only on the energy difference between the ionization potential and electron affinity for Na and HCl, respectively.

The electron transfer mechanism early in the reaction also explains the lack of a polarization dependence in the reaction. As noted by Rettner and Zare,[10] the alignment of the P orbital for the general C_s symmetry of Na + HCl is not expected to affect the probability of electron transfer at the crossing point. The $Na^+ + HCl^-(^2\Sigma^+)$ state can cross all the Na(3P) + $HCl(^1\Sigma)$ states. If the Na(3P) + HCl states are not substantially repulsive (<5 kc/m) at the crossing distance, the lack of an observable effect on the product angular or velocity distributions from the initial P orbital alignment is expected, since each initial molecular collision state must go through the same $Na^+(^1S) + HCl^-(^2\Sigma^+)$ intermediate surface to reach the $NaCl(^1\Sigma^+)$ + $H(^2S)$ products. The orbital alignment dependence seen by Rettner and Zare[10] for $Ca(^1P)$ + HCl resulted from the polarized ion core formed at the electron transfer, and a number of low lying, accessible, excited Ca^+ states. The $Na^+(^1S)$ core can have no alignment, and only one low lying $Na^+ + HCl^-$ ion pair state is accessible.

The large reaction cross section implies that significant initial orbital angular momentum (L) is present. The additional $1\hbar$ of angular momentum from the orbital electronic motion, when circularly polarized light is used in the optical pumping, cannot have a large effect on the differential cross section, as is observed.

The transformation from space to body fixed frames of reference is predicted to occur at substantial distances for the dominating long

range, $1/R^5$, dipole-quadrupole interaction of Na(3P) + HCl. From Eq. (2), the impact parameter dependence of the body fixed frame locking distance is

$$R_L(\text{Å}) = 11.2*b(\text{Å})^{-1/3} \tag{18}$$

for the 5.38 kc/m collision energy. The $V_\sigma - V_\pi$ splitting was calculated from the formula of Buckingham.[36] Even if there is an adiabatic transfer from the space to body fixed axes, the ion pair intermediate will not be sensitive to the P orbital alignment, unless one of the excited potential surfaces is strongly repulsive so that it does not cross the charge transfer curve at the 5.38 kc/m collision energy. Such is not expected, nor observed.

The product energy and angular distributions, containing the most detailed information on the reaction mechanism, are more difficult to relate directly to the electron transfer model. The dominance of backward scattering suggests an early release of the reaction exothermicity. This is opposite that observed for Li(2S) + HCl[24], where strong forward scattering was seen. The decrease in the angular distributions at 0° and 180° center-of-mass scattering angles, and the slightly structured, non-monotonic T(θ) seem to rule out a long lived collision complex or coplanar reaction geometry. The latter might be expected by the mass combination of this reaction, with substantial initial orbital angular momentum and a low product reduced mass. The moderate enhancement at the forward scattering angles near $\theta_{cm} = 60°$

is also peculiar, especially since this matches the features seen for the Li(2S) + HCl$\rightarrow$LiCl + H reaction[24].

The geometry of the transition state is unknown for this reaction. The large cross section, small product reduced mass, and direct mechanism based on the structured T(θ) would seem to preclude a tightly-bound, linear geometry. A bent, or loose transition state seems more probable, since sinθ weighting of T(θ) shows broad sideways NaCl scattering. Noting that the NaCl(v=o) internuclear separation is 2.36Å and the HCl(v=o) separation is 1.27Å, for a 90° transition state geometry, product exit parameters of 1.5Å are reasonable. Taking the average product translational energy of 25 kc/m, the product orbital angular momentum is 34ħ. For 3.5Å impact parameters at the 5.38 kc/m collision energy, the total initial angular momentum is ~160ħ, implying an average 127ħ must be in NaCl rotations. Neglecting centrifugal distortion, this is an average 8.9 kc/m of product rotational energy, leaving an additional 15 kc/m for product vibrational energy. The slower, forward scattered product seen in the 25° and 30° laboratory TOF would be a consequence of larger NaCl rotational excitation, necessary to satisfy angular momentum conservation if the forward scattering correlates with larger impact parameter collisions. For the broad product translational energy distribution observed, the utility of an average product translational energy is dubious.

The early release of the reaction exothermicity is expected, since HCl is known to dissociate by low energy electrons to H + Cl^-.[37] Hence, at the transfer distance, the slow electron will initiate the H

atom departure by dissociate attachment. The extent of the interaction between the forming $Na^+ Cl^-$ molecule and departing H atom is not known. The large product translational energy suggests this exit channel coupling is small. Conversely, the forward scattering of the product angular distribution in alkali-halogen reactions has been related to charge migration [4b]. This involves significant interaction among all three atoms. The current case of a light hydrogen atom leaving is expected to reduce the three particle interaction times considerably.

A more detailed analysis of the P(E), T(θ) distributions must wait until more is known about the PES of this reaction.

G. CONCLUSION

The crossed-molecular beams technique has measured the NaCl product center-of-mass scattering distribution for the reaction

$$Na(3^2P_{3/2}) + HCl(^1\Sigma^+) \longrightarrow NaCl(^1\Sigma^+) + H(^2S)$$

at a collision energy of 5.38 kc/m. The enhanced cross section for reaction of Na(3P) vs. Na(3S) atoms and the lack of an observable polarization dependence for the reaction is consistent with the <u>expected</u> electron transfer reaction mechanism. The product energy and angular distributions indicate a predominance of sideways scattering, unlike the Li(2S) + HCl⟶LiCl + H reaction[24], where forward scattering was observed. The large initial orbital angular momentum does correlate predominately (~80 percent) with product rotation as expected for this mass combination. Significant product translational energy is favored by the repulsive energy release initiated by dissociate attachment of HCl from the transfer of the sodium P orbital electron.

REFERENCES

1. Berichte der Bunsen-Gesellschaft fur Physikalische Chemie, R. E. Wyatt, J. McNutt, M. Redmon, Proceedings of "50 Years Molecular Dynamics," Berlin, 1981.

2. A. Kuppermann, in "Potential Energy Surfaces and Dynamics Calculations," ed. D. Truhlar, Plenum, (1981) p. 375.

3. F. Bartoszek, B. Blackwell, J. Polanyi, and J. Sloan, J. Chem. Phys., 74, 3400 (1981) and references therein.

4. (a) P. J. Kuntz, E. M. Nemeth, J. C. Polanyi, J. Chem. Phys., 50, 4607 (1969).

   (b) P. J. Kuntz, M. H. Mok, J. C. Polanyi, J. Chem. Phys., 50, 4623 (1969).

5. Robin Hennessy, Yoko Ono, and J. P. Simons, Mol. Phys., 43, 181 (1981).

6. R. Buss, P. Casavecchia, T. Hirooka, S. Sibener, Y. T. Lee, Chem. Phys. Lett., 82, 386 (1981).

7. M. Prisant, C. Rettner, and R. Zare, Chem. Phys. Lett., 88, 271 (1982).

8. M. Prisant, C. Rettner, and R. Zare, J. Chem. Phys., 75, 2222 (1981).

9. C. Rettner and R. Zare, J. Chem. Phys., 75, 3636 (1981).

10. C. Rettner and R. Zare, J. Chem. Phys. 77, 2416 (1982).

11. R. C. Esther and R. N. Zare, JACS, 100, 1324 (1978).

12. H. Schmidt, A. Bahring, E. Meyer, and B. Miller, Phys. Rev. Lett., 48, 1008 (1982).

13. N. Reiland, C. Schulz, H. Tittes, and I. Hertel, Chem. Phys. Lett., 91, 329 (1982).

14. W. Reiland, G. Jamieson, H. Tittes, and I. Hertel, Z. Phys. A., 307, 51 (1982).

15. W. Reiland, H. Tittes, I. Hertel, V. Bonacic-Koufecky, and Maurizio Persico, J. Chem. Phys., 77, 1908 (1982).

16. P. Botschwina, W. Meyer, I. Hertel, and W. Reiland, J. Chem. Phys., 75, 5438 (1901).

17. W. Reiland, H. Tittes, and I. Hertel, Phys. Rev. Lett., 48, 1389 (1982).

18. A. Fischer, I. Hertel, Z. Phys. A., 304, 103 (1982).

19. I. Hertel and W. Stoll, J. App. Phys., 47, 214 (1976).

20. I. Hertel and W. Stoll, Adv. Atomic Mol. Phys., 13, 113 (1978).

21. H. Hermann and I. Hertel, Comments At. Mol. Phys., 12, 61, 85 (1982).

22. F. Heismann and H. Loesch, Chem. Phys., 64, 43 (1982).

23. M. Hoffmeister, L. Potthast, and H. J. Loesch, preprint of "State selected molecular beam reaction dynamics of K with HF(v=1, j=5, 6, 7)."

24. C. Becker, P. Casavecchia, P. Tiedemann, J. Valentini, Y. T. Lee, J. Chem. Phys., 73, 2833 (1980).

25. M. Chen, H. S. Schaefer, J. Chem. Phys., 72, 4376 (1980).

26. M. Shapiro and Y. Zeiri, J. Chem. Phys., 70, 5264 (1979).

27. I. Nourbakha, N. Sathyamorthy, Chem. Phys., 77, 67 (1983) and references therein.

28. N. Hijazi and J. Polanyi, Chem. Phys., 11, 1 (1975).

29. K. Schulten, R. G. Gordon, J. Chem. Phys., 64, 2918 (1976)

30. B. Blackwell, J. C. Polanyi, and J. C. Sloan, Chem. Phys., 30, 299 (1978).

31. J. Barker, R. Weston, J. Chem. Phys., 65, 1427 (1976).

32. Thermocoax Heating Elements, application information, Amperex, Inc.

33. G. Comsa, R. David, B. Schumacher, Rev. Sci. Instr., 52, 789 (1981).

34. H. Schmidt, private communication.

35. R. Buss, Phd. thesis, Univ. of Calif., Berkeley,1979.

36. A. D. Buckingham, in "Intermolecular Forces," J. D. Hirschfelder, ed., Adv. Chem. Phys., XII, p. 107 (1967) Interscience.

37. J. N. Bardsley and J. M. Wadehra, J. Chem. Phys., 78, 7227 (1983).

38. F. E. Bartoszek, B. A. Blackwell, J. C. Polanyi, and J. J. Sloan, J. Chem. Phys., 74, 3400 (1981).

FIGURE CAPTIONS

Fig. 1. Schematic representation of how different laser beam E and k vector directions relative to the collision plane determine the initial, asymptotic distribution of P orbitals. On the left hand side, the laser propagates in the scattering plane. When the E vector is perpendicular to the collision plane (top), $|p\pi^-\rangle$ states are preferred with negative reflection symmetry. With the E vector in the collision plane, a mixture of $|p\pi^+\rangle$ and $|p\sigma\rangle$ states are formed, depending on the angle between the relative velocity vector and the laser E vector. On the right hand side, the laser beam propagates perpendicularly to the collision plane. The top (bottom) figure shows that if the E vector is perpendicular (parallel) to the relative velocity vector, $|p\pi^+\rangle$ ($|p\sigma\rangle$) states are preferred.

Fig. 2. Cross section of the seeded Na atom source. Components are (a) Main Na reservoir, (b) Reservoir heating cables, (c) gas inlet tube, (d) ceramic support posts for inlet tube radiation heater, (e) flow constrictor, (f) nozzle tube, (g) nozzle tube heating elements, (h) nozzle disk, (i) oven copper support block, (j) nozzle alignment bolts, (k) heated skimmer, (l) skimmer heaters, (m) pre-skimmer, (n) pre-skimmer heaters, (o) defining slits, (p) radiation shields, (q) beam flag, (r) reservoir thermocouple, (s) nozzle chamber bulkhead.

Fig. 3. Cross sectional view of HCl keyed beam source; (a) nozzle, (b) nozzle heater block, (c) nozzle alignment fixture, (d) gas inlet tube, (e) skimmer, (f) nozzle bulkhead.

Fig. 4. $Na(3^2S_{1/2})$, $Na(3^2P_{1/2})$, and $Na(3^2P_{3/2})$ electronic state hyperfine structure. The double headed arrow shows the two level system used for optically pumping a steady state fraction of Na atoms to the $3^2P_{3/2}$ state.

Fig. 5. Doppler shifted fluorescence for He (top) and Ne (bottom) seeded Na atom beams. Δf measures the $F=2 \rightarrow F'=3$ transition shift. The bottom trace is a relative frequency standard derived from an etalon.

Fig. 6. Na(3S) + HCl scattering angular distributions measured at the two collision energies at mass 23 (top) and mass 58 (bottom). The signal is measured in units of the experimentally observed count rates.

Fig. 7. Calculated and observed NaCl product angular distribution for the Na(3S) + HCl reaction. A constant product energy and recoil angle distribution was assumed. The good fit to the data indicates that the recoil velocity is so small, that no information on the structure of the center-of-mass scattering distribution can be obtained of this energy at the current apparatus resolution.

Fig. 8. Newton diagrams for the Na(3P) + HCl system at the two collision energies measured in the experiment. The hatched areas show the FWHM velocity distributions at each beam, and

the distribution of center-of-mass angles resulting from the reactant beam velocity spreads. The maximal NaCl product velocity is restricted to the circle drawn about the center-of-mass by conservation of energy. The laboratory angles tangent to these circles are the nominal maximum scattering angles for observation of NaCl product.

Fig. 9. Mass 23 angular distributions corrected for fragmentation of NaCl reaction product assuming different fragmentation ratios.

Fig. 10. Angular distributions observed with laser on and off at mass 23 (top) and mass 58 (bottom) at the two experimental collision energies. At mass 23 and 5.38 kc/m collision energy, the enhancement of the signal caused by the laser excitation is clear, while at mass 58 and 19.4 kc/m collision energy, the enhancement is barely observable.

Fig. 11. Na(3P) + HCl scattering angular distributions measured at the two collision energies at mass 23 (top) and mass 58 (bottom). Error bars are 1 standard deviation of the mean. The signal is in units of the observed count rates.

Fig. 12. Na(3P) + HCl mass 23 angular distributions, corrected for NaCl product fragmentation assuming different fragmentation ratios.

Fig. 13. Experimental laser correlated time-of-flight distributions at mass 23 for the indicated laboratory angles. At 25° and 30°, elastic scattering of Na(3P) atoms can be easily seen.

The slow, broader peak at all angles is assigned to NaCl product which fragments in the electron impact ionizer to Na^+.

Fig. 14. Experimental laser correlated time-of-flight distributions of mass 58 at the indicated laboratory angles.

Fig. 15. Laser induced scattering as a function of the resonance fluorescence intensity. If the experiment is operating correctly, the data should fall on a straight line. The straight line is an "eyeball" fit to the data indicating that, to first order, this is true.

Fig. 16. Newton diagram showing the laboratory angular range accessible to the inelastic Na(3P) + HCl quenching channel, or the NaH product reaction channel. The inelastic channel is labeled by the vibrational product state of the HCl, and the maximum HCl rotational level accessible for that vibrational state. The two circles showing NaH product are based on different values for the NaH bond energy.

Fig. 17 Calculated and observed laboratory angular distributions for the 5.38 kc/m collision energy, Na(3P) +HCl reaction using a 5 term legendre expansion in the center-of-mass scattering angle and an RRK function for the translational energy.

Fig. 18 Calculated and observed laboratory product arrival distributions for selected laboratory angles for the 5 term legendre expansion of fig 17.

Fig. 19 Best fit P(E) and T(θ) distributions for the 5 term legendre series. The shaded areas and hatch marks delimit the allowed range of the functions with essentially no discernable change in the quality of the fit to the data.

Fig. 20 Contour product flux map for the distributions of fig. 19.

Fig. 21 Calculated and observed angular distributions for a 7 term legendre series.

Fig. 22 Calculated and observed TOF data for the 7 term legendre series.

Fig. 23 Best fit T(θ) and P(E) functions for the 7 term legendre series.

Fig. 24 Contour product flux map for the 7 term legendre series.

Fig. 25 Laboratory angular distributions for the best fit center-of-mass scattering distributions with forward-backward symmetry. The poor quality of the fits show that the reaction is definitely backward scattered.

Fig. 26 TOF data observed and calculated for the forward-backward symmetric scattering distribution.

Fig. 27 Best fit T(θ) and P(E) functions for the forward-backward symmetric scattering distribution.

Fig. 28 Product flux contour map for the forward-backward symmetric best fit distributions of fig. 27. Note that the symmetric case shows an increase in the intensity near 60°, similar to the 5 and 7 term legendre expansions.

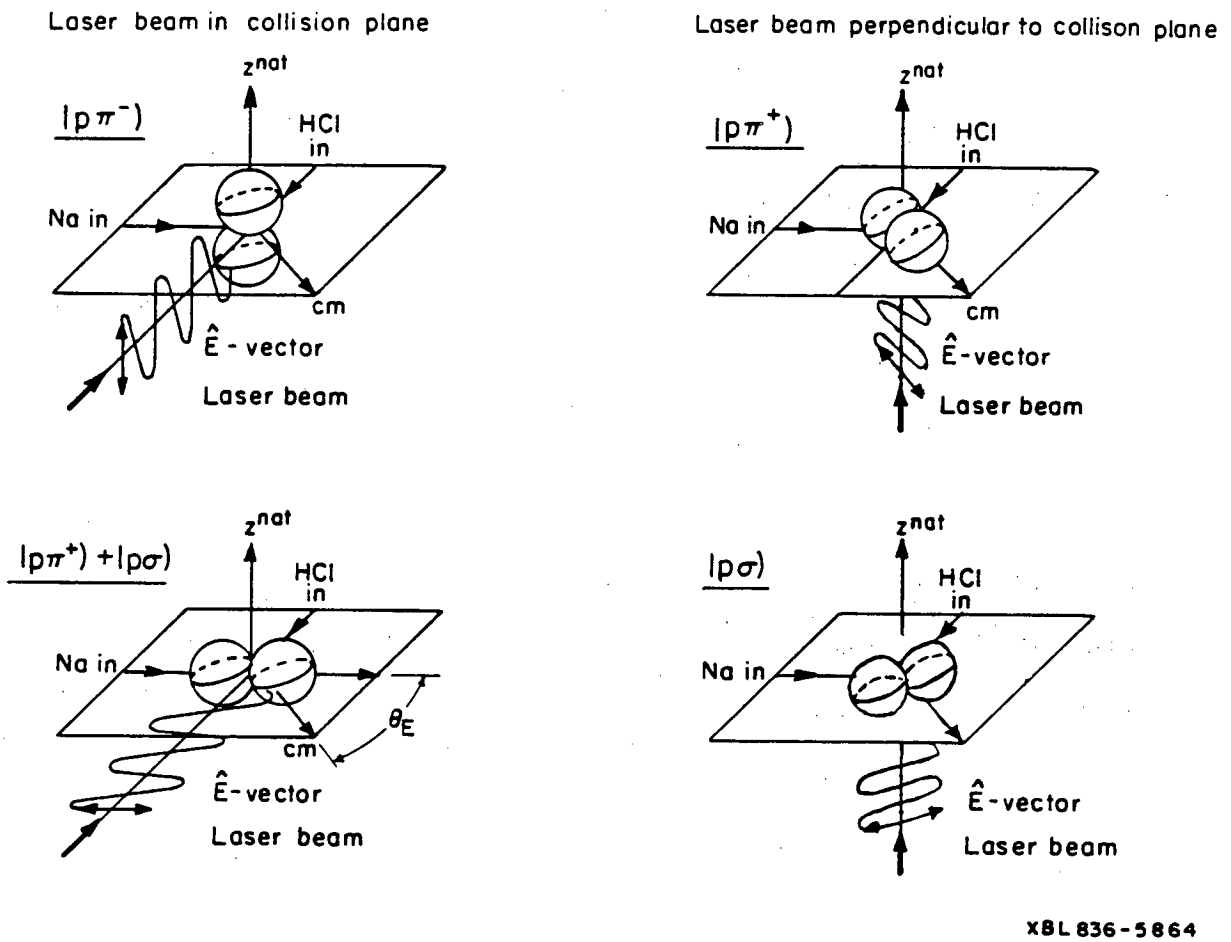
Laser beam in collision plane
Laser beam perpendicular to collison plane
z^{nat}
$|p\pi^-)$
HCl in
Na in
cm
$\hat{E}$ - vector
Laser beam
$|p\pi^+)$
$|p\pi^+) + |p\sigma)$
θ_E
$|p\sigma)$
XBL 836-5864

Fig. 1

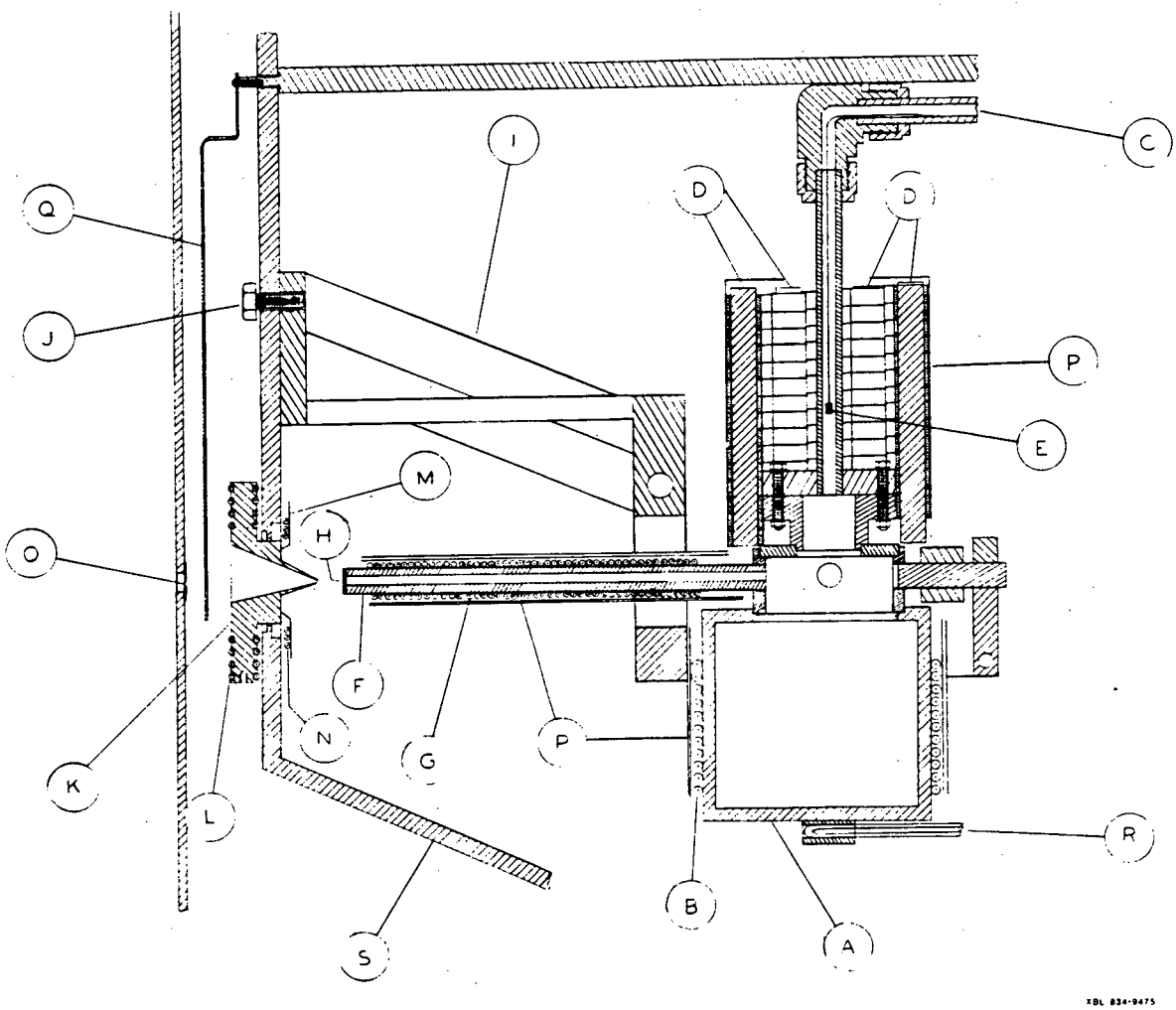

Fig. 2

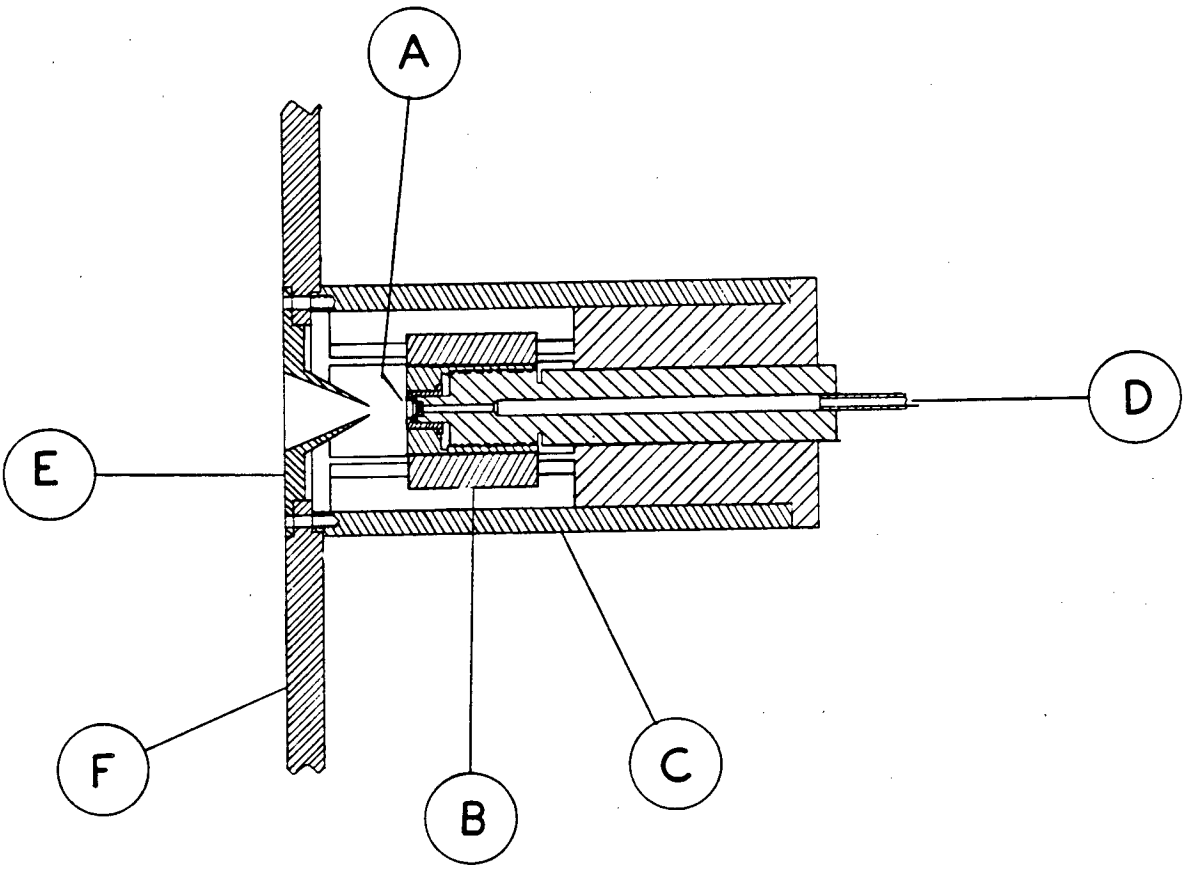

XBL 834-9474

Fig. 3

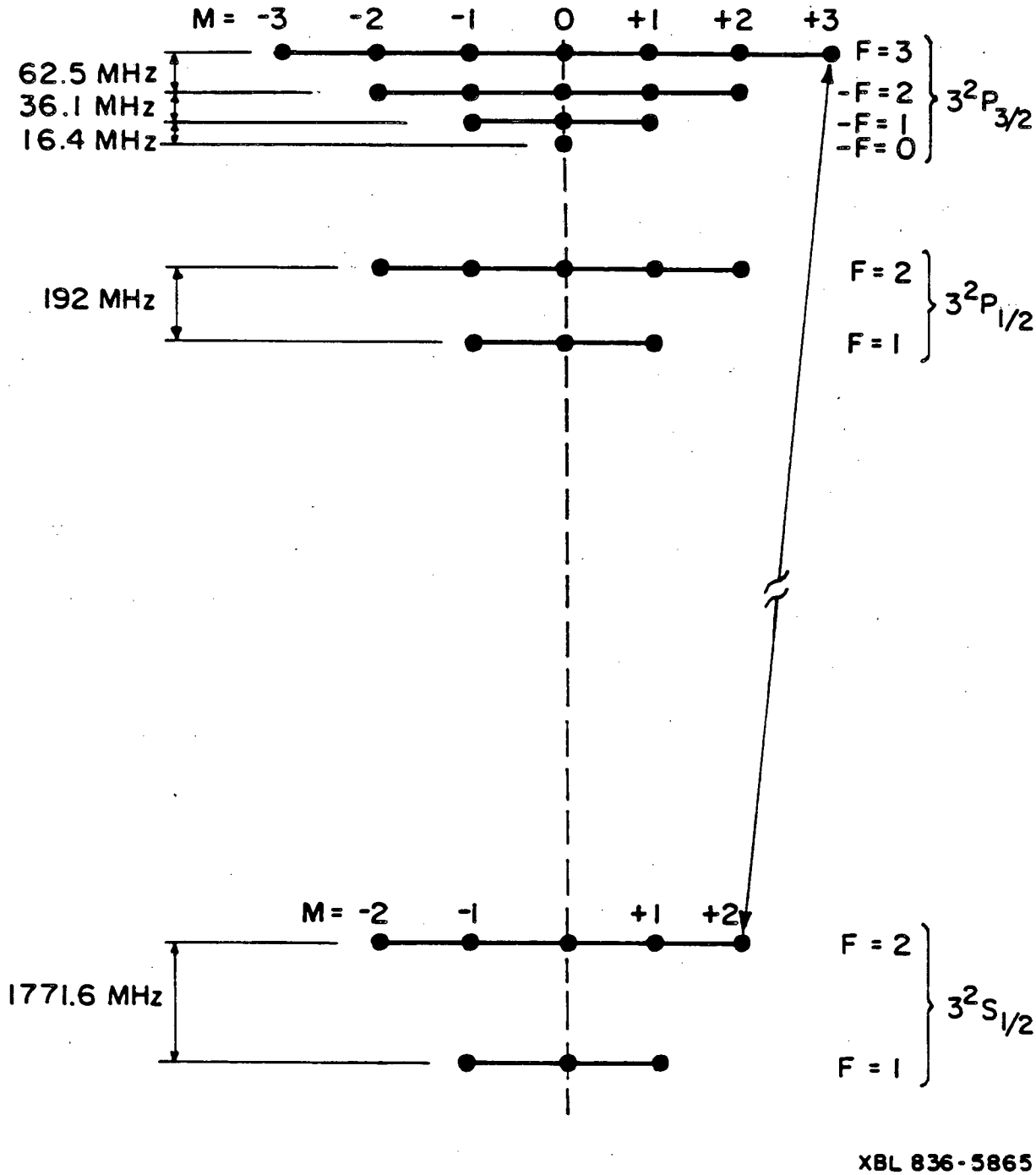
M = -3 -2 -1 0 +1 +2 +3
62.5 MHz
36.1 MHz
16.4 MHz
F = 3
-F = 2
-F = 1
-F = 0
$3^2P_{3/2}$
192 MHz
F = 2
F = 1
$3^2P_{1/2}$
M = -2 -1 +1 +2
1771.6 MHz
F = 2
F = 1
$3^2S_{1/2}$
XBL 836-5865

Fig. 4

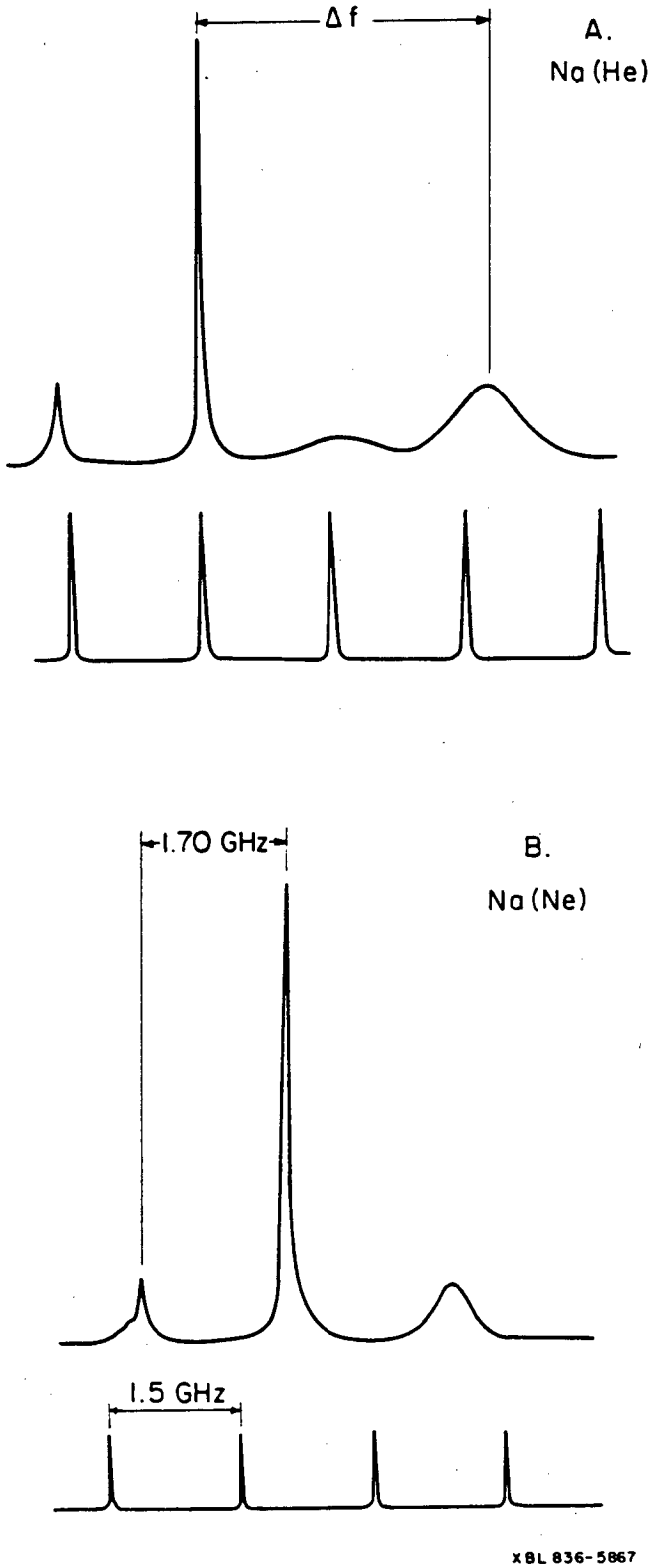

Fig. 5

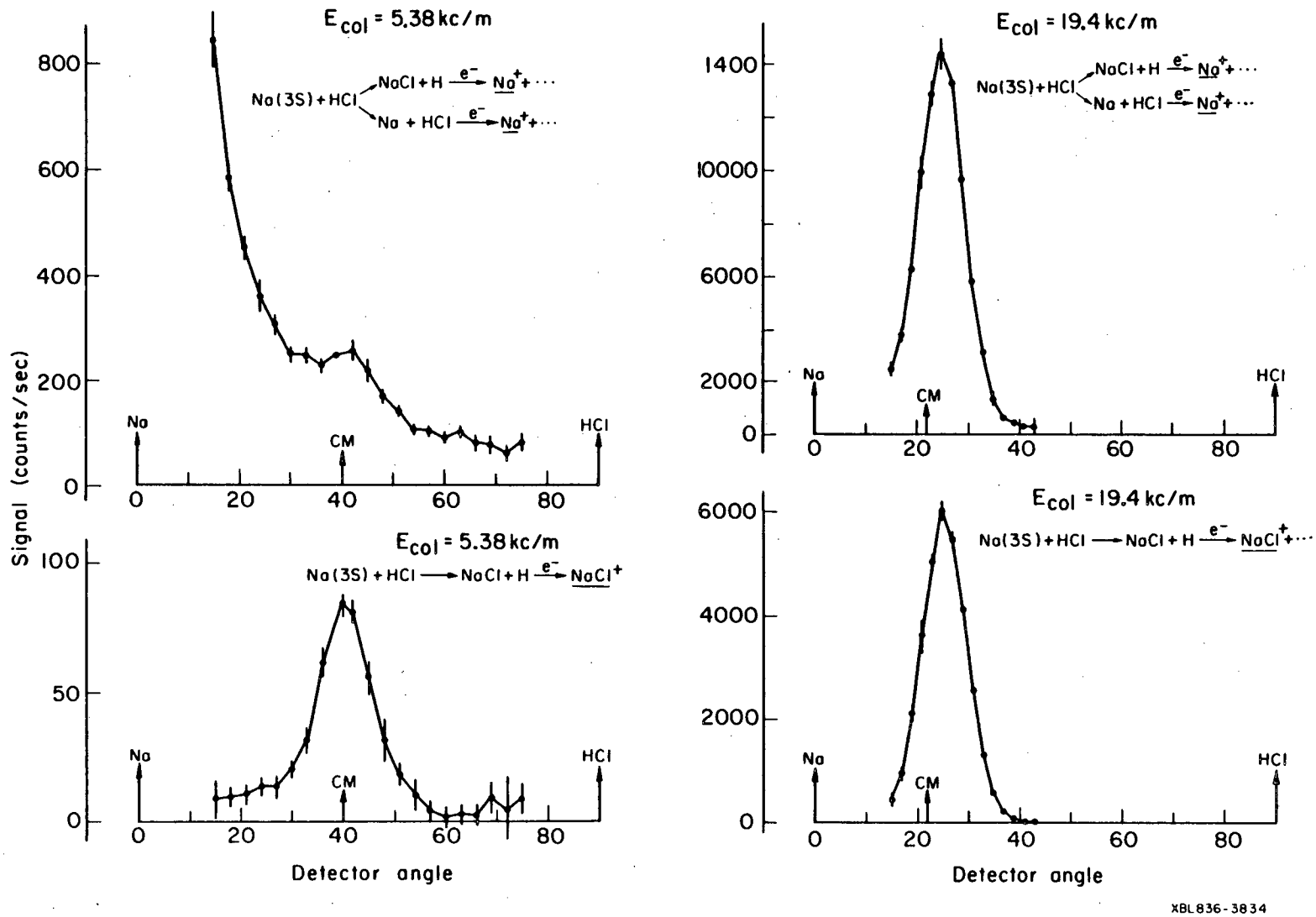
E_{col} = 5.38 kc/m
Na(3S) + HCl → NaCl + H $\xrightarrow{e^-}$ Na^+ + ···
Na + HCl $\xrightarrow{e^-}$ Na^+ + ···
Signal (counts/sec)
Na
CM
HCl
E_{col} = 5.38 kc/m
Na(3S) + HCl → NaCl + H $\xrightarrow{e^-}$ $NaCl^+$
Detector angle
E_{col} = 19.4 kc/m
Na(3S) + HCl → NaCl + H $\xrightarrow{e^-}$ Na^+ + ···
Na + HCl $\xrightarrow{e^-}$ Na^+ + ···
E_{col} = 19.4 kc/m
Na(3S) + HCl → NaCl + H $\xrightarrow{e^-}$ $NaCl^+$ + ···
Detector angle
XBL836-3834

Fig. 6

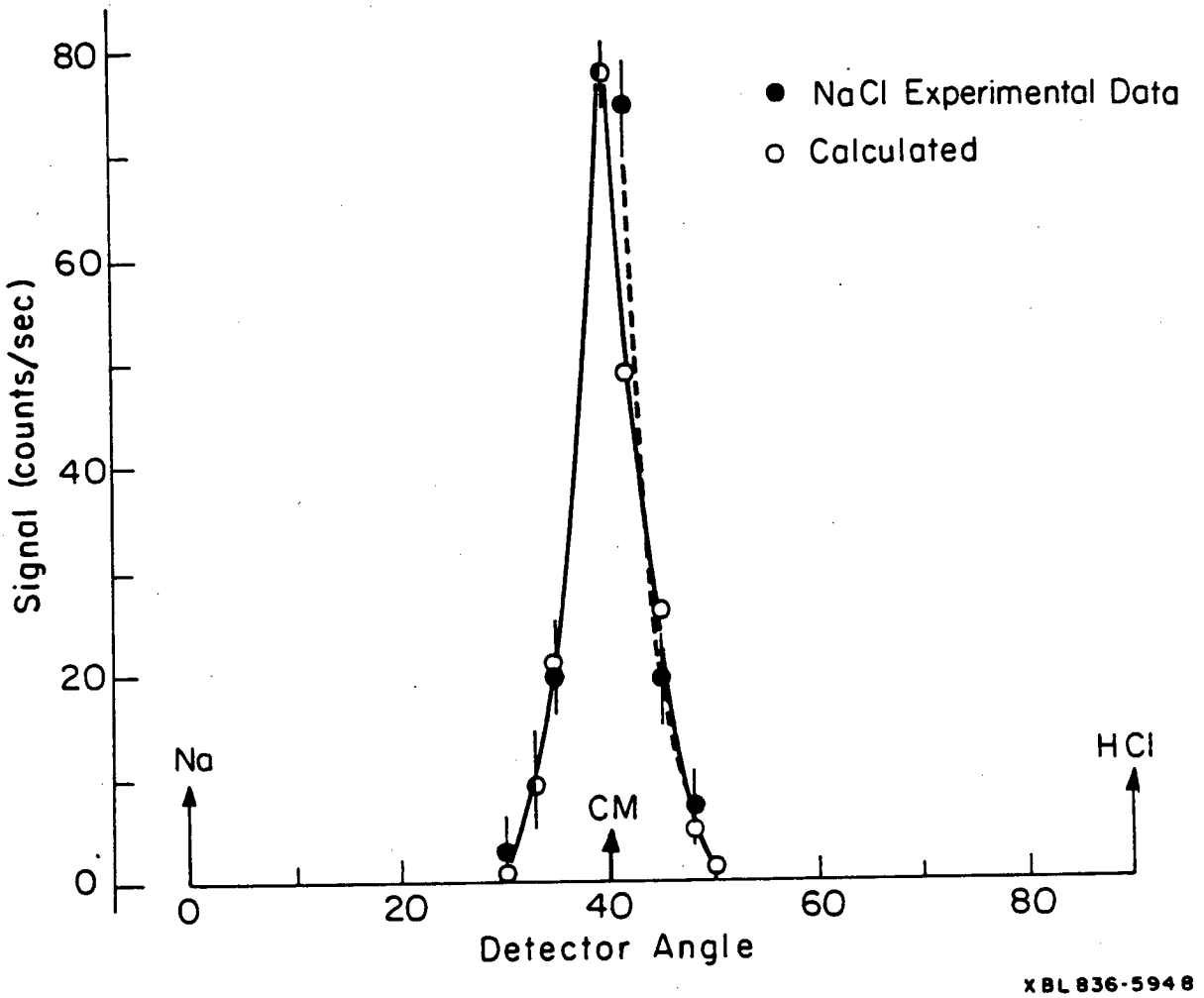
80
60
40
20
0
Signal (counts/sec)
NaCl Experimental Data
Calculated
Na
CM
HCl
0
20
40
60
80
Detector Angle
XBL 836-5948

Fig. 7

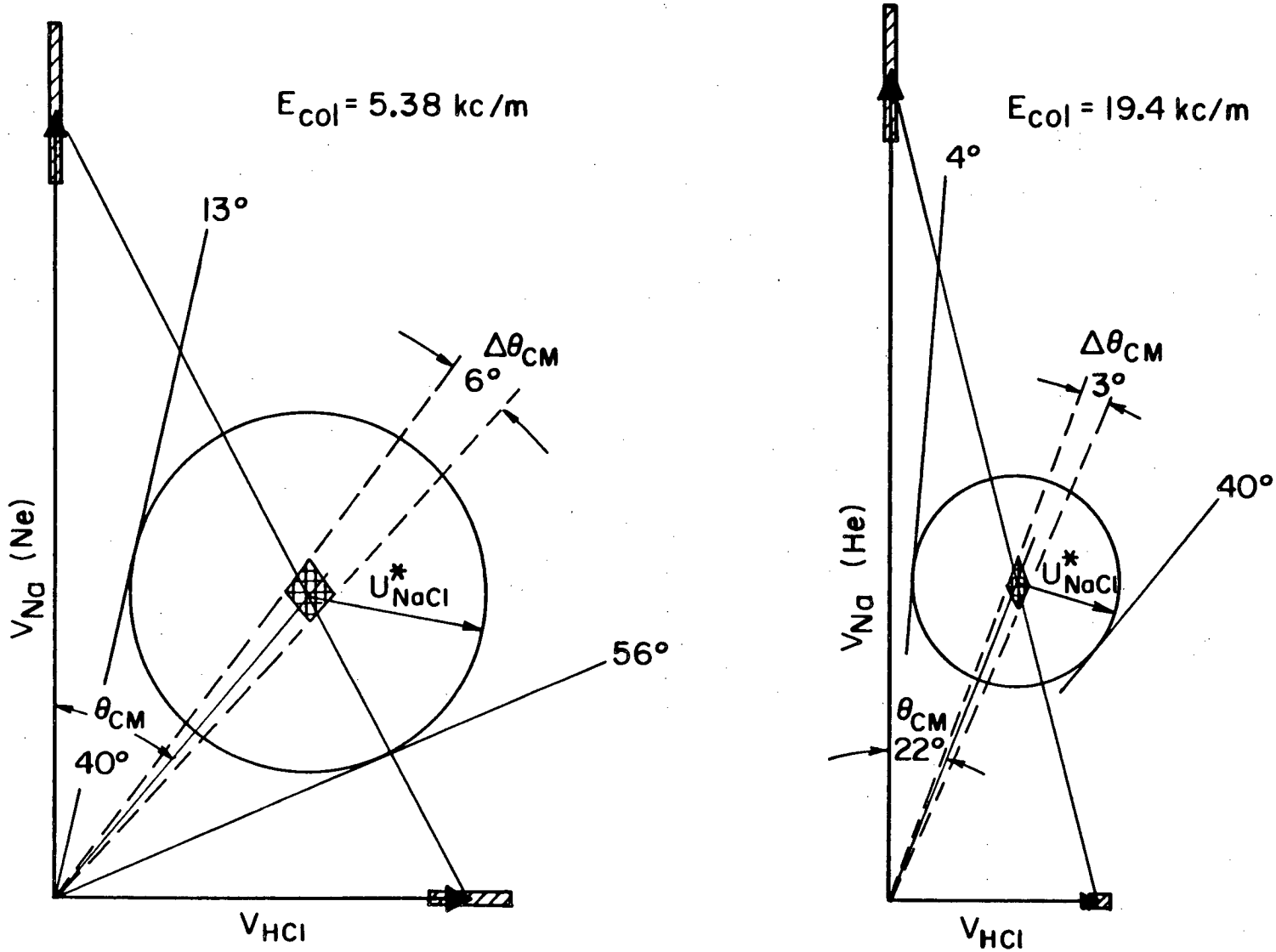

Fig. 8

XBL836-3831

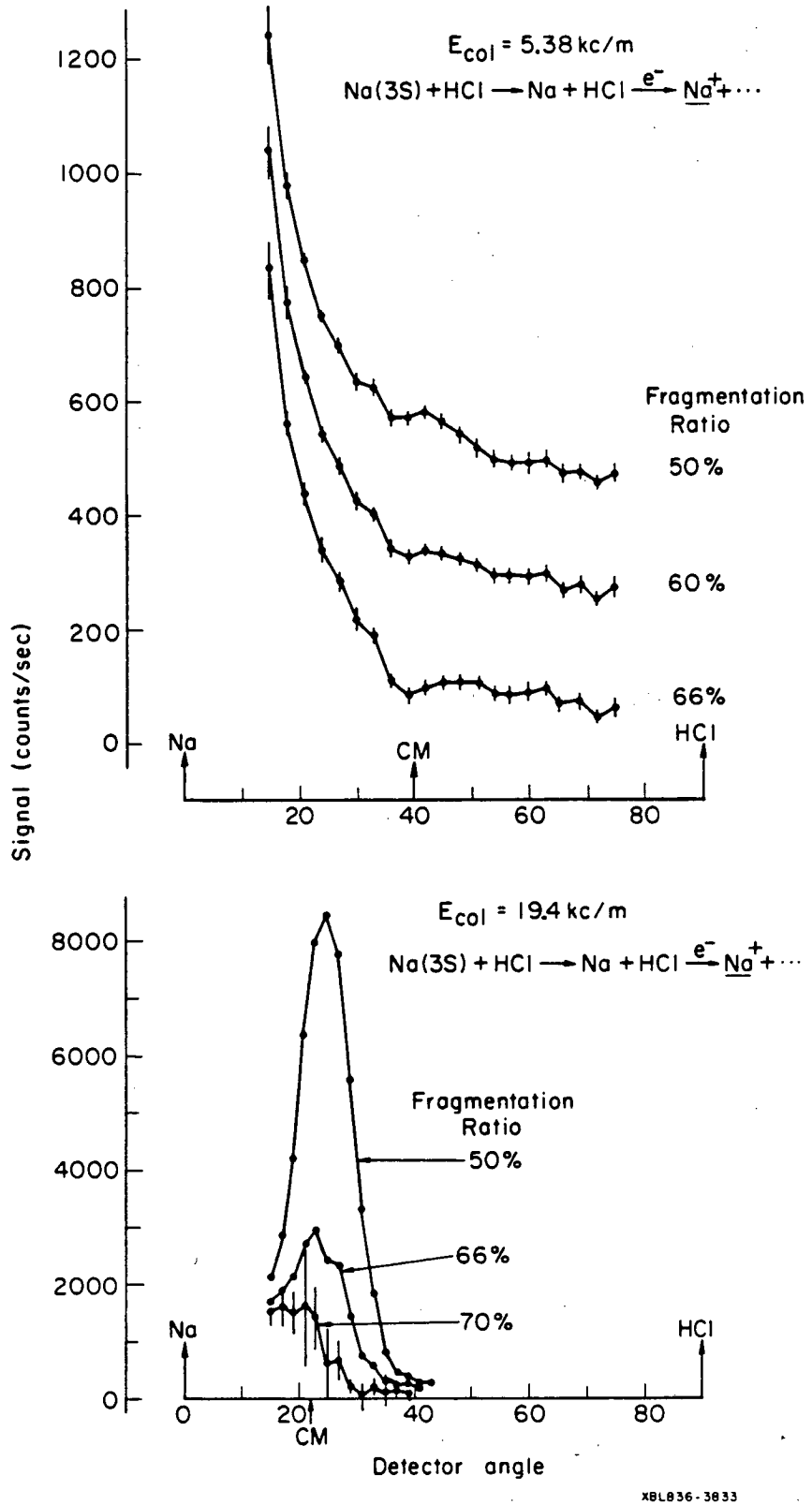
E_{col} = 5.38 kc/m
Na(3S) + HCl → Na + HCl $\xrightarrow{e^-}$ $\underline{Na}^+$ + ···
Fragmentation Ratio
50%
60%
66%
Na
CM
HCl
Signal (counts/sec)
E_{col} = 19.4 kc/m
Na(3S) + HCl → Na + HCl $\xrightarrow{e^-}$ $\underline{Na}^+$ + ···
Fragmentation Ratio
50%
66%
70%
Detector angle
XBL836-3833

Fig. 9

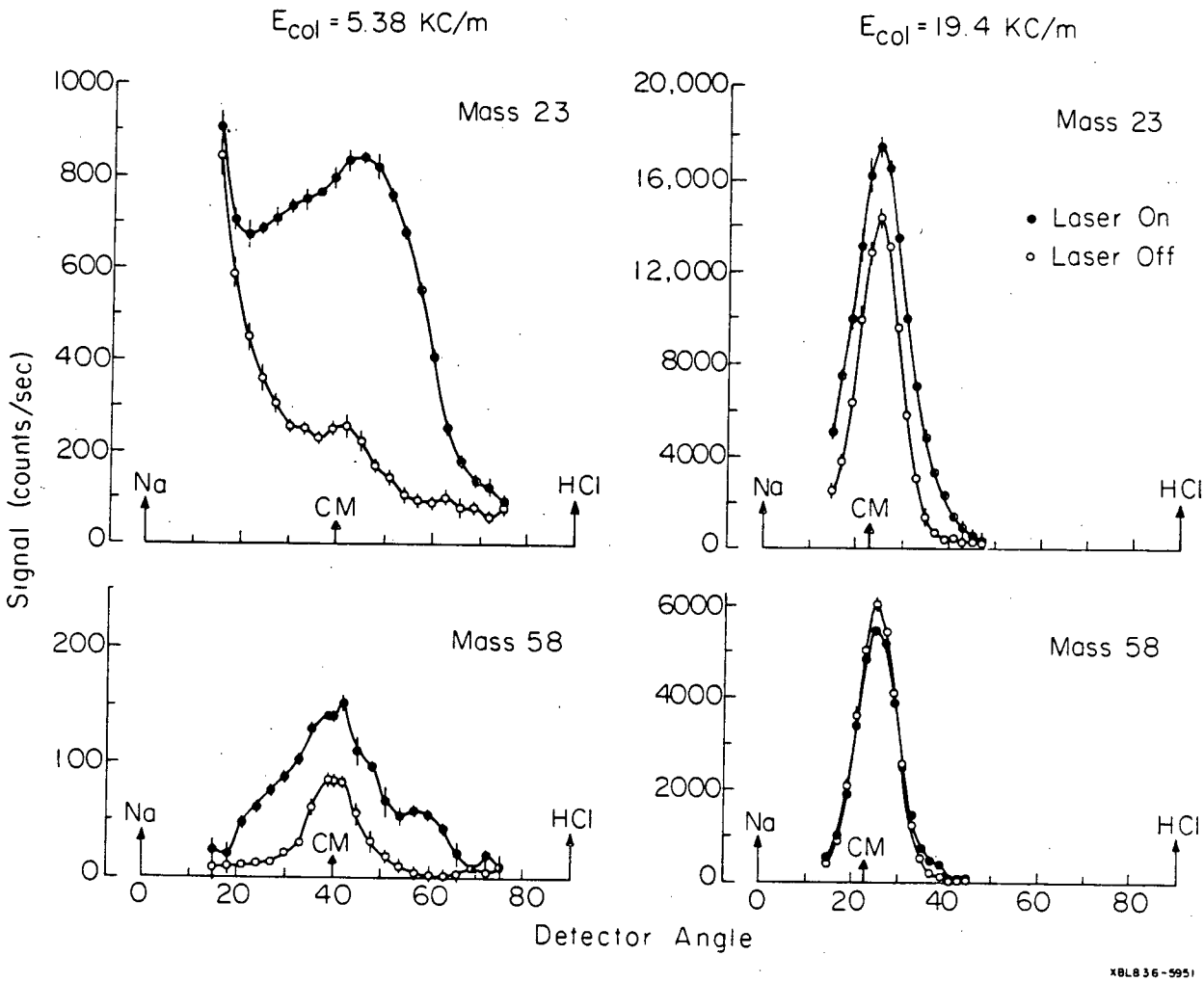
E_{col} = 5.38 KC/m
E_{col} = 19.4 KC/m
Mass 23
Mass 58
Laser On
Laser Off
Na
CM
HCl
Signal (counts/sec)
Detector Angle
XBL836-5951

Fig. 10

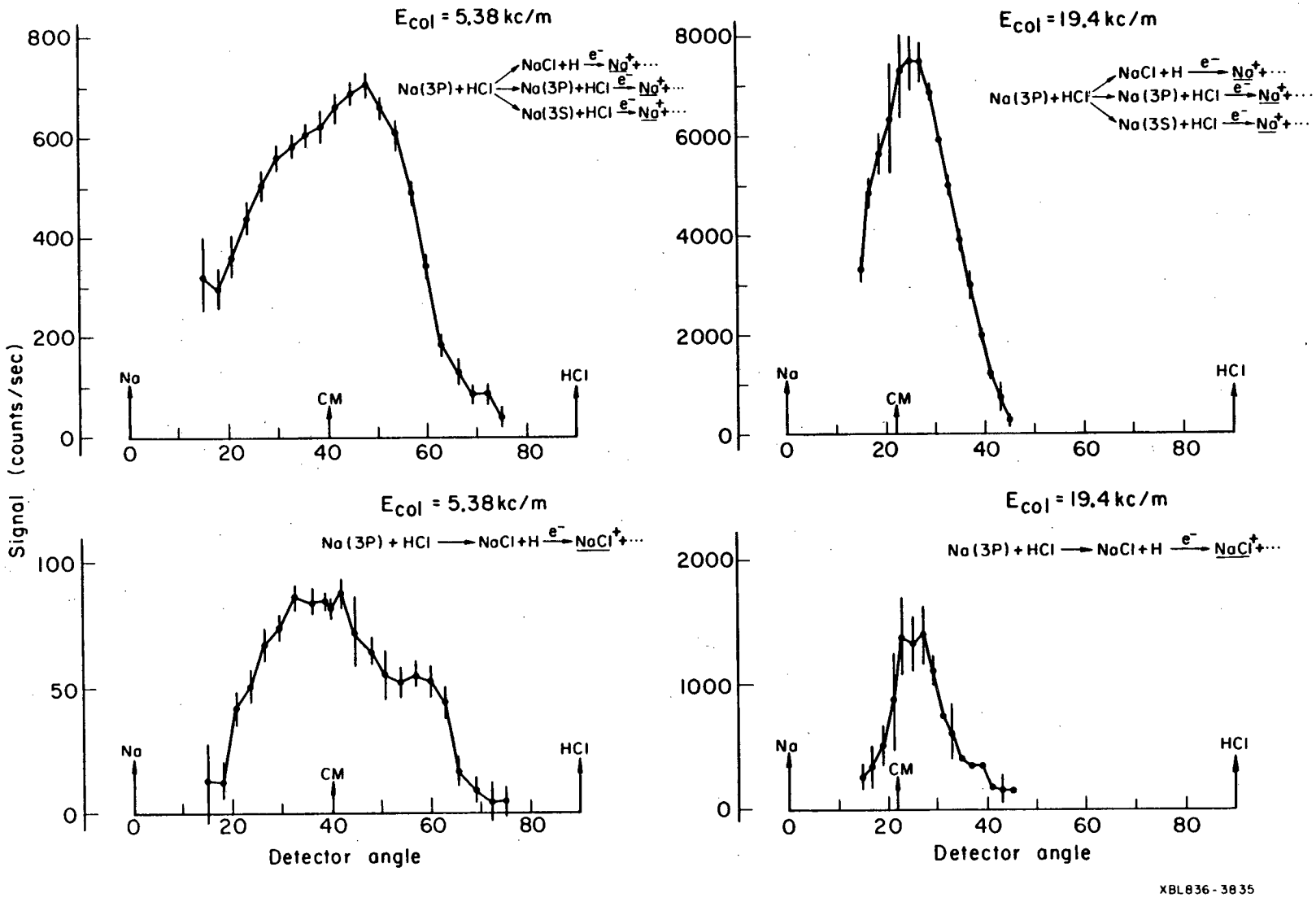
E_{col} = 5.38 kc/m
Na(3P)+HCl → NaCl+H $\xrightarrow{e^-}$ Na^++···
Na(3P)+HCl → Na(3P)+HCl $\xrightarrow{e^-}$ Na^++···
Na(3S)+HCl $\xrightarrow{e^-}$ Na^++···
E_{col} = 19.4 kc/m
Na(3P)+HCl → NaCl+H $\xrightarrow{e^-}$ Na^++···
Na(3P)+HCl → Na(3P)+HCl $\xrightarrow{e^-}$ Na^++···
Na(3S)+HCl $\xrightarrow{e^-}$ Na^++···
E_{col} = 5.38 kc/m
Na(3P) + HCl → NaCl+H $\xrightarrow{e^-}$ $NaCl^+$+···
E_{col} = 19.4 kc/m
Na(3P) + HCl → NaCl+H $\xrightarrow{e^-}$ $NaCl^+$+···
Signal (counts/sec)
Detector angle
Na
CM
HCl
XBL836-3835

Fig. 11

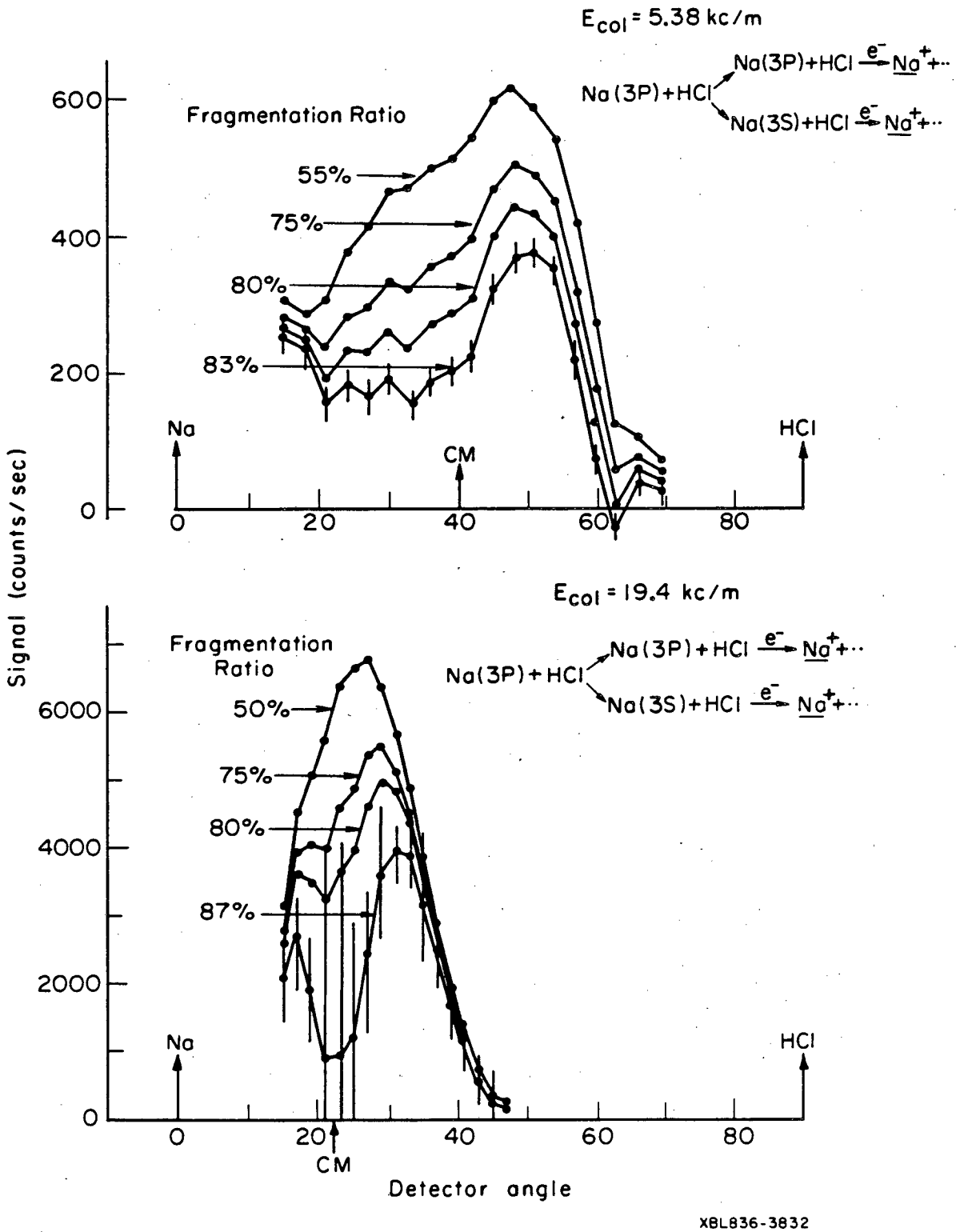
E_{col} = 5.38 kc/m
Na(3P)+HCl → Na(3P)+HCl $\xrightarrow{e^-}$ Na^++··
Na(3P)+HCl → Na(3S)+HCl $\xrightarrow{e^-}$ Na^++··
Fragmentation Ratio
55%
75%
80%
83%
Na
CM
HCl
0
20
40
60
80
0
200
400
600
Signal (counts/sec)
E_{col} = 19.4 kc/m
Fragmentation Ratio
Na(3P)+HCl → Na(3P)+HCl $\xrightarrow{e^-}$ Na^++··
Na(3P)+HCl → Na(3S)+HCl $\xrightarrow{e^-}$ Na^++··
50%
75%
80%
87%
Na
HCl
CM
0
2000
4000
6000
Detector angle
XBL836-3832

Fig. 12

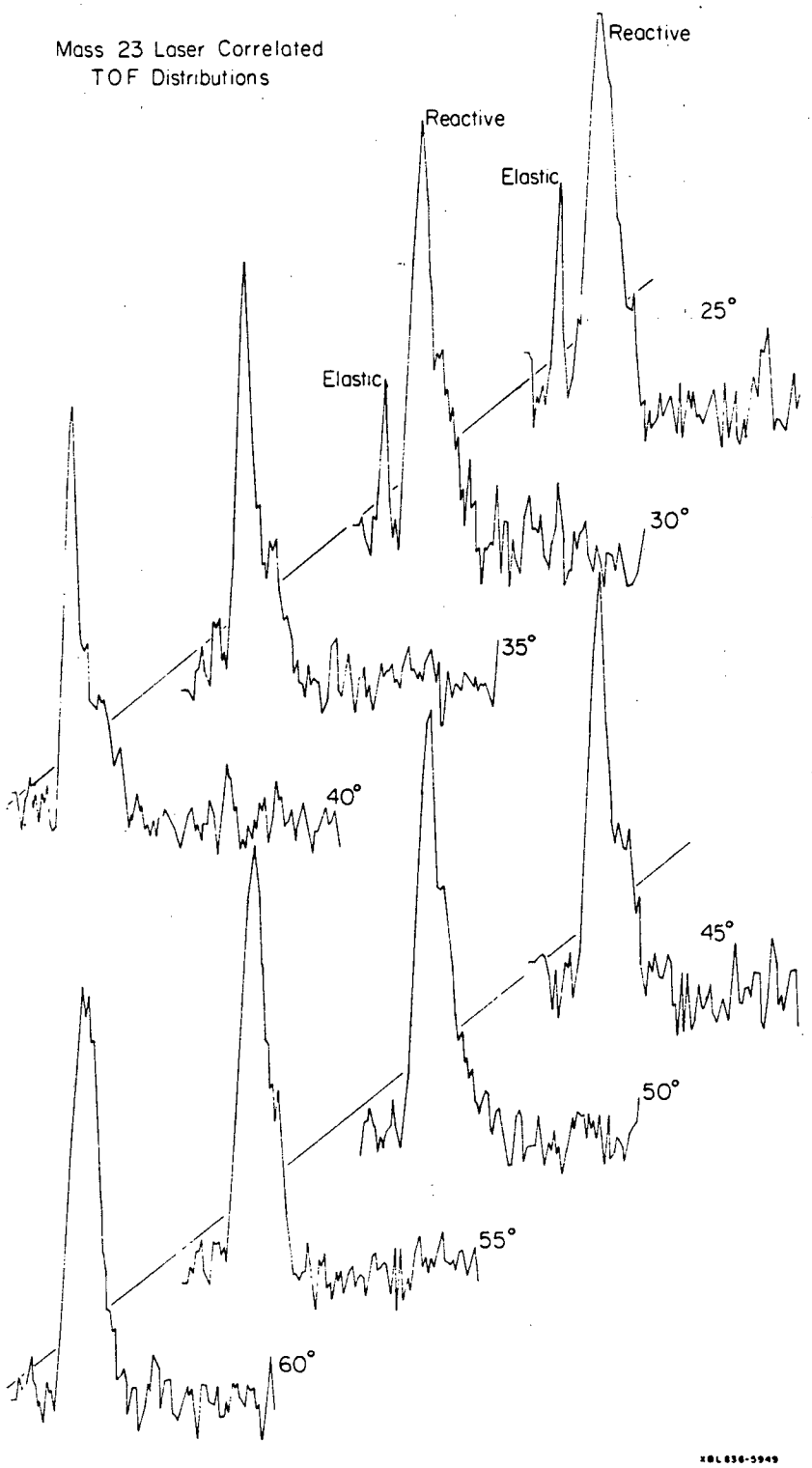
Mass 23 Laser Correlated
TOF Distributions
Reactive
Reactive
Elastic
Elastic
25°
30°
35°
40°
45°
50°
55°
60°
XBL 836-5949

Fig. 13

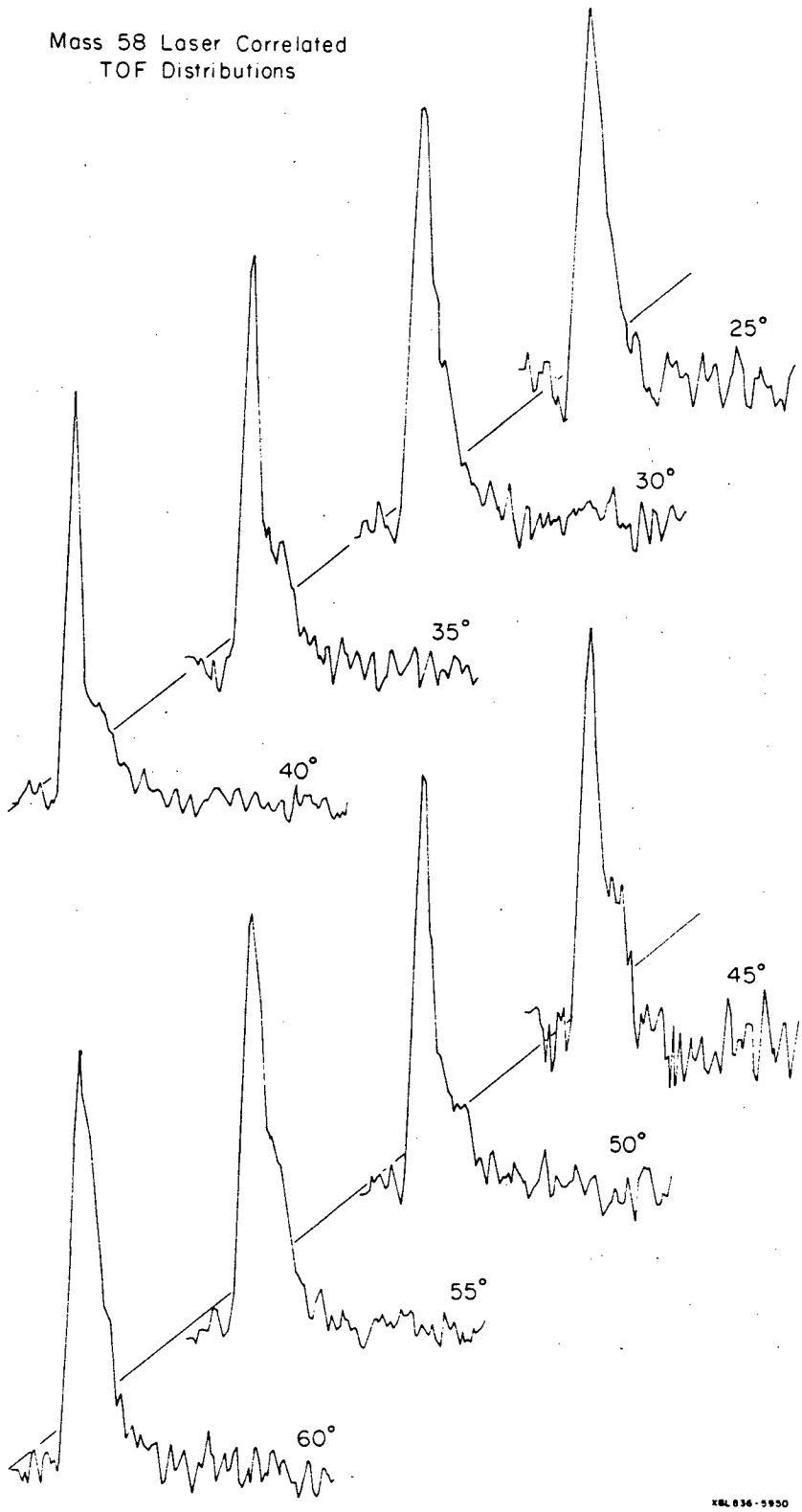
Mass 58 Laser Correlated
TOF Distributions
25°
30°
35°
40°
45°
50°
55°
60°
XBL 836-5950

Fig. 14

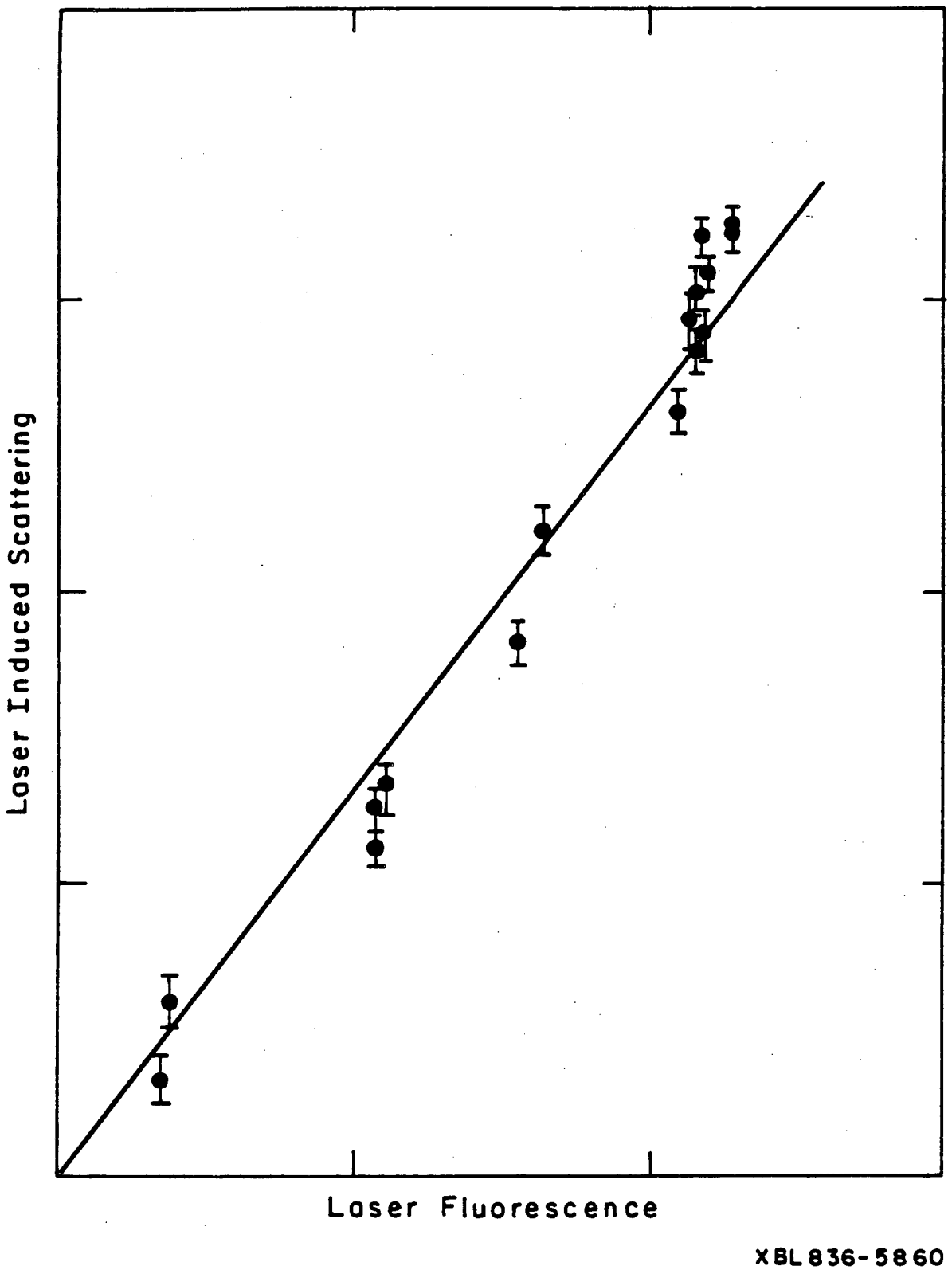

Fig. 15

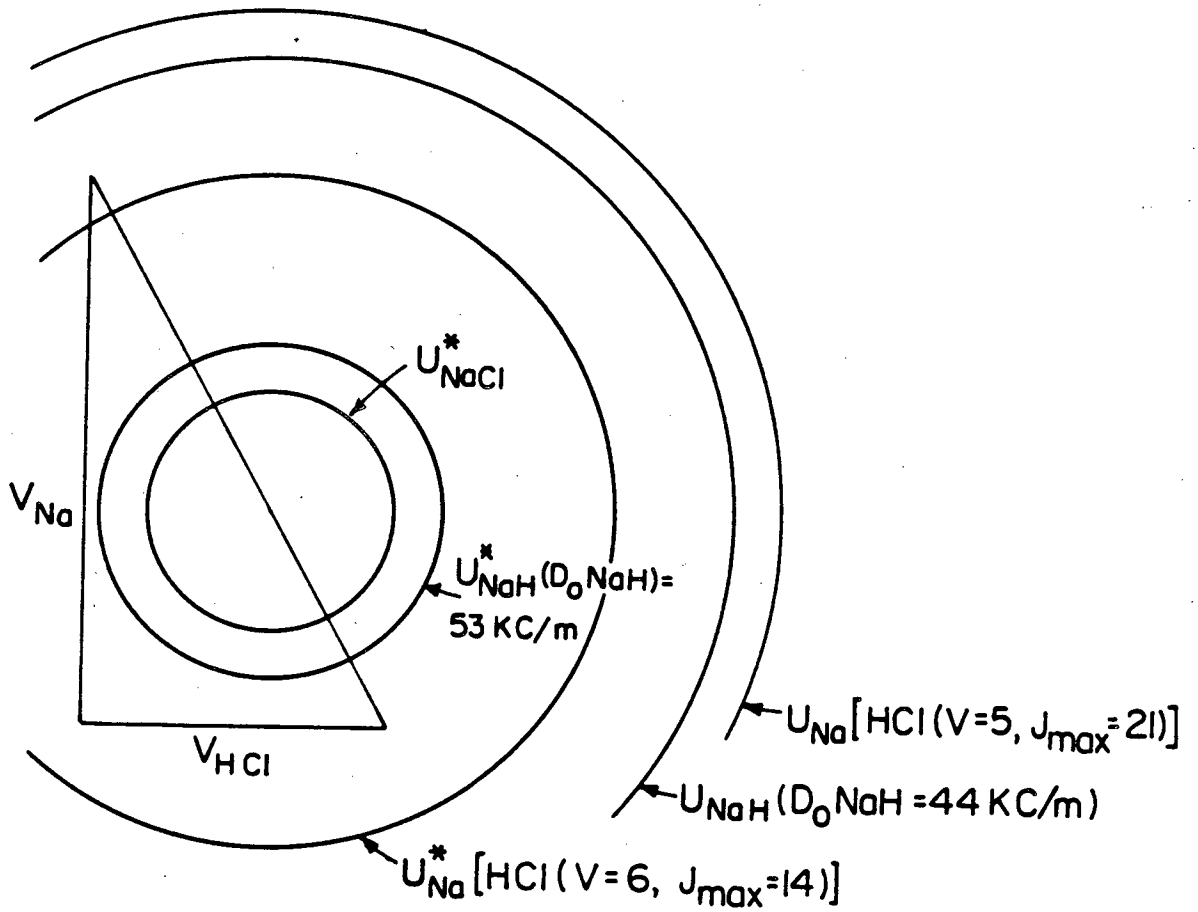

XBL 836-5947

Fig. 16

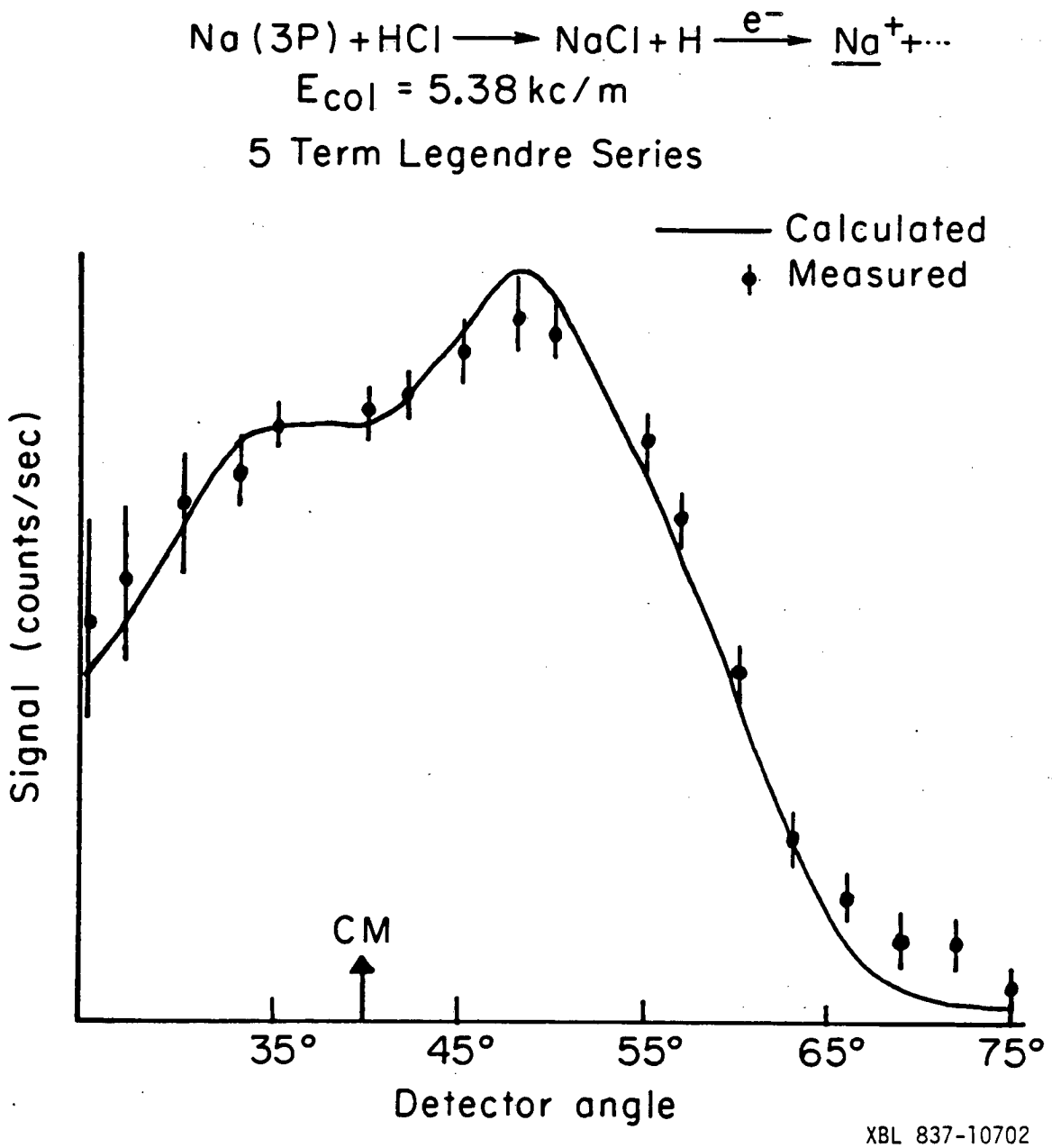
Na (3P) + HCl → NaCl + H $\xrightarrow{e^-}$ Na$^+$ + ···
E_{col} = 5.38 kc/m
5 Term Legendre Series
Calculated
Measured
Signal (counts/sec)
CM
35°
45°
55°
65°
75°
Detector angle
XBL 837-10702

Fig. 17

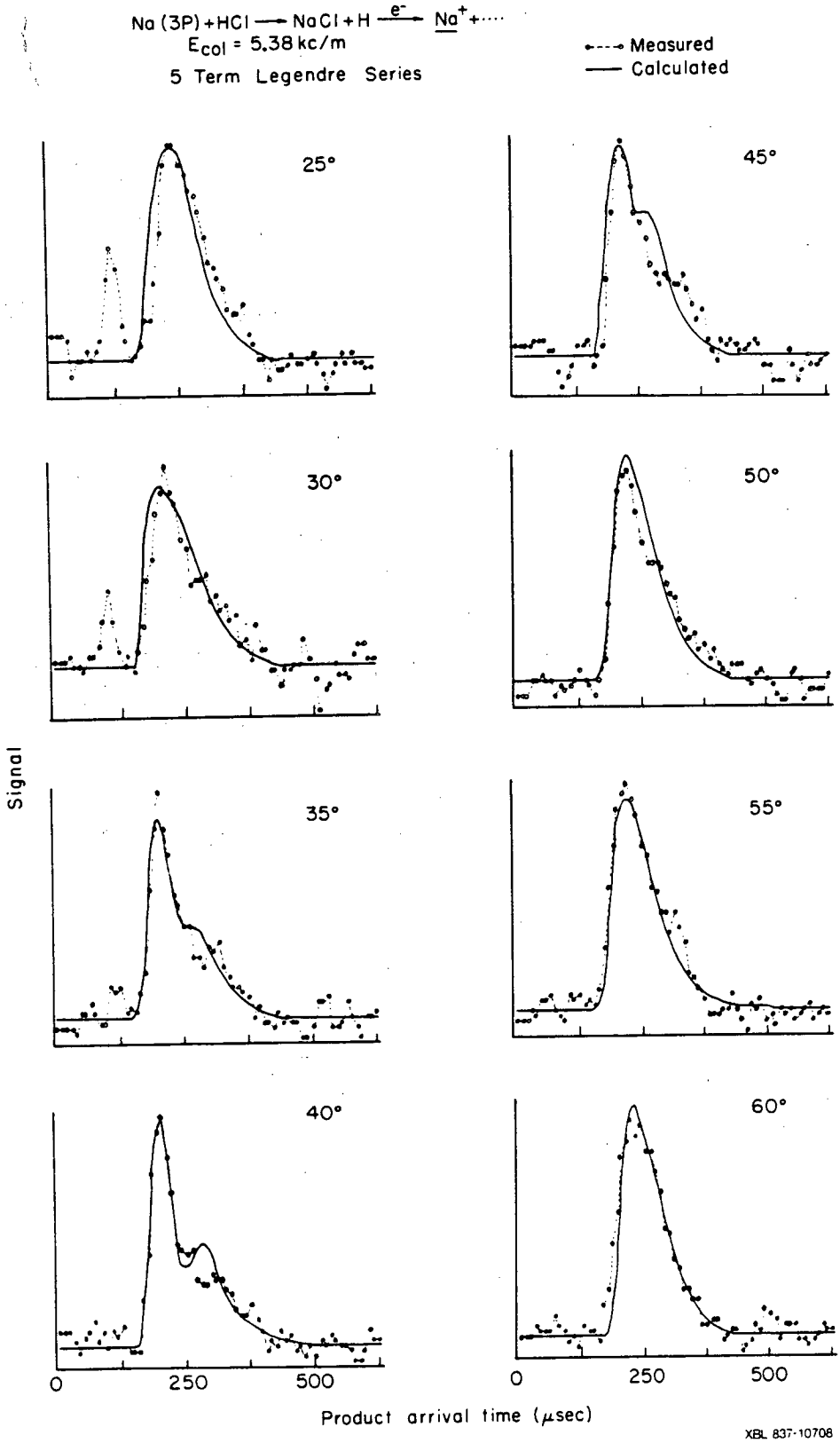
Na (3P) + HCl → NaCl + H $\xrightarrow{e^-}$ Na$^+$ + ...
E_{col} = 5.38 kc/m
5 Term Legendre Series
Measured
Calculated
25°
45°
30°
50°
35°
55°
40°
60°
Signal
0
250
500
0
250
500
Product arrival time (μsec)
XBL 837-10708

Fig. 18

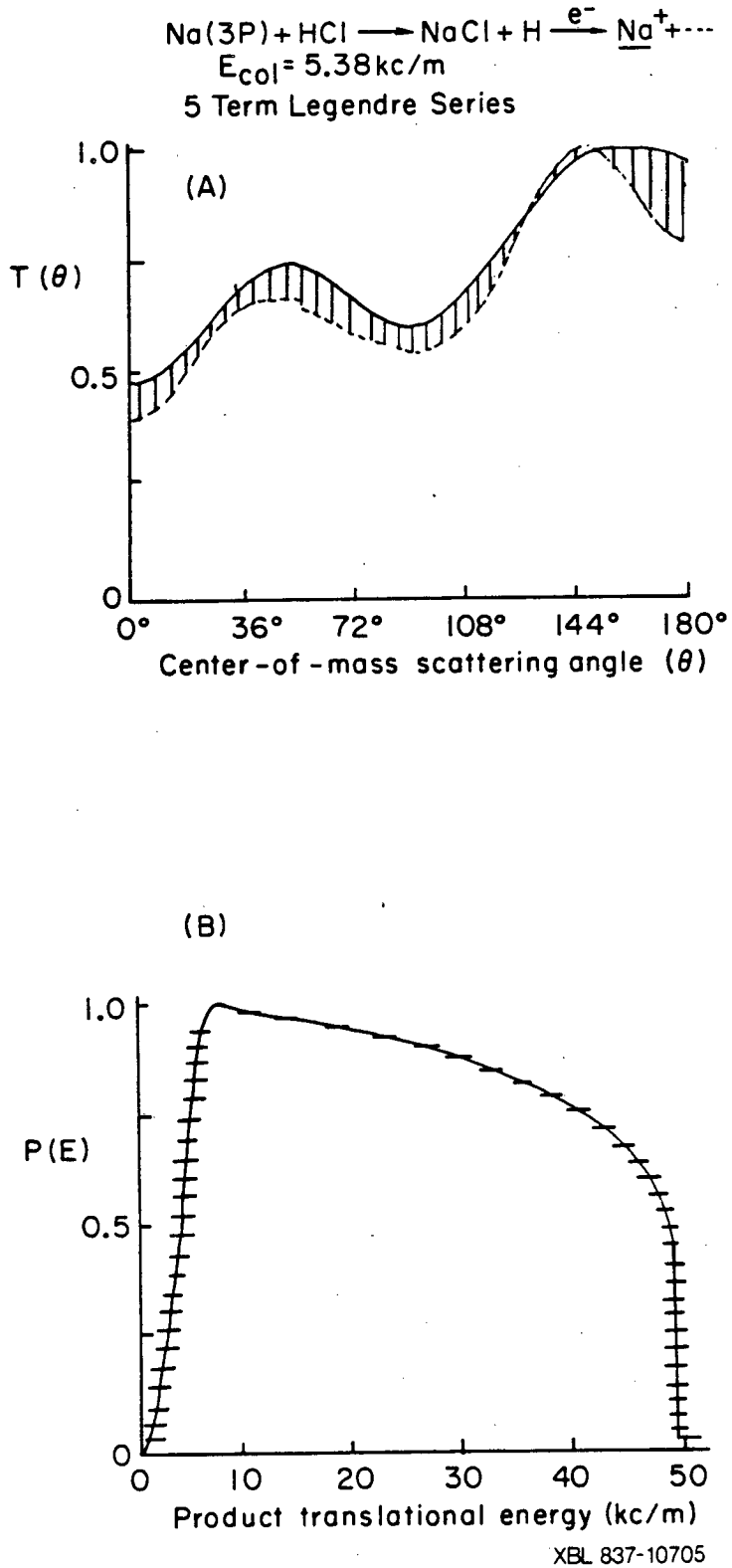
Na(3P) + HCl → NaCl + H $\xrightarrow{e^-}$ Na$^+$ + ···
E_{col} = 5.38 kc/m
5 Term Legendre Series
(A)
T (θ)
1.0
0.5
0
0°
36°
72°
108°
144°
180°
Center-of-mass scattering angle (θ)
(B)
P(E)
1.0
0.5
0
0
10
20
30
40
50
Product translational energy (kc/m)
XBL 837-10705

Fig. 19

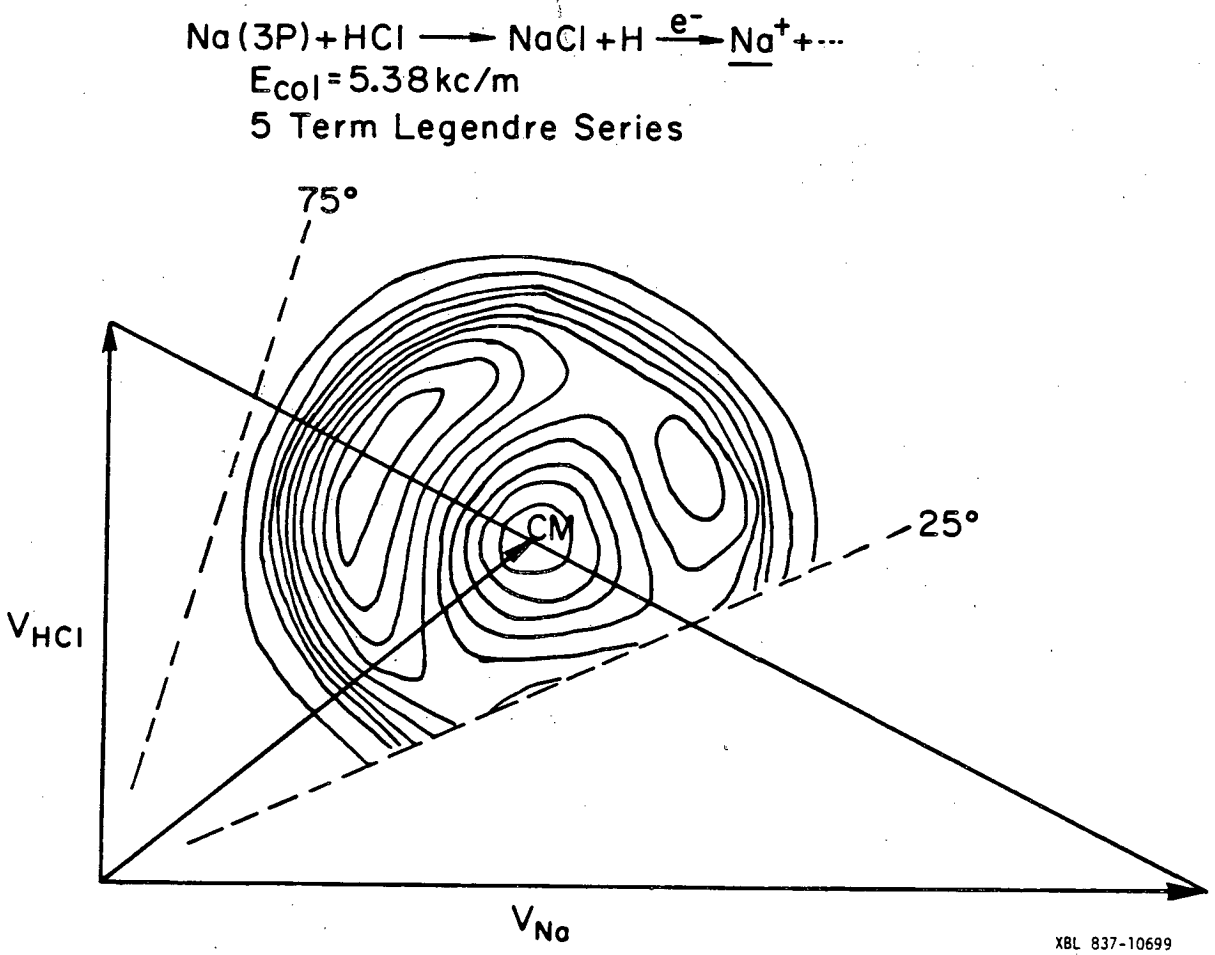
Na(3P)+HCl → NaCl+H $\xrightarrow{e^-}$ Na$^+$+···
E_{col}=5.38kc/m
5 Term Legendre Series
75°
25°
CM
V_{HCl}
V_{Na}
XBL 837-10699

Fig. 20

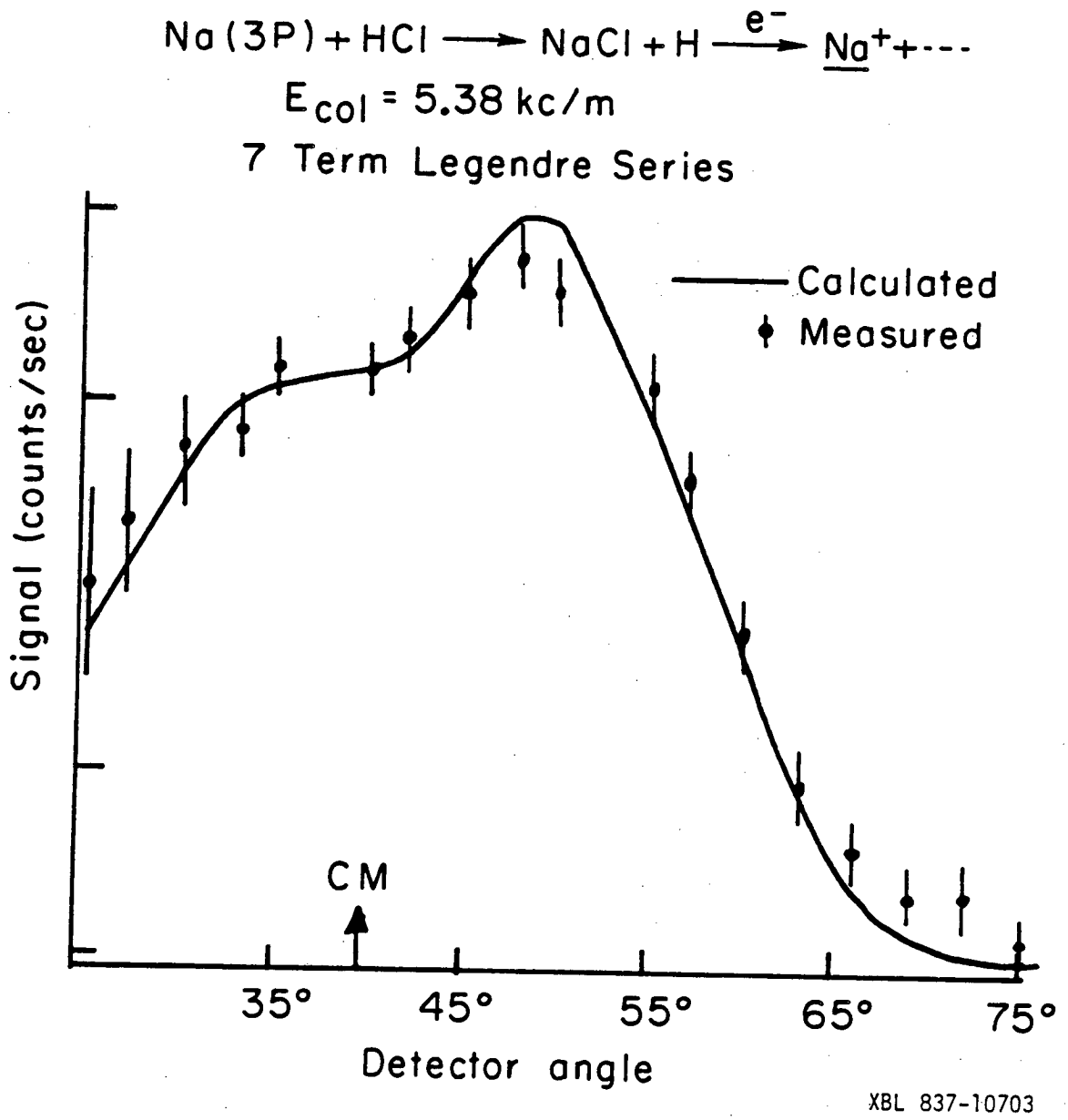
Na(3P) + HCl → NaCl + H $\xrightarrow{e^-}$ Na⁺+---
E_{col} = 5.38 kc/m
7 Term Legendre Series
Calculated
Measured
Signal (counts/sec)
CM
35°
45°
55°
65°
75°
Detector angle
XBL 837-10703

Fig. 21

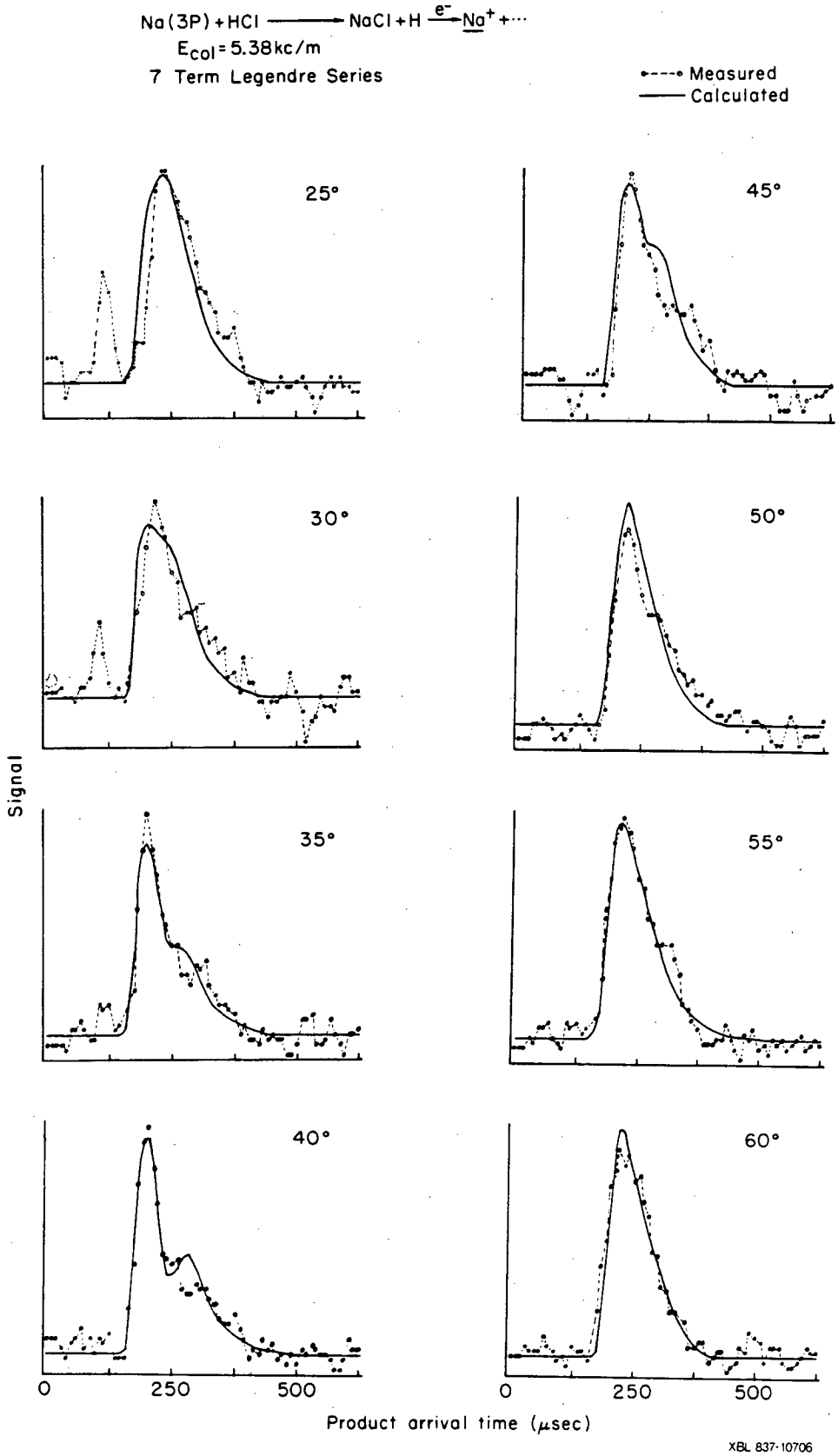
Na(3P) + HCl → NaCl + H $\xrightarrow{e^-}$ Na$^+$ + ···
E_{col} = 5.38kc/m
7 Term Legendre Series
Measured
Calculated
25°
45°
30°
50°
35°
55°
40°
60°
Signal
0
250
500
0
250
500
Product arrival time (μsec)
XBL 837-10706

Fig. 22

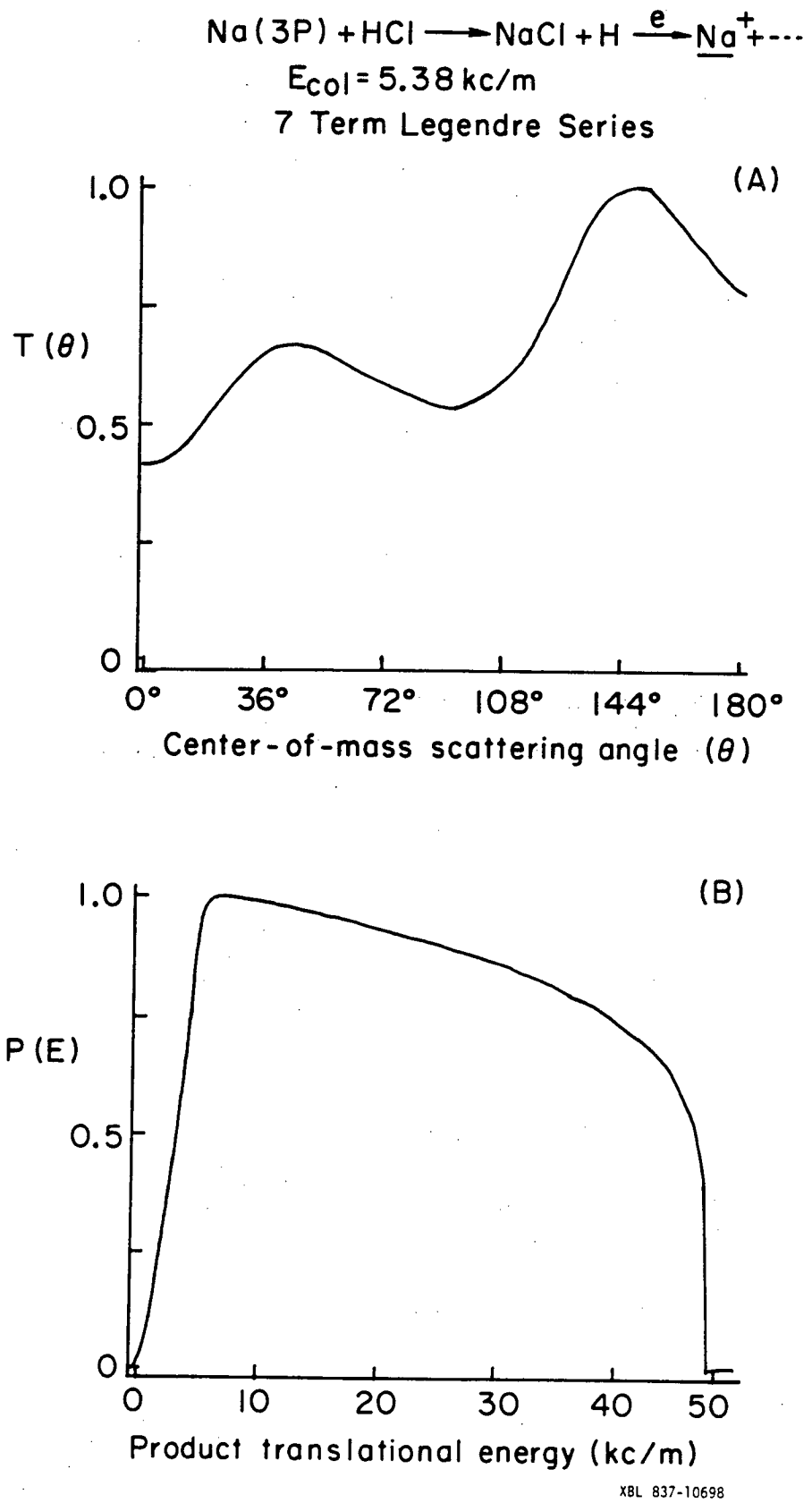
Na(3P) + HCl → NaCl + H $\xrightarrow{e}$ Na$^+$ + ---
E_{col} = 5.38 kc/m
7 Term Legendre Series
(A)
1.0
T (θ)
0.5
0
0°
36°
72°
108°
144°
180°
Center-of-mass scattering angle (θ)
(B)
1.0
P (E)
0.5
0
0
10
20
30
40
50
Product translational energy (kc/m)
XBL 837-10698

Fig. 23

$$Na(3P) + HCl \longrightarrow NaCl + H \xrightarrow{e^-} \underline{Na}^+ + \cdots$$

$E_{col} = 5.38$ kc/m

7 Term Legendre Series

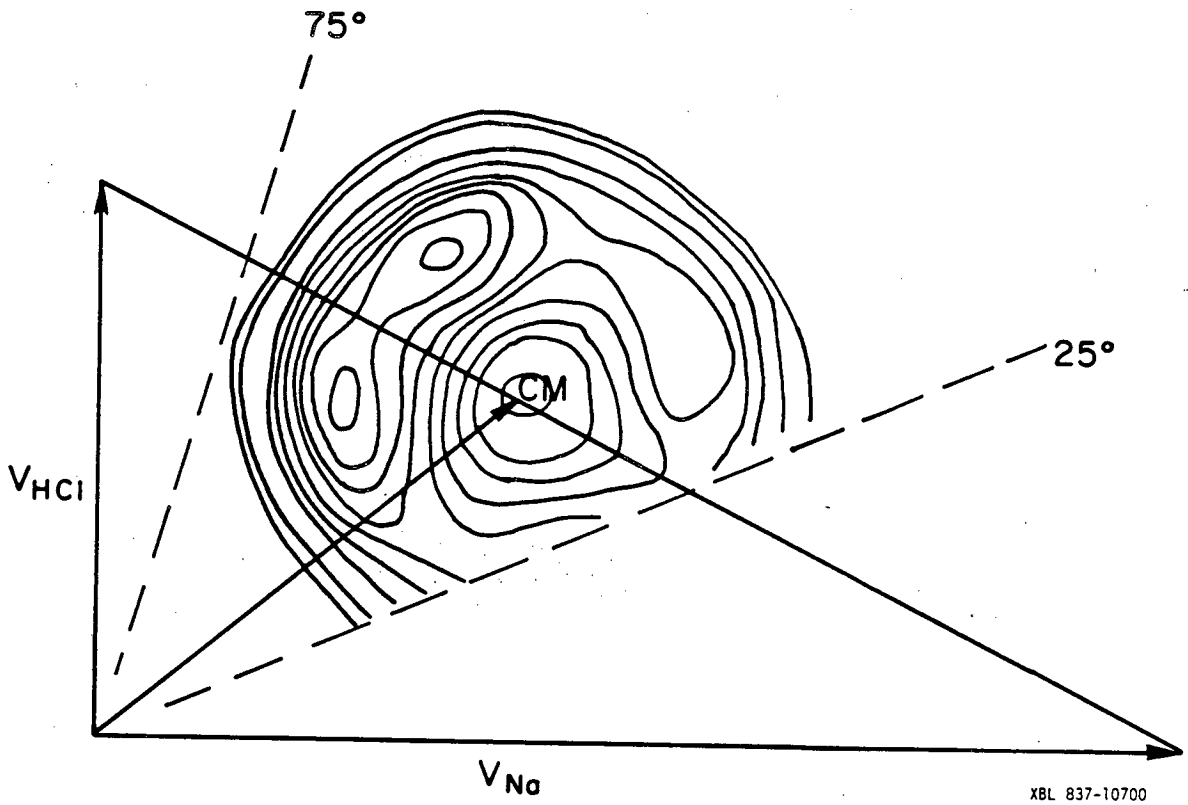

Fig. 24

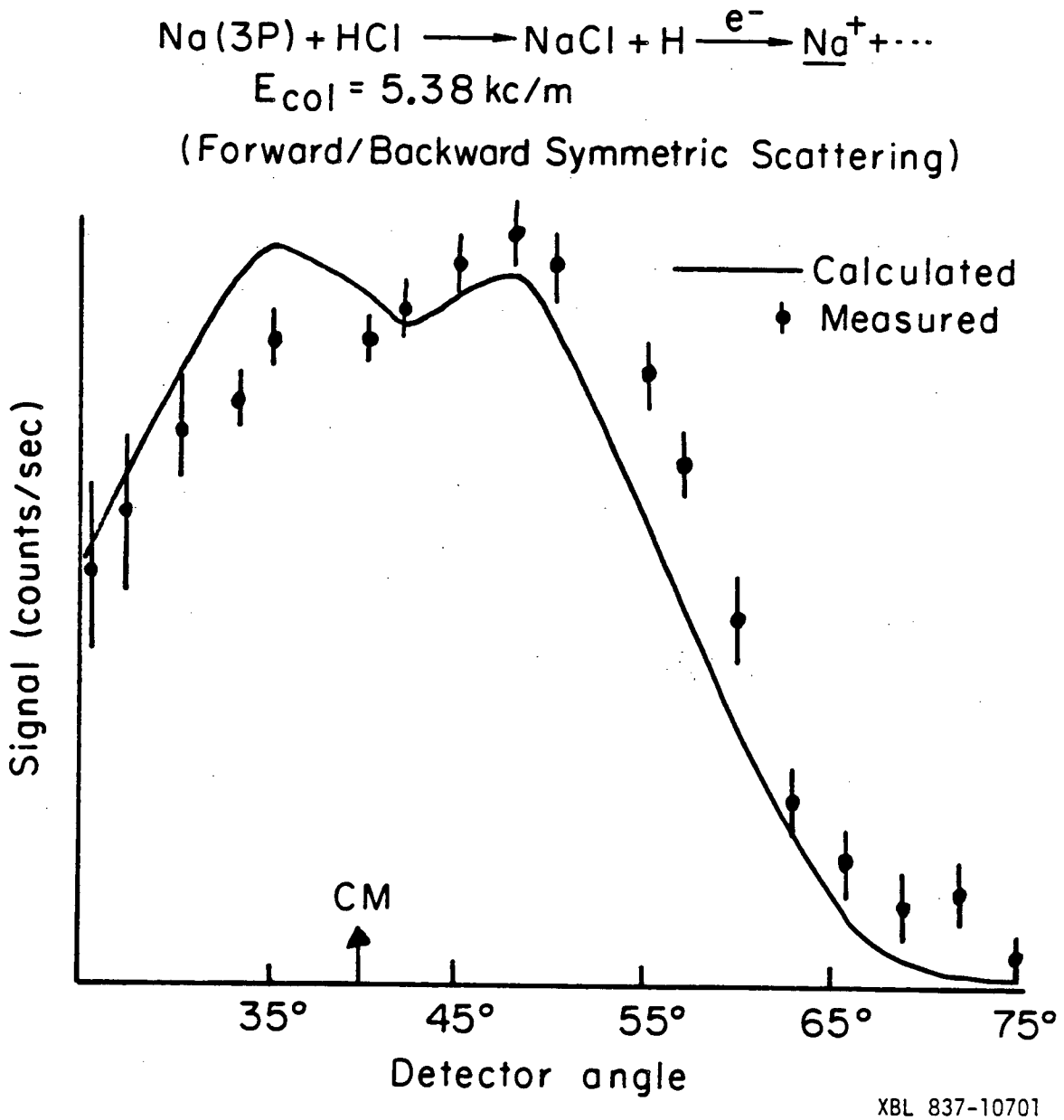
Na(3P) + HCl → NaCl + H $\xrightarrow{e^-}$ Na$^+$ + ···
E_{col} = 5.38 kc/m
(Forward/Backward Symmetric Scattering)
Calculated
Measured
Signal (counts/sec)
CM
35°
45°
55°
65°
75°
Detector angle
XBL 837-10701

Fig. 25

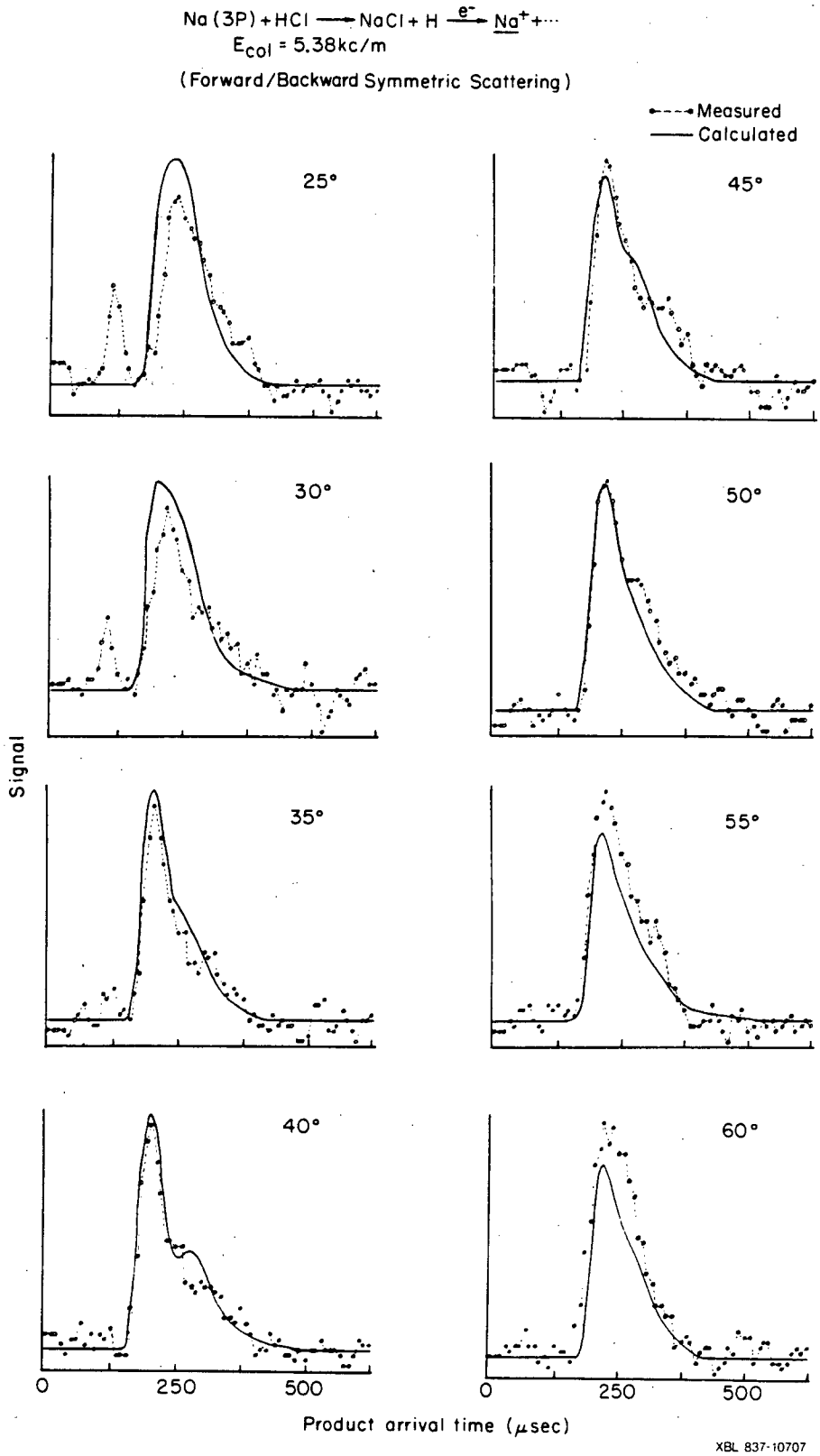
Na (3P) + HCl → NaCl + H $\xrightarrow{e^-}$ Na$^+$ + ···
E_{col} = 5.38kc/m
(Forward/Backward Symmetric Scattering)
Measured
Calculated
25°
45°
30°
50°
35°
55°
40°
60°
Signal
0
250
500
Product arrival time (μsec)
XBL 837-10707

Fig. 26

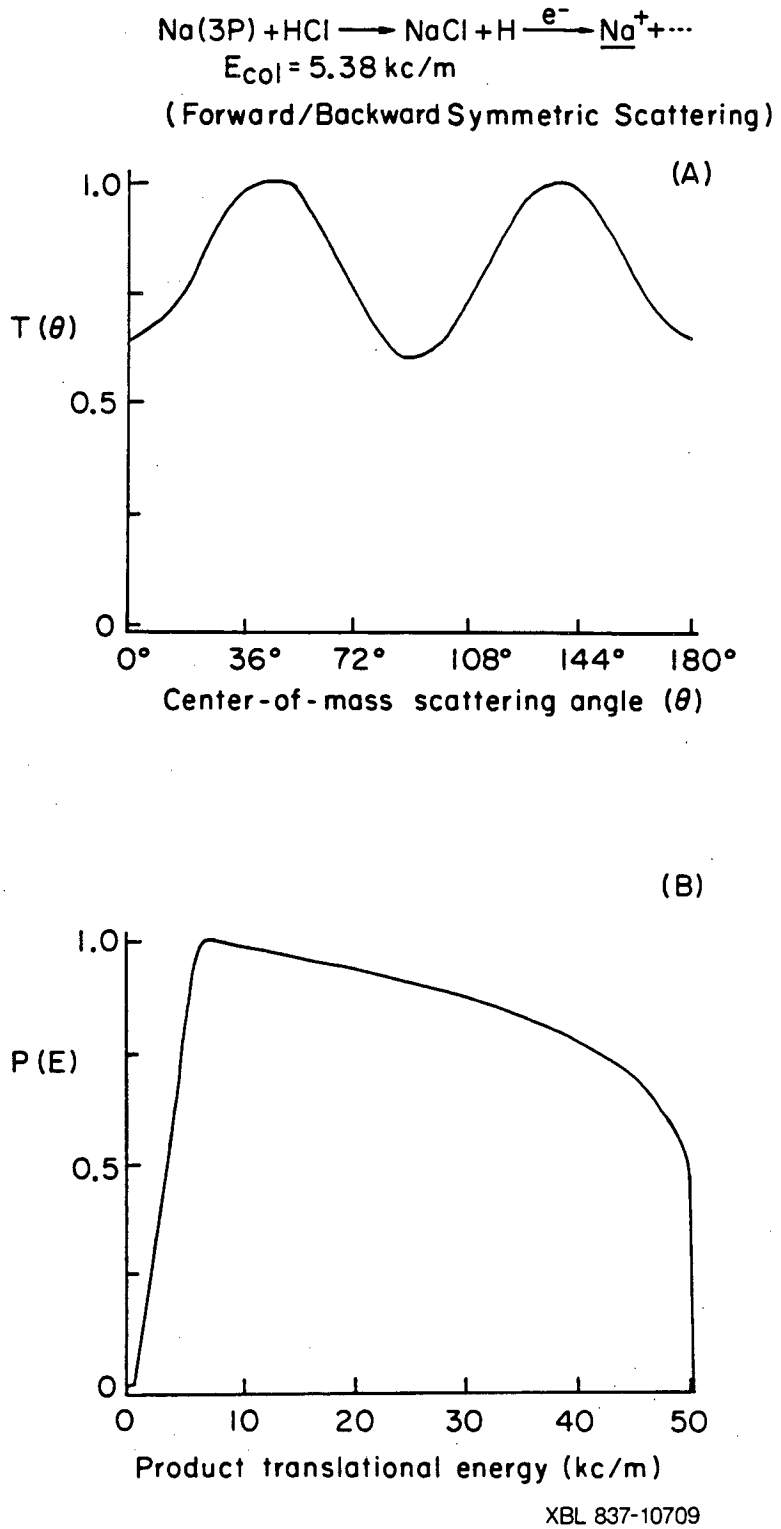
Na(3P) + HCl → NaCl + H $\xrightarrow{e^-}$ Na$^+$ + ···
E_{col} = 5.38 kc/m
(Forward/Backward Symmetric Scattering)
(A)
1.0
T (θ)
0.5
0
0°
36°
72°
108°
144°
180°
Center-of-mass scattering angle (θ)
(B)
1.0
P (E)
0.5
0
0
10
20
30
40
50
Product translational energy (kc/m)
XBL 837-10709

Fig. 27

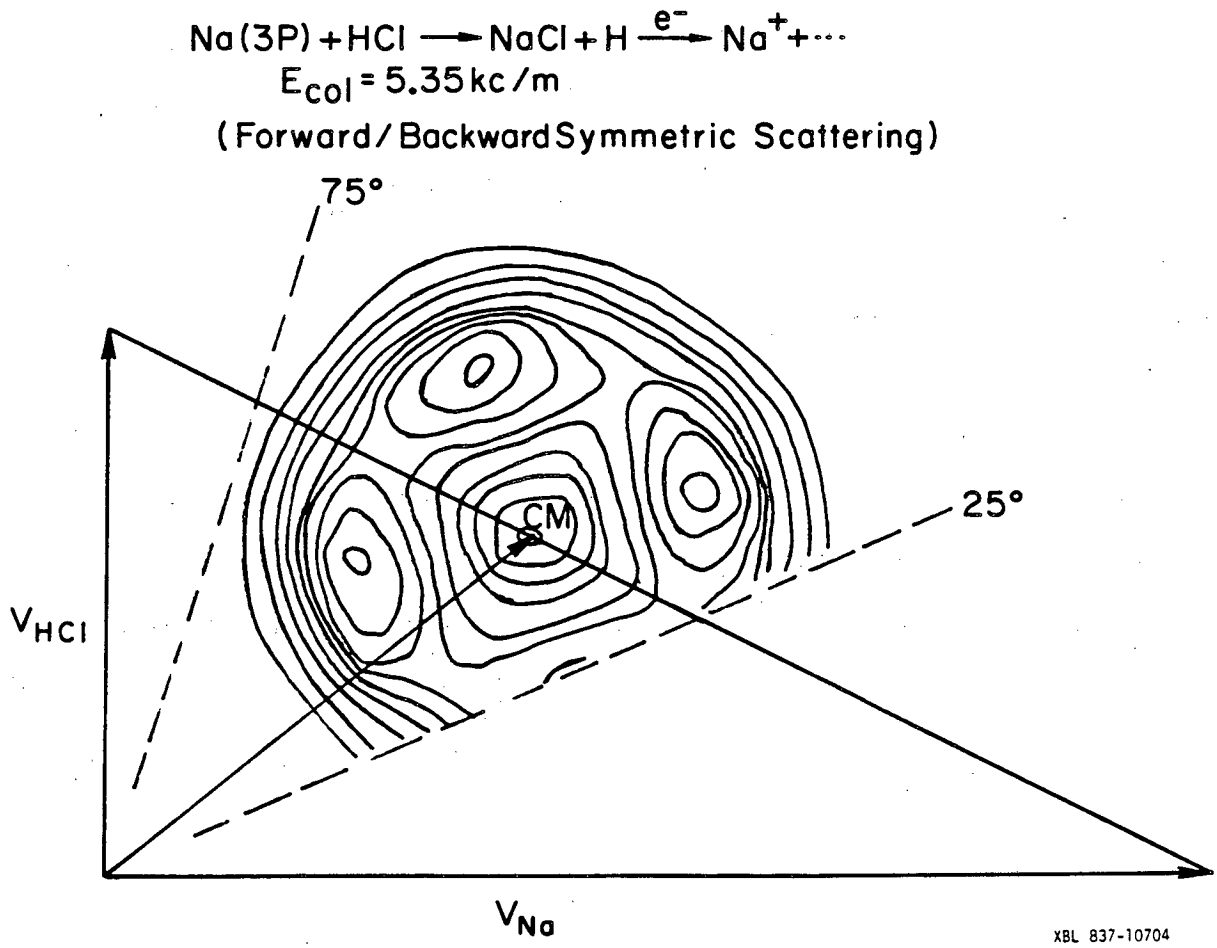
Na(3P) + HCl → NaCl + H $\xrightarrow{e^-}$ Na$^+$ + ···
E_{col} = 5.35 kc/m
(Forward/Backward Symmetric Scattering)
75°
25°
CM
V_{HCl}
V_{Na}
XBL 837-10704

Fig. 28

APPENDIX III. OPTICAL PUMPING STUDIES OF THE Li 2S→2P AND Na 3S→3P TRANSITIONS

A major problem in studying the collision dynamics of excited atomic states is the creation of a large fraction of the atoms in the excited state. Because most atoms have a multiplicity of hyperfine levels in the ground electronic state, a single laser frequency is unable to produce, in general, a steady state fraction of the atoms in the excited state. Usually, the excited state can decay by spontaneous emission to ground state hyperfine levels not resonant with the laser frequency. Consequently, after a few spontaneous emission cycles, initially resonant atoms will no longer be excited by the laser. The usable fraction of excited state atoms in the collision volume will be less than 1 percent.

To study excited state atom reactions for atoms other than sodium, it is necessary to develop optical pumping schemes matched to their ground state hyperfine structure. In this appendix, the results of a preliminary study of the feasibility of creating a steady state excited population of Li(2P) is presented. Lithium was chosen because its small number of electrons make its reactions attractive for *ab initio* electronic structure calculations of the reaction potential energy surfaces. Such calculations compare experimental results with basic theory, deepening the understanding of the collision process. As will be shown below, creating excited state Li atoms also represents the next stage in experimental complexity.

Let us begin by reviewing how sodium can be efficiently excited to

the $3^2P_{3/2}$ state. First, the transition intensity is strong and can be saturated with available cw lasers. Second, the frequency of the 3S$\longrightarrow$3P transition is near the peak of the rhodamine 6G dye emission curve. With readily obtained commercial laser hardware and a minimum of effort, the long term stability of the dye laser power and wavelength insured that this component of a molecular beam experiment is dependable. Third, by simply controlling the laser frequency, 30 percent of the sodium beam can be continuously excited when the transition is saturated. As discussed in Chapter 3, this was a consequence of the selection rules on the total angular momentum for spontaneous emission. When the 3S(F=2)$\longrightarrow$3P(F'=3) transition is excited, and the laser bandwidth and power broadening are less than the 3P(F'=2)-3P (F'=3) 65 MHZ splitting, an isolated, two-level system results

Now consider the example of optically pumping the $3^2P_{1/2}$ spin orbit level. Figure 1 shows the level structure for this transition. If the laser were tuned to excite the F=2$\longrightarrow$F'=1 transition, and the light linearly polarized, the $|M|=2$ magnetic sublevels of the F=2 ground state would not be excited to the F'=1 level because of the selection rule $\Delta M=0$. However, spontaneous emission connects the $3^2P_{1/2}$ (F'=1), $|M|=1$ magnetic sublevels to these "dark," $3^2S_{1/2}$ (F=2),$|M|=2$ magnetic sublevels. Consequently, after a very few spontaneous emission cycles, all of the atoms would be in the $3^2S_{1/2}$ (F=2),$|M|=2$ sublevels, <u>even</u> if there were no spontaneous decay to the $3^2S_{1/2}$ (F=1) ground state hpf level.

Let us then suppose that <u>both</u> the $3^2S_{1/2}$ (F=1,2)$\longrightarrow 3^2P_{1/2}$ (F'=2) transitions are pumped with two linearly polarized lasers. In this

case, the $3^2S_{1/2}$ (F=2),M=0 magnetic sublevel is a trap because it has no transition moment to the $3^2P_{1/2}$ (F'=2) state for linearly polarized light. An additional laser, tuned to the $3^2S_{1/2}$ (F=2)$\rightarrow 3^2P_{1/2}$ (F'=1) transition, is needed. In this manner, one can show that no combination of two laser frequencies of circular or linear polarization can optically pump a steady fraction into the $3^2P_{1/2}$ spin orbit state.[1]

Pritchard[2] has suggested that the application of a weak magnetic field perpendicular to the laser polarization axis is sufficient to remove the M=0 trap. (The Larmour precession frequency, if fast on the time scale of a few spontaneous emission cycles, will mix the M sublevels and stop population accumulation in the M=0 sublevel). In a scattering experiment with Na + Ar[2], a 17 percent reduction in the scattered Na intensity was observed when two laser frequencies were used to excite the $3^2P_{1/2}$ spin orbit state. This was taken as a measure of the fraction of sodium atoms pumped. To create the two frequencies, a molecular beam of sodium atoms was crossed nonorthogonally by a laser beam which was reflected upon itself. These two counterpropogating laser beams, if the angle between the laser and molecular beams is chosen correctly, are doppler shifted by the ground state hpf splitting of 1.77 Ghz, and for some fraction of the atomic beam, the two resonance conditions are met.

The above problem for optical pumping of the $3^2P_{1/2}$ spin orbit level was a consequence of the upper level having less than or equal total angular momentum than the ground state levels, and integral values for the total angular momentum. An additional problem, coherence trapping, can arise when two ground states are connected to a common

upper level by resonant cw radiation <u>even if there are no magnetic sublevel traps</u>. Much theoretical work on coherence trapping has recently appeared,[3-6] as well as some experimental verification.[3,7] Figure 2a shows the three state level structure called a lamda system. If two monochromatic resonant fields are used to pump both ground states to the excited state, and both are at resonance, then it can be shown that the steady state population in the upper state is zero.[3] The two laser fields create a coherence between the two ground state levels, such that the phases between the ground state amplitudes in the complete wavefunction uncouples the system from the driving fields. An alternative view shows that the system executes Raman transitions between the two ground state levels, with the excited level acting as a virtual state.

In an experiment, before the atoms enter the laser fields, there is no coherence between the two ground states. In the presence of the laser fields, two new ground basis states can be formed which are linear combinations of the original states. One of these states is coupled, the other uncoupled, from the laser fields.[3] As spontaneous decay occurs, the atoms in the optically coupled state are continuously depleted. Two laser frequencies are no better than one in producing a steady state excited population.

A theoretical study of the effects of laser bandwidth and detuning for a three level lamda system driven by two laser fields has been reported by Knight.[5] In particular, he examined the effects of phase correlation between the two laser fields on the coherence trapping. The individual laser fields were allowed to have phase fluctuations,

but the field amplitudes (and Rabi frequencies) were assumed constant. In this model, the constant field amplitude approximation enables a final separation of the atomic variables from the field equations. With the inclusion of uncorrelated fluctuations for each of the applied fields, the coherence trapping is reduced by the off-resonant frequency components from the fluctuating phases. If, however, both fields are critically cross-correlated, that is, the phase fluctuations between the two fields are dependent, then the coherence trapping is preserved, even in the presence of the fluctuations from the individual fields.

In this appendix, the model developed by Knight is extended to consider the asymptotic state distributions for a three level lambda system driven by two nearly resonant, phase fluctuating laser fields with variable cross-correlation. This model is applied to experimental observations of fluorescence and ionization yields when the ^{6}Li isotope is optically pumped by two, cw, single-mode optical fields, one derived from the other by acousto-optic modulation. The acoustic modulation frequency is set equal to the $2^2S_{1/2}$ (F=1/2)-(F=3/2), 228 Mhz hpf splitting. The modulator stability is quite high, and since the two frequencies are derived from the same laser, they have precisely the same phase fluctuations. In this way, the two laser fields have a fixed frequency difference which is independent of the laser bandwidth, i.e., they are critically cross correlated. The hyperfine structure of the ^{6}Li, $^2P_{3/2}$ level is shown in Fig. 2(b). Unlike ^{23}Na, the ^{6}Li hyperfine structure is overlapped within the 6 Mhz radiative linewidth. A single mode, single frequency dye laser is unable to create a steady state $^2P_{3/2}$ population, as spontaneous emission will connect the

overlapped $^2P_{3/2}$ levels with both ground state hyperfine levels. However, ^6Li, with half integral total angular momentum, has no M level traps and the Li(2S-->2P) transition is located near the maximum of the DCM dye laser emission. Experimentally, sufficient laser power (80 mW) and stability are readily obtained such that if the intrinsically overlapped excited state hyperfine structure and coherence trapping problems can be solved, ^6Li $^2P_{3/2}$ scattering experiments should be straightforward.

We now derive the steady state populations of a three level lamda system, beginning with the optical Bloch equations obtained by Knight and Dalton.[5] These equations were derived from a quantized treatment of the laser fluctuations, which are modeled as a stochastic process. The Bloch equations were obtained by using a reduced density matrix for the atom-laser system, making the usual rotating wave approximation. Lamb shifts of the atomic levels and the variation of the Rabi frequency with the laser coherent states (field amplitudes) are ignored. As we are only concerned with the atomic level populations, irrespective of the state of the laser field, the Bloch equations reduce to a simple set of linear coupled differential equations with constant coefficients.

For the time independent solution to these equations, we follow the method of Stroud.[8] For ease of computer calculation, we also redefine the off-diagonal density matrix elements into their real and imaginary parts. Additionally, we define two new diagonal elements which are the sum and difference of the populations in the two ground

state levels. As noted by Stroud, the nine differential equations for the density matrix elements are dependent when the time derivative is set to zero. We reduce this to a non-singular set of equations, by defining new variables which are the old variables divided by the sum of the populations in the two ground states. This sum is never zero. The equation involving the sum variable is discarded. The solution is easily provided by available software. The actual equations are given by Eq. (1). In Eq. (1), γ_{12} and γ_{10} are the spontaneous decay rates from level 1 to levels 2 and 0, respectively, δ_a and δ_b are the detunings from resonance for the fields a and b, ζ_a and ζ_b are the Rabi frequencies for the two laser fields, Δ_{aa} and Δ_{bb} are the uncorrelated phase fluctuation bandwidths for the fields a and b, and Δ_{ab} is the cross-correlated bandwidth. D is the difference between the two ground state populations normalized to their sum i.e., $D = (\sigma_{22}-\sigma_{oo})/(\sigma_{22}+\sigma_{oo})$. R_{ij} and I_{ij} are the real and imaginary off-diagonal density matrix elements, normalized to the two ground state populations, viz,

$$R_{ij} = \frac{\sigma_{ij}+\sigma_{ji}}{2(\sigma_{00}+\sigma_{22})} \quad , \quad I_{ij} = \frac{\sigma_{ij}-\sigma_{ji}}{2(\sigma_{00}+\sigma_{22})} \quad . \tag{2}$$

Finally, $\sigma_{11}' = \sigma_{11}/(\sigma_{00}+\sigma_{22})$, where σ_{11} is the excited state population.

Figure 3 shows the dependence of the excited state population on the detunings from resonance of each of the fields, on the Rabi frequencies of the applied fields, and on the amount of cross-

$$
\begin{bmatrix}
0 & \left(\frac{\gamma_{12}-\gamma_{10}}{2}\right) & -\zeta_{a/2} & 0 & 0 & \zeta_{b/2} & 0 \\
0 & -(\gamma_{10}+\gamma_{12}) & -\zeta_{a} & 0 & 0 & 0 & 0 \\
\zeta_{a/2} & \zeta_{a/2} & -\left(\Delta_{aa} + \left(\frac{\gamma_{10}+\gamma_{12}}{2}\right)\right) & -\delta_{a} & 0 & 0 & 0 \\
0 & 0 & \delta_{a} & -\left(\Delta_{aa} + \left(\frac{\gamma_{10}+\gamma_{12}}{2}\right)\right) & -\zeta_{b/2} & 0 & 0 \\
0 & 0 & \zeta_{b/2} & 0 & -(\delta_{a}+\delta_{b}) & \zeta_{a/2} & 0 \\
0 & 0 & 0 & \zeta_{b/2} & -(\Delta_{aa}+\Delta_{bb}-2\Delta_{ab}) & 0 & \zeta_{a/2} \\
-\zeta_{b/2} & \zeta_{b/2} & 0 & 0 & 0 & -\left(\Delta_{bb} + \frac{\gamma_{10}+\gamma_{12}}{2}\right) & -\delta_{b} \\
0 & 0 & 0 & 0 & -\zeta_{a/2} & \delta_{b} & -\left(\Delta_{bb} + \frac{\gamma_{10}+\gamma_{12}}{2}\right)
\end{bmatrix}
\begin{bmatrix} D \\ \sigma_{11}' \\ R_{01} \\ I_{01} \\ R_{02} \\ I_{02} \\ R_{12} \\ I_{12} \end{bmatrix}
=
\begin{bmatrix} 0 \\ 0 \\ \zeta_{a/2} \\ 0 \\ 0 \\ 0 \\ \zeta_{b/2} \\ 0 \end{bmatrix}
\qquad (1)
$$

correlation between the two laser fields. The unit of frequency is taken as the total spontaneous emission rate from the excited state.

The experimental configuration of Fig. 4 was used to investigate the optical pumping of Li. A similar study was done by Baum, et al.[9] In the present experiment, a heated tantalum oven, similar to that used in a previous molecular beam study,[10] creates a Li atomic beam which is illuminated at right angles by two, coaxial cw laser beams, of spot size 2mm. The two frequencies were obtained by passing the output of a commercial single mode dye laser (operating with DCM dye and tuned to the 2S$\longrightarrow$2P transition at 6709 angstroms), through a commercial acoustic-optic modulator (Intra-Action) set for the 228 MHZ ground state hpf splitting. The applied frequency was measured with a microwave counter. The two frequencies were recombined on a Glan-Thompson prism by rotating the polarization of one of the beams. The beams were made coaxial by overlapping them at two points separated by thirty feet, with the molecular beam intersection point approximately midway between the alignment points. The beams are linearly polarized, with their polarizations at right angles to each other. The power in each beam could be adjusted with filters, and the frequency shift changed over the range 200-230 MHZ with the acoustic-optic modulator. The laser bandwidth was estimated using a scanning Fabrey-Perot with 1.5 GHZ FSR, finesse 200, and found to be less than 10 MHZ.

Measurements consisted of monitoring the fluorescence from the illumination zone and scanning the dye laser frequency. The fluorescence is proportional to the excited state population. As the laser

is scanned, the absolute frequency is not recorded, so the position of maximum fluorescence relative to the transition resonance is not known. To compare with the calculations, we use the maximum seen during the frequency scan. Figure 5 shows typical fluorescence scans with and without the second laser beam. As the fluorescence is polarized, and the photomultiplier views only a small solid angle of the total emission, and the two laser beam's polarizations are orthogonal, the fluorescence induced by each laser is not detected with equal efficiency.

The results of the experiments show that the expected increase from the presence of the second laser was not realized. Given the Li atom velocity and the laser beam diameter, the atoms spend approximately 50 spontaneous lifetimes in the laser beam. If the second beam was able to saturate the three level system as expected, the fluorescence should have increased by at least one order of magnitude. Instead, only a 50 percent non-additive increase was observed. The model calculations would explain this (assuming the maximum possible cross-correlation was present between the two fields) if the laser power in one beam was sufficient to pump both transitions. In Fig. 3, the population in the upper level is shown for different laser powers assuming that only one field drives the transitions. The calculations, with cross-correlation, show that at high power, both the one and two frequency experiments are able to excite near the maximal fraction. However, the two frequency case is ten times more efficient at low powers. In the experiments, no improvement was seen with the second laser frequency at lower powers.

To understand the deviations of the observations from the model predictions, we reconsider the assumptions of the optical pumping model which would invalidate the predictions we have made. First, the model calculations assume that the power broadening is not commensurate with the ground state hpf splitting. This is definitely not the case at the high powers of some of the experiments. In particular, see Fig. 5(a). Second, the phase fluctuation model also predicts a Lorentzian laser lineshape which overestimates the power in the wings of the laser line. The result of this error is to overestimate the effectiveness of the off-resonance pumping. Third, we have assumed the two laser frequencies are critically cross correlated. The experimental results appear closer to the uncorrelated model calculations. If this were the case, the excited state population would be substantial. Finally, the approximation of the ^{6}Li, $^2S_{1/2}$(F=1/2, 3/2)$\rightarrow$$^2P_{3/2}$(F=5/2, 3/2, 1/2) level structure as a 3 level lamda system is also incorrect. Instead, there are 18 levels, with several sets of inter-connected lamda systems. The presence of the other, slightly non-degenerate, F levels in the $^2P_{3/2}$ state may effectively dephase the coherence in the individual lamda systems, in effect, uncorrelating the laser fields. A more elaborate density matrix treatment is necessary, incorporating all m sublevels, to ascertain the importance of this approximation.

To check the hypothesis that the three level system was already saturated by one strong field, a second set of experiments was done using a pulsed dye laser in addition to the optical pumping laser. To measure the excited state population without resorting to relative

fluorescence yields, we chose to ionize the 2P population by resonant multi-photon ionization through the 3D intermediate state as outlined by Payne.[11] The pulsed laser, of 10 nanosecond duration, takes a "snapshot" of the $2^2P_{3/2}$ population. If this ionization step can be saturated, then the ion yield, as a function of the parameters of the optical pumping cw laser, will provide us with the required information about our pumping scheme.

As an absolute calibration, the pulsed laser can be used to ionize the ground state by the sequence Li (2S)$\rightarrow$3P$\rightarrow$$Li^+$ + e-. The 2S$\rightarrow$3P photon is obtained by doubling pulsed, visible light. The residual pulsed visible light is sufficiently energetic to ionize the 3P state. If the ion yield can be saturated with respect to both the visible and doubled wavelengths, then the ion yield from the ground state ionization scheme will measure the density of Li atoms at the crossing of the cw laser. Comparing the ion yield for the ground and excited states will provide directly the fraction pumped.

The ground state signal was ionized and saturated, as shown in Fig. 6. However, no significant signal was seen from the excited state (i.e., <.1 percent of the ground state signal), with one or both cw frequencies present.

As a check, the same experiment was performed for Na, where we know that a large fraction of the atoms can be excited. The results are shown in Fig. 7. Here, the overlap of the cw and pulsed beams was done by maximizing the ion signal from the 3P state. The cw beam was unfocused so it would be larger than the cross section of the pulsed

beam. The pulsed beam was unfocused, and its cross section determined by an aperture. Once the 3P$\longrightarrow$$Na^+$ ion signal was maximized with respect to the cw laser beam position, only the dyes were changed in the pulsed laser to measure the ground state signal. Again, all signals were saturated and resonant as expected. (In regard to this last point, care was taken to be sure that the pulsed laser was operating with a low level of amplified spontaneous emission. Initial experiments indicated that the intermediate state (4D or 4P) resonance was quite broad. This was found to be from amplified spontaneous emission and the large oscillator strengths of these transitions.) The absolute determination of the 3P/3S ratio for sodium was very small by this technique. Additionally, no depletion of the ground state ion signal by optical pumping with the cw laser to the 3P state was seen.

If the Rabi frequency of the cw 3S-3P transition is large compared to the time duration of the ionization laser pulse, then it might be possible to so strongly saturate the ionization step, that as the atoms cycle between the 3S and 3P states, they can all be removed by the ionization laser. To check this, the uv power was reduced so the ion signal was several orders of magnitude lower than when saturated. Again, no depletion was obtained. If the Na beam was blocked, the ion signal disappeared.

To explain the results, we are forced to assume either an error in the experiment, or in our naive model for the ionization process. With regard to the former, the apertures in the vacuum chamber near to the

ion collector were efficient at ion production if the pulsed laser was not properly aligned. Back reflections from the optical windows also produced ion signal if the laser beam was not aligned properly. It is known that aromatic compounds are ionized efficiently and sometimes dissociatively by uv light. The silicone pumping fluid could then contribute some signal, but the resonant conditions for the ionizing frequencies cast doubt on this interpretation. Most probably, the total ion yield, which depends on the knowledge of the system for the duration of the pulsed laser excitation, is not simply a matter of our naive view of 30 percent of the population in the 3P state. Instead, it might depend on the amount of 3S character in the wavefunction. More elaborate experiments and models will be needed to check the behavior of Na or Li atoms in the presence of several saturated resonant fields and with access to a continuum decay.

REFERENCES

1. H. J. Gerritsen, G. Nienhuis, App. Phys. Lett., 26, 347 (1975).
2. G. Carter, D. Pritchard, I. Ducas, App. Phys. Lett., 27, 498 (1975).
3. H. R. Gray, R. Whitley, C. Stroud, Opt. Lett., 3, 218 (1978).
4. G. Orriols, Nuovo Cimento, 53B, 1 (1979).
5. B. Dalton, P. Knight, "The effects of laser field fluctuations on coherent population trapping," sub. to J. Phys. B (1982).
6. P. Radmore, P. Knight, J. Phys. B, 15, 561 (1982).
7. J. Thomas, P. Hemmer, S. Ezekiel, C. Leiby, R. Picard, C. Willis, Phys. Rev. Lett., 48, 867 (1982).
8. R. Whitley and C. Stroud, Phys. Rev. A, 14, 1498 (1976).
9. G. Baum, C. Caldwell, W. Schroder, App. Phys. 21, 121 (1980).
10. C. Becker, P. Casavecchia, P. Tiedemann, J. Valentini, Y. T. Lee, J. Chem. Phys. 73, 2833 (1980).
11. S. Kramer, J. Young, G. Hurst, M. Payne, Opt. Comm., 30, 47 (1979).

FIGURE CAPTIONS

Fig. 1. ^{23}Na hyperfine structure for the $3^2S_{1/2}$ and $3^2P_{1/2}$ electronic states. The solid lines with double headed arrows show the m levels connected by simulated emission by the two, linearly polarized lasers tuned to the $^2S_{1/2}$ (F=1,2)$\longrightarrow$$^2P_{1/2}$ (F'=1) transitions. The wavy, single headed arrows show which ground state m sublevels are connected to the F'=1, M=-1 sublevel by spontaneous emission. It can be seen that the $3^2S_{1/2}$(F=2), M = -2 sublevel is a trap by this optical pumping scheme.

Fig. 2. (a). Three level lamda system. δ_a and δ_b are the frequency offsets of the two applied fields (whose frequencies are W_1 and W_2) from the 0$\longrightarrow$1 and 2$\longrightarrow$1 transition resonances. Γ_{10} and Γ_{12} are the spontaneous emission rates from level 1 to levels 0 and 2 respectively.

(b). Hyperfine structure of the $2^2S_{1/2}$ and $2^2P_{3/2}$ states for ^6Li.

Fig. 3. (a). Fraction 1, steady state population in the excited level of the lamda system shown in Fig. 2(a). ζ is the rabi frequency of the fields, in units of the total spontaneous decay rate from state 1. Δ_{ab}=1 and 0 are the limits of full or no cross-correlation between the laser fields. The family of curves on each graph shows the dependence of the excited state population as one frequency is scanned with the other held fixed at different frequency offsets from resonance. The offset frequency is the location of the node in the curves.

(b). Power dependence of the excited state asymptotic population when one laser field is scanned through the lamda system. The $\delta_a - \delta_b$ frequency offset corresponds to the ^{6}Li $2^2S_{1/2}$ hyperfine splitting.

Fig. 4. Experimental arrangement used to study the optical pumping and ionization of Li and Na atoms. An Ar ion laser pumps a commercial dye laser, which passes through an acousto-optic modular (AOM). The two output frequencies are recombined on a prism, then orthogonally cross the atomic beam. The fluorescence is imaged onto a photomultiplier by a lens/spatial filter combination.

Fig. 5. Frequency dependence of ^{6}Li fluorescence observed for several different laser powers. The curves on the left hand side are for a single laser frequency. The curves on the right hand side were observed when both laser frequencies derived from the acousto-optic modulator excited the Li beam.

Fig. 6. Li^+ ion yield vs. laser power for the 2S$\longrightarrow$3P transition (solid line) and the 3P$\longrightarrow$4D transition (dashed line).

Fig. 7. Na^+ ion yield vs. laser power for the 3S$\longrightarrow$3P transition (solid line) and the 3P$\longrightarrow$4D transition (dashed line).

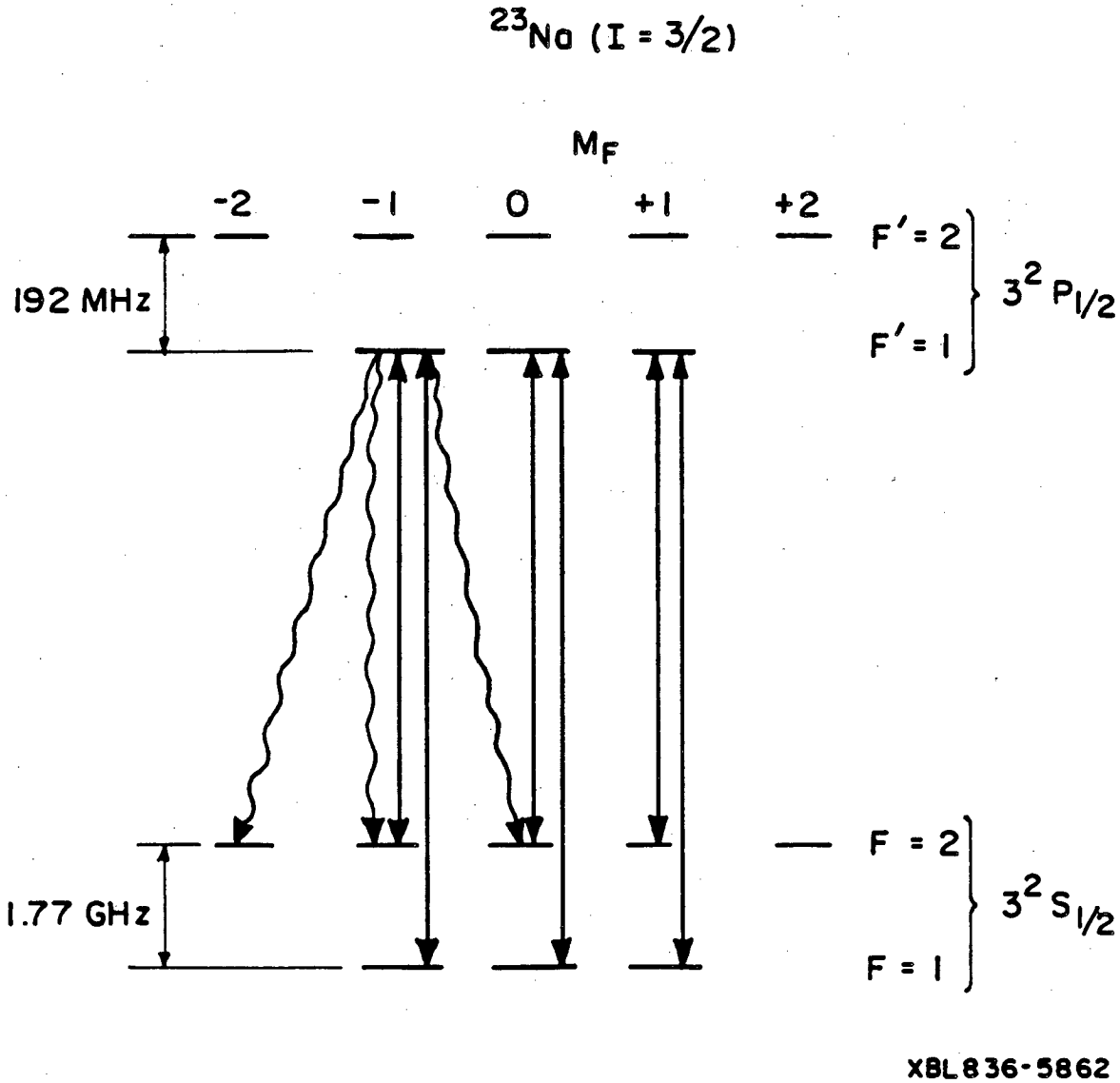
^{23}Na (I = 3/2)
M_F
-2
-1
0
+1
+2
192 MHz
F′ = 2
F′ = 1
$3^2P_{1/2}$
1.77 GHz
F = 2
F = 1
$3^2S_{1/2}$
XBL836-5862

Fig. 1

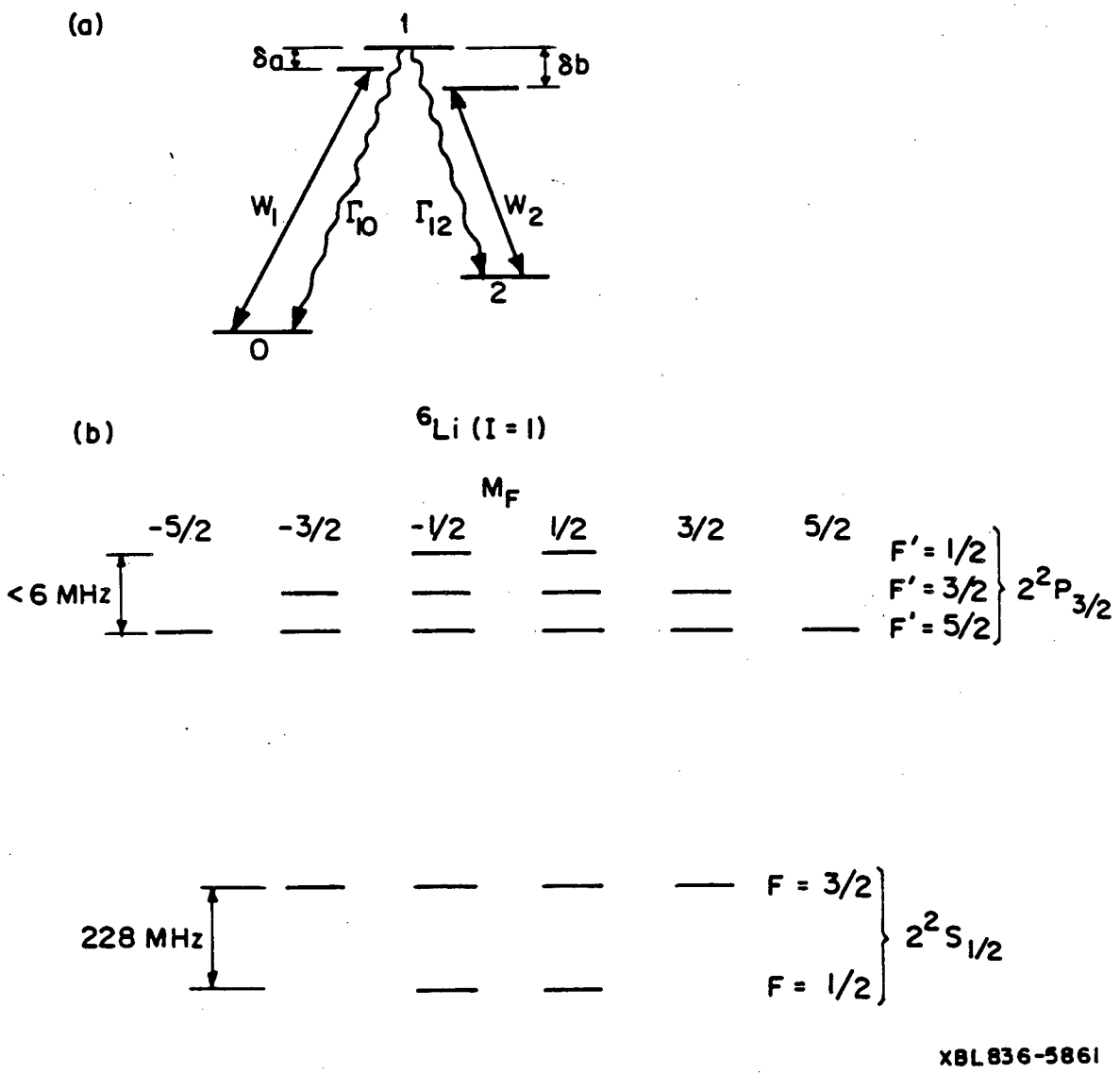
(a)
1
δa
δb
W1
Γ10
Γ12
W2
2
0
(b)
6Li (I = 1)
MF
-5/2
-3/2
-1/2
1/2
3/2
5/2
F' = 1/2
F' = 3/2
F' = 5/2
2²P3/2
< 6 MHz
228 MHz
F = 3/2
F = 1/2
2²S1/2
XBL836-5861

Fig. 2

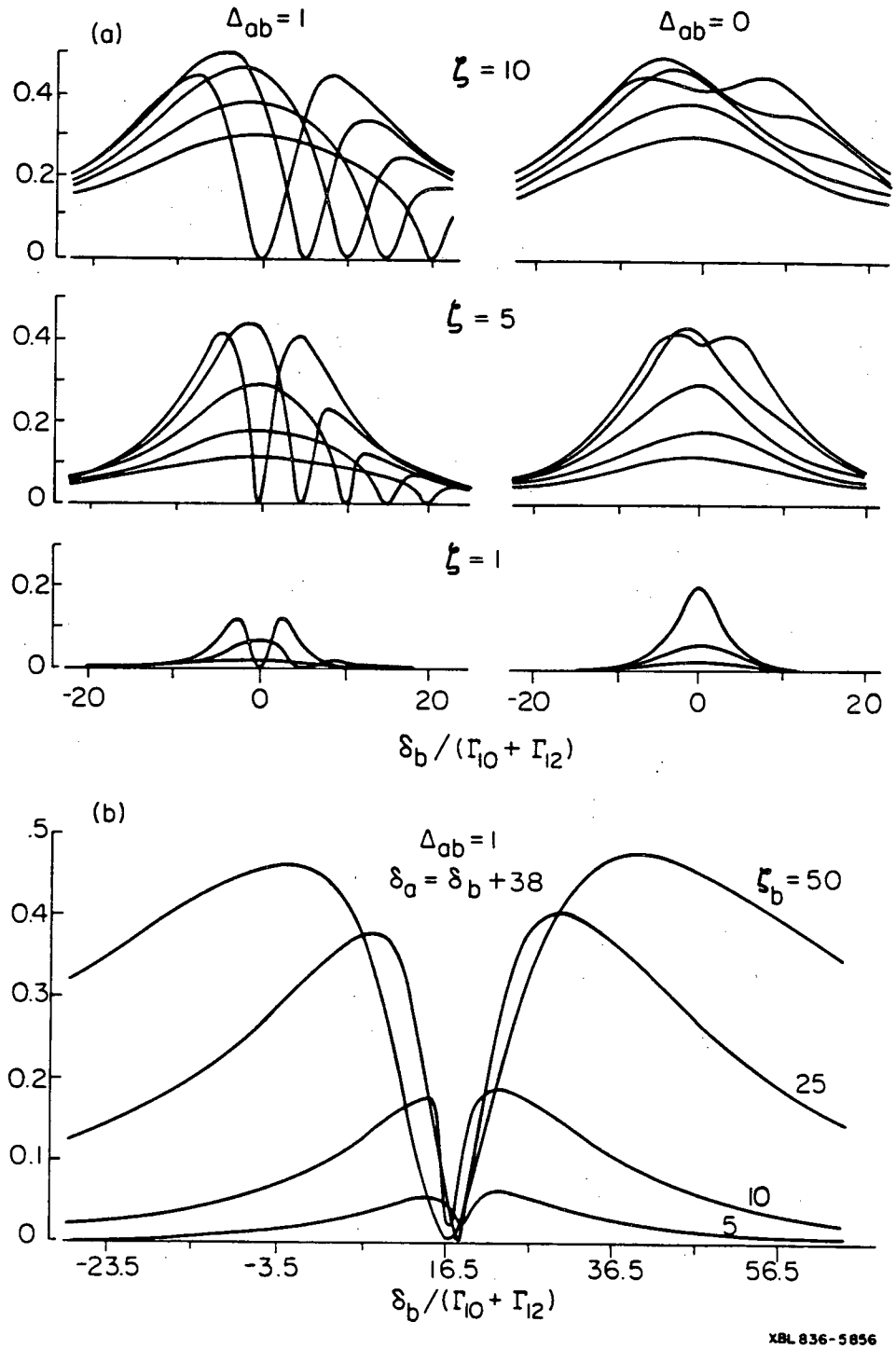
(a)
$\Delta_{ab} = 1$
$\Delta_{ab} = 0$
$\zeta = 10$
$\zeta = 5$
$\zeta = 1$
0.4
0.2
0
-20
0
20
$\delta_b / (\Gamma_{10} + \Gamma_{12})$
(b)
$\Delta_{ab} = 1$
$\delta_a = \delta_b + 38$
$\zeta_b = 50$
25
10
5
.5
0.4
0.3
0.2
0.1
0
-23.5
-3.5
16.5
36.5
56.5
$\delta_b / (\Gamma_{10} + \Gamma_{12})$
XBL 836-5856

Fig. 3

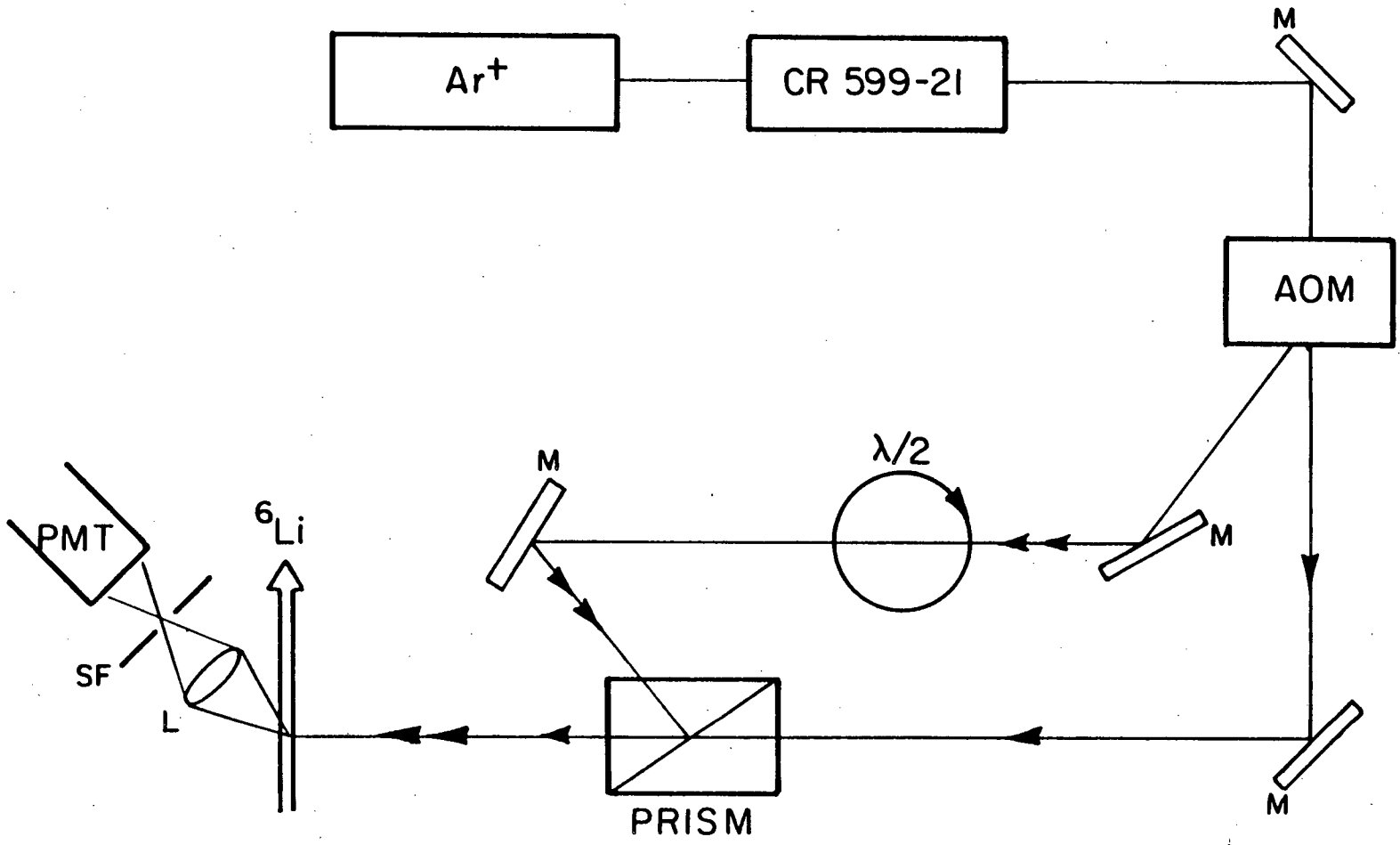

Fig. 4

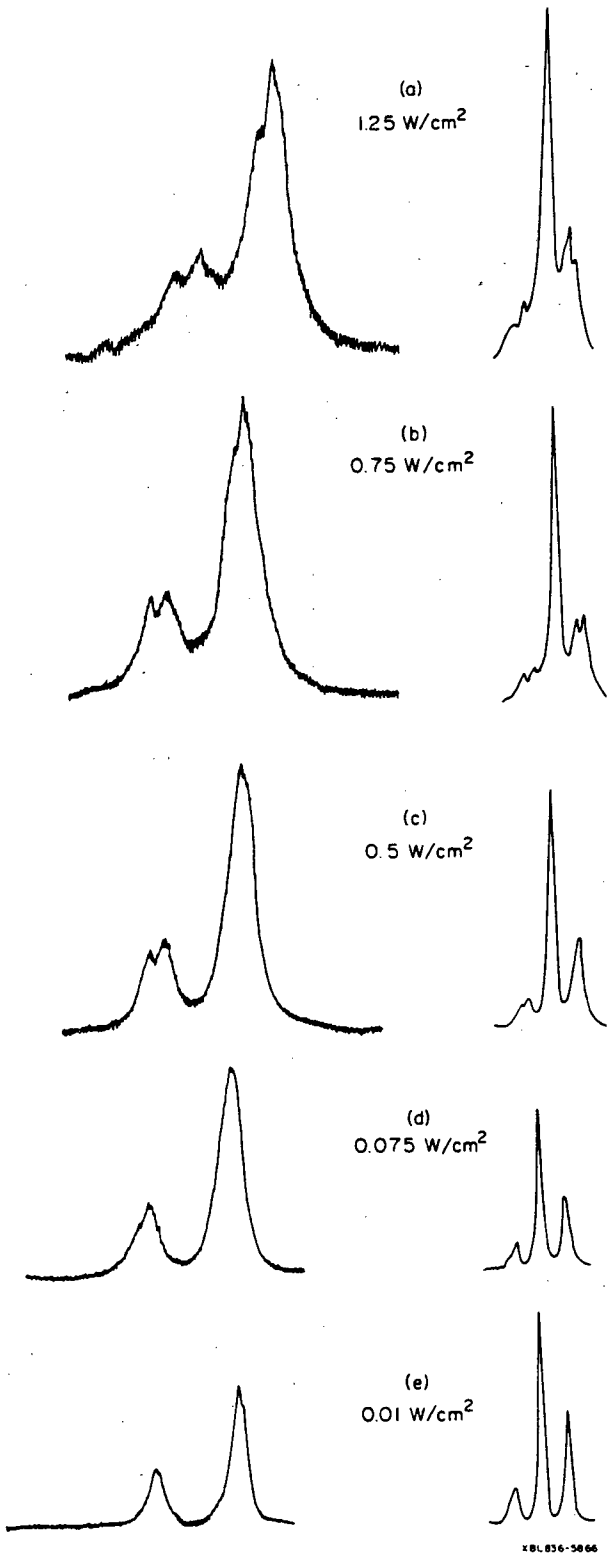
(a)
1.25 W/cm²
(b)
0.75 W/cm²
(c)
0.5 W/cm²
(d)
0.075 W/cm²
(e)
0.01 W/cm²
XBL 836-5866

Fig. 5

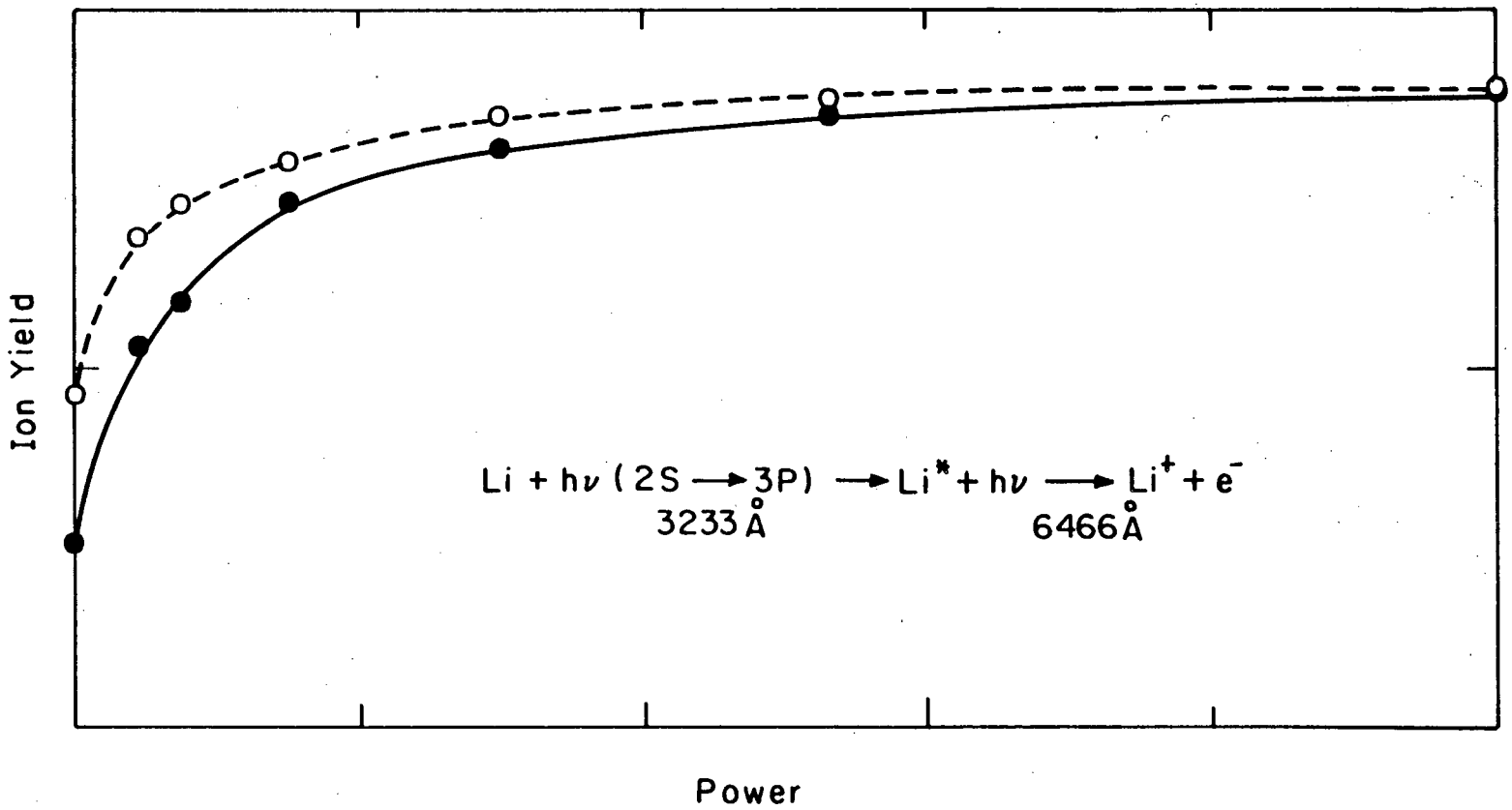

XBL 836-5858

Fig. 6

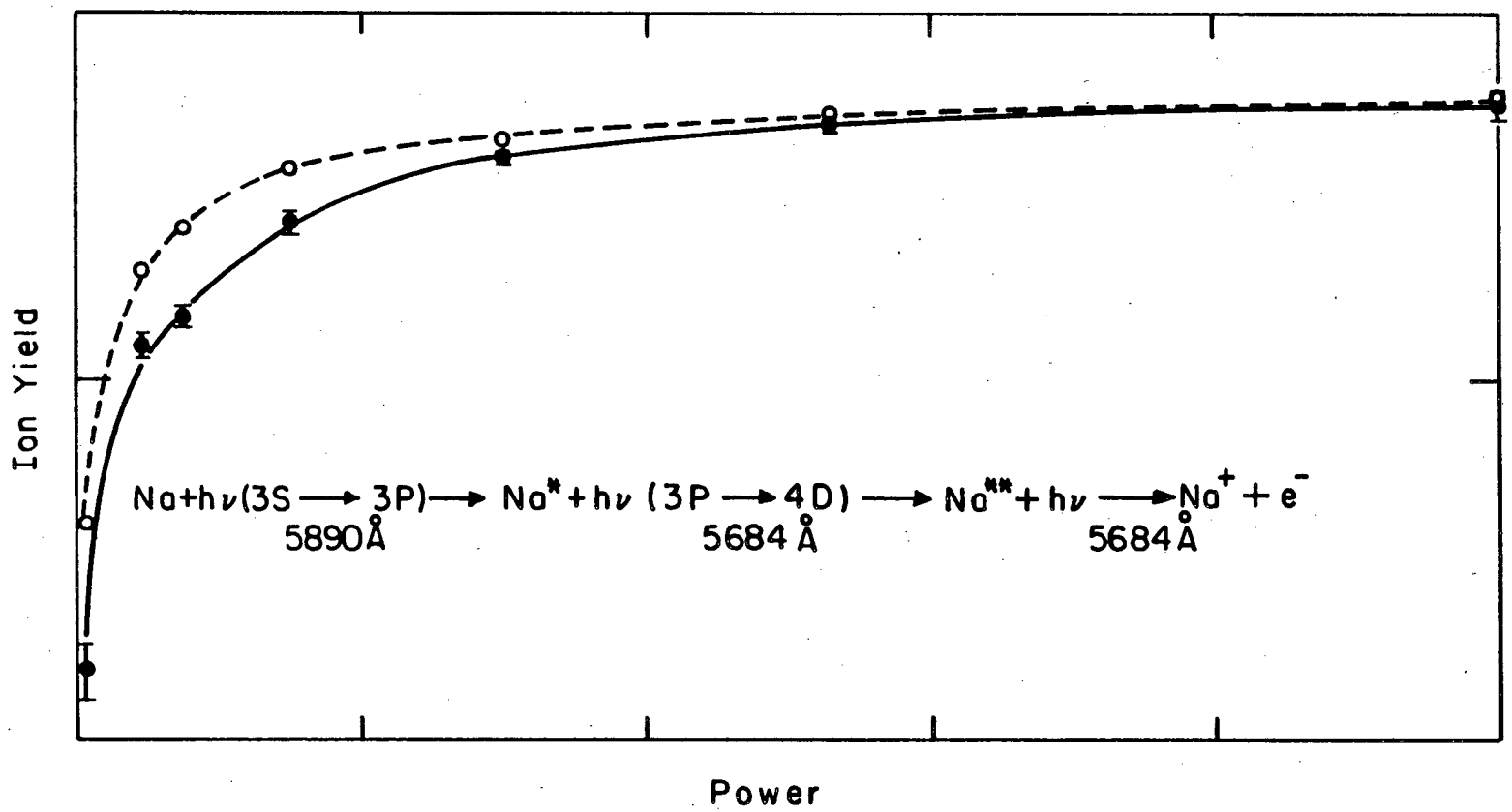

XBL836-5857

Fig. 7

This report was done with support from the Department of Energy. Any conclusions or opinions expressed in this report represent solely those of the author(s) and not necessarily those of The Regents of the University of California, the Lawrence Berkeley Laboratory or the Department of Energy.

Reference to a company or product name does not imply approval or recommendation of the product by the University of California or the U.S. Department of Energy to the exclusion of others that may be suitable.

TECHNICAL INFORMATION DEPARTMENT
LAWRENCE BERKELEY LABORATORY
UNIVERSITY OF CALIFORNIA
BERKELEY, CALIFORNIA 94720